# DNA DAMAGE, GENOME STABILITY AND HUMAN DISEASE

EDITED BY: Yuejin Hua, Hari S. Misra and Anthony Davis
PUBLISHED IN: Frontiers in Genetics, Frontiers in Cell and Developmental Biology and Frontiers in Pediatrics

frontiers Research Topics

# frontiers



ISSN 1664-8714
ISBN 978-2-88974-194-6
DOI 10.3389/978-2-88974-194-6

## About Frontiers

Frontiers is more than just an open-access publisher of scholarly articles: it is a pioneering approach to the world of academia, radically improving the way scholarly research is managed. The grand vision of Frontiers is a world where all people have an equal opportunity to seek, share and generate knowledge. Frontiers provides immediate and permanent online open access to all its publications, but this alone is not enough to realize our grand goals.

## Frontiers Journal Series

The Frontiers Journal Series is a multi-tier and interdisciplinary set of open-access, online journals, promising a paradigm shift from the current review, selection and dissemination processes in academic publishing. All Frontiers journals are driven by researchers for researchers; therefore, they constitute a service to the scholarly community. At the same time, the Frontiers Journal Series operates on a revolutionary invention, the tiered publishing system, initially addressing specific communities of scholars, and gradually climbing up to broader public understanding, thus serving the interests of the lay society, too.

## Dedication to Quality

Each Frontiers article is a landmark of the highest quality, thanks to genuinely collaborative interactions between authors and review editors, who include some of the world's best academicians. Research must be certified by peers before entering a stream of knowledge that may eventually reach the public - and shape society; therefore, Frontiers only applies the most rigorous and unbiased reviews.
Frontiers revolutionizes research publishing by freely delivering the most outstanding research, evaluated with no bias from both the academic and social point of view. By applying the most advanced information technologies, Frontiers is catapulting scholarly publishing into a new generation.

## What are Frontiers Research Topics?

Frontiers Research Topics are very popular trademarks of the Frontiers Journals Series: they are collections of at least ten articles, all centered on a particular subject. With their unique mix of varied contributions from Original Research to Review Articles, Frontiers Research Topics unify the most influential researchers, the latest key findings and historical advances in a hot research area! Find out more on how to host your own Frontiers Research Topic or contribute to one as an author by contacting the Frontiers Editorial Office: frontiersin.org/about/contact

# DNA DAMAGE, GENOME STABILITY AND HUMAN DISEASE

Topic Editors:
**Yuejin Hua,** Zhejiang University, China
**Hari S. Misra,** Bhabha Atomic Research Centre (BARC), India
**Anthony Davis,** University of Texas Southwestern Medical Center, United States

**Citation:** Hua, Y., Misra, H. S., Davis, A., eds. (2022). DNA Damage, Genome Stability and Human Disease. Lausanne: Frontiers Media SA.
doi: 10.3389/978-2-88974-194-6

# Table of Contents

frontiers in Genetics

ORIGINAL RESEARCH
published: 10 September 2020
doi: 10.3389/fgene.2020.01036

# Combining PARP and DNA-PK Inhibitors With Irradiation Inhibits HPV-Negative Head and Neck Cancer Squamous Carcinoma Growth

*Ling Zeng[1†], Drexell Hunter Boggs[1†], Chuan Xing[1], Zhuo Zhang[1], Joshua C. Anderson[1], Narendra Wajapeyee[2,3], Chris Veale[1], Markus Bredel[1], Lewis Z. Shi[1], James A. Bonner[1], Christopher D. Willey[1,2,3,4] and Eddy S. Yang[1,3,4,5]**

[1] Department of Radiation Oncology, University of Alabama at Birmingham School of Medicine, Birmingham, AL, United States, [2] Department of Biochemistry and Molecular Genetics, University of Alabama at Birmingham School of Medicine, Birmingham, AL, United States, [3] O'Neal Comprehensive Cancer Center, University of Alabama at Birmingham School of Medicine, Birmingham, AL, United States, [4] Department of Cell, Developmental, and Integrative Biology, University of Alabama at Birmingham School of Medicine, Birmingham, AL, United States, [5] Department of Pharmacology and Toxicology, University of Alabama at Birmingham School of Medicine, Birmingham, AL, United States

OPEN ACCESS

**Edited by:**
Anthony Davis,
University of Texas Southwestern Medical Center, United States

**Reviewed by:**
Tomasz Skorski,
Temple University, United States
Stephen B. Keysar,
University of Colorado Denver, United States

***Correspondence:**
Eddy S. Yang
eyang@uab.edu

[†] These authors have contributed equally to this work

**Specialty section:**
This article was submitted to Genetics of Common and Rare Diseases, a section of the journal Frontiers in Genetics

**Received:** 16 June 2020
**Accepted:** 11 August 2020
**Published:** 10 September 2020

**Citation:**
Zeng L, Boggs DH, Xing C, Zhang Z, Anderson JC, Wajapeyee N, Veale C, Bredel M, Shi LZ, Bonner JA, Willey CD and Yang ES (2020) Combining PARP and DNA-PK Inhibitors With Irradiation Inhibits HPV-Negative Head and Neck Cancer Squamous Carcinoma Growth. Front. Genet. 11:1036. doi: 10.3389/fgene.2020.01036

Novel targeted agents to inhibit DNA repair pathways to sensitize tumors to irradiation (IR) are being investigated as an alternative to chemoradiation for locally advanced human papilloma virus negative (HPV-negative) head and neck squamous cell carcinoma (HNSCC). Two well-characterized targets that, when inhibited, exhibit potent IR sensitization are PARP1 and DNA-PKcs. However, their cooperation in sensitizing HPV-negative HNSCC to IR remains to be explored given that PARP1 and DNA-$Pk_{CS}$ bind to unresected stalled DNA replication forks and cooperate to recruit XRCC1 to facilitate double-strand break repair. Here, we show that the combination of the DNA-PK inhibitor NU7441 and the PARP inhibitor olaparib significantly decrease proliferation (61–78%) compared to no reduction with either agent alone ($p < 0.001$) in both SCC1 and SCC6 cell lines. Adding IR to the combination further decreased cell proliferation (91–92%, $p < 0.001$) in SCC1 and SCC6. Similar results were observed using long-term colony formation assays [dose enhancement ratio (DER) 2.3–3.2 at 4Gy, $p < 0.05$]. Reduced cell survival was attributed to increased apoptosis and G2/M cell cycle arrest. Kinomic analysis using tyrosine (PTK) and serine/threonine (STK) arrays reveals that combination treatment results in the most potent inhibition of kinases involved in the CDK and ERK pathways compared to either agent alone. *In vivo*, a significant delay of tumor growth was observed in UM-SCC1 xenografts receiving IR with olaparib and/or NU7441, which was similar to the cisplatin-IR group. Both regimens were less toxic than cisplatin-IR as assessed by loss of mouse body weight. Taken together, these results demonstrate that the combination of NU7441 and olaparib with IR enhances HPV-negative HNSCC inhibition in both cell culture and in mice, suggesting a potential innovative combination for effectively treating patients with HPV-negative HNSCC.

**Keywords: DNA repair, DNA damage, PARP inhibitors, DNA-PK inhibitors, non-homologous end-joining, homologous recombination**

## INTRODUCTION

Current organ preservation treatment strategies for patients with head and neck squamous cell carcinoma (HNSCC) involve concurrent chemoradiation, which enhances radiation (IR)-induced DNA damage. Repair of this damage utilizes either single-strand break (SSB) or double-strand break (DSB) repair pathways. We and others have previously shown that inhibition of poly (ADP) ribose polymerase-1 (PARP1), a member of the SSB base excision repair pathway, is a potent sensitizer of tumor cells to IR (Nowsheen et al., 2011b; Swindall et al., 2013) in HNSCC cells.

Similarly, inhibition of deoxyribonucleic acid protein kinase catalytic subunit (DNA-Pk$_{CS}$), a key player in the DSB non-homologous end joining (NHEJ) repair also radiosensitizes cells (Azad et al., 2014; Ying et al., 2016; Brown et al., 2017; Lee et al., 2019). NHEJ is involved in ˜80% of DSB repairs induced by radiation in cancer cells (Kakarougkas and Jeggo, 2014), and DNA-Pk$_{cs}$ inhibitors, such as the oral inhibitor M3814, can potentiate the antitumor activity of IR in HNSCC cell lines *in vivo* (Zenke et al., 2020).

Previous work shows that PARP1 and DNA-Pk$_{CS}$ bind unresected stalled DNA replication forks and cooperate to recruit XRCC1 to facilitate DSB repair (Spagnolo et al., 2012; Azad et al., 2014; Ying et al., 2016; Fok et al., 2019). Additionally, combined inhibition of PARP1 and DNA-PK may increase genomic instability due to differing mechanisms by each inhibitor (Fok et al., 2019). Combination of PARP1 and DNA-PK inhibitors has also been shown to decrease cell growth by 20% *in vitro* and 60% *in vivo* in HNSCC cell lines compared to monotherapy of either agent (Fok et al., 2019). Because unrepaired IR-induced DNA damage may also cause replication stress and mitotic catastrophe (Mahaney et al., 2009), we hypothesized that, due to the crosstalk of these pathways, combining DNA-PK and PARP inhibitors could potentiate IR-induced damage leading to enhanced IR sensitivity in HNSCC cells.

To test this hypothesis, we investigated the *in vitro* and *in vivo* effects of the DNA-PK inhibitor NU7441 and the PARP inhibitor olaparib with irradiation in HPV-negative HNSCC cell lines. Indeed, combining NU7441 and olaparib with IR significantly reduced cell survival compared to IR with either agent alone. Cytotoxicity was due to increased apoptosis and G2/M cell cycle arrest. Mechanistically, kinomic analysis revealed that combination treatment resulted in the greatest inhibition of kinases involved in the CDK and ERK pathways compared to either agent alone. A significant tumor growth delay was observed *in vivo* in UM-SCC1 xenografts receiving IR with olaparib and/or NU7441. These results support the further testing of combining DNA-PK and PARP inhibitors with irradiation in patients with HNSCC.

## MATERIALS AND METHODS

### Cell Lines and Inhibitors

The HPV-negative UM-SCC1 and UM-SCC6 cell lines were obtained courtesy of Dr. Thomas E. Carey (University of Michigan, Ann Arbor, MI). UM-SCC1-luciferase was obtained from Dr. Eben Rosenthal (Stanford University, Stanford, CA, United States). These cell lines have been previously described (Weaver et al., 2015; Zeng et al., 2017). UM-SCC1 and UM-SCC6 cell lines were maintained in DMEM growth medium (Sigma) supplemented with 10% FBS (SAFC Biosciences) and 1% penicillin/streptomycin (Gibco). The DNA-Pk$_{CS}$ inhibitor NU7441 (Tocris Cat #3712) was used at 0.5 μM *in vitro* and 2, 4, and 8 mg/kg *in vivo*. The PARP inhibitors olaparib (LC laboratories Cat #763113-22-0) was used at 3 μM *in vitro* and 25 mg/kg *in vivo*. MK4827 (Selleckchem Cat #S2741), another PARP inhibitor, was used at 100 nM *in vitro*. Cisplatin was used at 4 mg/kg *in vivo*.

### Measurement of Cell Proliferation

Cell proliferation assays were performed as described previously (Weaver et al., 2015; Zeng et al., 2017). Briefly, cells were seeded in 24-well plates and harvested at 72 and 96 h after treatment. Cells were washed with PBS, trypsinized, and diluted 1:20 in isotonic saline solution (RICCA Chemical, catalog #7210-5). Diluted cells were counted using a Beckman Z1 Coulter particle counter. Cell counts were represented as cells/mL.

### Colony Formation Assay

Clonogenic survival was assessed by the colony formation assay as described previously (Nowsheen et al., 2011b, 2012; Zeng et al., 2017). Cells were treated accordingly and remained undisturbed for 2 weeks. Media was not replaced throughout the experiment. Cells were fixed and stained in 25% glutaraldehyde/12 mmol/L crystal violet solution, and the numbers of colonies were counted. Survival fraction was calculated as follows: (number of colonies counted in experimental plate/number of cells seeded in experimental plate)/(number of colonies counted in control plate/number of cells seeded in control plate). A dose-enhancement ratio (DER) was also calculated to illustrate the magnitude of radiation sensitization. The DER is defined as the ratio of the radiation dose required to obtain a surviving fraction (SF) of 0.5, without drug pretreatment, to that required to obtain the same SF after drug pretreatment.

### Cell Cycle

Cell-cycle distribution was measured as previously described (Nowsheen et al., 2011b, 2012; Zeng et al., 2017). Cells were seeded in 100 mm$^2$ dishes and treated accordingly. Twenty-four and 48 h after treatment, cells were collected, fixed, treated with RNAse (Sigma, catalog #R-4875), stained with propidium iodide (PI), and read on FACS Calibur using Cell Quest. Data were analyzed using ModFit LT (Verity Software Inc.).

### Measurement of Apoptosis

Apoptosis was analyzed using the Annexin V-FITC Apoptosis Detection kit (BioVision Research Products, 3K101-400) according to the manufacturer's instructions and was previously described (Nowsheen et al., 2011b, 2012; Zeng et al., 2017).

## Western Blot Analysis

Protein was analyzed by SDS-PAGE as previously described (Nowsheen et al., 2011b, 2012; Zeng et al., 2017). The following primary antibodies from Cell Signaling Technology were used at manufacturer-recommended dilutions for immunoblotting: phosphor-(Thr) MAPK/CDK substrate (#2321), phosphor-erk1/2 (#9101), total erk1/2 (#9102). Actin (Santa Cruz Biotechnology, catalog #sc-47778) was included as a loading control. Species-specific horseradish peroxidase–conjugated secondary antibodies (Santa Cruz Biotechnology) were used at 1:20,000 dilution.

## Kinomic Analysis

Lysates from UM-SCC1 treated with 2Gy IR, with and without 3 μM olaparib and/or 0.5 μM NU7441, were collected immediately after treatment and lysed in MPER lysis buffer with Halt's protease and phosphatase inhibitors as described previously. After BCA-based protein quantification, lysates were then analyzed with 15 μg of protein on the tyrosine (PTK) arrays and 2 ug of protein on the serine/threonine (STK) arrays as previously described using a PamStation12 (PamGene, The Netherlands) (Jarboe et al., 2012; Anderson et al., 2014; Isayeva et al., 2015). Phosphorylation data was collected over multiple computer-controlled pumping cycles and exposure times (10–200 ms) for ∼144–196 substrates per array. Comparative analysis of kinases upstream of altered peptide prediction was performed in BioNavigator v6.3 using PTK and STK UpKin PamApps (v 6.0).

Whole chip comparative analysis identified that combined olaparib and NU7441 altered kinase activity as compared to IR alone (summarized in **Supplementary Table S1**). Olaparib- and NU7441-altered kinases were uploaded to GeneGo (portal.genego.com, Clarivate Analytics) to identify biological networks, using indicated maximum node size with an AutoExpand model, canonical pathways, reactions, metabolites, and orphan nodes deselected or excluded.

## Animal Studies

All animal procedures were approved and in accordance with the UAB Institutional Animal Care and Use Committee guidelines. Four-week-old, 20 g, female athymic nude mice (Charles River Laboratories) were allowed to acclimatize for 1 week before experiments. For the orthotopic UM-SCC1-luc model, 100,000 cells were injected into the oral tongue, and tumors were imaged biweekly using a luciferase bioluminescence assay starting at day 4 after injection. Mice received intraperitoneal injections of D-luciferin substrate (150 mg/kg) 15 min before imaging, and luminescence was measured in photons per second. A pilot study was performed to assess potential dose-related toxicities of DNA-PK inhibitor NU7441 (2, 4, or 8 mg/kg IP once daily) in combination with PARP inhibitor olaparib (25 mg/kg, oral gavage twice a day) and irradiation (2 Gy, twice weekly). Treatments were given for three cycles over a total of 15 days. Tumor growth was determined via luciferase, and body weight or any other signs of treatment-related toxicities were recorded. The optimal does of DNA-PK inhibitor NU7441 (4 mg/kg) was selected for the combination treatment in the tumor growth delay study. Cisplatin (4 mg/kg) was also used as a comparison control.

## Statistical Analysis

Data were analyzed by analysis of variance (ANOVA) followed by Bonferroni post-test using GraphPad Prism version 4.02 (GraphPad Software, San Diego, CA, United States). Data are presented as average ± SE.

# RESULTS

## Combining DNA-PK and PARP Inhibition With or Without IR Inhibits HNSCC Growth in Cell Culture

The potent radiosensitization properties of DNA-PK and PARP inhibitors as well as the interactions of DNA-PK and PARP1 in replication stress repair suggest the potential for increased efficacy by combining these inhibitors with IR. We, therefore, tested the cell proliferation effects of DNA-PK inhibitor, NU7441, and PARP inhibitor olaparib with or without IR in UM-SCC1 or UM-SCC6 head and neck cancer cells. As shown in **Figure 1**, the combination of NU7441 and olaparib without irradiation significantly decreased proliferation by 60.7% compared to no reduction with either agent alone in UM-SCC1 (**Figure 1A**) and by 78% in UM-SCC6 (**Figure 1B**) cells at 96 h. The addition of 4 Gy IR to the combination further reduced cell growth (UM-SCC1: 60.7 vs. 91.3%, $p < 0.001$; UM-SCC6: 78 vs. 92%, $p < 0.001$). To verify the efficacy of this combination, we also performed long-term colony-formation assays. As shown in **Figures 1C,D**, a 92.2% reduction in clonogenic survival in UM-SCC1 cells was observed (DER = 3.2 at 4 Gy) and 98.8% reduction in UM-SCC6 cells (DER = 2.3 at 4 Gy). Similar inhibition of cell proliferation and inhibition of clonogenic survival was observed with another PARP inhibitor MK4827 (**Supplementary Figure S1**).

## NU7441 and Olaparib Induce Apoptosis and G2/M Cell Cycle Arrest

One of the major mechanisms of DNA damage-induced cytotoxicity by IR is cell cycle redistribution. Therefore, we next assessed the effects of the various treatments on the cell cycle at 24 and 48 h post IR (4 Gy). At 24 and 48 h post IR, minimal changes in cell cycle distribution were observed with NU7441, olaparib, or IR alone in the UM-SCC1 cells (**Figure 2A**). Interestingly, combining NU7441 with IR resulted in greater accumulation of SCC1 cells in the G2/M cell cycle compared to NU7441 alone (13.3 vs. 57.4%, $p < 0.001$). However, the addition of olaparib to this combination did not further increase the percentage of cells in G2/M. Similar results were observed with MK4827, which revealed that cells treated with IR accumulate in G2/M, and that is further increased by drug treatment at 12 h post IR. Cells treated with IR alone recover by 24 h post IR although combination groups continue to accumulate in G2/M (**Supplementary Figure S2**).

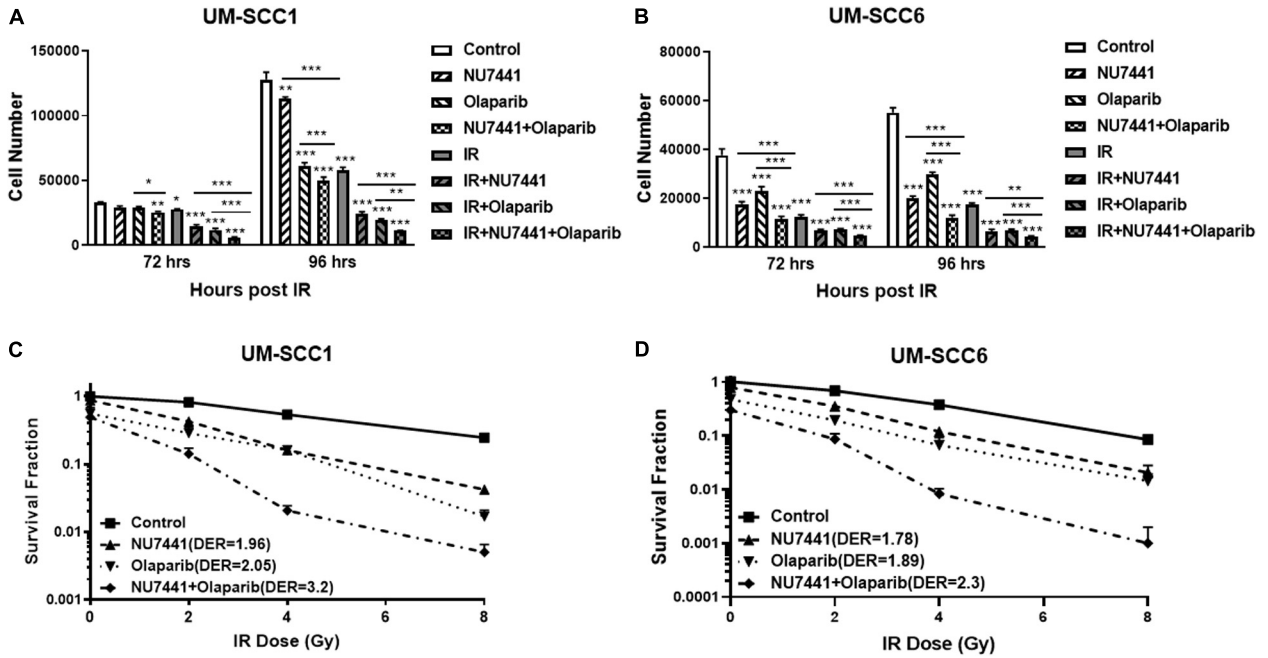


**FIGURE 1 |** Combination treatment with NU7441 (DNAPKi), Olaparib (PARPi), and IR suppresses **(A,B)** cell proliferation and **(C,D)** clonogenic survival in **(A,C)** UM-SCC1, and **(B,D)** UM-SCC6 head and neck cancer cell lines. For cell proliferation assays, cells were treated with either vehicle or 0.5 μM or 1 μM NU7441 for 16 h, then 3 μM olaparib for 2 h, followed by sham or 2 Gy or 4 Gy IR. Cell numbers were counted at 72 and 96 h after IR using a Beckman Z1 Coulter counter. Shown is the mean ± SEM from at least two independent experiments performed in triplicate; $^{*}p < 0.05$; $^{**}p < 0.01$; $^{***}p < 0.001$. For clonogenic assays, cells were treated with NU7441 and olaparib accordingly, then followed by 0, 2, 4, and 8 Gy IR. Media was left unchanged for 2 weeks. Cells were fixed, and the number of colonies were counted. Experiments were performed at least in triplicate. Each group showed statistically significant differences ($p < 0.05$).

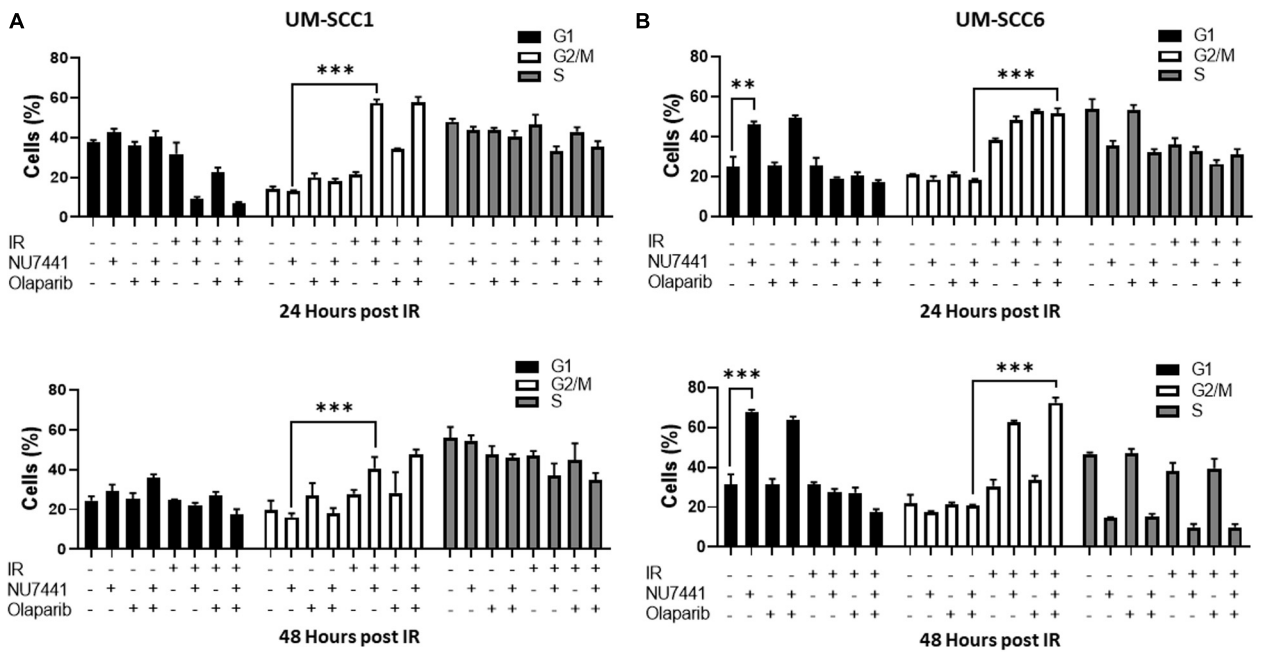


**FIGURE 2 |** Cell cycle redistribution 24 and 48 h after IR (4 Gy) with NU7441 (DNAPKi) and Olaparib (PARPi) in **(A)** UM-SCC1 and **(B)** UM-SCC6 head and neck cancer cell lines. Cells were treated with either vehicle or 1 μM NU7441 for 16 h, then 3 μM olaparib for 2 h, followed by sham or 4 Gy IR. Cells were stained with propidium iodide at 24 and 48 h after IR and analyzed for cell cycle distribution by flow cytometry. Shown is the mean ± SEM from at least two independent experiments performed in triplicate; $^{**}p < 0.01$; $^{***}p < 0.001$.

In contrast, at 24 h post-IR in the UM-SCC6 cells, NU7441 appeared to cause G1 phase accumulation (25 vs. 46%, $p = 0.0023$, **Figure 2B**). This effect was further magnified at 48 h post-IR. The addition of IR to NU7441 or olaparib or both NU7441 and olaparib induced G2/M accumulation at 24 h post-IR (18.4 vs. 51.6%, $p < 0.001$) and was further sustained at 48 h post-IR with the triple combination (**Figure 2B**).

To investigate the effects of NU7441 and/or olaparib with and without IR on apoptosis, we performed annexin V assays. As shown in **Figure 3, NU7441** and **olaparib** alone did not show a substantial increase in apoptosis in the UM-SCC1 (**Figure 3A**) or UM-SCC6 (**Figure 3B**) cells. However, in both cell lines, a statistically significant increase in apoptosis was observed at 24 and 48 h with IR in combination with NU7441 or olaparib alone, and that is further increased with the triple combination (UM-SCC1, $p = 0.003$; UM-SCC6, $p = 0.0001$).

## NU7441 and Olaparib Reduce CDK, MAPK, and ERK Signaling

We and others have previously reported crosstalk between the DNA damage response (DDR) and receptor tyrosine kinase cell signaling pathways (Dittmann et al., 2005, 2008, 2010; Golding et al., 2007, 2009; Nowsheen et al., 2011a, 2012; Jarboe et al., 2012). To perform an unbiased analysis of potential alterations in cell signaling events with our treatments, we performed kinomic analysis using the PamStation12, which allows for real-time detection and kinetic data on kinase/substrate interactions. As shown in **Figure 4A**, combining NU7441, olaparib, and IR resulted in inhibition of kinases involved in a network centering around CDK and ERK. To validate the kinomic data, we performed western blot analysis in the UM-SCC1 cells treated with various combinations of IR, NU7441, and olaparib. As shown in **Figure 4B**, the triple combination resulted in the greatest reduction of the levels of phospho-ERK1/2 supporting the kinomic data. The triple combination also suppressed the levels of phospho-MAPK/CDK substrates (**Supplementary Figure S3**).

## Combination NU7441, Olaparib, and IR Is Well Tolerated and Delays Tumor Growth in HNSCC Xenografts

To test the *in vivo* effects of NU7441, olaparib, and RT, tumor growth delay was measured using orthotopic tongue HPV-negative UM-SCC1 xenografts. An initial pilot dose-finding study was performed to determine the tolerability and optimal dose of NU7441 to combine with a fixed dose of olaparib (**Supplementary Figure S4**). As shown in **Figure 5A**, a significant tumor growth delay was observed in all treatment groups combined with IR ($p < 0.01$). Although not statistically significant, cisplatin-IR trended worse compared to the targeted therapy combinations with IR ($p = 0.075$). Body weight increases were statistically larger with DNAPKi + IR, PARPi + IR, and combination + IR compared to IR alone or IR plus cisplatin, suggesting that combinations of targeted agents with IR is better tolerated compared to cisplatin-IR (**Figure 5B**).

# DISCUSSION

Since the FDA approval of cetuximab in 2006, no targeted therapeutic combination with IR has been approved for the definitive treatment of HNSCC. Cetuximab, a monoclonal antibody against the epidermal growth factor receptor, is shown to inhibit both NHEJ and HR (Dittmann et al., 2005, 2008, 2010; Nowsheen et al., 2011a, 2012), the 2 major DNA DSB repair pathways. IR-induced DNA damage repair via NHEJ is found to be stimulated by EGFR nuclear translocation and binding to DNA-PK (Dittmann et al., 2005). For HR, EGFR is found to bind BRCA1 (Nowsheen et al., 2011a, 2012). Given the roles of these key DNA repair enzymes in resolution of IR-induced DNA damage, the potent radiosensitizing effects of either the DNA-PK inhibitor or PARP inhibitor in HNSCC is previously reported (Nowsheen et al., 2011b; Forster et al., 2012; Weaver et al., 2015; Kwon et al., 2016; Fok et al., 2019; Lee et al., 2019; Hernandez et al., 2020). DNA-PK inhibition is shown to demonstrate superior radiosensitivity to PARP inhibition in HNSCC cell lines although their combinatorial effect with IR was not tested (Fok et al., 2019; Lee et al., 2019).

PARP inhibition is also shown to inhibit EGFR nuclear translocation following IR, and an induced synthetic lethality is found with combined EGFR and PARP inhibition (Nowsheen et al., 2011a,b, 2012). Recent evidence also reveals a cooperation between DNA-PK and PARP1 at sites of replication fork instability to recruit XRCC1 and coordinate DNA repair at stalled replication forks to effectively protect, repair, and restart stalled replication forks (Spagnolo et al., 2012; Ying et al., 2016). These mechanisms reveal the crosstalk between the EGFR, DNA-PK, and PARP pathways and their putative roles in NHEJ and HR. They also provide the rationale for testing the combination of DNA-PK and PARP inhibition with IR.

Differential effects of DNA-PK and PARP inhibitors on cell cycle distribution are observed between the cell lines. DNA-PK and PARP inhibitors are shown to increase G2/M accumulation (Lee et al., 1997; Carrozza et al., 2009; Jelinic and Levine, 2014; Fok et al., 2019). DNA-PK activity is also essential for resumption of the cell cycle beyond IR-induced G2 checkpoint arrest, and cells exposed to the DNA-PK inhibitor AMA37 demonstrate irreversible G2 accumulation (Sturgeon et al., 2006). We observe a more prominent effect on cell cycle distribution in the UM-SCC6 cells compared to the UM-SCC1 cells, especially a potential senescence-like phenotype in UM-SCC6 cells (**Figure 2**: increased G1, reduced S at 24 h post IR). Although this is not surprising, due to the heterogeneity of cancer cell lines, the different effects we observe may be due to p53 status. As p53 is an important regulator of the DDR checkpoints (Gadhikar et al., 2013; Dobbelstein and Sorensen, 2015), including the G1/S phase transition, the more pronounced cell cycle redistribution in the UM-SCC6 cells may be due to its wild-type p53 status. Furthermore, it is recently reported that DNA-PK inhibition alone or in combination with PARP inhibition results in accelerated senescence in irradiated cancer cells that is dependent on p53 (Azad et al., 2011, 2014).

Interestingly, kinomic analysis of the combination treatments demonstrates the greatest suppression of CDK and MAPK/ERK

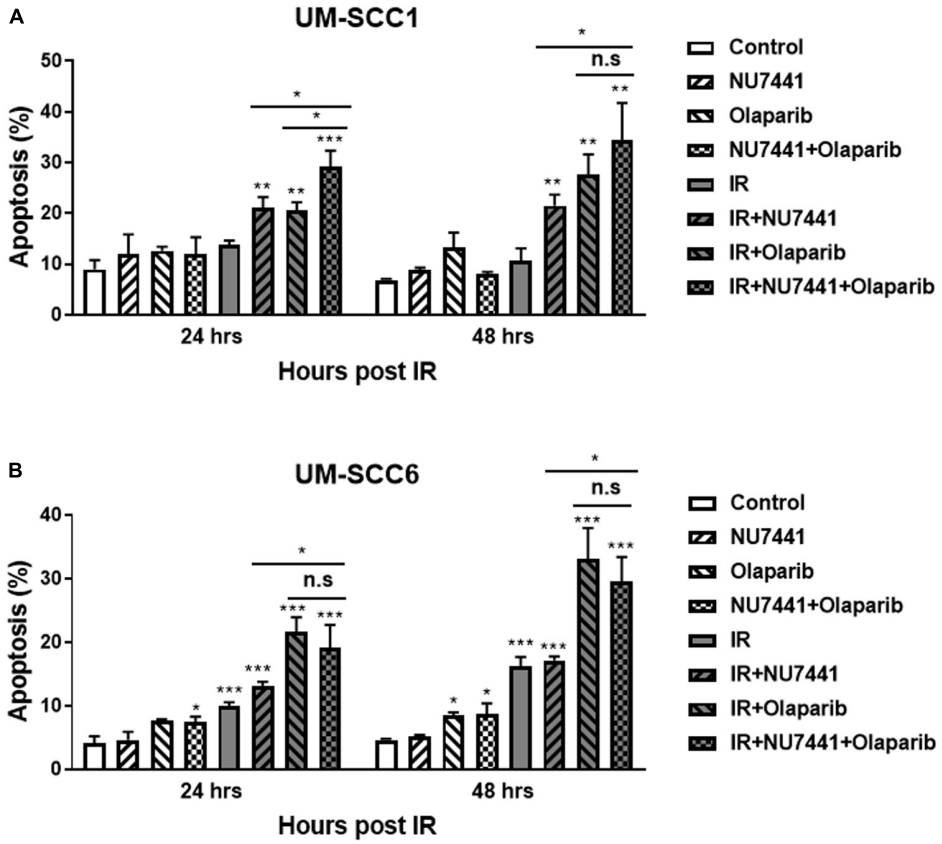


**FIGURE 3 |** NU7441 and olaparib with IR increases apoptosis in the **(A)** UM-SCC1 and **(B)** UM-SCC6 head and neck cancer cell lines. Cells were treated with vehicle or 1 μM NU7441 for 16 h, then 3 μM olaparib for 2 h, followed by sham or 2 Gy IR. Cells were harvested at 24 and 48 h after IR and evaluated for Annexin V positivity by flow cytometry. Shown is the mean ± SEM from at least two independent experiments performed in triplicate; $*p < 0.05$; $**p < 0.01$; $***p < 0.001$.

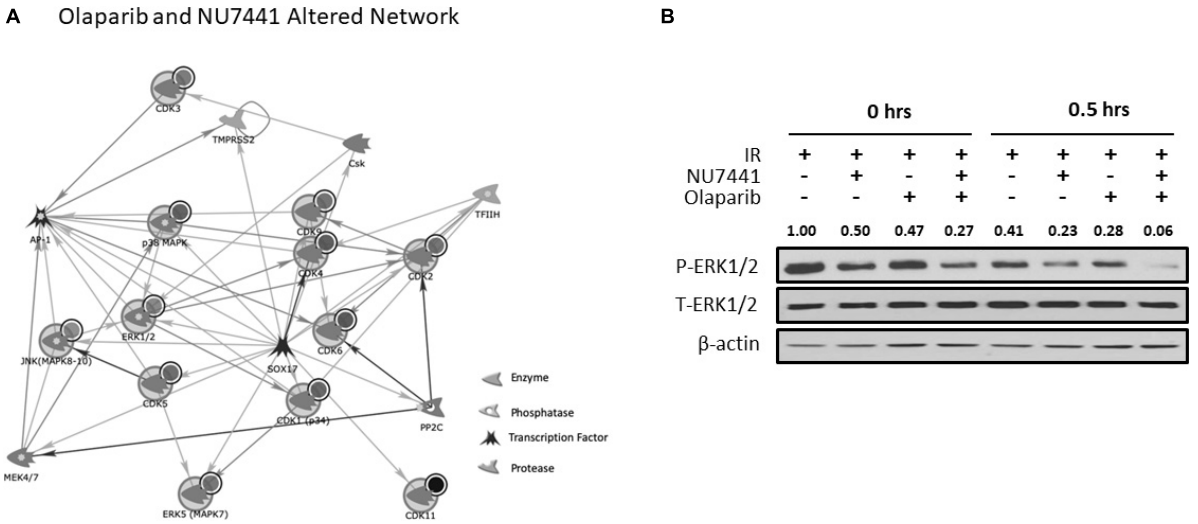


**FIGURE 4 |** Kinomic analysis following NU7441, olaparib, and IR reveal suppression of CDK and ERK signaling. **(A)** Network of kinases altered by olaparib + NU7441 combination treatment immediately post-IR. Kinases were uploaded by Uniprot ID and overlaid on literature-annotated interactions (portal.genego.com, Clarivate analytics) in a network model displaying centrally effected nodes (AutoExpand < 50 nodes, CDK/ERK centric). Interactions are indicated with lines and arrowheads for directionality. Nodes that are circled indicate input data. **(B)** Phospho- and total ERK status were validated at 0 and 30 min after IR via Western blot. Normalized densitometry values for phosphor-ERK1/2 are also shown.

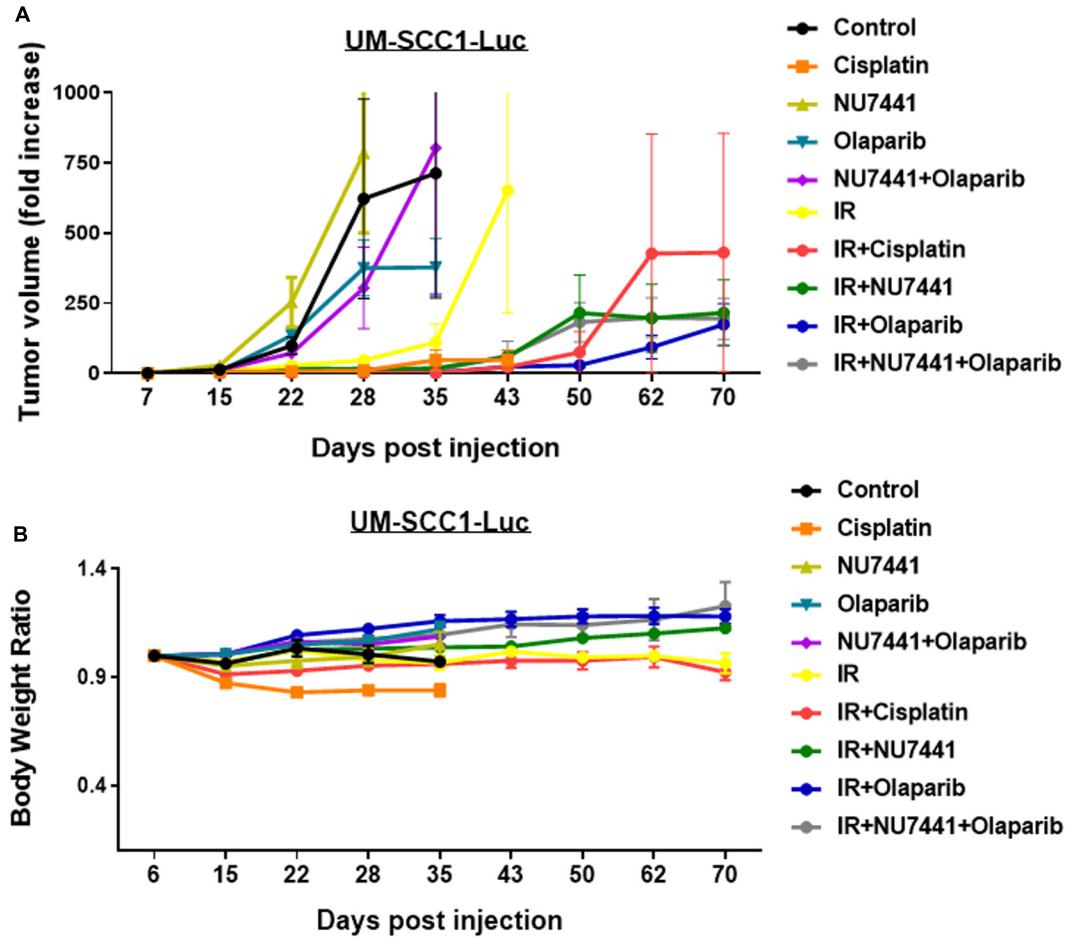


**FIGURE 5 |** The combination of NU7441 (DNAPKi), olaparib (PARP1), and IR **(A)** reduces *in vivo* tumor growth of UM-SCC1-Luc orthotopic xenografts and **(B)** is well tolerated as measured by body weight. The tongue of athymic nude mice were injected with UM-SCC1 luciferase-expressing cells (UM-SCC1), and tumor volume was measured by bioluminescence imaging twice weekly. Fold changes in each group are shown normalized to luminescence at the start of treatment on day 7. Shown is the mean fold change in tumor volume ± SEM. $N = 5$ mice for all treatment group. $^{**}p < 0.01$.

pathways. The involvement of these pathways in DNA repair is previously reported (Golding et al., 2007, 2009; Sharma et al., 2007; Khalil et al., 2011; Dean et al., 2012; Zalmas et al., 2013; Wang et al., 2018; Liu et al., 2020). Upon DNA damage, CDK2 activates the DNA damage response, and CDK2 knockout or deficiency increases sensitivity to radiation (Liu et al., 2020). Furthermore, inhibition of CDK4/6 modulates DNA repair (Dean et al., 2012). These actions are likely due to reduced E2F-mediated transcription of DNA repair enzymes (Sharma et al., 2007; Zalmas et al., 2013; Wang et al., 2018). The MAPK/ERK pathways also play key roles in DNA repair (Golding et al., 2007, 2009; Khalil et al., 2011). ERK signaling enhances both NHEJ and HR repair that is dependent on ATM, and blockade of ERK1/2 sensitizes cells to IR. Inhibitors of ERK signaling pathways are shown to block NHEJ-mediated DSB repair as demonstrated through EGFR mutant cell lines by Golding et al.

Our kinomic results also point to potential DNA repair-independent roles of DNA-PK and PARP, as the MAPK/ERK and CDK pathways regulate other cellular processes, including epithelial-mesenchymal transition (EMT). The MAPK/ERK and CDK pathways are implicated in EMT through various mechanisms (Shin et al., 2010) [reviewed in Thiery (2002)]. We have previously reported that, in HNSCC patients, high expression of DNA-PKcs is correlated with recurrence (Weaver et al., 2016). Preclinically, knockdown of DNA-PK in HNSCC cell lines reduces migration and invasion (Weaver et al., 2016). Similarly, DNA-PK is also shown to stimulate tumor cell invasion in head and neck cancer cells with a defective Fanconi Anemia pathway (Romick-Rosendale et al., 2016). A role of DNA-PK and PARP cooperativity in driving ERG-mediated gene transcriptional activation of genes involved in invasion and metastasis is also reported, where the activity of both enzymes is required in these processes (Brenner et al., 2011).

Through its interactions with the cytoskeletal machinery, PARP1 directly regulates cell motility and invasion (Rodriguez et al., 2013; Rom et al., 2016). PARP1 is shown to

impact invasion of ovarian cancer cells stimulated by HGF (Wei et al., 2018). In patients with gastric cancer, high PARP1 expression is shown to be associated with increased depth of tumor invasion and lymphatic invasion (Liu et al., 2016). Interestingly, inhibition of PARP reduces motility and invasion of BRAF-mutated melanoma cells (Rodriguez et al., 2013). These results suggest the role of DNA-PK and PARP in EMT, and the connection between DNA-PK, PARP, CDK, and MAPK/ERK pathways may be a mechanism through which the enhanced effects of the triple combination are occurring.

Targeting the DDR has been an attractive strategy in cancer treatment, especially for patients with HR-deficient tumors. In addition to PARP and DNA-PK inhibitors, ATR, CHK1, and WEE1 inhibitors are under development and being tested in current clinical trials alone or in combination with chemotherapy (Brown et al., 2017). Furthermore, combinations of DNA repair inhibitors, such as with PARP and RAD52 combinations, are being developed based on exciting preclinical results (Sullivan-Reed et al., 2018). In this study, we demonstrated that combining DNA-PK inhibition and PARP inhibition with IR in HNSCC results in further reduction in cell proliferation and clonogenic survival. Mechanistically, we show that the triple combination results in the greatest suppression of ERK and CDK signaling that is associated with induced G2/M phase cell cycle accumulation, persistent DNA damage, and increased apoptosis. The results from this study support the testing of this combination with IR in a phase 1b trial as a potential alternative to cisplatin-based chemoradiotherapy to potentially improve the therapeutic index. Combined inhibition of DNA-PK and PARP without radiation is currently being tested in a clinical trial (NCT03907969).

## DATA AVAILABILITY STATEMENT

All datasets generated for this study are included in the article/**Supplementary Material**.

## ETHICS STATEMENT

The animal study was reviewed and approved by the UAB Institutional Animal Care and Use Committee.

## AUTHOR CONTRIBUTIONS

EY: study conceptualization and supervision. EY, LZ, and DB: study design. LZ, DB, CX, ZZ, and JA: data collection. All authors contributed to data interpretation and manuscript writing.

## FUNDING

This study was supported through a Pilot Grant from UL1TR003096 (DB and EY) and Laboratory Funds from the Department of Radiation Oncology (EY).

## SUPPLEMENTARY MATERIAL

The Supplementary Material for this article can be found online at: https://www.frontiersin.org/articles/10.3389/fgene.2020.01036/full#supplementary-material

## REFERENCES

Anderson, J. C., Duarte, C. W., Welaya, K., Rohrbach, T. D., Bredel, M., Yang, E. S., et al. (2014). Kinomic exploration of temozolomide and radiation resistance in Glioblastoma multiforme xenolines. *Radiother. Oncol.* 111, 468–474. doi: 10.1016/j.radonc.2014.04.010

Azad, A., Bukczynska, P., Jackson, S., Haupt, Y., Cullinane, C., McArthur, G. A., et al. (2014). Co-targeting deoxyribonucleic acid-dependent protein kinase and poly(adenosine diphosphate-ribose) polymerase-1 promotes accelerated senescence of irradiated cancer cells. *Int. J. Radiat. Oncol. Biol. Phys.* 88, 385–394. doi: 10.1016/j.ijrobp.2013.10.043

Azad, A., Jackson, S., Cullinane, C., Natoli, A., Neilsen, P. M., Callen, D. F., et al. (2011). Inhibition of DNA-dependent protein kinase induces accelerated senescence in irradiated human cancer cells. *Mol. Cancer Res.* 9, 1696–1707. doi: 10.1158/1541-7786.mcr-11-0312

Brenner, J. C., Ateeq, B., Li, Y., Yocum, A. K., Cao, Q., Asangani, I. A., et al. (2011). Mechanistic rationale for inhibition of poly(ADP-ribose) polymerase in ETS gene fusion-positive prostate cancer. *Cancer Cell* 19, 664–678.

Brown, J. S., O'Carrigan, B., Jackson, S. P., and Yap, T. A. (2017). Targeting DNA repair in cancer: beyond PARP inhibitors. *Cancer Discov.* 7, 20–37. doi: 10.1158/2159-8290.cd-16-0860

Carrozza, M. J., Stefanick, D. F., Horton, J. K., Kedar, P. S., and Wilson, S. H. (2009). PARP inhibition during alkylation-induced genotoxic stress signals a cell cycle checkpoint response mediated by ATM. *DNA Repair* 8, 1264–1272. doi: 10.1016/j.dnarep.2009.07.010

Dean, J. L., McClendon, A. K., and Knudsen, E. S. (2012). Modification of the DNA damage response by therapeutic CDK4/6 inhibition. *J. Biol. Chem.* 287, 29075–29087. doi: 10.1074/jbc.m112.365494

Dittmann, K., Mayer, C., Kehlbach, R., and Rodemann, H. P. (2008). Radiation-induced caveolin-1 associated EGFR internalization is linked with nuclear EGFR transport and activation of DNA-PK. *Mol. Cancer* 7:69. doi: 10.1186/1476-4598-7-69

Dittmann, K., Mayer, C., and Rodemann, H. P. (2005). Inhibition of radiation-induced EGFR nuclear import by C225 (Cetuximab) suppresses DNA-PK activity. *Radiother. Oncol.* 76, 157–161. doi: 10.1016/j.radonc.2005.06.022

Dittmann, K., Mayer, C., and Rodemann, H. P. (2010). Nuclear EGFR as novel therapeutic target: insights into nuclear translocation and function. *Strahlenther. Onkol.* 186, 1–6. doi: 10.1007/s00066-009-2026-4

Dobbelstein, M., and Sorensen, C. S. (2015). Exploiting replicative stress to treat cancer. *Nat. Rev. Drug Discov.* 14, 405–423. doi: 10.1038/nrd4553

Fok, J. H L., Ramos-Montoya, A., Vazquez-Chantada, M., Wijnhoven, P. W G., et al. (2019). AZD7648 is a potent and selective DNA-PK inhibitor that enhances radiation, chemotherapy and olaparib activity. *Nat. Commun.* 10:5065.

Forster, M., Mendes, R., and Fedele, S. (2012). Synthetic lethality and PARP-inhibitors in oral and head & neck cancer. *Curr. Pharm. Des.* 18, 5431–5441. doi: 10.2174/138161212803307608

Gadhikar, M. A., Sciuto, M. R., Alves, M. V., Pickering, C. R., Osman, A. A., Neskey, D. M., et al. (2013). Chk1/2 inhibition overcomes the cisplatin resistance of head and neck cancer cells secondary to the loss of functional p53. *Mol. Cancer Ther.* 12, 1860–1873. doi: 10.1158/1535-7163.mct-13-0157

Golding, S. E., Morgan, R. N., Adams, B. R., Hawkins, A. J., Povirk, L. F., and Valerie, K. (2009). Pro-survival AKT and ERK signaling from EGFR and mutant EGFRvIII enhances DNA double-strand break repair in human glioma cells. *Cancer Biol. Ther.* 8, 730–738. doi: 10.4161/cbt.8.8.7927

Golding, S. E., Rosenberg, E., Neill, S., Dent, P., Povirk, L. F., and Valerie, K. (2007). Extracellular signal-related kinase positively regulates ataxia telangiectasia mutated, homologous recombination repair, and the DNA damage response. *Cancer Res.* 67, 1046–1053. doi: 10.1158/0008-5472.can-06-2371

Hernandez, A. L., Young, C. D., Bian, L., Weigel, K., Nolan, K., Frederick, B., et al. (2020). PARP inhibition enhances radiotherapy of SMAD4 deficient human head and neck squamous cell carcinomas in experimental models. *Clin. Cancer Res.* 26, 3058–3070. doi: 10.1158/1078-0432.ccr-19-0514

Isayeva, T., Xu, J., Ragin, C., Dai, Q., Cooper, T., Carroll, W., et al. (2015). The protective effect of p16(INK4a) in oral cavity carcinomas: p16(Ink4A) dampens tumor invasion-integrated analysis of expression and kinomics pathways. *Mod. Pathol.* 28, 631–653. doi: 10.1038/modpathol.2014.149

Jarboe, J. S., Jaboin, J. J., Anderson, J. C., Nowsheen, S., Stanley, J. A., Naji, F., et al. (2012). Kinomic profiling approach identifies Trk as a novel radiation modulator. *Radiother. Oncol.* 103, 380–387. doi: 10.1016/j.radonc.2012.03.014

Jelinic, P., and Levine, D. A. (2014). New insights into PARP inhibitors' effect on cell cycle and homology-directed DNA damage repair. *Mol. Cancer Ther.* 13, 1645–1654. doi: 10.1158/1535-7163.mct-13-0906-t

Kakarougkas, A., and Jeggo, P. A. (2014). DNA DSB repair pathway choice: an orchestrated handover mechanism. *Br. J. Radiol.* 87:20130685. doi: 10.1259/bjr.20130685

Khalil, A., Morgan, R. N., Adams, B. R., Golding, S. E., Dever, S. M., Rosenberg, E., et al. (2011). ATM-dependent ERK signaling via AKT in response to DNA double-strand breaks. *Cell Cycle* 10, 481–491. doi: 10.4161/cc.10.3.14713

Kwon, M., Jang, H., Kim, E. H., and Roh, J. L. (2016). Efficacy of poly (ADP-ribose) polymerase inhibitor olaparib against head and neck cancer cells: predictions of drug sensitivity based on PAR-p53-NF-kappaB interactions. *Cell Cycle* 15, 3105–3114.

Lee, S. E., Mitchell, R. A., Cheng, A., and Hendrickson, E. A. (1997). Evidence for DNA-PK-dependent and -independent DNA double-strand break repair pathways in mammalian cells as a function of the cell cycle. *Mol. Cell. Biol.* 17, 1425–1433. doi: 10.1128/mcb.17.3.1425

Lee, T. W., Wong, W. W., Dickson, B. D., Lipert, B., Cheng, G. J., Hunter, F. W., et al. (2019). Radiosensitization of head and neck squamous cell carcinoma lines by DNA-PK inhibitors is more effective than PARP-1 inhibition and is enhanced by SLFN11 and hypoxia. *Int. J. Radiat. Biol.* 95, 1597–1612. doi: 10.1080/09553002.2019.1664787

Liu, Q., Gao, J., Zhao, C., Guo, Y., Wang, S., Shen, F., et al. (2020). To control or to be controlled? Dual roles of CDK2 in DNA damage and DNA damage response. *DNA Repair*. 85:102702. doi: 10.1016/j.dnarep.2019.102702

Liu, Y., Zhang, Y., Zhao, Y., Gao, D., Xing, J., and Liu, H. (2016). High PARP-1 expression is associated with tumor invasion and poor prognosis in gastric cancer. *Oncol Lett.* 12, 3825–3835. doi: 10.3892/ol.2016.5169

Mahaney, B. L., Meek, K., and Lees-Miller, S. P. (2009). Repair of ionizing radiation-induced DNA double-strand breaks by non-homologous end-joining. *Biochem. J.* 417, 639–650. doi: 10.1042/bj20080413

Nowsheen, S., Bonner, J. A., Lobuglio, A. F., Trummell, H., Whitley, A. C., Dobelbower, M. C., et al. (2011a). Cetuximab augments cytotoxicity with poly (adp-ribose) polymerase inhibition in head and neck cancer. *PLoS One* 6:e24148. doi: 10.1371/journal.pone.0024148

Nowsheen, S., Bonner, J. A., and Yang, E. S. (2011b). The poly(ADP-Ribose) polymerase inhibitor ABT-888 reduces radiation-induced nuclear EGFR and augments head and neck tumor response to radiotherapy. *Radiother. Oncol.* 99, 331–338. doi: 10.1016/j.radonc.2011.05.084

Nowsheen, S., Cooper, T., Stanley, J. A., and Yang, E. S. (2012). Synthetic lethal interactions between EGFR and PARP inhibition in human triple negative breast cancer cells. *PLoS One* 7:e46614. doi: 10.1371/journal.pone.0046614

Rodriguez, M. I., Peralta-Leal, A., O'Valle, F., Rodriguez-Vargas, J. M., Gonzalez-Flores, A., Majuelos-Melguizo, J., et al. (2013). PARP-1 regulates metastatic melanoma through modulation of vimentin-induced malignant transformation. *PLoS Genet* 9:e1003531. doi: 10.1371/journal.pgen.1003531

Rom, S., Zuluaga-Ramirez, V., Reichenbach, N. L., Dykstra, H., Gajghate, S., Pacher, P., et al. (2016). PARP inhibition in leukocytes diminishes inflammation via effects on integrins/cytoskeleton and protects the blood-brain barrier. *J Neuroinflammation* 13:254.

Romick-Rosendale, L. E., Hoskins, E. E., Privette Vinnedge, L. M., Foglesong, G. D., Brusadelli, M. G., Potter, S. S., et al. (2016). Defects in the fanconi anemia pathway in head and neck cancer cells stimulate tumor cell invasion through DNA-PK and Rac1 signaling. *Clin. Cancer Res.* 22, 2062–2073. doi: 10.1158/1078-0432.ccr-15-2209

Sharma, A., Comstock, C. E., Knudsen, E. S., Cao, K. H., Hess-Wilson, J. K., Morey, L. M., et al. (2007). Retinoblastoma tumor suppressor status is a critical determinant of therapeutic response in prostate cancer cells. *Cancer Res.* 67, 6192–6203. doi: 10.1158/0008-5472.can-06-4424

Shin, S. Y., Rath, O., Zebisch, A., Choo, S. M., Kolch, W., and Cho, K. H. (2010). Functional roles of multiple feedback loops in extracellular signal-regulated kinase and Wnt signaling pathways that regulate epithelial-mesenchymal transition. *Cancer Res.* 70, 6715–6724. doi: 10.1158/0008-5472.can-10-1377

Spagnolo, L., Barbeau, J., Curtin, N. J., Morris, E. P., and Pearl, L. H. (2012). Visualization of a DNA-PK/PARP1 complex. *Nucleic Acids Res.* 40, 4168–4177. doi: 10.1093/nar/gkr1231

Sturgeon, C. M., Knight, Z. A., Shokat, K. M., and Roberge, M. (2006). Effect of combined DNA repair inhibition and G2 checkpoint inhibition on cell cycle progression after DNA damage. *Mol. Cancer Ther.* 5, 885–892. doi: 10.1158/1535-7163.mct-05-0358

Sullivan-Reed, K., Bolton-Gillespie, E., Dasgupta, Y., Langer, S., Siciliano, M., Nieborowska-Skorska, M., et al. (2018). Simultaneous Targeting of PARP1 and RAD52 Triggers Dual Synthetic Lethality in BRCA-Deficient Tumor Cells. *Cell Rep.* 23, 3127–3136. doi: 10.1016/j.celrep.2018.05.034

Swindall, A. F., Stanley, J. A., and Yang, E. S. (2013). PARP-1: friend or Foe of DNA damage and repair in tumorigenesis? *Cancers* 5, 943–958. doi: 10.3390/cancers5030943

Thiery, J. P. (2002). Epithelial-mesenchymal transitions in tumour progression. *Nat. Rev. Cancer* 2, 442–454. doi: 10.1038/nrc822

Wang, L., Chen, H., Wang, C., Hu, Z., and Yan, S. (2018). Negative regulator of E2F transcription factors links cell cycle checkpoint and DNA damage repair. *Proc. Natl. Acad. Sci. U.S.A.* 115, E3837–E3845.

Weaver, A. N., Burch, M. B., Cooper, T. S., Della Manna, D. L., Wei, S., Ojesina, A. I., et al. (2016). Notch signaling activation is associated with patient mortality and increased FGF1-mediated invasion in squamous cell carcinoma of the oral cavity. *Mol. Cancer Res.* 14, 883–891. doi: 10.1158/1541-7786.mcr-16-0114

Weaver, A. N., Cooper, T. S., Rodriguez, M., Trummell, H. Q., Bonner, J. A., Rosenthal, E. L., et al. (2015). DNA double strand break repair defect and sensitivity to poly ADP-ribose polymerase (PARP) inhibition in human papillomavirus 16-positive head and neck squamous cell carcinoma. *Oncotarget* 6, 26995–27007. doi: 10.18632/oncotarget.4863

Wei, W., Lv, S., Zhang, C., and Tian, Y. (2018). Potential role of HGF-PARP-1 signaling in invasion of ovarian cancer cells. *Int. J. Clin. Exp. Pathol.* 11, 3310–3317.

Ying, S., Chen, Z., Medhurst, A. L., Neal, J. A., Bao, Z., Mortusewicz, O., et al. (2016). DNA-PKcs and PARP1 bind to unresected stalled DNA replication forks where they recruit XRCC1 to mediate repair. *Cancer Res.* 76, 1078–1088. doi: 10.1158/0008-5472.can-15-0608

Zalmas, L. P., Coutts, A. S., Helleday, T., and La Thangue, N. B. (2013). E2F-7 couples DNA damage-dependent transcription with the DNA repair process. *Cell Cycle* 12, 3037–3051. doi: 10.4161/cc.26078

Zeng, L., Beggs, R. R., Cooper, T. S., Weaver, A. N., and Yang, E. S. (2017). Combining Chk1/2 inhibition with cetuximab and radiation enhances in vitro and in vivo cytotoxicity in head and neck squamous cell carcinoma. *Mol. Cancer Ther.* 16, 591–600. doi: 10.1158/1535-7163.mct-16-0352

Zenke, F. T., Zimmermann, A., Sirrenberg, C., Dahmen, H., Kirkin, V., Pehl, U., et al. (2020). Pharmacologic inhibitor of DNA-PK, M3814, potentiates radiotherapy and regresses human tumors in mouse models. *Mol. Cancer Ther.* 19, 1091–1101. doi: 10.1158/1535-7163.mct-19-0734

**Conflict of Interest:** EY has served on the advisory board of Astrazeneca, Eli Lilly, Clovis, Strata Oncology, and Bayer and has received honoraria from them. DB received honoraria for speaking engagements and research support for Varian Medical Systems. He also received research support from Novocure.

The remaining authors declare that the research was conducted in the absence of any commercial or financial relationships that could be construed as a potential conflict of interest.

frontiers in Genetics

CASE REPORT
published: 27 October 2020
doi: 10.3389/fgene.2020.594078

# Case Report: Compound Heterozygous Phosphatidylinositol-Glycan Biosynthesis Class N (*PIGN*) Mutations in a Chinese Fetus With Hypotonia-Seizures Syndrome 1

*Shi-qi Xiao[1], Mei-hui Li[2], Yi-lin Meng[2], Chuang Li[2], Hai-long Huang[2], Cai-xia Liu[2,3], Yuan Lyu[2,3] and Quan Na[2]**

[1] Department of Nursing, Shengjing Hospital of China Medical University, Shenyang, China, [2] Department of Obstetrics and Gynecology, Shengjing Hospital of China Medical University, Shenyang, China, [3] Key Laboratory of Maternal-Fetal Medicine of Liaoning Province, Key Laboratory of Obstetrics and Gynecology of Higher Education of Liaoning Province, Shenyang, China

OPEN ACCESS

**Edited by:**
Hari S. Misra,
Bhabha Atomic Research Centre (BARC), India

**Reviewed by:**
Fan Jin,
Zhejiang University, China
Fulya Taylan,
Karolinska Institutet (KI), Sweden

***Correspondence:**
Quan Na
naquan@163.com

**Specialty section:**
This article was submitted to Genetics of Common and Rare Diseases, a section of the journal Frontiers in Genetics

**Received:** 12 August 2020
**Accepted:** 06 October 2020
**Published:** 27 October 2020

**Citation:**
Xiao S, Li M, Meng Y, Li C, Huang H, Liu C, Lyu Y and Na Q (2020) Case Report: Compound Heterozygous Phosphatidylinositol-Glycan Biosynthesis Class N (PIGN) Mutations in a Chinese Fetus With Hypotonia-Seizures Syndrome 1. Front. Genet. 11:594078. doi: 10.3389/fgene.2020.594078

Multiple congenital anomalies-hypotonia-seizures syndrome 1 (MCAHS1) caused by phosphatidylinositol-glycan biosynthesis class N (*PIGN*) mutations is an autosomal recessive disease involving many systems of the body, such as the urogenital, cardiovascular, gastrointestinal, and central nervous systems. Here, compound heterozygous variants NM_012327.6:c.2427-2A > G and c.963G > A in *PIGN* were identified in a Chinese proband with MCAHS1. The features of the MCAHS1 family proband were evaluated to understand the mechanism of the *PIGN* mutation leading to the occurrence of MCAHS1. Ultrasound was conducted to examine the fetus, and his clinical manifestations were evaluated. Genetic testing was performed by whole-exome sequencing and the results were verified by Sanger sequencing of the proband and his parents. Reverse transcription-polymerase chain reaction was performed, and the products were subjected to Sanger sequencing. Quantitative PCR (Q-PCR) was conducted to compare gene expression between the patient and wild-type subjects. The compound heterozygous mutation NM_012327.6:c.2427-2A > G and c.963G > A was identified by whole-exome sequencing and was confirmed by Sanger sequencing. The NM_012327.6:c.2427-2A > G mutation led to skipping of exon 26, which resulted in a low expression level of the gene, as measured by Q-PCR. These findings provided a basis for genetic counseling and reproduction guidance in this family. Phenotype-genotype correlations may be defined by an expanded array of mutations.

**Keywords: *PIGN*, multiple congenital anomalies-hypotonia-seizures syndrome 1, reproduction guidance, prenatal diagnosis, glycosylphosphatidylinositol-anchor biosynthesis pathway**

## INTRODUCTION

Multiple congenital anomalies-hypotonia-seizures syndrome 1 (MCAHS1) is an autosomal recessive disease characterized by hypotonia, seizures, facial anomalies, and developmental delay, and involves various systems, such as the gastrointestinal tract, cardiovascular system, urogenital system, and central nervous system (Khayat et al., 2016). The etiology of MCAHS1 is based on mutations in phosphatidylinositol-glycan biosynthesis class N (*PIGN*). *PIGN* is one of more than 20 genes involved in the glycosylphosphatidylinositol (GPI)-anchor biosynthesis pathway (Couser et al., 2015). To date, eight genes [phosphatidylinositol glycan class A (*PIGA*), phosphatidylinositol glycan anchor biosynthesis class L (*PIGL*), phosphatidylinositol glycan anchor biosynthesis class M (*PIGM*), *PIGN*, phosphatidylinositol glycan anchor biosynthesis class O (*PIGO*), phosphatidylinositol glycan anchor biosynthesis class V (*PIGV*), phosphatidylinositol glycan anchor biosynthesis class T (*PIGT*), and post-GPI attachment to proteins 2 (*PGAP2*)] in this pathway are reported to be associated with neural abnormalities (Khayat et al., 2016). As *PIGN* is expressed in many tissues, several body systems are affected by mutations in this gene, leading to severe developmental delay (Couser et al., 2015). Here, we report a fetus with head and neck hygroma that subsequently disappeared and tetralogy of Fallot in a Chinese family. To clarify the genotype-phenotype relationship and provide a basis for genetic counseling, whole-exome sequencing (WES), Sanger sequencing, and reverse transcription-polymerase chain reaction (RT-PCR) were performed. The compound heterozygous *PIGN* mutation NM_012327.6:c.2427-2A > G was identified in the fetus. The transcription product of c.2427-2A > G mutation was found to result in skipping of exon 26.

## CASE DESCRIPTION

### Pedigree and Clinical Evaluations

Gestational ultrasound at 12 weeks and 3 days revealed a neck hygroma approximately 32 mm × 17 mm in size, trunk edema, as well as nuchal translucency of 6.6 mm. Other measurements included biparietal diameter that was approximately 21 mm, femur length that was approximately 7 mm, and crown-lump length that was approximately 70 mm. The head and neck hygroma disappeared at 16 weeks. At 24 weeks, systematic ultrasound revealed tetralogy of Fallot in the fetus. Amniocentesis revealed a normal karyotype. After explaining the disease condition and related risks to the patient's parents, they voluntarily requested the induction of labor. This study was approved by the ethics committee of Shengjing Hospital of China Medical University (ethics approval number: 2013PS33K).

### Identification and Functional Characterization of Variants

Peripheral blood samples were collected from the proband's family members and tissue was collected from the proband. Genomic DNA was extracted using a TIANamp Blood DNA Kit (TIANGEN, Beijing, China) and subjected to WES. Targeted exon sequences plus flanking sequences were captured and enriched using an array-based hybridization chip (xGen Exome Research Panel v1.0, Integrated DNA Technologies, Coralville, IA, United States) followed by HiSeq X10 sequencing (Illumina, San Diego, CA, United States). All variants on autosomes and sex chromosomes were annotated using the Annotate Variation tool. The pathogenicity of variants was annotated using the Human Gene Mutation Database[1], ClinVar database[2], and Standards and Guidelines for the Interpretation of Sequence Variants of the American College of Medical Genetics and Genomics (ACMG) (Richards et al., 2015). A series of *in silico* impact score procedures, including Mendelian Clinically Applicable Pathogenicity[3], Sorting Intolerant from Tolerant[4], Polymorphism Phenotyping v2[5], Likelihood Ratio Test[6], MutationTaster[7], Combined Annotation Dependent Depletion (CADD)[8], Functional Analysis through Hidden Markov Models[9], and Protein Variation Effect Analyzer[10] were used to prioritize all variants according to the ACMG guidelines. Variants with minor allele frequencies <0.01 in any of the databases used [Single Nucleotide Polymorphism Database, Exome Aggregation Consortium (ExAC), 1000 Genomes Project, Genome Aggregation Database (gnomAD), and an in-house database] were selected. The WES results were validated by Sanger sequencing of the patient and his family members. RT-PCR using total RNA extracted from fetal tissue was performed. Briefly, total RNA was extracted using the RNeasy Plus Mini kit (QIAGEN, Hilden, Germany) from lymphoblastoid cell lines with or without incubation in 30 μM cycloheximide (Sigma, St. Louis, MO, United States) for 4 h. Four micrograms of total RNA were subjected to reverse transcription, and 2 μL cDNA was used for PCR. Primer sequences were ex29-F (5′-TCAAGCCAGCTGCCATAATC-3′) and ex22-R (5′-GTGCCACTACTGAGTTCTCCA-3′). PCR products were electrophoresed on a 10% polyacrylamide gel, bands were purified using an E.Z.N.A. poly-Gel DNA Extraction kit (Omega Bio-Tek, Norcross, GA, United States), and sequenced. RT-PCR products were sequenced using Sanger sequencing and quantitative PCR (Q-PCR) of the gene transcripts was performed.

High throughput sequencing of the patient revealed a synonymous mutation: c.963G > A/p.Gln321 = showing compound heterozygosity with a novel splicing mutation: c.2427-2 A > G. Sanger sequencing of the patient and his family members validated these results (**Figure 1A**). Mutations in *PIGN* were acquired from both parents separately. According to the ACMG standards, both mutations were defined as likely

[1]http://www.hgmd.cf.ac.uk/ac/index.php
[2]https://www.ncbi.nlm.nih.gov/clinvar/
[3]http://bejerano.stanford.edu/MCAP/
[4]https://sift.bii.a-star.edu.sg/
[5]http://genetics.bwh.harvard.edu/pph2/
[6]http://www.genetics.wustl.edu/jflab/lrt_query.html
[7]http://www.mutationtaster.org/
[8]https://cadd.gs.washington.edu/
[9]http://fathmm.biocompute.org.uk/inherited.html
[10]http://provean.jcvi.org/index.php

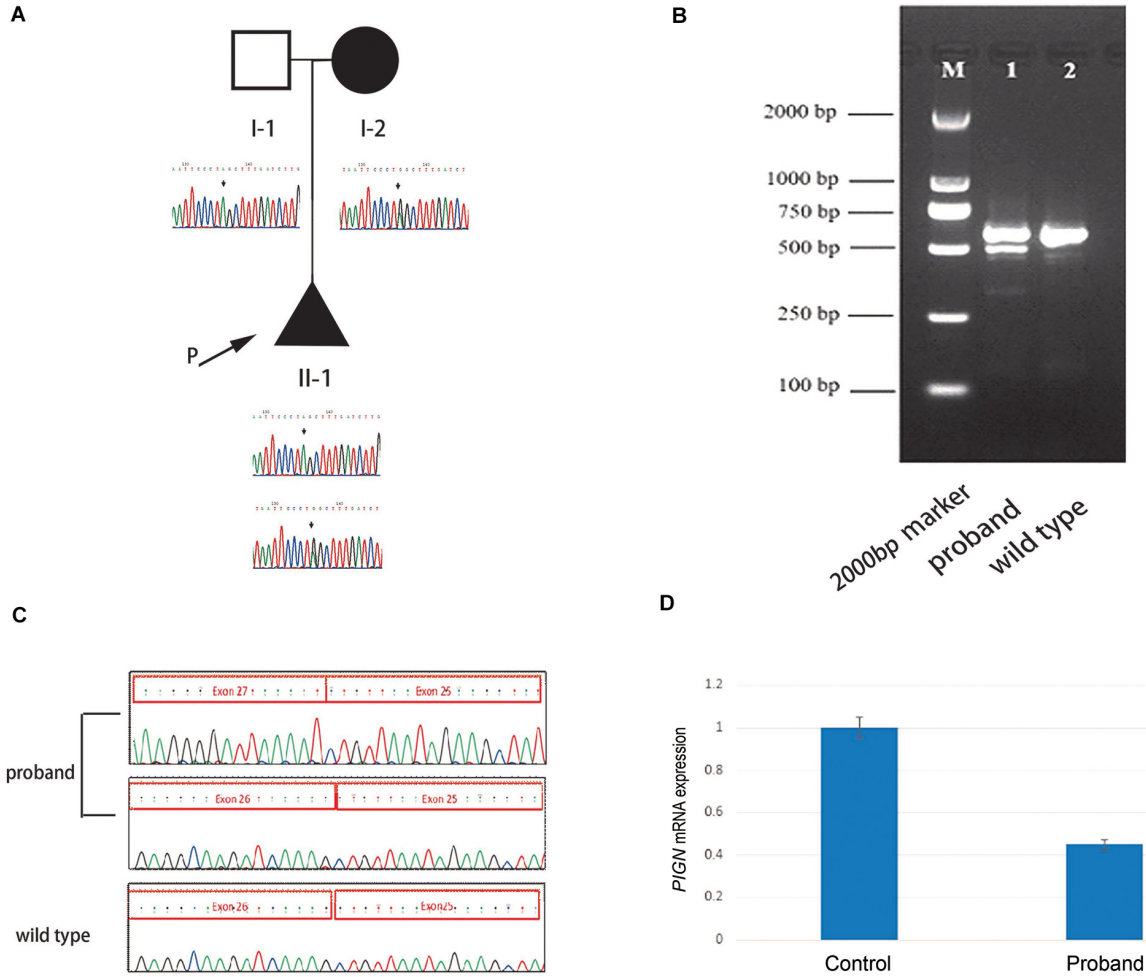


**FIGURE 1 | (A)** Pedigree of the family and Sanger sequencing results of each family member. **(B)** The proband's polymerase chain reaction (PCR) product contains two electrophoretic bands: 569 and 493 bp; the wild-type has only one band: 596 bp. **(C)** Sanger sequencing results of the reverse transcription (RT)-PCR product of the fetus and the wild-type, respectively. **(D)** Quantitative-PCR of phosphatidylinositol-glycan biosynthesis class N (*PIGN*) reveals lower expression in the patient than in the normal control.

pathogenic. c.963G > A/p.Gln321 = is a synonymous mutation located in exon 10. The two mutations had a very low carrying rate in the ExAC and gnomAD databases (**Table 1**). c.2427-2 A > G is a splicing mutation located in intron 25 and may lead to abnormal mRNA splicing that influences protein expression. This mutation is predicted to cause loss of function of the protein. Sanger sequencing of the RT-PCR product revealed that the splicing mutation c.2427-2 A > G led to skipping of exon 26 (**Figures 1B,C**). A hazardous assessment of the mutation: c.963G > A/p.Gln321 = was conducted. The CADD score was 32, Genomic Evolutionary Rate Profiling (GERP) score was 5.56, DANN score was 0.995, and the PhyloP100way vertebrate Score was 6.812. The splicing mutation c.2427-2 A > G CADD score was 24, GERP score was 6.16, DANN score was 0.998, and the PhyloP100way vertebrate Score was 5.693. Q-PCR of the *PIGN* transcript revealed that levels of the patient mRNA were decreased compared to those in the normal control subjects (**Figure 1D**).

## DISCUSSION

The MCAHS1 phenotype always includes congenital anomalies, seizures, developmental delay, and hypotonia; cerebellar atrophy, nystagmus, and diaphragmatic hernia may also be present (**Table 2**). The etiology of MCAHS1 involves *PIGN* mutations. Early onset and focal seizures appear to be a common feature of patients with *PIGN* mutation (Brady et al., 2014; Jiao et al., 2020). The clinical severity of cases is predicted to be associated with the severity of functional loss resulting from mutations in *PIGN*. Patients with biallelic truncated *PIGN* variants show a severe clinical phenotype, including early onset of intractable seizures and death *in utero* or shortly after birth, indicating that truncated variants are likely related to the severe phenotype (Thiffault et al., 2017). It is difficult to predict MCAHS1 by ultrasound examination because rare cases do not show abnormalities during gestation. However, in this study, the patient initially showed head and neck hygroma, which then disappeared. Additionally,

**TABLE 1 |** Summary of all phosphatidylinositol-glycan biosynthesis class N (*PIGN*) mutations leading to multiple congenital anomalies-hypotonia-seizures syndrome 1 (MCAHS1).

| | Mutation | Age | Sex | Birth | | Dysmorphic features | | | Congenital anomalies | | | Neurologic | | | | | | Brain MRI | | |
|---|---|---|---|---|---|---|---|---|---|---|---|---|---|---|---|---|---|---|---|---|
| | | | | weight | OFC | Palate | Ears | Fingers | Cardiac | Urinary | intestinal malrotation, anal stenosis or atresia | development delay | hypotonia | Nystagmus | Tremor | Seizure | Feeding | Corpus callosum | Cerebellar atrophy | Cerebral volume loss |
| Maydan et al., 2011 | c.2126 G > A (p.R709Q) | 29 months | M | 3566 | 37 | + | + | + | + | + | + | + | + | + | + | + | NR | – | – | + |
| | | 14 months | M | 4065 | 37 | + | + | + | + | + | + | + | + | + | + | – | NR | | | |
| | | 1 month | M | 3850 | 35.5 | NR | + | + | + | + | + | + | + | – | + | + | NR | | | |
| | | 5 months | F | 3410 | 34.5 | – | + | – | + | – | + | + | + | + | + | + | – | + | + | – |
| | | 3 months | F | 4250 | NR | – | + | – | – | – | – | + | + | + | + | + | – | + | – | + |
| | | 17 months | F | 4300 | NR | – | + | + | + | – | – | + | + | + | – | + | + | | | |
| | | 39 months | M | 4800 | NR | other | + | + | – | – | – | + | + | + | – | + | + | | | |
| Ohba et al., 2014 | c.808 T > C; c.963 G > A | 9 years | F | 3390 | 35 | + | + | + | – | + | + | + | + | + | + | + | + | | | |
| | | 2 years | M | 3252 | 35 | + | + | + | – | – | – | + | + | + | + | + | NR | | | |
| Brady et al., 2014 | c.1574?1G > A | 16 weeks | M | NA | NA | + | + | + | + | + | + | NA | NA | NA | NA | NA | NA | | | |
| Couser et al., 2015 | c.406T > G; c.2576C > G | 2 years | M | 4271 | 36.8 | NR | + | + | + | + | + | + | + | – | – | + | + | | | |
| Fleming et al., 2016 | c.2340 T > A; c.1434 + 5 G > A | 30 months | F | 3350 | 35 | + | + | – | – | – | + | + | + | + | – | + | + | | | |
| | | 18 months | F | 3147 | 36.5 | + | + | – | – | – | + | + | + | + | – | + | + | | | |
| | c.709 G > A; c.2411_2412delTAinsAG | 14 years | F | 2756 | NA | + | – | – | – | – | – | + | + | – | – | + | – | + | – | + |
| | c.548_549?6del | 4 months | F | 4008 | 36 | + | + | + | – | – | + | + | + | + | – | + | + | | – | – |
| Khayat et al., 2016 | c.755A > T | 5 years | F | 3300 | NA | – | + | + | – | – | – | + | + | + | – | + | – | – | – | + |
| Nakagawa et al., 2016 | c.808T > C | 6 years | M | 2880 | 33 | – | – | – | – | – | – | + | + | + | – | – | – | – | + | – |
| Jezela-Stanek et al., 2016 | c.790G > A; c.932T > G | 2 months | F | 4300 | 34 | – | – | – | – | – | – | + | + | + | + | + | – | – | + | – |
| Pagnamenta et al., 2017 | c.932T > G; c.694 > T | NA | F | NA | NA | NA | NA | – | NA | NA | NA | + | – | – | – | + | NA | – | – | + |
| Jiao et al., 2020 | c.2122C > T; c.2557A > C | 2 years | M | NA | NA | NA | NA | NA | – | – | – | + | + | – | NA | + | – | – | – | – |
| | c.2759_2760del; c.1172 + 1G > A | 4 years 9 months | M | NA | NA | + | – | – | – | – | – | + | + | – | NA | + | – | – | – | – |
| | c.1109A > C; c.694A > T | 3 years 6 months | M | NA | NA | – | – | – | – | – | – | + | + | – | NA | + | – | – | – | – |
| | c.1694G > A; c.2663 T > C;c.963G > A | 2 years 8 months | F | NA | NA | + | – | + | – | – | – | + | + | – | NA | + | – | + | – | – |
| | c.343G > C; c.1694G > T | 1 year 7 months | M | NA | NA | – | – | – | – | – | – | + | + | + | NA | + | – | – | – | – |
| | c.505C > T; c.769 T > G | 2 years | M | NA | NA | – | – | – | – | – | – | + | – | – | NA | + | – | – | – | – |
| | c.895 C > T; c.629 T > C | 2 years 5 months | F | NA | NA | – | – | – | – | – | – | + | + | – | NA | + | – | – | + | – |

**TABLE 2 |** The allele frequencies in different databases of the two variants.

| *PIGN* Variations | Allele frequency in gnomAD | Allele frequency in 1000 genomes | Allele frequency in ExAC | Allele frequency in dbSNP | Allele frequency in in-house database |
|---|---|---|---|---|---|
| NM_012327.6: c.2427-2A > G | 0.00008806 (East Asian) | No records | No records | 0.00003 (Asian) | No records |
| NM_012327.6: c.963G > A | 0.001109 (East Asian) | No records | 0.0012 (East Asian) | 0.00 (East Asian) | 0.00098232 |

the fetal system ultrasound displayed tetralogy of Fallot for which the phenotype spectrum was enriched during gestation. This finding enabled the prenatal diagnosis of MCAHS1. Eight genes (*PIGA*, *PIGL*, *PIGM*, *PIGN*, *PIGO*, *PIGV*, *PIGT*, and *PGAP2*) in this pathway are associated with neural abnormalities (Krawitz et al., 2012; Freeze, 2013; Hansen et al., 2013). Alkaline phosphatase (ALP) is a useful marker for suspected GPI anchor-synthesis pathway deficiencies caused by mutations in *PIGV*, *PIGO*, and *PGAP2*. Additionally, a recent study has reported that elevated ALP in patient serum may be useful in screening for *PIGN* mutations and MCAHS1 (Jiao et al., 2020).

Located on chromosome 18q21.33, *PIGN* is composed of 30 exons and encodes 931 amino acids (Hong et al., 1999). *PIGN* biallelic variants cause MCAHS1, which shows great clinical heterogeneity and autosomal recessive inheritance. Since PIGN is abundantly expressed in various tissues, mutation results in diverse phenotypes and involves various systems (Paulick and Bertozzi, 2008; Nakagawa et al., 2016). Additionally, *PIGN* mutations in a mouse model result in a holoprosencephaly like phenotype (McKean and Niswander, 2012). Yeast Mcd4 (a *PIGN* ortholog) mutants display defective bud emergence, polarized growth, marked morphological defects, and defective transportation from the endoplasmic reticulum to the Golgi specific for GPI-anchored proteins (Gaynor et al., 1999). The GPI backbone consists of alternating phosphoethanolamine and sugar moieties bound to phosphatidylinositol. *PIGN* is involved in GPI anchor biosynthesis; *PIGN* encodes GPI ethanolamine phosphate transferase, is expressed in the endoplasmic reticulum, and transfers phosphoethanolamine to the first mannose of the GPI anchor (Freeze et al., 2012). GPI anchors sort transport signals from the GPI-anchored protein at their site of synthesis, the endoplasmic reticulum, to their final destination, the cell surface, and enable GPI-anchored proteins to anchor in the cell membrane by covalent linkage to GPI (Kinoshita et al., 2008; Muñiz and Riezman, 2016). *PIGN* mutations lead to low expression of GPI-anchored proteins, which have roles in cell adhesion, signal transduction, and antigen presentation (Fujita and Jigami, 2008; Paulick and Bertozzi, 2008). Maydan et al. (2011) have reported that *PIGN* mutations lead to low expression of GPI-anchored proteins, particularly CD59, on the surface of patient fibroblasts.

In this study, the synonymous mutation c.963G > A was found in exon 10 of *PIGN*, which has been reported previously (Ohba et al., 2014). The synonymous mutation c.963G > A leads to abnormal transcription because this site is located at the last nucleotide of exon 10. The abnormal transcription contains two new sequences: one with a 53 bp insertion of intron 10 sequences and one with a 41 bp deletion of the entire exon 10, both leading to a frameshift mutation, and to two premature stop codons (p. Ala322Valfs*24 and p. Glu308Glyfs*2) (Ohba et al., 2014). The synonymous mutation c.963G > A results in extremely low expression of GPI-anchored proteins on patient granulocytes, specifically CD16 and CD24, suggesting severe and complete loss of PIGN activity. The degree of CD16 and CD24 deficiency is sufficient to cause severe neurological phenotypes (Ohba et al., 2014). c.2427-2 A > G is a splicing mutation in intron 25. This mutation may lead to intron loss, intron shortening, intron transfer to exons, effects on protein expression, and the production of a non-functional protein. The RT-PCR and Sanger sequencing results revealed that the mutation led to the skipping of exon 26 during transcription, and to the low expression of *PIGN*; possibly because the abnormal mRNA was degraded by non-sense-mediated mRNA decay.

In this study, two mutations in *PIGN* were identified. These findings provided reproduction guidance for this family, a basis for prenatal diagnosis, and broadened the gene and phenotype spectrum of MCAHS1.

## DATA AVAILABILITY STATEMENT

The datasets for this article are not publicly available due to concerns regarding participant/patient anonymity. Requests to access the datasets should be directed to the corresponding author.

## ETHICS STATEMENT

The studies involving human participants were reviewed and approved by the Ethics Committee of Shengjing Hospital of China Medical University (ethics approval number: 2013PS33K). Written informed consent to participate in this study was provided by the participants' legal guardian/next of kin. Written informed consent was obtained from the minor(s)' legal guardian/next of kin for the publication of any potentially identifiable images or data included in this article.

## AUTHOR CONTRIBUTIONS

SX and QN conceived and designed the experiments. ML, YL, and CL helped recruit the patients and their family members. CL, HH, and YL performed the experiments and

helped with the genetic analysis. ML, YM, QN, and YL wrote the manuscript. All authors contributed to the article and approved the submitted version.

## FUNDING

This work was supported by the National Key Research and Development Program of China (Nos. 2018YFC1002904 and 2016YFC1000408), the National Natural Science Foundation of China (No. 81701462), and the 345 Talent Project.

## ACKNOWLEDGMENTS

We appreciate the participation of the proband and his family in the study.

## REFERENCES

Brady, P. D., Moerman, P., De Catte, L., Deprest, J., Devriendt, K., and Vermeesch, J. R. (2014). Exome sequencing identifies a recessive PIGN splice site mutation as a cause of syndromic congenital diaphragmatic hernia. *Eur. J. Med. Genet.* 57, 487–493. doi: 10.1016/j.ejmg.2014.05.001

Couser, N. L., Masood, M. M., and Strande, N. T. (2015). The phenotype of multiple congenital anomalies-hypotonia-seizures syndrome 1: report and review. *Am. J. Med. Genet. A* 167A, 2176–2181. doi: 10.1002/ajmg.a.37129

Fleming, L., Lemmon, M., Beck, N., Johnson, M., Mu, W., Murdock, D., et al. (2016). Genotype-phenotype correlation of congenital anomalies in multiple congenital anomalies hypotonia seizures syndrome (MCAHS1)/PIGN-related epilepsy. *Am. J. Med. Genet. A* 170A, 77–86. doi: 10.1002/ajmg.a.37369

Freeze, H. H. (2013). Understanding human glycosylation disorders: biochemistry leads the charge. *J. Biol. Chem.* 288, 6936–6945. doi: 10.1074/jbc.r112.429274

Freeze, H. H., Eklund, E. A., Ng, B. G., and Patterson, M. C. (2012). Neurology of inherited glycosylation disorders. *Lancet Neurol.* 11, 453–466. doi: 10.1016/s1474-4422(12)70040-6

Fujita, M., and Jigami, Y. (2008). Lipid remodeling of GPI-anchored proteins and its function. *Biochim. Biophys. Acta* 1780, 410–420. doi: 10.1016/j.bbagen.2007.08.009

Gaynor, E. C., Mondésert, G., Grimme, S. J., Reed, S. I., Orlean, P., and Emr, S. D. (1999). MCD4 encodes a conserved endoplasmic reticulum membrane protein essential for glycosylphosphatidylinositol anchor synthesis in yeast. *Mol. Biol. Cell* 10, 627–648. doi: 10.1091/mbc.10.3.627

Hansen, L., Tawamie, H., and Murakami, Y. (2013). Hypomorphic mutations in PGAP2, encoding a GPI-anchor-remodeling protein, cause autosomal-recessive intellectual disability. *Am. J. Hum. Genet.* 92, 575–583. doi: 10.1016/j.ajhg.2013.03.008

Hong, Y., Maeda, Y., Watanabe, R., Ohishi, K., Mishkind, M., Riezman, H., et al. (1999). Pig-n, a mammalian homologue of yeast Mcd4p, is involved in transferring phosphoethanolamine to the first mannose of the glycosylphosphatidylinositol. *J. Biol. Chem.* 274, 35099–35106. doi: 10.1074/jbc.274.49.35099

Jezela-Stanek, A., Ciara, E., Piekutowska-Abramczuk, D., Trubicka, J., Jurkiewicz, E., Rokicki, D., et al. (2016). Congenital disorder of glycosylphosphatidylinositol (GPI)-anchor biosynthesis–the phenotype of two patients with novel mutations in the PIGN and PGAP2 genes. *Eur. J. Paediatr. Neurol.* 20, 462–473. doi: 10.1016/j.ejpn.2016.01.007

Jiao, X., Xue, J., and Gong, P. (2020). Analyzing clinical and genetic characteristics of a cohort with multiple congenital anomalies-hypotonia-seizures syndrome (MCAHS). *Orphanet J Rare Dis.* 15:78.

Khayat, M., Tilghman, J. M., Chervinsky, I., Zalman, L., Chakravarti, A., and Shalev, S. A. (2016). A PIGN mutation responsible for multiple congenital anomalies-hypotonia-seizures syndrome 1 (MCAHS1) in an Israeli-Arab family. *Am. J. Med. Genet. A* 170A, 176–182. doi: 10.1002/ajmg.a.37375

Kinoshita, T., Fujita, M., and Maeda, Y. (2008). Biosynthesis, remodelling and functions of mammalian GPI-anchored proteins: recent progress. *J. Biochem.* 144, 287–294. doi: 10.1093/jb/mvn090

Krawitz, P. M., Murakami, Y., and Hecht, J. (2012). Mutations in PIGO, a member of the GPI-anchor-synthesis pathway, cause hyperphosphatasia with mental retardation. *Am. J. Hum. Genet.* 91, 146–151. doi: 10.1016/j.ajhg.2012.05.004

Maydan, G., Noyman, I., and Har-Zahav, A. (2011). Multiple congenital anomalies-hypotonia-seizures syndrome is caused by a mutation in PIGN. *J. Med. Genet.* 48, 383–389. doi: 10.1136/jmg.2010.087114

McKean, D. M., and Niswander, L. (2012). Defects in GPI biosynthesis perturb Cripto signaling during forebrain development in two new mouse models of holoprosencephaly. *Biol. Open* 1, 874–883. doi: 10.1242/bio.20121982

Muñiz, M., and Riezman, H. (2016). Trafficking of glycosylphosphatidylinositol anchored proteins from the endoplasmic reticulum to the cell surface. *J. Lipid Res.* 57, 352–360. doi: 10.1194/jlr.r062760

Nakagawa, T., Taniguchi-Ikeda, M., Murakami, Y., Nakamura, S., Motooka, D., Emoto, T., et al. (2016). A novel PIGN mutation and prenatal diagnosis of inherited glycosylphosphatidylinositol deficiency. *Am. J. Med. Genet. A* 170A, 183–188.

Ohba, C., Okamoto, N., Murakami, Y., Suzuki, Y., Tsurusaki, Y., Nakashima, M., et al. (2014). PIGN mutations cause congenital anomalies, developmental delay, hypotonia, epilepsy, and progressive cerebellar atrophy. *Neurogenetics* 15, 85–92. doi: 10.1007/s10048-013-0384-7

Pagnamenta, A. T., Murakami, Y., and Taylor, J. M. (2017). Analysis of exome data for 4293 trios suggests GPI-anchor biogenesis defects are a rare cause of developmental disorders. *Eur. J. Hum. Genet.* 25, 669–679. doi: 10.1038/ejhg.2017.32

Richards, S., Aziz, N., Bale, S., Bick, D., Das, S., Gastier-Foster, J., et al. (2015). Standards and guidelines for the interpretation of sequence variants: a joint consensus recommendation of the american college of medical genetics and genomics and the association for molecular pathology. *Genet. Med.* 17, 405–424. doi: 10.1038/gim.2015.30

Paulick, M. G., and Bertozzi, C. R. (2008). The glycosylphosphatidylinositol anchor: a complex membrane-anchoring structure for proteins. *Biochemistry* 47, 6991–7000. doi: 10.1021/bi8006324

Thiffault, I., Zuccarelli, B., Welsh, H., Yuan, X., Farrow, E., Zellmer, L., et al. (2017). Hypotonia and intellectual disability without dysmorphic features in a patient with PIGN-related disease. *BMC Med. Genet.* 18:124. doi: 10.1186/s12881-017-0481-9

**Conflict of Interest:** The authors declare that the research was conducted in the absence of any commercial or financial relationships that could be construed as a potential conflict of interest.

frontiers in Genetics

ORIGINAL RESEARCH
published: 27 November 2020
doi: 10.3389/fgene.2020.561687

# Xeroderma Pigmentosum C (XPC) Mutations in Primary Fibroblasts Impair Base Excision Repair Pathway and Increase Oxidative DNA Damage

*Nour Fayyad[1], Farah Kobaisi[1,2,3], David Beal[1], Walid Mahfouf[4], Cécile Ged[4,5], Fanny Morice-Picard[5], Mohammad Fayyad-Kazan[2], Hussein Fayyad-Kazan[2], Bassam Badran[2], Hamid R. Rezvani[4,5] and Walid Rachidi[1,3]**

[1] University Grenoble Alpes, SyMMES/CIBEST UMR 5819 UGA-CNRS-CEA, Grenoble, France, [2] Laboratory of Cancer Biology and Molecular Immunology, Faculty of Sciences I, Lebanese University, Hadath, Lebanon, [3] University Grenoble Alpes, CEA, Inserm, BIG-BGE U1038, Grenoble, France, [4] Université de Bordeaux, Inserm, BMGIC, U1035, Bordeaux, France, [5] Centre de Référence pour les Maladies Rares de la Peau, CHU de Bordeaux, Bordeaux, France

OPEN ACCESS

**Edited by:**
Yuejin Hua,
Zhejiang University, China

**Reviewed by:**
Bixia Zheng,
Nanjing Children's Hospital, China
Julien H. Park,
University of Münster, Germany

***Correspondence:**
Walid Rachidi
walid.rachidi@univ-grenoble-alpes.fr

**Specialty section:**
This article was submitted to Genetics of Common and Rare Diseases, a section of the journal Frontiers in Genetics

**Received:** 26 May 2020
**Accepted:** 28 October 2020
**Published:** 27 November 2020

**Citation:**
Fayyad N, Kobaisi F, Beal D, Mahfouf W, Ged C, Morice-Picard F, Fayyad-Kazan M, Fayyad-Kazan H, Badran B, Rezvani HR and Rachidi W (2020) Xeroderma Pigmentosum C (XPC) Mutations in Primary Fibroblasts Impair Base Excision Repair Pathway and Increase Oxidative DNA Damage. Front. Genet. 11:561687. doi: 10.3389/fgene.2020.561687

Xeroderma Pigmentosum C (XPC) is a multi-functional protein that is involved not only in the repair of bulky lesions, post-irradiation, via nucleotide excision repair (NER) *per se* but also in oxidative DNA damage mending. Since base excision repair (BER) is the primary regulator of oxidative DNA damage, we characterized, post-Ultraviolet B-rays (UVB)-irradiation, the detailed effect of three different XPC mutations in primary fibroblasts derived from XP-C patients on mRNA, protein expression and activity of different BER factors. We found that XP-C fibroblasts are characterized by downregulated expression of different BER factors including *OGG1*, *MYH*, *APE1*, *LIG3*, *XRCC1*, and *Pol*β. Such a downregulation was also observed at OGG1, MYH, and APE1 protein levels. This was accompanied with an increase in DNA oxidative lesions, as evidenced by 8-oxoguanine levels, immediately post-UVB-irradiation. Unlike in normal control cells, these oxidative lesions persisted over time in XP-C cells having lower excision repair capacities. Taken together, our results indicated that an impaired BER pathway in XP-C fibroblasts leads to longer persistence and delayed repair of oxidative DNA damage. This might explain the diverse clinical phenotypes in XP-C patients suffering from cancer in both photo-protected and photo-exposed areas. Therapeutic strategies based on reinforcement of BER pathway might therefore represent an innovative path for limiting the drawbacks of NER-based diseases, as in XP-C case.

**Keywords: Xeroderma Pigmentosum C, nucleotide excision repair, base excision repair, ultra violet (UV) light, oxidative DNA damage, oxidative stress, skin cancer**

## INTRODUCTION

Skin is considered a first line of defense protecting the human body against several chemical and physical stressors (such as microbial infections, irradiation, toxic substances, pollutants) that can generate molecular DNA lesions at a rate of 1,000 to 1,000,000 lesions per cell per day (Kelley, 2012). Such lesions could be repaired via different repair systems [such as base excision repair (BER), nucleotide excision repair (NER), mismatch repair (MMR)] that are specialized to remove DNA

damage and maintain genome integrity. Ultraviolet B rays (UVB) (280–315 nm), an environmental stress, could act as a carcinogen that triggers tumor-initiation, -promotion, and progression. UVB, by inducing both direct and indirect DNA damage, is capable of causing genomic instability, thus leading to acute- or delayed-skin lesions (D'Orazio et al., 2013; Melis et al., 2013a). Direct lesions, including pyrimidine (6–4) pyrimidone photoproducts [(6–4) PPs] and cyclobutane pyrimidine dimers (CPDs), can cause UV-signature mutations (C > T and CC > TT transition mutations). Such mutations usually contribute to a dominant phenotype as in the case of *p53* gene mutations that are dominant in skin cancer (Ravanat et al., 2001; Kemp et al., 2017). Indirect damages, such as 8-oxoguanine (8-oxoGua), are oxidative DNA damage occurring at a rate of $10^4$ hits per cell per day in humans and are usually triggered by UV-induced reactive oxygen species (ROS) that will also damage protein and lipid cellular molecules. However, unlike these molecules, DNA lesions are not replaced with new molecules rather repaired (Ravanat et al., 2001; Rezvani et al., 2006; Melis et al., 2013b). If left unrepaired, 8-oxoGua may give rise to the oxidative stress hallmark, GC→TA transversion mutation, subsequently, sporadic and hereditary cancerogenesis (Hegde et al., 2008). Therefore, these oxidized bases are repaired via BER pathway for maintaining genome integrity and survival, consequently preventing cancer and aging (David et al., 2007; Hegde et al., 2008; Krokan and Bjørås, 2013). In general, BER corrects small base lesions from oxidation, deamination and alkylation in the nucleus and mitochondria. First, depending on the type of lesions and cell's physiological state, a selective DNA glycosylase will recognize and remove the base lesion, leaving an abasic site that is further processed by short-patch or long-patch repair. The subsequent steps are incision, end-processing, repair synthesis, and ligation (Krokan and Bjørås, 2013). Meanwhile, direct bulky photoproducts (CPDs and (6–4) PPs) are removed by NER pathway to prevent UV-mediated mutagenesis and maintain cell and tissue viability post-stress. NER is regulated by DNA damage-induced signaling pathway (DDR pathway) and subdivided into global genome NER (GG-NER) and RNA-polymerase dependent transcriptional coupled NER (TC-NER) (Park and Kang, 2016; Kemp et al., 2017). Both sub-pathways differ in their recognition step, speed, and efficiency. Hereditary alterations in NER-genes may result in severe diseases, such as Cockayne syndrome, Trichothiodystrophy, and Xeroderma Pigmentosum (XP) (Park and Kang, 2016).

Xeroderma Pigmentosum is a rare, recessive, cancer-prone, autosomal genodermatosis with an incidence rate of 1 in 250,000 in North America, and 1 in 1,000,000 in Europe (Lehmann et al., 2011; Pázmándi et al., 2019). Its prevalent symptoms include photosensitivity, cutaneous atrophy, dry pigmented-freckled skin, and a 2,000 and 10,000-fold incidence increase of melanoma and non-melanoma skin cancers, respectively. It is characterized by the accumulation of mutations either in proto-oncogenes (such as *BRAF* and *MYC*) or tumor suppressor genes (such as *P53* and *PTCH1*) that persist due to NER defect whereby neither DNA repair nor apoptosis occurs (Daya-Grosjean and Sarasin, 2004; Murray et al., 2016; Zebian et al., 2019). Amongst XP patients, XPC patients have a lost or mutated XPC protein, the main initiator of GG-NER. Not only do they suffer from cancer in photo-exposed areas, but also XP-C patients are characterized by a 10 to 20-fold increased risk of developing internal malignancies in photo-protected sites (Zebian et al., 2019). Analysis of these internal tumors indicated that mutations are most likely caused by unrepaired oxidative DNA damages (Melis et al., 2013b). Remarkably, primary internal tumors (such as lung, uterus, thyroid, breast, and thyroid malignancies) have also been reported in XP-C patients (Hosseini et al., 2015). This predicts that XPC is involved in pathways other than NER. In this context, it has been demonstrated that NER is engaged in processing oxidative DNA lesions that are usually repaired by the BER pathway (Hutsell and Sancar, 2005). It is suggested that this role could be done by XPC (Murray et al., 2016). Researchers had started to suggest a direct link between XPC, BER, and oxidative DNA damage. For instance, it has been reported that XPC mutation leads to 8-oxoguanine (8-oxoGua) persistence, where this effect can be inverted by XPC-overexpression (D'Errico et al., 2006). Moreover, it has been demonstrated that XPC knockdown in normal keratinocytes leads to metabolism alterations through NADPH-oxidase-1 (NOX1) and ROS upregulation (Rezvani et al., 2011). Furthermore, a previous study proposed that XPC recognizes oxidative DNA damage directly, and thus it will be recruited solely without other GG-NER factors (Hosseini et al., 2015). Others demonstrated that XPC stimulates the activities of distinct glycosylases (such as OGG1 and MPG) (Zebian et al., 2019). This may explain the different cancer etiology in patients where increased intracellular oxidative DNA damage may function synergistically with altered DNA repair response to promote tumorigenesis and/or premature aging (one of the major XP-C disorder's clinical features) (Hosseini et al., 2014, 2015).

In this study, we deciphered, post-UVB-irradiation, the effect of three different XPC mutations on the expression status and activity levels of different components of BER pathway. This unraveled the adaptation of BER components to XPC mutations and could enable: (1) better understanding of skin and internal cancers' etiology; (2) identification of risk factors in XP-C patients; and (3) provide better insights toward designing novel therapeutic or preventive strategies.

## MATERIALS AND METHODS

### Primary Fibroblasts Isolation and Culture

Three unrelated patients clinically classified as classical XP-C with no associated neurologic or extracutaneous findings were included in this study (**Supplementary Table S1**). After the concerned Ethical Committee agreed to perform the analysis and the patients' parents gave their informed consent, XP-C fibroblasts were isolated from punch biopsies obtained from non-exposed patients' body sites followed by their sequencing as previously described (Soufir et al., 2010). These cells are compatible with our aim in explaining the reason for cancer development in photo-protected areas of XP-C patients. They were compared to normal primary fibroblasts ($n$ = 3) extracted by our laboratory (SyMMES, CIBEST, CEA).

Fibroblasts were cultured in DMEM medium (DMEM, high glucose, GlutaMAX$^{TM}$ Supplement, +Pyruvate, Thermo

Fisher Scientific) with 10% SVF and 1% penicillin/streptomycin in falcon flasks (75 $cm^2$) at 37°C in 5% CO2 incubator. 3000 cells/$cm^2$ were seeded 7 days to reach 80% confluency.

## Short-Term Cytotoxicity Assay, MTT

3-(4,5-dimethylthiazol-2-yl)-2,5-diphenyltetrazolium bromide (MTT) assay (SIGMA) was used to evaluate cell viability 24 h post-UVB-irradiation. 200 μL MTT (5 mg/mL)/well were added to six well-plates followed by a 2 h-incubation at 37°C and discarding the supernatant. Next, 2 mL DMSO/well was added along with 20 min shaking. Solutions were then transferred to 96 well microplates and the absorbance of formazan crystals at 560 nm was measured by a spectrophotometer (Spectramax M2; from Molecular Devices) allowing us to quantify the number of living cells. All data were normalized by comparison with the yield of MTT conversion in non-irradiated control samples set at 100% viability.

## Immunofluorescence and Associated Microscopy

Cells were seeded in 96 well microplates, after that exposed to UVB-irradiation at a dose of 0.03 J/$cm^2$. Following that, cells were fixed at different time points (0 and 24 h) with 4% paraformaldehyde, and then permeabilized with 0.2% Triton X-100. After washing with PBS, DNA was denatured with 2 M HCL, followed by blocking with 3% FBS in PBS. The primary anti-pyrimidine (6–4) pyrimidone photoproducts (64M-2, Cosmo Bio) and secondary antibodies (Alexa Fluor 488 goat anti-mouse, Invitrogen) were diluted in 1% FBS and incubated with three washing steps between them. Finally, nuclear DNA was counter-stained with Hoechst (Sigma-Aldrich). Cell images were acquired by the Cell-insight NXT high content screening platform at 10× magnification. Data were normalized against non-irradiated samples.

## Treatment and Cell-Pellets Preparation

Sub-confluent cells (80%) were either exposed or not to 0.05 J/$cm^2$ UVB-irradiation. Fibroblasts were harvested 4 h post-irradiation [real-time quantitative PCR (qRT-PCR) assay, western blot], centrifuged, and rinsed with PBS (Invitrogen, Carlsbad, CA, United States). Pellets were rapidly frozen at −80°C until further use.

For comet assay, cells were either exposed or not to 0.05 J/$cm^2$ UVB-irradiation then harvested after 0, 2, and 24 h. Cells were then centrifuged, rinsed with PBS, and dissolved in freezing buffer (pH = 7.6) to be stored at −80°C.

## Reverse Transcription and Real-Time Quantitative PCR (qRT-PCR) Analysis

Total RNA was isolated using GenElute™ Mammalian Total RNA Miniprep kit (Sigma-Aldrich) and then quantified using Nanodrop 1000 from Thermo scientific to check its integrity. Another method for assessing RNA integrity was to add 5 μL of sample/well (each sample tube consisted of 1 μL RNA, 9 μL water, and 2 μL DNA gel loading dye) in agarose gel using LT4 DNA ladder. Total RNA was considered intact when two acute 28S and 18S bands were visualized.

RNA (2 μg) was reversely transcribed to cDNA (Superscript® III Reverse Transcriptase, Invitrogen, Carlsbad, CA, United States) in the presence of random primers (100 ng/μL, Promega, Charbonnières, France), dNTP mix (10 mM, Sigma-Aldrich, Saint-Quentin-Fallavier, France), 5×-First-strand buffer (Invitrogen, Carlsbad, CA, United States), DTT (0.1 M, Invitrogen, Carlsbad, CA, United States), ribonuclease inhibitor (45 U/μL, Sigma-Aldrich, Saint-Quentin-Fallavier, France) and SuperScript III enzyme (200 units, Invitrogen, Carlsbad, CA, United States).

Next, 5 μL of each cDNA (25 ng/μL) was used in qPCR reactions with gene-specific primers (**Supplementary Table S2**), and qPCR was performed by MESA Blue qPCR MasterMix Plus for SYBR® Assay with low ROX (Eurogenetic, Angers, France). Samples were run in triplicates through Bio-Rad CFX96™ Real-time Sys (C1000 Touch™ Thermal Cycler). At the end of each run, the integrity of amplification was verified by a single melt-curve peak per product. Expression levels of target genes were normalized to those of the housekeeping gene glyceraldehyde-3-phosphate dehydrogenase (GAPDH). Calculations for determining the relative level of gene expression were made using the ΔΔCT method for quantification as reported by Livak and Schmittgen (2001).

## Western Blot

Total proteins were extracted from fibroblasts upon adding 100 μL of lysis buffer to the cell pellet followed by vortexing and incubation on ice for 30 min (vortexed every 10 min). The mixture was then transferred to 1.5 mL eppendorf and centrifuged at 16000 rpm for 15 min at 4°C. Total proteins were dosed by microBC assay protein quantification kit according to the manufacturers' instructions. Western blotting was performed as previously described (D'Errico et al., 2006). Briefly, equal amounts of proteins were resolved by SDS-PAGE and transferred to nitrocellulose membrane (*Trans*-Blot® Turbo™ Transpack, Bio-Rad), followed by blocking the membrane with 5% lyophilized milk and the addition of 1/1000 diluted primary anti-XPC (mouse monoclonal antibody; Thermo Fisher Scientific), 1/50000 diluted primary anti-OGG1 (rabbit monoclonal antibody; Abcam), 1/250 diluted primary anti-MYH (rabbit monoclonal antibody; Novus Biologicals), and 1/1000 diluted primary anti-APE1 (rabbit monoclonal antibody; Sigma Aldrich). Incubation at 4°C for overnight was done, followed by incubation with mouse or rabbit anti-HRP (1/10000 diluted secondary antibody) and the addition of clarity™ western ECL substrate (Bio-Rad). The membrane was visualized through Bio-Rad Molecular Imager® ChemiDoc™ XRS + using Image Lab™ software. After a stain-free total protein detection, target proteins' expression was normalized to the total protein extract.

## Comet Assay ± FPG

Comet assay is a single-cell gel electrophoresis assay that is used to measure the DNA lesions of cell extracts, and consequently, can monitor the excision repair capacity when it is employed at various time points post-treatment of cells. More specifically,

upon adding FormamidoPyrimidine [fapy]-DNA Glycosylase (FPG) enzyme, we were able to detect 8-oxoguanine excision activity. Hydrogen peroxide ($H_2O_2$, 400 μM) was used as an internal positive control. Cells were plated in 100 mm dishes as triplicates and irradiated with 0.05 J/cm$^2$ UVB-irradiation then collected after 0, 2, and 24 h. Immediately following treatment, cells were harvested, counted, and suspended at a concentration of 200,000 cells in 100 μL freezing buffer. Samples were stored at −80°C until use.

Briefly, slides were prepared with normal agarose coating 1 day in advance. On the day of the experiment, cells were deposited on the slides with 0.6% solution of low-melting agarose followed by adding a coverslip, immersing in lysis buffer, and incubation for 1 h after which a three times wash with Tris–HCL 0.4 M (neutralizing buffer) was done. FPG 0.05 u/μL (1.25 μL/slide) was then prepared in which 100 μL FPG solution with or without FPG enzyme was deposited on the slides and covered with coverslips. The slides were set on a humidified bed and added in a 37°C incubator for 40 min. The reaction was stopped by incubation for a few minutes on ice. After digestion, the slides were transferred to an electrophoresis tank filled with electrophoresis buffer pre-chilled at 4°C. The slides were left at room temperature for 30 min, and electrophoresis was subsequently done for 30 min at 25 V and 300 mA. The slides were then rinsed 3 times with Tris–HCL 0.4 M. 50 μL of Gel Red was added per slide, and a coverslip was added for reading the next day. We read the slides using a 10× objective microscope and Comet Assay IV software (Perceptive Instruments, Suffolk, United Kingdom). 50 randomly selected nuclei were scored in each slide and triplicate slides were processed for each experimental point. The extent of damage was evaluated by the Tail DNA value defined as the percentage of DNA in the tail of the comet. The normalization was done by doing a ratio of irradiated/non-irradiated at each condition.

## Statistical Analysis

The data were expressed as mean ± SEM for three independent experiments. Statistical significance of data was assessed using the student's-*t*-test (GraphPad Prism 8) after checking variance homogeneity with the Levene's test and normality by normality test. Student paired-*t*-test allows us to compare each sample between two different conditions while student unpaired-*t*-test allows us to compare different samples at each condition. Results were considered significant for $p$-value $\leq 0.05$.

# RESULTS

## Characterization of Normal and XP-C Primary Fibroblasts

### Dysregulated XPC mRNA and Protein Expression Levels in XP-C Fibroblasts Compared to Normal

We first examined using qRT-PCR the mRNA levels of *XPC* in the normal versus XP-C fibroblasts at basal state. As shown in **Figure 1A**, XP-C1, XP-C2, and XP-C3 exhibited a drastically significant ($p < 0.0001$) lower *XPC* mRNA levels than normal fibroblasts ($n = 3$) (∼ 8, 4, and 3-fold downregulation,

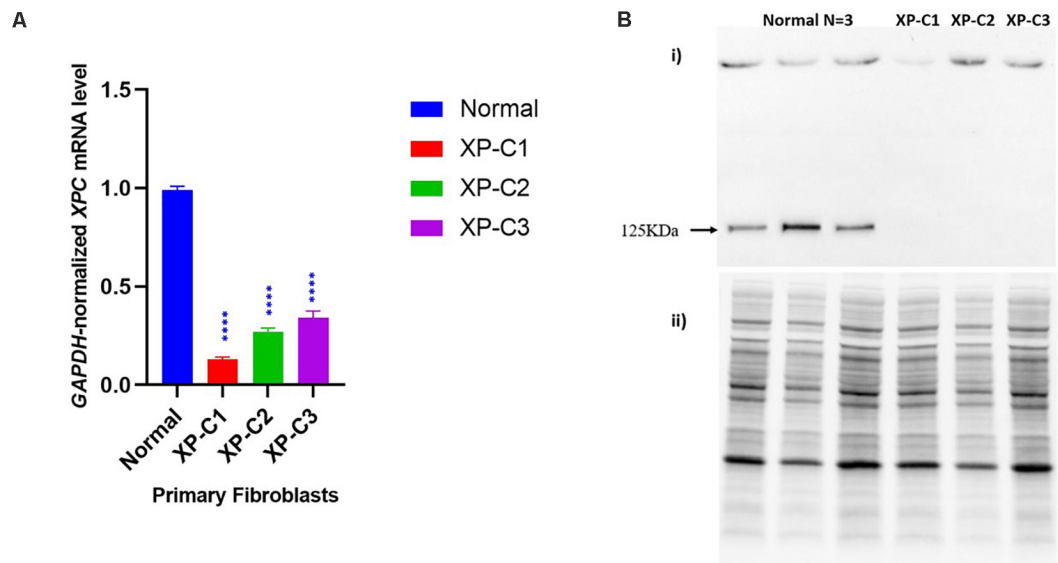


**FIGURE 1 |** Impaired *XPC* mRNA and protein levels in XP-C primary fibroblasts at basal level. **(A)** *XPC* mRNA level is downregulated in XP-C primary fibroblasts compared to normal control at basal level. Upon qRT-PCR, all three XP-C fibroblasts exhibited a significantly reduced *XPC* gene transcription compared to the normal ($n = 3$). ($p < 0.0001$ ****, Unpaired-*t*-test, GraphPad Prism 8). The data were normalized relative to the GAPDH mRNA levels, where GAPDH was used as an endogenous control. The results are the mean ± SEM from three independent experiments, $n = 3$. **(B)** XPC protein was not expressed in XP-C primary fibroblasts at basal level. Although XPC protein was readily observed in all three normal fibroblasts, it was undetectable in the three XP-C fibroblasts at MW = 125 KDa. The results correspond to the mean ± SEM from three independent experiments, $n = 3$. (i) membrane with XPC bands upon hybridization with anti-XPC (ii) total protein-membrane used for normalization.

respectively). In a next step, western blot was performed to validate this expression profile at protein level. As seen in **Figure 1B**, XPC protein (band size = 125 KDa) was detected in normal cells but was totally absent in the three XP-C fibroblasts. This indicates that all the three different XPC mutations led to an impairment in XPC gene expression and absence at the protein level.

### Similar Photosensitivity Between Normal and XP-C Primary Fibroblasts

We checked whether XP-C and normal fibroblasts differ in their photosensitivity as the former are suspected to be hyper-photosensitive. Hence, we did a cytotoxicity test 24 h post-UVB-irradiation. The viability of the different cells was gradually decreasing in a manner dependent on the increasing UVB doses. Generally, there was no significant difference in photosensitivity between the control and XP-C fibroblasts (**Figure 2**). At the highest dose (1.5 J/cm$^2$), less than 20% of cells survived.

The $LD_{50}$ was determined for all primary fibroblasts (**Supplementary Table S3**) using regression analysis.

Based on this cytotoxicity test, we decided to perform our experiments at 0.05 J/cm$^2$ UVB dose. It is a moderate cytotoxic dose which kills <50% of cells and is thus suitable for the investigation of DNA oxidative lesions and their repair.

### Dysregulated Photoproducts' Repair in XP-C Primary Fibroblasts Compared to Normal

Xeroderma Pigmentosum C protein does not recognize the lesion itself but rather binds to the associated helix distortion. Hence, XPC binds with a high affinity to pyrimidine (6–4) pyrimidone photoproducts [(6–4) PPs], inducing high helical alterations (Nemzow et al., 2015). For that, we were interested in following the kinetics of repair of (6–4) PPs by immunocytochemistry, where an anti-(6–4) PP was used to detect (6–4) PPs at 0 and 24 h. 24 h post-UVB-irradiation around 70% of lesions were repaired in normal fibroblasts. However, this was not the case in the three XP-C fibroblasts where elevated levels persisted. Almost 20% were repaired in XP-C1, XP-C2, and XP-C3 as shown in **Figure 3** and **Supplementary Figure S1**. This lesion persistence was significant in XP-C1, XP-C2, and XP-C3 compared to normal fibroblasts ($p < 0.001$, $p < 0.001$, $p < 0.05$, respectively).

## Dysregulated BER-Associated Gene Expression in XP-C Fibroblasts Compared to Normal, Post-UVB-Irradiation

We examined the mRNA levels of a series of genes involved in BER between normal and XP-C primary fibroblasts 4 h post-UVB-irradiation (**Figure 4**). We scanned the whole BER pathway starting from the initiation and base removal steps (*OGG1*, *MYH*), passing by abasic sites removal (*APE1*), and to newly synthesized nucleotide (*PolB*) and ligation (*LIG3*, *XRCC1*).

We observed that 8-oxoguanine glycosylase (*OGG1*), MutY Adenine DNA Glycosylase (*MYH*), apurinic endonuclease 1 (*APE1*), ligase 3 (*LIG3*), and X-ray repair cross-complementing 1, LIG3's cofactor, (*XRCC1*) were characterized by a significantly lower mRNA levels in all three XP-C fibroblasts compared to normal cells ($p < 0.01$). On the other hand, *PolB* transcription levels were significantly downregulated in XP-C1 and XP-C3 ($p < 0.01$) but not XP-C2.

## Dysregulated BER-Associated Protein Expression in XP-C Fibroblasts Compared to Normal, Post-UVB-Irradiation

To better understand the effect of XPC mutation on BER's regulation, we studied the difference in OGG1, MYH, and APE1 protein levels between normal and XP-C primary fibroblasts 4 h post-UVB-irradiation (**Figure 5** and **Supplementary Figure S2**). Such proteins were selected due to their main role in initiating BER of oxidative damage. OGG1 and MYH were characterized by a significantly ($p < 0.05$) lower protein levels in all three XP-C fibroblasts compared to normal cells. Meanwhile, APE1 protein expression was significantly downregulated in XP-C2 ($p < 0.0001$) but not XP-C1 and XP-C3.

## Lower Intrinsic Base Excision-Repair Capacities in XP-C Primary Fibroblasts Compared to Normal

Standard alkaline comet (−FPG) is a genotoxic assay that measures DNA single-strand breaks (SSBs) and alkali-labile sites (ALS). Once FPG glycosylase is added, oxidized purines (including 8-oxoguanine) can be evaluated. This is done by the excision of FPG-sensitive sites (oxidized purines) converting abasic sites into DNA SSBs. The net cleavage sites (oxidized purines) generated by FPG activity are calculated by subtracting the value of DNA damage at alkaline conditions from that with FPG treatment (as presented in **Figure 6C**). This FPG enzyme is functionally similar to OGG1 where both recognize oxidized purines, majorly Fapy and 8-oxoGua (Hu et al., 2005).

**Figure 6A** shows an example of comets done ± FPG in normal and XP-C1 fibroblasts, and the positive control, $H_2O_2$. The head of comet represents intact DNA, meanwhile, the tail represents damaged DNA.

### In Absence of FPG

Ultraviolet B rays-irradiation increased SSBs to the maximum at time = 0 h in all primary fibroblasts. However, this was significantly higher in XP-C1 and XP-C2 compared to the control ($p < 0.01$, **). On the contrary, the increase of DNA damages in XP-C3 was not significant compared to the control. During the course of the experiment, lesions were repaired faster in the normal fibroblasts. Similarly, at times = 2 and 24 h, XP-C1 and XP-C2 had significantly higher DNA lesions compared to normal ($p < 0.01$ and $p < 0.05$, respectively) (**Figure 6B**).

### In Presence of FPG

Upon adding FPG,% mean tail intensity increased due to more breaks in DNA where FPG will specifically excise oxidized purines (oxidative DNA lesions, as 8-oxoguanine and Fapy). This was clearly demonstrated upon a significant increase in intensity when comparing the samples with/without FPG at times = 0 and

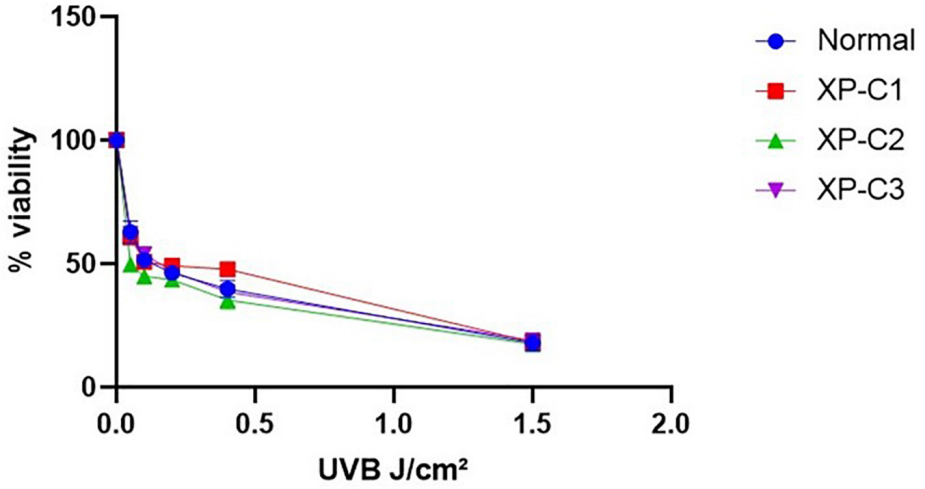


**FIGURE 2 |** Similar Photosensitivity between normal and XP-C primary fibroblasts. Short-term cytotoxicity test (MTT) was done 24 h post-UVB-irradiation. This was done by comparing the cellular viability between normal and XP-C fibroblasts at each UVB dose condition. Each sample was normalized by its non-irradiated value (100% viability). Unpaired-*t*-test was used to compare photosensitivity between normal and each XP-C fibroblast at each UVB dose (GraphPad Prism 8). The results are the mean ± SEM from three independent experiments, $n = 3$.

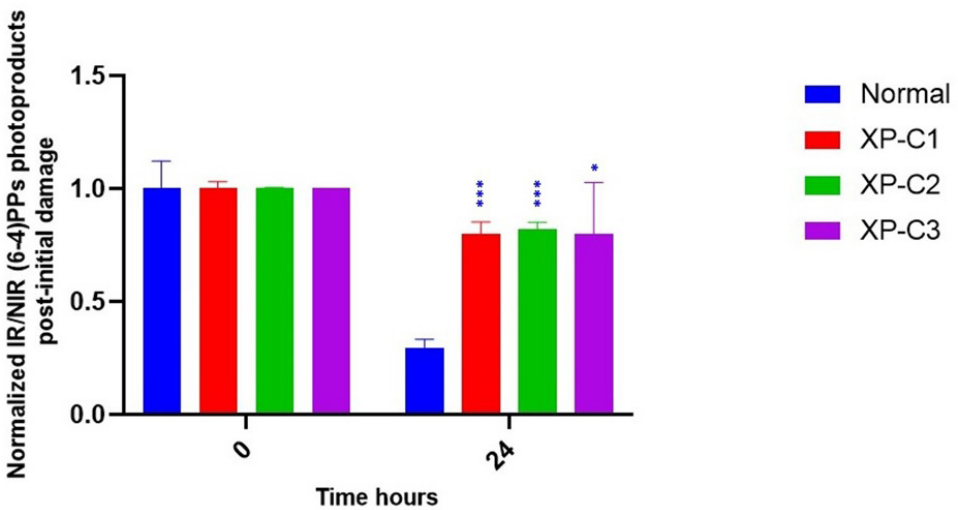


**FIGURE 3 |** Downregulated repair of (6–4) PPs, bulky photoproducts, in XP-C fibroblasts compared to normal control. Immunocytochemistry was done to detect (6–4) PPs by fixation instantaneously at 0 and 24 h post-UVB-irradiation (0.03 J/cm$^2$). An absence of primary antibody was used as negative control. The nuclei were stained with Hoechst and the (6–4) PPs were detected by green fluorescently labeled primary antibody. Images were shown upon merging both fluorescence, thereby, lesions were quantified (fluorescence signal) and normalized by non-irradiated conditions. XP-C1, XP-C2, and XP-C3 showed a significant persistence of lesion repair at 24 h compared to normal ($p < 0.001$,***; $p < 0.001$,**; $p < 0.05$,* respectively). Unpaired-*t*-test was used to compare normalized IR/NIR lesion between normal and each XP-C fibroblast at each UVB dose (0 and 24 h) (GraphPad Prism 8). The results are the mean ± SEM from two independent experiments, $n = 2$ (each experiment is done as a triplicate). IR, irradiated, NIR, non-irradiated.

2 h ($p < 0.05$, \$). When comparing control cells to each XP-C fibroblast: significantly higher DNA lesions were observed in XP-C1 and XP-C2 at $t = 0$, 2 and 24 h. Meanwhile, XP-C3's higher DNA lesions were only significant at $t = 0$ h ($p < 0.05$, μ) (**Figure 6B**).

**Figure 6C** is a zoom in to **Figure 6B**. It represents oxidized purines present in each sample and its kinetic repair follow up. At $t = 0$ h, XP-C1, XP-C2, and XP-C3 had higher oxidized purines compared to normal control ($p < 0.01$, $p < 0.001$, and $p < 0.05$, respectively). Similarly, at $t = 2$ and 24 h, XP-C fibroblasts showed significantly higher oxidized purines compared to control ($p < 0.05$); except for XP-C3 at 24 h.

On the contrary to Berra et al. (2013), the repair was not similar between XP-C deficient and XP-C-proficient fibroblasts (normal control). Induction of single strand breaks and oxidized purines was more prominent and persistent (slower rate of

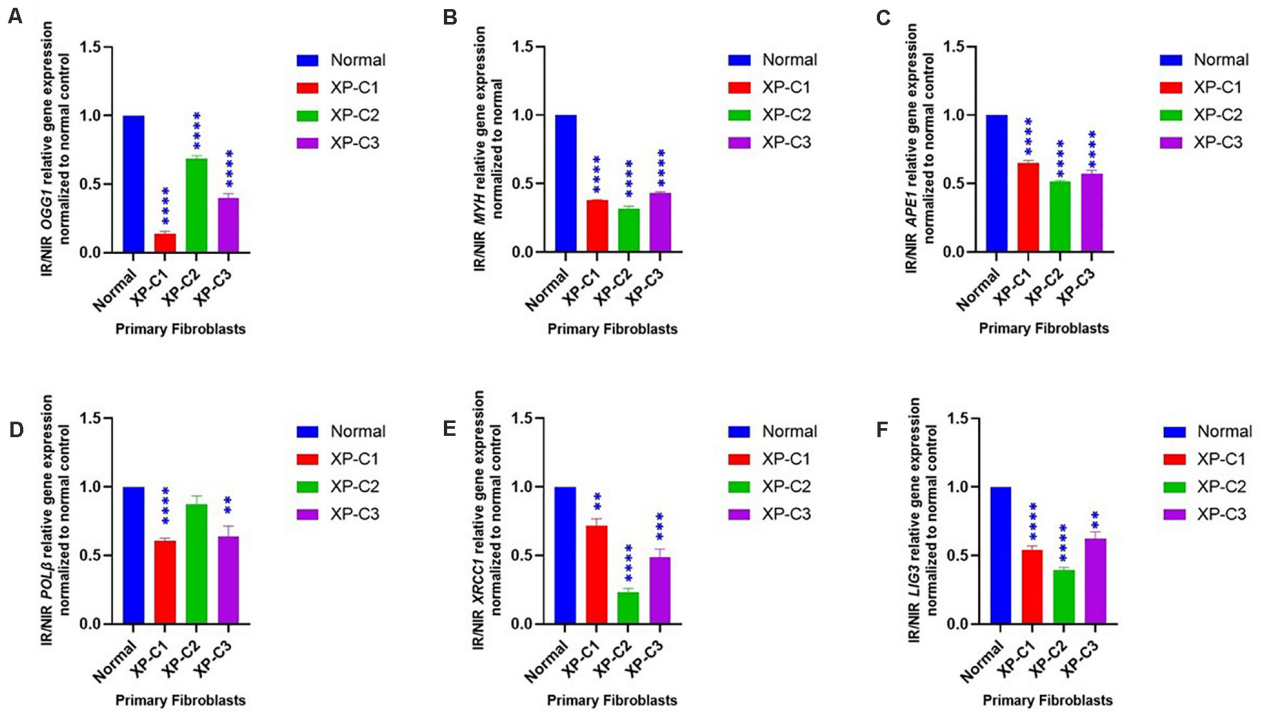


**FIGURE 4 |** Downregulated BER-associated gene transcription in normal and XP-C fibroblasts, post-UVB-irradiation. Gene transcription was investigated by qRT-PCR experiments in XP-C vs. control fibroblasts 4 h post-UVB dose (0.05 J/cm$^2$). Total RNA extraction was followed by reverse transcription. QRT-PCR was carried out to assess gene expression. Shown values are the mean ± SEM from three independent experiments, $n = 3$. The used calibrator was non-irradiated normal fibroblast where expression ratios were normalized by that of control. Ratio of IR/NIR was used in analysis. Panel **(A)** shows the significant downregulation of normalized IR/NIR *OGG1* gene expression in XP-C fibroblasts compared to normal ($p < 0.0001$,****). Panel **(B)** shows the significant downregulation of normalized IR/NIR *MYH* gene expression in XP-C fibroblasts compared to normal ($p < 0.0001$,****). Panel **(C)** shows the significant downregulation of normalized IR/NIR *APE1* gene expression in XP-C fibroblasts compared to normal ($p < 0.0001$,****). Panel **(D)** XP-C1 and XP-C3 showed a significant *Pol*β downregulation compared to normal ($p < 0.0001$,**** and $p < 0.01$,** respectively) while no significant difference was observed while comparing XP-C2 to the control. Panel **(E)** shows the significant downregulation of normalized IR/NIR *XRCC1* gene expression in XP-C1, XP-C2, and XP-C3 compared to normal ($p < 0.01$,**; $p < 0.0001$,**** and $p < 0.001$,*** respectively). Panel **(F)** shows the significant downregulation of normalized IR/NIR *LIG3* gene expression in XP-C1, XP-C2, and XP-C3 compared to normal ($p < 0.0001$,****; $p < 0.0001$,**** and $p < 0.01$,** respectively). This was done by unpaired-*t*-test that allows the comparison between normal and each XP-C fibroblast (GraphPad Prism 8). IR, irradiated; NIR, Non-Irradiated.

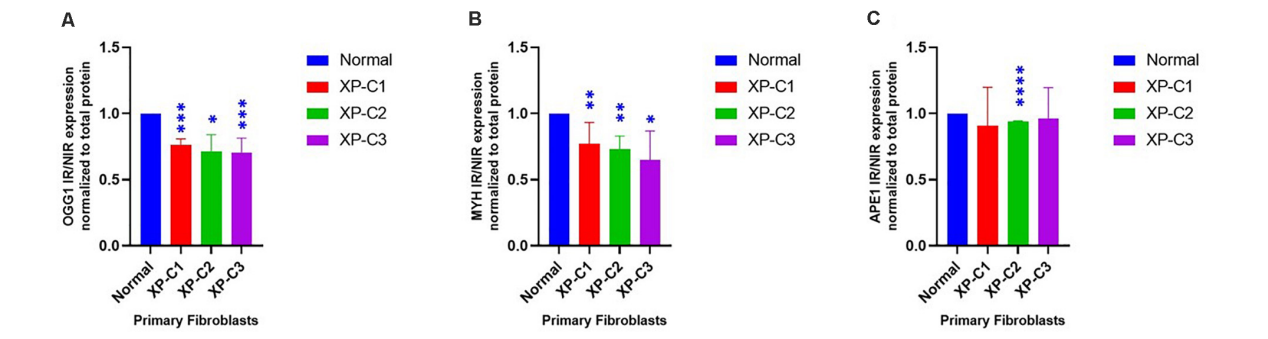


**FIGURE 5 |** Downregulated BER-associated protein levels in normal and XP-C fibroblasts, post-UVB-irradiation. Protein level was investigated in XP-C vs. control fibroblasts 4 h post-UVB-irradiation (0.05 J/cm$^2$). Total protein was extracted followed by western blot to evaluate protein expression. Values shown are the mean ± SEM from three independent experiments, $n = 3$. Ratio of IR/NIR was used in analysis after normalization by the total protein. Panel **(A)** shows the significant downregulation of normalized IR/NIR OGG1 protein expression in XP-C1, XP-C2, and XP-C3 compared to normal ($p < 0.001$,***; $p < 0.05$,*; and $p < 0.001$,***). Panel **(B)** shows the significant downregulation of normalized IR/NIR MYH protein expression in XP-C1, XP-C2, and XP-C3 compared to normal ($p < 0.01$,**; $p < 0.01$,** and $p < 0.05$,* respectively). Panel **(C)** shows the significant downregulation of normalized IR/NIR *APE1* gene expression in XP-C2 fibroblast compared to normal ($p < 0.0001$,****). Statistical analysis was done by unpaired-*t*-test that allows the comparison between normal and each XP-C fibroblast (GraphPad Prism 8). IR, irradiated; NIR, Non-Irradiated.

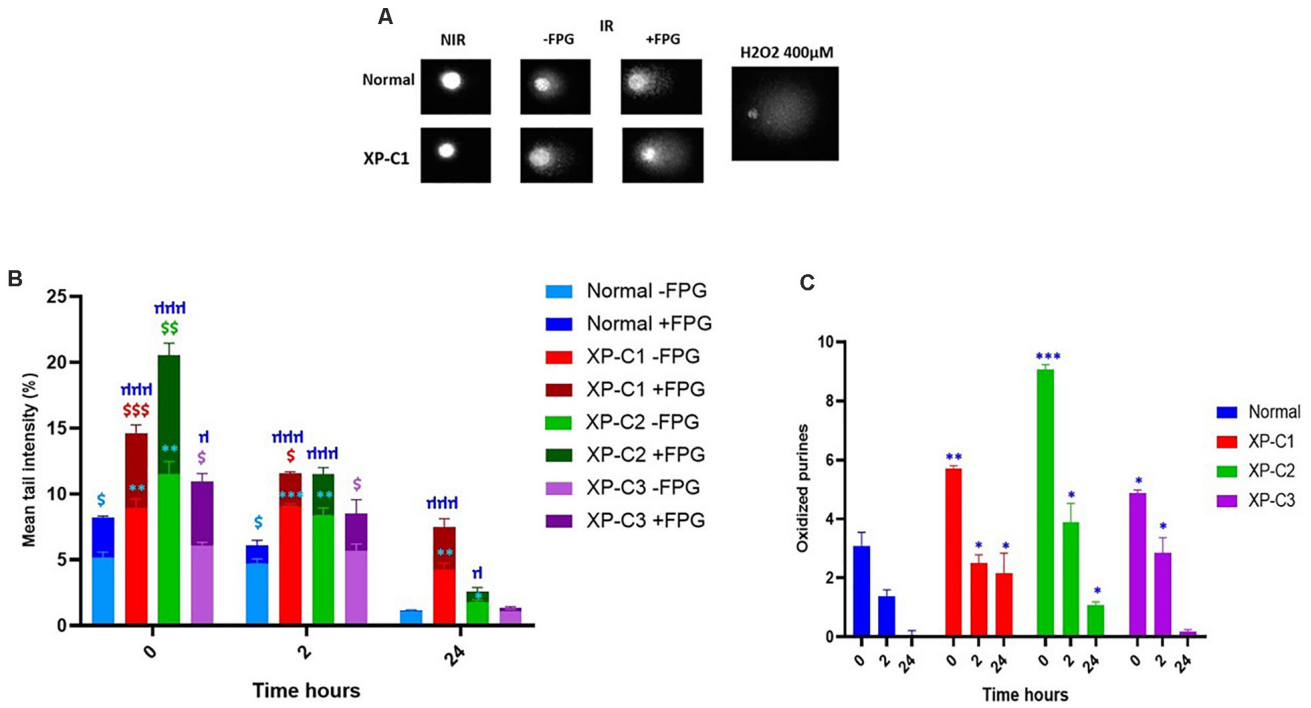


**FIGURE 6 |** Low intrinsic base excision excision-repair capacities in XP-C primary fibroblasts. Comet ± FPG was done to detect single-strand breaks (SSB), alkali-labile sites (ALS), and oxidative purines (including 8-oxoGua) in each sample at each condition. **(A)** Illustrates the undamaged (comet head) and damaged (comet tail) DNA ± FPG in normal and XP-C1 fibroblasts and positive control $H_2O_2$; the% tail intensity and length are proportional to the DNA damage. **(B)** The graphical representation displays the mean tail intensities (%) for each sample, for both FPG active sites (dark-colored) and SSB/ALS (light-colored) post-UVB-irradiation (0.05 J/cm$^2$). All fibroblasts were able to repair; however, the XP-C fibroblasts had a downregulated and dwindled repair activity. We did a ratio of IR/NIR ± FPG for each fibroblast at three kinetic points = 0, 2, and 24 h. The results are the mean ± SEM from three independent experiments. Paired-*t*-test was done to compare each sample with two conditions (FPG–ve or FPG+ve). Unpaired-*t*-test was done to compare different samples within the same condition (GraphPad Prism 8). $ Sample significantly ($p < 0.05$) higher in its tail intensity with presence of FPG (+FPG) compared to its absence (–FPG). *XP-C fibroblast significantly ($p < 0.05$) higher in its tail intensity compared to normal fibroblast, at –FPG condition. μ XP-C fibroblast significantly ($p < 0.05$) higher in its tail intensity compared to normal fibroblast, at +FPG condition. **(C)** The graphical representation displays oxidized purines repair (8-oxoGua and Fapy) in normal compared to XP-C fibroblasts. These oxidized purines were detected upon subtracting values +FPG from values –FPG for each sample. As expected, oxidized purines were downregulated in all fibroblasts. At $t = 0$ h, XP-C1, XP-C2, and XP-C3 had higher oxidized purines compared to normal fibroblasts ($p < 0.01$,**; $p < 0.001$,*** and $p < 0.05$,** respectively). Similarly was shown at $t = 2$ and 24 h for XP-C1, XP-C2, and XP-C3; except for XP-C3 at 24 h. Shown values correspond to the mean ± SEM from three independent experiments. Unpaired-*t*-test was done to compare different samples within the same condition (GraphPad Prism 8). *XP-C fibroblast significantly ($p < 0.05$) higher in its oxidized purines compared to normal fibroblast. –FPG = FPG alkaline buffer without the enzyme. +FPG = FPG alkaline buffer and FPG enzyme. IR, irradiated, NIR, Non-Irradiated.

repair) in XP-C fibroblasts compared to control at 0, 2, and 24 h where both lesion types are usually repaired by BER.

## DISCUSSION

It is well described that several cancer-prone diseases result from defective nucleotide excision DNA repair. This is well known for XPC mutations that are associated with high rate of basal cell carcinomas (BCCs), squamous cell carcinomas (SCCs), and melanoma in photo-exposed skin (De Boer and Hoeijmakers, 2000).

In a previous report, Agar et al. was able to detect 8-oxoGua and its correlated G:C→T:A transversion, thus indicating the contribution of such oxidative DNA damage to skin cancer (D'Errico et al., 2006). Hence, they speculated that the increased UV-induced skin cancer could be attributed not only to reduced NER but also to impaired BER, the foremost oxidative DNA damage repair system (D'Errico et al., 2006). Besides, XP patients also suffer from internal cancers that could be contributed to ROS accumulation and oxidative stress. Indeed, exploiting the long term follow-up of XP patients at NIH (National Institute of Health) from 1971 to 2009, Bradford et al. (2010) have reported that internal cancers (17%, $n = 5$) could be considered as the third factor [besides skin cancer (34%, $n = 10$) and neurologic degeneration (31%, $n = 9$)] leading to XP patients' death. Of note, among XP patients in their cohort, only patients belonging to XP-C group (6 out of 12) died due to internal cancers, including central nervous system cancers ($n = 3$), peripheral nerve cancer ($n = 1$), lung cancer ($n = 1$) and endocervical adenocarcinoma of the uterus ($n = 1$). Furthermore, Live imaging data has shown that XPC is rapidly recruited to the oxidized bases, independent on the recruitment of downstream NER factors (Menoni et al., 2012).

Thus, our study aimed to assess the effect of different XPC-mutations on BER in order to decipher how its phenotype is linked to a defect in BER's DNA repair capacity.

## Characterization of Normal and XP-C Primary Fibroblasts

In this study, we used fibroblasts isolated from patients with different clinical manifestations. XP-C1 had frame-shift mutation (c.1643_1644del). Meanwhile, XP-C2 and XP-C3 patients were compound heterozygotes for *XPC* mutations (**Supplementary Table S1**). As shown in **Figure 1**, while the full-length XPC protein was undetectable in fibroblasts from the three XP-C patients, XPC mRNA was expressed in these cells although at a significantly lower level than that of control fibroblasts. This suggests that XPC-mutated mRNAs may contain premature termination codons (PTCs) that induce non-sense mediated mRNA decay (NMD pathway) as a protective method to prevent deleterious-truncated proteins' expression. Our observations are in agreement with what was described by Chavanne et al. (2000); Khan et al. (2005), and Senhaji et al. (2012) who reported that mutations in the *XPC* gene are expected to cause protein truncations as a result of non-sense, frameshift, and deletion events. Thus, XPC mRNA levels may be considered as a predictive-diagnostic biological marker protecting from skin cancer since its low expression level is linked to an increased susceptibility to cancer in XPC-mutation carriers (Khan et al., 2005).

Even though photosensitivity is a XP-linked symptom, it was not the case when we did the short-term cytotoxicity test on XP-C fibroblasts. Similarly to De Waard et al. (2008), all fibroblasts shared similar moderate UVB-photosensitivity. It was clearly demonstrated that *XPC* mutations and deletions do not shorten lifespan in mice rather perhaps could be early events that induce late onset, slow growth/progression of tumor (Hollander et al., 2005). This suggests that cells harboring accumulated UVB-induced DNA damage are not eliminated with apoptosis. In agreement, Hollander et al. (2005) had shown that $Xpc^{-/-}$ mice develop spontaneous lung tumors at old age, due to an overtime accumulating effect passing the threshold of cancer risks. Also, Rezvani et al. (2006) showed that XP-C cells underwent spontaneous tumoral transformation owing to their susceptibility to accumulate DNA damage. XPC protein is not essential for cellular viability, proliferation or development as its dysfunction does not result in stalling RNA replication fork; hence, the difference between normal and mutated fibroblasts is the persistence of mutations in the latter arising to genomic instability and abnormal survival. In accordance, XP-C patients have been reported to suffer less from acute burning on minimal sun exposure than other XP complementary groups (Chavanne et al., 2000; Sethi et al., 2013). Indeed, it has been suggested that XP-C patients are diagnosed later in their life owing to their normal sunburn reactivity compared to the other XP groups. Consequently, XP-C patients are less likely to adhere to ultra-violet radiation protection and precaution early in their lives. As the inevitable consequence, they later develop a more aggressive phenotype compared to other XP-groups (Fassihi et al., 2016). This implies that sensitivity to sunburn may not always be an adequate clinical marker of an individual's skin cancer risk rather NER capacity, GG-NER in particular, may be a better predictor (Berg et al., 1998).

Hence, we monitored the repair of bulky lesions in normal and XP-C fibroblasts to investigate XPC mutations' effect on GG-NER repair activity. XPC protein's binding affinity to DNA correlates with the extent of helical distortions. Although it recognizes (6–4) PPs and CPDs, it binds with more specificity to the former that are bulkier than CPDs (Melis et al., 2008). Thus, we decided to study the effect of XPC mutations on the repair of (6–4) PPs at 0 and 24 h post-UVB-irradiation. Repair synthesis in XPC-mutated cells ranges between 10 and 20% compared to normal (Chavanne et al., 2000). In agreement with that, we showed that only ∼20% of pyrimidine (6–4) pyrimidone photoproducts' [(6–4) PPs] were repaired in XP-C fibroblasts after 24 h. This is consistent with what Courdavault et al. (2004) had published. (6–4) PPs were repaired efficiently within less than 24 h in cultured dermal human primary fibroblasts.

## Downregulation of Different BER-Associated Gene and Protein Levels in XP-C Fibroblasts Compared to Normal

Besides skin cancers, XP patients have a 10 to 20-fold increased risk of developing internal malignancies, such as lung, tongue, brain, and liver cancer (Bowden, 2004; DiGiovanna and Kraemer, 2012; Zhang et al., 2015; Murray et al., 2016; Zebian et al., 2019). These incidences cannot be explained unless XPC acts as a multi-functional protein involved in roles beyond GG-NER initiation. It recognizes both NER targeted lesions and base lesions which may provide it the power of determining the eventual repair type. Once cells are irradiated by UVB, stress-mediated alterations in mitochondrial and nuclear functions and oxidative unbalance will arise since almost 50% of UVB-induced lesions attribute to the formation of ROS, consequently oxidative DNA damage and cancer. These events are highly pronounced once XPC protein is dysregulated (Rezvani et al., 2011; Wölfle et al., 2011; Melis et al., 2013a; Hosseini et al., 2014; Zhang et al., 2015). For instance, there is an association between the increased lung tumor incidence and oxidative stress in *Xpc*-knock out mice (Liu et al., 2010). D'Errico et al. (2006) showed that primary keratinocytes and fibroblasts derived from XP-C patients are hypersensitive to DNA-oxidizing agents and that could be inverted by the re-expression of XPC. In good agreement, the activity of catalase, an enzyme protecting the cell from oxidative DNA damage through the conversion of $H_2O_2$ into oxygen and water, was found to be decreased in XP patients (Rezvani et al., 2006). XPC has been reported to affect oxidative and energy metabolism. For instance, *in vitro* studies displayed an elevated sensitivity in $Xpc^{-/-}$ mouse embryonic fibroblasts (MEFs) to oxidative DNA-damaging agents compared to control (Melis et al., 2008). It is estimated that up to 100,000 8-oxoGua lesions can be formed daily in DNA per cell (Ba and Boldogh, 2018). They are recognized by OGG1 and MYH. The former excise 8-oxoGua directly, meanwhile, the latter removes misincorporated adenines

in front of 8-oxoguanine (8-oxoGua) during DNA replication. These excision activities will result in an AP site that will be cleaved by APE1 for the synthesis and ligation to be carried out by POLβ and LIG3, respectively (Campalans et al., 2015). It has been shown that MYH-OGG1 deficient cells are sensitive to oxidants and ROS (Xie et al., 2008). As ROS accumulation negatively regulates the activity of several important DNA repair proteins, including OGG1, its production may lead to the increase of DNA damage which supports the important role of ROS in carcinogenesis. Not only it induces oxidative DNA damage but also prevents its repair (Srinivas et al., 2018). Mutations in the *OGG1* gene can lead to lung and kidney tumors and the S326C polymorphism appears to be associated with an increased risk of esophageal, lung and prostate cancers (Thibodeau et al., 2019). In parallel, mutations in the *MYH* gene are associated with lung, colorectal and breast cancers (Hollander et al., 2005; Viel et al., 2017; Thibodeau et al., 2019). In light of these studies, several questions arise. Would this occur through lack of XPC-BER interaction? If yes, how profound is XPC's influence on BER effectiveness and expression?

Therefore, we were interested in highlighting the role of XPC as an interplay between NER and BER. For that, real-time-qPCR was done where primers anneal to each of the following BER components: *OGG1*, *MYH*, *APE1*, *POL*β, *XRCC1*, and *LIG3*. Afterward, we did western blot analysis on OGG1, MYH, and APE1. These proteins were selected due to their essential role in initiating oxidative DNA lesions' repair.

OGG1, MYH gene and protein expressions were significantly inhibited upon UVB-irradiation ($p < 0.05$). Although APE1 showed a significantly inhibited gene expression in all XP-C fibroblasts ($p < 0.0001$), such an inhibition was not significant at protein level except in XP-C2. These results indicate a downregulation in stimulation. In agreement with our results, it has been shown that XPC is recruited to 8-oxoguanine lesions to induce a partial removal of the oxidative DNA damage and regulate cellular stress-response (Zhou et al., 2001; Miccoli et al., 2007). This is done by stimulating OGG1's protein expression and catalytic activity and physically interacting with APE1 (D'Errico et al., 2006; De Melo et al., 2016). Hence, XPC mutation affects them directly. For example, there is an evidence that *XPC* P334H substitution can prevent stimulation of BER factor OGG1 (Melis et al., 2013b). However, little is mentioned in the literature about the effect of XPC on *MYH*, *LIG3*, *POLB*, and *XRCC1*. Perhaps MYH was barely studied because it is an indirect secondary actor in the repair of 8-oxoGua, functioning downstream of OGG1 and removing adenine bases misincorporated opposite 8-oxoGua (Forestier et al., 2012). However, due to its role, there might be a direct link between MYH and XPC. This was seen at both gene and protein levels. Meanwhile, other BER factors' mRNA downregulation could be explained by the fact that an interaction and cross-talks amongst BER factors is crucial for the recruitment to the site of repair and optimum repair efficiency (Campalans et al., 2015). Hence, since, as shown in our results, OGG1, MYH, and APE1 are affected, a stimulation to trigger the expression of downstream factors could be inhibited or slowed down where the coordination amongst the protein complexes is similar to passing of the baton, where the repair product is handed over from an enzyme to the next one.

## Downregulation in Excision Activity of BER-Associated Enzymes in XP-C Fibroblasts Compared to Normal

Some studies have demonstrated that ROS-induced 8-oxoguanine formation, primarily in guanine-rich gene regulatory regions, inactivates OGG1's enzymatic activity (Hao et al., 2018), resulting in GC to TA transversion mutations (De Rosa et al., 2012). Hence, 8-oxoGua accumulation might be considered as a diagnostic marker for BER malfunction (Tinaburri et al., 2018). For example, OGG1-Cys enzymatic activity decreases under oxidative stress due to redox-sensitive residues in accordance with our results where there is a reverse correlation between OGG1 activity and oxidative stress (Bravard et al., 2009; De Rosa et al., 2012; Tinaburri et al., 2018). Moreover, D'Errico et al. (2006) had shown that XPC plays a role as a cofactor for the efficient 8-oxoGua excision by OGG1. XPC/P334H mutation weakens the interaction between OGG1 and XPC, resulting in a decreased glycosylase activity and turn-over (Melis et al., 2013b). Additionally, studies had demonstrated that APE1 and XRCC1 are involved in the repair of SSBs containing 3′-8-oxoGua and SSBs, respectively in human cell extracts (Okano et al., 2000; Parsons et al., 2005). Both were shown, in our data, to be downregulated at mRNA level in absence of XPC. Decreased expression of several BER factors in XP-C cells could explain why at time = 0 h, more single strand breaks and oxidative DNA damage were found in these cells compared to control. Our results also showed that repair of the oxidative damage was much lower and slower in XP-C cells than normal cells. In agreement, it had been shown that XPC deficiency impairs the repair of oxidative DNA damage induced by visible light and methylene blue where XPC had been proven to bind much better oxidative base damage than direct SSBs (Menoni et al., 2012; Melis et al., 2013b). Similarly, the level of 8-oxoGua in cells treated with KBrO3 (40 mM) at different time points after exposure was much higher in XP-C cells compared to their control counterparts (D'Errico et al., 2006). Despite the dysregulation in BER's efficiency in XP-C fibroblasts, a bashful repair occurred. This could be explained by two complement scenarios: Although OGG1 is the main preferred actor in BER, other multiple of backup-glycosylases will step up once it is function becomes incompetent (Hegde et al., 2008). On the other hand, as mentioned before, XPC enhances OGG1's turnover i.e., efficiency of activity (De Melo et al., 2016). In the absence of XPC, OGG1 is stable and able to remove oxidized lesions with a less competency and slower rate.

These results suggest that increased susceptibility to internal tumors in XP-C patients and spontaneous tumors in *Xpc* mice may be due to incompetent oxidative DNA lesions repair.

It is evident now that repair of both endogenous and induced oxidative DNA damage are essential for maintaining genomic integrity and homeostasis. This involves complex interactions among BER proteins and between them and other proteins, mainly XPC (Hegde et al., 2008).

## CONCLUSION

The difference in XPC mutations among our samples allowed us to have a general and more confirmed conclusion about the effect of such protein on the expression and activity status of distinct BER system components to repair oxidized DNA damage.

Characterization of the interplay between BER factors and XPC may provide new insights about the occurrence of non-skin cancer upon XPC-deficiency. Furthermore, the synergic effects of amassed oxidative DNA damage and impaired BER could explain heterogeneity in the clinical spectrum of XP-C patients.

## DATA AVAILABILITY STATEMENT

All datasets generated for this study are included in the article/**Supplementary Material**. For further inquiries contact the corresponding author.

## AUTHOR CONTRIBUTIONS

NF performed all the experiments (cell culture, short-term cytotoxicity assay, qRT-PCR, western blot, Immunocytochemistry, and comet ± FPG assay) and wrote the manuscript. WR conceived the project, grant funding, supervised the project, and revised the manuscript. HRR contributed to formal analysis and manuscript editing and revision. MF-K and BB aided in the manuscript revision. HF-K participated in the statistical analysis and manuscript revision. FK assisted in the immunocytochemistry experiment. DB assisted in certain experiments. WM prepared the XP-C fibroblasts. They were sequenced and had their mutation identified by CG and FM-P. All authors read and approved the final version of the manuscript.

## FUNDING

NF is a Ph.D. student supported by a grant from UGA-L'Ecole Doctorale Ingénierie pour la Santé, la Cognition et l'Environnement (EDISCE). WR's contribution was funded by ANR grant PG2HEAL (ANR-18-CE17-0017) and supported by the French National Research Agency in the framework of the "Investissements d'avenir" program (ANR-15-IDEX-02).

## ACKNOWLEDGMENTS

HRR gratefully acknowledges support from the patients' support group "Les Enfants de La Lune."

## SUPPLEMENTARY MATERIAL

The Supplementary Material for this article can be found online at: https://www.frontiersin.org/articles/10.3389/fgene.2020.561687/full#supplementary-material

## REFERENCES

Ba, X., and Boldogh, I. (2018). 8-Oxoguanine DNA glycosylase 1: beyond repair of the oxidatively modified base lesions. *J. Redox Biol.* 14, 669–678. doi: 10.1016/j.redox.2017.11.008

Berg, R. J., Ruven, H. J., Sands, A. T., De Gruijl, F. R., and Mullenders, L. H. (1998). Defective global genome repair in XPC mice is associated with skin cancer susceptibility but not with sensitivity to UVB induced erythema and edema. *J. Invest. Dermatol.* 110, 405–409. doi: 10.1111/j.1523-1747.1998.00173.x

Berra, C. M., De Oliveira, C. S., Garcia, C. C., Rocha, C. R., Lerner, L. K., Lima, L. C., et al. (2013). Nucleotide excision repair activity on DNA damage induced by photoactivated methylene blue. *J. Free Radic. Biol. Med.* 61, 343–356. doi: 10.1016/j.freeradbiomed.2013.03.026

Bowden, G. T. (2004). Prevention of non-melanoma skin cancer by targeting ultraviolet-B-light signalling. *J. Nat. Rev. Cancer* 4, 23–35. doi: 10.1038/nrc1253

Bradford, P. T., Goldstein, A. M., Tamura, D., Khan, S. G., Ueda, T., Boyle, J., et al. (2010). Cancer and neurologic degeneration in xeroderma pigmentosum: long term follow-up characterises the role of DNA repair. *J. Med. Genet.* 48, 168–176. doi: 10.1136/jmg.2010.083022

Bravard, A., Vacher, M., Moritz, E., Vaslin, L., Hall, J., Epe, B., et al. (2009). Oxidation status of human OGG1-S326C polymorphic variant determines cellular DNA repair capacity. *J. Cancer Res.* 69, 3642–3649. doi: 10.1158/0008-5472.CAN-08-3943

Campalans, A., Moritz, E., Kortulewski, T., Biard, D., Epe, B., and Radicella, J. P. (2015). Interaction with OGG1 is required for efficient recruitment of XRCC1 to base excision repair and maintenance of genetic stability after exposure to oxidative stress. *J. Mol. Cell Biol.* 35, 1648–1658. doi: 10.1128/MCB.00134-15

Chavanne, F., Broughton, B. C., Pietra, D., Nardo, T., Browitt, A., Lehmann, A. R., et al. (2000). Mutations in the XPC gene in families with xeroderma pigmentosum and consequences at the cell, protein, and transcript levels. *J. Cancer Res.* 60, 1974–1982.

Courdavault, S., Baudouin, C., Sauvaigo, S., Mouret, S., Candéias, S., Charveron, M., et al. (2004). Unrepaired cyclobutane pyrimidine dimers do not prevent proliferation of UV-B-irradiated cultured human fibroblasts. *J. Photochem. Photobiol.* 79, 145–151. doi: 10.1562/0031-8655(200)4079<0145:ucpddn<2.0.co;2

David, S. S., O'Shea, V. L., and Kundu, S. (2007). Base-excision repair of oxidative DNA damage. *J. Nat.* 447, 941–950. doi: 10.1038/nature05978

Daya-Grosjean, L., and Sarasin, A. (2004). The role of UV induced lesions in skin carcinogenesis: an overview of oncogene and tumor suppressor gene modifications in xeroderma pigmentosum skin tumors. *J. Mutat. Res.* 571, 43–56. doi: 10.1016/j.mrfmmm.2004.11.013

De Boer, J., and Hoeijmakers, J. H. (2000). Nucleotide excision repair and human syndromes. *J. Carcinogen.* 21, 453–460. doi: 10.1093/carcin/21.3.453

De Melo, J. T., De Souza Timoteo, A. R., Lajus, T. B., Brandão, J. A., De Souza-Pinto, N. C., Menck, C. F., et al. (2016). XPC deficiency is related to APE1 and OGG1 expression and function. *J. Mutat Res.* 784, 25–33. doi: 10.1016/j.mrfmmm.2016.01.004

De Rosa, V., Erkekoğlu, P., Forestier, A., Favier, A., Hincal, F., Diamond, A. M., et al. (2012). Low doses of selenium specifically stimulate the repair of oxidative DNA damage in LNCaP prostate cancer cells. *J. Free Radic. Res.* 46, 105–116. doi: 10.3109/10715762.2011.647009

De Waard, H., Sonneveld, E., De Wit, J., Esveldt-van Lange, R., Hoeijmakers, J. H., Vrieling, H., et al. (2008). Cell-type-specific consequences of nucleotide excision repair deficiencies: embryonic stem cells versus fibroblasts. *J. DNA Rep.* 7, 1659–1669. doi: 10.1016/j.dnarep.2008.06.009

D'Errico, M., Parlanti, E., Teson, M., De Jesus, B. M., Degan, P., Calcagnile, A., et al. (2006). New functions of XPC in the protection of human skin cells from oxidative damage. *Embo J.* 25, 4305–4315. doi: 10.1038/sj.emboj.7601277

DiGiovanna, J. J., and Kraemer, K. H. (2012). Shining a light on xeroderma pigmentosum. *J. Invest. Dermatol.* 132(3 Pt 2), 785–796. doi: 10.1038/jid.2011.426

D'Orazio, J., Jarrett, S., Amaro-Ortiz, A., and Scott, T. (2013). UV radiation and the skin. *Int. J. Mol. Sci.* 14, 12222–12248. doi: 10.3390/ijms140612222

Fassihi, H., Sethi, M., Fawcett, H., Wing, J., Chandler, N., Mohammed, S., et al. (2016). Deep phenotyping of 89 xeroderma pigmentosum patients reveals unexpected heterogeneity dependent on the precise molecular defect. *J. Proc. Natl. Acad. Sci. U.S.A.* 113, E1236–E1245. doi: 10.1073/pnas.1519444113

Forestier, A., Douki, T., Sauvaigo, S., De Rosa, V., Demeilliers, C., and Rachidi, W. (2012). Alzheimer's disease-associated neurotoxic peptide amyloid-β impairs base excision repair in human neuroblastoma cells. *Int. J. Mol. Sci.* 13, 14766–14787. doi: 10.3390/ijms131114766

Hao, W., Qi, T., Pan, L., Wang, R., Zhu, B., Aguilera-Aguirre, L., et al. (2018). Effects of the stimuli-dependent enrichment of 8-oxoguanine DNA glycosylase1 on chromatinized DNA. *J. Redox Biol.* 18, 43–53. doi: 10.1016/j.redox.2018.06.002

Hegde, M. L., Hazra, T. K., and Mitra, S. (2008). Early steps in the DNA base excision/single-strand interruption repair pathway in mammalian cells. *J. Cell Res.* 18, 27–47. doi: 10.1038/cr.2008.8

Hollander, M. C., Philburn, R. T., Patterson, A. D., Velasco-Miguel, S., Friedberg, E. C., Linnoila, R. I., et al. (2005). Deletion of XPC leads to lung tumors in mice and is associated with early events in human lung carcinogenesis. *J. Proc. Natl. Acad. Sci. U.S.A.* 102, 13200–13205. doi: 10.1073/pnas.0503133102

Hosseini, M., Ezzedine, K., Taieb, A., and Rezvani, H. R. (2015). Oxidative and energy metabolism as potential clues for clinical heterogeneity in nucleotide excision repair disorders. *J. Invest. Dermatol.* 135, 341–351. doi: 10.1038/jid.2014.365

Hosseini, M., Mahfouf, W., Serrano-Sanchez, M., Raad, H., Harfouche, G., Bonneu, M., et al. (2014). Premature skin aging features rescued by inhibition of NADPH oxidase activity in XPC-deficient mice. *J. Invest. Dermatol.* 135, 1108–1118. doi: 10.1038/jid.2014.511

Hu, J., De Souza-Pinto, N. C., Haraguchi, K., Hogue, B. A., Jaruga, P., Greenberg, M. M., et al. (2005). Repair of formamidopyrimidines in DNA involves different glycosylases: role of the OGG1, NTH1, and NEIL1 enzymes. *J. Biol. Chem.* 280, 40544–40551. doi: 10.1074/jbc.M508772200

Hutsell, S. Q., and Sancar, A. (2005). Nucleotide excision repair, oxidative damage, DNA sequence polymorphisms, and cancer treatment. *J. Clin. Cancer Res.* 11, 1355–1357. doi: 10.1158/1078-0432.CCR-05-0024

Kelley, M. R. (2012). *DNA Repair in Cancer Therapy*, 1st Edn. Amsterdam: Elsevier.

Kemp, M. G., Spandau, D. F., and Travers, J. B. (2017). Impact of age and insulin-like growth factor-1 on DNA damage responses in UV-irradiated human skin. *J. Mol.* 22:356. doi: 10.3390/molecules22030356

Khan, S. G., Oh, K. S., Shahlavi, T., Ueda, T., Busch, D. B., Inui, H., et al. (2005). Reduced XPC DNA repair gene mRNA levels in clinically normal parents of xeroderma pigmentosum patients. *J. Carcinogen.* 27, 84–94. doi: 10.1093/carcin/bgi204

Krokan, H. E., and Bjørås, M. (2013). Base excision repair. *J. Cold Spring Harb. Perspect. Biol.* 5:a012583. doi: 10.1101/cshperspect.a012583

Lehmann, A. R., McGibbon, D., and Stefanini, M. (2011). Xeroderma pigmentosum. *Orphanet J. Rare Dis.* 6:70. doi: 10.1186/1750-1172-6-70

Liu, S. Y., Wen, C. Y., Lee, Y. J., and Lee, T. C. (2010). XPC silencing sensitizes glioma cells to arsenic trioxide via increased oxidative damage. *J. Toxicol. Sci.* 116, 183–193. doi: 10.1093/toxsci/kfq113

Livak, K. J., and Schmittgen, T. D. (2001). Analysis of relative gene expression data using real-time quantitative PCR and the 2(-Delta Delta C(T)) Method. *Methods* 25, 402–408. doi: 10.1006/meth.2001.1262

Melis, J. P., Kuiper, R. V., Zwart, E., Robinson, J., Pennings, J. L., Van Oostrom, C. T., et al. (2013a). Slow accumulation of mutations in Xpc-/- mice upon induction of oxidative stress. *J. DNA Rep.* 12, 1081–1086. doi: 10.1016/j.dnarep.2013.08.019

Melis, J. P., Van Steeg, H., and Luijten, M. (2013b). Oxidative DNA damage and nucleotide excision repair. *J. Antioxid. Redox Signal.* 18, 2409–2419. doi: 10.1089/ars.2012.5036

Melis, J. P., Wijnhoven, S. W., Beems, R. B., Roodbergen, M., van den Berg, J., Moon, H., et al. (2008). Mouse models for xeroderma pigmentosum group A and group C show divergent cancer phenotypes. *J. Cancer Res.* 68, 1347–1353. doi: 10.1158/0008-5472.CAN-07-6067

Menoni, H., Hoeijmakers, J. H., and Vermeulen, W. (2012). Nucleotide excision repair-initiating proteins bind to oxidative DNA lesions in vivo. *J. Cell Biol.* 199, 1037–1046. doi: 10.1083/jcb.201205149

Miccoli, L., Burr, K. L., Hickenbotham, P., Friedberg, E. C., Angulo, J. F., and Dubrova, Y. E. (2007). The combined effects of xeroderma pigmentosum C deficiency and mutagens on mutation rates in the mouse germ line. *J. Cancer Res.* 67, 4695–4699. doi: 10.1158/0008-5472.CAN-06-3844

Murray, H. C., Maltby, V. E., Smith, D. W., and Bowden, N. A. (2016). Nucleotide excision repair deficiency in melanoma in response to UVA. *Exp. Hematol. Oncol.* 5:6. doi: 10.1186/s40164-016-0035-4

Nemzow, L., Lubin, A., Zhang, L., and Gong, F. (2015). XPC: going where no DNA damage sensor has gone before. *J. DNA Rep.* 36, 19–27. doi: 10.1016/j.dnarep.2015.09.004

Okano, S., Kanno, S., Nakajima, S., and Yasui, A. (2000). Cellular responses and repair of single-strand breaks introduced by UV damage endonuclease in mammalian cells. *J Biol. Chem.* 275, 32635–32641. doi: 10.1074/jbc.M004085200

Park, J. M., and Kang, T. H. (2016). Transcriptional and posttranslational regulation of nucleotide excision repair: the guardian of the genome against ultraviolet radiation. *Int. J. Mol. Sci.* 17:1840. doi: 10.3390/ijms17111840

Parsons, J. L., Dianova, I. I., and Dianov, G. L. (2005). APE1-dependent repair of DNA single-strand breaks containing 3'-end 8-oxoguanine. *J. Nucleic Acids Res.* 33, 2204–2209. doi: 10.1093/nar/gki518

Pázmándi, K., Sütö, M., Fekete, T., Varga, A., Boldizsár, E., Boldogh, I., et al. (2019). Oxidized base 8-oxoguanine, a product of DNA repair processes, contributes to dendritic cell activation. *J. Free Radic. Biol. Med.* 143, 209–220. doi: 10.1016/j.freeradbiomed.2019.08.010

Ravanat, J. L., Douki, T., and Cadet, J. (2001). Direct and indirect effects of UV radiation on DNA and its components. *J. Photochem. Photobiol. B* 63, 88–102. doi: 10.1016/s1011-1344(01)00206-8

Rezvani, H. R., Kim, A. L., Rossignol, R., Ali, N., Daly, M., Mahfouf, W., et al. (2011). XPC silencing in normal human keratinocytes triggers metabolic alterations that drive the formation of squamous cell carcinomas. *J. Clin. Invest.* 121, 195–211. doi: 10.1172/JCI40087

Rezvani, H. R., Mazurier, F., Cario-André, M., Pain, C., Ged, C., Taïeb, A., et al. (2006). Protective effects of catalase overexpression on UVB-induced apoptosis in normal human keratinocytes. *J. Biol. Chem.* 281, 17999–18007. doi: 10.1074/jbc.M600536200

Senhaji, M. A., Abidi, O., Nadifi, S., Benchikhi, H., Khadir, K., Ben Rekaya, M., et al. (2012). c.*1643*_1644delTG XPC mutation is more frequent in Moroccan patients with xeroderma pigmentosum. *J. Arch. Dermatol. Res.* 305, 53–57. doi: 10.1007/s00403-012-1299-0

Sethi, M., Lehmann, A. R., Fawcett, H., Stefanini, M., Jaspers, N., Mullard, K., et al. (2013). Patients with xeroderma pigmentosum complementation groups C, E and V do not have abnormal sunburn reactions. *Br. J. Dermatol.* 169, 1279–1287. doi: 10.1111/bjd.12523

Soufir, N., Ged, C., Bourillon, A., Austerlitz, F., Chemin, C., Stary, A., et al. (2010). A prevalent mutation with founder effect in xeroderma pigmentosum group C from north Africa. *J. Invest. Dermatol.* 130, 1537–1542. doi: 10.1038/jid.2009.409

Srinivas, U. S., Tan, B. W. Q., Vellayappan, B. A., and Jeyasekharan, A. D. (2018). ROS and the DNA damage response in cancer. *J. Redox Biol.* 25:101084. doi: 10.1016/j.redox.2018.101084

Thibodeau, M. L., Zhao, E. Y., Reisle, C., Ch'ng, C., Wong, H. L., Shen, Y., et al. (2019). Base excision repair deficiency signatures implicate germline and somatic *MUTYH* aberrations in pancreatic ductal adenocarcinoma and breast cancer oncogenesis. *J. Cold Spring Harb. Mol. Case Stud.* 5:a003681. doi: 10.1101/mcs.a003681

Tinaburri, L., D'Errico, M., Sileno, S., Maurelli, R., Degan, P., Magenta, A., et al. (2018). miR-200a modulates the expression of the DNA repair protein OGG1 playing a role in aging of primary human keratinocytes. *J. Oxid. Med. Cell Longev.* 2018:9147326. doi: 10.1155/2018/9147326

Viel, A., Bruselles, A., Meccia, E., Fornasarig, M., Quaia, M., Canzonieri, V., et al. (2017). A specific mutational signature associated with DNA 8-Oxoguanine persistence in MUTYH-defective colorectal cancer. *J. EBioMed.* 20, 39–49. doi: 10.1016/j.ebiom.2017.04.022

Wölfle, U., Esser, P. R., Simon-Haarhaus, B., Martin, S. F., Lademann, J., and Schempp, C. M. (2011). UVB-induced DNA damage, generation of reactive oxygen species, and inflammation are effectively attenuated by the flavonoid

luteolin in vitro and in vivo. *J. Free Radic. Biol. Med.* 50, 1081–1093. doi: 10.1016/j.freeradbiomed.2011.01.027

Xie, Y., Yang, H., Miller, J. H., Shih, D. M., Hicks, G. G., Xie, J., et al. (2008). Cells deficient in oxidative DNA damage repair genes Myh and Ogg1 are sensitive to oxidants with increased G2/M arrest and multinucleation. *J. Carcinogen.* 29, 722–728. doi: 10.1093/carcin/bgn033

Zebian, A., Shaito, A., Mazurier, F., Rezvani, H. R., and Zibara, K. (2019). XPC beyond nucleotide excision repair and skin cancers. *J. Mutat. Res.* 782:108286. doi: 10.1016/j.mrrev.2019.108286

Zhang, X., He, N., Gu, D., Wickliffe, J., Salazar, J., Boldogh, I., et al. (2015). Genetic evidence for XPC-KRAS interactions during lung cancer development. *J. Genet. Genomics* 42, 589–596. doi: 10.1016/j.jgg.2015.09.006

Zhou, J., Ahn, J., Wilson, S. H., and Prives, C. (2001). A role for p53 in base excision repair. *Embo J.* 20, 914–923. doi: 10.1093/emboj/20.4.914

**Conflict of Interest:** The authors declare that the research was conducted in the absence of any commercial or financial relationships that could be construed as a potential conflict of interest.

frontiers in Cell and Developmental Biology

MINI REVIEW
published: 18 January 2021
doi: 10.3389/fcell.2020.609714

# PprI: The Key Protein in Response to DNA Damage in *Deinococcus*

*Huizhi Lu and Yuejin Hua**

*MOE Key Laboratory of Biosystems Homeostasis and Protection, Institute of Biophysics, College of Life Sciences, Zhejiang University, Hangzhou, China*

Deoxyribonucleic acid (DNA) damage response (DDR) pathways are essential for maintaining the integrity of the genome when destabilized by various damaging events, such as ionizing radiation, ultraviolet light, chemical or oxidative stress, and DNA replication errors. The PprI–DdrO system is a newly identified pathway responsible for the DNA damage response in *Deinococcus*, in which PprI (also called IrrE) acts as a crucial component mediating the extreme resistance of these bacteria. This review describes studies about PprI sequence conservation, regulatory function, structural characteristics, biochemical activity, and hypothetical activation mechanisms as well as potential applications.

**Keywords: PprI, DNA damage response, switch, PprI-DdrO system, *Deinococcus***

OPEN ACCESS

***Edited by:***
*Brian C. Schaefer, Uniformed Services University of the Health Sciences, United States*

***Reviewed by:***
*Lydia Contreras, University of Texas at Austin, United States*
*Elena K. Gaidamakova, Henry M Jackson Foundation for the Advancement of Military Medicine (HJF), United States*
*Sangyong Lim, Korea Atomic Energy Research Institute (KAERI), South Korea*

***Correspondence:**
*Yuejin Hua*
*yjhua@zju.edu.cn*

***Specialty section:***
*This article was submitted to Cell Death and Survival, a section of the journal Frontiers in Cell and Developmental Biology*

***Received:*** *22 October 2020*
***Accepted:*** *17 December 2020*
***Published:*** *18 January 2021*

***Citation:***
*Lu H and Hua Y (2021) PprI: The Key Protein in Response to DNA Damage in Deinococcus. Front. Cell Dev. Biol. 8:609714. doi: 10.3389/fcell.2020.609714*

## INTRODUCTION

Deoxyribonucleic acid (DNA) damage occurs when the genome is exposed to exogenous and endogenous hazards, leading to imperfection and instability of the genetic information (Pilzecker et al., 2019). If not repaired in a timely and accurate manner, accumulating mutations will result in severe effects, such as cancer, and even lead to cell death. To cope with DNA damage, organisms have evolved various DNA damage repair pathways, including nucleotide excision repair, non-homologous end joining, homologous recombination, mismatch repair, and base excision repair (Boulton et al., 2002).

The SOS response involves a common mechanism that is induced after DNA damage occurs in various bacteria (Radman, 1975; Butala et al., 2008, 2011). In the SOS response system, LexA functions as a transcriptional repressor that mediates the transcription of *recA* and other SOS genes. When sensing DNA damage, RecA forms filaments with ssDNA in the presence of ATP, causing the autocleavage of LexA. The decrease in the cellular pool of LexA leads to dissociation of SOS box-bound LexA, thus initiating SOS gene transcription. The upregulation of SOS genes is repressed by abundant LexA after the damage is repaired (Butala et al., 2008, 2011; **Figure 1**).

As one of the most radio-resistant organisms on Earth, bacteria belonging to the genus *Deinococcus* can withstand a series of environmental stresses, such as high doses of ionizing radiation, UV radiation, oxidation, mitomycin C, and long periods of desiccation, due to their extraordinary antioxidant system and DNA repair capability (Cox and Battista, 2005; Makarova et al., 2007; Blasius et al., 2008; Slade and Radman, 2011; Lim et al., 2019; Qi et al., 2020). Indeed, members of *Deinococcus* produce several antioxidants, including catalase, peroxidase, superoxide dismutase, carotenoids, and manganese ion antioxidant complex, to deal with oxidative stresses (Slade and Radman, 2011; Sharma et al., 2017). *Deinococcus* seldom invoke translesion synthesis and non-homologous end joining, but rather adopt homologous recombination to guarantee the fidelity of DNA repair (Slade and Radman, 2011). Several proteins, such as PprI, PprA, DrRRA, and

OxyR, have been identified involving in the DNA damage response: PprI is the switch mediating the transcription of DDR genes, PprA contributes to UV radiation resistance and interacts with both DraTopoIB and the Gyrase A subunit, DrRRA cooperates with PprI and functions in gamma radiation resistance, and OxyR senses the presence of reactive oxygen species to regulate the antioxidant system (Chen et al., 2008; Wang et al., 2008, 2012, 2015; Bauermeister et al., 2009; Selvam et al., 2013; Kota et al., 2014).

However, unlike in most bacteria, the two encoded LexA in *Deinococcus radiodurans* do not participate in the induction of *recA*, although the autocleavage activity remains unchanged, indicating the malfunction of the classic SOS response system (Narumi et al., 2001; Sheng et al., 2004; Jolivet et al., 2006). Instead of the SOS system, a novel pathway has been found to be responsible for the DNA damage response in *Deinococcus*: two conserved proteins, DdrO—the repressor and PprI—the derepressor, comprise this unique response system (Devigne et al., 2015; Wang et al., 2015; **Figure 1**). To activate DDR genes participating in pathways such as DNA replication and stress response, PprI cleaves DdrO to deprive its DNA-binding ability after sensing DNA damage signals by unclear activation mechanisms (Wang et al., 2015).

This article summarizes the research progress on PprI in the last few years, mainly covering its structure and function. Potential applications and probable activation mechanisms of PprI in response to DNA damage as well as other oxidative stresses are also discussed.

## PprI STRUCTURE REVEALS THREE DISTINCT DOMAINS

As reported before, *pprI* from *D. deserti* shares 73 and 64% sequence identity with *D. geothermalis* and *D. radiodurans* homologs and can complement the loss of radiation resistance of *pprI* deletion in *D. radiodurans* (Vujicic-Zagar et al., 2009). It is also demonstrated that PprI from either *D. geothermalis* or *D. radiodurans* can cleave DdrO from either *D. geothermalis* or *D. radiodurans*, further demonstrating that PprI cleavage of DdrO as well as the PprI–DdrO response system is conserved among *Deinococcus* species (Lu et al., 2019).

The crystal structure of PprI from *D. deserti* was solved by Vujicic-Zagar et al. (2009), revealing that the protein consists of three domains: one zinc peptidase-like domain, one helix-turn-helix motif, and one GAF-like domain. The N-terminal domain of PprI exhibits a zinc metallopeptidase fold and contains a conserved HEXXH sequence (Vujicic-Zagar et al., 2009). Ludanyi et al. (2014) and Wang et al. (2015) later proved that PprI functions as a protease targeting DdrO. Subsequent research on HEXXH-related residues has indicated that H82, E83, H86, and E113 are indispensable for metal ion binding as well as the PprI protease function (Wang et al., 2015).

The middle region of PprI comprises an HTH domain that is usually responsible for DNA binding. Although some researchers doubt the DNA-binding ability of PprI based on the structural domain arrangement and alignment with ParB-DNA structure, Lu verified the promoter-binding ability of PprI *in vitro* and *in vivo* (Vujicic-Zagar et al., 2009; Lu et al., 2012). He also proved that DNA binding is important for PprI function in response to DNA damage, and truncation of the HTH domain leads to loss of DNA affinity in PprI and the failure of RecA induction after radiation, as well as a decrease in stress resistance in *D. radiodurans* (Lu et al., 2012).

The C-terminus of PprI forms a GAF-like domain, which is one of the most widespread small molecule-binding domains responsible for binding allosteric regulatory molecules, named after a series of proteins consisting of GAF domains: cGMP-specific phosphodiesterases, adenylyl cyclases, and FhlA (Aravind and Ponting, 1997). Structural alignments revealed that the C-terminus is similar to the GAF domain in the *Thermotoga maritima* transcription factor IclR, *Klebsiella pneumoniae* CitA28, and *Escherichia coli* PDE2A that always participate in the binding of regulatory molecules such as cAMP and cGMP for the stress response. The comparison indicated that the C-terminus may be responsible for signal transduction, although this possibility needs further verification (Martinez et al., 2002; Sevvana et al., 2008).

## PprI IS A GENERAL SWITCH REGULATING DDR GENES

Seventeen years ago, both Earl and Hua found that the *pprI* (also called *irrE*) gene can regulate the expression of *recA* gene and that its deletion would lead to the sensitivity of *D. radiodurans* to radiation (Earl et al., 2002; Hua et al., 2003; Gao et al., 2005). The disruption of *pprI* led to the decrease in resistance to gamma radiation, UV radiation, $H_2O_2$, and mitomycin C and left DdrO un-cleaved after radiation, while similar phenotypes were also detected in *D. deserti* (Vujicic-Zagar et al., 2009; Lu et al., 2012; Ludanyi et al., 2014; Wang et al., 2015).

To uncover the function role and regulation pathways of *pprI* in *Deinococcus*, proteomics and transcriptomics studies have been conducted. Proteomics research has revealed that various proteins are significantly upregulated by PprI after exposure to a low dose of gamma radiation. These proteins are involved in several different pathways, including DNA replication and repair, stress response, energy metabolism, transcriptional regulation, signal transduction, protein turnover, and chaperone functions (Lu et al., 2009). Later, microarrays and time-course sampling were applied to analyze the dynamic transcription of the *pprI* mutant strains compared with wild type. A total of 210 genes were found to be significantly induced in irradiated wild-type *D. radiodurans* but not in the irradiated *pprI* mutant strains. Consistent with the proteomics data, these genes participate in various pathways, indicating that *pprI* is a global regulator (Lu et al., 2012). Part of these genes are regulated by PprI directly, such as *pprA*, *ssB*, and *recA*, whose promoter contains RDRM (radiation/desiccation response motif) site and repressed by DdrO (Liu et al., 2003; Makarova et al., 2007). Genes like *DR0997* (*ddrI*) and *DR1114* (*hsp20*) that are also regulated by PprI without the conserved RDRM site are classified as indirectly regulated by PprI (Makarova et al., 2007; Lu et al., 2009; Singh et al., 2014;

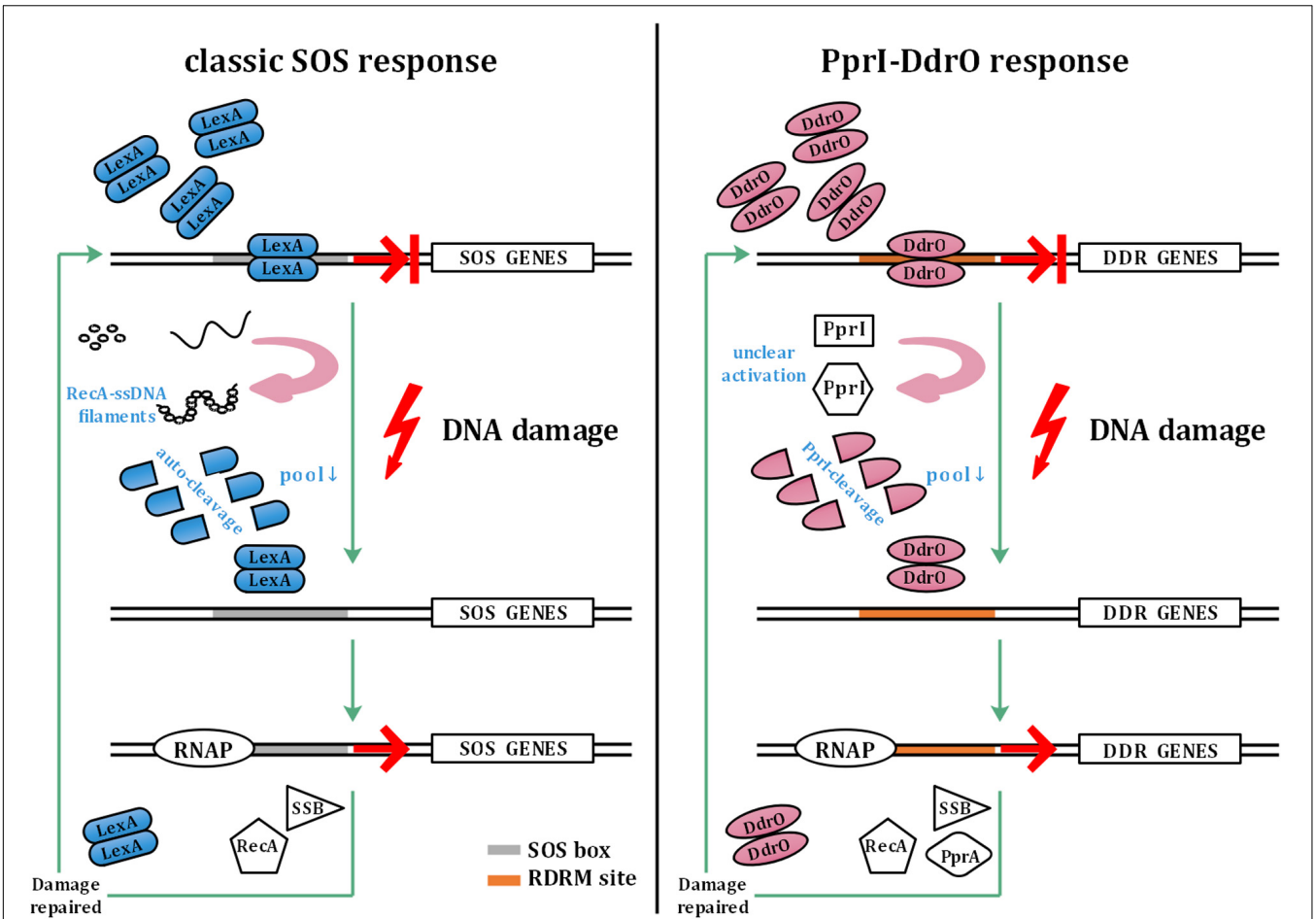


**FIGURE 1 |** Model of the classic SOS response and PprI–DdrO response. The left panel shows the model of the classic SOS response. LexA inhibits the transcription of SOS genes under normal conditions. Sensing DNA damage, RecA forms filaments with ssDNA and activates autocleavage of LexA. With the decrease in the cellular pool of LexA, SOS box-bound LexA dissociates to initiate the transcription of SOS genes by RNAP (RNA polymerase), which are repressed again by abundant LexA after the damage is repaired. The right panel shows the model of the PprI–DdrO response for comparison. Similar to LexA, DdrO represses the transcription of DDR genes before stresses occur. PprI is activated to efficiently cleave DdrO through an unclear mechanism after sensing DNA damage signals. DDR genes such as *recA*, *ssB*, and *pprA* are upregulated until the damage is repaired.

Yang et al., 2016). Moreover, Wang reported that DrRRA and PprI may collaborate to defend against environmental stresses (Wang et al., 2008, 2012).

## REPRESSION AND DEREPRESSION MECHANISMS OF THE PprI–DdrO SYSTEM

It is reported that proteins of COG2856, such as YdcM, tend to fuse with XRE (xenobiotic-response element) family proteins to form operons regulating cascade downstream. PprI is also belonging to COG2856, indicating the cooperation with an XRE family protein similar to other proteins in toxin–antitoxin systems (TAS) (Bose et al., 2008; Makarova et al., 2009). The mechanism by which PprI regulates a series of DDR genes is revealed along with the discovery of its action on the transcription repressor DdrO (Ludanyi et al., 2014; Wang et al., 2015). DdrO, a component in this DNA damage response system, belonging to the XRE family, is a transcriptional repressor that forms dimers and specifically binds to the promoter region of DDR genes, including *ddrO* itself, to repress DDR gene transcription under normal conditions (de Groot et al., 2019; Lu et al., 2019). These promoter regions contain a conserved 17-bp palindromic motif named RDRM (Makarova et al., 2007). After sensing DNA damage, DdrO is cleaved by PprI, which in turn relieves the transcriptional repression of DNA damage response genes. Thus, the repressor DdrO, in coordination with the protease PprI, constitutes the novel pathway mediating the DNA damage response in *Deinococcus*.

The detail of how the repressor DdrO works in the system remained unclear until the structure of DdrO was determined. The crystal structure of DdrO from *D. geothermalis* was solved by Lu et al. (2019). The results showed that DdrO is composed of eight α-helices, containing an HTH-containing N-terminal domain and a novel fold of C-terminal domain. Although the

structure of DdrO and promoter DNA in complex is not yet available, comparison of DdrO with other XRE family protein complexes and biochemical studies have revealed a conserved binding mode and recognition/binding residues in the HTH motif. It is verified in the article that the solvent-exposed residues such as R22, R28, K30, Y42, and D45 in DG-DdrO are essential for binding affinity. As for the RDRM sequence recognition and binding, both variation of the conserved base pairs and length shortening impaired the binding of DG-DdrO. In conclusion, the extended dimeric interaction in DdrO is essential for binding to RDRM-containing sequences (Makarova et al., 2007; Lu et al., 2019; Chen et al., 2020). Besides, apart from this NTD dimerization, Arjan de Groot also revealed a CTD dimerization of DdrO that is quite different to the already known XRE family proteins such as SinR (de Groot et al., 2019).

Analysis of the novel fold in the DdrO C-terminus exhibits enrichment of hydrophobic residues forming a stable hydrophobic core. The cleavage destabilizes the C-terminal hydrophobic core and disrupts the DdrO dimer, terminating the transcriptional repression of DDR genes as the specific DNA affinity of DdrO requires its dimeric conformation (Lu et al., 2019). Arjan de Groot and colleagues solved the crystal structure of DdrO from *D. deserti* and reported similar conclusions (de Groot et al., 2019). In a manner similar to the derepression of LexA, it is found by Laurence Blanchard that cleavage by PprI decreases the intracellular pool of unbound DdrO, resulting in dissociation of RDRM-bound DdrO and leading to DDR gene transcription (Blanchard et al., 2017).

## HYPOTHETIC MECHANISMS OF PprI ACTIVATION

In contrast to most genes related to the DNA damage response, the transcriptomic study by Liu et al. (2003) detected a constant level of *pprI* transcription during the early, middle, and late phases of recovery in *D. radiodurans* after acute irradiation at 15 kGy, indicating an unclear activation mechanism of PprI. Several hypotheses have been proposed that might explain the activation of PprI since the activation mechanism of PprI after irradiation remained unknown (**Figure 2A**).

### The Release of $Zn^{2+}$/$Mn^{2+}$ Caused by Radiation or Oxidative Stress

Blanchard discovered that the protease activity of PprI from *D. deserti* could be restored in the presence of $Zn^{2+}$, $Mn^{2+}$, or $Fe^{2+}$ *in vitro* (Blanchard et al., 2017). As radiation and oxidative stress can result in the rapid release of $Zn^{2+}$ from cysteine-containing zinc sites, Qi suggested that the level of intracellular $Zn^{2+}$ may be responsible for the activation of PprI (Maret, 2006; Kroncke and Klotz, 2009; Qi et al., 2020). Yet, it has to be demonstrated whether the level of intracellular $Zn^{2+}$ increases. However, Wang reported that the protease activity of PprI from *D. radiodurans* depends on $Mn^{2+}$ and that stimulation of PprI activity may rely on the alteration between $Mn^{2+}$ and other ions (Wang et al., 2015).

### Posttranslational Modifications

Posttranslational modification (PTM) has always been thought to be responsible for activating protein function in DNA damage response pathways, such as phosphorylation of H2A.X and ubiquitylation of Ku in DNA damage signaling and the NHEJ pathway, respectively (Kinner et al., 2008; Postow et al., 2008). Recently, Zhou et al. revealed the succinylome of *D. radiodurans* that is involved in its extreme resistance. *In vitro* assays have verified that glutamate substitution of Lys185 (K185E) in PprI, which mimics lysine succinylation, results in decreased enzymatic activity but that K185A exhibits enhanced protease activity (Zhou et al., 2019; **Figure 2A**). Whether other kinds of modification exist in PprI and affect the activation need further research.

### Small Molecules Binding to the GAF-Like Domain

The GAF domains always bind small molecules such as cAMP and cGMP, which participate as secondary messengers in many cellular signal transduction pathways. The C-terminus of PprI exhibits a GAF-like domain, the function of which has not yet been demonstrated. Li proved that the addition of dGMP significantly enhanced *D. radiodurans* tolerance to $H_2O_2$ and gamma radiation by stimulating the activity of KatA and inducing the transcription of an extracellular nuclease (Dr_b0067) (Li et al., 2013). Based on the results, it is tempting to propose that PprI might be activated via a signaling molecule such as dGMP interacting with the GAF-like domain (**Figure 2A**). Regardless, the GAF domain of *D. deserti* PprI exhibits a "closed gate" (the long loop from residue 201 to residue 211 that connects the second and third strands), blocking the access to the hydrophobic pocket, which may function as a small molecule binding site (Vujicic-Zagar et al., 2009). Although this blocking may be caused by crystal stacking, unless the loop region is moved aside, otherwise, small molecules would be rejected into the pocket to activate PprI.

## POTENTIAL APPLICATIONS OF PprI IN GENETIC ENGINEERING

It is meaningful to increase the resistance of organisms, especially industrial microbes and crops grown in extreme environments. In addition to mutant selection, overexpression of heterologous genes like the global regulator *pprI* from *Deinococcus* can help increase resistance to environmental stresses in organisms (Jin et al., 2019; Wang et al., 2019).

For example, Gao and Pan expressed *Dr_pprI* in *Escherichia coli*, which resulted in enhanced tolerances to radiation, salt, osmotic, reactive oxygen species (ROS) and other stresses. For example, the $D_{10}$ dose of ionizing radiation increased from 50 to 250 Gy, although it is quite far from that of *Deinococcus* (Gao et al., 2003; Pan et al., 2009). Ma also found that transduction of *Dr_pprI* into ethanologenic *E. coli* increases the ethanol production by 14.7 and 26.3% from glucose and xylose, respectively (Ma et al., 2011). Similarly, Dong produced a lactic

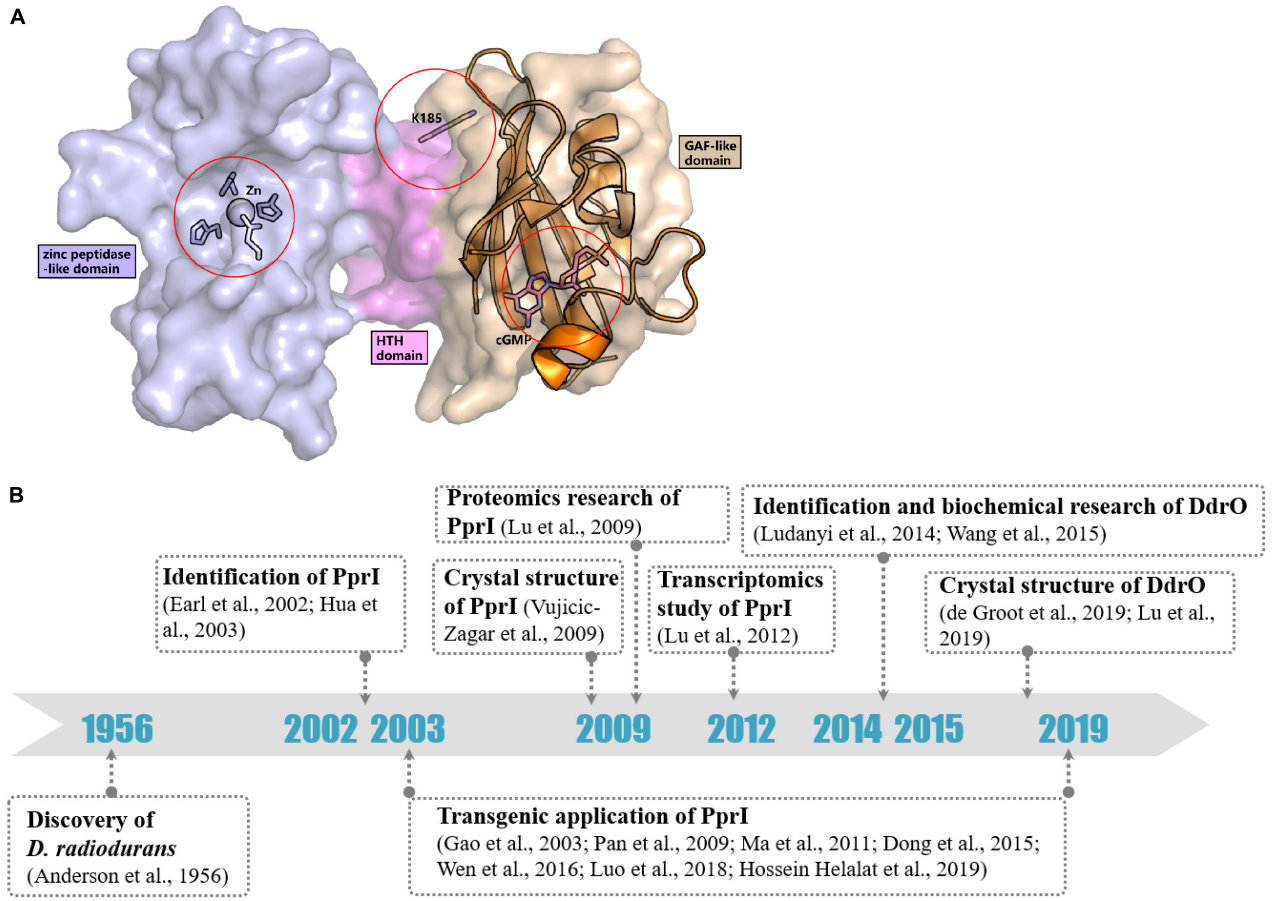


**FIGURE 2 |** Activation hypotheses and timeline of important discoveries of PprI. **(A)** Three hypotheses of the PprI activation are present on the structure of DR_PprI, which is from the homolog modeling (Swiss model) using *D. deserti* protein (PDB: 3DTE) as the starting model. DR_PprI is shown as surface, and the zinc peptidase-like domain, helix-turn-helix motif and GAF-like domain are colored in light blue, magenta, and wheat, respectively. Related residues are shown as sticks. The aligned structure of PDE2A (RCSB PDB code 1MC0) is shown as cartoon. The four residues and metal ion in the NTD zinc peptidase-like domain represent the metal hypothesis. The Lys185 residue represents the posttranscriptional modification hypothesis. The cGMP in the GAF-like pocket by alignment represents the small molecule hypothesis. **(B)** Timeline of the important discoveries of PprI.

acid high-yield and stress-tolerant strain of *Lactococcus lactis* by expression of *pprI* from *D. radiodurans*. The increment of lactic acid reached even up to threefold especially under salt stress (Dong et al., 2015). Luo explored the effects of introducing *pprI* into the electrochemically active bacterium *Pseudomonas aeruginosa* PAO1 and achieved an increase in power density by 71% higher than that of the control strain (Luo et al., 2018). The transduction of *pprI* works even in eukaryotes. Hossein Helalat reported that the heterologous expression of the *pprI* gene generated a 1.5-fold alcohol and salt stress-tolerant strain of *Saccharomyces cerevisiae* (Hossein Helalat et al., 2019). Furthermore, Wen attempted to introduce *pprI* cloned in the pEGFP-c1 vector into mouse and human cells, and showed that its expression relieved acute radiation-induced damage to different organs and increased nearly 30% the survival rate by regulating expression of Rad51 (Wen et al., 2016). The detailed mechanism of how PprI affects the stress tolerance of other organisms remains unknown so far. One possible explanation is the similarity in analogous stress regulon systems. Adding PprI from *Deinococcus* may increase the amount of PprI-like protease copies and improve the survival in extreme environments to some point. The transcriptome and proteome in *E. coli* expressing PprI revealed the regulation of gene response not only to DNA damage but also to pH stress, and osmotic and oxidative stress, which also indicated the analogous stress regulon systems in *E. coli* (Zhou et al., 2011; Chen et al., 2012; Zhao et al., 2015). What is more, researchers have also inferred that PprI has other functions in addition to acting as a protease to derepress transcription in response to DNA damage. Further study will help to better reveal its functional mechanisms and can be applied to various human production activities.

## CONCLUSION

Identified nearly 64 years ago, *D. radiodurans* has been designated as one of the most radio-resistant organisms on Earth (Anderson et al., 1956). The reason for its robust viability has been revealed

with research progresses of the antioxidant system and DNA damage repair, especially when the essential of *pprI* for the stress resistance and its orchestrating on DNA damage genes such as *recA* are confirmed (Earl et al., 2002; Hua et al., 2003; Longtin, 2003).

In the past 17 years, the *pprI* gene has been studied by genomics, transcriptomics, proteomics, bioinformatics, molecular biology, and structural biology approaches, revealing its structural and functional characteristics (**Figure 2B**). Structural data reveal the composition of three domains, suggesting its function as a protease, which was later demonstrated with the discovery of its specific substrate, DdrO. DNA microarrays and proteomics analysis have revealed that the *pprI* gene is responsible for regulating various genes participating in transcription, translation, metabolism, and DNA damage repair. However, transcriptomics data also suggest that the DNA damage response mediated by PprI does not rely on the induction of protein translation but on an unclear activation mechanism that needs further research.

Comparison of the PprI–DdrO response system with the SOS response system reveals distinctions between them. For one thing, the dimerization of the two repressors depends on the interaction from both NTD and CTD, while the interface of DdrO is much more extensive and CTD dependent (Lu et al., 2019; Chen et al., 2020). For another, the dissociation of LexA relies on the autocleavage, which is promoted by the stabilization of autocleavage conformation when RecA is activated after sensing DNA damage and form RecA-ssDNA-ATP filaments (Butala et al., 2008, 2011). On this occasion, the cleavage conducted by PprI is much more direct and efficient compared with the co-protease activity of RecA.

The efficiency of the PprI–DdrO response system also relies on the antioxidant intracellular environment protecting the proteome, which is provided and kept by the extraordinary antioxidant system (Daly et al., 2004, 2010; Slade and Radman, 2011). The domestication of the high-resistant *E. coli* by 100-cycle selection exhibits reduced level of hydroxylation, which further indicates the relationship between DNA damage repair and antioxidant system (Bruckbauer et al., 2020). In other words, both DDR system and antioxidant system are important, without which the radiation resistance will be greatly impaired.

DNA damage occurs throughout the entire life cycle, inducing mutation, cancer and cell death, which are prevented by the DNA damage response that includes a series of activities such as DNA repair, cell cycle checkpoints, and apoptosis. Studies on the DNA damage response can contribute to the development of new drugs for cancer therapy, such as small molecule inhibitors that target key proteins in DNA damage response and repair pathways (Li et al., 2020). Furthermore, greater knowledge of DNA damage response mechanisms may help to prevent cancer-inducing habits and guide healthy living. Research on the DNA damage response, such as the SOS and PprI–DdrO response systems, can help in elucidating the extraordinary resistance of *Deinococcus* and the mechanisms of organisms that can survive environmental stresses. Regardless, much work is needed to fully understand the multiple DNA damage response systems.

## AUTHOR CONTRIBUTIONS

HL and YH reviewed the literature and wrote the manuscript. Both authors contributed to the article and approved the submitted version.

## FUNDING

This work was supported by the National Key Research and Development Program of China (2017YFA0503900), the grants from National Natural Science Foundation of China (31670065 and 31870051), and China Postdoctoral Science Foundation (2020M671699).

## REFERENCES

Anderson, A. W., Nordan, H. C., Cain, R. F., Parrish, G., and Duggan, D. (1956). Studies on a radio-resistant micrococcus .1. Isolation, morphology, cultural characteristics, and resistance to gamma radiation. *Food Technol.* 10, 575–578.

Aravind, L., and Ponting, C. P. (1997). The GAF domain: an evolutionary link between diverse phototransducing proteins. *Trends Biochem. Sci.* 22, 458–459. doi: 10.1016/s0968-0004(97)01148-1

Bauermeister, A., Bentchikou, E., Moeller, R., and Rettberg, P. (2009). Roles of PprA, IrrE, and RecA in the resistance of *Deinococcus radiodurans* to germicidal and environmentally relevant UV radiation. *Arch. Microbiol.* 191, 913–918. doi: 10.1007/s00203-009-0522-7

Blanchard, L., Guerin, P., Roche, D., Cruveiller, S., Pignol, D., Vallenet, D., et al. (2017). Conservation and diversity of the IrrE/DdrO-controlled radiation response in radiation-resistant *Deinococcus* bacteria. *Microbiologyopen* 6:e00477. doi: 10.1002/mbo3.477

Blasius, M., Sommer, S., and Hubscher, U. (2008). *Deinococcus radiodurans*: what belongs to the survival kit? *Crit. Rev. Biochem. Mol. Biol.* 43, 221–238. doi: 10.1080/10409230802122274

Bose, B., Auchtung, J. M., Lee, C. A., and Grossman, A. D. (2008). A conserved anti-repressor controls horizontal gene transfer by proteolysis. *Mol. Microbiol.* 70, 570–582. doi: 10.1111/j.1365-2958.2008.06414.x

Boulton, S. J., Gartner, A., Reboul, J., Vaglio, P., Dyson, N., Hill, D. E., et al. (2002). Combined functional genomic maps of the C. elegans DNA damage response. *Science* 295, 127–131. doi: 10.1126/science.1065986

Bruckbauer, S. T., Martin, J., Minkoff, B. B., Veling, M. T., Lancaster, I., Liu, J., et al. (2020). Physiology of highly radioresistant *Escherichia coli* after experimental evolution for 100 cycles of selection. *Front. Microbiol.* 11:582590. doi: 10.3389/fmicb.2020.582590

Butala, M., Klose, D., Hodnik, V., Rems, A., Podlesek, Z., Klare, J. P., et al. (2011). Interconversion between bound and free conformations of LexA orchestrates the bacterial SOS response. *Nucleic Acids Res.* 39, 6546–6557. doi: 10.1093/nar/gkr265

Butala, M., Žgur-Bertok, D., and Busby, S. J. W. (2008). The bacterial LexA transcriptional repressor. *Cellular and Molecular Life Sciences* 66, 82–93. doi: 10.1007/s00018-008-8378-6

Chen, H., Xu, G., Zhao, Y., Tian, B., Lu, H., Yu, X., et al. (2008). A novel OxyR sensor and regulator of hydrogen peroxide stress with one cysteine residue in *Deinococcus radiodurans*. *PLoS One* 3:e1602. doi: 10.1371/journal.pone.0001602

Chen, T., Wang, J., Zeng, L., Li, R., Li, J., Chen, Y., et al. (2012). Significant rewiring of the transcriptome and proteome of an *Escherichia coli* strain harboring a tailored exogenous global regulator IrrE. *PLoS One* 7:e37126. doi: 10.1371/journal.pone.0037126

Chen, Z., Tang, Y., Hua, Y., and Zhao, Y. (2020). Structural features and functional implications of proteins enabling the robustness of *Deinococcus radiodurans*. *Comput. Struct. Biotechnol. J.* 18, 2810–2817. doi: 10.1016/j.csbj.2020.09.036

Cox, M. M., and Battista, J. R. (2005). *Deinococcus radiodurans* - the consummate survivor. *Nat. Rev. Microbiol.* 3, 882–892. doi: 10.1038/nrmicro1264

Daly, M. J., Gaidamakova, E. K., Matrosova, V. Y., Kiang, J. G., Fukumoto, R., Lee, D. Y., et al. (2010). Small-molecule antioxidant proteome-shields in *Deinococcus radiodurans*. *PLoS One* 5:e12570. doi: 10.1371/journal.pone.0012570

Daly, M. J., Gaidamakova, E. K., Matrosova, V. Y., Vasilenko, A., Zhai, M., Venkateswaran, A., et al. (2004). Accumulation of Mn(II) in *Deinococcus radiodurans* facilitates gamma-radiation resistance. *Science* 306, 1025–1028. doi: 10.1126/science.1103185

de Groot, A., Siponen, M. I., Magerand, R., Eugenie, N., Martin-Arevalillo, R., Doloy, J., et al. (2019). Crystal structure of the transcriptional repressor DdrO: insight into the metalloprotease/repressor-controlled radiation response in *Deinococcus*. *Nucleic Acids Res.* 47, 11403–11417. doi: 10.1093/nar/gkz883

Devigne, A., Ithurbide, S., Bouthier de la Tour, C., Passot, F., Mathieu, M., Sommer, S., et al. (2015). DdrO is an essential protein that regulates the radiation desiccation response and the apoptotic-like cell death in the radioresistant *Deinococcus radiodurans* bacterium. *Mol. Microbiol.* 96, 1069–1084. doi: 10.1111/mmi.12991

Dong, X., Tian, B., Dai, S., Li, T., Guo, L., Tan, Z., et al. (2015). Expression of PprI from *Deinococcus radiodurans* improves lactic acid production and stress tolerance in *Lactococcus lactis*. *PLoS One* 10:e0142918. doi: 10.1371/journal.pone.0142918

Earl, A. M., Mohundro, M. M., Mian, I. S., and Battista, J. R. (2002). The IrrE protein of *Deinococcus radiodurans* R1 is a novel regulator of recA expression. *J. Bacteriol.* 184, 6216–6224. doi: 10.1128/jb.184.22.6216-6224.2002

Gao, G., Tian, B., Liu, L., Sheng, D., Shen, B., and Hua, Y. (2003). Expression of *Deinococcus radiodurans* PprI enhances the radioresistance of *Escherichia coli*. *DNA Repair.* 2, 1419–1427. doi: 10.1016/j.dnarep.2003.08.012

Gao, G. J., Lu, H. M., Huang, L. F., and Hua, Y. J. (2005). Construction of DNA damage response gene pprI function-deficient and function-complementary mutants in *Deinococcus radiodurans*. *Chin. Sci. Bull.* 50, 311–316. doi: 10.1360/982004-719

Hossein Helalat, S., Bidaj, S., Samani, S., and Moradi, M. (2019). Producing alcohol and salt stress tolerant strain of *Saccharomyces cerevisiae* by heterologous expression of *pprI* gene. *Enzyme Microb. Technol.* 124, 17–22. doi: 10.1016/j.enzmictec.2019.01.008

Hua, Y., Narumi, I., Gao, G., Tian, B., Satoh, K., Kitayama, S., et al. (2003). PprI: a general switch responsible for extreme radioresistance of *Deinococcus radiodurans*. *Biochem. Biophys. Res. Commun.* 306, 354–360. doi: 10.1016/s0006-291x(03)00965-3

Jin, M., Xiao, A., Zhu, L., Zhang, Z., Huang, H., and Jiang, L. (2019). The diversity and commonalities of the radiation-resistance mechanisms of *Deinococcus* and its up-to-date applications. *AMB Express* 9:138. doi: 10.1186/s13568-019-0862-x

Jolivet, E., Lecointe, F., Coste, G., Satoh, K., Narumi, I., Bailone, A., et al. (2006). Limited concentration of RecA delays DNA double-strand break repair in *Deinococcus radiodurans* R1. *Mol. Microbiol.* 59, 338–349. doi: 10.1111/j.1365-2958.2005.04946.x

Kinner, A., Wu, W., Staudt, C., and Iliakis, G. (2008). Gamma-H2AX in recognition and signaling of DNA double-strand breaks in the context of chromatin. *Nucleic Acids Res.* 36, 5678–5694. doi: 10.1093/nar/gkn550

Kota, S., Charaka, V. K., Ringgaard, S., Waldor, M. K., and Misra, H. S. (2014). PprA contributes to *Deinococcus radiodurans* resistance to nalidixic acid, genome maintenance after DNA damage and interacts with deinococcal topoisomerases. *PLoS One* 9:e85288. doi: 10.1371/journal.pone.0085288

Kroncke, K. D., and Klotz, L. O. (2009). Zinc fingers as biologic redox switches? *Antioxid Redox Signal.* 11, 1015–1027. doi: 10.1089/ARS.2008.2269

Li, M., Sun, H., Feng, Q., Lu, H., Zhao, Y., Zhang, H., et al. (2013). Extracellular dGMP enhances *Deinococcus radiodurans* tolerance to oxidative stress. *PLoS One* 8:e54420. doi: 10.1371/journal.pone.0054420

Li, L., Kumar, A. K., Hu, Z., and Guo, Z. (2020). Small molecule inhibitors targeting the key proteins in DNA damage response for cancer therapy. *Curr. Med. Chem.* 27, 1–21. doi: 10.2174/0929867327666200224102309

Lim, S., Jung, J. H., Blanchard, L., and de Groot, A. (2019). Conservation and diversity of radiation and oxidative stress resistance mechanisms in *Deinococcus* species. *FEMS Microbiol. Rev.* 43, 19–52. doi: 10.1093/femsre/fuy037

Liu, Y., Zhou, J., Omelchenko, M. V., Beliaev, A. S., Venkateswaran, A., Stair, J., et al. (2003). Transcriptome dynamics of *Deinococcus radiodurans* recovering from ionizing radiation. *Proc. Natl. Acad. Sci. U.S.A.* 100, 4191–4196. doi: 10.1073/pnas.0630387100

Longtin, R. (2003). Deinoccocus radiodurans: getting a better fix on DNA repair. *J. Natl. Cancer Inst.* 95, 1270–1271. doi: 10.1093/jnci/95.17.1270

Lu, H., Chen, H., Xu, G., Shah, A. M., and Hua, Y. (2012). DNA binding is essential for PprI function in response to radiation damage in *Deinococcus radiodurans*. *DNA Repair.* 11, 139–145. doi: 10.1016/j.dnarep.2011.10.013

Lu, H., Gao, G., Xu, G., Fan, L., Yin, L., Shen, B., et al. (2009). *Deinococcus radiodurans* PprI switches on DNA damage response and cellular survival networks after radiation damage. *Mol. Cell Proteomics* 8, 481–494. doi: 10.1074/mcp.M800123-MCP200

Lu, H., Wang, L., Li, S., Pan, C., Cheng, K., Luo, Y., et al. (2019). Structure and DNA damage-dependent derepression mechanism for the XRE family member DG-DdrO. *Nucleic Acids Res.* 47, 9925–9933. doi: 10.1093/nar/gkz720

Ludanyi, M., Blanchard, L., Dulermo, R., Brandelet, G., Bellanger, L., Pignol, D., et al. (2014). Radiation response in *Deinococcus deserti*: IrrE is a metalloprotease that cleaves repressor protein DdrO. *Mol. Microbiol.* 94, 434–449. doi: 10.1111/mmi.12774

Luo, J., Wang, T., Li, X., Yang, Y., Zhou, M., Li, M., et al. (2018). Enhancement of bioelectricity generation via heterologous expression of IrrE in *Pseudomonas aeruginosa*-inoculated MFCs. *Biosens. Bioelectron.* 117, 23–31. doi: 10.1016/j.bios.2018.05.052

Ma, R., Zhang, Y., Hong, H., Lu, W., Lin, M., Chen, M., et al. (2011). Improved osmotic tolerance and ethanol production of ethanologenic *Escherichia coli* by IrrE, a global regulator of radiation-resistance of *Deinococcus radiodurans*. *Curr. Microbiol.* 62, 659–664. doi: 10.1007/s00284-010-9759-2

Makarova, K. S., Omelchenko, M. V., Gaidamakova, E. K., Matrosova, V. Y., Vasilenko, A., Zhai, M., et al. (2007). *Deinococcus geothermalis*: the pool of extreme radiation resistance genes shrinks. *PLoS One* 2:e955. doi: 10.1371/journal.pone.0000955

Makarova, K. S., Wolf, Y. I., and Koonin, E. V. (2009). Comprehensive comparative-genomic analysis of type 2 toxin-antitoxin systems and related mobile stress response systems in prokaryotes. *Biol. Direct,* 4:19. doi: 10.1186/1745-6150-4-19

Maret, W. (2006). Zinc coordination environments in proteins as redox sensors and signal transducers. *Antioxid Redox Signal.* 8, 1419–1441. doi: 10.1089/ars.2006.8.1419

Martinez, S. E., Wu, A. Y., Glavas, N. A., Tang, X. B., Turley, S., Hol, W. G., et al. (2002). The two GAF domains in phosphodiesterase 2A have distinct roles in dimerization and in cGMP binding. *Proc. Natl. Acad. Sci. U.S.A,* 99, 13260–13265. doi: 10.1073/pnas.192374899

Narumi, I., Satoh, K., Kikuchi, M., Funayama, T., Yanagisawa, T., Kobayashi, Y., et al. (2001). The LexA protein from *Deinococcus radiodurans* is not involved in RecA induction following gamma irradiation. *J. Bacteriol.* 183, 6951–6956. doi: 10.1128/JB.183.23.6951-6956.2001

Pan, J., Wang, J., Zhou, Z., Yan, Y., Zhang, W., Lu, W., et al. (2009). IrrE, a global regulator of extreme radiation resistance in *Deinococcus radiodurans*, enhances salt tolerance in *Escherichia coli* and Brassica napus. *PLoS One* 4:e4422. doi: 10.1371/journal.pone.0004422

Pilzecker, B., Buoninfante, O. A., and Jacobs, H. (2019). DNA damage tolerance in stem cells, ageing, mutagenesis, disease and cancer therapy. *Nucleic Acids Res.* 47, 7163–7181. doi: 10.1093/nar/gkz531

Postow, L., Ghenoiu, C., Woo, E. M., Krutchinsky, A. N., Chait, B. T., and Funabiki, H. (2008). Ku80 removal from DNA through double strand break-induced ubiquitylation. *J. Cell Biol.* 182, 467–479. doi: 10.1083/jcb.200802146

Qi, H. Z., Wang, W. Z., He, J. Y., Ma, Y., Xiao, F. Z., and He, S. Y. (2020). Antioxidative system of *Deinococcus radiodurans*. *Res. Microbiol.* 171, 45–54. doi: 10.1016/j.resmic.2019.11.002

Radman, M. (1975). SOS repair hypothesis: phenomenology of an inducible DNA repair which is accompanied by mutagenesis. *Basic Life Sci.* 5A, 355–367. doi: 10.1007/978-1-4684-2895-7_48

Selvam, K., Duncan, J. R., Tanaka, M., and Battista, J. R. (2013). DdrA, DdrD, and PprA: components of UV and mitomycin C resistance in *Deinococcus radiodurans* R1. *PLoS One* 8:e69007. doi: 10.1371/journal.pone.0069007

Sevvana, M., Vijayan, V., Zweckstetter, M., Reinelt, S., Madden, D. R., Herbst-Irmer, R., et al. (2008). A ligand-induced switch in the periplasmic domain of sensor histidine kinase CitA. *J. Mol. Biol.* 377, 512–523. doi: 10.1016/j.jmb.2008.01.024

Sharma, A., Gaidamakova, E. K., Grichenko, O., Matrosova, V. Y., Hoeke, V., Klimenkova, P., et al. (2017). Across the tree of life, radiation resistance is governed by antioxidant Mn(2+), gauged by paramagnetic resonance. *Proc. Natl. Acad. Sci. U.S.A.* 114, E9253–E9260. doi: 10.1073/pnas.1713608114

Sheng, D., Zheng, Z., Tian, B., Shen, B., and Hua, Y. (2004). LexA analog (dra0074) is a regulatory protein that is irrelevant to recA induction. *J. Biochem.* 136, 787–793. doi: 10.1093/jb/mvh188

Singh, H., Appukuttan, D., and Lim, S. (2014). Hsp20, a small heat shock protein of *Deinococcus radiodurans*, confers tolerance to hydrogen peroxide in *Escherichia coli*. *J. Microbiol. Biotechnol.* 24, 1118–1122. doi: 10.4014/jmb.1403.03006

Slade, D., and Radman, M. (2011). Oxidative stress resistance in *Deinococcus radiodurans*. *Microbiol. Mol. Biol. Rev.* 75, 133–191. doi: 10.1128/MMBR.00015-10

Vujicic-Zagar, A., Dulermo, R., Le Gorrec, M., Vannier, F., Servant, P., Sommer, S., et al. (2009). Crystal structure of the IrrE protein, a central regulator of DNA damage repair in deinococcaceae. *J. Mol. Biol.* 386, 704–716. doi: 10.1016/j.jmb.2008.12.062

Wang, L., Xu, G., Chen, H., Zhao, Y., Xu, N., Tian, B., et al. (2008). DrRRA: a novel response regulator essential for the extreme radioresistance of *Deinococcus radiodurans*. *Mol. Microbiol.* 67, 1211–1222. doi: 10.1111/j.1365-2958.2008.06113.x

Wang, L. Y., Yin, L. F., Xu, G. Z., Li, M. F., Zhang, H., Tian, B., et al. (2012). Cooperation of PprI and DrRRA in response to extreme ionizing radiation in *Deinococcus radiodurans*. *Chin. Sci. Bull.* 57, 98–104. doi: 10.1007/s11434-011-4790-7

Wang, W., Ma, Y., He, J., Qi, H., Xiao, F., and He, S. (2019). Gene regulation for the extreme resistance to ionizing radiation of *Deinococcus radiodurans*. *Gene* 715:144008. doi: 10.1016/j.gene.2019.144008

Wang, Y., Xu, Q., Lu, H., Lin, L., Wang, L., Xu, H., et al. (2015). Protease activity of PprI facilitates DNA damage response: Mn2+-dependence and substrate sequence-specificity of the proteolytic reaction. *PLoS One* 10:e0122071. doi: 10.1371/journal.pone.0122071

Wen, L., Yue, L., Shi, Y., Ren, L., Chen, T., Li, N., et al. (2016). *Deinococcus radiodurans* pprI expression enhances the radioresistance of eukaryotes. *Oncotarget* 7, 15339–15355. doi: 10.18632/oncotarget.8137

Yang, S., Xu, H., Wang, J., Liu, C., Lu, H., Liu, M., et al. (2016). Cyclic AMP Receptor Protein Acts as a Transcription Regulator in Response to Stresses in *Deinococcus radiodurans*. *PLoS One* 11:e0155010. doi: 10.1371/journal.pone.0155010

Zhao, P., Zhou, Z., Zhang, W., Lin, M., Chen, M., and Wei, G. (2015). Global transcriptional analysis of *Escherichia coli* expressing IrrE, a regulator from *Deinococcus radiodurans*, in response to NaCl shock. *Mol. Biosyst.* 11, 1165–1171. doi: 10.1039/c5mb00080g

Zhou, C., Dai, J., Lu, H., Chen, Z., Guo, M., He, Y., et al. (2019). Succinylome analysis reveals the involvement of lysine succinylation in the extreme resistance of *Deinococcus radiodurans*. *Proteomics* 19:e1900158. doi: 10.1002/pmic.201900158

Zhou, Z., Zhang, W., Chen, M., Pan, J., Lu, W., Ping, S., et al. (2011). Genome-wide transcriptome and proteome analysis of *Escherichia coli* expressing IrrE, a global regulator of *Deinococcus radiodurans*. *Mol. Biosyst.* 7, 1613–1620. doi: 10.1039/c0mb00336k

**Conflict of Interest:** The authors declare that the research was conducted in the absence of any commercial or financial relationships that could be construed as a potential conflict of interest.

frontiers in Genetics

ORIGINAL RESEARCH
published: 27 January 2021
doi: 10.3389/fgene.2020.609758

# *ANKLE1* as New Hotspot Mutation for Breast Cancer in Indian Population and Has a Role in DNA Damage and Repair in Mammalian Cells

*Divya Bakshi[1], Archana Katoch[2,3], Souneek Chakraborty[2,3], Ruchi Shah[1], Bhanu Sharma[1], Amrita Bhat[1], Sonali Verma[1], Gh. Rasool Bhat[1], Ashna Nagpal[1], Samantha Vaishnavi[4], Anindya Goswami[2,3] and Rakesh Kumar[1]**

[1] Shri Mata Vaishno Devi University, Katra, India, [2] Cancer Pharmacology Division, Indian Institute of Integrative Medicine (CSIR) Jammu, Jammu, India, [3] Academy of Scientific and Innovative Research (AcSIR), New Delhi, India, [4] Department of Botany, Central University of Jammu, Jammu, India

OPEN ACCESS

**Edited by:**
Hari S. Misra,
Bhabha Atomic Research Centre (BARC), India

**Reviewed by:**
Manoj Kumar Kashyap,
Amity University Gurgaon, India
Roberto Scarpato,
University of Pisa, Italy

***Correspondence:**
Rakesh Kumar
kumar.rakesh@smvdu.ac.in

**Specialty section:**
This article was submitted to Genetics of Common and Rare Diseases, a section of the journal Frontiers in Genetics

**Received:** 24 September 2020
**Accepted:** 30 November 2020
**Published:** 27 January 2021

**Citation:**
Bakshi D, Katoch A, Chakraborty S, Shah R, Sharma B, Bhat A, Verma S, Bhat GR, Nagpal A, Vaishnavi S, Goswami A and Kumar R (2021) ANKLE1 as New Hotspot Mutation for Breast Cancer in Indian Population and Has a Role in DNA Damage and Repair in Mammalian Cells. Front. Genet. 11:609758. doi: 10.3389/fgene.2020.609758

Breast cancer has replaced cervical cancer as being the most common and having the highest mortality among women in India. *ANKLE* gene is conserved among organisms during evolutionary succession and is a member of LEM family proteins in lower metazoans and is involved in critical functions in the nuclear architecture, gene expression and cell signaling. *ANKLE1* is the human orthologous of LEM-3 and is involved in DNA damage response and DNA repair. Whole Exome Sequencing (WES) of paired breast cancer samples was performed and *ANKLE1* was found to be a new possible hotspot for predisposition of breast cancer. The mass array genotyping for breast cancer variant rs2363956 further confirmed the *ANKLE1* association with the studied population of breast cancer. To elucidate the role of *ANKLE1* in DNA damage, it was knocked down in MCF-7 breast cancer cell line and the expression of γH2AX was assessed. *ANKLE1* knockdown cells displayed elevated levels of γ-H2AX foci in response to the cisplatin induced replication stress. The localization pattern of *ANKLE1* further emphasized the role of *ANKLE1* in DNA repair process. We observed that *ANKLE1* is required for maintaining genomic stability and plays a role in DNA damage and repair process. These findings provided a molecular basis for the suspected role of *ANKLE1* in human breast cancer and suggested an important role of this gene in controlling breast cancer development among women in India.

**Keywords: *ANKLE-1*, γH2AX, cancer, breast cancer, MCF-7 cell line, DNA damage**

## INTRODUCTION

Cancer development is a multistage process involving several genetic alterations (Takashi et al., 1992). Plethora of carcinogens like ultraviolet radiations, ionizing radiations and toxic chemicals attack the DNA and create DNA lesions (Roos and Kaina, 2013). If unrepaired, the accumulation of these lesions might lead to precarious oncogenic progressions in the cell and enhance the cancer risk (Hoeijmakers, 2001). The development of cancers involves lacunae in the DNA repair pathways

that are now being targeted for treatment processes (Gomes et al., 2017). Breast cancer is the most frequent type of cancer among women worldwide and is the leading cause of cancer related deaths (Miranda and Fidier, 2018). Breast cancer shares 14% of the cancer mortality burden worldwide and affects 1.3 million women worldwide (Lam et al., 2014). The most frequent mutations in breast cancer are associated with DNA repair mechanisms in the cell (Ciriello et al., 2013). Several genes *BRCA1*, *BRCA2, PALB2, CHEK2, PTEN, RAD51, RAD52, XRCC1, XRCC2* have been characterized for their involvement in hereditary or sporadic breast cancers (Walsh et al., 2006; Majidinia and Yousefi, 2017). In the recent years, the genome-wide association studies (GWAS) have helped in identification of many breast cancer susceptibility loci (Douglas et al., 2007). The breast cancer is found to be polygenic (Paul et al., 2002). The common alleles discovered by GWAS in the general population confer a higher risk in *BRCA1* and *BRCA2* mutations (Simon et al., 2007). Inherited mutations in these genes confer a lifetime risk of breast cancer (Paula et al., 2009). BRCA family of genes plays critical role in DNA Damage response and Repair.

SNP genotyping provides a powerful tool for identifying the contributors in complex disorders (Brookes, 1999). Mass array genotyping using MALDI-TOF spectrometry allows rapid genotyping of several hundred SNPs in the cost-effective manners (Oeth et al., 2009). Genotyping studies have highlighted several variations in the genes that might contribute in the breast cancer development. Exome sequencing has helped to decipher the genetic basis of several sporadic cancers and other human inherited diseases (Rabbani et al., 2012). In various cancer studies, the exome sequencing succeeded in identifying novel mutations of hereditary nature (Noetzli et al., 2015). Recent studies have indicated toward an increased predisposition to breast and ovarian cancer with small nucleotide polymorphisms in the human *ANKLE1* gene (Kristen et al., 2011; Lawrenson et al., 2016). The expression of *ANKLE1* in breast epithelial cells (Rosenbloom et al., 2012) and its presence in ovarian cancer indicated that *ANKLE1* might be regulating women cancers through hormonal mechanisms (Bolton et al., 2016). Whole exome sequencing has helped in identifying several loci within the *ANKLE1* gene, which account for autoimmunity disorders (Johar et al., 2015). The LEM family proteins are involved in nuclear architecture, gene expression, cell signaling etc. The mammalian genome study has spotted genes belonging to the LEM family termed as LEM3 and LEM4 also called the ankyrin repeat and LEM domain containing proteins 1 and 2, respectively (Brachner et al., 2011). *ANKLE1* or the *LEM3* protein is present in the hematopoietic tissue and cells. It is an evolutionarily conserved non membrane bound protein transported between cytoplasm and nucleus (Lacy et al., 2016). In *C. elegans*, the mutation in the *LEM-3* gene (mammalian orthologous of *ANKLE1* gene) has shown to develop extreme sensitivity to DNA damaging agents (Brachner and Foisner, 2014). The up-regulated expression of *ANKLE1* in DNA damage conditions confirms the role of *ANKLE1* under stress conditions. These studies suggest that *ANKLE1* might be a relevant factor in DNA damage response and DNA repair. Detailed studies on *ANKLE1* involvement in breast cancer for Indian population are unknown.

Here we report the detailed studies on WES and mass array genotypic of variant rs2363956 and observed that genetic variations in *ANKLE1* is associated with breast cancer population in India. Further, we provided evidence that *ANKLE1* is involved in DNA repair process in MCF-7 cell lines as the absence of *ANKLE1* resulted in an increased DNA damage. The cells exposed to DNA damaging agents showed *ANKLE1* localization in nucleus. These results together suggested that *ANKLE1* plays an important role in breast cancer development in Indian population most likely by regulation DNA repair in breast cancer cell lines.

# METHODOLOGY

## Study Materials

The recruitment of subjects of breast cancer cases was confirmed by histopathological examination, and those with any other type of cancer were excluded. A small number of samples were analyzed through WES. For SNP Mass Array Genotyping a total of 550 blood and tissue samples were recruited (150 cases and 400 controls). The details of the samples have been mentioned in **Supplementary Table 1**. The MCF-7 (Michigan Cancer Foundation-7) breast cancer cell line was used for the study. These cell lines were obtained from ATCC (American Type Culture Collection) United States. Gibco$^{TM}$ RPMI 1640 (Roswell Park Memorial Institute) media was used for the MCF-7 cell culture. The media was supplemented with 10% FBS and 1% penicillin. The cells were grown at a temperature of 37°C in a 5% $CO_2$ incubator up to 75–80% confluence. The study was approved by the Institutional Ethics Review Board (IERB) of SMVDU (SMVDU/IERB/18/70).

## Mutation Detection and Analysis

The samples were outsourced for WES at the Xcelris Labs Pvt. Limited, Ahmedabad, Gujarat, India. About 3 μg of the DNA isolated, using the Qaigen DNA isolation kit (Cat. No. 69504) was sent for whole exome sequencing. Illumina HiSeq 2000 with paired-end 100-bp reads was used for the Whole Exome Sequencing. For the tissue samples, DNA isolation was done using the Nectera rapid capture exome kit. 50 ng of DNA was then used for sequencing using Illumina HiSeq 2500 sequencer. Based on plethora of hotspots elucidated in WES and after validation through various bioinformatic tools, *ANKLE1* gene was chosen. The main criterion for the gene selection was its consistent presence in Breast Cancer samples.

Similarly, the mass array for SNP genotyping was carried out for rs2363956 variant within the *ANKLE1* gene by using Sequenom Mass Array iPLEX. The 550 samples were employed (150 breast cancer cases and 400 control samples) and studied for the genotypes at the location rs2363956 on the *ANKLE1* gene. Genotypes were analyzed based on the ratio of MALDI-TOF spectrometer. SNP genotyping and SNP allele frequency were calculated using software.

## Cell Lysate Preparation and Western Blotting

The cells were given 25 μM cisplatin treatment and rested for time intervals of 0, 4, 8, 16 and 24 h. After the respective treatments, the cells were centrifuged and mixed with a lysis buffer to obtain the cell lysate. The total protein concertation was determined using Lowry method. The equal amount of total proteins was separated on SDS-PAGE, immunoblotted using antibodies against *ANKLE1* (Merck Inc.) (Cat. No. HPA073498-100UL), γ-H2AX and β-Actin using methods as described (Merck, 2020). In brief, proteins separated on SDS-PAGE were transferred to nitrocellulose membrane and blocked with 5% BSA. Thereafter adding primary antibodies in the dilution of 1:1,000, the blots were washed and probed with the respective secondary antibodies (Merck Inc.) coupled with horseradish peroxidase (Merck Inc.). The secondary antibody in a dilution of 1:2,000 was used. The bands were developed using the chemiluminescence reagent (Millipore) and captured onto Biomax light film (Eastman Kodak Co., Rochester, NY).

## Immunocytochemistry (ICC)

The cells were subjected to ICC to assess the localization and expression of *ANKLE1* and γH2AX. The cells cultured in chambered slides were fixed using paraformaldehyde. After washing the cells with PBS, permeabilization was done using 0.3% of Triton-X for 10 min. The cells were then subjected to primary anti-Rabbit and anti- Mouse antibody (*ANKLE1*, Merck Inc.) treatment overnight for 3 h, at 4°C, washed and then incubated with secondary antibody for *ANKLE1* and γH2AX for 2 h. at RT. DAPI was used as a counter stain. After pouring the mounting media and coverslip placement the visualization was done with 2X Floid® microscope (FLoid Cell Imaging Station).

## *ANKLE1* siRNA Knockdown

MCF-7 cells were seeded in six well chamber slides and transfected using X-treme Gene$^{TM}$ (Merck Inc.). *ANKLE1* siRNA (Merck Inc.) was employed to knockdown the gene expression. RNA scramble was used as siRNA control. These cells were checked for expression of *ANKLE1* immunoblotting. Following the siRNA treatment, the cells were treated with cisplatin and the cell lysates were obtained and used for immunoblotting and immunocytochemistry. **Supplementary Table 3** shows the siRNA sequences used.

## Statistical Analysis

The values were subjected to densitometry analysis and *t*-test to analyze their statistical significance. All images were representative of three fields. The relative increase in the protein expression of *ANKLE1* at 4–24 h duration, for the western blot, were checked for statistical significance and found to be statistically significant with $p < 0.0001$. The relative decrease in the γH2AX expression with the increase in the *ANKLE1* expression was found to be statistically significant ($p < 0.0001$).

## Ethical Clearance

The study was approved by the Institutional Ethics Review Board (IERB) of Shri Mata Vaishno Devi University (SMVDU) (SMVDU/IERB/18/70). Written informed consent was obtained from each participant before conducting the study. All experimental protocols were conducted according to the guidelines and regulations set by IERB, SMVDU.

# RESULTS

## WES Analysis Showed Mutant in *ANKLE1*

Plenitude of variations outside of the limited known pool are involved to impede the DNA repair processes. To better understand these variants that might be directly or indirectly involved in the DNA damage process, thus allying cancer progression, we performed the whole exome sequencing of the breast cancer samples. The effect of the variation was predicted based on their score levels. We assessed several gene variants and observed certain variants to be consistent in several samples. Located on chromosome 19, *ANKLE1* showed varied exonic, intronic, intergenic and upstream variations (**Supplementary Table 2**).

## Mass Array SNP Genotyping Showed Higher Frequency of GT Over GG in *rs2363956*

We next sought to determine the other potential repetitive variant locus of *ANKLE1* gene, rs2363956. Another locus on the *ANKLE1* elucidated in the whole exome sequencing was studied through the SNP Mass array genotyping. The studied variant rs2363956, on the *ANKLE1* gene, is a missense type of variant with T > G change. On comparing the difference of expression between genotypes GT and GG at rs2363956 in *ANKLE1* gene through the mass array SNP genotyping of subjects, we found that the genotype GT confers protection to the individual as compared to the genotype GG. It was found that the allele T within the rs2363956, with an OR of 0.7011 indicated a low risk of breast cancer. The allele frequency of allele T in cases was 0.37 and 0.45 in controls. The allele frequency of allele G was 0.63 in cases and 0.55 in controls. Thus, the genotype GT confers protection to the individual as compared to the GG genotype. The genotypes followed the Hardy Weinberg equilibrium (H.W.E, *p*-value 0.732) and were statistically significant ($p = 0.02246$) to our population. Data suggests that breast cancer is more frequent in patients carrying rs2363956 GT genotype than those carrying GG genotype.

## DNA Damage Responsive Increase in ANKLE1 Protein in MCF-7 Cells

We further explored the functional significance of *ANKLE1* gene after treatment with cisplatin, a known DNA damaging drug. MCF-7 cell line was treated with 25 μM cisplatin for different time intervals: 0, 4, 8, 16, and 24 h. Along with the increase in the treatment time of cisplatin, a slight increase in the cell volume, that is indicative of DNA damage, was seen. After encountering

the stress stimulus triggered by cisplatin, the cells increase in volume and swell (Fulda et al., 2010). Cisplatin acts as a DNA damaging agent thus a potent stress signal for the cells. **Figure 1A** shows the images of the cells captured at different time interval of treatment. Cells treated at 0 h serve as control, whereas the cells captured at 24 h treatment seem to be inflated.

To investigate the contribution of *ANKLE1* gene in DNA repair in relation to breast cancer we assessed the expression levels under different exposure time intervals. Treated cells were analyzed for protein expression through western blotting. It was found that with the increase in the time of cisplatin treatment the expression of *ANKLE1* protein subsequently increased in the cells. The expression of *ANKLE1* was found to be gradually increasing with the increase in the treatment time, highest being at 24 h. However, the expression of γH2AX was inversely related to the *ANKLE1* expression levels. A high γH2AX was found where the *ANKLE1* expression was low and vice versa. The increased expression of γH2AX signals for DNA damage, however, with the increase in the *ANKLE1* expression the γH2AX was found to be relative decreased (**Figure 1B**). β-Actin served as a control and had a leveled expression. The values were subjected to *t*-test to analyze their statistical significance. The relative decrease in the γH2AX expression with the increase in the *ANKLE1* expression was studied. **Figure 1C** represents the statistical values of *ANKLE1* and γH2AX expression. The values were found to be statistically significant ($p < 0.0001$).

## DNA Damage Changes ANKLE1 Protein Localization

Given the key role of *ANKLE1* in breast cancer, we speculated that *ANKLE1* might be localized near the nuclear membrane considering its shuttling property inside the cytoplasm and nucleus. To analyze the localization and expression of the proteins under study, immunocytochemistry was performed. Vehicle served as the control, i.e., cells without the cisplatin treatment. Anti-Rabbit secondary antibody was used for *ANKLE1* and florescence was observed at 488λ (green color). Anti-Mouse secondary antibody was used for γH2AX and florescence was observed at 488λ. DAPI served as the counter stain and stained the nucleus (blue color).

As shown in **Figure 2B**, the expression of *ANKLE1* increased substantially, when the cells were treated with 25 μm of cisplatin, as compared to the vehicle. The overlay images showed the expression of *ANKLE1* inside the nucleus and in the cytoplasm, being highest around the nuclear membrane. **Figure 2A** shows that the expression of γH2AX was mitigated in cells that were treated with 25 μm cisplatin (with a higher expression of *ANKLE1*) as compared to the untreated cells. DAPI served as the counter stain and stained the nucleus. The overlay images showed the expression of γH2AX in the nucleus. The decrease in the expression of γH2AX corresponded to the increase in the *ANKLE1* expression.

## Knockdown of *ANKLE1* Gene Using si*ANKLE1*

The *ANKLE1* gene was knocked down using si*ANKLE1* and the expression of the proteins was studied. We found that as compared to the vehicle or the control, the expression of *ANKLE1* was increased when the cells were treated with 25 μm cisplatin (**Figure 3A**). The expression of the scramble was equivalent to the expression of the control. The si*ANKLE1* treated cells showed a decreased level expression of *ANKLE1* as compared to the

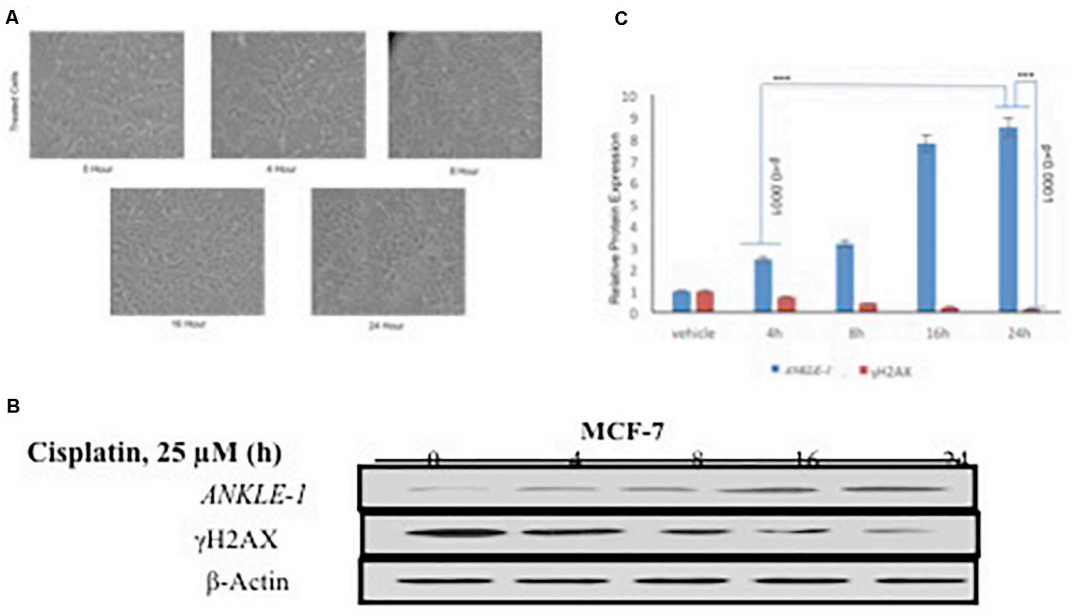


**FIGURE 1 | (A)** MCF-7 Breast Cancer cell line at different time interval of cisplatin treatment. **(B)** Western blotting for *ANKLE1*, γH2AX and β-Actin. **(C)** Expression levels of *ANKLE1* & γH2AX at different time intervals.

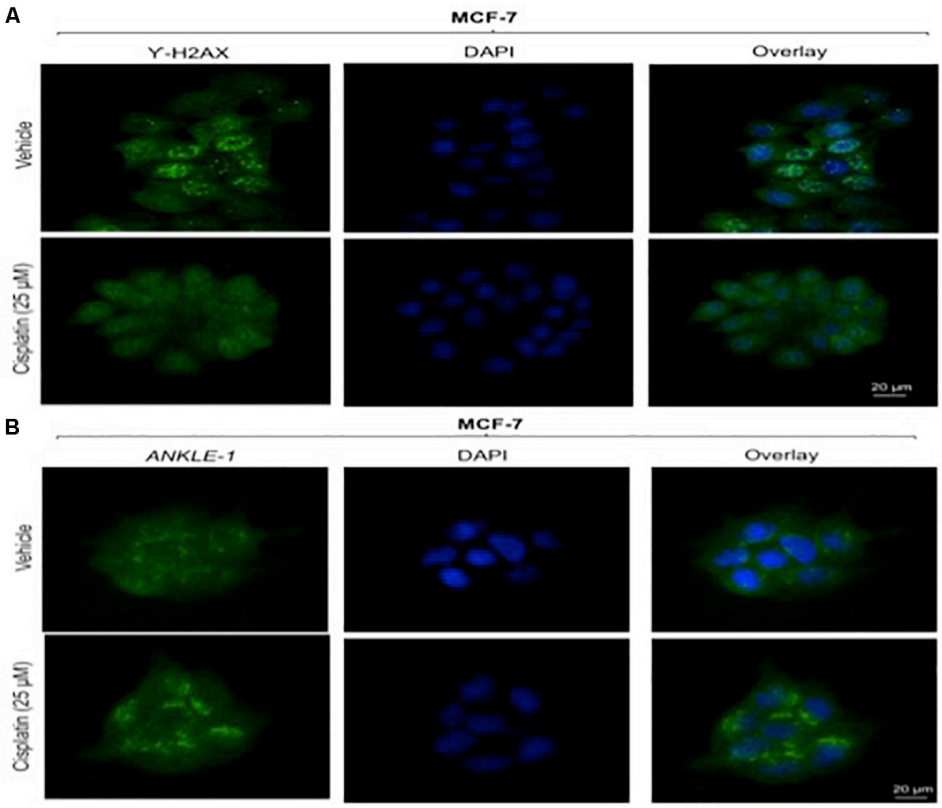


**FIGURE 2 | (A)** Image showing ICC images of γH2AX in vehicle and treated cells. **(B)** Image showing ICC images of *ANKLE1* in vehicle and treated cells. ICC was performed to check the expression and localization of the proteins. The cells were fixed using 4% paraformaldehyde for 15 min at RT. Permeabilization was done using 0.3% Triton X for 10 min at RT and Blocking was done using PBS for 30 min. After addition of primary antibody (1:100) and secondary antibody (1:500) visualization was done in FLoid© Cell Imaging Station.

vehicle/control. The *ANKLE1* expression failed to increase when the si*ANKLE1* treated cells were treated with 25 μm cisplatin. The expression of γH2AX was decreased when the cells were treated with 25 μm cisplatin. However, when the cells were treated with si*ANKLE1* the expression of the γH2AX increased and elevated further when the si*ANKLE1* treated cells were treated with 25 μm cisplatin, nuancing toward an enhanced DNA damage in absence of *ANKLE1* protein.

Adequate levels of β-Actin were observed in the cells and served as a positive control. As shown in **Figure 3B**, the values were found to be statistically significant ($p < 0.0001$).

## Immunocytochemistry (ICC) Analysis After Treatment With si*ANKLE1*

To further test whether the ability of the expression of the protein was affected we performed immunocytochemistry. The knockdown of the target gene was performed using si*ANKLE1* and immunocytochemistry study was done. **Figure 3B** shows the *ANKLE1* protein's expression in the treated and untreated cells, in the absence and presence of *siANKLE1*. As compared to the vehicle/control the treated cells showed an increased expression of *ANKLE1* protein. The scramble had a comparable expression to the control. When the cells were treated with si*ANKLE1*, the expression of *ANKLE1* lowered and further decreased when si*ANKLE1* cells were treated with 25 μm cisplatin (**Figure 4B**).

Also, the expression of γH2AX was analyzed when the cells were treated with si*ANKLE1* (**Figure 4A**). γH2AX expression, as verified previously, decreased when the cells were treated with 25 μm cisplatin. However, its expression was elevated when the cells were treated with si*ANKLE1* and was increased further when the si*ANKLE1* cells were treated with 25 μm cisplatin showing a higher DNA damage in the cells. The merged images show the presence of γH2AX in nucleus by staining with DAPI, which stains the nucleus. ICC images correlated with the expression levels of si*ANKLE1* and γH2AX and highlighted the si*ANKLE1* location inside the nucleus and around the nuclear membrane.

# DISCUSSION

The aim of the study was to evaluate the role of *ANKLE1,* identified through whole exome sequencing, in DNA repair process. We have reported the role of *ANKLE1* in DNA repair process, it's mitigating action on the DNA damage in MCF-7 cell lines and an elevated DNA damage with knockdown of *ANKLE1* gene. In the present study we also studied the polymorphic variant of *ANKLE1* or the LEM3 gene. Whole-exome sequencing

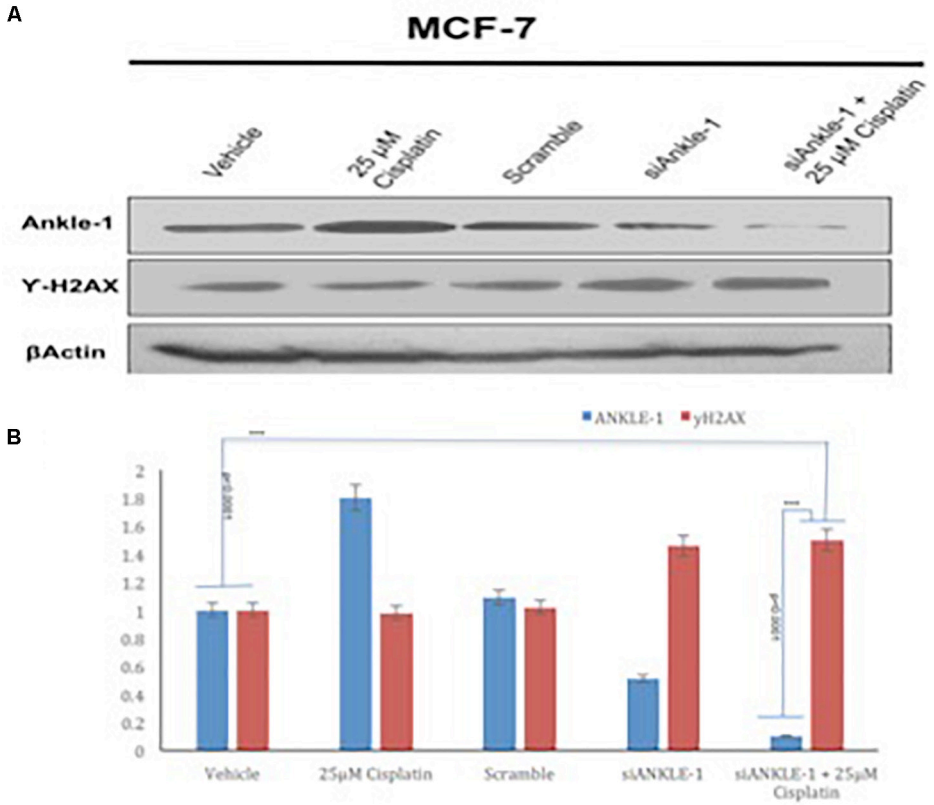


**FIGURE 3 | (A)** Western blot for *ANKLE1*, γH2AX and β-Actin. **(B)** Expression levels of *ANKLE1* & γH2AX subsequent to treatments.

is a diagnostic approach for the identification of molecular defects in patients with suspected genetic disorders (Yang et al., 2013). *ANKLE1* gene is the human ortholog of LEM-3 gene and is conserved among species. *ANKLE1* contains a GIY-YIG endonuclease domain that is also present in the endonuclease SLX-1. *ANKLE1* like SLX-1 is involved in resolving the holliday-junction (Wyatt and West, 2014) through it's resolvase activity and takes part in the Homologous recombination process of DNA repair (Saito et al., 2013). Several studies have implicated the mutations in *ANKLE1* gene to the development of breast and ovarian cancers indication its role in the DNA damage repair process (Bolton et al., 2010; Stevens et al., 2011). In this study we have demonstrated that *ANKLE1*, a potential DNA repair candidate, repairs the DNA damage caused by the treatment of MCF-7 cells with cisplatin. The role of H2AX is conspicuous with it being a biomarker of the DNA damage in the cells (Linda and Yang, 2008). The double strand break in the DNA leads to the phosphorylation of H2AX into γH2AX triggering it as being a initiator DNA damage repair machinery (Kobayashi, 2004). The phosphorylation of serine 139 on histone H2AX (Emmy et al., 1997) is rapid process, propagating swiftly from double stranded breaks (Lowndes and Toh, 2005). Interestingly, we found that when the cells were treated with cisplatin, a DNA damaging agent, the γH2AX subsequently decreased in the cells. This decrease in the γH2AX was relatable to the corresponding increase in the *ANKLE1* expression in the cells. *ANKLE1* is involved in the DNA damage response and DNA repair pathways (Brachner and Foisner, 2014). Our studies showed that when expression of *ANKLE1* was knocked down, the expression of γH2AX got elevated, indicating a higher DNA damage in absence of *ANKLE1* protein. Although it would be over ambitious to imply that *ANKLE1* is directly involved in DNA repair process, however, we suggest a collaborative effort of DNA repair proteins, working in conjugation to achieve the DNA repair target. *ANKLE1* has been shown to bind with the BAF family of proteins, which are shown to be involved in gene regulation processes (Brachner et al., 2012). The induction of DNA damage by cisplatin potentially triggered the *ANKLE1* for the DNA damage repair and lowered the expression of γH2AX. Since γH2AX gives the measure of DNA damage in the cell, we can state the role of *ANKLE1* in DNA repair process. The *ANKLE1* gene offers a magnanimous prospect in the cancer therapeutics. The overexpression of *ANKLE1* in mammalian cells has shown to trigger the DNA damage response, whereas, knocking out the LEM-3 gene which is ortholog of *ANKLE1*, in *C. elegans* attributes to an increased sensitivity to DNA damaging agents (Brachner and Foisner, 2014). Thus *ANKLE1* poses to be a promising candidate to explore for curtailing the extensive spread of the neoplastic disease.

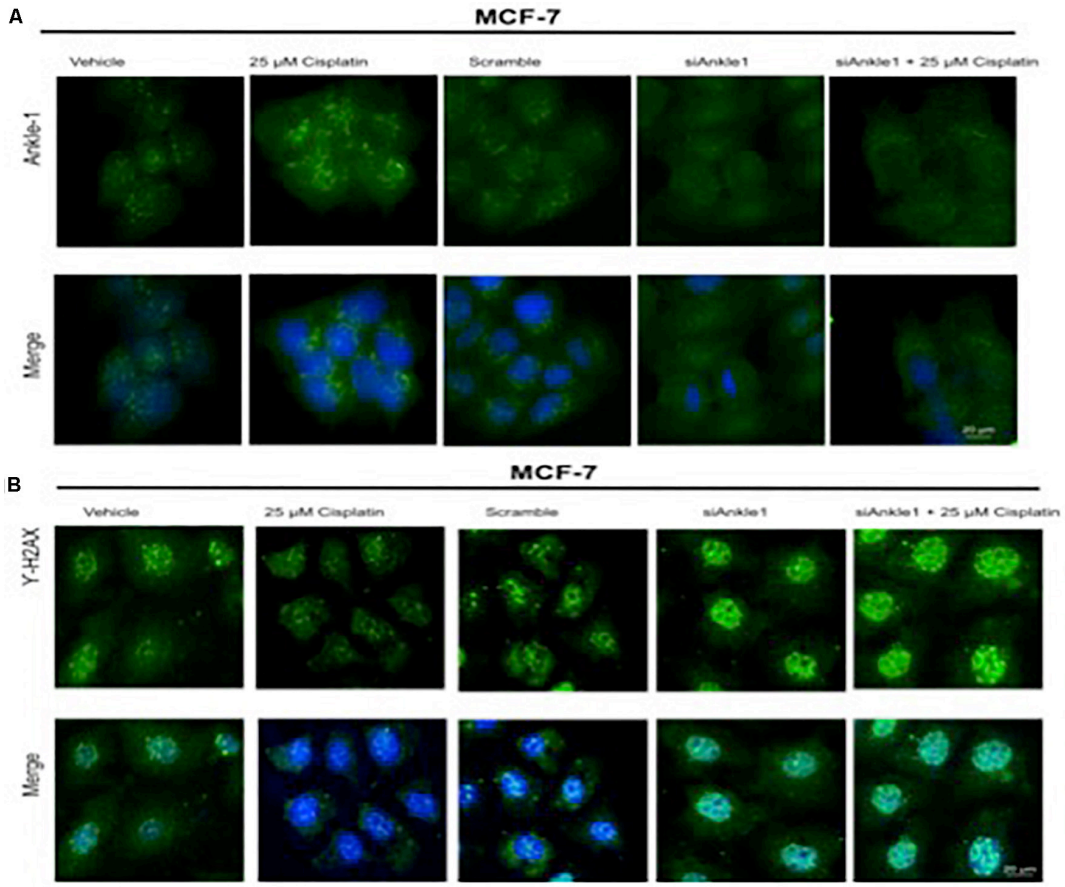


**FIGURE 4 | (A)** Image showing ICC images of *ANKLE1* in vehicle and treated cells. **(B)** Image showing ICC images of γH2AX in vehicle and treated cells. The cells were treated with siANKLE1 and their expression was analyzed. The treated cells were fixed on the chamber slides by using 4% paraformaldehyde for 15 min at RT. The cells were permeabilized using 0.3 Triton X for 10 min at RT and Blocking was done using PBS for 30 min. After addition of primary antibody (1:100) and secondary antibody (1:500) visualization was done in FLoid® Cell Imaging Station.

## CONCLUSION

Breast cancer is a multifactorial disease that has become the most common cancer in Indian women. Despite its common prevalence there is a lacuna in the data regarding the genetic framework of the disease especially in the population of Jammu and Kashmir. The Whole Exome Sequence study gave us an insight into thousands of single nucleotide variations in the genome of breast cancer patients. Few variants were found to be consistent in numerous samples under study. Through the mass array genotyping we confirmed the disease-associated genotype in 550 samples The knockdown study performed with siRNA *ANKLE1*, highlighted the increase in *ANKLE1* expression with the DNA damaging agent cisplatin, however, with the si*ANKLE1* (siRNA *ANKLE1*) treatment, the *ANKLE1* expression decreased. γH2AX was conversely related to the *ANKLE1* expression degree. The siRNA *ANKLE1* treated cells showed a basal expression of *ANKLE1*, which failed to increase with the cisplatin treatment. On the contrary, when treated with siRNA *ANKLE1*, the γH2AX expression was found to be elevated in the cells indicating a high DNA damage. The localization of the *ANKLE1* protein was found to be concentrated near the nuclear membrane congruent with its property of shuffling between nucleus and cytoplasm. Since only few proteins associated with DNA organization or repair have the NIS (Nucleus Import signal) enter the nucleus, this property further establishes the role of *ANKLE1* in DNA damage response. Since *ANKLE1* has been a player before in some cancers, further intensive study could be done to investigate the role of *ANKLE1* and its potential role in DNA repair mechanism in various cancers. *ANKLE1* gene be further validated and exploited for developing a novel approach toward breast cancer diagnosis and treatment. Further the limitations of this study should be catered to by studying the expression of *ANKLE1* in triple negative cells along with the checking the co-occurrence of other markers like ATM, P53, NF-κB, and TWIST.

## DATA AVAILABILITY STATEMENT

The original contributions presented in the study are included in the article/**Supplementary Material**, further inquiries can be directed to the corresponding author/s.

## ETHICS STATEMENT

The studies involving human participants were reviewed and approved by the Institutional Ethical Review Board (IERB) (SMVDU/IERB/18/70) of Shri Mata Vaishno Devi University. The patients/participants provided their written informed consent to participate in this study. Written informed consent was obtained from the individual(s) for the publication of any potentially identifiable images or data included in this article.

## AUTHOR CONTRIBUTIONS

RK designed the study. DB and AK performed the experiments and extrapolated results. DB wrote the manuscript. SC helped with the experimental work. AN, RS, SV, AB, GB, and BS helped in sample collection. AG and SV helped in guiding the study. All authors contributed to the article and approved the submitted version.

## ACKNOWLEDGMENTS

We were grateful to Dr. Swarkar Sharma for his help in genotype analysis. RK and DB acknowledge research grants SERB/YSS/2014/00659 and DST/SSTP/J&K/459.

## SUPPLEMENTARY MATERIAL

The Supplementary Material for this article can be found online at: https://www.frontiersin.org/articles/10.3389/fgene.2020.609758/full#supplementary-material

## REFERENCES

Bolton, K. L., Tyrer, J., Song, H., Ramus, S. J., Notaridou, M., Jones, C., et al. (2010). Common variants at 19p13 are associated with susceptibility to ovarian cancer. *Nat. Genet.* 42, 880–884.

Bolton, K. L., Tyrer, J., Song, H., Ramus, S. J., Notaridou, M., Jones, C., et al. (2016). Corrigendum: common variants at 19p13 are associated with susceptibility to ovarian cancer. *Nat. Genet.* 48:101.

Brachner, A., Braun, J., Ghodgaonkar, M., Castor, D., Zlopasa, L., Ehrlich, V., et al. (2012). The endonuclease Ankle1 requires its LEM and GIY-YIG motifs for DNA cleavage in vivo. *J. Cell Sci.* 125(Pt 4), 1048–1057. doi: 10.1242/jcs.098392

Brachner, A., and Foisner, R. (2014). Lamina-associated polypeptide (LAP)2α and other LEM proteins in cancer biology. *Adv. Exper. Med. Biol.* 773, 143–163. doi: 10.1007/978-1-4899-8032-8_7

Brachner, A., Medini, G., Dennis, C., Livija, Z., Veronika, E., and Josef, G. (2011). The endonuclease Ankle1 requires its LEM and GIY-YIG motifs for DNA cleavage in vivo. *J. Cell Sci.* 125(Pt 4), 1048–1057.

Brookes, A. J. (1999). The essence of SNPs. *Gene* 234, 177–186. doi: 10.1016/s0378-1119(99)00219-x

Ciriello, G., Miller, M. L., Aksoy, B. A., Senbabaoglu, Y., Schultz, N., and Sander, C. (2013). Emerging landscape of oncogenic signatures across human cancers. *Nat. Genet.* 45, 1127–1133. doi: 10.1038/ng.2762

Douglas, F. E., Karen, A. P., and Alison, D. M. (2007). Genome-wide association study identifies novel breast cancer susceptibility loci. *Nature* 447, 1087–1093.

Emmy, P. R., Pilch, D. R., Orr, A. H., Ivanova, V. S., and Bonner, W. M. (1997). DNA Double-stranded breaks induce histone H2AX phosphorylation on Serine 139. *J. Biol. Chem.* 273, 5858–5868. doi: 10.1074/jbc.273.10.5858

Fulda, S., Gorman, A. M., Hori, O., and Samali, A. (2010). Cellular stress responses: cell survival and cell death. *Int. J. Cell Biol.* 2010:214074.

Gomes, L. R., Menck, C. F. M., and Leandro, G. S. (2017). Autophagy roles in the modulation of DNA repair pathways. *Int. J. Mol. Sci.* 18:2351. doi: 10.3390/ijms18112351

Hoeijmakers, J. H. J. (2001). Genome maintenance mechanisms for preventing cancer. *Nature* 411, 366–374. doi: 10.1038/35077232

Johar, A. S., Adriana, R. V., Hardip, R. P., Aaron, C., Kaiman, P., and Angela, H. (2015). Novel and rare functional genomic variants in multiple autoimmune syndrome and Sjögren's syndrome. *J. Transl. Med.* 13:173.

Kobayashi, J. (2004). Molecular mechanism of the recruitment of NBS1/hMRE11/hRAD50 complex to DNA double-strand breaks: NBS1 binds to γ-H2AX through FHA/BRCT domain. *J. Radiat. Res.* 45, 473–478. doi: 10.1269/jrr.45.473

Kristen, N. S., Adam, M. L., Susan, S., Timothy, L., Curtis, O., and Peter, A. F. (2011). Common breast cancer susceptibility loci are associated with triple-negative breast cancer. *Cancer Res.* 71, 6240–6249.

Lacy, J. B., Alexey, A. S., and Pamela, K. G. (2016). Networking in the nucleus: a spotlight on LEM-domain proteins. *Curr. Opin. Cell Biol.* 34, 1–8. doi: 10.1016/j.ceb.2015.03.005

Lam, S. W., Jimenez, C. R., and Boven, E. (2014). Breast cancer classification by proteomic technologies: current state of knowledge. *Cancer Treat. Rev.* 40, 129–138. doi: 10.1016/j.ctrv.2013.06.006

Lawrenson, K., Kar, S., McCue, K., Kuchenbaeker, K., Michailidou, K., Tyrer, J., et al. (2016). Functional mechanisms underlying pleiotropic risk alleles at the 19p13.1 breast-ovarian cancer susceptibility locus. *Nat. Commun.* 7:12675.

Linda, J., and Yang, L. (2008). γ-H2AX - a novel biomarker for DNA double-strand breaks. *In Vivo* 22, 305–309.

Lowndes, N. F., and Toh, G. W. (2005). DNA repair: the importance of phosphorylating histone H2AX. *Curr. Biol.* 15, R99–R102.

Majidinia, M., and Yousefi, B. (2017). DNA repair and damage pathways in breast cancer development and therapy. *DNA Repair.* 54, 22–29. doi: 10.1016/j.dnarep.2017.03.009

Merck (2020). *SDS-Polyacrylamide Gel Electrophoresis (PAGE)*. Available at https://www.sigmaaldrich.com/life-science/molecular-biology/molecular-biologyproducts.html?TablePage=9622721&gclid=EAIaIQobChMIx5eb1WF6gIVin0rCh2FSgTeEAAYASAAEgJo0vD_BwE

Miranda, M., and Fidier, F. B. I. S. (2018). The global cancer burden and human development: a review. *Scand. J. Public Health* 46, 27–36. doi: 10.1177/1403494817715400

Noetzli, L., Lo, R. W., Lee-Sherick, A. B., Callaghan, M., Noris, P., Savoia, A., et al. (2015). Germline mutations in ETV6 are associated with thrombocytopenia, red cell macrocytosis and predisposition to lymphoblastic leukemia. *Nat. Genet.* 47, 535–538. doi: 10.1038/ng.3253

Oeth, P., Mistro, Gd, Marnellos, G., Shi, T., and Boom, D. (2009). Qualitative and quantitative genotyping using single base primer extension coupled with matrix-assisted laser Desorption/ionization time-of-flight mass spectrometry (MassARRAY) Single nucleotide polymorphisms. *Methods Mol. Biol.* 578, 307–343. doi: 10.1007/978-1-60327-411-1_20

Paul, D. P., Pharoah, A. A., Martin, B., Ron, L. Z., Douglas, F. E., and Bruce, A. J. P. (2002). Polygenic susceptibility to breast cancer and implications for prevention. *Nat. Genet.* 31, 33–36. doi: 10.1038/ng853

Paula, S., Lesley, M., and Douglas, F. E. (2009). A genome wide linkage search for breast cancer susceptibility gene. *Genes Chromosom. Cancer* 45, 646–655.

Rabbani, B., Mahdieh, N., Hosomichi, K., Nakaoka, H., and Inoue, I. (2012). Next-generation sequencing: impact of exome sequencing in characterizing Mendelian disorders. *J. Hum. Genet.* 57, 621–632. doi: 10.1038/jhg.2012.91

Roos, W. P., and Kaina, B. (2013). DNA damage-induced cell death: from specific DNA lesions to the DNA damage response and apoptosis. *Cancer Lett.* 332, 237–248. doi: 10.1016/j.canlet.2012.01.007

Rosenbloom, K. R., Timothy, R. D., and Jeffrey, C. L. (2012). ENCODE whole-genome data in the UCSC genome browser: update 2012. *Nucleic Acids Res.* 40, D912–D917.

Saito, T. T., Lui, D. Y., Kim, H. M., Meyer, K., and Colaiacovo, M. P. (2013). Interplay between structure-specific endonucleases for crossover control during *Caenorhabditis elegans* meiosis. *PLoS Genet.* 9:e1003586. doi: 10.1371/journal.pgen.1003586

Simon, N. S., Andrei, M., Patrick, S., Thorunn, R., and Julius, G. (2007). Common variants on chromosomes 2q35 and 16q12 confer susceptibility to estrogen receptor-positive breast cancer. *Nat. Genet.* 39, 865–869. doi: 10.1038/ng2064

Stevens, K. N., Vachon, C. M., Lee, A. M., Slager, S., Lesnick, T., Olswold, C., et al. (2011). Common breast cancer susceptibility loci are associated with triple-negative breast cancer. *Cancer Res.* 71, 6240–6249.

Takashi, S., Terada, M., Jun, Y., Setsuo, H., and Keiji, W. (1992). Multiple gene alterationsin human carcinogenesis. *Environ. Health Perspect.* 98, 5–12.

Walsh, T., Coats, K. H., Swisher, E., Stray, S. M., Higgins, J., and Kevin, C. R. (2006). Spectrum of mutations in BRCA1, BRCA2, CHEK2, and TP53 in families at high risk of breast cancer. *Am. Med. Assoc.* 295, 1379–1388. doi: 10.1001/jama.295.12.1379

Wyatt, H. D., and West, S. C. (2014). Holliday junction resolvases. *Cold Spring Harb. Perspect. Biol.* 6:a023192.

Yang, Y., Muzny, D. M., Reid, J. G., Bainbridge, M. N., Willis, A., Ward, P. A., et al. (2013). Clinical whole-exome sequencing for the diagnosis of mendelian disorders. *N. Engl. J. Med.* 369, 1502–1511.

**Conflict of Interest:** The authors declare that the research was conducted in the absence of any commercial or financial relationships that could be construed as a potential conflict of interest.

frontiers in Genetics

ORIGINAL RESEARCH
published: 04 February 2021
doi: 10.3389/fgene.2021.634615

# Effects of Conserved Wedge Domain Residues on DNA Binding Activity of *Deinococcus radiodurans* RecG Helicase

OPEN ACCESS

**Edited by:**
*Hari S. Misra, Bhabha Atomic Research Centre (BARC), India*

**Reviewed by:**
*Issay Narumi, Toyo University, Japan*
*Huiming Lu, University of Texas Southwestern Medical Center, United States*
*Joanna Timmins, UMR5075 Institut de Biologie Structurale (IBS), France*

***Correspondence:**
*Sangyong Lim*
*saylim@kaeri.re.kr*

*†These authors have contributed equally to this work*

**Specialty section:**
*This article was submitted to Genetics of Common and Rare Diseases, a section of the journal Frontiers in Genetics*

**Received:** *06 December 2020*
**Accepted:** *18 January 2021*
**Published:** *04 February 2021*

**Citation:**
*Jeong S-W, Kim M-K, Zhao L, Yang S-K, Jung J-H, Lim H-M and Lim S (2021) Effects of Conserved Wedge Domain Residues on DNA Binding Activity of Deinococcus radiodurans RecG Helicase. Front. Genet. 12:634615. doi: 10.3389/fgene.2021.634615*

***Sun-Wook Jeong*[1,2†], *Min-Kyu Kim*[1†], *Lei Zhao*[1], *Seul-Ki Yang*[1], *Jong-Hyun Jung*[1,3], *Heon-Man Lim*[2] *and Sangyong Lim*[1,3*]**

[1]*Radiation Research Division, Korea Atomic Energy Research Institute, Jeongeup, South Korea,* [2]*Department of Biological Sciences, College of Biological Sciences and Biotechnology, Chungnam National University, Daejeon, South Korea,* [3]*Department of Radiation Science and Technology, University of Science and Technology, Daejeon, South Korea*

*Deinococcus radiodurans* is extremely resistant to ionizing radiation and has an exceptional ability to repair DNA damage caused by various DNA-damaging agents. *D. radiodurans* uses the same DNA-repair strategies as other prokaryotes, but certain proteins involved in the classical DNA repair machinery have characteristics different from their counterparts. RecG helicase, which unwinds a variety of branched DNA molecules, such as Holliday junctions (HJ) and D-loops, plays important roles in DNA repair, recombination, and replication. Primary sequence analysis of RecG from a number of bacterial species revealed that three amino acids (QPW) in the DNA-binding wedge domain (WD) are well-conserved across the *Deinococcus* RecG proteins. Interactions involving these conserved residues and DNA substrates were predicted in modeled domain structures of *D. radiodurans* RecG (DrRecG). Compared to the WD of *Escherichia coli* RecG protein (EcRecG) containing FSA amino acids corresponding to QPW in DrRecG, the HJ binding activity of DrRecG-WD was higher than that of EcRecG-WD. Reciprocal substitution of FSA and QPW increased and decreased the HJ binding activity of the mutant WDs, EcRecG-$WD_{QPW}$, and DrRecG-$WD_{FSA}$, respectively. Following $\gamma$-irradiation treatment, the reduced survival rate of DrRecG mutants (Δ*recG*) was fully restored by the expression of DrRecG, but not by that of EcRecG. $EcRecG_{QPW}$ also enhanced $\gamma$-radioresistance of Δ*recG*, whereas $DrRecG_{FSA}$ did not. Δ*recG* cells complemented *in trans* by DrRecG and $EcRecG_{QPW}$ reconstituted an intact genome within 3 h post-irradiation, as did the wild-type strain, but Δ*recG* with EcRecG and $DrRecG_{FSA}$ exhibited a delay in assembly of chromosomal fragments induced by $\gamma$-irradiation. These results suggested that the QPW residues facilitate the association of DrRecG with DNA junctions, thereby enhancing the DNA repair efficiency of DrRecG.

**Keywords: *Deinococcus radiodurans*, radiation resistance, DNA repair, RecG helicase, wedge domain**

## INTRODUCTION

*Deinococcus radiodurans* is well known for its extreme resistance to lethal doses of ionizing radiation (IR) and many other DNA damaging agents, including mitomycin C (MMC), UV-C radiation, and desiccation (Slade and Radman, 2011). This remarkable resistance is thought to be attributed to its highly efficient DNA repair capacity and various anti-oxidative systems (Lim et al., 2019). In *D. radiodurans*, extensive IR-induced DNA double-strand breaks (DSBs), which are the most lethal form of DNA damage, can be mended within a few hours (Zahradka et al., 2006). The rapid reconstruction of an intact genome from hundreds of chromosomal fragments is achieved through extended synthesis-dependent strand annealing (ESDSA), followed by homologous recombination (HR; Zahradka et al., 2006).

ATP-dependent duplex DNA unwinding enzymes, termed DNA helicases, are prevalent in all kingdoms of life and play important roles in the processes of DNA replication, repair, recombination, etc. (Brosh and Matson, 2020). The human genome encodes for 31 nonredundant DNA helicases (Umate et al., 2011). Given their fundamental roles in DNA metabolism, mutations in some of these genes are associated with certain human diseases characterized by premature aging and cancer, including Xeroderma Pigmentosum, Cockayne Syndrome, and Werner Syndrome (Uchiumi et al., 2015). Since DNA helicase was first discovered in the model bacterium *Escherichia coli* (Brosh and Matson, 2020), the *E. coli* helicases have been intensively studied, and their function has been compared to that of counterparts identified in different organisms. In *E. coli*, HR initiation follows the RecBCD pathway. The RecBCD complex binds to double-stranded DNA (dsDNA) ends and unwinds and degrades the DNA by using a combination of helicase and nuclease activities, which promotes the repair of DSB (Rocha et al., 2005). *D. radiodurans* is devoid of RecB and RecC proteins but possesses a RecD homolog named RecD2 (Wang and Julin, 2004). Since RecD2 is present in *recBC*-minus organisms, it is not associated with RecBC (Montague et al., 2009). The *D. radiodurans* RecD2 protein is a DNA helicase with 5'-3' polarity and low processivity (Wang and Julin, 2004). *recD2* mutants are more sensitive than wild type cells to the cytotoxic effect of γ-irradiation, UV light, and hydrogen peroxide ($H_2O_2$; Servinsky and Julin, 2007; Zhou et al., 2007), but *recD2* mutations does not alter the sensitivity of *D. radiodurans* to treatment with mitomycin C (MMC), methyl methanesulfonate, and hydroxyurea (Servinsky and Julin, 2007; Montague et al., 2009). *D. radiodurans* lacks not only RecBC, but also exonuclease I (SbcB), hence DSBs in *D. radiodurans* are repaired by the RecFOR pathway, which is significantly more common than RecBCD in bacterial genomes (Rocha et al., 2005). RecFOR-dependent DSB repair is initiated by unwinding duplex DNA, followed by DNA end resection that degrades the broken ends in the 5'–3' direction to obtain 3' single-stranded DNA (ssDNA) tails (Rocha et al., 2005).

In *E. coli*, RecQ is the major helicase implicated in the RecFOR pathway and in nucleolytic degradation catalyzed by RecJ; however, in *D. radiodurans*, RecQ is dispensable (Bentchikou et al., 2010). Different results have been reported with respect to *recQ* mutant phenotypes: a *recQ* mutant strain was reported to be sensitive to γ-irradiation, UV, $H_2O_2$, and MMC (Huang et al., 2007), whereas another study showed that *recQ* mutant cells display wild-type resistance to γ-irradiation (Bentchikou et al., 2010). Recently, RecD2 and RecQ proteins from *D. radiodurans* were reported to be able to unwind guanine quadruplex (G4) DNA structures (Khairnar et al., 2019; Xue et al., 2020). Instead of RecQ, in *D. radiodurans*, the UvrD helicase, which can unwind duplex DNA in both the 3'–5' and 5'–3' directions (Stelter et al., 2013), plays a critical role in DSB repair and reconstitution of the genome following IR exposure (Bentchikou et al., 2010). However, the *uvrD* mutant still retained significant radio-resistance as compared to a repair-deficient *recA* mutant strain, suggesting that the redundant activity of other helicase(s) is responsible for the residual DNA repair capacity observed (Bentchikou et al., 2010).

The RecFOR complex loads RecA onto ssDNA substrates, thereby resulting in the formation of a RecA nucleoprotein filament that searches for homology and then invades the double-stranded homologous DNA (Bentchikou et al., 2010). RecA-mediated strand invasion creates a D-loop, and primes DNA polymerase III (Pol III)- and/or Pol I-dependent DNA synthesis (Slade et al., 2009). DNA synthesis proceeds *via* a migrating D-loop, in which the unwinding of the dsDNA template may be mediated by UvrD, RecD2, RecQ, RuvAB, and/or other helicases (Slade and Radman, 2011). The RuvABC system can displace and resolve a four-way DNA intermediate named the Holliday junction (HJ). The RuvAB and RuvC proteins catalyze branch migration and the resolution of HJ recombination intermediates, respectively (Rocha et al., 2005). The *D. radiodurans ruvB* mutant is modestly sensitive to UV light, γ-irradiation, and MMC (Kitayama et al., 1997). However, the fact that inactivation of both *ruv* and *recG* resulted in a more dramatic increase in the sensitivity of cells to DNA damaging-agents has led to the suggestion that RecG and RuvABC are part of two overlapping pathways for processing intermediates in HR and DNA repair (Lloyd and Rudolph, 2016). The deletion of *recG* resulted in a growth delay and a decrease in the resistance of *D. radiodurans* to γ-irradiation and $H_2O_2$ (Wu et al., 2009).

RecG, a monomeric dsDNA translocase that unwinds a variety of branched DNA molecules, such as replication forks, HJs, D-, and R-loops (Lloyd and Rudolph, 2016), consists of an N-terminal wedge domain (WD), two RecA-like helicase domains, and a C-terminal translocation in RecG (TRG) motif (Fairman-Williams et al., 2010). The WD, which is not found in other DNA helicases, provides specificity for binding branched DNA structures (Rudolph et al., 2010). Amino acid sequence analysis of WDs of RecGs from *Deinococcus* species revealed that a "Gln(Q)-Pro(P)-Trp(W)" residue motif is highly conserved in *Deinococus* RecG proteins. In this study, we found that QPW residues contributed to strong binding of RecG to HJ and, consequently, enhanced the ability of RecG to repair DNA damage in *D. radiodurans*.

# MATERIALS AND METHODS

## Bacterial Strains and Culture Conditions

*Deinococus radiodurans* R1 (ATCC13939) and its isogenic *recG* mutant strains (Δ*recG*), which had been previously constructed (Jeong et al., 2016), were cultivated at 30°C in TGY broth (0.5% tryptone, 0.1% glucose, and 0.3% yeast extract) with aeration or on TGY plates supplemented with 1.5% Bacto-agar. The *E. coli* strain DH5α was used for routine cloning experiments. *Escherichia coli* strains were grown at 37°C in Luria-Bertani (LB) medium or on LB plates solidified with 1.5% Bacto-agar. Antibiotics were added to the medium if necessary: ampicillin, 100 μg/ml (*E. coli*), and chloramphenicol, 3 μg/ml (*D. radiodurans*).

## Plasmid Construction

The pRADZ3 shuttle vector, which functions in *E. coli* as well as in *D. radiodurans*, contains the *groEL* promoter for constitutive gene expression (Jeong et al., 2016). Complete *recG* coding sequences were PCR-amplified from genomic DNA of *D. radiodurans* R1 and *E. coli* MG1655 by using DR1916F/R and B3652F/R primer pairs, respectively, carrying the SpeI and BamHI restriction sites. The PCR products were cloned into pRADZ3 at the *Spe*I and *Bam*HI sites to generate the plasmids pDrRecG and pEcRecG, respectively. These plasmids were transformed into Δ*recG* for complementation studies. For transformation, *D. radiodurans* cells from exponentially growing cultures were collected by centrifugation and concentrated 50-fold in TGY supplemented with 30 mM $CaCl_2$. The cell mixture (100 μl) containing the constructed plasmid DNAs was held on ice for 30 min and then incubated at 32°C for 90 min. The transformation mixture was diluted 10-fold with TGY broth and incubated at 30°C for 5 h with aeration, prior to being plated on drug-selective agar. The partial nucleotide sequence of *recG* encoding DrRecG lacking the N-terminal region (residues 1–99) was PCR-amplified using DR1916-ΔNF/-ΔNR primer pairs and cloned into pRADZ3 to generate $pDrRecG_{\Delta N99}$ as described above. To produce RecG mutant proteins, EcRecG with QPW instead of $^{99}$FSA$^{101}$ and DrRecG with FSA instead of $^{201}$QPW$^{203}$, mutagenesis was carried out using fusion PCR techniques. Complementary primer pairs, EcQPW-F/-R and DrFSA-F/-R, were designed to contain the desired mutations in the middle of the primers. To introduce the triple point mutation "QPW" into EcRecG, in the first step, two fragments were amplified using the primer pairs B3652F/EcQPW-R and EcQPW-F/B3652R, respectively. In the second step, the two PCR products were annealed at their overlapping homologous regions and were amplified by the 3652F/R primer pair. The fusion PCR product was cloned into pRADZ3 to generate $pEcRecG_{QPW}$ as described above. The plasmid $pDrRecG_{FSA}$ was constructed using primer pairs DR1916F/DrFSA-R and DrFSA-F/DR1916R. The plasmid constructs were transformed into Δ*recG*. The plasmids were verified by DNA sequencing. Primers used in this study are listed in **Supplementary Table S1**.

## Construction and Purification of RecG Wedge Domain

A maltose-binding protein (MBP)-RecG-WD fusion was constructed using the pMAL-c2x vector, in which the *E. coli malE* gene encoding MBP was expressed *via* an IPTG-inducible promoter. The WD regions of *recG* genes were amplified using the DrWD-F/-R and EcWD-F/-R primer sets (**Supplementary Table S1**) by using *D. radiodurans* and *E. coli* genomic DNA as template, respectively. The PCR products were digested with EcoRI and HindIII and cloned into pMAL-c2x for purification of the wild-type WDs, named $DrRecG\text{-}WD_{WT}$ and $EcRrecG\text{-}WD_{WT}$, respectively. To generate mutant RecG-WDs, $DrRecG\text{-}WD_{FSA}$, and $EcRecG\text{-}WD_{QPW}$, the WD regions were amplified from plasmids $pDrRecG_{FSA}$ and $pEcRecG_{QPw}$, respectively, and then cloned into pMAL-c2x as described above. The resulting plasmids were transformed into *E. coli* strain BL21 (DE3) for purification of the RecG-WDs fused to MBP. Cells were grown in 500 ml of LB broth at 37°C. IPTG (0.1 mM) was added to the culture when the cells reached an optical density at 600 nm ($OD_{600}$) of 0.5 and were further grown at 16°C overnight. The cells were harvested by centrifugation and resuspended in buffer A (20 mM Tris-HCl, pH 7.5; 0.2 M NaCl; and 1 mM EDTA, pH 8.0). Following sonication on ice, cell debris was removed by centrifugation, and the supernatant was loaded onto a 5 ml amylose column. The column was washed with five column volumes of buffer A. The MBP-RecG-WD fusion protein was eluted with 5 ml of buffer B (buffer A containing 10 mM maltose). Following 10% SDS PAGE, fractions containing the approximately 51-kDa fusion protein were collected and concentrated by ultrafiltration using Amicon® Ultra Filters (Merck Millipore, Darmstadt, Germany). Protein concentrations were determined using the Bradford protein assay with bovine serum albumin as the standard.

## DNA Binding Assay

To create the HJ DNA substrate, four complementary oligonucleotides (oligo 1, 5'-GTCGGATCCTCTAGACAGCT CCATGATCACTGGCACTGGTAGAATTCGGC-3'; oligo 2, 5'-CAACGTCATAGACGATT ACATTGCTACATGGAGCTGTC TAGAGGATCCGA-3'; oligo 3, 5'-TGCCGAATTCTACCAGT GCCAGTGATGGACATCTTTGCCACGTTGACCC-3'; oligo 4, 5'-TGGGTCAACGTGGGCAAGATGTCCTAGCAATGTAATC GTCTATGACGT-3') were synthesized as described previously (McGlynn et al., 2000). The oligonucleotides were denatured for 15 min at 95°C and allowed to anneal at 25°C for 45 min. To examine the DNA binding activity of RecG-WD, an electrophoretic mobility shift assay kit (Invitrogen, Carlsbad, CA, United States) was used. Purified recombinant RecG-WD proteins and 100 nM of HJ DNA substrates were mixed in binding buffer containing 50 mM Tris-HCl (pH 8.0), 5 mM EDTA, 1 mM dithiothreitol, 100 μg/ml bovine serum albumin, and 6% glycerol (v/v) and incubated on ice for 15 min as described previously (McGlynn et al., 1997; Briggs et al., 2005). The DNA binding reaction was terminated by the addition of 2 μl of 2× loading dye. Samples were loaded onto 6%

polyacrylamide gels in low-ionic strength buffer at 120 V for 35 min at room temperature, and the electrophoresed DNA-protein complexes were visualized using a ChemiDoc™ Touch imaging system (Bio-Rad, Hercules, CA, United States). Reaction products were quantified using Image Lab Software (Bio-Rad).

## Growth and Survival Assays

A stationary-phase culture that had grown overnight was used as a seed culture. The seed culture was inoculated into 25 ml of TGY broth at 1:100 dilution, and cell growth was monitored at $OD_{600}$ by using a spectrophotometer. For survival studies, cells grown to log phase ($OD_{600} \approx 1.0$, corresponding to ~$10^8$ CFU/ml) in TGY broth were adjusted to $OD_{600} \approx 0.1$ with TGY. After γ-irradiation treatment, cells were serially diluted 10-fold in saline (0.85% NaCl), spotted onto TGY plates, and incubated at 30°C for 3 days to allow colony formation.

## Quantitative Real-Time PCR Assay

A 5 ml culture grown to mid-log phase was harvested by centrifugation. RNA preparation and cDNA synthesis were performed as described previously (Jeong et al., 2016). The quantitative real-time PCR (qRT-PCR) was performed on a CFX Connect real-time PCR system (Bio-Rad) using SYBR Premix Ex Taq (Takara Bio Inc., Otsu, Japan). PCR reactions were performed as follows one cycle of 95°C for 5 min and then 40 cycles of 95°C for 10 s and 60°C for 15 s. The housekeeping gene *dr1343* encoding glyceraldehyde-3-phosphate dehydrogenase was used as an internal control. Primers used in qRT-PCR are denoted with the prefix "RT-" in **Supplementary Table S1**.

## Pulsed Field Gel Electrophoresis

Irradiated (6 kGy) and unirradiated cells were diluted in 50 ml TGY broth to an $OD_{600}$ of 0.25, and incubated at 30°C. At the indicated times, 1.5, 3, 4.5, 6, and 8 h after re-inoculation, cells (~ $5 \times 10^8$ CFU/ml) were harvested and washed with 10 mM phosphate buffer (pH 7.0). The cells were resuspended in 0.125 M EDTA (pH 8.0) and mixed with low-melt agarose (Bio-Rad) to obtain a final concentration of 0.8% agarose. The DNA plugs were incubated overnight at 37°C in 0.05 M EDTA (pH 7.5) containing 1 mg/ml lysozyme, placed in proteinase K solution at 50°C for 16 h, and washed once with 1 × washing buffer containing 1 mM phenylmethylsulfonyl fluoride (PMSF) and then three times with 1× washing buffer. The prepared DNA plugs were digested with 30 U of NotI restriction enzyme overnight at 37°C and then subjected to pulsed field gel electrophoresis (PFGE). DNA fragments were separated on 1% (wt/vol) agarose gels in 0.5 × TBE. Electrophoresis was performed using a CHEF-Mapper apparatus (Bio-Rad) under the following conditions: pulse ramping from 10 to 60 s, angle of 120°, current of 6 V/cm, and 22 h run time at 12°C. Gels were stained with 0.5 × TBE containing 0.5 μg/ml ethidium bromide for 30 min, destained for 10 min in deionized water, and then visualized using a ChemiDoc™ Touch imaging system (Bio-Rad).

# RESULTS

## QPW Residues Are Highly Conserved in the WD of Deinococcal RecG Proteins

In general, RecG proteins largely consist of an N-terminal WD critical to DNA binding, helicase core domains, including seven motifs common to DNA helicases, and the signature RecG TRG motif (Fairman-Williams et al., 2010). Compared to the *E. coli* RecG protein (EcRecG), the *D. radiodurans* RecG protein (DrRecG) has an extended region with 99 amino acids at the N-terminus (**Figure 1A**). When the C-terminal regions containing the helicase domain and TRG motif are considered, sequence identity between the two proteins approaches 53%, whereas there is no significant similarity in the WD (**Figure 1A**; **Supplementary Figure S1**). The crystal structure of RecG from *Thermatoga maritima* (TmRecG) revealed that $Phe^{204}$ and $Tyr^{208}$ in its WD are important for the binding of branched DNA molecules (Singleton et al., 2001). Multiple sequence alignment of the WD showed that the phenylalanine residue was highly conserved, and the tyrosine residue was replaced with another aromatic amino acid, tryptophan, in all deinococcal RecG proteins (**Figure 1B**; **Supplementary Figure S2**). Interestingly, glutamine (Q), proline (P), and tryptophan (W) at positions 201, 202, and 203, respectively (*D. radiodurans* numbering) were found in all deinococcal RecGs (**Supplementary Figure S2**).

## Comparative Modeling of RecG Proteins

To gain insight into the forked-DNA binding mode of DrRecG, we generated structural models of DrRecG and EcRecG with SWISS-MODEL (Biasini et al., 2014) by using the crystal structure of TmRecG (PDB id: 1gm5) as a template. TmRecG (780 amino acids) shares 36.5 and 32.3% sequence identities with DrRecG (784 amino acids) and EcRecG (693 amino acids), respectively. We predicted structural models for DrRecG comprising of 735 amino acid residues (10–744) and EcRecG comprising of 635 amino acids (6–660), respectively. The modeled structures were validated by using QMEAN and ProSA (**Supplementary Figure S3**) and were superimposed onto the TmRecG-DNA complex structure. Our analyses suggested that $Phe^{199}$ and $Trp^{203}$ in DrRecG, which are likely to be equivalent to $Phe^{204}$ and $Tyr^{208}$, respectively, in TmRecG, may have roles in the stabilization of the leading and lagging strand templates by base stacking interactions between nucleotide bases and aromatic side chains, whereas $Gln^{201}$ corresponding to $Gln^{206}$ in TmRecG could interact with nucleotide bases by electrostatic interactions, thereby participating in the binding of DrRecG to DNA (**Figure 2**). In the case of EcRecG, only $Phe^{97}$, corresponding to $Phe^{204}$ in TmRecG, seemed to directly interact with a DNA base (**Figure 2**). $Phe^{96}$ in EcRecG is also required for interaction with branched DNA molecules because it may have a stabilizing effect similar to that of $Trp^{203}$ in TmRecG, which is partially buried in WD hydrophobic core and preserves WD conformation as a whole (Briggs et al., 2005). $Phe^{96}$ in EcRecG, $Trp^{203}$ in TmRecG, and $Trp^{198}$

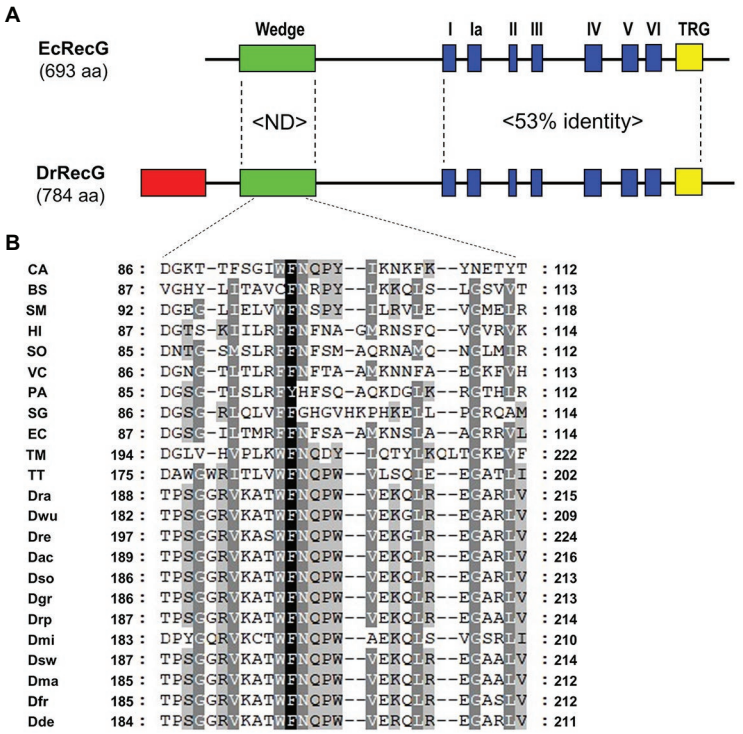


**FIGURE 1 |** Alignment of *Escherichia coli* RecG (EcRecG) and *Deinococcus radiodurans* RecG (DrRecG). **(A)** Schematic comparison of the domain structures of EcRecG and DrRecG. EcRecG and DrRecG are aligned *via* wedge (green), helicase (blue), and TRG (yellow) motifs. The N-terminal extended region of DrRecG is shown as a red box. The percentages of conservation of amino acid sequences between EcRecG and DrRecG are indicated for wedge domain (ND, not determined) and helicase and TRG motifs (53% identity). **(B)** Multiple alignment of amino acid sequences containing the conserved phenylalanine (F) residue within the wedge domain. The program Genedoc (www.psc.edu/biomed/genedoc) was used to visualize the alignment in quantify mode, which highlights residues most-frequently found in each column of the alignment. Gaps introduced to maximize alignment are indicated by dash. Black and white letters on gray shading represent ≥60 and ≥80% identity, respectively. White letters on black shading represent 100% identity. Wedge domain sequences were obtained from RecGs of *Clostridium acetobutylicum*, CA; *Bacillus subtilis*, BS; *Streptobacillus moniliformis*, SM; *Haemophilus influenza*, HI; *Shewanella oneidensis*, SO; *Vibrio cholera*, VC; *Pseudomonas aeruginosa*, PA; *Streptomyces griseus*, SG; *Escherichia coli*, EC; *Thermatoga maritima*, TM; *Thermus thermophilus*, TT; *D. radiodurans*, Dra; *D. wulumuqiensis*, Dwu; *D. reticulitermitis*, Dre; *D. actinosclerus*, Dac; *D. soli*, Dso; *D. grandis*, Dgr; *D. radiopugnans*, Drp; *D. maricopensis*, Dmi; *D. swuensis*, Dsw; *D. marmoris*, Dma; *D. frigensis*, Dfr; and *D. deserti*, Dde.

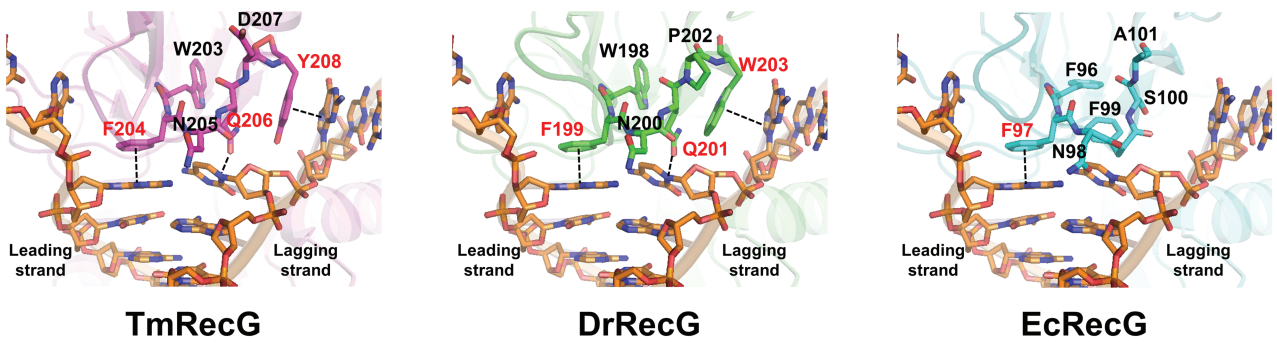


**FIGURE 2 |** Structural model of RecG wedge domains in complex with a partial replication fork. The modeled wedge domains of RecG from *Thermatoga maritima* (TmRecG), DrRecG, and EcRecG are shown in purple, green, and cyan, respectively. DNA molecules are displayed in an orange stick model. Nitrogen, oxygen, and phosphorous atoms are colored in blue, red, and orange, respectively.

in DrRecG, which is equivalent to $Trp^{203}$ in TmRecG, are located in the same position (**Figure 2**). Taken together, our homology models obtained for DrRecG and EcRecG fit well with the crystal structure of TmRecG. It can thus be assumed that QPW residues may play important roles in the DNA binding of deinococcal RecGs.

## QPW Residues Enhance RecG DNA Binding Activity

The isolated WD can bind to HJ structures, although its affinity is lower than that of full-length RecG (Briggs et al., 2005). To test whether the QPW residues could affect the DNA binding activity of RecG, we cloned partial *recG* gene fragments encoding the WD into the expression vector pMAL-c2x to produce an MBP-RecG-WD fusion protein. The constructs encompassed residues 59–135 of EcRecG, and 158–235 of DrRecG (**Supplementary Figure S1**). We also constructed mutant versions of RecG-WD by replacing the QPW of DrRecG with FSA of EcRecG corresponding to QPW in DrRecG (**Figure 1B**), and vice versa. DNA binding assays involving the four different kinds of WDs, EcRecG-$WD_{WT}$, EcRecG-$WD_{QPW}$, DrRecG-$WD_{WT}$, and DrRecG-$WD_{FSA}$, were performed using HJ structures formed by annealing four complementary oligonucleotides, as previously described (McGlynn et al., 2000). As shown in **Figure 3**, DrRecG-$WD_{WT}$ almost reached a saturation of the total DNA binding at 160 nM protein, whereas EcRecG-$WD_{WT}$ did not even at higher concentrations (to 640 nM). The substitution of QPW with FSA (DrRecG-$WD_{FSA}$) dramatically reduced binding ability, but EcRecG-$WD_{QPW}$ exhibited a significant increase compared to EcRecG-$WD_{WT}$ (**Figure 3**). These results clearly indicated that the QPW signature motif in deinococcal RecGs plays a role in enhancing the DNA-binding affinity of RecG.

## N-Terminal Extended Region Deletion Does Not Affect DrRecG Activity

*Deinococcus radiodurans* RecG has an extended region, with 99 amino acids in the N-terminus compared to EcRecG (**Figure 1A**). We constructed plasmid pDrRecG$_{\Delta N99}$ expressing the N-terminal deletion mutant (residues 100–784) of DrRecG, with $Ala^{100}$ converted to methionine, and transformed it into a DrRecG mutant strain (Δ*recG*). Disruption of *recG* is known to result in *D. radiodurans* cell growth defects (Wu et al., 2009). Thus, we first monitored the growth of the wild-type *D. radiodurans* strain (WT) and Δ*recG* by measuring their $OD_{600}$ values over time. Δ*recG* exhibited delayed growth relative to WT, and expression of the native DrRecG protein (pDrRecG) was able to complement the growth defects. Interestingly, the growth of Δ*recG* harboring pDrRecG$_{\Delta N99}$ was comparable to that of Δ*recG* harboring pDrRecG (**Figure 4A**). In addition, the resistance of Δ*recG* to γ-irradiation was fully restored to the levels of WT by DrRecG$_{\Delta N99}$ provided *in trans* (data not shown). These observations indicate that the N-terminal extended region is not involved in the Δ*recG* phenotypes, growth defect, and increased γ-irradiation sensitivity, under the experimental conditions tested here.

## The QPW Motif Increases RecG DNA Repair Capacity

Because the N-terminal extended region was not essential for DrRecG activity (**Figure 4A**), and EcRecG displays a high degree of sequence conservation with DrRecG in the helicase and TRG motifs (**Supplementary Figure S1**), we introduced the pEcRecG plasmid carrying the *E. coli recG* gene into Δ*recG* cells and measured cell survival rates following γ-irradiation to determine if EcRecG can functionally replace DrRecG. Compared to WT, Δ*recG* showed approximately 0.25-, 0.5-, and 1-log reductions in survival at 6, 9, and 12 kGy of γ-irradiation, respectively, and these reductions were completely restored by DrRecG. However, EcRecG was able to partially restore the γ-irradiation-sensitive phenotype of Δ*recG* only at 12 kGy of γ-irradiation (**Figure 4B**). To test the functional role of the QPW residues, we constructed pEcRecG$_{QPW}$ encoding an EcRecG mutant in which $^{99}FSA^{101}$ was substituted with QPW, and pDrRecG$_{FSA}$ encoding a DrRecG mutant in which $^{201}QPW^{203}$ was substituted with FSA. The resulting plasmids were transformed into Δ*recG* cells, which were then exposed

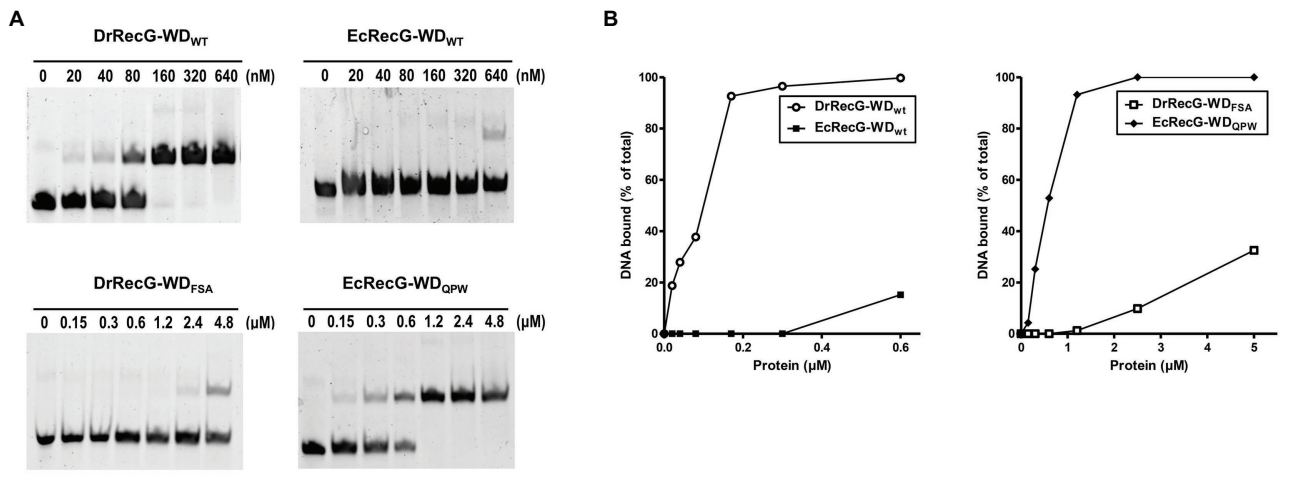


**FIGURE 3 |** DNA binding activity of RecG wedge domains (RecG-WDs). **(A)** Binding affinities of RecG-WDs as measured in band shift assays with Holiday junction (HJ) substrate. Native RecG-WDs, DrRecG-$WD_{WT}$ and EcRecG-$WD_{WT}$ from *D. radiodurans* and *E. coli*, respectively, and their mutants, DrRecG-$WD_{FSA}$ and EcRecG-$WD_{QPW}$ were used in this assay. Reactions contained 100 nM HJ DNA and native RecG-WDs or mutant RecG-WDs at as shown. **(B)** Quantification of the binding activity of RecG-WDs. The formation of RecG-WD complexes with HJ in **(A)** was quantified and plotted as a function of increasing concentration of RecG-WDs.

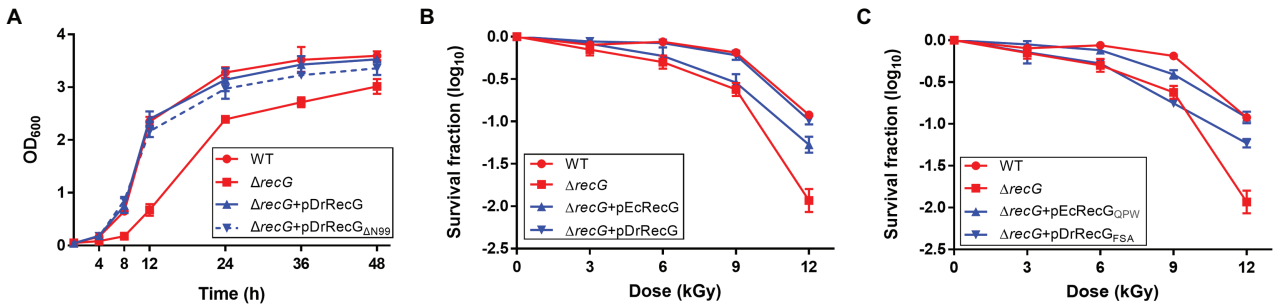


**FIGURE 4 |** Growth and survival assays of the *D. radiodurans recG* mutant strain (Δ*recG*). **(A)** Growth curves of *D. radiodurans* strains. Optical density ($OD_{600}$) measurements were employed to estimate the growth of *D. radiodurans* R1 (WT), Δ*recG*, and Δ*recG* harboring the plasmids pDrRecG and pDrRecGΔ$_{N99}$, which encode the full-length DrRecG and the N-terminal truncation mutant of DrRecG, respectively. Survival curves for Δ*recG* with pEcRecG and pDrRecG **(B)** and with pEcRecG$_{QPW}$ and pDrRecG$_{FSA}$ **(C)**. Cells grown to log phase were exposed to γ-irradiation and spotted onto TGY plates. The survival fraction was calculated by dividing the colony-forming units (CFUs) of γ-irradiation-treated cells by the CFUs of unirradiated cells. The error bars represent the SD of three independent experiments conducted in duplicate ($n$ = 3).

to γ-irradiation. There was no significant difference in *recG* mRNA levels between Δ*recG* harboring pDrRecG and pDrRecG$_{FSA}$ (**Supplementary Figure S4**), but resistance to γ-irradiation was not recovered by DrRecG$_{FSA}$ (**Figure 4C**). In contrast, EcRecG$_{QPW}$ restored the Δ*recG* survival in a similar way as DrRecG, although the restoration levels were somewhat different at 9 kGy (**Figures 4B,C**). These results showed that substituting the three amino acids in the WD between EcRecG and DrRecG is sufficient to exchange their abilities to complement the loss-of-function phenotype of Δ*recG* after γ-irradiation.

To investigate the role of DrRecG in DSB, the DNA repair kinetics of cells subjected to γ-irradiation were examined using PFGE. DNA fragmented by γ-irradiation was reconstructed within 3 h in WT, whereas Δ*recG* was able to compete the repair of shattered genomes 4.5 h after γ-irradiation (**Figure 5**). Δ*recG* harboring pDrRecG and pEcRecG showed repair kinetics similar to those observed in WT and Δ*recG*, respectively. Compared to Δ*recG* with pEcRecG$_{QPW}$, the process of genome reassembly was delayed by 1.5 h in Δ*recG* with pDrRecG$_{FSA}$ (**Figure 5**). The similar patterns of results shown in survival assays and PFGE analysis, which are caused by the reciprocal swapping of the three amino acid motifs between DrRecG and EcRecG, strongly suggest that the QPW residues enhance DNA-binding activity, thereby leading to efficient DNA repair in *D. radiodurans*.

## DISCUSSION

Analysis of the genome sequence of *D. radiodurans* identifies the typical complement of prokaryotic DNA repair proteins, suggesting the possibility that *D. radiodurans* uses the same DNA-repair strategies as other prokaryotes, but it does so in a manner that is somehow much more effective than that observed in other species to retain the extraordinary tolerance to DNA damage (Battista et al., 1999; White et al., 1999). A series of biochemical and structural analyses of *D. radiodurans* proteins involved in DNA repair systems have revealed unusual features distinguishing them from their counterparts in other prokaryotic species. Uracil-DNA glycosylase (UNG) removes uracil from DNA molecules, formed as a result of cytosine deamination, and represents part of the base-excision repair pathway. The uracil-DNA *N*-glycosylase DrUNG (DR_0689), the main UNG in *D. radiodurans*, possesses a much higher catalytic efficiency than human UNG, which is attributed to the high substrate affinity caused by an increased number of positively charged residues close to the DNA binding site (Pedersen et al., 2015). Mismatch-specific UNG (MUG) also removes uracil from DNA. The overall structure of DrMUG is similar to that of EcMUG, but DrMUG possesses a novel catalytic residue (Asp-93) that can provide DrMUG with broad substrate specificity (Moe et al., 2006). The novel catalytic residue identified in DrMUG is conserved in other deinococcal MUG proteins (Lim et al., 2019). The *D. radiodurans* X family DNA polymerase (DrPolX), which not only has polymerase activity, but also exerts strong $Mn^{2+}$-dependent 3'→5' exonuclease activity affects DSB repair efficiency in *D. radiodurans* (Blasius et al., 2006). At the active site of the polymerase catalytic domain, the "DXD" motif conserved in almost all pol X-family members is replaced by an "AAE" motif in *D. radiodurans* (Leulliot et al., 2009; Bienstock et al., 2014). RecA is a critical enzyme in HR for DSB repair. Unlike canonical RecAs, DrRecA first forms a filament on dsDNA and then takes up a homologous single strand to initiate DNA strand exchange, which is the exact inverse of the major pathway seen with other proteins of the RecA family (Kim and Cox, 2002). Although the overall fold of DrRecA is similar to EcRecA, there are a few key amino acid changes in the DrRecA C-terminal domain that interacts with dsDNA. One of the key differences, $Phe^{303}$ in DrRecA, equivalent to $Trp^{290}$ in EcRecA, would seem to be a likely candidate in dictating a possible specificity for binding to dsDNA (Rajan and Bell, 2004). It has also been observed that a single amino acid mutation at the C-terminus of EcRecA alters its activity. The RecA variants found in radioresistant *E. coli* strain CB2000 have mutations at residue 276 (D276A and D276N), which increase the rates of filament nucleation on DNA, and promote DNA strand exchange more efficiently than wild-type RecA proteins (Piechura et al., 2015). These studies imply that DNA repair proteins with altered substrate

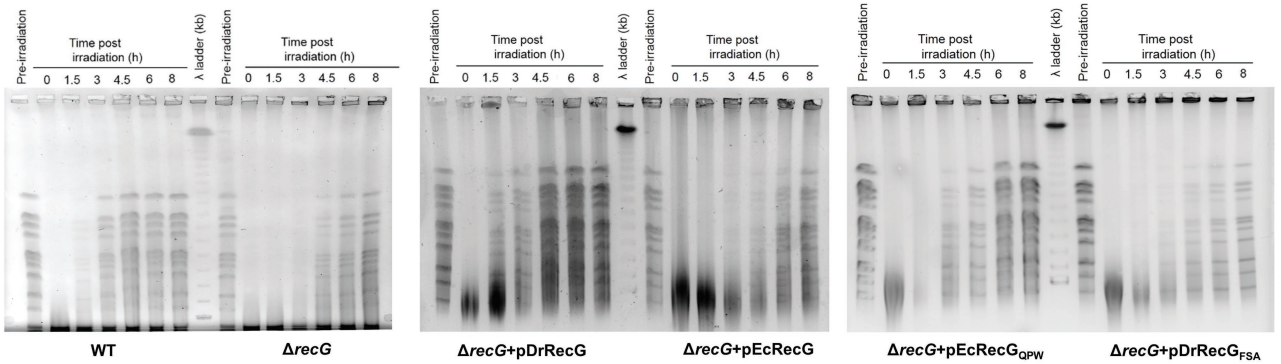


**FIGURE 5 |** DNA repair in Δ*recG* and Δ*recG* cells harboring plasmids encoding the native (pDrRecG and pEcRecG) and mutant (pDrRecG$_{FSA}$ and pEcRecG$_{QPW}$) RecG proteins. Exponentially growing cells were exposed to 6 kGy of γ-irradiation and then recovered in TGY liquid media. At the indicated times (0–8 h), samples were removed, and genomic DNA was isolated. The amount of DNA double-strand breaks (DSBs) was analyzed by pulsed-field gel electrophoresis (PFGE). Pre-irradiation indicates unirradiated cells.

specificity and enhanced catalytic activity, which might be attributed to unique amino acid residues, likely contribute to the improved DNA repair capacity of *D. radiodurans* to survive DNA damage caused by γ-irradiation. In this aspect, the highly conserved QPW residues in the WD can be assumed to affect the binding activity of deinococcal RecGs.

The WD found in the N-terminal region of RecG is a DNA-binding domain that has an oligonucleotide/oligosaccharide binding-fold (OB-fold) motif ranging between 70 and 150 amino acids in length (Theobald et al., 2003). The phenylalanine residue, which is critical for RecG binding of branched DNA molecules, is conserved in the WDs (Briggs et al., 2005; **Figure 1B**). This residue is regarded to stabilize the orphan base of the leading strand template by base stacking, effectively capping the parental duplex (Singleton et al., 2001; **Figure 2**). In *Mycobacterium tuberculosis* RecG, substitution of Phe$^{99}$ corresponding to Phe$^{204}$ in TmRecG to Ala was seen to significantly lower the DNA binding activity compared to that of wild-type RecG protein (Zegeye et al., 2014). In this study, protein structure modeling analysis showed that two other amino acids, Gln$^{206}$ and Tyr$^{208}$ in TmRecG and Gln$^{201}$ and Trp$^{203}$ in DrRecG, interacted with the nucleotide bases of the leading and lagging forked-DNA strands, together with the key residues, Phe$^{204}$ in TmRecG, and Phe$^{199}$ in DrRecG, respectively (**Figure 2**). The aromatic side-chain of Tyr participates in DNA binding of the WD through hydrophobic interactions such as base stacking (Singleton et al., 2001). Tyr was not observed in DrRecG, but it was substituted with an equivalent aromatic residue, Trp (**Figure 2**), suggesting that Trp$^{203}$ may play a similar role in the stabilization of the lagging DNA strand duplex. Of the 79 deinococcal RecGs analyzed in this study, only two species *Deinococcus ruber* and *Deinococcus aquiradiocola*, have QAW instead of the signature QPW residues (**Supplementary Figure S2**). However, it is noteworthy that Q and W are strictly conserved. EcRecG does not have a signature motif with an aromatic residue in the corresponding position ($^{99}$FSA$^{101}$ in EcRecG). Comparisons of the DrRecG and EcRecG models suggested that the conserved QPW residues in the WD confer greater RecG-DNA interaction compared to FSA because of the additional charge interactions and base packing through Gln and Trp, respectively (**Figure 2**; **Supplementary Figure S5**). Indeed, DrRecG-WD$_{WT}$ and EcRecG-WD$_{QPW}$ exhibited enhanced affinities for HJ compared to EcRecG-WD$_{WT}$ and DrRecG-WD$_{FSA}$ (**Figure 3**). Full-length DrRecG and EcRecG$_{QPW}$ restored resistance to γ-irradiation and DNA repair capacity of Δ*recG* to that of WT (**Figures 4, 5**).

Also noteworthy is the N-terminal extended region of DrRecG (**Figure 1A**). This feature is shared with RecG proteins from thermophilic bacteria, *Thermotoga maritima* and *Aquifex aeolicus*, and a number of cyanobacteria, and is longer than in many other RecG proteins such as EcRecG (Wen et al., 2005). RecG from the extreme thermophile *A. aeolicus* unwinds DNA well at high temperature (60°C), whereas the N-terminal extension present in this protein is dispensable for activity and thermostability (Wen et al., 2005). In *D. radiodurans*, the N-/C-terminal extension (or variation) is found not only in RecG, but also in other helicases, including RecD2 and RecQ. DrRecD2 contains an additional N-terminal region of approximately 200 amino acids, which is longer than the corresponding feature in *E. coli* RecD protein (RecD1; Montague et al., 2009). In contrast to most other RecQ proteins composed of the helicase, RecQ-C-terminal (RQC), and helicase-and-RNaseD-like-C terminal (HRDC) domains, DrRecQ contains three tandem HRDC domains in the C-terminus (Killoran and Keck, 2006). Full-length DrRecD2 restored the $H_2O_2$-resistant phenotype of *recD2* mutants, whereas the N-terminal truncation mutant of DrRecD2 could not, suggesting that the N-terminal domain is necessary for the role of DrRecD2 in antioxidant pathways (Zhou et al., 2007). The three tandem HRDC domains increase the efficiency of DNA unwinding and ATPase activities of DrRecQ (Huang et al., 2007), and could work together with other functional motifs to enhance DrRecQ interactions with DNA (Liu et al., 2013). Considering that Δ*recG* cells are sensitive to γ-irradiation and $H_2O_2$ (Wu et al., 2009; **Figure 4**), and DrRecG is also involved in catalase gene *katE1* regulation (Jeong et al., 2016), further research is

needed to determine the role of the additional DrRecG N-terminal region, although it seems not to be implicated in DNA repair under the experimental conditions tested in this study.

RecG provides a more general defense against pathological DNA replication, e.g., the rescue of stalled or damaged replication forks, and is associated with a number of additional cellular processes (Rudolph et al., 2010; Azeroglu et al., 2016; Lloyd and Rudolph, 2016; Romero et al., 2020). Recently, it has become increasingly clear that RecG is an enzyme responsible for regression of stalled DNA replication forks that can be induced by various types of lesions, including single-strand breaks and DSB. RecG is directly loaded onto the forks by binding to ssDNA-binding protein (SSB) and reverses the stalled forks, leading to the formation of HJ-type structures. PriA helicase then targets the repaired fork to reload and assemble a DNA replication machinery (the replisome complex), enabling DNA replication to restart (Lloyd and Rudolph, 2016; Bianco and Lyubchenko, 2017). During HR for DSB repair, RecG is proposed to re-model branched intermediates of recombination to direct the correct binding of PriA and subsequent DNA synthesis (Azeroglu et al., 2016). These studies indicate that SSB-mediated RecG loading onto DNA plays an important role in facilitating stalled replication fork rescue. *D. radiodurans* SSB (DrSSB) is different from that of the prototype *E. coli* SSB (EcSSB), in that DrSSB (301 amino acids) contains two OB folds per monomer, and functions as homodimers, in contrast to the homotetrameric EcSSB (178 amino acids), with each monomer encoding a single OB fold (Bernstein et al., 2004). In *E. coli*, SSB-RecG interactions occur *via* the WD of RecG and the PXXP motifs within the SSB linker domain. In particular, the SSB binding site on RecG overlaps the residues of the binding site for the leading strand arm of the fork in RecG (Ding et al., 2020). Thus, it is likely that these different features do not enable DrSSB to deliver EcRecG to the fork with an efficiency equal to that of DrRecG, which may explain why EcRecG does not confer resistance to Δ*recG* (**Figure 4B**). EcRecG also partially complements *Helicobacter pylori recG* mutants but not to the same extent as the *H. pylori* RecG protein, suggesting that the host context appears to be critical in defining the function of RecG (Kang et al., 2004). In this aspect, the QPW residues found in the WD of DrRecG might be interpreted as the result of evolutionary adaptation to cooperate with the unique DrSSB. *D. radiodurans* is most closely related to *Thermus thermophilus*, and the two genera *Deinococcus* and *Thermus* belong to a distinct bacterial clade called the *Deinococcus-Thermus* group (Omelchenko et al., 2005). Regarding RecG and SSB, they share common features. *Thermus* RecG proteins have either QPW or QTW (**Supplementary Figure S6**), and the dimeric SSBs like DrSSB are discovered in the *Deinococcus-Thermus* group (Zhang et al., 2014), supporting that RecG and SSB might be evolutionarily related. *T. thermophilus* is a thermophile, which is relatively sensitive to IR, whereas *D. radiodurans* is a mesophile, which is highly IR-resistant (Omelchenko et al., 2005). However, considering that the mechanisms employed by thermophiles to overcome DNA damage by high temperature may also be employed in repair of damage caused by IR (Ranawat and Rawat, 2017), the coevolution between RecG and SSB, which likely occurred in the *Deinococcus-Thermus* group, may contribute to the enhanced abilities of the *Deinococcus* and *Thermus* lineages to survive different kinds of environmental stresses. Further research is warranted to investigate the effects of QPW on RecG-SSB interactions.

## DATA AVAILABILITY STATEMENT

The original contributions presented in the study are included in the article/**Supplementary Material**, further inquiries can be directed to the corresponding author.

## AUTHOR CONTRIBUTIONS

S-WJ performed the experiments and wrote a first draft. M-KK performed the comparative protein structure modeling and revised the first draft. LZ and S-KY constructed the plasmids and performed the survival assays. M-KK, J-HJ, and H-ML guided the experiments and interpreted the results. SL conceived the study and was in charge of overall direction and planning. All authors reviewed and edited the manuscript, and approved the final version.

## FUNDING

This research was supported by the Nuclear R&D program of the Ministry of Science and ICT (MSIT), South Korea.

## SUPPLEMENTARY MATERIAL

The Supplementary Material for this article can be found online at: https://www.frontiersin.org/articles/10.3389/fgene.2021.634615/full#supplementary-material

## REFERENCES

Azeroglu, B., Mawer, J. S., Cockram, C. A., White, M. A., Hasan, A. M., Filatenkova, M., et al. (2016). RecG directs DNA synthesis during double-strand break repair. *PLoS Genet.* 12:e1005799. doi: 10.1371/journal.pgen.1005799

Battista, J. R., Earl, A. M., and Park, M. J. (1999). Why is *Deinococcus radiodurans* so resistant to ionizing radiation? *Trends Microbiol.* 7, 362–365. doi: 10.1016/S0966-842X(99)01566-8

Bentchikou, E., Servant, P., Coste, G., and Sommer, S. (2010). A major role of the RecFOR pathway in DNA double-strand-break repair through ESDSA in *Deinococcus radiodurans*. *PLoS Genet.* 6:e1000774. doi: 10.1371/journal.pgen.1000774

Bernstein, D. A., Eggington, J. M., Killoran, M. P., Misic, A. M., Cox, M. M., and Keck, J. L. (2004). Crystal structure of the *Deinococcus radiodurans* single-stranded DNA-binding protein suggests a mechanism for coping with DNA damage. *Proc. Natl. Acad. Sci. U. S. A.* 101, 8575–8580. doi: 10.1073/pnas.0401331101

Bianco, P. R., and Lyubchenko, Y. L. (2017). SSB and the RecG DNA helicase: an intimate association to rescue a stalled replication fork. *Protein Sci.* 26, 638–649. doi: 10.1002/pro.3114

Biasini, M., Bienert, S., Waterhouse, A., Arnold, K., Studer, G., Schmidt, T., et al. (2014). SWISS-MODEL: modelling protein tertiary and quaternary structure using evolutionary information. *Nucleic Acids Res.* 42, W252–W258. doi: 10.1093/nar/gku340

Bienstock, R. J., Beard, W. A., and Wilson, S. H. (2014). Phylogenetic analysis and evolutionary origins of DNA polymerase X-family members. *DNA Repair* 22, 77–88. doi: 10.1016/j.dnarep.2014.07.003

Blasius, M., Shevelev, I., Jolivet, E., Sommer, S., and Hübscher, U. (2006). DNA polymerase X from *Deinococcus radiodurans* possesses a structure-modulated 3′→5′ exonuclease activity involved in radioresistance. *Mol. Microbiol.* 60, 165–176. doi: 10.1111/j.1365-2958.2006.05077.x

Briggs, G. S., Mahdi, A. A., Wen, Q., and Lloyd, R. G. (2005). DNA binding by the substrate specificity (wedge) domain of RecG helicase suggests a role in processivity. *J. Biol. Chem.* 280, 13921–13927. doi: 10.1074/jbc.M412054200

Brosh, R. M. Jr., and Matson, S. W. (2020). History of DNA helicases. *Gene* 11:255. doi: 10.3390/genes11030255

Ding, W., Tan, H. Y., Zhang, J. X., Wilczek, L. A., Hsieh, K. R., Mulkin, J. A., et al. (2020). The mechanism of single strand binding protein-RecG binding: implications for SSB interactome function. *Protein Sci.* 29, 1211–1227. doi: 10.1002/pro.3855

Fairman-Williams, M. E., Guenther, U. P., and Jankowsky, E. (2010). SF1 and SF2 helicases: family matters. *Curr. Opin. Struct. Biol.* 20, 313–324. doi: 10.1016/j.sbi.2010.03.011

Huang, L., Hua, X., Lu, H., Gao, G., Tian, B., Shen, B., et al. (2007). Three tandem HRDC domains have synergistic effect on the RecQ functions in *Deinococcus radiodurans*. *DNA Repair* 6, 167–176. doi: 10.1016/j.dnarep.2006.09.006

Jeong, S. W., Seo, H. S., Kim, M. K., Choi, J. I., Lim, H. M., and Lim, S. (2016). PprM is necessary for up-regulation of *katE1*, encoding the major catalase of *Deinococcus radiodurans*, under unstressed culture conditions. *J. Microbiol.* 54, 426–431. doi: 10.1007/s12275-016-6175-8

Kang, J., Tavakoli, D., Tschumi, A., Aras, R. A., and Blaser, M. J. (2004). Effect of host species on *recG* phenotypes in *Helicobacter pylori* and *Escherichia coli*. *J. Bacteriol.* 186, 7704–7713. doi: 10.1128/JB.186.22.7704-7713.2004

Khairnar, N. P., Maurya, G. K., Pandey, N., Das, A., and Misra, H. S. (2019). DrRecQ regulates guanine quadruplex DNA structure dynamics and its impact on radioresistance in *Deinococcus radiodurans*. *Mol. Microbiol.* 112, 854–865. doi: 10.1111/mmi.14321

Killoran, M. P., and Keck, J. L. (2006). Three HRDC domains differentially modulate *Deinococcus radiodurans* RecQ DNA helicase biochemical activity. *J. Biol. Chem.* 281, 12849–12857. doi: 10.1074/jbc.M600097200

Kim, J. I., and Cox, M. M. (2002). The RecA proteins of *Deinococcus radiodurans* and *Escherichia coli* promote DNA strand exchange via inverse pathways. *Proc. Natl. Acad. Sci. U. S. A.* 99, 7917–7921. doi: 10.1073/pnas.122218499

Kitayama, S., Kohoroku, M., Takagi, A., and Itoh, H. (1997). Mutation of *D. radiodurans* in a gene homologous to *ruvB* of *E. coli*. *Mutat. Res.* 385, 151–157. doi: 10.1016/s0921-8777(97)00048-7

Leulliot, N., Cladière, L., Lecointe, F., Durand, D., Hübscher, U., and van Tilbeurgh, H. (2009). The family X DNA polymerase from *Deinococcus radiodurans* adopts a non-standard extended conformation. *J. Biol. Chem.* 284, 11992–11999. doi: 10.1074/jbc.M809342200

Lim, S., Jung, J. H., Blanchard, L., and de Groot, A. (2019). Conservation and diversity of radiation and oxidative stress resistance mechanisms in *Deinococcus* species. *FEMS Microbiol. Rev.* 43, 19–52. doi: 10.1093/femsre/fuy037

Liu, S., Zhang, W., Gao, Z., Ming, Q., Hou, H., Lan, W., et al. (2013). NMR structure of the N-terminal-most HRDC1 domain of RecQ helicase from *Deinococcus radiodurans*. *FEBS Lett.* 587, 2635–2642. doi: 10.1016/j.febslet.2013.06.048

Lloyd, R. G., and Rudolph, C. J. (2016). 25 years on and no end in sight: a perspective on the role of RecG protein. *Curr. Genet.* 62, 827–840. doi: 10.1007/s00294-016-0589-z

McGlynn, P., Al-Deib, A. A., Liu, J., Marians, K. J., and Lloyd, R. G. (1997). The DNA replication protein PriA and the recombination protein RecG bind D-loops. *J. Mol. Biol.* 270, 212–221. doi: 10.1006/jmbi.1997.1120

McGlynn, P., Mahdi, A. A., and Lloyd, R. G. (2000). Characterisation of the catalytically active form of RecG helicase. *Nucleic Acids Res.* 28, 2324–2332. doi: 10.1093/nar/28.12.2324

Moe, E., Leiros, I., Smalås, A. O., and McSweeney, S. (2006). The crystal structure of mismatch-specific uracil-DNA glycosylase (MUG) from *Deinococcus radiodurans* reveals a novel catalytic residue and broad substrate specificity. *J. Biol. Chem.* 281, 569–577. doi: 10.1074/jbc.M508032200

Montague, M., Barnes, D., Smith, H. O., Chuang, R. -Y., and Vashee, S. (2009). The evolution of RecD outside of the RecBCD complex. *J. Mol. Evol.* 69, 360–371. doi: 10.1007/s00239-009-9290-x

Omelchenko, M. V., Wolf, Y. I., Gaidamakova, E. K., Matrosova, V. Y., Vasilenko, A., Zhai, M., et al. (2005). Comparative genomics of *Thermus thermophilus* and *Deinococcus radiodurans*: divergent routes of adaptation to thermophily and radiation resistance. *BMC Evol. Biol.* 5:57. doi: 10.1186/1471-2148-5-57

Pedersen, H. L., Johnson, K. A., McVey, C. E., Leiros, I., and Moe, E. (2015). Structure determination of uracil-DNA N-glycosylase from *Deinococcus radiodurans* in complex with DNA. *Acta Crystallogr. D Biol. Crystallogr.* 71, 2137–2149. doi: 10.1107/S1399004715014157

Piechura, J. R., Tseng, T. L., Hsu, H. F., Byrne, R. T., Windgassen, T. A., Chitteni-Pattu, S., et al. (2015). Biochemical characterization of RecA variants that contribute to extreme resistance to ionizing radiation. *DNA Repair* 26, 30–43. doi: 10.1016/j.dnarep.2014.12.001

Rajan, R., and Bell, C. E. (2004). Crystal structure of RecA from *Deinococcus radiodurans*: insights into the structural basis of extreme radioresistance. *J. Mol. Biol.* 344, 951–963. doi: 10.1016/j.jmb.2004.09.087

Ranawat, P., and Rawat, S. (2017). Radiation resistance in thermophiles: mechanisms and applications. *World J. Microbiol. Biotechnol.* 33:112. doi: 10.1007/s11274-017-2279-5

Rocha, E. P., Cornet, E., and Michel, B. (2005). Comparative and evolutionary analysis of the bacterial homologous recombination systems. *PLoS Genet.* 1:e15. doi: 10.1371/journal.pgen.0010015

Romero, Z. J., Chen, S. H., Armstrong, T., Wood, E. A., van Oijen, A., Robinson, A., et al. (2020). Resolving toxic DNA repair intermediates in every *E. coli* replication cycle: critical roles for RecG, Uup and RadD. *Nucleic Acids Res.* 48, 8445–8460. doi: 10.1093/nar/gkaa579

Rudolph, C. J., Upton, A. L., Briggs, G. S., and Lloyd, R. G. (2010). Is RecG a general guardian of the bacterial genome? *DNA Repair* 9, 210–223. doi: 10.1016/j.dnarep.2009.12.014

Servinsky, M. D., and Julin, D. A. (2007). Effect of a *recD* mutation on DNA damage resistance and transformation in *Deinococcus radiodurans*. *J. Bacteriol.* 189, 5101–5107. doi: 10.1128/JB.00409-07

Singleton, M. R., Scaife, S., and Wigley, D. B. (2001). Structural analysis of DNA replication fork reversal by RecG. *Cell* 107, 79–89. doi: 10.1016/S0092-8674(01)00501-3

Slade, D., Lindner, A. B., Paul, G., and Radman, M. (2009). Recombination and replication in DNA repair of heavily irradiated *Deinococcus radiodurans*. *Cell* 136, 1044–1055. doi: 10.1016/j.cell.2009.01.018

Slade, D., and Radman, M. (2011). Oxidative stress resistance in *Deinococcus radiodurans*. *Microbiol. Mol. Biol. Rev.* 75, 133–191. doi: 10.1128/MMBR.00015-10

Stelter, M., Acajjaoui, S., McSweeney, S., and Timmins, J. (2013). Structural and mechanistic insight into DNA unwinding by *Deinococcus radiodurans* UvrD. *PLoS One* 8:e77364. doi: 10.1371/journal.pone.0077364

Theobald, D. L., Mitton-Fry, R. M., and Wuttke, D. S. (2003). Nucleic acid recognition by OB-fold proteins. *Annu. Rev. Biophys. Biomol. Struct.* 32, 115–133. doi: 10.1146/annurev.biophys.32.110601.142506

Uchiumi, F., Seki, M., and Furuichi, Y. (2015). Helicases and human diseases. *Front. Genet.* 6:39. doi: 10.3389/fgene.2015.00039

Umate, P., Tuteja, N., and Tuteja, R. (2011). Genome-wide comprehensive analysis of human helicases. *Commun. Integr. Biol.* 4, 118–137. doi: 10.4161/cib.4.1.13844

Wang, J., and Julin, D. A. (2004). DNA helicase activity of the RecD protein from *Deinococcus radiodurans*. *J. Biol. Chem.* 279, 52024–52032. doi: 10.1074/jbc.M408645200

Wen, Q., Mahdi, A. A., Briggs, G. S., Sharples, G. J., and Lloyd, R. G. (2005). Conservation of RecG activity from pathogens to hyperthermophiles. *DNA Repair* 4, 23–31. doi: 10.1016/j.dnarep.2004.07.008

White, O., Eisen, J. A., Heidelberg, J. F., Hickey, E. K., Peterson, J. D., Dodson, R. J., et al. (1999). Genome sequence of the radioresistant bacterium *Deinococcus radiodurans* R1. *Science* 286, 1571–1577. doi: 10.1126/science.286.5444.1571

Wu, Y., Chen, W., Zhao, Y., Xu, H., and Hua, Y. (2009). Involvement of RecG in $H_2O_2$-induced damage repair in *Deinococcus radiodurans*. *Can. J. Microbiol.* 55, 841–848. doi: 10.1139/W09-028

Xue, Z. Y., Wu, W. Q., Zhao, X. C., Kumar, A., Ran, X., Zhang, X. H., et al. (2020). Single-molecule probing the duplex and G4 unwinding patterns of a RecD family helicase. *Int. J. Biol. Macromol.* 164, 902–910. doi: 10.1016/j.ijbiomac.2020.07.158

Zahradka, K., Slade, D., Bailone, A., Sommer, S., Averbeck, D., Petranovic, M., et al. (2006). Reassembly of shattered chromosomes in *Deinococcus radiodurans*. *Nature* 443, 569–573. doi: 10.1038/nature05160

Zegeye, E. D., Balasingham, S. V., Laerdahl, J. K., Homberset, H., Kristiansen, P. E., and Tonjum, T. (2014). Effects of conserved residues and naturally occurring mutations on *Mycobacterium tuberculosis* RecG helicase activity. *Microbiology* 160, 217–227. doi: 10.1099/mic.0.072140-0

Zhang, J., Zhou, R., Inoue, J., Mikawa, T., and Ha, T. (2014). Single molecule analysis of *Thermus thermophilus* SSB protein dynamics on single-stranded DNA. *Nucleic Acids Res.* 42, 3821–3832. doi: 10.1093/nar/gkt1316

Zhou, Q., Zhang, X., Xu, H., Xu, B., and Hua, Y. (2007). A new role of *Deinococcus radiodurans* RecD in antioxidant pathway. *FEMS Microbiol. Lett.* 271, 118–125. doi: 10.1111/j.1574-6968.2007.00703.x

**Conflict of Interest:** The authors declare that the research was conducted in the absence of any commercial or financial relationships that could be construed as a potential conflict of interest.

frontiers in Cell and Developmental Biology

ORIGINAL RESEARCH
published: 15 February 2021
doi: 10.3389/fcell.2021.630777

# Mrc1-Dependent Chromatin Compaction Represses DNA Double-Stranded Break Repair by Homologous Recombination Upon Replication Stress

*Poyuan Xing, Yang Dong, Jingyu Zhao, Zhou Zhou, Zhao Li, Yu Wang, Mengfei Li, Xinghua Zhang and Xuefeng Chen**

*Hubei Key Laboratory of Cell Homeostasis and the Institute for Advanced Studies, College of Life Sciences, Wuhan University, Wuhan, China*

OPEN ACCESS

**Edited by:**
*Anthony Davis, University of Texas Southwestern Medical Center, United States*

**Reviewed by:**
*James Daley, The University of Texas Health Science Center at San Antonio, United States*
*Ella L. Kim, Johannes Gutenberg University Mainz, Germany*

***Correspondence:**
*Xuefeng Chen*
*xfchen@whu.edu.cn*

**Specialty section:**
*This article was submitted to Cell Death and Survival, a section of the journal Frontiers in Cell and Developmental Biology*

**Received:** *19 November 2020*
**Accepted:** *06 January 2021*
**Published:** *15 February 2021*

**Citation:**
*Xing P, Dong Y, Zhao J, Zhou Z, Li Z, Wang Y, Li M, Zhang X and Chen X (2021) Mrc1-Dependent Chromatin Compaction Represses DNA Double-Stranded Break Repair by Homologous Recombination Upon Replication Stress. Front. Cell Dev. Biol. 9:630777. doi: 10.3389/fcell.2021.630777*

The coordination of DNA replication and repair is critical for the maintenance of genome stability. It has been shown that the Mrc1-mediated S phase checkpoint inhibits DNA double-stranded break (DSB) repair through homologous recombination (HR). How the replication checkpoint inhibits HR remains only partially understood. Here we show that replication stress induces the suppression of both Sgs1/Dna2- and Exo1-mediated resection pathways in an Mrc1-dependent manner. As a result, the loading of the single-stranded DNA binding factor replication protein A (RPA) and Rad51 and DSB repair by HR were severely impaired under replication stress. Notably, the deletion of *MRC1* partially restored the recruitment of resection enzymes, DSB end resection, and the loading of RPA and Rad51. The role of Mrc1 in inhibiting DSB end resection is independent of Csm3, Tof1, or Ctf4. Mechanistically, we reveal that replication stress induces global chromatin compaction in a manner partially dependent on Mrc1, and this chromatin compaction limits the access of chromatin remodeling factors and HR proteins, leading to the suppression of HR. Our study reveals a critical role of the Mrc1-dependent chromatin structure change in coordinating DNA replication and recombination under replication stress.

**Keywords: replication checkpoint, Mrc1, DNA double-stranded breaks, homologous recombination, replication stress**

## INTRODUCTION

Maintenance of genome stability relies on checkpoint signaling pathways that perceive DNA damage or replication stress to initiate a cellular response that coordinates DNA replication, repair with the cell cycle progression. During the S phase, cells are particularly vulnerable since the progression of replication forks can be impeded by numerous physical, chemical, or genetic perturbations, such as the hard-to-replicate regions, natural pausing sites, chromatin-bound proteins, secondary DNA structures, active transcription, or DNA replication inhibitors (Giannattasio and Branzei, 2017; Pardo et al., 2017). These barriers can cause the uncoupling of DNA helicase and replicative polymerases or between leading or lagging strand synthesis, leading to the accumulation of single-stranded DNA (ssDNA) (Garcia-Rodriguez et al., 2018).

Replication protein A (RPA), the first responder of ssDNA, binds the exposed ssDNA, leading to the recruitment of the checkpoint kinase Mec1–Ddc2 complex and the activation of the S phase checkpoint (Zou and Elledge, 2003; Chen and Wold, 2014).

In yeast, the S phase checkpoint pathway is comprised of two branches: the DNA damage checkpoint and the DNA replication checkpoint (Pardo et al., 2017). Both pathways are initiated by the sensor kinase Mec1 and converge on the effector kinase Rad53 (Pardo et al., 2017). However, they differ in the mediator proteins. The DNA damage checkpoint relies on the adaptor protein Rad9, while the replication checkpoint depends on the replisome component Mrc1 (Claspin in human) (Alcasabas et al., 2001; Prado, 2014; Pardo et al., 2017). Upon replication stress, Mrc1 is phosphorylated by Mec1, and the modified Mrc1 interacts with the FHA domain of Rad53 to promote its activation (Tanaka and Russell, 2001; Smolka et al., 2006; Xu et al., 2006). Activation of the replication checkpoint turns on a cassette of events, leading to stabilization of stalled forks, suppression of late fired origins, induction of DNA damage response genes, upregulation of dNTP pools, and arrest of the cell cycle (Pardo et al., 2017).

Mrc1 is also a replisome component traveling with replication forks, and it interacts with DNA polymerase epsilon and Mcm6 (Katou et al., 2003; Lou et al., 2008; Komata et al., 2009). Mrc1 forms a complex with Csm3 and Tof1 at normal or stalled forks (Katou et al., 2003; Noguchi et al., 2004; Calzada et al., 2005). The complex fulfills a structural role required for normal replication fork progression in addition to its role in the S phase checkpoint activation (Calzada et al., 2005; Szyjka et al., 2005; Tourriere et al., 2005; Bando et al., 2009; Pardo et al., 2017). One of the essential functions of the replication checkpoint is to stabilize forks and preserve the ability of forks to synthesize DNA after exposure to genotoxic stress (Cortez, 2015). In the absence of a functional replication checkpoint, replication can be terminated irreversibly upon methyl methanesulfonate (MMS) or hydroxyurea (HU) treatment (Tercero and Diffley, 2001; Tercero et al., 2003; Lopes et al., 2006), leading to the accumulation of pathological structures at forks, such as ssDNA gaps and reversed, collapsed, or broken forks (Sogo et al., 2002; Cobb et al., 2003, 2005; Cortez, 2015; Rossi et al., 2015; Pardo et al., 2017). These structures can generate DNA double-stranded breaks (DSBs), a highly deleterious form of DNA lesion threatening genome stability. Homologous recombination (HR) is an essential pathway for the recovery of stalled or collapsed forks and the repair of DSBs (Kowalczykowski, 2015; Haber, 2016; Kramara et al., 2018).

HR utilizes a homologous template, usually a sister chromatid, to direct the repair and generally produces accurate repair products (Kowalczykowski, 2015; Haber, 2016). Deficiencies in HR cause genome instability and cancer (Prakash et al., 2015). During HR, the 5′-ends of DSBs are initially processed by the Mre11–Rad50–Xrs2 complex (MRE11-RAD50-NBS1 in mammals) in conjunction with Sae2 (CtIP in mammals) (Cannavo and Cejka, 2014). Further nucleolytic degradation of the 5′-ends is carried out by the exonuclease Exo1 or the Sgs1 helicase (BLM or WRN in mammals) and Dna2 nuclease (Mimitou and Symington, 2008; Zhu et al., 2008; Cejka et al., 2010; Niu et al., 2010). The 3′-tail ssDNA revealed by resection recruits the conserved ssDNA binding factor RPA. The recombinase Rad51 subsequently replaces RPA on ssDNA with the assistance of the mediator protein Rad52 (BRCA2 in mammals). This leads to the formation of Rad51–ssDNA nucleofilament that performs homology search and strand invasion of homologous duplex DNA (Kowalczykowski, 2015). The DNA synthesis primed by the 3′-end of the invading strand extends D-loop to complete the repair (Kowalczykowski, 2015).

In support of the role of HR in the recovery of stalled forks or in the repair of broken forks, cells deficient in members of the Rad52 epistasis group are sensitive to replication inhibitors (Chang et al., 2002; Lundin et al., 2005). However, paradoxically, multiple evidence showed that the replication checkpoint plays a role in inhibiting HR repair during the S phase. First, Mec1 prevents the formation of Rad52 foci upon HU or MMS treatment in the S phase in an Mrc1-dependent manner (Lisby et al., 2004; Alabert et al., 2009; Gonzalez-Prieto et al., 2013). Second, DSB end resection and HR repair were inhibited when the replication checkpoint is activated by HU or MMS treatment (Alabert et al., 2009; Barlow and Rothstein, 2009). The resection enzyme Exo1 is also negatively regulated by Rad53 to suppress its activity (Cotta-Ramusino et al., 2005; Smolka et al., 2007; Morin et al., 2008). To reconcile these conflicting observations, Alabert et al. (2009) proposed that the DNA replication checkpoint differentially regulates recombination at DSBs and stalled forks (Alabert et al., 2009; Prado, 2014). This differential regulation on HR repair appears to be critical for preserving the integrity of stalled forks (Pardo et al., 2017). However, a critical question that remains unclear is how HR repair is suppressed by replication stress.

In this study, we showed that the Mrc1-dependent replication stress signaling plays a critical role in repressing the 5′-end resection of the HO endonuclease-induced DSB and HR repair. We found that both Sgs1/Dna2 and Exo1 resection pathways are suppressed, and this suppression is relieved by the deletion of *MRC1*, but not *RAD9*. The suppression of resection is specifically mediated by Mrc1 since it is independent of Csm3, Tof1, or Ctf4. Finally, we showed that replication stress induces global chromatin compaction, which blocks the recruitment of the chromatin remodeling factors Ino80, RSC, and Fun30 that are known to function in resection. Our studies provide insight into how HR repair is repressed by replication stress and reveal a critical role of Mrc1-mediated chromatin compaction in coordinating replication and recombination.

# MATERIALS AND METHODS

## Yeast Strains

The yeast strains used in this study are derivatives of JKM139 (*ho MAT**a** hml::ADE1 hmr::ADE1 ade1-100 leu2-3,112 trp1::hisG' lys5 ura3-52 ade3::GAL::HO*) or tGI354 (*MATa-inc arg5,6::MATa-HPH ade3::GAL::HO hmr::ADE1 hml::ADE1 ura3-52*). The genotypes for these strains are listed in **Supplementary Table 1**. The yeast strains were constructed with standard genetic manipulation.

## Analysis of 5′-End Resection by Southern Blot

Yeast cells were grown overnight in the pre-induction YEP–raffinose medium (1% yeast extract, 2% peptone, and 2% raffinose) to a density of $\sim 1 \times 10^7$ cells/ml. DSB induction was initiated by adding 2% galactose. For testing the resection under replication stress, 200 mM HU (final concentration) was added to each sample when starting the galactose induction. Samples were collected at different time points following break induction. DNA isolated by glass bead disruption using a standard phenol extraction method was digested with *E*coRI and separated on 0.8% agarose gels. The resolved DNA was transferred onto a Nylon hybridization transfer membrane (Perkin Elmer). Radiolabeling of DNA probes was carried out according to the manufacturer's instructions (Takara). Southern blotting and hybridization were carried out as described previously (Chen et al., 2012). The signal on the phosphor screen was captured by scanning with an OptiQuant Cyclone Plus machine (Perkin Elmer). Quantities of DNA loaded on gels for each time point were normalized using the *TRA1* DNA probe. The resulting values were further normalized to that of the control sample (uncut). Three independent experiments were performed for each strain.

## Analysis of Ectopic Recombination

To examine the repair kinetics of ectopic recombination, we cultured yeast cells in the pre-induction medium (YEP–Raffinose) overnight to the early log phase. Then, 2% of galactose was added to induce the HO cut that generates a single DSB on chromosome V. Samples were collected at different time points. Genomic DNA was extracted using a standard phenol extraction method and digested with *E*coRI. Purified DNA was resolved on 0.8% agarose gel followed by transfer onto a positively charged nylon membrane (Perkin Elmer). Southern blotting and hybridization with radiolabeled DNA probes were performed as described previously (Zhu et al., 2008; Chen et al., 2012). The blot was exposed in a phosphor screen. The signal on the screen was captured by scanning in an OptiQuant Cyclone Plus machine (Perkin Elmer). We quantified and normalized the pixel intensity of target bands to that of corresponding parental bands on blots. The resulting values were further normalized to that of the control sample (uncut). Three independent experiments were performed for each strain.

## Drug Sensitivity Test

Yeast cells were grown in YEPD-rich medium overnight to saturation. Undiluted cell culture and 1/10 serial dilutions of each cell culture were spotted onto YPD plates containing different DNA-damaging agents at indicated concentrations. The plates were incubated at 30°C for 3 days before analysis.

## Chromatin Immunoprecipitation

Chromatin immunoprecipitation assays were carried out as previously described (Chen et al., 2012). Cultures were grown to a density of about $1 \times 10^7$ cells/ml in the pre-induction medium (YEP–raffinose), and the expression of HO endonuclease was induced by adding 2% galactose. The cells were fixed with 1% formaldehyde and incubated for 10 min at room temperature with rotation. The reaction was quenched by adding 125 mM of glycine, followed by incubating at room temperature for 5 min with rotation. The cells were lysed with glass beads in lysis buffer (50 mM HEPES, pH 7.5, 1 mM EDTA, 140 mM NaCl, 1% Triton X-100, 0.1% NaDOC, 1 mg/ml bacitracin, 1 mM benzamidine, and 1 mM PMSF) supplemented with protease inhibitors. The whole-cell extracts were sonicated with a Bioruptor (Diagenode) to shear the DNA to an average size of 0.5 kb. After centrifugation, the supernatant was collected and incubated with anti-Myc (Sigma M4439) or anti-FLAG (CST) antibody overnight at 4°C, followed by incubating with protein G-agarose beads for 3 h at 4°C. The protein-bound beads were washed twice with lysis buffer, twice with lysis buffer containing 500 mM NaCl, twice in wash buffer (10 mM Tris-HCl, pH 8.0, 1 mM EDTA, 0.25 M LiCl, 0.5% NP-40 substitute, and 0.5% NaDOC), and twice in ×1 TE. The protein–DNA complexes were eluted with elution buffer (10 mM Tris-HCl, pH 8.0, 10 mM EDTA, pH 8.0, and 1% SDS) and incubated at 65°C overnight to reverse crosslinking. The samples were digested with proteinase K at 37°C for 12 h. DNA was purified by phenol extraction and ethanol precipitation. The purified DNA samples were analyzed by real-time quantitative PCR, with primers that specifically anneal to DNA sequences located at indicated distances from the DSB, using the following conditions: 95°C for 10 min and 40 cycles of 95°C for 15 s and 60°C for 1 min.

## Western Blotting

Whole-cell yeast extracts were prepared using the trichloroacetic acid method as previously described (Chen et al., 2012). The pelleted cells from 5 ml of culture were washed once with water and resuspended in 10% trichloroacetic acid. The cells were lysed by vortexing with glass beads, and the protein lysates were pelleted by centrifugation at 12,000 g for 15 min. The pellets were washed with ice-cold 80% acetone, and proteins were dissolved in ×2 SDS sample loading buffer by boiling for 5 min. The samples were centrifuged for 5 min at 12,000 g, and the supernatant was retained as protein extract. The samples were resolved on 8% SDS-PAGE gel and transferred onto a polyvinylidene difluoride membrane (Immobilon-P; Millipore) using a semi-dry method. Anti-Myc and anti-FLAG antibodies were purchased from MBL. GAPDH was purchased from GeneTex. Anti-mouse and rabbit IgG HRP-conjugated secondary antibodies were purchased from Santa Cruz Biotechnology. Blots were developed using the Western Blotting substrate (Bio-Rad).

## MNase Digestion

MNase digestion of chromatin was performed as described (Chen et al., 2012). Yeast cells from 80 ml of culture ($\sim 2 \times 10^7$ ml$^{-1}$) were collected and washed with sterilized $H_2O$. The cells were resuspended in 900 μl of sorbitol solution (1 M sorbitol, 50 mM Tris-Cl, pH 7.5), followed by the addition of 0.56 μl of β-mercaptoethanol (14.3 M) and 100 μl of zymolase 20T stock (dissolved in sorbitol solution, 25 mg/ml). The samples were incubated at 30°C with rotation for 25–40 min to digest the cell wall. Spheroplasts were collected by centrifugation at 12,000 g for 2 min and washed twice with ice-cold sorbitol solution. The pellet

was resuspended with lysis buffer (0.5 mM spermidine, 1 mM β-mercaptoethanol, 0.075% Nonidet P-40, 50 mM NaCl, 10 mM Tris-HCl, pH 8.0, 5 mM $MgCl_2$, 5 mM $CaCl_2$, plus protease inhibitors). Then, 100 unit/ml of micrococcal nuclease (NEB, M0247) was added to each sample. After mixing, 200 μl of nuclei suspension was immediately taken out as an undigested control. The remaining samples were subjected to MNase digestion at 37°C. Aliquots of nuclei suspension were taken out at indicated time points, and the reactions were stopped by the addition of 20 mM EDTA, pH 8.0, and 1% SDS. The supernatants were collected by centrifugation at 12,000 g for 10 min, followed by Proteinase K digestion (0.1 mg/ml) at 50°C for 3 h. DNA was purified by phenol–chloroform extraction and precipitated by ethanol precipitation. DNA pellet was dissolved in ×1 TE and digested with RNase A. Equal amounts of total DNA were resolved on 1.5% agarose gels and visualized by ethidium bromide staining.

# RESULTS

## Replication Stress Inhibits DSB End Resection, RPA Loading, and HR Repair

Previous studies have revealed that resection of 5′-ends of DSBs is inhibited upon HU treatment that causes replication stress by reducing the dNTP level (Alabert et al., 2009; Barlow and Rothstein, 2009). To verify this result, we employed a haploid yeast system wherein a single unrepairable DSB is generated at the *MAT*a locus on chromosome III upon induction of the HO endonuclease by galactose (Zhu et al., 2008). The donor sequences *HML* and *HMR* were deleted so that the cells cannot repair the DSB by HR. We compared the resection kinetics for the wild-type (WT) cells in the presence or absence of HU treatment. In unperturbed cells, the 5′-end resection proceeded normally as reported previously (Zhu et al., 2008; Chen et al., 2012). However, in the presence of constant HU treatment (200 mM), resection was completely blocked in the initial 2–4 h no matter at proximal ends or at 5 or 10 kb distal ends (**Figures 1A–D**). However, resection started to occur at proximal ends after 4 h and at 5 or 10 kb location after 6 h (**Figures 1A–D**). Therefore, the regulation of resection under constant HU treatment can be divided into two stages. In the initial 2–4 h, resection is severely suppressed, but the suppression becomes alleviated afterwards even in the presence of constant HU treatment. This is consistent with the observation that cells can bypass the S phase checkpoint and proceed through the cell cycle after prolonged HU incubation (Uzunova et al., 2014).

As a consequence, recruitment of the ssDNA binding proteins RPA and Rad51 was severely impaired within the initial 4 h, while their recruitment started to occur after 4 h (**Figure 1E**). Next, we evaluated DSB repair by ectopic recombination using a repair system in which a single HO-induced DSB is repaired by using the homologous sequence on chromosome III as a donor (**Figure 1F**) (Ira et al., 2003; Prakash et al., 2009). By Southern blot analysis, we found that the repair proceeded much slower in the presence of HU compared to that in the unperturbed cells (**Figures 1G,H**). Interestingly, the level of crossover products was reduced under replication stress (**Figure 1I**). These results together indicate that HU-induced replication stress represses resection and DSB repair by HR.

## Both Sgs1–Dna2 and Exo1 Pathways Are Repressed

Long-range resection is carried out by two partially redundant pathways mediated by Sgs1–Dna2 or Exo1 (Mimitou and Symington, 2008; Zhu et al., 2008; Cejka et al., 2010; Niu et al., 2010). To delineate which pathway was inhibited by replication stress, we compared the resection rate for *sgs1Δ* or *exo1Δ* mutant in the absence or presence of HU treatment. Compared to the unperturbed condition, replication stress severely impaired resection in the *exo1Δ* mutant, indicating that the Sgs1–Dna2 pathway was suppressed (**Figures 2A,B**). Similarly, resection in *sgs1Δ* cells was also severely impaired under HU treatment, indicating that the Exo1-mediated pathway was also suppressed. Consistently, recruitment of the resection enzymes Sgs1, Dna2, and Exo1 was nearly abolished at 4 h under replication stress compared to the unperturbed condition (**Figure 2C**). These results indicate that replication stress impairs the recruitment of the resection enzymes, thereby repressing DSB end resection.

## Mrc1 Is Critical to Mediate the Suppression of Resection Upon Replication Stress

Mrc1 travels with the replisome and is essential to sense and activate the checkpoint upon replication stress (Tanaka and Russell, 2001; Katou et al., 2003; Smolka et al., 2006; Xu et al., 2006; Lou et al., 2008; Komata et al., 2009). We tested whether Mrc1 mediates the HU-induced repression of DSB end resection. Interestingly, we found that, in unperturbed conditions, the *mrc1Δ* mutant exhibited faster resection at proximal or distal ends when compared to WT cells (**Figures 3A,B**), suggesting that Mrc1 plays a role in limiting resection in cycling cells. In the presence of HU treatment, resection in *mrc1Δ* cells became slower as compared to unperturbed conditions. However, when compared to the HU-treated WT cells, resection was much faster in HU-treated *mrc1Δ* mutant cells (**Figures 3A,B**), indicating an important role of Mrc1 in mediating the suppression of resection. Consistently, the deletion of *MRC1* partially restored the recruitment of Dna2 and Exo1 and the loading of RPA and Rad51 4 h after HU treatment (**Figures 3C,D**). The levels of these proteins are comparable between WT and *mrc1Δ* cells, suggesting that the differences in their loading were not due to any changes in their protein levels (**Supplementary Figure 1**). Although resection occurred at late hours, the Mrc1-deficient cells still failed to repair DSBs by ectopic recombination in the presence of HU and showed hypersensitivity to HU or MMS (**Supplementary Figure 2**). This may reflect the role of Mrc1 in mediating the replication checkpoint and in ensuring fork progression or restart at stalled forks.

## The Replication Checkpoint Is Essential to Maintain Suppression

Next, we asked whether the Mrc1-mediated replication checkpoint is required to maintain the suppression on resection.

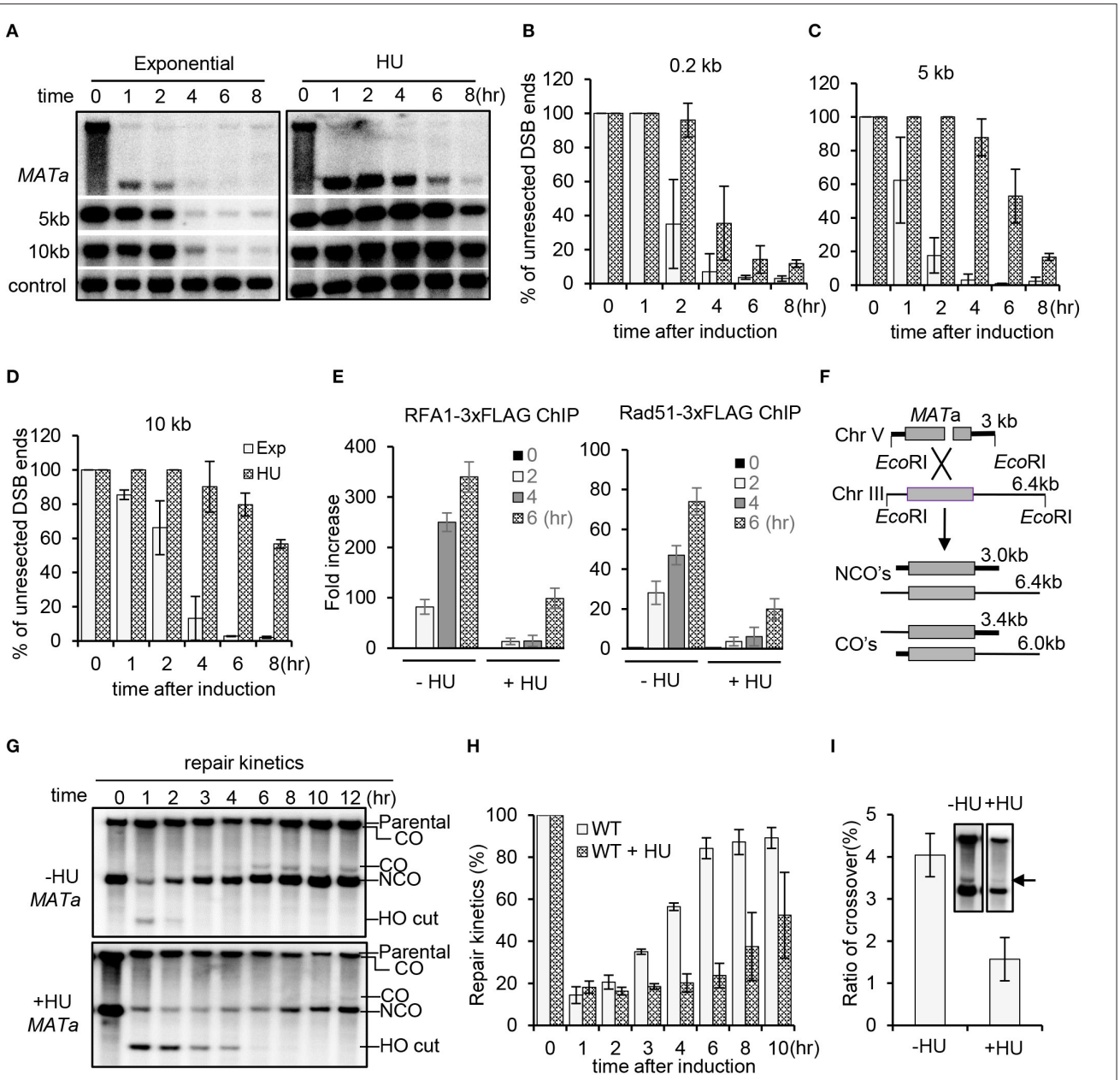


**FIGURE 1 |** Replication stress inhibits DSB end resection and homologous recombination repair. **(A)** Southern blot analysis of resection kinetics for wild-type (WT) cells with or without hydroxyurea (HU) treatment. The location of probes is indicated. The *TRA1* probe was used as a loading control. The HO cut was induced by adding 2% galactose to early-log-phase cells grown in YP-raffinose. To induce replication stress, 200 mM HU was added into each cell culture when initiating DSB induction, and the cells were cultured under constant HU treatment. Samples were taken at indicated time points. Exp, exponential cells (without HU treatment). **(B–D)** Quantification of Southern blot presented in **(A)**. **(E)** Chromatin immunoprecipitation analysis of the recruitment of RPA−3xFLAG or Rad51–3xFLAG at DSB ends (1 kb location). DSB induction and HU treatment were carried out as described above. **(F)** Scheme showing an ectopic recombination system. CO, crossover; NCO, non-crossover. **(G,H)** Southern blot analysis and quantification of repair kinetics for WT cells with or without HU treatment. DSB induction and HU treatment were carried out as described in **(A)**. **(I)** Southern blot and quantification showing the levels of crossover products (12 h). The arrow indicates crossover products. Error bars represent the standard deviation from three independent experiments.

To this end, the WT cells were first treated with HU for 2 h. Half of the culture was washed and allowed to recover in fresh medium without HU, while the other half remained with constant HU treatment. We monitored the kinetics of checkpoint activation and the progression of DSB end resection. The replication checkpoint was activated within 1 h following HU treatment as indicated by the phosphorylation of Mrc1 and Rad53 (**Figure 4A**). After removing HU, the checkpoint

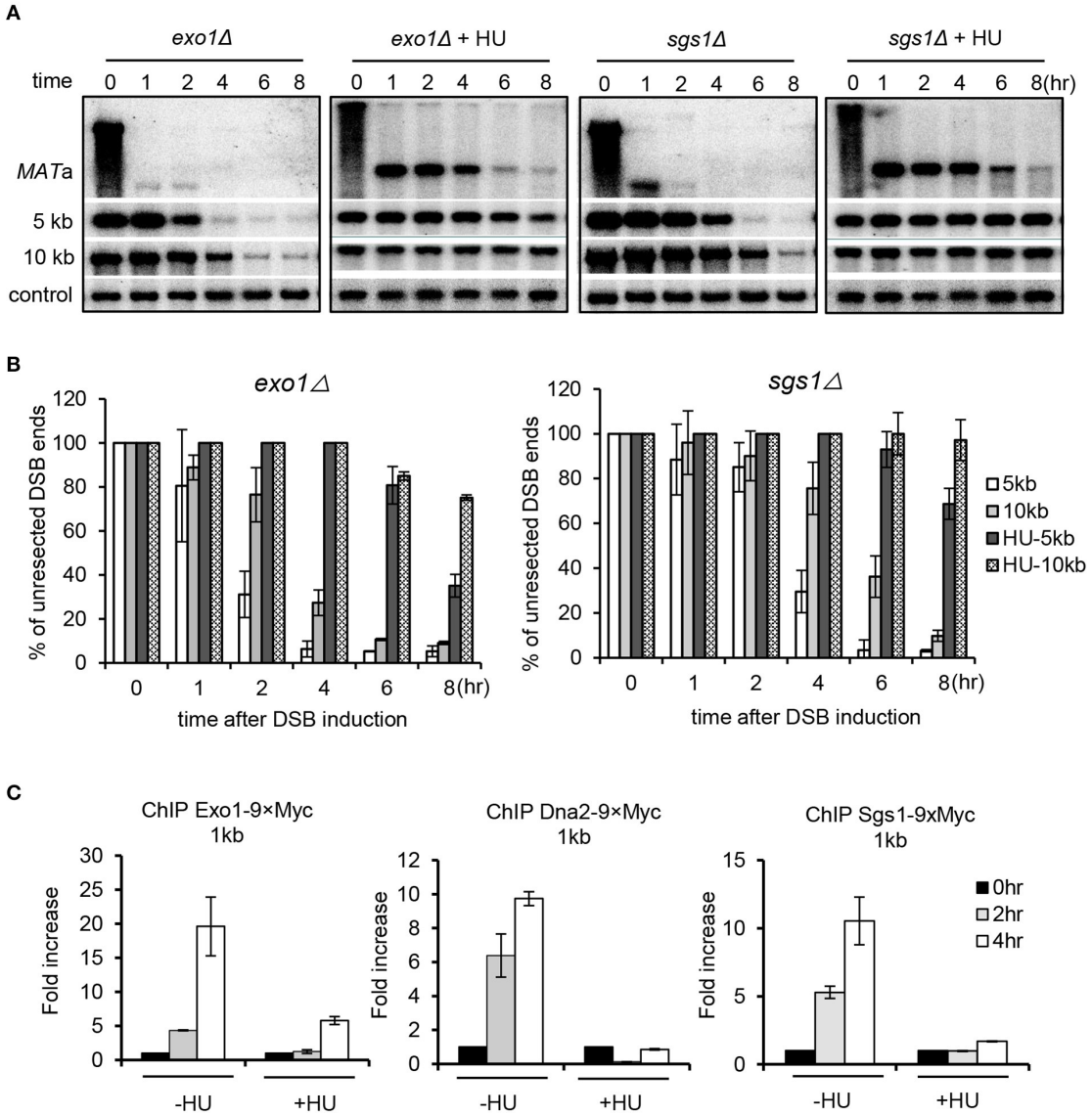


**FIGURE 2 |** Replication stress inhibits both Sgs1/Dna2 and Exo1 resection pathways. **(A,B)** Southern blot analysis and quantification of DSB end resection for the indicated mutant cells with indicated probes. **(C)** Chromatin immunoprecipitation analysis of the recruitment of Exo1–9xMyc, Dna2–9xMyc, or Sgs1–3xFLAG at DSB ends (1 kb location). DSB induction and hydroxyurea treatment for experiments in this figure were performed as described in **Figure 1A**. Samples were collected at indicated time points. Error bars represent the standard deviation from three independent experiments.

was quickly turned off since both Mrc1 and Rad53 were dephosphorylated (**Figure 4A**). Importantly, we observed that the removal of HU also quickly alleviated the suppression of resection (**Figures 4B,C**). However, under constant HU treatment, Rad53 dephosphorylation was apparently slower. Accordingly, the suppression of resection was sustained longer (**Figures 4B,C**). Thus, the suppression of resection correlates with the status of replication checkpoint activation. These results suggest that the Mrc1-mediated replication checkpoint signaling is essential to suppress DNA end resection and to maintain this suppression.

## Mrc1-Mediated Suppression of Resection Is Independent of Csm3, Tof1, or Ctf4

The checkpoint proteins Mrc1, Csm3, and Tof1 can form a heterotrimeric complex that travels with the replication fork and mediates the activation of replication checkpoint (Katou et al., 2003; Noguchi et al., 2004; Calzada et al., 2005). We tested whether Csm3 and Tof1 are involved in the suppression of resection. We monitored resection for the *csm3Δ* or *tof1Δ* mutant cells with constant HU treatment. The result showed that the resection rate in the *csm3Δ* or *tof1Δ* mutant resembles that of WT cells, and it was significantly

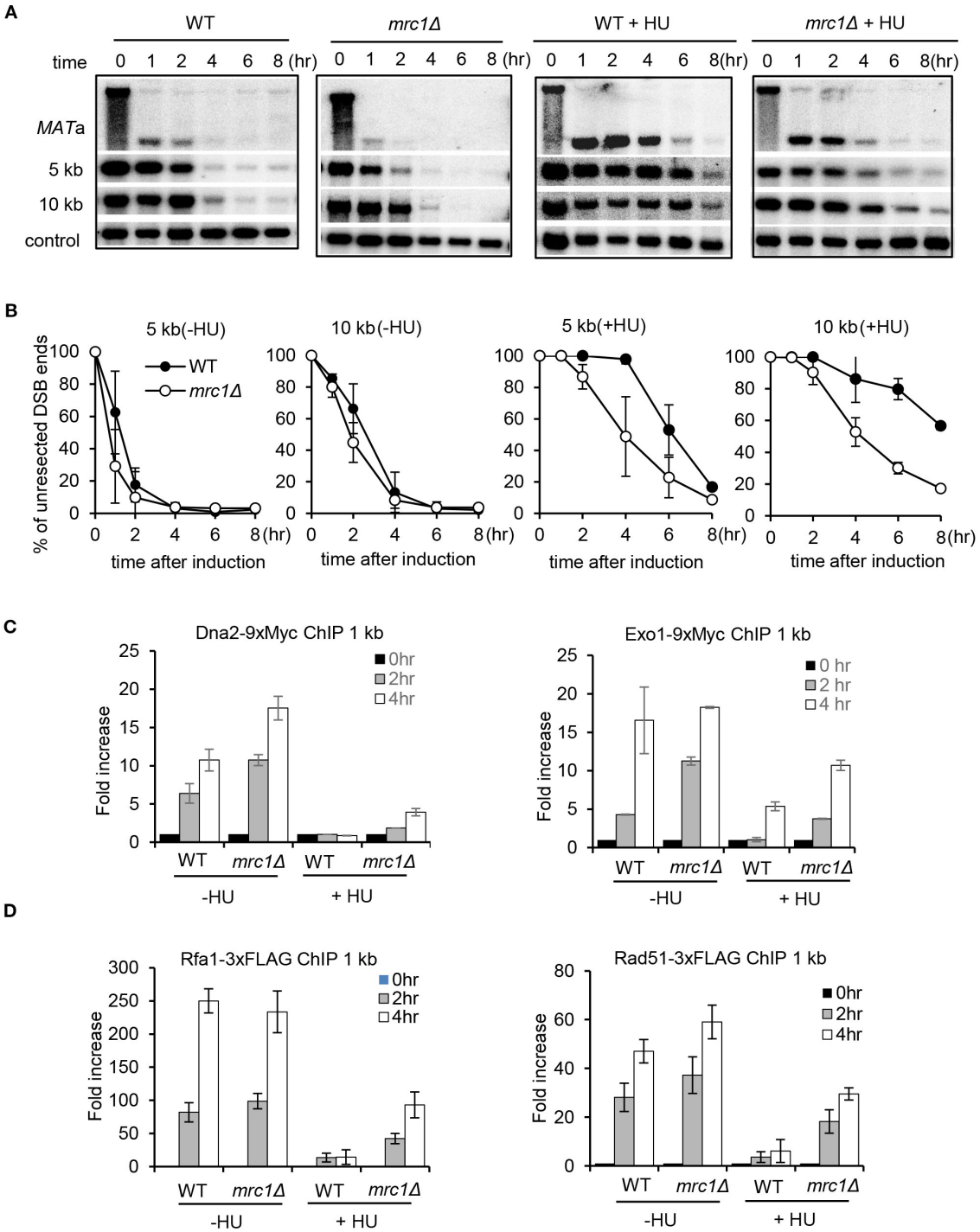


**FIGURE 3 |** Mrc1 mediates the HU-induced inhibition on DSB end resection. **(A,B)** Southern blot analysis and quantification of DSB end resection for wild-type or *mrc1Δ* mutant cells with or without HU treatment. The location of probes is indicated. **(C,D)** Chromatin immunoprecipitation analysis of the recruitment of Dna2–9xMyc, Exo1–9xMyc, Rfa1–3xFLAG, or Rad51–3xFLAG at DSBs in indicated cells with or without HU treatment. For HU treatment in **(A–D)**, 200 mM HU was added into each sample when starting DSB induction, and the cells were cultured under constant HU treatment. Samples were collected at indicated time points after DSB induction. Error bars denote standard deviation from three independent experiments.

slower than that observed in *mrc1Δ* cells (**Figures 5A,B**). It was recently reported that the replisome component Ctf4 functions as a key regulator suppressing DSB end resection at arrested forks in rDNA region (Sasaki and Kobayashi, 2017). We examined whether it affects DSB end resection under replication stress. We found that deletion of *CTF4* did not

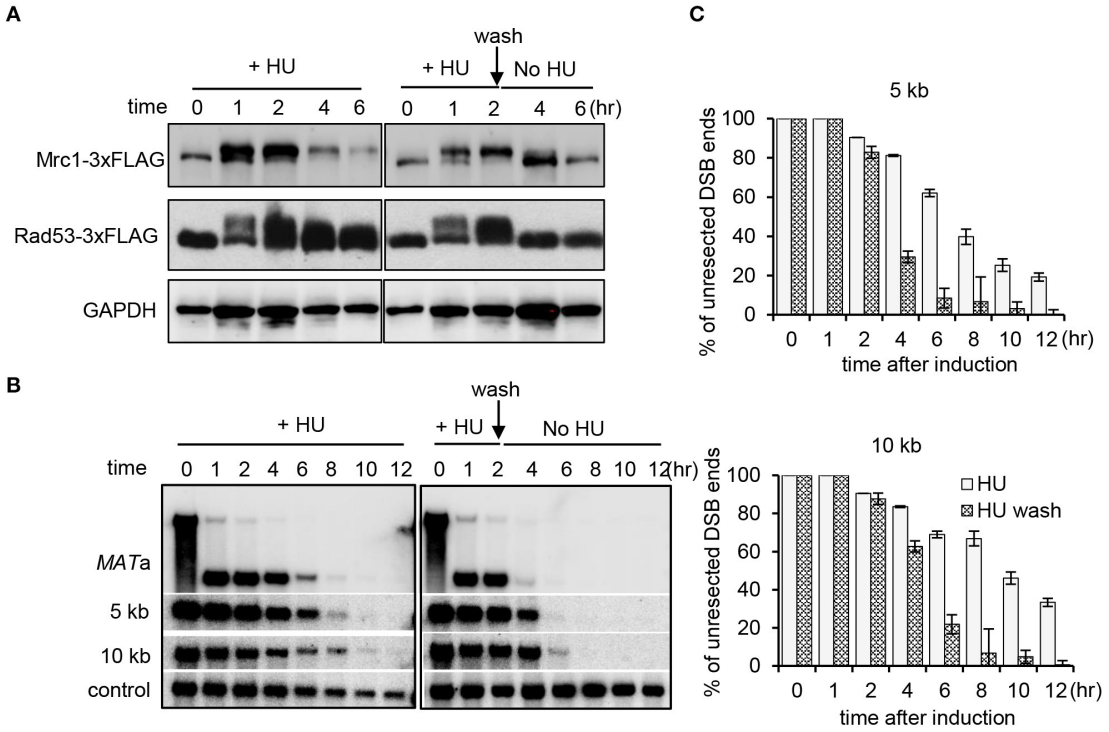


**FIGURE 4 |** Mrc1-mediated replication checkpoint is essential for the maintenance of inhibition on resection. **(A)** Western blot showing replication checkpoint activation as indicative of the phosphorylation of Mrc1 and Rad53. GAPDH serves as a loading control. The WT cells were first treated with HU for 2 h. Then, half of the culture was washed and allowed to recover in fresh medium without HU, while the other half remained with constant HU treatment. **(B)** Southern blot analysis of double-stranded break end resection for WT cells with HU treatment or during the recovery. HU treatment was performed as described in **(A)**. Samples were taken at indicated time points. **(C)** Quantification of the Southern blot is presented in **(B)**. Error bars denote standard deviation from three independent experiments.

alleviate the inhibition on resection (**Figures 5A,B**). These results together suggest that the Mrc1-mediated suppression of resection under replication stress is largely independent of Csm3, tof1, or Ctf4.

## The Deletion of *RAD9* Fails to Restore Resection Under Replication Stress

Rad9, the mediator protein for the DNA damage checkpoint, is known to form a physical barrier suppressing resection at DSB ends (Lazzaro et al., 2008; Chen et al., 2012). Rad9 is recruited to damaged chromatin *via* associating with Dpb11, histone H3 methylated on K79, or H2A phosphorylated on Serine 129 (Wysocki et al., 2005; Toh et al., 2006; Grenon et al., 2007; Puddu et al., 2008; Pfander and Diffley, 2011). Consistent with previous studies, we found that lack of either Rad9 or Dot1, the methyltransferase for H3K79 methylation, resulted in faster resection as compared to WT cells in unperturbed conditions (**Figures 6A,C**) (Lazzaro et al., 2008; Chen et al., 2012). We then tested whether deletion of *RAD9* or *DOT1* could bypass the suppression on resection under replication stress. However, we found that resection in both *rad9Δ* and *dot1Δ* mutant cells remained inhibited in the presence of HU as seen in WT cells (**Figures 6B,D**). Thus, the replication stress-induced suppression of resection cannot be bypassed by removing H3K79 methylation or Rad9. However, we noted that Rad9 was not recruited properly at DSBs under replication stress as compared to that in unperturbed conditions (**Figure 6E**). These results together reveal a unique role of Mrc1-mediated replication checkpoint in inhibiting DSB end resection.

## Replication Stress Induces Global Chromatin Compaction and Impairs the Recruitment of Chromatin Remodeling Factors

In fission yeast, it was recently reported that replication stress induces the deacetylation of H2B-K33Ac and tri-methylation on H3K79, thereby triggering chromatin compaction (Feng et al., 2019). We compared the chromatin structure of WT cells in the presence or absence of HU treatment using the MNase digestion. We observed that, compared to untreated cells, HU treatment (2 h) led to the apparent compaction of chromatin as reflected by the poor digestion of chromatin DNA by MNase (**Figure 7A**). Importantly, we noted that HU treatment also resulted in chromatin compaction in the *mrc1Δ* mutant, but it

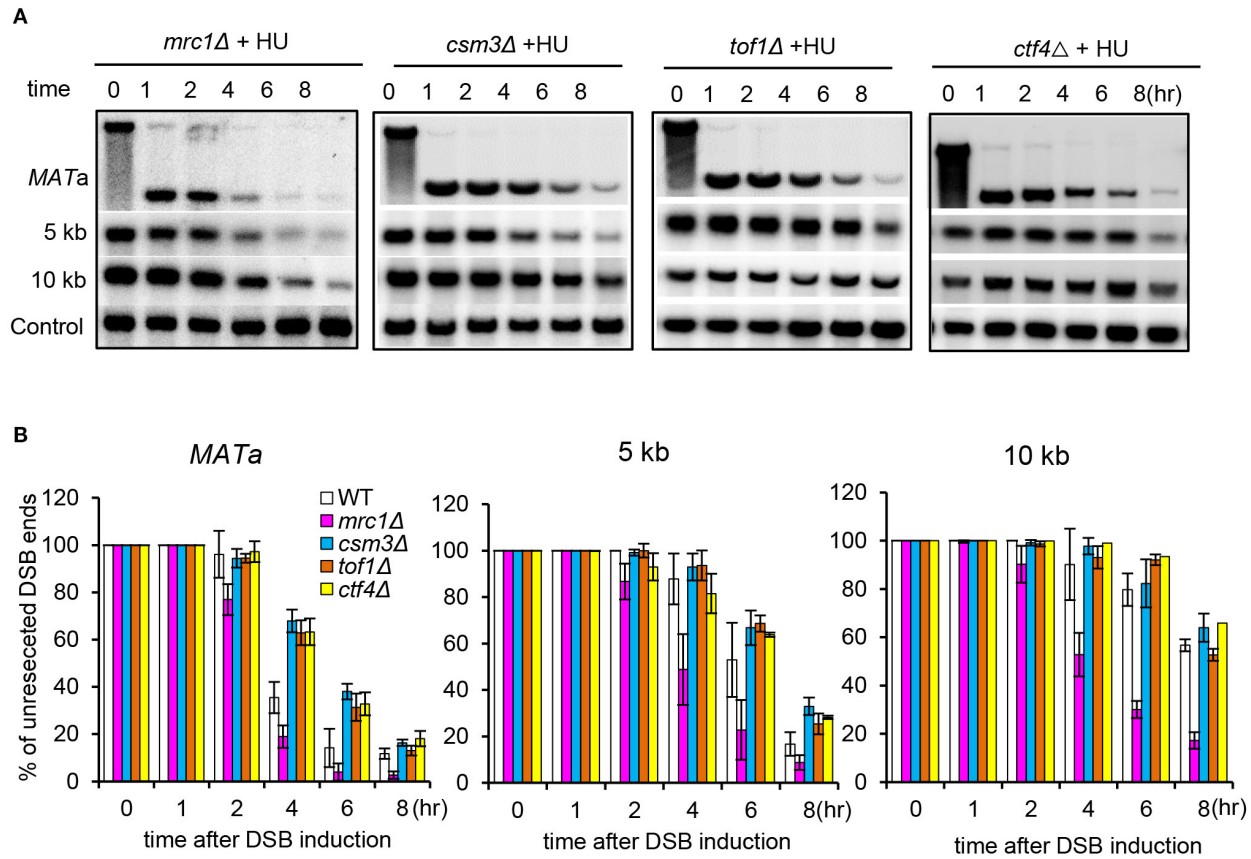


**FIGURE 5 |** Mrc1-mediated suppression of resection is independent of Csm3, Tof1, or Ctf4. **(A,B)** Southern blot analysis and quantification of DSB end resection at indicated locations for the indicated mutant cells with HU treatment. For HU treatment, 200 mM HU was added into each sample when initiating DSB induction, and the cells were cultured under constant HU treatment. Samples were collected at indicated time points after DSB induction. Error bars denote standard deviation from three independent experiments.

was less severe than that in WT cells, suggesting that Mrc1 is required to induce condensed chromatin under replication stress.

Several ATP-dependent chromatin remodelers are recruited to DSBs, where they act to remodel local chromatin structure and to promote DSB repair (Chai et al., 2005; Shim et al., 2007; Chen et al., 2012; Costelloe et al., 2012; Seeber et al., 2013; Wiest et al., 2017). Consistently, we observed enrichment of the chromatin remodelers Ino80, RSC, Fun30, or Snf5 at DSB ends 4 h following break induction in the absence of HU (**Figure 7B**). However, their enrichment was significantly reduced in cells with constant HU treatment. Next, we tested whether the loading of Mre11, which recognizes DNA breaks, was affected under replication stress. We noted that Mre11–3xFLAG was efficiently recruited to DSBs in unperturbed cells, while its recruitment was slightly impaired in HU-treated cells at 4 h after DSB induction, suggesting that recognition of DSBs by Mre11 on the compacted chromatin was modestly affected (**Figure 7C**). These results together suggest that the Mrc1-mediated replication checkpoint induces global chromatin condensation that limits the access of chromatin remodelers, resection machinery, and repair proteins to the damaged site, leading to the suppression of HR repair.

## DISCUSSION

Cells in the S phase are particularly vulnerable to genotoxic stresses that can lead to replication stress and genome instability, which are hallmarks of cancer. It is known that HR proteins are important to protect and restart stressed forks (Prado, 2014; Branzei and Szakal, 2017; Pardo et al., 2017). Paradoxically, the Mrc1-dependent checkpoint was shown to prevent HR repair at DSBs or arrested forks (Prado, 2014; Garcia-Rodriguez et al., 2018). How the replication checkpoint inhibits HR remains unclear. In this study, we showed that the replication stress-induced checkpoint mediated by Mrc1 represses both Sgs1/Dna2 and Exo1 resection pathways, leading to defective RPA and Rad51 loading and HR repair. Mechanistically, we found that the Mrc1-dependent checkpoint induces global compaction of chromatin that blocks the access of multiple chromatin remodeling factors and resection machinery. We also show that the suppression of resection in the S phase is specifically mediated by the replication checkpoint mediator Mrc1 but is independent of the replisome components Csm3, Tof1, or Ctf4 or the DNA damage checkpoint mediator Rad9.

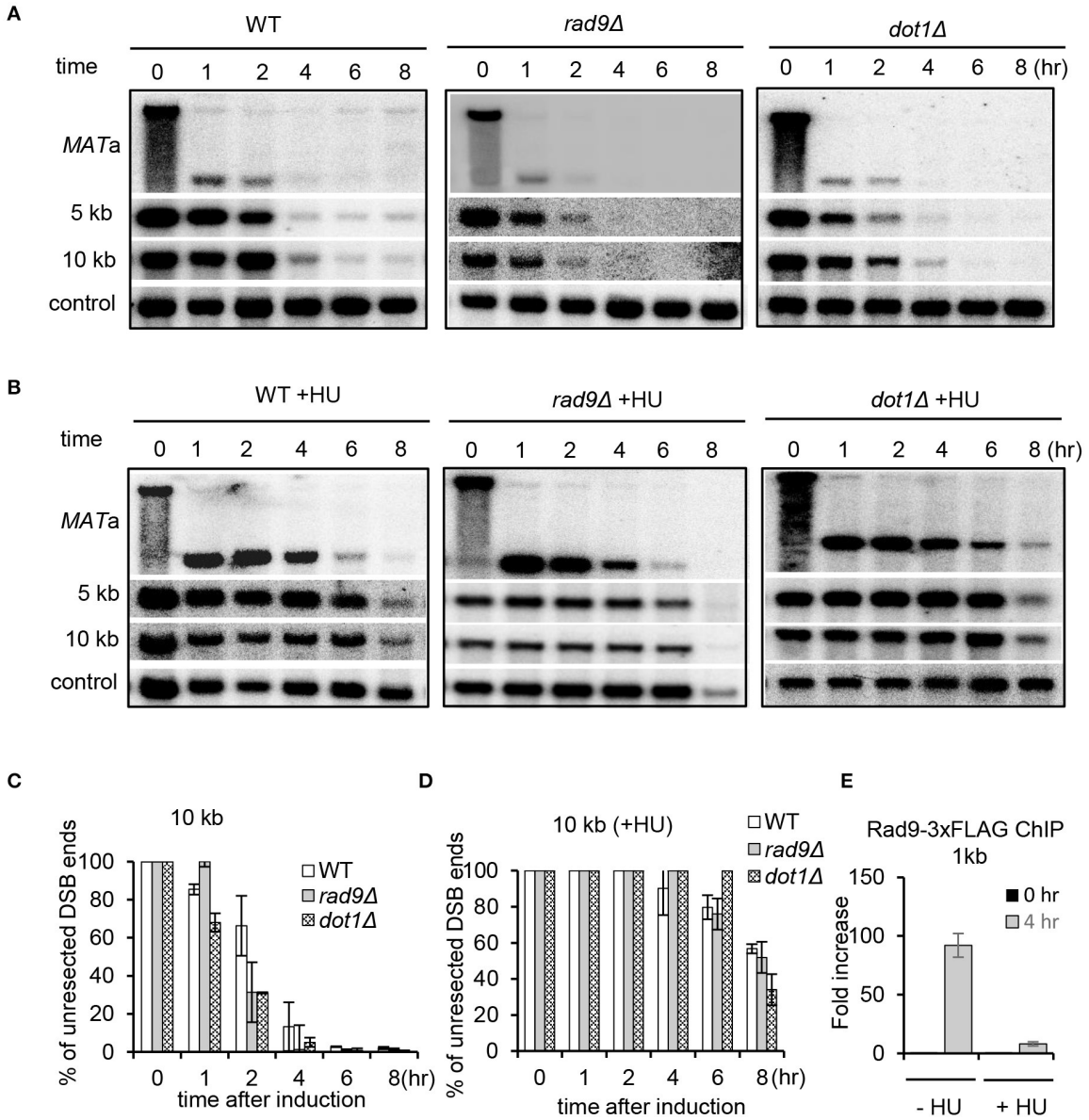


**FIGURE 6 |** The deletion of *RAD9* fails to increase resection under replication stress. **(A,B)** Southern blot analysis and quantification of DSB end resection for the indicated mutant cells with or without HU treatment. HU treatment was performed as described in **Figure 1A**. **(C,D)** Quantification of the Southern blot shown in **(A)** and **(B)**. **(E)** Chromatin immunoprecipitation analysis of Rad9–3xFLAG recruitment at DSB ends (1 kb) in the absence or presence of HU treatment. Error bars denote standard deviation from three independent experiments.

Why do cells inhibit HR repair, given that HR proteins are required to protect or restart stressed forks? It was proposed that the replication checkpoint may differentially regulate recombination at DSBs and replication forks (Alabert et al., 2009). Cells must prevent undesired or premature HR repair that can lead to errors, loss of heterozygosity, or genome arrangement, especially when it is initiated with templates other than the sister chromatid (Alcasabas et al., 2001; Branzei and Szakal, 2017). The suppression of HR provides a time window of opportunity to protect and stabilize the forks, allowing repair or bypass of the DNA lesion before fork restart (Barlow and Rothstein, 2009). The spatial–temporal separation of HR at DSBs and stressed forks allow cells to repair the damaged DNA after completing the S phase, whereupon the stress is relieved (Pardo et al., 2017).

We provided evidence that the replication stress-induced suppression of resection depends on Mrc1, but not Rad9. Consistently, we found that Rad9 is not recruited to DSBs under HU treatment (**Figure 6E**). These two mediators play distinct functions in sensing the checkpoint in the S phase. The Mrc1-dependent pathway primarily monitors the state of the replisome

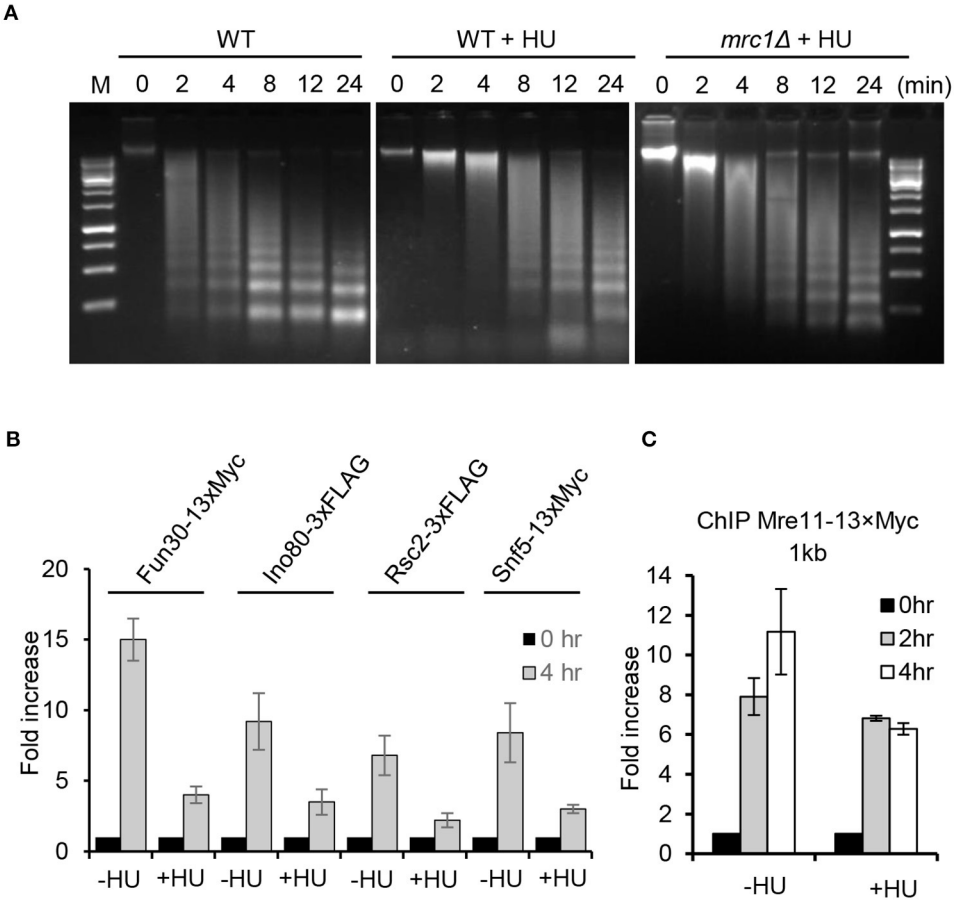


**FIGURE 7 |** Replication stress induces global chromatin compaction. **(A)** MNase digestion of chromatin DNA for the indicated cells with or without HU treatment. For HU treatment, the cells were treated with 200 mM HU for 2 h. Chromatin samples were collected after different time points of MNase digestion. **(B,C)** Chromatin immunoprecipitation analysis of Fun30–13xMyc, Ino80–3xFLAG, Rsc2–3xFLAG, Snf5–13xMyc, or Mre11–13xMyc recruitment at double-stranded break ends (1 kb) in the absence or presence of HU treatment. For HU treatment, the cells were cultured in the presence of 200 mM HU for 2 or 4 h. Samples were taken at indicated time points. Error bars denote standard deviation from three independent experiments.

and is considered to be associated closely with replication forks (Garcia-Rodriguez et al., 2018). This pathway is independent of the exonuclease Exo1 that is involved in expanding ssDNA gaps (Garcia-Rodriguez et al., 2018). In contrast, more ssDNA is accumulated behind the fork upon MMS or UV exposure, which activates the Rad9-dependent pathway. This pathway senses DNA lesions in the daughter-strand gap left behind the replisome and in an Exo1-dependent manner (Garcia-Rodriguez et al., 2018).

Mrc1 forms a complex with Csm3 and Tof1, and the association of Mrc1 with replication forks partially depends on Csm3 and Tof1 (Tourriere et al., 2005; Bando et al., 2009; Prado, 2014; Pardo et al., 2017). This complex is critical for proper activation of the replication checkpoint and protection or restart of stalled forks (Tourriere et al., 2005; Bando et al., 2009; Prado, 2014; Pardo et al., 2017). However, there are multiple pieces of evidence showing that these proteins also have non-overlapping functions. For example, Mrc1-deficient cells are more sensitive to HU than *tof1Δ* mutant cells (Tourriere et al., 2005). Compared to Tof1, Mrc1 is more important in preventing the fragility and instability of long CAG repeats (Gellon et al., 2019). Notably, it was reported that Mrc1 plays a major role in the activation of the replication checkpoint, while Tof1 likely only plays an indirect role in this process (Tourriere et al., 2005). These differences may explain why the replication stress-induced suppression of resection depends on Mrc1, but not Csm3, Tof1, or Ctf4.

Notably, we observed that HU treatment induces global chromatin compaction that partially depends on Mrc1, leading to the blockage of the access of chromatin remodeling factors and resection machinery (**Figures 7A,B**). This is consistent with the observation that replication stress also triggers chromatin compaction in fission yeast (Feng et al., 2019). It was reported that replication stress induces the deacetylation of histone H2B-K33ac by Clr6 and the enrichment of H3K9 tri-methylation at stalled forks, which contributes to the formation of a compacted chromatin environment (Feng et al., 2019). Constitutive mimic acetylation of H2B-K33ac leads to uncoupling of replicative helicase and DNA polymerases and

replication fork instability (Feng et al., 2019). Thus, replication stress-triggered chromatin compaction is likely a conserved cellular response. However, whether Mrc1-dependent chromatin compaction in yeast is affected by similar histone modifications remains to be determined.

Chromatin compaction can also result from other mechanisms. For example, in mammalian cells, DSBs can induce temporary chromatin compaction that involves the macro-histone variant macroH2A1 and demethylation of H3-K9 (Khurana et al., 2014; Oberdoerffer, 2015). This change facilitates the accumulation of BRCA1 at DSBs (Khurana et al., 2014; Oberdoerffer, 2015). In yeast mitosis, chromatin compaction can be defined as two mechanistically distinct processes (Kruitwagen et al., 2015): one is called chromatin compaction, mediated by Ipl1-dependent H3S10 phosphorylation that recruits the deacetylase Hst2 to remove H4K16 acetylation, leading to a tighter packing of neighboring nucleosomes (Wilkins et al., 2014; Kruitwagen et al., 2015); the other is a condensin-dependent axial chromosome contraction process that promotes the long-range contraction of chromosomes (Kruitwagen et al., 2015; Hirano, 2016). It was also reported that lack of HMO1, the mobile chromatin-binding protein, confers chromatin hypersensitivity to nuclease and creates a more accessible chromatin state (Panday and Grove, 2017). Therefore, it is important to determine whether the replication stress-induced chromatin compaction in yeast is related to these factors.

## DATA AVAILABILITY STATEMENT

The original contributions presented in the study are included in the article/**Supplementary Material**, further inquiries can be directed to the corresponding author/s.

## AUTHOR CONTRIBUTIONS

PX designed and conducted the majority of the experiments. YD, JZ, ZZ, ZL, YW, and ML constructed some yeast strains and participated in DNA extraction. XC supervised the study. PX and XC wrote the manuscript. XZ discussed the data and critically read the manuscript. All authors contributed to the article and approved the submitted version.

## FUNDING

This work was supported by the National Natural Science Foundation of China (32070573, 31872808, and 31671294) and Advanced Genetics Course grant by Wuhan University Graduate School to XC.

## SUPPLEMENTARY MATERIAL

The Supplementary Material for this article can be found online at: https://www.frontiersin.org/articles/10.3389/fcell.2021.630777/full#supplementary-material

## REFERENCES

Alabert, C., Bianco, J. N., and Pasero, P. (2009). Differential regulation of homologous recombination at DNA breaks and replication forks by the Mrc1 branch of the S-phase checkpoint. *EMBO J.* 28, 1131–1141. doi: 10.1038/emboj.2009.75

Alcasabas, A. A., Osborn, A. J., Bachant, J., Hu, F., Werler, P. J., Bousset, K., et al. (2001). Mrc1 transduces signals of DNA replication stress to activate Rad53. *Nat. Cell Biol.* 3, 958–965. doi: 10.1038/ncb1101-958

Bando, M., Katou, Y., Komata, M., Tanaka, H., Itoh, T., Sutani, T., et al. (2009). Csm3, Tof1, and Mrc1 form a heterotrimeric mediator complex that associates with DNA replication forks. *J. Biol. Chem.* 284, 34355–34365. doi: 10.1074/jbc.M109.065730

Barlow, J. H., and Rothstein, R. (2009). Rad52 recruitment is DNA replication independent and regulated by Cdc28 and the Mec1 kinase. *EMBO J.* 28, 1121–1130. doi: 10.1038/emboj.2009.43

Branzei, D., and Szakal, B. (2017). Building up and breaking down: mechanisms controlling recombination during replication. *Crit. Rev. Biochem. Mol. Biol.* 52, 381–394. doi: 10.1080/10409238.2017.1304355

Calzada, A., Hodgson, B., Kanemaki, M., Bueno, A., and Labib, K. (2005). Molecular anatomy and regulation of a stable replisome at a paused eukaryotic DNA replication fork. *Gene Dev.* 19, 1905–1919. doi: 10.1101/gad.337205

Cannavo, E., and Cejka, P. (2014). Sae2 promotes dsDNA endonuclease activity within Mre11-Rad50-Xrs2 to resect DNA breaks. *Nature* 514, 122–125. doi: 10.1038/nature13771

Cejka, P., Cannavo, E., Polaczek, P., Masuda-Sasa, T., Pokharel, S., Campbell, J. L., et al. (2010). DNA end resection by Dna2-Sgs1-RPA and its stimulation by Top3-Rmi1 and Mre11-Rad50-Xrs2. *Nature* 467, 112–116. doi: 10.1038/nature09355

Chai, B., Huang, J., Cairns, B. R., and Laurent, B. C. (2005). Distinct roles for the RSC and Swi/Snf ATP-dependent chromatin remodelers in DNA double-strand break repair. *Gene Dev.* 19, 1656–1661. doi: 10.1101/gad.1273105

Chang, M., Bellaoui, M., Boone, C., and Brown, G. W. (2002). A genome-wide screen for methyl methanesulfonate-sensitive mutants reveals genes required for S phase progression in the presence of DNA damage. *Proc. Natl. Acad. Sci. U.S.A.* 99, 16934–16939. doi: 10.1073/pnas.262669299

Chen, R., and Wold, M. S. (2014). Replication protein A: single-stranded DNA's first responder: dynamic DNA-interactions allow replication protein A to direct single-strand DNA intermediates into different pathways for synthesis or repair. *BioEssays* 36, 1156–1161. doi: 10.1002/bies.201400107

Chen, X., Cui, D., Papusha, A., Zhang, X., Chu, C. D., Tang, J., et al. (2012). The Fun30 nucleosome remodeller promotes resection of DNA double-strand break ends. *Nature* 489, 576–580. doi: 10.1038/nature11355

Cobb, J. A., Bjergbaek, L., Shimada, K., Frei, C., and Gasser, S. M. (2003). DNA polymerase stabilization at stalled replication forks requires Mec1 and the RecQ helicase Sgs1. *EMBO J.* 22, 4325–4336. doi: 10.1093/emboj/cdg391

Cobb, J. A., Schleker, T., Rojas, V., Bjergbaek, L., Tercero, J. A., and Gasser, S. M. (2005). Replisome instability, fork collapse, and gross chromosomal rearrangements arise synergistically from Mec1 kinase and RecQ helicase mutations. *Gene Dev.* 19, 3055–3069. doi: 10.1101/gad.361805

Cortez, D. (2015). Preventing replication fork collapse to maintain genome integrity. *DNA Repair* 32, 149–157. doi: 10.1016/j.dnarep.2015.04.026

Costelloe, T., Louge, R., Tomimatsu, N., Mukherjee, B., Martini, E., Khadaroo, B., et al. (2012). The yeast Fun30 and human SMARCAD1 chromatin remodellers promote DNA end resection. *Nature* 489, 581–584. doi: 10.1038/nature11353

Cotta-Ramusino, C., Fachinetti, D., Lucca, C., Doksani, Y., Lopes, M., Sogo, J., et al. (2005). Exo1 processes stalled replication forks and counteracts fork reversal in checkpoint-defective cells. *Mol. Cell* 17, 153–159. doi: 10.1016/j.molcel.2004.11.032

Feng, G., Yuan, Y., Li, Z., Wang, L., Zhang, B., Luo, J., et al. (2019). Replication fork stalling elicits chromatin compaction for the stability of stalling replication forks. *Proc. Natl. Acad. Sci. U.S.A.* 116, 14563–14572. doi: 10.1073/pnas.1821475116

Garcia-Rodriguez, N., Morawska, M., Wong, R. P., Daigaku, Y., and Ulrich, H. D. (2018). Spatial separation between replisome- and template-induced replication stress signaling. *EMBO J.* 37:e98369. doi: 10.15252/embj.201798369

Gellon, L., Kaushal, S., Cebrian, J., Lahiri, M., Mirkin, S. M., and Freudenreich, C. H. (2019). Mrc1 and Tof1 prevent fragility and instability at long CAG repeats by their fork stabilizing function. *Nucleic Acid. Res.* 47, 794–805. doi: 10.1093/nar/gky1195

Giannattasio, M., and Branzei, D. (2017). S-phase checkpoint regulations that preserve replication and chromosome integrity upon dNTP depletion. *Cell. Mol. Life Sci.* 74, 2361–2380. doi: 10.1007/s00018-017-2474-4

Gonzalez-Prieto, R., Munoz-Cabello, A. M., Cabello-Lobato, M. J., and Prado, F. (2013). Rad51 replication fork recruitment is required for DNA damage tolerance. *EMBO J.* 32, 1307–1321. doi: 10.1038/emboj.2013.73

Grenon, M., Costelloe, T., Jimeno, S., O'Shaughnessy, A., Fitzgerald, J., Zgheib, O., et al. (2007). Docking onto chromatin via the *Saccharomyces cerevisiae* Rad9 tudor domain. *Yeast* 24, 105–119. doi: 10.1002/yea.1441

Haber, J. E. (2016). A Life Investigating Pathways That Repair Broken Chromosomes. *Annu. Rev. Genet.* 50, 1–28. doi: 10.1146/annurev-genet-120215-035043

Hirano, T. (2016). Condensin-based chromosome organization from bacteria to vertebrates. *Cell* 164, 847–857. doi: 10.1016/j.cell.2016.01.033

Ira, G., Malkova, A., Liberi, G., Foiani, M., and Haber, J. E. (2003). Srs2 and Sgs1-Top3 suppress crossovers during double-strand break repair in yeast. *Cell* 115, 401–411. doi: 10.1016/S0092-8674(03)00886-9

Katou, Y., Kanoh, Y., Bando, M., Noguchi, H., Tanaka, H., Ashikari, T., et al. (2003). S-phase checkpoint proteins Tof1 and Mrc1 form a stable replication-pausing complex. *Nature* 424, 1078–1083. doi: 10.1038/nature01900

Khurana, S., Kruhlak, M. J., Kim, J., Tran, A. D., Liu, J., Nyswaner, K., et al. (2014). A macrohistone variant links dynamic chromatin compaction to BRCA1-dependent genome maintenance. *Cell Rep.* 8, 1049–1062. doi: 10.1016/j.celrep.2014.07.024

Komata, M., Bando, M., Araki, H., and Shirahige, K. (2009). The direct binding of Mrc1, a checkpoint mediator, to Mcm6, a replication helicase, is essential for the replication checkpoint against methyl methanesulfonate-induced stress. *Mol. Cell. Biol.* 29, 5008–5019. doi: 10.1128/MCB.01934-08

Kowalczykowski, S. C. (2015). An overview of the molecular mechanisms of recombinational DNA repair. *Cold Spring Harb. Perspect. Biol.* 7:a016410. doi: 10.1101/cshperspect.a016410

Kramara, J., Osia, B., and Malkova, A. (2018). Break-induced replication: the where, the why, and the how. *Trend. Genet.* 34, 518–531. doi: 10.1016/j.tig.2018.04.002

Kruitwagen, T., Denoth-Lippuner, A., Wilkins, B. J., Neumann, H., and Barral, Y. (2015). Axial contraction and short-range compaction of chromatin synergistically promote mitotic chromosome condensation. *eLife* 4:e1039. doi: 10.7554/eLife.10396.014

Lazzaro, F., Sapountzi, V., Granata, M., Pellicioli, A., Vaze, M., Haber, J. E., et al. (2008). Histone methyltransferase Dot1 and Rad9 inhibit single-stranded DNA accumulation at DSBs and uncapped telomeres. *EMBO J.* 27, 1502–1512. doi: 10.1038/emboj.2008.81

Lisby, M., Barlow, J. H., Burgess, R. C., and Rothstein, R. (2004). Choreography of the DNA damage response: spatiotemporal relationships among checkpoint and repair proteins. *Cell* 118, 699–713. doi: 10.1016/j.cell.2004.08.015

Lopes, M., Foiani, M., and Sogo, J. M. (2006). Multiple mechanisms control chromosome integrity after replication fork uncoupling and restart at irreparable UV lesions. *Mol. Cell* 21, 15–27. doi: 10.1016/j.molcel.2005.11.015

Lou, H., Komata, M., Katou, Y., Guan, Z., Reis, C. C., Budd, M., et al. (2008). Mrc1 and DNA polymerase epsilon function together in linking DNA replication and the S phase checkpoint. *Mol. Cell* 32, 106–117. doi: 10.1016/j.molcel.2008.08.020

Lundin, C., North, M., Erixon, K., Walters, K., Jenssen, D., Goldman, A. S., et al. (2005). Methyl methanesulfonate (MMS) produces heat-labile DNA damage but no detectable *in vivo* DNA double-strand breaks. *Nucleic Acid. Res.* 33, 3799–3811. doi: 10.1093/nar/gki681

Mimitou, E. P., and Symington, L. S. (2008). Sae2, Exo1 and Sgs1 collaborate in DNA double-strand break processing. *Nature* 455, 770–U773. doi: 10.1038/nature07312

Morin, I., Ngo, H. P., Greenall, A., Zubko, M. K., Morrice, N., and Lydall, D. (2008). Checkpoint-dependent phosphorylation of Exo1 modulates the DNA damage response. *EMBO J.* 27, 2400–2410. doi: 10.1038/emboj.2008.171

Niu, H., Chung, W. H., Zhu, Z., Kwon, Y., Zhao, W., Chi, P., et al. (2010). Mechanism of the ATP-dependent DNA end-resection machinery from *Saccharomyces cerevisiae*. *Nature* 467, 108–111. doi: 10.1038/nature09318

Noguchi, E., Noguchi, C., McDonald, W. H., Yates, J. R. 3rd, and Russell, P. (2004). Swi1 and Swi3 are components of a replication fork protection complex in fission yeast. *Mol. Cell. Biol.* 24, 8342–8355. doi: 10.1128/MCB.24.19.8342-8355.2004

Oberdoerffer, P. (2015). Stop relaxing: how DNA damage-induced chromatin compaction may affect epigenetic integrity and disease. *Mol. Cell Oncol.* 2:e970952. doi: 10.4161/23723548.2014.970952

Panday, A., and Grove, A. (2017). Yeast HMO1: linker histone reinvented. *Microbiol. Mol. Biol. Rev.* 81:e00037-16. doi: 10.1128/MMBR.00037-16

Pardo, B., Crabbe, L., and Pasero, P. (2017). Signaling pathways of replication stress in yeast. *FEMS Yeast Res.* 17, 1–11. doi: 10.1093/femsyr/fow101

Pfander, B., and Diffley, J. F. (2011). Dpb11 coordinates Mec1 kinase activation with cell cycle-regulated Rad9 recruitment. *EMBO J.* 30, 4897–4907. doi: 10.1038/emboj.2011.345

Prado, F. (2014). Genetic instability is prevented by Mrc1-dependent spatio-temporal separation of replicative and repair activities of homologous recombination: homologous recombination tolerates replicative stress by Mrc1-regulated replication and repair activities operating at S and G2 in distinct subnuclear compartments. *BioEssays* 36, 451–462. doi: 10.1002/bies.201300161

Prakash, R., Satory, D., Dray, E., Papusha, A., Scheller, J., Kramer, W., et al. (2009). Yeast Mph1 helicase dissociates Rad51-made D-loops: implications for crossover control in mitotic recombination. *Gene Dev.* 23, 67–79. doi: 10.1101/gad.1737809

Prakash, R., Zhang, Y., Feng, W., and Jasin, M. (2015). Homologous recombination and human health: the roles of BRCA1, BRCA2, and associated proteins. *Cold Spring Harb. Perspect. Biol.* 7:a016600. doi: 10.1101/cshperspect.a016600

Puddu, F., Granata, M., Di Nola, L., Balestrini, A., Piergiovanni, G., Lazzaro, F., et al. (2008). Phosphorylation of the budding yeast 9-1-1 complex is required for Dpb11 function in the full activation of the UV-induced DNA damage checkpoint. *Mol. Cell. Biol.* 28, 4782–4793. doi: 10.1128/MCB.00330-08

Rossi, S. E., Ajazi, A., Carotenuto, W., Foiani, M., and Giannattasio, M. (2015). Rad53-mediated regulation of Rrm3 and Pif1 DNA Helicases contributes to prevention of aberrant fork transitions under replication stress. *Cell Rep.* 13, 80–92. doi: 10.1016/j.celrep.2015.08.073

Sasaki, M., and Kobayashi, T. (2017). Ctf4 Prevents genome rearrangements by suppressing DNA double-strand break formation and its end resection at arrested replication forks. *Mol. Cell* 66, 533–545.e535. doi: 10.1016/j.molcel.2017.04.020

Seeber, A., Hauer, M., and Gasser, S. M. (2013). Nucleosome remodelers in double-strand break repair. *Curr. Opin. Genet. Dev.* 23, 174–184. doi: 10.1016/j.gde.2012.12.008

Shim, E. Y., Hong, S. J., Oum, J. H., Yanez, Y., Zhang, Y., and Lee, S. E. (2007). RSC mobilizes nucleosomes to improve accessibility of repair machinery to the damaged chromatin. *Mol. Cell. Biol.* 27, 1602–1613. doi: 10.1128/MCB.01956-06

Smolka, M. B., Albuquerque, C. P., Chen, S. H., and Zhou, H. (2007). Proteome-wide identification of *in vivo* targets of DNA damage checkpoint kinases. *Proc. Natl. Acad. Sci. U.S.A.* 104, 10364–10369. doi: 10.1073/pnas.0701622104

Smolka, M. B., Chen, S. H., Maddox, P. S., Enserink, J. M., Albuquerque, C. P., Wei, X. X., et al. (2006). An FHA domain-mediated protein interaction network of Rad53 reveals its role in polarized cell growth. *J. Cell Biol.* 175, 743–753. doi: 10.1083/jcb.200605081

Sogo, J. M., Lopes, M., and Foiani, M. (2002). Fork reversal and ssDNA accumulation at stalled replication forks owing to checkpoint defects. *Science* 297, 599–602. doi: 10.1126/science.1074023

Szyjka, S. J., Viggiani, C. J., and Aparicio, O. M. (2005). Mrc1 is required for normal progression of replication forks throughout chromatin in *S. cerevisiae*. *Mol. Cell* 19, 691–697. doi: 10.1016/j.molcel.2005.06.037

Tanaka, K., and Russell, P. (2001). Mrc1 channels the DNA replication arrest signal to checkpoint kinase Cds1. *Nat. Cell Biol.* 3, 966–972. doi: 10.1038/ncb1101-966

Tercero, J. A., and Diffley, J. F. (2001). Regulation of DNA replication fork progression through damaged DNA by the Mec1/Rad53 checkpoint. *Nature* 412, 553–557. doi: 10.1038/35087607

Tercero, J. A., Longhese, M. P., and Diffley, J. F. (2003). A central role for DNA replication forks in checkpoint activation and response. *Mol. Cell* 11, 1323–1336. doi: 10.1016/S1097-2765(03)00169-2

Toh, G. W., O'Shaughnessy, A. M., Jimeno, S., Dobbie, I. M., Grenon, M., Maffini, S., et al. (2006). Histone H2A phosphorylation and H3 methylation are required for a novel Rad9 DSB repair function following checkpoint activation. *DNA Repair* 5, 693–703. doi: 10.1016/j.dnarep.2006.03.005

Tourriere, H., Versini, G., Cordon-Preciado, V., Alabert, C., and Pasero, P. (2005). Mrc1 and Tof1 promote replication fork progression and recovery independently of Rad53. *Mol. Cell* 19, 699–706. doi: 10.1016/j.molcel.2005.07.028

Uzunova, S. D., Zarkov, A. S., Ivanova, A. M., Stoynov, S. S., and Nedelcheva-Veleva, M. N. (2014). The subunits of the S-phase checkpoint complex Mrc1/Tof1/Csm3: dynamics and interdependence. *Cell Div*. 9:4. doi: 10.1186/1747-1028-9-4

Wiest, N. E., Houghtaling, S., Sanchez, J. C., Tomkinson, A. E., and Osley, M. A. (2017). The SWI/SNF ATP-dependent nucleosome remodeler promotes resection initiation at a DNA double-strand break in yeast. *Nucleic Acid. Res*. 45, 5887–5900. doi: 10.1093/nar/gkx221

Wilkins, B. J., Rall, N. A., Ostwal, Y., Kruitwagen, T., Hiragami-Hamada, K., Winkler, M., et al. (2014). A cascade of histone modifications induces chromatin condensation in mitosis. *Science* 343, 77–80. doi: 10.1126/science.1244508

Wysocki, R., Javaheri, A., Allard, S., Sha, F., Cote, J., and Kron, S. J. (2005). Role of Dot1-dependent histone H3 methylation in G1 and S phase DNA damage checkpoint functions of Rad9. *Mol. Cell. Biol*. 25, 8430–8443. doi: 10.1128/MCB.25.19.8430-8443.2005

Xu, Y. J., Davenport, M., and Kelly, T. J. (2006). Two-stage mechanism for activation of the DNA replication checkpoint kinase Cds1 in fission yeast. *Gene. Dev*. 20, 990–1003. doi: 10.1101/gad.1406706

Zhu, Z., Chung, W. H., Shim, E. Y., Lee, S. E., and Ira, G. (2008). Sgs1 helicase and two nucleases Dna2 and Exo1 resect DNA double-strand break ends. *Cell* 134, 981–994. doi: 10.1016/j.cell.2008.08.037

Zou, L., and Elledge, S. J. (2003). Sensing DNA damage through ATRIP recognition of RPA-ssDNA complexes. *Science* 300, 1542–1548. doi: 10.1126/science.1083430

**Conflict of Interest:** The authors declare that the research was conducted in the absence of any commercial or financial relationships that could be construed as a potential conflict of interest.

frontiers in Cell and Developmental Biology

REVIEW
published: 25 February 2021
doi: 10.3389/fcell.2021.640755

# Human RecQ Helicases in DNA Double-Strand Break Repair

*Huiming Lu* and Anthony J. Davis**

*Division of Molecular Radiation Biology, Department of Radiation Oncology, UT Southwestern Medical Center, Dallas, TX, United States*

RecQ DNA helicases are a conserved protein family found in bacteria, fungus, plants, and animals. These helicases play important roles in multiple cellular functions, including DNA replication, transcription, DNA repair, and telomere maintenance. Humans have five RecQ helicases: RECQL1, Bloom syndrome protein (BLM), Werner syndrome helicase (WRN), RECQL4, and RECQL5. Defects in BLM and WRN cause autosomal disorders: Bloom syndrome (BS) and Werner syndrome (WS), respectively. Mutations in RECQL4 are associated with three genetic disorders, Rothmund–Thomson syndrome (RTS), Baller–Gerold syndrome (BGS), and RAPADILINO syndrome. Although no genetic disorders have been reported due to loss of RECQL1 or RECQL5, dysfunction of either gene is associated with tumorigenesis. Multiple genetically independent pathways have evolved that mediate the repair of DNA double-strand break (DSB), and RecQ helicases play pivotal roles in each of them. The importance of DSB repair is supported by the observations that defective DSB repair can cause chromosomal aberrations, genomic instability, senescence, or cell death, which ultimately can lead to premature aging, neurodegeneration, or tumorigenesis. In this review, we will introduce the human RecQ helicase family, describe in detail their roles in DSB repair, and provide relevance between the dysfunction of RecQ helicases and human diseases.

**Keywords: RecQ helicase, RECQL1, BLM, WRN, RECQL4, RECQL5, DNA double-strand break repair, genome stability**

OPEN ACCESS

***Edited by:***
*Binfeng Lu,*
*University of Pittsburgh, United States*

***Reviewed by:***
*Sudha Sharma,*
*Howard University, United States*
*Matthew Bochman,*
*Indiana University, United States*

****Correspondence:***
*Huiming Lu*
*huiming.lu@utsouthwestern.edu*
*Anthony J. Davis*
*anthony.davis@utsouthwestern.edu*

***Specialty section:***
*This article was submitted to Cell Death and Survival, a section of the journal Frontiers in Cell and Developmental Biology*

***Received:*** *12 December 2020*
***Accepted:*** *29 January 2021*
***Published:*** *25 February 2021*

***Citation:***
*Lu H and Davis AJ (2021) Human RecQ Helicases in DNA Double-Strand Break Repair. Front. Cell Dev. Biol. 9:640755. doi: 10.3389/fcell.2021.640755*

## DNA DOUBLE-STRAND BREAKS AND REPAIR PATHWAYS

A number of elegant mechanisms have evolved that repair the vast number of DNA lesions an organism encounters each day. DNA repair mechanisms are described as guardians of the human genome because DNA is the template for the fundamental processes of replication and transcription, and preserving the integrity of genomic DNA ensures faithful propagation of genetic material and transmission to daughter cells (Hoeijmakers, 2009; Ciccia and Elledge, 2010; Tubbs and Nussenzweig, 2017). Arguably, the most important DNA repair mechanisms are those that repair DNA double-strand breaks (DSBs) (Ciccia and Elledge, 2010; Ceccaldi et al., 2016; Scully et al., 2019). DSBs are generated during endogenous events such as after the collapse of replication forks (Bouwman and Crosetto, 2018), SPO11-induced DSB formation during meiosis (Tock and Henderson, 2018), V(D)J (variable, diversity, and joining) recombination (Chi et al., 2020), and *via* reactive oxygen species generated during metabolism, as well as from various exogenous stresses which include ionizing radiation (IR) and cancer chemotherapeutic agents (Tubbs and Nussenzweig, 2017) (**Figure 1**). Unrepaired or misrepaired DSBs can cause chromosomal

aberrations, genomic instability, senescence, or cell death, further leading to premature aging, neurodegeneration, or tumorigenesis (**Figure 1**) (White and Vijg, 2016; Tubbs and Nussenzweig, 2017; Taylor et al., 2019). To overcome severe consequences from DSBs, mammalian cells have evolved at least four pathways to repair this type of DNA lesion, termed non-homologous end joining (NHEJ), homologous recombination (HR), and the alternative end-joining pathways, microhomology-mediated end joining (MMEJ) and single-strand annealing (SSA) (**Figure 2**). In the following sections, we will give a brief overview of each DSB repair pathway.

## Non-homologous End Joining

Non-homologous end joining (NHEJ) is the major pathway responsible for the repair of two-ended DSBs generated by IR, restriction enzymes, and those intentionally generated for V(D)J and class switch recombination during T and B cell lymphocyte development (Davis and Chen, 2013; Davis et al., 2014; Scully et al., 2019). NHEJ is a flexible process that directs re-ligation of the broken DNA molecule in a template-independent manner and is active in all phases of the cell cycle (Davis et al., 2014; Pannunzio et al., 2018). Initiation of NHEJ occurs when the ring-shaped Ku heterodimer, composed of the Ku70 and Ku80 proteins, recognizes and binds to the DSB in a sequence-independent manner (Fell and Schild-Poulter, 2015). Once bound to the DSB ends, Ku then functions as a scaffold to recruit the NHEJ machinery to the damage site. In particular, Ku70/80 directly recruits DNA-dependent protein kinase catalytic subunit (DNA-$PK_{cs}$) to the DNA ends to form the DNA-PK complex, resulting in the activation of DNA-$PK_{cs}$ kinase activity (Davis et al., 2014). DNA-$PK_{cs}$ promotes NHEJ and phosphorylates the histone H2AX and the chromatin remodeler KAP1 to promote chromatin relaxation proximal to the DSB to facilitate recruitment of the DNA damage response and repair machinery to the DNA damage site (Lu et al., 2019). If the ends of the DSB are not compatible for ligation, different enzymes are required, including those that resect DNA ends, fill in gaps, or remove blocking end groups, to process the DNA ends to allow ligation (Pannunzio et al., 2018). The terminal step in NHEJ is the ligation of the broken DNA ends by the DNA ligase IV(LIG4)/X-ray cross-complementing protein 4 (XRCC4) complex with the assistance of the XRCC4-like factor (XLF) (Ellenberger and Tomkinson, 2008). NHEJ is not intrinsically inaccurate, but the quality of end joining is dictated by the structure of the DSB ends as small insertions or deletions can be generated if end processing by nucleases and polymerases is required (Davis and Chen, 2013; Pannunzio et al., 2018; Scully et al., 2019).

## Homologous Recombination

Homologous recombination (HR) requires a homologous DNA sequence to serve as a template for DNA synthesis-dependent repair. It is an accurate process as it employs DNA sequences homologous to/near the broken ends to drive repair, predominantly using the sister chromatid as a template for DSB repair rather than the homologous chromosome. As a sister chromatid is available after DNA replication, HR predominantly occurs in mid-S to the early G2 phase of the cell cycle (Ceccaldi et al., 2016; Hustedt and Durocher, 2016). HR is initiated by the MRE11/RAD50/NBS1 (MRN) complex in conjunction with CtIP *via* the endonuclease and 3′–5′ exonuclease activities of MRE11 (Lengsfeld et al., 2007; Sartori et al., 2007; Garcia et al., 2011; Cannavo and Cejka, 2014; Deshpande et al., 2020). The endonuclease activity of MRE11 generates a nick in the double-stranded DNA (dsDNA) near the DSB site, followed by its 3′–5′ exonuclease activity generating a short section of single-stranded DNA (ssDNA) next to the nick. This is followed by extensive resection by exonuclease 1 (EXO1) and/or the nuclease DNA2 with the RECQ helicase Bloom syndrome protein (BLM) to produce a long 3′ overhang (Mimitou and Symington, 2008; Nimonkar et al., 2011; Symington, 2014; Ronato et al., 2020). The resulting 3′ ssDNA is rapidly coated by the ssDNA-binding protein replication protein A (RPA), which is subsequently replaced by RAD51 *via* assistance by BRCA2 and DSS1 (Gudmundsdottir et al., 2004; Yang et al., 2005; Jensen et al., 2010; Thorslund et al., 2010; Zhao et al., 2015). RAD51 binds to ssDNA, forming a helical RAD51–ssDNA nucleoprotein filament that is capable of homology search and invasion of a homologous DNA sequence. If sufficient base pairing occurs between the invading RAD51-coated strand and the invaded DNA molecule, the non-base-paired strand of the invaded molecule is displaced in the form of a displacement loop (D-loop). A DNA polymerase extends the 3′-end of the invasion strand past the break using the invaded homologous strand as a template, followed by resolution of the Holliday junction from the extended D-loop by resolvases and dissolution by BLM-TOP3a-RMI1/2 complex, annealing, and ligation of the extended invasion strand to the other end of the DSB on the original DNA molecule (Wright et al., 2018; Scully et al., 2019).

## Alternative End-Joining Pathways

Non-homologous end joining and HR are the dominant DSB repair pathways, but there are two minor alternative end joining pathways called microhomology-mediated end joining (MMEJ) and single-strand annealing (SSA). MMEJ and SSA were initially identified in cells that were deficient in NHEJ and/or HR, and thus, both were believed to be strictly "backup pathways" (Fairman et al., 1992; Boulton and Jackson, 1996; Mason et al., 1996; Kabotyanski et al., 1998), but it has been found that, even in NHEJ- and HR-proficient cells, a small percentage of DSBs are repaired by these alternative pathways (Truong et al., 2013). Similar to NHEJ, the MMEJ and SSA pathways terminate with direct ligation of the two ends of the broken DNA, but MMEJ and SSA are distinct from NHEJ as they function completely independently of the Ku heterodimer and DNA-$PK_{cs}$, require components of the HR machinery, and require longer tracts of microhomology to mediate repair (Sallmyr and Tomkinson, 2018). The factors and processes required for MMEJ and SSA are not well defined, but both initiate with the binding of PARP1 to the DSB ends and each requires DNA end resection (Bennardo et al., 2008; Xie et al., 2009; Lee-Theilen et al., 2011; Zhang and Jasin, 2011; Truong et al., 2013). Similar to HR, DNA end resection is initiated by the MRN–CtIP complex in MMEJ and SSA, but the enzymes required for long DNA

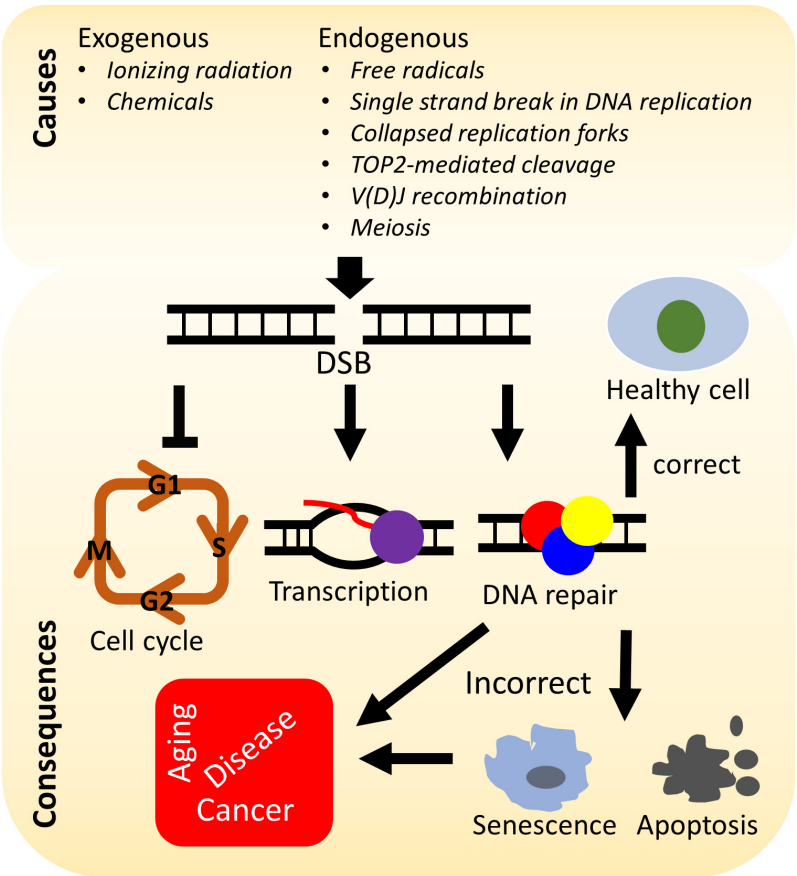


**FIGURE 1 |** Causes and consequences of DNA double-strand breaks (DSBs). DSBs arise from various stresses by endogenous or exogenous factors and can lead to arrest of the cell cycle, transcription, activation of the DNA damage response, and repair of the DNA damage. Incorrectly repaired or unrepaired DSBs can result in cellular senescence, apoptosis, premature aging, genetic disorders, and/or tumorigenesis.

end resection are not clearly defined, with speculation being that EXO1 and/or DNA2/BLM mediate this process (Sallmyr and Tomkinson, 2018). Each alternative end-joining pathway requires differing amounts of sequence homology to align the DNA. MMEJ requires a short region of complimentary sequence, 2–20 nucleotides, called microhomology sequences, whereas SSA needs >25 nucleotides of homologous sequence, which typically reside within tandem repeats (Bhargava et al., 2016). During SSA, the generated 3′ ssDNAs are annealed by RAD52 *via* alignment of homologous sequences, whereas multiple enzymes are responsive for end bridging and annealing in MMEJ, including the MRN complex, PARP1, and Polθ (Sallmyr and Tomkinson, 2018). Once aligned, the non-complementary sequences generate 3′ ssDNA overhangs that are removed by nucleases. Both MMEJ and SSA complete with gap filling and DNA ligation by DNA polymerases and DNA ligases, but the exact enzymes and mechanisms that drive these processes are not well defined (Sallmyr and Tomkinson, 2018; Patterson-Fortin and D'Andrea, 2020). The repair of DSBs by MMEJ and SSA are intrinsically mutagenic as they cause deletions and rearrangements, resulting in genomic instability (Sallmyr and Tomkinson, 2018; Patterson-Fortin and D'Andrea, 2020).

## HUMAN RecQ HELICASES

Helicases are a ubiquitous family of molecular motors that unwind DNA, RNA, and DNA–RNA duplexes. They play essential roles in DNA and RNA metabolism, including DNA replication, transcription, DNA repair, translation, RNA maturation, ribosome synthesis, and splicing. A conserved helicase family is the RecQ family, which is named after the prototypical member found in *Escherichia coli* called RecQ (Cobb and Bjergbaek, 2006; Croteau et al., 2014). RecQ helicases possess 3′ to 5′ directionality and can unwind a variety of DNA structures including B-form DNA, forked DNA duplexes, D-loops, DNA junctions, and G-quadruplexes (Croteau et al., 2014). Furthermore, they promote the annealing of complementary ssDNAs and branch migration of Holliday junctions. Each RecQ helicase shares the highly conserved core helicase domain (DEAD/DEAH box, helicase conserved C-terminal domain), with the majority of the family members containing the RecQ C-terminal (RQC) domain, and the helicase and RNase D-like C-terminal (HRDC) domain is shared among members (**Figure 3**). An important function of RecQ helicases is that they are essential to maintain genome stability as they act

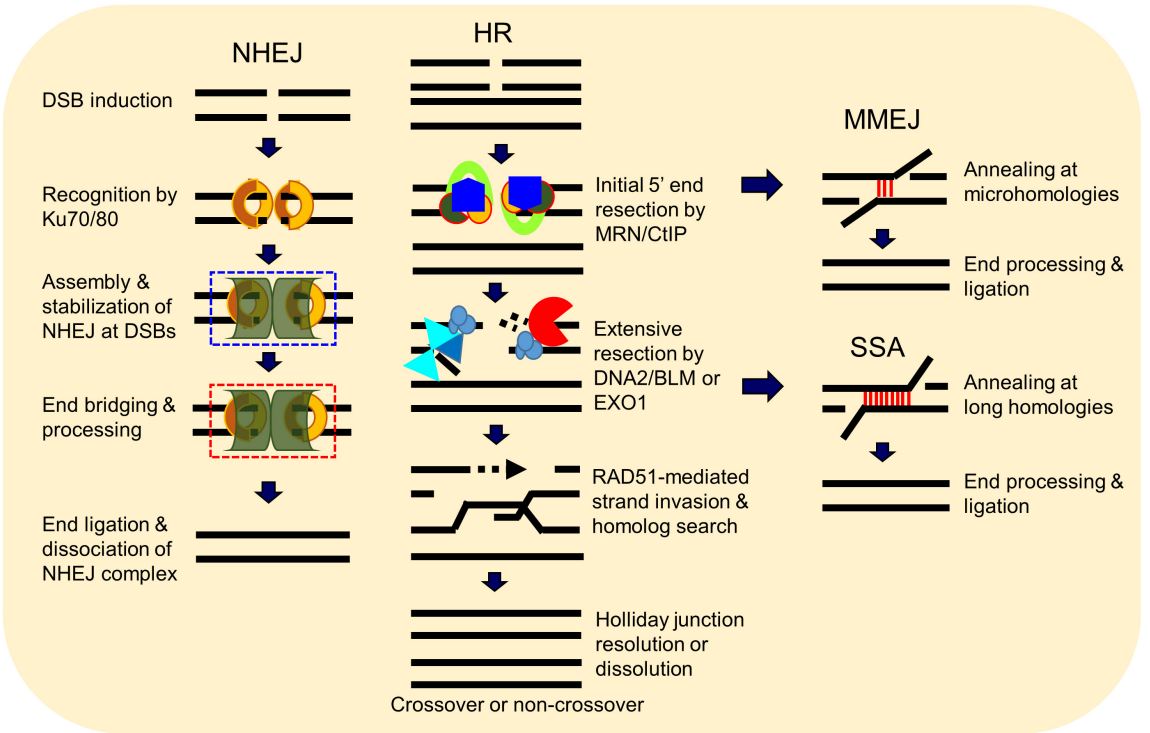


**FIGURE 2 |** Double-strand break (DSB) repair pathways. DSBs in mammalian cells are able to be repaired by at least four pathways, including non-homologous end joining (NHEJ), homologous recombination (HR), microhomology-mediated end joining (MMEJ), and single-strand annealing (SSA). HR and NHEJ are the dominant DSB repair pathways in normal cells, but the two minor pathways SSA and MMEJ can occur under certain circumstances. Choice between these repair pathways is tightly regulated.

at the interface between DNA replication, DNA recombination, DNA repair, telomere maintenance, and transcription (Bohr, 2008; Croteau et al., 2014; Urban et al., 2017). Besides RecQ, *E. coli* has another RecQ-like helicase, named RqlH, which does not appear in the K12 strain of *E. coli* but in many other strains (Russell and Mulvey, 2015). Two RecQ helicases, Sgs1 and Hrq1, have been identified in the budding yeast *Saccharomyces cerevisiae* as homologs to human BLM and RECQL4, respectively (Watt et al., 1996; Choi et al., 2013; Bochman et al., 2014; Rogers et al., 2017). Human cells have five distinct RecQ helicases, named RECQL1, BLM, Werner syndrome helicase (WRN), RECQL4, and RECQL5. All of them have the conserved helicase core domain, but only BLM and WRN possess the HRDC domain, and RECQL1, BLM, and WRN have the typical RQC domain (**Figure 3**). Notably, the human RecQ helicases play important functions in nearly all DNA repair pathways, in particular those required for the repair of DSBs (Hickson, 2003; Bohr, 2008; Croteau et al., 2014). The role of human RecQ helicases in DSB repair is supported by the observation that defects in these enzymes result in a number of distinct human genetic disorders, premature aging, and/or carcinogenesis, which may be driven due to defective DSB repair (Datta et al., 2020; Oshima et al., 2018). These RecQ helicases participate in multiple DSB repair pathways by physically and functionally interacting with key players in these pathways (**Table 1**). In this review, we will focus on the important roles of human RecQ helicases in DSB repair and maintenance of genome stability, as well as the biological relevance between these cellular functions and the mechanisms underlying RecQ-associated disorders and cancers.

## RECQL1

RECQL1, also known as RECQL and RECQ1, is the most abundant member of the five human RecQ helicases (Sharma and BroshJr., 2008). It is encoded by the *RECQL1* gene, which is located at chromosome 12p12. RECQL1 consists of 649 amino acid residues, and it possesses the conserved core helicase domain, RecQ $Zn^{2+}$ binding motif, and the RQC domain (**Figure 3**). RECQL1 can unwind 3′ overhang dsDNA, forked duplexes, 3′ or 5′ flap dsDNA, D-loops, bubble-structured dsDNA, and Holliday junctions, and its helicase activity is stimulated by RPA (Cui et al., 2003; Sharma et al., 2005). RECQL1 plays important roles in DNA repair, restart of stalled replication, and telomere maintenance (Sharma and BroshJr., 2007; Popuri et al., 2012a, 2014; Berti et al., 2013; Banerjee et al., 2015; Parvathaneni and Sharma, 2019).

### RECQL1 and NHEJ

A role for RECQL1 in DSB repair was initially identified *via* the observation that *Recql1* knockout mouse embryonic fibroblasts (MEFs) are highly sensitive to IR and that knockdown of RECQL1 in human cells results in increased cell death to IR

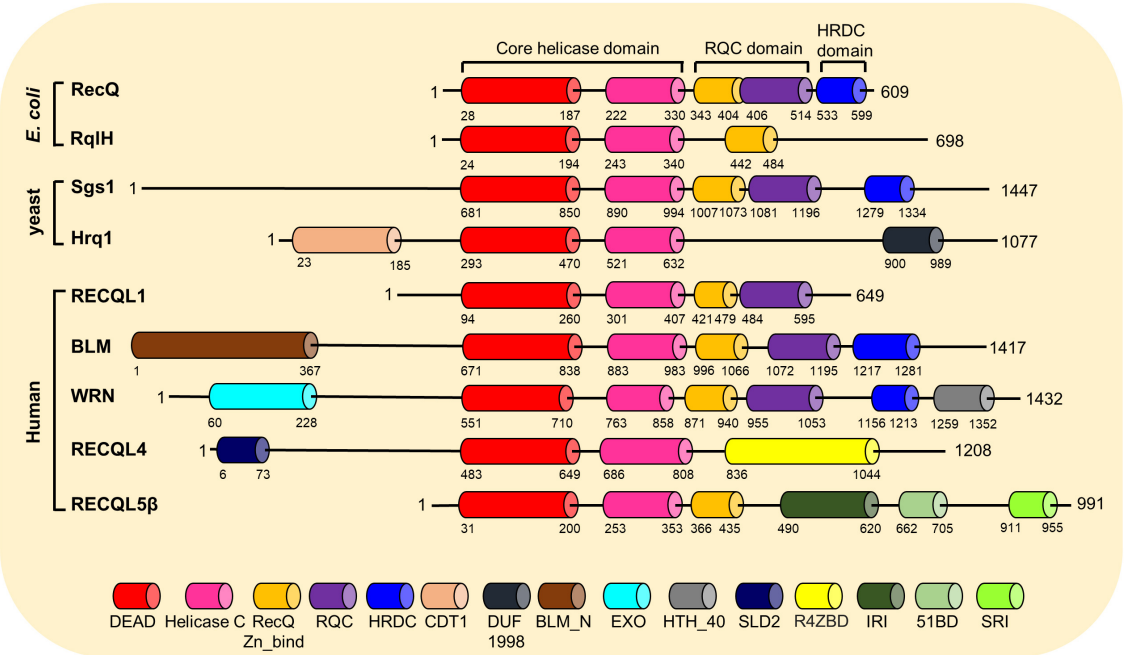


**FIGURE 3 |** Conserved motifs and domains of RecQ helicases from *Escherichia coli*, budding yeast, and humans. The RecQ helicases' motifs and domains are presented mainly based on the annotations by the GenomeNet Database (https://www.genome.jp/), with information from published literatures. *DEAD*, DEAD/DEAH box helicase; *Helicase C*, helicase conserved C-terminal motif; *RecQ-Zn-Bind*, RecQ $Zn^{2+}$-binding motif; *RQC*, RecQ-C-terminal domain; *HRDC*, helicase and RNase D-like C-terminal domain; *CDT1*, DNA replication factor CDT1 like; *DUF1998*, domain of unknown function (DUF1998); *BLM_N*, N-terminal region of Bloom syndrome protein; *EXO*, DNA_POLA_EXO1, 3′–5′ exonuclease domain; *HTH_40*, helix-turn-helix domain; *SLD2*, DNA replication and checkpoint protein; *R4ZBD*, RECQL4-$Zn^{2+}$-binding motif; *IRI*, internal RNAPII-interacting domain; *51BD*, RAD51-binding domain; *SRI*, SET2-RPB1 interaction motif.

and the topoisomerase 1 (TOP1) inhibitor camptothecin (CPT) (Sharma and BroshJr., 2007; Sharma et al., 2007). Interestingly, RECQL1 is phosphorylated following exposure to IR and accumulates at IR-damaged chromatin (Sharma and BroshJr., 2007), but the IR-induced phosphorylation site(s) and the kinase(s) mediating the RECQL1 phosphorylation have not been identified. A key piece of evidence supporting RECQL1 functions in NHEJ is that it directly interacts with the Ku heterodimer, and does so independently of DNA-$PK_{cs}$, and that RECQL1 and Ku70/80 can simultaneously bind linearized plasmid DNA *in vitro* (Parvathaneni et al., 2013). Furthermore, RECQL1 can unwind Ku-bound DNA duplex in a manner that is dependent on intrinsic RECQL1 ATPase activity and RECQL1 modulates end joining in cell-free extracts (Parvathaneni et al., 2013). A reporter-based assay with small interfering RNA (siRNA) library targeting DNA damage response and repair proteins showed that RECQL1 siRNA treatment resulted in a loss of NHEJ efficiency by approximately 25% (Howard et al., 2015). However, exactly how RECQL1 directs end joining and its role in NHEJ *in vivo* are still undefined.

## RECQL1 and HR

RECQL1 has also been implicated to play a role in HR, as the depletion of RECQL1 by siRNA resulted in increased sister chromatid exchanges in HeLa cells (LeRoy et al., 2005; Sharma and BroshJr., 2007). In addition, RECQL1 forms a complex with RAD51 (Sharma and BroshJr., 2007) and promotes the processing of Holliday junctions by promoting branch migration (LeRoy et al., 2005; Mazina et al., 2012), indicating that RECQL1 functions in resolving HR intermediates. However, knockdown of RECQL1 in U2OS cells did not significantly reduce HR efficiency, as assessed using a green fluorescent protein (GFP)-based reporter assay (Sharma et al., 2012). RECQL1, similar to RAD51, protects stalled replication forks from MRE11-dependent degradation (Berti et al., 2013; Mason et al., 2019), suggesting that RECQL1 may play an indirect role in the protection and/or repair of one-ended DSBs at replication forks and is not directly required for strand invasion or homology search in HR at two-ended DSBs. Further studies are required to define the mechanism of RECQL1 in the repression of sister chromatid exchanges and its role in HR.

## RECQL1 and Cancers

The data support that RECQL1 is important for the maintenance of the genome as MEFs from *Recql1* knockout mice show evaluated levels of chromosomal structural aberrations and aneuploidy, and loss of human RECQL1 also causes increased sister chromatid exchanges (LeRoy et al., 2005; Sharma and BroshJr., 2007; Sharma et al., 2007). Although no genetic disorders have been identified with mutations in RECQL1, germline mutations in RECQL1 are reported to be linked with an increased risk of breast cancer, suggesting that RECQL1 is a breast cancer susceptibility gene (Cybulski et al., 2015; Kwong et al., 2016; Sun J. et al., 2017; Sun et al., 2015;

**TABLE 1 |** RecQ helicase-interacting proteins in DSB repair pathways.

| | Pathway | Interacting proteins | Function | References |
|---|---|---|---|---|
| RECQL1 | NHEJ | Ku70, Ku80, SHDL2 | Promotes NHEJ by interacting with Ku70/80 | Parvathaneni et al., 2013; Howard et al., 2015; Findlay et al., 2018 |
| | HR | RAD51 | Undefined function in HR | Sharma and BroshJr., 2007 |
| | MMEJ | PARP1 | Promotes MMEJ by an unknown mechanism | Sharma et al., 2012; Berti et al., 2013; Howard et al., 2015 |
| BLM | HR | DNA2, EXO1, RPA, TOP3A, RMI1, RMI2 | Promotes HR by stimulating 5′ end resection and dissolution of Holliday junction | Doherty et al., 2005; Gravel et al., 2008; Nimonkar et al., 2008; Nimonkar et al., 2011 |
| | | RAD51 | Inhibits unfavorable HR by melting D-loop | van Brabant et al., 2000; Wu et al., 2001; Bachrati et al., 2006; Bugreev et al., 2007 |
| | SSA | Unknown | Promotes SSA in HEK293 cells, but not in U2OS cells | Sturzenegger et al., 2014 |
| | MMEJ | 53BP1 | Inhibits MMEJ by interacting with 53BP in G1 cells | Grabarz et al., 2013; Truong et al., 2013 |
| WRN | NHEJ | Ku70, Ku80, DNA-PKcs, XRCC4-LIG4 | Promotes NHEJ by stimulating end processing and DNA end ligation | Cooper et al., 2000; Karmakar et al., 2002a; Kusumoto et al., 2008; Sallmyr et al., 2008; Lachapelle et al., 2011 |
| | HR | MRN, EXO1, DNA2, BLM, BRCA1, RPA | Promotes HR by stimulating 5′ end resection by MRN/DNA2 with RPA | Constantinou et al., 2000; Cheng et al., 2004, 2006; Sommers et al., 2005; Lachapelle et al., 2011; Sturzenegger et al., 2014 |
| | | RAD51, RAD54 | Disrupts potentially deleterious HR intermediates | Otterlei et al., 2006; Opresko et al., 2009 |
| | MMEJ | CtIP, MRE11, PARP1, LIG3 | Inhibits end resection by limiting the recruitment of MRE11 and CtIP to DSBs, especially in G1 cells | Sallmyr et al., 2008; Shamanna et al., 2016b |
| | SSA | DNA2, RAD52 | Promotes 5′ end resection and enhances the efficiency of RAD52-mediated strand annealing | Baynton et al., 2003; Sturzenegger et al., 2014 |
| RECQL4 | NHEJ | Ku70, Ku80 | Promotes NHEJ by interacting with Ku70/80 | Shamanna et al., 2014; Lu et al., 2017 |
| | HR | MRE11, NBS1, RAD50, CtIP, BLM, EXO1, DNA2, RAD51 | Promotes 5′ end resection by stimulating the recruitment of CtIP, BLM, DNA2, and EXO1 and nuclease activity of MRN | Petkovic et al., 2005; Singh et al., 2012; Lu et al., 2016, 2017 |
| | SSA | Unknown | Inhibits RAD52-mediated SSA | Kohzaki et al., 2020 |
| | MMEJ | Unknown | Promotes MMEJ with an unknown mechanism | Kohzaki et al., 2020 |
| RECQL5 | HR | MRN, RAD51 | Inhibits exonuclease of MRE11 and RAD51-mediated D-loop formation and displaces RAD51 from ssDNA | Hu et al., 2007; Zheng et al., 2009; Schwendener et al., 2010; Paliwal et al., 2014 |
| | SSA | Unknown | Promotes SSA with an unknown mechanisms in *Drosophila* | Chen et al., 2010 |

*DSB, double-strand break; BLM, Bloom syndrome protein; WRN, Werner syndrome helicase; NHEJ, non-homologous end joining; HR, homologous recombination; MMEJ, microhomology-mediated end joining; SSA, single-strand annealing.*

Tervasmaki et al., 2018). These accumulating clues suggest a tight association between RECQL1 dysfunction and the consequence of genome instability and cancer predisposition (Debnath and Sharma, 2020; Mojumdar, 2020).

## Bloom Syndrome Protein (BLM)

BLM helicase, encoded by the *BLM* gene that is located on chromosome 15q26.1, is a multifunctional protein consisting of 1,417 amino acids. BLM possesses a conserved helicase domain, the RQC domain, and the HRDC domain (**Figure 3**). BLM can unwind Y-structured dsDNA, bubble-like dsDNA, G-quadruplex, and Holliday junction and also disrupts mobile D-loops (Mohaghegh et al., 2001; Bachrati et al., 2006). The HRDC domain is important for BLM to direct the annealing of DNA strands and the dissolution of double Holliday junctions, but not for unwinding DNA substrates (Cheok et al., 2005; Wu et al., 2005; Gyimesi et al., 2012). An HRDC-dependent conformational change coupled with ATP hydrolysis/DNA translocation cycle promotes BLM to process complex DNA structures (Newman et al., 2015). The N-terminal domain of BLM is unique and conserved in vertebrates, and it is believed to regulate the oligomerization of BLM (Beresten et al., 1999; Janscak et al., 2003; Xu et al., 2012; Shi et al., 2017). BLM participates in different pathways required for DNA metabolism, which it achieves by interacting with many proteins *via* either its N-terminal domain or undefined C-terminal region (Croteau et al., 2014). BLM resolves complex secondary structures such as G-quadruplexes and hairpins during DNA replication and transcription and at telomeres (Schawalder et al., 2003; Johnson et al., 2010; Barefield and Karlseder, 2012; Grierson et al., 2012, 2013; Drosopoulos et al., 2015). BLM can also stabilize stalled replication forks and promote the restart of the stalled forks (Ralf et al., 2006; Pan et al., 2017). BLM functions in multiple DNA repair pathways, with its most-defined role in HR.

### BLM and HR

Bloom syndrome protein plays a multifaceted role in HR as it is required for the early phase of the pathway (DNA end resection) as well as one of the terminal steps (dissolution of Holliday junctions) (Croteau et al., 2014). Consistent with BLM playing a role at the early and later steps in HR, GFP-tagged BLM accumulates at laser-generated DSBs a few seconds after induction of damage, and it stays at the damage site for hours (Karmakar et al., 2006; Singh et al., 2010). As mentioned above,

HR initiates with 5′ DNA end resection by the MRN complex with CtIP and then the 3′ ssDNA is extended by further resection by EXO1 and/or this DNA2/BLM complex. During this step, BLM unwinds dsDNA after binding to 3′ ssDNA to facilitate the endonuclease activity of DNA2, resulting in the generation of an extended 3′ ssDNA (Gravel et al., 2008; Nimonkar et al., 2011). During this process, RPA interacts with BLM and promotes its helicase activity (BroshJr., Li et al., 2000; Doherty et al., 2005; Nimonkar et al., 2011; Soniat et al., 2019; Qin et al., 2020). A recent study reported that CtIP interacts with BLM and stimulates its helicase activity, further promoting DNA2/BLM-mediated extensive resection (Daley et al., 2017). Interestingly, in addition to working with DNA2, another biochemical study found that BLM, but not other RecQ helicases, promotes the nuclease activity of EXO1 on dsDNA (Nimonkar et al., 2008).

Resection-generated 3′ ssDNA is used by RAD51 for strand invasion and exchange with intact sister chromatid, resulting in the formation of a D-loop. BLM can displace the invading strand from the D-loop and thus can disrupt the RAD51–ssDNA filaments, which explains why BLM has also been termed an "anti-recombination" protein, which is a feature observed in Bloom syndrome (BS) patient cells (van Brabant et al., 2000; Wu et al., 2001; Bachrati et al., 2006; Bugreev et al., 2007). The role of BLM as an anti-recombinase is dependent on its helicase activity, but does not require association with DNA topoisomerase IIIα (Patel et al., 2017). BLM stimulates the strand exchange of active ATP-bound RAD51 filaments, but dismantles inactive ADP-bound filaments (Bugreev et al., 2007; Bugreev et al., 2009; Kikuchi et al., 2009), indicating that BLM may not be an actual anti-recombinase but is required to inspect nascent D-loops in order to drive proper HR (Manthei and Keck, 2013; Xue et al., 2019). Another important role of BLM in HR is to process double Holliday junction structures along with topoisomerase IIIα, RMI1, and RMI2, generating only non-crossover recombinant products, which is termed as "dissolution of the Holliday junction" (Wu and Hickson, 2003; Raynard et al., 2006; Wu et al., 2006; Singh et al., 2008; Xu et al., 2008).

### BLM and Alternative End-Joining Pathways

Although BLM possesses a strong ssDNA annealing activity and is crucial for extensive DNA end resection, its role in the alternative end-joining DSB repair pathways is unclear. Using a GFP-based reporter assay, depletion of BLM by siRNA reduces SSA in HEK293 cells, but not in U2OS cells (Sturzenegger et al., 2014). In contrast, depletion of BLM by short hairpin RNA (shRNA) leads to a significant increase in MMEJ in U2OS cells (Truong et al., 2013). Consistently, another study showed that BLM inhibits MMEJ and long-range CtIP/MRE11-dependent deletions by interacting with 53BP1 in G1 cells, suggesting that BLM plays a role in DSB repair pathway choice (Grabarz et al., 2013).

### BLM and Diseases

Mutations in BLM lead to a rare autosomal-recessive genetic disorder, Bloom syndrome (BS; OMIM#210900). BS is characterized by growth deficiency, insulin resistance, immune deficiency, photosensitive skin changes, and increased risk for diabetes, as well as high risk of cancer predisposition at a young age (Cunniff et al., 2017; de Renty and Ellis, 2017). Unfortunately, BS patients have a short life span (less than 30 years), and the major cause of death is cancer (Cunniff et al., 2017; de Renty and Ellis, 2017). In addition to BS, heterozygous deleterious mutations in BLM increase the risk of breast cancer (Thompson et al., 2012), prostate cancer (Ledet et al., 2020), and colorectal cancer (Gruber et al., 2002; Cleary et al., 2003; Baris et al., 2007; de Voer et al., 2015). The cells from BS patients display chromosomal instability, which is characterized by elevated rates of chromatid gaps, breaks, sister chromatid exchanges, and quadriradials (Ellis et al., 1995; German et al., 2007). In support of this, an increased frequency of sister chromatid exchanges of >10-fold is used for the standard diagnosis of BS (Chaganti et al., 1974).

## Werner Syndrome Helicase (WRN)

Werner syndrome helicase (WRN) is encoded by the *WRN* gene, which is located at chromosome 8p11-12 (Goto et al., 1992; Yu et al., 1996; Goto et al., 1997). WRN is a 1,432-amino acid-long protein with multiple functional domains, including 3′–5′ exonuclease, conserved helicase domain, RQC domain, and HRDC domain (Croteau et al., 2014; Oshima et al., 2017). The 3′–5′ exonuclease domain in the N-terminal region of WRN is required for multiple DNA repair pathways, and this domain can resolve various DNA substrates, such as fork-shaped duplex, flap-structured dsDNA, D-loops, bubble-structured duplex, Holliday junctions, and G-quadruplexes (Croteau et al., 2014; Oshima et al., 2017). WRN efficiently unwinds duplex DNA with 3′ or 5′ ssDNA tails that are >10 nucleotides long, as well as unwinding duplex DNA duplex with shorter 3′ ssDNA tails (BroshJr., Waheed and Sommers, 2002). The helicase activity of WRN is stimulated by a number of proteins, including RPA, the Ku heterodimer, MRN complex, and the telomere protein TRF2 (Cheng et al., 2004; Sommers et al., 2005; BroshJr., Opresko and Bohr, 2006). Interestingly, a recent study showed that the binding of multiple RPAs super boosts the unwinding activity of WRN so that this helicase can unidirectionally unwind a duplex with a size of >1 kb (Lee et al., 2018). The conserved RQC domain is critical for the substrate-specific DNA binding of WRN to initiate unwinding (Kitano et al., 2010; Tadokoro et al., 2012) and is also required for the ability of WRN to localize at telomere regions, but not at other genomic sites, after oxidative stress (Sun L. et al., 2017). The HRDC domain of WRN plays a role in DNA binding (von Kobbe et al., 2003; Kitano et al., 2007) and is important for the recruitment of WRN protein to DSBs (Lan et al., 2005). In addition, a small region between the RQC and HRDC domains promotes the ability of WRN to execute ssDNA annealing activity and oligomerization (Muftuoglu et al., 2008). The nuclear localization signal is located in the C-terminal region of WRN, and mutations in these sequence result in the translocation of WRN to the nucleolus and account for a significant portion of the mutations that drive the pathogenesis of Werner syndrome (WS) (Matsumoto et al., 1997; Suzuki et al., 2001). Each of these activities of WRN allows it to play

a role in multiple DNA-associated metabolisms, including DNA replication, recombination and repair, telomere maintenance, and transcription (Oshima et al., 2017; Shamanna et al., 2017; Mukherjee et al., 2018).

### Recruitment of WRN to DSB

The WRN plays various roles in NHEJ, HR, MMEJ, and SSA and does so by interacting with key participants in these pathways (Croteau et al., 2014; Shamanna et al., 2017). Cells isolated from WS patients or those with WRN knockdown are sensitive to DSB-inducing agents, including IR, CPT, etoposide, and chromium (Yannone et al., 2001; Imamura et al., 2002; Zecevic et al., 2009; Ammazzalorso et al., 2010). WRN quickly accumulates at laser-induced DSBs and is also retained at the damage sites for many hours (Lan et al., 2005; Singh et al., 2010). The recruitment of WRN to DSBs requires the presence of the HRDC domain, and its recruitment is independent of DSB sensors, such as PARP1, Ku80, DNA-PK$_{cs}$, NBS1, and histone H2AX (Lan et al., 2005). In line with WRN's involvement in multiple DSB repair pathways, the recruitment of this RecQ helicase to DSBs occurs in the G1, S, and G2 phases of the cell cycle (Shamanna et al., 2016b).

### WRN and NHEJ

The involvement of WRN in NHEJ is supported by the observations that the depletion of WRN results in a reduced *in vitro* ligation of DNA substrates with either blunt or sticky ends, as well as a decrease in NHEJ as monitored by an *in vivo* NHEJ GFP reporter assay (Chen et al., 2003; Shamanna et al., 2016b). WRN physically and functionally interacts with multiple members of the NHEJ machinery, including the Ku heterodimer, DNA-PK$_{cs}$, and the XRCC4–LIG4 complex (Cooper et al., 2000; Karmakar et al., 2002a; Kusumoto et al., 2008; Sallmyr et al., 2008; Lachapelle et al., 2011). WRN directly interacts with both subunits of the Ku70/80 heterodimer, which stimulates its exonuclease activity (Cooper et al., 2000; Li and Comai, 2000; Orren et al., 2001). Interestingly, Ku enables WRN to digest DNA containing 8-oxoadenine and 8-oxoguanine modifications, lesions that block the exonuclease activity of WRN in the absence of Ku (Orren et al., 2001). Two putative Ku-binding motifs are located in the N-terminus and C-terminus of WRN, and the interaction between WRN and Ku facilitates the nucleolytic processing of ends (Karmakar et al., 2002b). A recent study reported that these two Ku-binding motifs of WRN function cooperatively to bind the Ku heterodimer and that the N-terminal Ku-binding motif mediates Ku-dependent stimulation of WRN exonuclease activity, promoting DSB repair (Grundy et al., 2016). DNA-PK$_{cs}$, phosphorylates WRN at Ser440 and Ser467, and regulates the enzymatic activities of WRN (Yannone et al., 2001; Karmakar et al., 2002a; Kusumoto-Matsuo et al., 2014). The XRCC4-LIG4 complex also interacts with WRN and stimulates its exonuclease activity, but not helicase activity, to generate DNA ends suitable for XRCC4-LIG4-mediated ligation (Kusumoto et al., 2008). Another report indicates that WRN is involved in NHEJ indirectly by upregulating the transcription level of the key NHEJ factor XLF (Liu et al., 2014). Together, the data show that the enzymatic activities of WRN, in particular DNA end processing by the exonuclease activity of WRN, promote NHEJ.

### WRN and HR

In addition to NHEJ, WRN promotes HR-mediated DSB repair in multiple ways (Saintigny et al., 2002; Chen et al., 2003). WRN participates in DNA end resection during the early stages of HR. WRN interacts with MRE11 and NBS1, which is enhanced by IR, and results in the promotion of WRN helicase activity (Cheng et al., 2004). WRN also physically interacts with DNA2 and promotes extensive DNA end resection in an RPA-dependent matter (Sturzenegger et al., 2014; Pinto et al., 2016). Moreover, during the late S/G2 and M phases of the cell cycle, cyclin-dependent kinase 1 (CDK1) phosphorylates WRN to promote the long-range end resection by DNA2 at replication-associated DSBs, which stimulates HR and the recovery of collapsed replication forks and promotes the maintenance of chromosome stability (Palermo et al., 2016). Specifically, CDK1-dependent phosphorylation of WRN occurs at Ser1133, and this phosphorylation is required for the WRN–MRE11 interaction and promotes MRE11 foci formation at CPT-induced DSBs (Palermo et al., 2016). Moreover, BRCA1 also directly interacts with WRN and stimulates both the helicase and exonuclease activities of WRN, which likely promotes DNA end resection (Cheng et al., 2006). WRN processes intermediates during HR as it promotes the ATP-dependent translocation of Holliday junctions (Constantinou et al., 2000), disrupts mobile D-loop by promoting branch migration, and degrades the invading strand both prior to and after release from the D-loop (Opresko et al., 2009). WRN has also been found to interact with the following HR proteins: RAD51, RAD54, and RAD52 (Baynton et al., 2003; Otterlei et al., 2006; Lachapelle et al., 2011). In addition, the BRCA1/BARD1 complex interacts with WRN *in vivo* and stimulates WRN helicase activity toward forked and Holliday junction substrates (Cheng et al., 2006). RAD52 modulates WRN activity and inhibits its ability to unwind four-way Holliday junctions (Baynton et al., 2003). Collectively, WRN plays important roles in multiple steps during HR.

### WRN and Alternative End-Joining Pathways

As mentioned above, resected dsDNA with 3′ ssDNA overhangs can be used for HR, MMEJ, and SSA, which is initiated by MRN with the assistance of CtIP (Ronato et al., 2020). Interestingly, WRN actively inhibits DNA end resection by limiting the recruitment of MRE11 and CtIP to DSBs in the G1 phase of the cell cycle (Shamanna et al., 2016b). Accordingly, elevated MMEJ was observed in both WS and WRN-deficient cells, leading to telomere fusions (Shamanna et al., 2016b). In agreement with this finding, limiting MMEJ by depleting CtIP suppresses telomere fusions in WRN-deficient cells (Shamanna et al., 2016b).

WRN interacts with the key SSA player RAD52 and enhances the efficiency of RAD52-mediated strand annealing between non-duplex DNA and homologous sequences contained within a double-stranded plasmid (Baynton et al., 2003). The C-terminal region of WRN may be required for SSA (Muftuoglu et al., 2008). WRN deletion by siRNA causes a 25–50% reduction of SSA-mediated DSB repair in two human cell lines, indicating that WRN promotes SSA (Sturzenegger et al., 2014). However, many questions remain with regard to WRN's role in SSA, including whether it helps mediate the long resection required for SSA and

whether WRN is required for the RAD52-dependent annealing of ssDNA to drive SSA.

### WRN and Diseases

Mutations in WRN cause the autosomal-recessive disorder Werner syndrome (MIM #277700), which is a segmental progeria (Oshima et al., 2017; Shamanna et al., 2017; Lebel and MonnatJr., 2018). The average life span of WS patients is 54 years, and the major death causes of WS patients are cancer and myocardial infarction (Huang et al., 2006; Goto et al., 2013; Oshima et al., 2017). WS confers a strong predisposition to a diversity of neoplasia, and two thirds of these neoplasia are collectively thyroid neoplasms, malignant melanoma, meningioma, soft tissue sarcomas, leukemia and pre-leukemic conditions of the bone marrow, and primary bone neoplasms (Goto et al., 2013; Lauper et al., 2013). The elevated risk of these neoplasms ranges from 8.9-fold for thyroid epithelial neoplasms to 53.5-fold for melanoma compared to the normal population (Lauper et al., 2013). Meningioma frequently occurs in WS patients (Tsurubuchi et al., 2008; Huang et al., 2018; Pattankar et al., 2020), and this is likely a consequence of a reduced WRN expression due to the elevated methylation of the WRN promoter (Li et al., 2015). In addition, WRN mutations are also associated with other tumors, such as breast cancer (Romanowicz et al., 2017), oral squamous cell carcinoma (Kuribayashi et al., 2019), and colorectal cancer (Lee et al., 2017; Zhunussova et al., 2019; Zimmer et al., 2020). The cells from WS patients display an increased rate of somatic mutations, chromosome losses, deletions, and genomic rearrangements (Subino et al., 1982; Fukuchi et al., 1989; Oshima et al., 2002; Friedrich et al., 2010).

## RECQL4

*RECQL4*, located at chromosome 8q24.3, encodes a 1,208-amino acid protein, which possesses the highly conserved 3′ to 5′ helicase domain, but does not have the typical RQC and HRDC domains (**Figure 3**). A recent study identified a novel C-terminal domain containing a $Zn^{2+}$-binding site and two distinct winged-helix domains, which are not involved in canonical DNA binding or helicase activity (Kaiser et al., 2017). The N-terminus of RECQL4 contains multiple functional domains, including both nuclear and mitochondrial targeting sequences (Burks et al., 2007; Croteau et al., 2012a). Furthermore, an SLD2-like domain is located in the N-terminus of RECQL4, and it is important for DNA replication (Sangrithi et al., 2005; Xu et al., 2009). Many proteins interact with the N-terminal region of RECQ4 (Croteau et al., 2012b). In addition, functional phosphorylation and acetylation events have also been identified in this region (Dietschy et al., 2009; Lu et al., 2017). Consequently, the N-terminus of RECQL4 is essential for cell viability and for the cellular response to IR (Abe et al., 2011; Lu et al., 2017). The C-terminal region of RECQL4 is not well characterized, but is important for cells to survive IR (Kohzaki et al., 2012). The helicase activity of RECQL4 can unwind forked duplexes, D-loops, and bubble structures, but not duplex DNA or Holliday junctions (Rossi et al., 2010). Interestingly, a recent study identified an unwinding activity of RECQL4 and its yeast homolog Hrq1 on G-quadruplexes (Rogers et al., 2017). RECQL4 has a strong ssDNA annealing activity, which may mask the detection of unwound products (Rossi et al., 2010). The helicase activity is important for the role of RECQL4 in DNA repair and prevention of cellular senescence (Lu et al., 2014, 2016). Overall, RECQL4 is involved in various cellular functions, including DNA replication (Sangrithi et al., 2005), multiple repair pathways (Fan and Luo, 2008; Schurman et al., 2009; Singh et al., 2010; Duan et al., 2020), preservation of the mitochondrial genome (Croteau et al., 2012a), and telomere maintenance (Ghosh et al., 2012).

### Recruitment of RECQL4 to DSBs

RECQL4-depleted human cells and fibroblasts from Rothmund–Thomson syndrome (RTS) patients are sensitive to IR and other DSB-inducing chemicals, and these cells accumulate unrepaired DSBs, as indicated by elevated γH2AX and 53BP1 foci (Jin et al., 2008; Singh et al., 2010; Kohzaki et al., 2012; Shamanna et al., 2014; Lu et al., 2014, 2016). In *Xenopus* egg extracts, RECQL4 accumulates on chromatin containing *Eco*RI-induced DSBs *in vitro*, which is dependent on RPA, DNA-PK, and ataxia telangiectasia mutated (ATM), but not on DNA replication or RAD51 (Kumata et al., 2007). In human cells, GFP-tagged RECQL4 is recruited immediately to laser−induced DSBs and dissociates from DSBs much more quickly than WRN and BLM, suggesting that RECQL4 only functions at the early time points in DSB repair (Singh et al., 2010; Lu et al., 2016). The unique N−terminus between amino acids 363–492 is the region required for the recruitment of RECQL4 to DSBs (Singh et al., 2010). Moreover, the accumulation of RECQL4 at laser-induced DSBs occurs in both G1 and S/G2 cells (Lu et al., 2017). Inhibition of ATM or knockdown of BLM or WRN does not significantly alter the dynamics of RECQL4 to laser-induced DSBs in human cells (Singh et al., 2010; Lu et al., 2017). The accumulation of RECQL4 at DSBs is stimulated by both phosphorylation at Ser89 and Ser251 by CDK1 and CDK2 and ubiquitination by the DDB1-CUL4A E3 ubiquitin ligase (Lu et al., 2017). However, the ubiquitination sites on RECQL4 by DDB1-CUL4A E3 Ligase have not been identified.

### RECQL4 and NHEJ

A role for RECQL4 in NHEJ was first indicated when it was found that RECQL4 binds to restriction enzyme-generated DSBs near the Ku70-binding site and that RECQL4 is required for the repair of these DSBs in *Xenopus* extracts (Kumata et al., 2007). Depletion of RECQL4 reduced the end-joining activity on DNA substrates with either cohesive or non-cohesive ends *in vitro* and also decreased the end-joining activity of a GFP reporter plasmid *in vivo,* providing strong evidence that RECQL4 functions in NHEJ in human cells (Shamanna et al., 2014). Further investigations showed that RECQL4 forms a complex with the Ku70/Ku80 heterodimer through its N-terminal domain and stimulates the DNA binding of Ku70/Ku80 to a blunt-ended dsDNA substrate (Shamanna et al., 2014). Interestingly, the interaction of RECQL4 with the Ku complex is enhanced in the G1 phase of the cell cycle compared to that in S/G2 cells, indicating that RECQL4 promotes NHEJ in G1 cells (Lu et al., 2017).

### RECQL4 and HR

As an important protein in the assembly of DNA replication machinery, RECQL4 is highly expressed during the S phase, the cell cycle phase when HR is the dominant DSB repair pathway, and thus it was predicted that it would also play a role in HR (Sangrithi et al., 2005; Im et al., 2009; Xu et al., 2009; Singh et al., 2012). The initial study suggesting RECQL4 functions in HR reported that it forms a complex with RAD51 following treatment with etoposide (Petkovic et al., 2005). Its role was further elucidated when it was found that the depletion of RECQL4 by siRNAs caused a dramatic loss of HR efficiency, as monitored by a GFP reporter assay, and that RECQL4 is required for DNA end resection (Lu et al., 2016). Specifically, MRE1 regulates the recruitment of RECQL4 to DSBs and RECQL4 promotes the nuclease activity of MRE11 *in vitro*. In addition, RECQL4 also forms a complex with CtIP *via* its N-terminal domain and promotes the recruitment of CtIP to MRN at DSBs. Furthermore, the helicase activity of RECQL4 promotes DNA end processing and HR, and this process is regulated by CDK1/2-mediated phosphorylation (Lu et al., 2017). Specifically, CDK1 and CDK2 phosphorylate RECQL4 on serines 89 and 251, and this facilitates the interaction between MRE11 and RECQL4 as well as RECQL4 recruitment to DSBs (Lu et al., 2017). Interestingly, RECQL4 promotes and coordinates NHEJ and HR in a cell cycle-dependent manner (Lu et al., 2017). RECQL4 preferably interacts with Ku70 to promote NHEJ in G1 when the overall CDK activity is low. During the S/G2 phases, RECQL4 is phosphorylated by CDK1 and CDK2, which promotes the RECQL4–MRN interaction to stimulate HR. These findings indicate a role for RECQL4 in the regulation of DSB repair pathway choice.

### RECQL4 and Alternative End-Joining Pathways

A study recently discovered a role for RECQL4 in DSB repair pathway choice between MMEJ and SSA (Kohzaki et al., 2020). RECQL4ΔC HCT116 cells (lacking the C-terminal domain) exhibit increased SSA activity and decreased MMEJ activity, and ectopic expression of RECQL4 increased HR and MMEJ but repressed SSA (Kohzaki et al., 2020). Knockdown of RAD52 inhibits SSA in RECQL4ΔC HCT116 cells, but does not influence HR and MMEJ (Kohzaki et al., 2020). The involvement of RECQL4 in the initial end resection by MRN/CtIP may account for the pro-MMEJ role of RECQL4 since a short resected ssDNA is required for MMEJ. However, it is unclear how RECQL4 functions in repressing RAD52-mediated SSA.

### RECQL4 and Diseases

Mutations in RECQL4 are associated with three rare autosomal-recessive disorders: Rothmund–Thomson syndrome (RTS; OMIM #268400), RAPADILINO (RAPA; OMIM #266280), and Baller–Gerold syndrome (BGS; OMIM #218600) (Siitonen et al., 2009; Larizza et al., 2010, 2013). RTS is accompanied with an increased risk of malignant tumor osteosarcoma in childhood (Wang et al., 2003; Larizza et al., 2010; Lu et al., 2020). RAPADILINO patients develop lymphoma and osteosarcoma (Siitonen et al., 2009), while a BGS patient was reported with lymphoma (Debeljak et al., 2009). In addition, germline mutations of RECQL4 have also been identified to associate with several cancers, including prostate cancer (Paulo et al., 2018), colorectal cancer (Zhunussova et al., 2019), choroid plexus papilloma (Taher et al., 2019), and melanoma (Bodelon et al., 2012; Aoude et al., 2020). Chromosome aberrations, mainly mosaic trisomies and isochromosomes, frequently occur in RTS patient cells, leading to the cancer predisposition of these patients (Larizza et al., 2006). In line with this finding in human RTS cells, defective sister chromatid cohesion, aneuploidy, and cancer predisposition were observed in the cells from an RTS mouse model (Mann et al., 2005). Therefore, RECQL4 is crucial to maintain the integrity of the genome.

## RECQL5

RECQL5, encoded by the *RECQL5* gene at chromosome 17q25, exists in three isoforms generated by alternative splicing: RECQL5α, RECQL5β, and RECQL5γ. RECQL5α and RECQL5γ consist of 410 and 435 amino acids, respectively, while RECQL5β contains 991 amino acids (**Figure 3**) (Sekelsky et al., 1999; Shimamoto et al., 2000). All three isoforms have the core helicase domain, while only RECQL5β has helicase activity *in vitro* (Shimamoto et al., 2000). Additionally, RECQL5β (referred to as RECQL5 in the following text) has a $Zn^{2+}$-binding motif and a unique C-terminal region harboring multiple specific protein interaction domains: a RAD51-binding domain, internal RNAPII-interacting (IRI) domain, Set2-Rpb1-interacting (SRI) domain, RNA polymerase I (RNAPI)-binding domain, and a proliferating cell nuclear antigen (PCNA)-interacting protein (PIP) motif (Andrs et al., 2020). The $Zn^{2+}$-binding motif is essential for helicase activity and DNA binding (Ren et al., 2008). RECQL5 has intrinsic ssDNA strand annealing activity, which is inhibited by ATP (Garcia et al., 2004; Ren et al., 2008). However, a recent study showed that RECQL5 possesses a stronger annealing activity on long or small duplexed substrates compared to the other RecQ helicases, which is not inhibited by the presence of ATP (Khadka et al., 2016). RECQL5 efficiently catalyzes the annealing of RNA to DNA *in vitro* in the presence or absence of ATP (Khadka et al., 2016). However, the cellular function of this activity for RECQL5 is yet to be delineated.

### Recruitment of RECQL5 to DSBs

RECQL5-depleted cells accumulate persistent IR-induced 53BP1 foci, implicating a role for RECQL5 in DSB repair (Popuri et al., 2012b). RECQL5 is recruited quickly to laser-induced DSBs and remains for a shorter duration than BLM and WRN, but persists longer than RECQL4 (Zheng et al., 2009; Popuri et al., 2012b). Both the helicase and KIX domains are required for DNA damage recognition and the stable association of RECQL5 to DSB sites (Popuri et al., 2012b). The recruitment of RECQL5 requires MRE11, but not the exonuclease activity of MRE11, and its recruitment to DSB is independent of RNA polymerase II, BLM, WRN, ATM, MDC1, and CtIP (Zheng et al., 2009; Popuri et al., 2012b). RECQL5 interacts with Poly(ADP-ribose) (PAR) and Poly(ADP-ribose) polymerase 1 (PARP1), and PARylation by PARP1 stimulates the recruitment of RECQL5-GFP to laser-induced DSBs (Khadka et al., 2015).

### RECQL5 and HR

Deletion of RECQL5 increases HR in MEFs (Hu et al., 2007). Consistent with this, it was found that RECQL5 binds to RAD51, inhibits RAD51-mediated D-loop formation, and displaces RAD51 from ssDNA in assistance with ATP hydrolysis and RPA (Hu et al., 2007; Schwendener et al., 2010). Another study reported that RECQL5 counteracts the inhibitory effect of RAD51 on RAD52-mediated DNA annealing with its ATPase and RAD51-binding activity (Paliwal et al., 2014). Furthermore, RECQL5 deficiency causes an increased occupancy of RAD51 at DSBs and evaluated sister chromatid exchange when the Holliday junction dissolution pathway is inactivated or a high load of DNA damage is generated in the cell (Paliwal et al., 2014). Together, these findings suggest that RECQL5 functions during the postsynaptic phase of synthesis-dependent strand annealing to prevent the formation of aberrant RAD51 filaments on the extended invading strand and inappropriate HR events (Hu et al., 2007; Schwendener et al., 2010; Paliwal et al., 2014). RECQL5 forms a constitutive complex with MRN and specifically inhibits the exonuclease activity of MRE11 (Zheng et al., 2009), but it is unclear whether this activity plays a role in the ability of RECQL5 to suppress HR. Interestingly, it was reported that RECQL5 promotes HR-mediated repair with non-crossover products in a direct repeat GFP (DR-GFP) reporter assay in both U2OS and HEK293 cells (Paliwal et al., 2014; Khadka et al., 2015). RECQL5 deficiency in *Drosophila* causes sensitivity to IR and DSBs induced by the I-SceI endonuclease and impairs SSA-mediated DSB repair (Chen et al., 2010), but it is unknown whether RECQL5 modulates SSA in mammalian cells.

### RECQL5 and Cancers

The downregulation of RECQ5 leads to a transcription-dependent chromosome fragmentation during S phase of the cell cycle as well as the accumulation of chromosomal rearrangements with the breakpoints located in genes and common fragile sites, indicating the importance of this helicase in maintaining genome integrity (Li et al., 2011; Saponaro et al., 2014). Although defects in RECQL5 have not been associated with human genetic disorders, mutations in RECQL5 have been associated with tumorigenesis, including breast cancer (He et al., 2014), osteosarcoma (Zhi et al., 2014; Dong et al., 2015), NUT midline carcinoma (Stirnweiss et al., 2017), head and neck cancer (Das et al., 2018), and hereditary diffuse gastric cancer (Fewings et al., 2018).

## PERSPECTIVE REMARKS

A significant number of clues have uncovered the roles that the RecQ helicases play in DSB repair and the maintenance of genome stability. Furthermore, the evidence has started to reveal how defects in the RecQ helicases drive specific genetic disorders and carcinogenesis. However, many questions still remain, including: (1) a clear role for each RecQ helicase's enzymatic activity in DSB repair is yet to be demonstrated; (2) it is still unclear how BLM, WRN, and RECQL4 cooperate in 5′ DNA end resection during HR; (3) RECQL4 interacts with Ku70/80 heterodimers and is required for NHEJ, but its role in this pathway is unknown; (4) the role of RecQ helicases in MMEJ and SSA are also limited; (5) does RECQL5 play a role in RNA-mediated DSB repair; (6) do the RecQ helicases play a direct or passive role in DSB repair pathway choice; (7) what role does posttranslational modifications play in regulating the RecQ helicases; and (8) can RecQ helicases be targeted for specific cancer therapies. Among these questions, investigating the posttranslational modifications of RecQ helicases may shed light on many unknown mechanisms, including the enzymatic roles of RecQ helicases in specific steps of DSB repair pathways, coordination between the RecQ helicases during specific repair processes, and the role(s) of RecQ helicases in DSB repair pathway choice. Thanks to the great advance of mass spectrometry, hundreds of posttranslational modifications, including phosphorylation, acetylation, ubiquitination, etc., have been identified on RecQ helicases[1] (Hornbeck et al., 2012, 2015, 2019). However, the biological functions of these modifications are yet to be elucidated. Hence, it would be promising to investigate posttranslational modifications of RecQ helicases with the combination of spatial and temporal factors as well as stresses. Recently, WRN was identified as a synthetic lethal vulnerability in cancers with microsatellite instability (Chan et al., 2019; van Wietmarschen et al., 2020). Interestingly, CPT treatment leads to the degradation of WRN (Shamanna et al., 2016a; Li et al., 2020), suggesting that cancers with microsatellite instability may be a candidate target for CPT treatment to drive WRN-specific vulnerable tumors. These findings together demonstrate WRN as an important genome guardian to prevent diseases and as a potential drug target. Collectively, these and other unanswered questions drive us and others to understand the role of each RecQ helicase in DSB repair, how defects drive human disorders, and how these enzymes may be targets for therapy.

## AUTHOR CONTRIBUTIONS

HL and AD conceived the concept and wrote the manuscript together. Both authors contributed to the article and approved the submitted version.

## FUNDING

This research was supported by grants from the National Institutes of Health CA092584, CA162804, and GM04725 to AD and by an Initiative Seed Grant for Career Development from the Department of Radiation Oncology at UT Southwestern Medical Center to HL.

[1] www.phosphosite.org

## REFERENCES


Abe, T., Yoshimura, A., Hosono, Y., Tada, S., Seki, M., and Enomoto, T. (2011). The N-terminal region of RECQL4 lacking the Helicase domain is both essential and sufficient for the viability of vertebrate cells. Role of the N-terminal region of RECQL4 in cells. *Biochim. Biophys. Acta* 1813, 473–479. doi: 10.1016/j.bbamcr.2011.01.001

Ammazzalorso, F., Pirzio, L. M., Bignami, M., Franchitto, A., and Pichierri, P. (2010). ATR and ATM differently regulate WRN to prevent DSBs at stalled replication forks and promote replication fork recovery. *EMBO J.* 29, 3156–3169. doi: 10.1038/emboj.2010.205

Andrs, M., Hasanova, Z., Oravetzova, A., Dobrovolna, J., and Janscak, P. (2020). RECQ5: a mysterious Helicase at the interface of DNA replication and transcription. *Genes* 11:232. doi: 10.3390/genes11020232

Aoude, L. G., Bonazzi, V. F., Brosda, S., Patel, K., Koufariotis, L. T., Oey, H., et al. (2020). Pathogenic germline variants are associated with poor survival in stage III/IV melanoma patients. *Sci. Rep.* 10:17687.

Bachrati, C. Z., Borts, R. H., and Hickson, I. D. (2006). Mobile D-loops are a preferred substrate for the Bloom's syndrome Helicase. *Nucleic Acids Res.* 34, 2269–2279. doi: 10.1093/nar/gkl258

Banerjee, T., Sommers, J. A., Huang, J., Seidman, M. M., and Brosh, R. M. Jr. (2015). Catalytic strand separation by RECQ1 is required for RPA-mediated response to replication stress. *Curr. Biol.* 25, 2830–2838. doi: 10.1016/j.cub.2015.09.026

Barefield, C., and Karlseder, J. (2012). The BLM Helicase contributes to telomere maintenance through processing of late-replicating intermediate structures. *Nucleic Acids Res.* 40, 7358–7367. doi: 10.1093/nar/gks407

Baris, H. N., Kedar, I., Halpern, G. J., Shohat, T., Magal, N., Ludman, M. D., et al. (2007). Prevalence of breast and colorectal cancer in Ashkenazi Jewish carriers of Fanconi anemia and Bloom syndrome. *Isr. Med. Assoc. J.* 9, 847–850.

Baynton, K., Otterlei, M., Bjoras, M., von Kobbe, C., Bohr, V. A., and Seeberg, E. (2003). WRN interacts physically and functionally with the recombination mediator protein RAD52. *J. Biol. Chem.* 278, 36476–36486. doi: 10.1074/jbc.m303885200

Bennardo, N., Cheng, A., Huang, N., and Stark, J. M. (2008). Alternative-NHEJ is a mechanistically distinct pathway of mammalian chromosome break repair. *PLoS Genet.* 4:e1000110. doi: 10.1371/journal.pgen.1000110

Beresten, S. F., Stan, R., van Brabant, A. J., Ye, T., Naureckiene, S., and Ellis, N. A. (1999). Purification of overexpressed hexahistidine-tagged BLM N431 as oligomeric complexes. *Protein Expr. Purif.* 17, 239–248. doi: 10.1006/prep.1999.1135

Berti, M., Ray Chaudhuri, A., Thangavel, S., Gomathinayagam, S., Kenig, S., Vujanovic, M., et al. (2013). Human RECQ1 promotes restart of replication forks reversed by DNA topoisomerase I inhibition. *Nat. Struct. Mol. Biol.* 20, 347–354. doi: 10.1038/nsmb.2501

Bhargava, R., Onyango, D. O., and Stark, J. M. (2016). Regulation of single-strand annealing and its role in genome maintenance. *Trends Genet.* 32, 566–575. doi: 10.1016/j.tig.2016.06.007

Bochman, M. L., Paeschke, K., Chan, A., and Zakian, V. A. (2014). Hrq1, a homolog of the human RecQ4 Helicase, acts catalytically and structurally to promote genome integrity. *Cell Rep.* 6, 346–356. doi: 10.1016/j.celrep.2013.12.037

Bodelon, C., Pfeiffer, R. M., Bollati, V., Debbache, J., Calista, D., Ghiorzo, P., et al. (2012). On the interplay of telomeres, nevi and the risk of melanoma. *PLoS One* 7:e52466. doi: 10.1371/journal.pone.0052466

Bohr, V. A. (2008). Rising from the RecQ-age: the role of human RecQ Helicases in genome maintenance. *Trends Biochem. Sci.* 33, 609–620. doi: 10.1016/j.tibs.2008.09.003

Boulton, S. J., and Jackson, S. P. (1996). *Saccharomyces cerevisiae* Ku70 potentiates illegitimate DNA double-strand break repair and serves as a barrier to error-prone DNA repair pathways. *EMBO J.* 15, 5093–5103. doi: 10.1002/j.1460-2075.1996.tb00890.x

Bouwman, B. A. M., and Crosetto, N. (2018). Endogenous DNA double-strand breaks during DNA transactions: emerging insights and methods for genome-wide profiling. *Genes* 9:632. doi: 10.3390/genes9120632

Brosh, R. M. Jr., Li, J. L., Kenny, M. K., Karow, J. K., Cooper, M. P., Kureekattil, R. P., et al. (2000). Replication protein A physically interacts with the Bloom's syndrome protein and stimulates its Helicase activity. *J. Biol. Chem.* 275, 23500–23508. doi: 10.1074/jbc.m001557200

Brosh, R. M. Jr., Opresko, P. L., and Bohr, V. A. (2006). Enzymatic mechanism of the WRN Helicase/nuclease. *Methods Enzymol.* 409, 52–85. doi: 10.1016/s0076-6879(05)09004-x

Brosh, R. M. Jr., Waheed, J., and Sommers, J. A. (2002). Biochemical characterization of the DNA substrate specificity of Werner syndrome Helicase. *J. Biol. Chem.* 277, 23236–23245. doi: 10.1074/jbc.m111446200

Bugreev, D. V., Mazina, O. M., and Mazin, A. V. (2009). Bloom syndrome Helicase stimulates RAD51 DNA strand exchange activity through a novel mechanism. *J. Biol. Chem.* 284, 26349–26359. doi: 10.1074/jbc.m109.029371

Bugreev, D. V., Yu, X., Egelman, E. H., and Mazin, A. V. (2007). Novel pro- and anti-recombination activities of the Bloom's syndrome Helicase. *Genes Dev.* 21, 3085–3094. doi: 10.1101/gad.1609007

Burks, L. M., Yin, J., and Plon, S. E. (2007). Nuclear import and retention domains in the amino terminus of RECQL4. *Gene* 391, 26–38. doi: 10.1016/j.gene.2006.11.019

Cannavo, E., and Cejka, P. (2014). Sae2 promotes dsDNA endonuclease activity within Mre11-Rad50-Xrs2 to resect DNA breaks. *Nature* 514, 122–125. doi: 10.1038/nature13771

Ceccaldi, R., Rondinelli, B., and D'Andrea, A. D. (2016). Repair pathway choices and consequences at the double-strand break. *Trends Cell Biol.* 26, 52–64. doi: 10.1016/j.tcb.2015.07.009

Chaganti, R. S., Schonberg, S., and German, J. (1974). A manyfold increase in sister chromatid exchanges in Bloom's syndrome lymphocytes. *Proc. Natl. Acad. Sci. U.S.A.* 71, 4508–4512. doi: 10.1073/pnas.71.11.4508

Chan, E. M., Shibue, T., McFarland, J. M., Gaeta, B., Ghandi, M., Dumont, N., et al. (2019). WRN Helicase is a synthetic lethal target in microsatellite unstable cancers. *Nature* 568, 551–556.

Chen, L., Huang, S., Lee, L., Davalos, A., Schiestl, R. H., Campisi, J., et al. (2003). WRN, the protein deficient in Werner syndrome, plays a critical structural role in optimizing DNA repair. *Aging Cell* 2, 191–199. doi: 10.1046/j.1474-9728.2003.00052.x

Chen, Y., Dui, W., Yu, Z., Li, C., Ma, J., and Jiao, R. (2010). Drosophila RecQ5 is required for efficient SSA repair and suppression of LOH in vivo. *Protein Cell* 1, 478–490. doi: 10.1007/s13238-010-0058-2

Cheng, W. H., Kusumoto, R., Opresko, P. L., Sui, X., Huang, S., Nicolette, M. L., et al. (2006). Collaboration of Werner syndrome protein and BRCA1 in cellular responses to DNA interstrand cross-links. *Nucleic Acids Res.* 34, 2751–2760. doi: 10.1093/nar/gkl362

Cheng, W. H., von Kobbe, C., Opresko, P. L., Arthur, L. M., Komatsu, K., Seidman, M. M., et al. (2004). Linkage between Werner syndrome protein and the Mre11 complex via Nbs1. *J. Biol. Chem.* 279, 21169–21176. doi: 10.1074/jbc.m312770200

Cheok, C. F., Wu, L., Garcia, P. L., Janscak, P., and Hickson, I. D. (2005). The Bloom's syndrome Helicase promotes the annealing of complementary single-stranded DNA. *Nucleic Acids Res.* 33, 3932–3941. doi: 10.1093/nar/gki712

Chi, X. Y., Li, Y., and Qiu, X. Y. (2020). V(D)J recombination, somatic hypermutation and class switch recombination of immunoglobulins: mechanism and regulation. *Immunology* 160, 233–247. doi: 10.1111/imm.13176

Choi, D. H., Lee, R., Kwon, S. H., and Bae, S. H. (2013). Hrq1 functions independently of Sgs1 to preserve genome integrity in *Saccharomyces cerevisiae*. *J. Microbiol.* 51, 105–112. doi: 10.1007/s12275-013-3048-2

Ciccia, A., and Elledge, S. J. (2010). The DNA damage response: making it safe to play with knives. *Mol. Cell* 40, 179–204. doi: 10.1016/j.molcel.2010.09.019

Cleary, S. P., Zhang, W., Di Nicola, N., Aronson, M., Aube, J., Steinman, A., et al. (2003). Heterozygosity for the BLM(Ash) mutation and cancer risk. *Cancer Res.* 63, 1769–1771.

Cobb, J. A., and Bjergbaek, L. (2006). RecQ Helicases: lessons from model organisms. *Nucleic Acids Res.* 34, 4106–4114. doi: 10.1093/nar/gkl557

Constantinou, A., Tarsounas, M., Karow, J. K., Brosh, R. M., Bohr, V. A., Hickson, I. D., et al. (2000). Werner's syndrome protein (WRN) migrates Holliday junctions and co-localizes with RPA upon replication arrest. *EMBO Rep.* 1, 80–84. doi: 10.1093/embo-reports/kvd004

Cooper, M. P., Machwe, A., Orren, D. K., Brosh, R. M., Ramsden, D., and Bohr, V. A. (2000). Ku complex interacts with and stimulates the Werner protein. *Genes Dev.* 14, 907–912.

Croteau, D. L., Popuri, V., Opresko, P. L., and Bohr, V. A. (2014). Human RecQ Helicases in DNA repair, recombination, and replication. *Annu. Rev. Biochem.* 83, 519–552. doi: 10.1146/annurev-biochem-060713-035428

Croteau, D. L., Rossi, M. L., Canugovi, C., Tian, J., Sykora, P., Ramamoorthy, M., et al. (2012a). RECQL4 localizes to mitochondria and preserves mitochondrial DNA integrity. *Aging Cell* 11, 456–466. doi: 10.1111/j.1474-9726.2012.00803.x

Croteau, D. L., Singh, D. K., Hoh Ferrarelli, L., Lu, H., and Bohr, V. A. (2012b). RECQL4 in genomic instability and aging. *Trends Genet.* 28, 624–631. doi: 10.1016/j.tig.2012.08.003

Cui, S., Klima, R., Ochem, A., Arosio, D., Falaschi, A., and Vindigni, A. (2003). Characterization of the DNA-unwinding activity of human RECQ1, a Helicase specifically stimulated by human replication protein A. *J. Biol. Chem.* 278, 1424–1432. doi: 10.1074/jbc.m209407200

Cunniff, C., Bassetti, J. A., and Ellis, N. A. (2017). Bloom's syndrome: clinical spectrum, molecular pathogenesis, and cancer predisposition. *Mol. Syndromol.* 8, 4–23. doi: 10.1159/000452082

Cybulski, C., Carrot-Zhang, J., Kluzniak, W., Rivera, B., Kashyap, A., Wokolorczyk, D., et al. (2015). Germline RECQL mutations are associated with breast cancer susceptibility. *Nat. Genet.* 47, 643–646. doi: 10.1038/ng.3284

Daley, J. M., Jimenez-Sainz, J., Wang, W., Miller, A. S., Xue, X., Nguyen, K. A., et al. (2017). Enhancement of BLM-DNA2-mediated long-range DNA end resection by CtIP. *Cell Rep.* 21, 324–332. doi: 10.1016/j.celrep.2017.09.048

Das, R., Kundu, S., Laskar, S., Choudhury, Y., and Ghosh, S. K. (2018). Assessment of DNA repair susceptibility genes identified by whole exome sequencing in head and neck cancer. *DNA Repair.* 66–67, 50–63. doi: 10.1016/j.dnarep.2018.04.005

Datta, A., Dhar, S., Awate, S., and Brosh, R. M. Jr. (2020). Synthetic Lethal Interactions of RECQ Helicases. *Trends Cancer* 7, 146–161. doi: 10.1016/j.trecan.2020.09.001

Davis, A. J., Chen, B. P., and Chen, D. J. (2014). DNA-PK: a dynamic enzyme in a versatile DSB repair pathway. *DNA Repair.* 17, 21–29. doi: 10.1016/j.dnarep.2014.02.020

Davis, A. J., and Chen, D. J. (2013). DNA double strand break repair via non-homologous end-joining. *Transl. Cancer Res.* 2, 130–143.

de Renty, C., and Ellis, N. A. (2017). Bloom's syndrome: why not premature aging?: a comparison of the BLM and WRN Helicases. *Age. Res. Rev.* 33, 36–51.

de Voer, R. M., Hahn, M. M., Mensenkamp, A. R., Hoischen, A., Gilissen, C., Henkes, A., et al. (2015). Deleterious germline BLM mutations and the risk for early-onset colorectal cancer. *Sci. Rep.* 5:14060.

Debeljak, M., Zver, A., and Jazbec, J. (2009). A patient with Baller-gerold syndrome and midline NK/T lymphoma. *Am. J. Med. Genet. A* 149A, 755–759. doi: 10.1002/ajmg.a.32736

Debnath, S., and Sharma, S. (2020). RECQ1 Helicase in genomic stability and cancer. *Genes* 11:622. doi: 10.3390/genes11060622

Deshpande, R. A., Myler, L. R., Soniat, M. M., Makharashvili, N., Lee, L., Lees-Miller, S. P., et al. (2020). DNA-dependent protein kinase promotes DNA end processing by MRN and CtIP. *Sci. Adv.* 6:eaay0922. doi: 10.1126/sciadv.aay0922

Dietschy, T., Shevelev, I., Pena-Diaz, J., Huhn, D., Kuenzle, S., Mak, R., et al. (2009). p300-mediated acetylation of the Rothmund-Thomson-syndrome gene product RECQL4 regulates its subcellular localization. *J. Cell Sci.* 122, 1258–1267. doi: 10.1242/jcs.037747

Doherty, K. M., Sommers, J. A., Gray, M. D., Lee, J. W., von Kobbe, C., Thoma, N. H., et al. (2005). Physical and functional mapping of the replication protein a interaction domain of the werner and bloom syndrome Helicases. *J. Biol. Chem.* 280, 29494–29505. doi: 10.1074/jbc.m500653200

Dong, Y. Z., Huang, Y. X., and Lu, T. (2015). Single nucleotide polymorphism in the RECQL5 gene increased osteosarcoma susceptibility in a Chinese Han population. *Genet. Mol. Res.* 14, 1899–1902. doi: 10.4238/2015.march.13.18

Drosopoulos, W. C., Kosiyatrakul, S. T., and Schildkraut, C. L. (2015). BLM Helicase facilitates telomere replication during leading strand synthesis of telomeres. *J. Cell Biol.* 210, 191–208. doi: 10.1083/jcb.201410061

Duan, S., Han, X., Akbari, M., Croteau, D. L., Rasmussen, L. J., and Bohr, V. A. (2020). Interaction between RECQL4 and OGG1 promotes repair of oxidative base lesion 8-oxoG and is regulated by SIRT1 deacetylase. *Nucleic Acids Res.* 48, 6530–6546. doi: 10.1093/nar/gkaa392

Ellenberger, T., and Tomkinson, A. E. (2008). Eukaryotic DNA ligases: structural and functional insights. *Annu. Rev. Biochem.* 77, 313–338. doi: 10.1146/annurev.biochem.77.061306.123941

Ellis, N. A., Groden, J., Ye, T. Z., Straughen, J., Lennon, D. J., Ciocci, S., et al. (1995). The Bloom's syndrome gene product is homologous to RecQ Helicases. *Cell* 83, 655–666. doi: 10.1016/0092-8674(95)90105-1

Fairman, M. P., Johnson, A. P., and Thacker, J. (1992). Multiple components are involved in the efficient joining of double stranded DNA breaks in human cell extracts. *Nucleic Acids Res.* 20, 4145–4152. doi: 10.1093/nar/20.16.4145

Fan, W., and Luo, J. (2008). RecQ4 facilitates UV light-induced DNA damage repair through interaction with nucleotide excision repair factor xeroderma pigmentosum group A (XPA). *J. Biol. Chem.* 283, 29037–29044. doi: 10.1074/jbc.m801928200

Fell, V. L., and Schild-Poulter, C. (2015). The Ku heterodimer: function in DNA repair and beyond. *Mutat. Res. Rev. Mutat. Res.* 763, 15–29. doi: 10.1016/j.mrrev.2014.06.002

Fewings, E., Larionov, A., Redman, J., Goldgraben, M. A., Scarth, J., Richardson, S., et al. (2018). Germline pathogenic variants in PALB2 and other cancer-predisposing genes in families with hereditary diffuse gastric cancer without CDH1 mutation: a whole-exome sequencing study. *Lancet Gastroenterol. Hepatol.* 3, 489–498. doi: 10.1016/s2468-1253(18)30079-7

Findlay, S., Heath, J., Luo, V. M., Malina, A., Morin, T., Coulombe, Y., et al. (2018). SHLD2/FAM35A co-operates with REV7 to coordinate DNA double-strand break repair pathway choice. *EMBO J.* 37:e100158.

Friedrich, K., Lee, L., Leistritz, D. F., Nurnberg, G., Saha, B., Hisama, F. M., et al. (2010). WRN mutations in Werner syndrome patients: genomic rearrangements, unusual intronic mutations and ethnic-specific alterations. *Hum. Genet.* 128, 103–111. doi: 10.1007/s00439-010-0832-5

Fukuchi, K., Martin, G. M., and Monnat, R. J. Jr. (1989). Mutator phenotype of Werner syndrome is characterized by extensive deletions. *Proc. Natl. Acad. Sci. U.S.A.* 86, 5893–5897. doi: 10.1073/pnas.86.15.5893

Garcia, P. L., Liu, Y., Jiricny, J., West, S. C., and Janscak, P. (2004). Human RECQ5beta, a protein with DNA Helicase and strand-annealing activities in a single polypeptide. *EMBO J.* 23, 2882–2891. doi: 10.1038/sj.emboj.7600301

Garcia, V., Phelps, S. E., Gray, S., and Neale, M. J. (2011). Bidirectional resection of DNA double-strand breaks by Mre11 and Exo1. *Nature* 479, 241–244. doi: 10.1038/nature10515

German, J., Sanz, M. M., Ciocci, S., Ye, T. Z., and Ellis, N. A. (2007). Syndrome-causing mutations of the BLM gene in persons in the Bloom's syndrome registry. *Hum. Mutat.* 28, 743–753. doi: 10.1002/humu.20501

Ghosh, A. K., Rossi, M. L., Singh, D. K., Dunn, C., Ramamoorthy, M., Croteau, D. L., et al. (2012). RECQL4, the protein mutated in Rothmund-Thomson syndrome, functions in telomere maintenance. *J. Biol. Chem.* 287, 196–209. doi: 10.1074/jbc.m111.295063

Goto, M., Imamura, O., Kuromitsu, J., Matsumoto, T., Yamabe, Y., Tokutake, Y., et al. (1997). Analysis of helicase gene mutations in Japanese Werner's syndrome patients. *Hum. Genet.* 99, 191–193. doi: 10.1007/s004390050336

Goto, M., Ishikawa, Y., Sugimoto, M., and Furuichi, Y. (2013). Werner syndrome: a changing pattern of clinical manifestations in Japan (1917˜2008). *Biosci. Trends* 7, 13–22.

Goto, M., Rubenstein, M., Weber, J., Woods, K., and Drayna, D. (1992). Genetic linkage of Werner's syndrome to five markers on chromosome 8. *Nature* 355, 735–738. doi: 10.1038/355735a0

Grabarz, A., Guirouilh-Barbat, J., Barascu, A., Pennarun, G., Genet, D., Rass, E., et al. (2013). A role for BLM in double-strand break repair pathway choice: prevention of CtIP/Mre11-mediated alternative nonhomologous end-joining. *Cell Rep.* 5, 21–28. doi: 10.1016/j.celrep.2013.08.034

Gravel, S., Chapman, J. R., Magill, C., and Jackson, S. P. (2008). DNA Helicases Sgs1 and BLM promote DNA double-strand break resection. *Genes Dev.* 22, 2767–2772. doi: 10.1101/gad.503108

Grierson, P. M., Acharya, S., and Groden, J. (2013). Collaborating functions of BLM and DNA topoisomerase I in regulating human rDNA transcription. *Mutat. Res.* 743–744, 89–96. doi: 10.1016/j.mrfmmm.2012.12.002

Grierson, P. M., Lillard, K., Behbehani, G. K., Combs, K. A., Bhattacharyya, S., Acharya, S., et al. (2012). BLM Helicase facilitates RNA polymerase I-mediated ribosomal RNA transcription. *Hum. Mol. Genet.* 21, 1172–1183. doi: 10.1093/hmg/ddr545

Gruber, S. B., Ellis, N. A., Scott, K. K., Almog, R., Kolachana, P., Bonner, J. D., et al. (2002). BLM heterozygosity and the risk of colorectal cancer. *Science* 297:2013. doi: 10.1126/science.1074399

Grundy, G. J., Rulten, S. L., Arribas-Bosacoma, R., Davidson, K., Kozik, Z., Oliver, A. W., et al. (2016). The Ku-binding motif is a conserved module for recruitment and stimulation of non-homologous end-joining proteins. *Nat. Commun.* 7:11242.

Gudmundsdottir, K., Lord, C. J., Witt, E., Tutt, A. N., and Ashworth, A. (2004). DSS1 is required for RAD51 focus formation and genomic stability in mammalian cells. *EMBO Rep.* 5, 989–993. doi: 10.1038/sj.embor.7400255

Gyimesi, M., Harami, G. M., Sarlos, K., Hazai, E., Bikadi, Z., and Kovacs, M. (2012). Complex activities of the human Bloom's syndrome Helicase are encoded in a core region comprising the RecA and Zn-binding domains. *Nucleic Acids Res.* 40, 3952–3963. doi: 10.1093/nar/gks008

He, Y. J., Qiao, Z. Y., Gao, B., Zhang, X. H., and Wen, Y. Y. (2014). Association between RECQL5 genetic polymorphisms and susceptibility to breast cancer. *Tumour Biol.* 35, 12201–12204. doi: 10.1007/s13277-014-2528-2

Hickson, I. D. (2003). RecQ Helicases: caretakers of the genome. *Nat. Rev. Cancer* 3, 169–178. doi: 10.1038/nrc1012

Hoeijmakers, J. H. (2009). DNA damage, aging, and cancer. *N. Engl. J. Med.* 361, 1475–1485.

Hornbeck, P. V., Kornhauser, J. M., Latham, V., Murray, B., Nandhikonda, V., Nord, A., et al. (2019). 15 years of PhosphoSitePlus(R): integrating post-translationally modified sites, disease variants and isoforms. *Nucleic Acids Res.* 47, D433–D441.

Hornbeck, P. V., Kornhauser, J. M., Tkachev, S., Zhang, B., Skrzypek, E., Murray, B., et al. (2012). PhosphoSitePlus: a comprehensive resource for investigating the structure and function of experimentally determined post-translational modifications in man and mouse. *Nucleic Acids Res.* 40, D261–D270.

Hornbeck, P. V., Zhang, B., Murray, B., Kornhauser, J. M., Latham, V., and Skrzypek, E. (2015). PhosphoSitePlus, 2014: mutations, PTMs and recalibrations. *Nucleic Acids Res.* 43, D512–D520.

Howard, S. M., Yanez, D. A., and Stark, J. M. (2015). DNA damage response factors from diverse pathways, including DNA crosslink repair, mediate alternative end joining. *PLoS Genet.* 11:e1004943. doi: 10.1371/journal.pgen.1004943

Hu, Y., Raynard, S., Sehorn, M. G., Lu, X., Bussen, W., Zheng, L., et al. (2007). RECQL5/Recql5 Helicase regulates homologous recombination and suppresses tumor formation via disruption of Rad51 presynaptic filaments. *Genes Dev.* 21, 3073–3084. doi: 10.1101/gad.1609107

Huang, G., Feng, J., Hao, S., Li, D., Wang, K., Wang, L., et al. (2018). CASP8, XRCC1, WRN, NF2, and BRIP1 polymorphisms analysis shows their genetic susceptibility for meningioma risk and the association with tumor-related phenotype in a Chinese population. *World Neurosurg.* 114, e883–e891.

Huang, S., Lee, L., Hanson, N. B., Lenaerts, C., Hoehn, H., Poot, M., et al. (2006). The spectrum of WRN mutations in Werner syndrome patients. *Hum. Mutat.* 27, 558–567.

Hustedt, N., and Durocher, D. (2016). The control of DNA repair by the cell cycle. *Nat. Cell Biol.* 19, 1–9.

Im, J. S., Ki, S. H., Farina, A., Jung, D. S., Hurwitz, J., and Lee, J. K. (2009). Assembly of the Cdc45-Mcm2-7-GINS complex in human cells requires the Ctf4/And-1, RecQL4, and Mcm10 proteins. *Proc. Natl. Acad. Sci. U.S.A.* 106, 15628–15632. doi: 10.1073/pnas.0908039106

Imamura, O., Fujita, K., Itoh, C., Takeda, S., Furuichi, Y., and Matsumoto, T. (2002). Werner and Bloom Helicases are involved in DNA repair in a complementary fashion. *Oncogene* 21, 954–963. doi: 10.1038/sj.onc.1205143

Janscak, P., Garcia, P. L., Hamburger, F., Makuta, Y., Shiraishi, K., Imai, Y., et al. (2003). Characterization and mutational analysis of the RecQ core of the bloom syndrome protein. *J. Mol. Biol.* 330, 29–42. doi: 10.1016/s0022-2836(03)00534-5

Jensen, R. B., Carreira, A., and Kowalczykowski, S. C. (2010). Purified human BRCA2 stimulates RAD51-mediated recombination. *Nature* 467, 678–683. doi: 10.1038/nature09399

Jin, W., Liu, H., Zhang, Y., Otta, S. K., Plon, S. E., and Wang, L. L. (2008). Sensitivity of RECQL4-deficient fibroblasts from Rothmund-Thomson syndrome patients to genotoxic agents. *Hum. Genet.* 123, 643–653. doi: 10.1007/s00439-008-0518-4

Johnson, J. E., Cao, K., Ryvkin, P., Wang, L. S., and Johnson, F. B. (2010). Altered gene expression in the Werner and Bloom syndromes is associated with sequences having G-quadruplex forming potential. *Nucleic Acids Res.* 38, 1114–1122. doi: 10.1093/nar/gkp1103

Kabotyanski, E. B., Gomelsky, L., Han, J. O., Stamato, T. D., and Roth, D. B. (1998). Double-strand break repair in Ku86- and XRCC4-deficient cells. *Nucleic Acids Res.* 26, 5333–5342. doi: 10.1093/nar/26.23.5333

Kaiser, S., Sauer, F., and Kisker, C. (2017). The structural and functional characterization of human RecQ4 reveals insights into its Helicase mechanism. *Nat. Commun.* 8:15907.

Karmakar, P., Piotrowski, J., Brosh, R. M. Jr., Sommers, J. A., Miller, S. P., Cheng, W. H., et al. (2002a). Werner protein is a target of DNA-dependent protein kinase in vivo and in vitro, and its catalytic activities are regulated by phosphorylation. *J. Biol. Chem.* 277, 18291–18302. doi: 10.1074/jbc.m111523200

Karmakar, P., Snowden, C. M., Ramsden, D. A., and Bohr, V. A. (2002b). Ku heterodimer binds to both ends of the Werner protein and functional interaction occurs at the Werner N-terminus. *Nucleic Acids Res.* 30, 3583–3591. doi: 10.1093/nar/gkf482

Karmakar, P., Seki, M., Kanamori, M., Hashiguchi, K., Ohtsuki, M., Murata, E., et al. (2006). BLM is an early responder to DNA double-strand breaks. *Biochem. Biophys. Res. Commun.* 348, 62–69. doi: 10.1016/j.bbrc.2006.07.037

Khadka, P., Croteau, D. L., and Bohr, V. A. (2016). RECQL5 has unique strand annealing properties relative to the other human RecQ Helicase proteins. *DNA Repair.* 37, 53–66. doi: 10.1016/j.dnarep.2015.11.005

Khadka, P., Hsu, J. K., Veith, S., Tadokoro, T., Shamanna, R. A., Mangerich, A., et al. (2015). Differential and concordant roles for Poly(ADP-Ribose) Polymerase 1 and Poly(ADP-Ribose) in Regulating WRN and RECQL5 Activities. *Mol. Cell Biol.* 35, 3974–3989. doi: 10.1128/mcb.00427-15

Kikuchi, K., Abdel-Aziz, H. I., Taniguchi, Y., Yamazoe, M., Takeda, S., and Hirota, K. (2009). Bloom DNA Helicase facilitates homologous recombination between diverged homologous sequences. *J. Biol. Chem.* 284, 26360–26367. doi: 10.1074/jbc.m109.029348

Kitano, K., Kim, S. Y., and Hakoshima, T. (2010). Structural basis for DNA strand separation by the unconventional winged-helix domain of RecQ Helicase WRN. *Structure* 18, 177–187. doi: 10.1016/j.str.2009.12.011

Kitano, K., Yoshihara, N., and Hakoshima, T. (2007). Crystal structure of the HRDC domain of human Werner syndrome protein, WRN. *J. Biol. Chem.* 282, 2717–2728. doi: 10.1074/jbc.m610142200

Kohzaki, M., Chiourea, M., Versini, G., Adachi, N., Takeda, S., Gagos, S., et al. (2012). The Helicase domain and C-terminus of human RecQL4 facilitate replication elongation on DNA templates damaged by ionizing radiation. *Carcinogenesis* 33, 1203–1210. doi: 10.1093/carcin/bgs149

Kohzaki, M., Ootsuyama, A., Sun, L., Moritake, T., and Okazaki, R. (2020). Human RECQL4 represses the RAD52-mediated single-strand annealing pathway after ionizing radiation or cisplatin treatment. *Int. J. Cancer* 146, 3098–3113. doi: 10.1002/ijc.32670

Kumata, Y., Tada, S., Yamanada, Y., Tsuyama, T., Kobayashi, T., Dong, Y. P., et al. (2007). Possible involvement of RecQL4 in the repair of double-strand DNA breaks in Xenopus egg extracts. *Biochim. Biophys. Acta* 1773, 556–564. doi: 10.1016/j.bbamcr.2007.01.005

Kuribayashi, N., Uchida, D., Hamasaki, Y., and Kawamata, H. (2019). Oral squamous cell carcinoma arising in a patient with Werner syndrome. *Int. J. Oral. Maxillofac. Surg.* 48, 1394–1397. doi: 10.1016/j.ijom.2019.06.005

Kusumoto, R., Dawut, L., Marchetti, C., Wan Lee, J., Vindigni, A., Ramsden, D., et al. (2008). Werner protein cooperates with the XRCC4-DNA ligase IV complex in end-processing. *Biochemistry* 47, 7548–7556. doi: 10.1021/bi702325t

Kusumoto-Matsuo, R., Ghosh, D., Karmakar, P., May, A., Ramsden, D., and Bohr, V. A. (2014). Serines 440 and 467 in the Werner syndrome protein are phosphorylated by DNA-PK and affects its dynamics in response to DNA double strand breaks. *Aging* 6, 70–81. doi: 10.18632/aging.100629

Kwong, A., Shin, V. Y., Cheuk, I. W. Y., Chen, J., Au, C. H., Ho, D. N., et al. (2016). Germline RECQL mutations in high risk Chinese breast cancer patients. *Breast Cancer Res. Treat.* 157, 211–215. doi: 10.1007/s10549-016-3784-1

Lachapelle, S., Gagne, J. P., Garand, C., Desbiens, M., Coulombe, Y., Bohr, V. A., et al. (2011). Proteome-wide identification of WRN-interacting proteins in untreated and nuclease-treated samples. *J. Proteome Res.* 10, 1216–1227. doi: 10.1021/pr100990s

Lan, L., Nakajima, S., Komatsu, K., Nussenzweig, A., Shimamoto, A., Oshima, J., et al. (2005). Accumulation of Werner protein at DNA double-strand breaks in human cells. *J. Cell Sci.* 118, 4153–4162. doi: 10.1242/jcs.02544

Larizza, L., Magnani, I., and Roversi, G. (2006). Rothmund-Thomson syndrome and RECQL4 defect: splitting and lumping. *Cancer Lett.* 232, 107–120. doi: 10.1016/j.canlet.2005.07.042

Larizza, L., Roversi, G., and Verloes, A. (2013). Clinical utility gene card for: Rothmund-Thomson syndrome. *Eur. J. Hum. Genet.* 21:260.

Larizza, L., Roversi, G., and Volpi, L. (2010). Rothmund-Thomson syndrome. *Orphanet. J. Rare Dis.* 5:2.

Lauper, J. M., Krause, A., Vaughan, T. L., and Monnat, R. J. Jr. (2013). Spectrum and risk of neoplasia in Werner syndrome: a systematic review. *PLoS One* 8:e59709. doi: 10.1371/journal.pone.0059709

Lebel, M., and Monnat, R. J. Jr. (2018). Werner syndrome (WRN) gene variants and their association with altered function and age-associated diseases. *Age. Res. Rev* 41, 82–97. doi: 10.1016/j.arr.2017.11.003

Ledet, E. M., Antonarakis, E. S., Isaacs, W. B., Lotan, T. L., Pritchard, C., and Sartor, A. O. (2020). Germline BLM mutations and metastatic prostate cancer. *Prostate* 80, 235–237. doi: 10.1002/pros.23924

Lee, J. H., Kim, S. S., Kim, M. S., Yoo, N. J., and Lee, S. H. (2017). WRN, the Werner syndrome gene, exhibits frameshift mutations in gastric and colorectal cancers. *Pathol. Oncol. Res.* 23, 451–452. doi: 10.1007/s12253-016-0173-3

Lee, M., Shin, S., Uhm, H., Hong, H., Kirk, J., Hyun, K., et al. (2018). Multiple RPAs make WRN syndrome protein a superhelicase. *Nucleic Acids Res.* 46, 4689–4698. doi: 10.1093/nar/gky272

Lee-Theilen, M., Matthews, A. J., Kelly, D., Zheng, S., and Chaudhuri, J. (2011). CtIP promotes microhomology-mediated alternative end joining during class-switch recombination. *Nat. Struct. Mol. Biol.* 18, 75–79. doi: 10.1038/nsmb.1942

Lengsfeld, B. M., Rattray, A. J., Bhaskara, V., Ghirlando, R., and Paull, T. T. (2007). Sae2 is an endonuclease that processes hairpin DNA cooperatively with the Mre11/Rad50/Xrs2 complex. *Mol. Cell* 28, 638–651. doi: 10.1016/j.molcel.2007.11.001

LeRoy, G., Carroll, R., Kyin, S., Seki, M., and Cole, M. D. (2005). Identification of RecQL1 as a Holliday junction processing enzyme in human cell lines. *Nucleic Acids Res.* 33, 6251–6257. doi: 10.1093/nar/gki929

Li, B., and Comai, L. (2000). Functional interaction between Ku and the werner syndrome protein in DNA end processing. *J. Biol. Chem.* 275, 28349–28352. doi: 10.1074/jbc.c000289200

Li, M., Liu, B., Yi, J., Yang, Y., Wang, J., Zhu, W. G., et al. (2020). MIB1-mediated degradation of WRN promotes cellular senescence in response to camptothecin treatment. *FASEB J.* 34, 11488–11497. doi: 10.1096/fj.202000268rrr

Li, M., Xu, X., and Liu, Y. (2011). The SET2-RPB1 interaction domain of human RECQ5 is important for transcription-associated genome stability. *Mol. Cell Biol.* 31, 2090–2099. doi: 10.1128/mcb.01137-10

Li, P., Hao, S., Bi, Z., Zhang, J., Wu, Z., and Ren, X. (2015). Methylation of Werner syndrome protein is associated with the occurrence and development of invasive meningioma via the regulation of Myc and p53 expression. *Exp. Ther. Med.* 10, 498–502. doi: 10.3892/etm.2015.2519

Liu, D., Deng, X., Yuan, C., Chen, L., Cong, Y., and Xu, X. (2014). Werner syndrome protein positively regulates XRCC4-like factor transcription. *Mol. Med. Rep.* 9, 1648–1652. doi: 10.3892/mmr.2014.2030

Lu, H., Fang, E. F., Sykora, P., Kulikowicz, T., Zhang, Y., Becker, K. G., et al. (2014). Senescence induced by RECQL4 dysfunction contributes to Rothmund-Thomson syndrome features in mice. *Cell Death Dis.* 5:e1226. doi: 10.1038/cddis.2014.168

Lu, H., Saha, J., Beckmann, P. J., Hendrickson, E. A., and Davis, A. J. (2019). DNA-PKcs promotes chromatin decondensation to facilitate initiation of the DNA damage response. *Nucleic Acids Res.* 47, 9467–9479. doi: 10.1093/nar/gkz694

Lu, H., Shamanna, R. A., de Freitas, J. K., Okur, M., Khadka, P., Kulikowicz, T., et al. (2017). Cell cycle-dependent phosphorylation regulates RECQL4 pathway choice and ubiquitination in DNA double-strand break repair. *Nat. Commun.* 8:2039.

Lu, H., Shamanna, R. A., Keijzers, G., Anand, R., Rasmussen, L. J., Cejka, P., et al. (2016). RECQL4 promotes DNA end resection in repair of DNA double-strand breaks. *Cell Rep.* 16, 161–173. doi: 10.1016/j.celrep.2016.05.079

Lu, L., Jin, W., and Wang, L. L. (2020). RECQ DNA Helicases and Osteosarcoma. *Adv. Exp. Med. Biol.* 1258, 37–54.

Mann, M. B., Hodges, C. A., Barnes, E., Vogel, H., Hassold, T. J., and Luo, G. (2005). Defective sister-chromatid cohesion, aneuploidy and cancer predisposition in a mouse model of type II Rothmund-Thomson syndrome. *Hum. Mol. Genet.* 14, 813–825. doi: 10.1093/hmg/ddi075

Manthei, K. A., and Keck, J. L. (2013). The BLM dissolvasome in DNA replication and repair. *Cell Mol. Life Sci.* 70, 4067–4084. doi: 10.1007/s00018-013-1325-1

Mason, J. M., Chan, Y. L., Weichselbaum, R. W., and Bishop, D. K. (2019). Non-enzymatic roles of human RAD51 at stalled replication forks. *Nat. Commun.* 10:4410.

Mason, R. M., Thacker, J., and Fairman, M. P. (1996). The joining of non-complementary DNA double-strand breaks by mammalian extracts. *Nucleic Acids Res.* 24, 4946–4953. doi: 10.1093/nar/24.24.4946

Matsumoto, T., Shimamoto, A., Goto, M., and Furuichi, Y. (1997). Impaired nuclear localization of defective DNA Helicases in Werner's syndrome. *Nat. Genet.* 16, 335–336. doi: 10.1038/ng0897-335

Mazina, O. M., Rossi, M. J., Deakyne, J. S., Huang, F., and Mazin, A. V. (2012). Polarity and bypass of DNA heterology during branch migration of Holliday junctions by human RAD54, BLM, and RECQ1 proteins. *J. Biol. Chem.* 287, 11820–11832. doi: 10.1074/jbc.m112.341347

Mimitou, E. P., and Symington, L. S. (2008). Sae2, Exo1 and Sgs1 collaborate in DNA double-strand break processing. *Nature* 455, 770–774. doi: 10.1038/nature07312

Mohaghegh, P., Karow, J. K., Brosh, R. M. Jr., Bohr, V. A., and Hickson, I. D. (2001). The Bloom's and Werner's syndrome proteins are DNA structure-specific Helicases. *Nucleic Acids Res.* 29, 2843–2849. doi: 10.1093/nar/29.13.2843

Mojumdar, A. (2020). Mutations in conserved functional domains of human RecQ Helicases are associated with diseases and cancer: a review. *Biophys. Chem.* 265:106433. doi: 10.1016/j.bpc.2020.106433

Muftuoglu, M., Kulikowicz, T., Beck, G., Lee, J. W., Piotrowski, J., and Bohr, V. A. (2008). Intrinsic ssDNA annealing activity in the C-terminal region of WRN. *Biochemistry* 47, 10247–10254. doi: 10.1021/bi800807n

Mukherjee, S., Sinha, D., Bhattacharya, S., Srinivasan, K., Abdisalaam, S., and Asaithamby, A. (2018). Werner syndrome protein and DNA replication. *Int. J. Mol. Sci.* 19:3442. doi: 10.3390/ijms19113442

Newman, J. A., Savitsky, P., Allerston, C. K., Bizard, A. H., Ozer, O., Sarlos, K., et al. (2015). Crystal structure of the Bloom's syndrome Helicase indicates a role for the HRDC domain in conformational changes. *Nucleic Acids Res.* 43, 5221–5235. doi: 10.1093/nar/gkv373

Nimonkar, A. V., Genschel, J., Kinoshita, E., Polaczek, P., Campbell, J. L., Wyman, C., et al. (2011). BLM-DNA2-RPA-MRN and EXO1-BLM-RPA-MRN constitute two DNA end resection machineries for human DNA break repair. *Genes Dev.* 25, 350–362. doi: 10.1101/gad.2003811

Nimonkar, A. V., Ozsoy, A. Z., Genschel, J., Modrich, P., and Kowalczykowski, S. C. (2008). Human exonuclease 1 and BLM Helicase interact to resect DNA and initiate DNA repair. *Proc. Natl. Acad. Sci. U.S.A.* 105, 16906–16911. doi: 10.1073/pnas.0809380105

Opresko, P. L., Sowd, G., and Wang, H. (2009). The Werner syndrome Helicase/Exonuclease processes mobile D-loops through branch migration and degradation. *PLoS One* 4:e4825. doi: 10.1371/journal.pone.0004825

Orren, D. K., Machwe, A., Karmakar, P., Piotrowski, J., Cooper, M. P., and Bohr, V. A. (2001). A functional interaction of Ku with Werner exonuclease facilitates digestion of damaged DNA. *Nucleic Acids Res.* 29, 1926–1934. doi: 10.1093/nar/29.9.1926

Oshima, J., Huang, S., Pae, C., Campisi, J., and Schiestl, R. H. (2002). Lack of WRN results in extensive deletion at nonhomologous joining ends. *Cancer Res.* 62, 547–551.

Oshima, J., Kato, H., Maezawa, Y., and Yokote, K. (2018). RECQ Helicase disease and related progeroid syndromes: RECQ2018 meeting. *Mech. Age. Dev.* 173, 80–83. doi: 10.1016/j.mad.2018.05.002

Oshima, J., Sidorova, J. M., and Monnat, R. J. Jr. (2017). Werner syndrome: Clinical features, pathogenesis and potential therapeutic interventions. *Age. Res. Rev.* 33, 105–114. doi: 10.1016/j.arr.2016.03.002

Otterlei, M., Bruheim, P., Ahn, B., Bussen, W., Karmakar, P., Baynton, K., et al. (2006). Werner syndrome protein participates in a complex with RAD51, RAD54, RAD54B and ATR in response to ICL-induced replication arrest. *J. Cell Sci.* 119, 5137–5146. doi: 10.1242/jcs.03291

Palermo, V., Rinalducci, S., Sanchez, M., Grillini, F., Sommers, J. A., Brosh, R. M. Jr., et al. (2016). CDK1 phosphorylates WRN at collapsed replication forks. *Nat. Commun.* 7:12880.

Paliwal, S., Kanagaraj, R., Sturzenegger, A., Burdova, K., and Janscak, P. (2014). Human RECQ5 Helicase promotes repair of DNA double-strand breaks by synthesis-dependent strand annealing. *Nucleic Acids Res.* 42, 2380–2390. doi: 10.1093/nar/gkt1263

Pan, X., Drosopoulos, W. C., Sethi, L., Madireddy, A., Schildkraut, C. L., and Zhang, D. (2017). FANCM, BRCA1, and BLM cooperatively resolve the replication stress at the ALT telomeres. *Proc. Natl. Acad. Sci. U.S.A.* 114, E5940–E5949.

Pannunzio, N. R., Watanabe, G., and Lieber, M. R. (2018). Nonhomologous DNA end-joining for repair of DNA double-strand breaks. *J. Biol. Chem.* 293, 10512–10523. doi: 10.1074/jbc.tm117.000374

Parvathaneni, S., and Sharma, S. (2019). The DNA repair Helicase RECQ1 has a checkpoint-dependent role in mediating DNA damage responses induced by gemcitabine. *J. Biol. Chem.* 294, 15330–15345. doi: 10.1074/jbc.ra119.008420

Parvathaneni, S., Stortchevoi, A., Sommers, J. A., Brosh, R. M. Jr., and Sharma, S. (2013). Human RECQ1 interacts with Ku70/80 and modulates DNA end-joining of double-strand breaks. *PLoS One* 8:e62481. doi: 10.1371/journal.pone.0062481

Patel, D. S., Misenko, S. M., Her, J., and Bunting, S. F. (2017). BLM Helicase regulates DNA repair by counteracting RAD51 loading at DNA double-strand break sites. *J. Cell Biol.* 216, 3521–3534. doi: 10.1083/jcb.201703144

Pattankar, S., Churi, O., and Misra, B. K. (2020). Meningioma in a patient with Werner syndrome. *Neurol. India* 68, 483–486. doi: 10.4103/0028-3886.284350

Patterson-Fortin, J., and D'Andrea, A. D. (2020). Exploiting the microhomology-mediated end-joining pathway in cancer therapy. *Cancer Res.* 80, 72.

Paulo, P., Maia, S., Pinto, C., Pinto, P., Monteiro, A., Peixoto, A., et al. (2018). Targeted next generation sequencing identifies functionally deleterious germline mutations in novel genes in early-onset/familial prostate cancer. *PLoS Genet.* 14:e1007355. doi: 10.1371/journal.pgen.1007355

Petkovic, M., Dietschy, T., Freire, R., Jiao, R., and Stagljar, I. (2005). The human Rothmund-Thomson syndrome gene product, RECQL4, localizes to distinct nuclear foci that coincide with proteins involved in the maintenance of genome stability. *J. Cell Sci.* 118, 4261–4269. doi: 10.1242/jcs.02556

Pinto, C., Kasaciunaite, K., Seidel, R., and Cejka, P. (2016). Human DNA2 possesses a cryptic DNA unwinding activity that functionally integrates with BLM or WRN Helicases. *eLife* 5:e18574.

Popuri, V., Croteau, D. L., Brosh, R. M. Jr., and Bohr, V. A. (2012a). RECQ1 is required for cellular resistance to replication stress and catalyzes strand exchange on stalled replication fork structures. *Cell Cycle* 11, 4252–4265. doi: 10.4161/cc.22581

Popuri, V., Ramamoorthy, M., Tadokoro, T., Singh, D. K., Karmakar, P., Croteau, D. L., et al. (2012b). Recruitment and retention dynamics of RECQL5 at DNA double strand break sites. *DNA Repair.* 11, 624–635. doi: 10.1016/j.dnarep.2012.05.001

Popuri, V., Hsu, J., Khadka, P., Horvath, K., Liu, Y., Croteau, D. L., et al. (2014). Human RECQL1 participates in telomere maintenance. *Nucleic Acids Res.* 42, 5671–5688. doi: 10.1093/nar/gku200

Qin, Z., Bi, L., Hou, X. M., Zhang, S., Zhang, X., Lu, Y., et al. (2020). Human RPA activates BLM's bidirectional DNA unwinding from a nick. *eLife* 9:e54098.

Ralf, C., Hickson, I. D., and Wu, L. (2006). The Bloom's syndrome Helicase can promote the regression of a model replication fork. *J. Biol. Chem.* 281, 22839–22846. doi: 10.1074/jbc.m604268200

Raynard, S., Bussen, W., and Sung, P. (2006). A double holliday junction dissolvasome comprising BLM, topoisomerase IIIalpha, and BLAP75. *J. Biol. Chem.* 281, 13861–13864. doi: 10.1074/jbc.c600051200

Ren, H., Dou, S. X., Zhang, X. D., Wang, P. Y., Kanagaraj, R., Liu, J. L., et al. (2008). The zinc-binding motif of human RECQ5beta suppresses the intrinsic strand-annealing activity of its DExH Helicase domain and is essential for the Helicase activity of the enzyme. *Biochem. J.* 412, 425–433. doi: 10.1042/bj20071150

Rogers, C. M., Wang, J. C., Noguchi, H., Imasaki, T., Takagi, Y., and Bochman, M. L. (2017). Yeast Hrq1 shares structural and functional homology with the disease-linked human RecQ4 Helicase. *Nucleic Acids Res.* 45, 5217–5230. doi: 10.1093/nar/gkx151

Romanowicz, H., Pyziak, L., Jablonski, F., Brys, M., Forma, E., and Smolarz, B. (2017). Analysis of DNA repair genes polymorphisms in breast cancer. *Pathol. Oncol. Res.* 23, 117–123. doi: 10.1007/s12253-016-0110-5

Ronato, D. A., Mersaoui, S. Y., Busatto, F. F., Affar, E. B., Richard, S., and Masson, J. Y. (2020). Limiting the DNA double-strand break resectosome for genome protection. *Trends Biochem. Sci.* 45, 779–793. doi: 10.1016/j.tibs.2020.05.003

Rossi, M. L., Ghosh, A. K., Kulikowicz, T., Croteau, D. L., and Bohr, V. A. (2010). Conserved Helicase domain of human RecQ4 is required for strand annealing-independent DNA unwinding. *DNA Repair.* 9, 796–804. doi: 10.1016/j.dnarep.2010.04.003

Russell, C. W., and Mulvey, M. A. (2015). The extraintestinal pathogenic *Escherichia coli* factor RqlI constrains the genotoxic effects of the RecQ-Like Helicase RqlH. *PLoS Pathog.* 11:e1005317. doi: 10.1371/journal.ppat.1005317

Saintigny, Y., Makienko, K., Swanson, C., Emond, M. J., and Monnat, R. J. Jr. (2002). Homologous recombination resolution defect in werner syndrome. *Mol. Cell Biol.* 22, 6971–6978. doi: 10.1128/mcb.22.20.6971-6978.2002

Sallmyr, A., and Tomkinson, A. E. (2018). Repair of DNA double-strand breaks by mammalian alternative end-joining pathways. *J. Biol. Chem.* 293, 10536–10546. doi: 10.1074/jbc.tm117.000375

Sallmyr, A., Tomkinson, A. E., and Rassool, F. V. (2008). Up-regulation of WRN and DNA ligase IIIalpha in chronic myeloid leukemia: consequences for the repair of DNA double-strand breaks. *Blood* 112, 1413–1423. doi: 10.1182/blood-2007-07-104257

Sangrithi, M. N., Bernal, J. A., Madine, M., Philpott, A., Lee, J., Dunphy, W. G., et al. (2005). Initiation of DNA replication requires the RECQL4 protein mutated in Rothmund-Thomson syndrome. *Cell* 121, 887–898. doi: 10.1016/j.cell.2005.05.015

Saponaro, M., Kantidakis, T., Mitter, R., Kelly, G. P., Heron, M., Williams, H., et al. (2014). RECQL5 controls transcript elongation and suppresses genome instability associated with transcription stress. *Cell* 157, 1037–1049. doi: 10.1016/j.cell.2014.03.048

Sartori, A. A., Lukas, C., Coates, J., Mistrik, M., Fu, S., Bartek, J., et al. (2007). Human CtIP promotes DNA end resection. *Nature* 450, 509–514. doi: 10.1038/nature06337

Schawalder, J., Paric, E., and Neff, N. F. (2003). Telomere and ribosomal DNA repeats are chromosomal targets of the bloom syndrome DNA Helicase. *BMC Cell Biol.* 4:15. doi: 10.1186/1471-2121-4-15

Schurman, S. H., Hedayati, M., Wang, Z., Singh, D. K., Speina, E., Zhang, Y., et al. (2009). Direct and indirect roles of RECQL4 in modulating base excision repair capacity. *Hum. Mol. Genet.* 18, 3470–3483. doi: 10.1093/hmg/ddp291

Schwendener, S., Raynard, S., Paliwal, S., Cheng, A., Kanagaraj, R., Shevelev, I., et al. (2010). Physical interaction of RECQ5 Helicase with RAD51 facilitates its anti-recombinase activity. *J. Biol. Chem.* 285, 15739–15745. doi: 10.1074/jbc.m110.110478

Scully, R., Panday, A., Elango, R., and Willis, N. A. (2019). DNA double-strand break repair-pathway choice in somatic mammalian cells. *Nat. Rev. Mol. Cell Biol.* 20, 698–714. doi: 10.1038/s41580-019-0152-0

Sekelsky, J. J., Brodsky, M. H., Rubin, G. M., and Hawley, R. S. (1999). Drosophila and human RecQ5 exist in different isoforms generated by alternative splicing. *Nucleic Acids Res.* 27, 3762–3769. doi: 10.1093/nar/27.18.3762

Shamanna, R. A., Croteau, D. L., Lee, J. H., and Bohr, V. A. (2017). Recent advances in understanding Werner syndrome. *F1000Research* 6:1779. doi: 10.12688/f1000research.12110.1

Shamanna, R. A., Lu, H., Croteau, D. L., Arora, A., Agarwal, D., Ball, G., et al. (2016a). Camptothecin targets WRN protein: mechanism and relevance in clinical breast cancer. *Oncotarget* 7, 13269–13284. doi: 10.18632/oncotarget.7906

Shamanna, R. A., Lu, H., de Freitas, J. K., Tian, J., Croteau, D. L., and Bohr, V. A. (2016b). WRN regulates pathway choice between classical and alternative non-homologous end joining. *Na.t Commun.* 7:13785.

Shamanna, R. A., Singh, D. K., Lu, H., Mirey, G., Keijzers, G., Salles, B., et al. (2014). RECQ Helicase RECQL4 participates in non-homologous end joining and interacts with the Ku complex. *Carcinogenesis* 35, 2415–2424. doi: 10.1093/carcin/bgu137

Sharma, S., and Brosh, R. M. Jr. (2007). Human RECQ1 is a DNA damage responsive protein required for genotoxic stress resistance and suppression of sister chromatid exchanges. *PLoS One* 2:e1297. doi: 10.1371/journal.pone.0001297

Sharma, S., and Brosh, R. M. Jr. (2008). Unique and important consequences of RECQ1 deficiency in mammalian cells. *Cell Cycle* 7, 989–1000. doi: 10.4161/cc.7.8.5707

Sharma, S., Phatak, P., Stortchevoi, A., Jasin, M., and Larocque, J. R. (2012). RECQ1 plays a distinct role in cellular response to oxidative DNA damage. *DNA Repair.* 11, 537–549. doi: 10.1016/j.dnarep.2012.04.003

Sharma, S., Sommers, J. A., Choudhary, S., Faulkner, J. K., Cui, S., Andreoli, L., et al. (2005). Biochemical analysis of the DNA unwinding and strand annealing activities catalyzed by human RECQ1. *J. Biol. Chem.* 280, 28072–28084. doi: 10.1074/jbc.m500264200

Sharma, S., Stumpo, D. J., Balajee, A. S., Bock, C. B., Lansdorp, P. M., Brosh, R. M. Jr., et al. (2007). RECQL, a member of the RecQ family of DNA Helicases, suppresses chromosomal instability. *Mol. Cell Biol.* 27, 1784–1794. doi: 10.1128/mcb.01620-06

Shi, J., Chen, W. F., Zhang, B., Fan, S. H., Ai, X., Liu, N. N., et al. (2017). A helical bundle in the N-terminal domain of the BLM Helicase mediates dimer and potentially hexamer formation. *J. Biol. Chem.* 292, 5909–5920. doi: 10.1074/jbc.m116.761510

Shimamoto, A., Nishikawa, K., Kitao, S., and Furuichi, Y. (2000). Human RecQ5beta, a large isomer of RecQ5 DNA Helicase, localizes in the nucleoplasm and interacts with topoisomerases 3alpha and 3beta. *Nucleic Acids Res.* 28, 1647–1655. doi: 10.1093/nar/28.7.1647

Siitonen, H. A., Sotkasiira, J., Biervliet, M., Benmansour, A., Capri, Y., Cormier-Daire, V., et al. (2009). The mutation spectrum in RECQL4 diseases. *Eur. J. Hum. Genet.* 17, 151–158. doi: 10.1038/ejhg.2008.154

Singh, D. K., Karmakar, P., Aamann, M., Schurman, S. H., May, A., Croteau, D. L., et al. (2010). The involvement of human RECQL4 in DNA double-strand break repair. *Aging Cell* 9, 358–371. doi: 10.1111/j.1474-9726.2010.00562.x

Singh, D. K., Popuri, V., Kulikowicz, T., Shevelev, I., Ghosh, A. K., Ramamoorthy, M., et al. (2012). The human RecQ Helicases BLM and RECQL4 cooperate to preserve genome stability. *Nucleic Acids Res.* 40, 6632–6648. doi: 10.1093/nar/gks349

Singh, T. R., Ali, A. M., Busygina, V., Raynard, S., Fan, Q., Du, C. H., et al. (2008). BLAP18/RMI2, a novel OB-fold-containing protein, is an essential component of the Bloom Helicase-double Holliday junction dissolvasome. *Genes Dev.* 22, 2856–2868. doi: 10.1101/gad.1725108

Sommers, J. A., Sharma, S., Doherty, K. M., Karmakar, P., Yang, Q., Kenny, M. K., et al. (2005). p53 modulates RPA-dependent and RPA-independent WRN Helicase activity. *Cancer Res.* 65, 1223–1233. doi: 10.1158/0008-5472.can-03-0231

Soniat, M. M., Myler, L. R., Kuo, H. C., Paull, T. T., and Finkelstein, I. J. (2019). RPA phosphorylation inhibits DNA resection. *Mol. Cell* 75, 145–153.e145.

Stirnweiss, A., Oommen, J., Kotecha, R. S., Kees, U. R., and Beesley, A. H. (2017). Molecular-genetic profiling and high-throughput in vitro drug screening in NUT midline carcinoma-an aggressive and fatal disease. *Oncotarget* 8, 112313–112329. doi: 10.18632/oncotarget.22862

Sturzenegger, A., Burdova, K., Kanagaraj, R., Levikova, M., Pinto, C., Cejka, P., et al. (2014). DNA2 cooperates with the WRN and BLM RecQ helicases to mediate long-range DNA end resection in human cells. *J. Biol. Chem.* 289, 27314–27326. doi: 10.1074/jbc.m114.578823

Subino, S., Fiori, P. L., Lubinu, G., Scappaticci, S., and Cerimele, D. (1982). Immunofluorescence of the tubulin system in human skin fibroblasts in Werner's syndrome, Kaposi sarcoma, and psoriasis. *Arch. Dermatol. Res.* 272, 143–145. doi: 10.1007/bf00510405

Sun, J., Meng, H., Yao, L., Lv, M., Bai, J., Zhang, J., et al. (2017). Germline mutations in cancer susceptibility genes in a large series of unselected breast cancer patients. *Clin. Cancer Res.* 23, 6113–6119. doi: 10.1158/1078-0432.ccr-16-3227

Sun, L., Nakajima, S., Teng, Y., Chen, H., Yang, L., Chen, X., et al. (2017). WRN is recruited to damaged telomeres via its RQC domain and tankyrase1-mediated poly-ADP-ribosylation of TRF1. *Nucleic Acids Res.* 45, 3844–3859. doi: 10.1093/nar/gkx065

Sun, J., Wang, Y., Xia, Y., Xu, Y., Ouyang, T., Li, J., et al. (2015). Mutations in RECQL gene are associated with predisposition to breast cancer. *PLoS Genet.* 11:e1005228. doi: 10.1371/journal.pgen.1005228

Suzuki, T., Shiratori, M., Furuichi, Y., and Matsumoto, T. (2001). Diverged nuclear localization of Werner Helicase in human and mouse cells. *Oncogene* 20, 2551–2558. doi: 10.1038/sj.onc.1204344

Symington, L. S. (2014). End resection at double-strand breaks: mechanism and regulation. *Cold Spring Harb. Perspect. Biol.* 6:a016436. doi: 10.1101/cshperspect.a016436

Tadokoro, T., Kulikowicz, T., Dawut, L., Croteau, D. L., and Bohr, V. A. (2012). DNA binding residues in the RQC domain of Werner protein are critical for its catalytic activities. *Aging* 4, 417–429. doi: 10.18632/aging.100463

Taher, M. M., Hassan, A. A., Saeed, M., Jastania, R. A., Nageeti, T. H., Alkhalidi, H., et al. (2019). Next generation DNA sequencing of atypical choroid plexus papilloma of brain: identification of novel mutations in a female patient by Ion Proton. *Oncol. Lett.* 18, 5063–5076.

Taylor, A. M. R., Rothblum-Oviatt, C., Ellis, N. A., Hickson, I. D., Meyer, S., Crawford, T. O., et al. (2019). Chromosome instability syndromes. *Nat. Rev. Dis. Primers* 5:64.

Tervasmaki, A., Mantere, T., Hartikainen, J. M., Kauppila, S., Lee, H. M., Koivuluoma, S., et al. (2018). Rare missense mutations in RECQL and POLG associate with inherited predisposition to breast cancer. *Int. J. Cancer* 142, 2286–2292. doi: 10.1002/ijc.31259

Thompson, E. R., Doyle, M. A., Ryland, G. L., Rowley, S. M., Choong, D. Y., Tothill, R. W., et al. (2012). Exome sequencing identifies rare deleterious mutations in DNA repair genes FANCC and BLM as potential breast cancer susceptibility alleles. *PLoS Genet.* 8:e1002894. doi: 10.1371/journal.pgen.1002894

Thorslund, T., McIlwraith, M. J., Compton, S. A., Lekomtsev, S., Petronczki, M., Griffith, J. D., et al. (2010). The breast cancer tumor suppressor BRCA2 promotes the specific targeting of RAD51 to single-stranded DNA. *Nat. Struct. Mol. Biol.* 17, 1263–1265. doi: 10.1038/nsmb.1905

Tock, A. J., and Henderson, I. R. (2018). Hotspots for initiation of meiotic recombination. *Front. Genet.* 9:521. doi: 10.3389/fgene.2018.00521

Truong, L. N., Li, Y., Shi, L. Z., Hwang, P. Y., He, J., Wang, H., et al. (2013). Microhomology-mediated end joining and homologous recombination share the initial end resection step to repair DNA double-strand breaks in mammalian cells. *Proc. Natl. Acad. Sci. U.S.A.* 110, 7720–7725. doi: 10.1073/pnas.1213431110

Tsurubuchi, T., Yamamoto, T., Tsukada, Y., Matsuda, M., Nakai, K., and Matsumura, A. (2008). Meningioma associated with Werner syndrome–case report. *Neurol. Med. Chir.* 48, 470–473.

Tubbs, A., and Nussenzweig, A. (2017). Endogenous DNA damage as a source of genomic instability in cancer. *Cell* 168, 644–656. doi: 10.1016/j.cell.2017.01.002

Urban, V., Dobrovolna, J., and Janscak, P. (2017). Distinct functions of human RecQ helicases during DNA replication. *Biophys. Chem.* 225, 20–26. doi: 10.1016/j.bpc.2016.11.005

van Brabant, A. J., Ye, T., Sanz, M., German, I. J., Ellis, N. A., and Holloman, W. K. (2000). Binding and melting of D-loops by the Bloom syndrome Helicase. *Biochemistry* 39, 14617–14625. doi: 10.1021/bi0018640

van Wietmarschen, N., Sridharan, S., Nathan, W. J., Tubbs, A., Chan, E. M., Callen, E., et al. (2020). Repeat expansions confer WRN dependence in microsatellite-unstable cancers. *Nature* 586, 292–298. doi: 10.1038/s41586-020-2769-8

von Kobbe, C., Thoma, N. H., Czyzewski, B. K., Pavletich, N. P., and Bohr, V. A. (2003). Werner syndrome protein contains three structure-specific DNA binding domains. *J. Biol. Chem.* 278, 52997–53006. doi: 10.1074/jbc.m308338200

Wang, L. L., Gannavarapu, A., Kozinetz, C. A., Levy, M. L., Lewis, R. A., Chintagumpala, M. M., et al. (2003). Association between osteosarcoma and deleterious mutations in the RECQL4 gene in Rothmund-Thomson syndrome. *J. Natl. Cancer Inst.* 95, 669–674. doi: 10.1093/jnci/95.9.669

Watt, P. M., Hickson, I. D., Borts, R. H., and Louis, E. J. (1996). SGS1, a homologue of the Bloom's and Werner's syndrome genes, is required for maintenance of genome stability in *Saccharomyces cerevisiae*. *Genetics* 144, 935–945. doi: 10.1093/genetics/144.3.935

White, R. R., and Vijg, J. (2016). Do DNA double-strand breaks drive aging? *Mol. Cell* 63, 729–738. doi: 10.1016/j.molcel.2016.08.004

Wright, W. D., Shah, S. S., and Heyer, W. D. (2018). Homologous recombination and the repair of DNA double-strand breaks. *J. Biol. Chem.* 293, 10524–10535.

Wu, L., Bachrati, C. Z., Ou, J., Xu, C., Yin, J., Chang, M., et al. (2006). BLAP75/RMI1 promotes the BLM-dependent dissolution of homologous recombination intermediates. *Proc. Natl. Acad. Sci. U.S.A.* 103, 4068–4073. doi: 10.1073/pnas.0508295103

Wu, L., Chan, K. L., Ralf, C., Bernstein, D. A., Garcia, P. L., Bohr, V. A., et al. (2005). The HRDC domain of BLM is required for the dissolution of double Holliday junctions. *EMBO J.* 24, 2679–2687. doi: 10.1038/sj.emboj.7600740

Wu, L., Davies, S. L., Levitt, N. C., and Hickson, I. D. (2001). Potential role for the BLM Helicase in recombinational repair via a conserved interaction with RAD51. *J. Biol. Chem.* 276, 19375–19381. doi: 10.1074/jbc.m009471200

Wu, L., and Hickson, I. D. (2003). The Bloom's syndrome Helicase suppresses crossing over during homologous recombination. *Nature* 426, 870–874. doi: 10.1038/nature02253

Xie, A., Kwok, A., and Scully, R. (2009). Role of mammalian Mre11 in classical and alternative nonhomologous end joining. *Nat. Struct. Mol. Biol.* 16, 814–818. doi: 10.1038/nsmb.1640

Xu, D., Guo, R., Sobeck, A., Bachrati, C. Z., Yang, J., Enomoto, T., et al. (2008). RMI, a new OB-fold complex essential for Bloom syndrome protein to maintain genome stability. *Genes Dev.* 22, 2843–2855. doi: 10.1101/gad.1708608

Xu, X., Rochette, P. J., Feyissa, E. A., Su, T. V., and Liu, Y. (2009). MCM10 mediates RECQ4 association with MCM2-7 Helicase complex during DNA replication. *EMBO J.* 28, 3005–3014. doi: 10.1038/emboj.2009.235

Xu, Y. N., Bazeille, N., Ding, X. Y., Lu, X. M., Wang, P. Y., Bugnard, E., et al. (2012). Multimeric BLM is dissociated upon ATP hydrolysis and functions as monomers in resolving DNA structures. *Nucleic Acids Res.* 40, 9802–9814. doi: 10.1093/nar/gks728

Xue, C., Daley, J. M., Xue, X., Steinfeld, J., Kwon, Y., Sung, P., et al. (2019). Single-molecule visualization of human BLM Helicase as it acts upon double- and single-stranded DNA substrates. *Nucleic Acids Res.* 47, 11225–11237. doi: 10.1093/nar/gkz810

Yang, H., Li, Q., Fan, J., Holloman, W. K., and Pavletich, N. P. (2005). The BRCA2 homologue Brh2 nucleates RAD51 filament formation at a dsDNA-ssDNA junction. *Nature* 433, 653–657. doi: 10.1038/nature03234

Yannone, S. M., Roy, S., Chan, D. W., Murphy, M. B., Huang, S., Campisi, J., et al. (2001). Werner syndrome protein is regulated and phosphorylated by DNA-dependent protein kinase. *J. Biol. Chem.* 276, 38242–38248. doi: 10.1074/jbc.m101913200

Yu, C. E., Oshima, J., Fu, Y. H., Wijsman, E. M., Hisama, F., Alisch, R., et al. (1996). Positional cloning of the Werner's syndrome gene. *Science* 272, 258–262.

Zecevic, A., Menard, H., Gurel, V., Hagan, E., DeCaro, R., and Zhitkovich, A. (2009). WRN Helicase promotes repair of DNA double-strand breaks caused by aberrant mismatch repair of chromium-DNA adducts. *Cell Cycle* 8, 2769–2778. doi: 10.4161/cc.8.17.9410

Zhang, Y., and Jasin, M. (2011). An essential role for CtIP in chromosomal translocation formation through an alternative end-joining pathway. *Nat. Struct. Mol. Biol.* 18, 80–84. doi: 10.1038/nsmb.1940

Zhao, W., Vaithiyalingam, S., San Filippo, J., Maranon, D. G., Jimenez-Sainz, J., Fontenay, G. V., et al. (2015). Promotion of BRCA2-dependent homologous recombination by DSS1 via RPA targeting and Dna Mimicry. *Mol. Cell* 59, 176–187. doi: 10.1016/j.molcel.2015.05.032

Zheng, L., Kanagaraj, R., Mihaljevic, B., Schwendener, S., Sartori, A. A., Gerrits, B., et al. (2009). MRE11 complex links RECQ5 Helicase to sites of DNA damage. *Nucleic Acids Res.* 37, 2645–2657. doi: 10.1093/nar/gkp147

Zhi, L. Q., Ma, W., Zhang, H., Zeng, S. X., and Chen, B. (2014). Association of RECQL5 gene polymorphisms and osteosarcoma in a Chinese Han population. *Tumour Biol.* 35, 3255–3259. doi: 10.1007/s13277-013-1425-4

Zhunussova, G., Afonin, G., Abdikerim, S., Jumanov, A., Perfilyeva, A., Kaidarova, D., et al. (2019). Mutation spectrum of cancer-associated genes in patients with early onset of colorectal cancer. *Front. Oncol.* 9:673. doi: 10.3389/fonc.2019.00673

Zimmer, K., Puccini, A., Xiu, J., Baca, Y., Spizzo, G., Lenz, H. J., et al. (2020). WRN-mutated colorectal cancer is characterized by a distinct genetic phenotype. *Cancers* 12:1319. doi: 10.3390/cancers12051319

**Conflict of Interest:** The authors declare that the research was conducted in the absence of any commercial or financial relationships that could be construed as a potential conflict of interest.

frontiers in Genetics

BRIEF RESEARCH REPORT
published: 09 March 2021
doi: 10.3389/fgene.2021.603195

# Molecular Diagnosis of Neurofibromatosis by Multigene Panel Testing

*Zeng-Yun-Ou Zhang[1,2†], Yuan-Yuan Wu[1,2†], Xin-ying Cai[1,2], Wen-Liang Fang[3*] and Feng-Li Xiao[1,2,4*]*

[1] Department of Dermatology, First Affiliated Hospital of Anhui Medical University, Hefei, China, [2] Key Laboratory of Dermatology, Ministry of Education, Anhui Medical University, Hefei, China, [3] Clinical College, Anhui Medical University, Hefei, China, [4] The Center for Scientific Research of Anhui Medical University, Hefei, China

OPEN ACCESS

**Edited by:**
Yuejin Hua,
Zhejiang University, China

**Reviewed by:**
Priyanka Upadhyai,
Manipal Academy of Higher Education, India
Cecilia Mancini,
Rare Diseases and Medical Genetics Unit, Bambino Gesù Children Hospital (IRCCS), Italy

***Correspondence:**
Feng-Li Xiao
xiaofengli@126.com
Wen-Liang Fang
fangwenliang@ahmu.edu.cn

† These authors have contributed equally to this work

**Specialty section:**
This article was submitted to Genetics of Common and Rare Diseases, a section of the journal Frontiers in Genetics

**Received:** 05 September 2020
**Accepted:** 02 February 2021
**Published:** 09 March 2021

**Citation:**
Zhang Z-Y-O, Wu Y-Y, Cai X-y, Fang W-L and Xiao F-L (2021) Molecular Diagnosis of Neurofibromatosis by Multigene Panel Testing. Front. Genet. 12:603195. doi: 10.3389/fgene.2021.603195

Neurofibromatosis (NF) is an autosomal genetic disorder for which early and definite clinical diagnoses are difficult. To identify the diagnosis, five affected probands with suspected NF from unrelated families were included in this study. Molecular analysis was performed using multigene panel testing and Sanger sequencing. Ultradeep sequencing was used to analyze the mutation rate in the tissues from the proband with mosaic mutations. Three different pathogenic variants of the *NF1* gene were found in three probands who mainly complained of café-au-lait macules (CALMs), including one frameshift variant c.5072_5073insTATAACTGTAACTCCTGGGTCAGGGAGTACACCAA:p.Tyr1692Ilefs in exon 37, one missense variant c.3826C > T:p.Arg1276Ter in exon 28, and one splicing variant c.4110 + 1G > T at the first base downstream of the 3′-end of exon 30. One *NF1* gene mosaic variant was found in a proband who complained of cutaneous neurofibroma with the frameshift variant c.495_498del:p.Thr165fs in exon 5, and ultradeep sequencing showed the highest mutation rate of 10.81% in cutaneous neurofibromas. A frameshift variant, c.36_39del:p.Ser12fs in exon 1 of the *NF2* gene, was found in a proband who presented with skin plaques and intracranial neurogenic tumors. All of these pathogenic variants were heterozygous, one was not reported, and one not in Chinese before. This study expands the pathogenic variant spectrum of NF and demonstrates the clinical diagnosis.

**Keywords: neurofibromatosis type 1·NF1, neurofibromatosis type 2·NF2, mosaic neurofibromatosis type 1·MNF1, multi-gene panel testing, ultra-deep sequencing**

## INTRODUCTION

Neurofibromatosis (NF) is characterized by abnormal development of the nervous system, bones, and skin. It can be divided into the following three different clinical types: NF type 1 (NF1), NF type 2 (NF2), and schwannomatosis. The most common form is NF1 (96%), followed by NF2 (3%) and the lesser known form schwannomatosis (Kresak and Walsh, 2016). The incidence rates of NF1, NF2, and schwannomatosis are 1:3,000, 1:60,000, and 1:70,000 in the general population, respectively (Dhamija et al., 1993; Evans, 1993; Friedman, 1993).

The clinical manifestations of NF are complex. Superficial features of NF1 include axillary, inguinal freckling, cafè-au-lait macules (CALMs), multiple cutaneous neurofibromas, and iris Lisch nodules. NF2 is characterized by bilateral vestibular schwannomas (VSs) with associated symptoms of hearing loss, tinnitus, and balance dysfunction (Evans, 1993). Schwannomatosis is prone to peripheral nerve sheath tumors. Histological features of cutaneous neurofibromas showed tumoral nodules with wavy spindle cell changes. The expression of the S100 protein in the cytoplasm and nucleus highlights Schwann cell elements, while CD34 showed a specialized fibroblastic component forming a net-like pattern and presenting NF architectures (Miettinen et al., 2017).

Neurofibromatosis is an autosomal-dominant disorder. Approximately 50% of individuals inherit it from a parent, while in others it is caused by a spontaneous mutation (Friedman, 1993). NF1 and NF2 are caused by mutations in *NF1* at 17q11.2 and *NF2* at 22q12, respectively. Mosaic NF type 1 (MNF1) is a somatic mosaicism of NF1 that is uncommon (Garcia-Romero et al., 2016). The clinical manifestations of MNF are similar to those of NF1. It is not easy to distinguish NF clinically because it has multiple and complicated phenotypes. Thus, molecular investigation is useful to identify pathogenic variants and improve diagnosis (Louvrier et al., 2018).

Next-generation sequencing (NGS) is a high-output sequencing method that can rapidly sequence exomes, transcriptomes, and genomes (Levy and Myers, 2016; Le Gallo et al., 2017). NGS, especially multigene panel testing, has promoted rapid progress, allowing for the simultaneous analysis of many genes and improvements in the detection rate of mutations (Shin et al., 2020). In this study, we applied multigene panel testing combined with Sanger sequencing testing to five families suspected of having NF and made clear diagnoses.

## MATERIALS AND METHODS

### Study Subjects

Five probands suspected of having NF and nine relatives were from the outpatient department of the First Affiliated Hospital of Anhui Medical University. Clinical samples were collected, including peripheral blood, skin lesions, hair, oral mucosa, and cutaneous tissue. The study was approved by the Institutional Review Board of our hospital. Informed consent was obtained from all participants or their guardians for the collection of data and samples. The samples collected from the probands' families are shown in **Supplementary Table 1**.

There were six patients in five families (**Supplementary Figure 1**). Three probands, including a 3-year-old girl (III-1) from family 1, a 2-year-old girl (II-1) from family 2, and a 2.8-year-old boy (II-1) from family 3, presented with scattered CALMs throughout the body (**Figures 1A,C,D**), and the father (III-1) of the proband from family 1 exhibited CALMs in the trunk area (**Figure 1B**). These patients were born with CALMs that gradually increased with age. These patients showed no other abnormalities. Reflectance confocal microscopy (RCM) (**Supplementary Figure 2A**) and dermoscopy (**Supplementary Figure 2B**) of the probands from family 2 and family 3 revealed significantly increased pigment contents in the stratum basal and regular sepia grid-like pigmentation with clear boundaries.

A 62-year-old man in family 4 (II-4) presented with cutaneous neurofibromas of the left back, chest, and abdomen at the age of 58 years (**Figure 1E**). No other abnormalities were found. Histological evaluation of the cutaneous neurofibromas showed a large and isolated tumoral nodule that presented wavy spindle cell changes (**Supplementary Figures 3A,D**). Immunohistochemical analysis showed scattered S100 positivity in tumor cell nuclei (**Supplementary Figures 3C,F**) and strong and diffuse CD34 positivity in the tumor cell cytoplasm (**Supplementary Figures 3B,E**). No abnormalities were found in the rest of the family members.

A 4-year-old female proband in family 5 (II-1) mainly presented with skin plaques, amblyopia in her right eye, and an intracranial neurogenic tumor by MRI. The skin plaque was present on her right foot when she was born and developed into six skin lesions as she grew up (**Figure 1F**). These lesions were distributed in the trunk area, left hip, right calf front knee, right ankle, and left foot back and consisted of well-circumscribed and slightly pigmented plaques. There were no obvious differences in learning ability and intelligence between her and her peers during her growth. Cranial MRI examination showed an intracranial neurogenic tumor located in the cerebellum medulla oblongata pool of the right side. Histological evaluation of the skin plaques showed multiple nodules forming well-circumscribed interconnected masses of different sizes (**Supplementary Figure 4A**). These multiple nodules presented swirly spindle cell changes (**Supplementary Figure 4D**). Immunohistochemical analysis showed strong and diffuse S100 positivity in the tumor cell nuclei (**Supplementary Figures 4C,F**) and weak and scattered CD34 positivity in the tumor cell cytoplasm (**Supplementary Figures 4B,E**). Other family members did not show similar symptoms.

All clinical manifestations in the NF families are shown in **Table 1**.

### DNA Isolation of Samples

Genomic DNA was extracted from the peripheral blood, skin lesions, hair, oral mucosa, and tumor tissues separately using the AxyPrep Blood Genomic DNA Miniprep Kit (Axygen, Corning, Jiangsu, China) and DNeasy Blood & Tissue Kit (Qiagen, Germany). The DNA purity was determined using a NanoDrop one spectrophotometer and quantified with a Qubit 2.0 Fluorometer using the Qubit dsDNA HS Assay Kit (Life Technologies, Thermo Fisher Scientific, Inc.) according to the manufacturer's recommendations. DNA samples were then preserved at −20°C for further experiments.

### Multigene Panel Testing

To explore the genetic properties of the patients, the capture probe from the Roche NimbleGen Sequence Capture SeqCap EZ Library was used to capture a total of 569 genes associated with hereditary dermatosis. Firstly, DNA was cropped into approximately 300-bp fragments using focused ultrasonicators (Covaris M220, United States) and used to construct the DNA

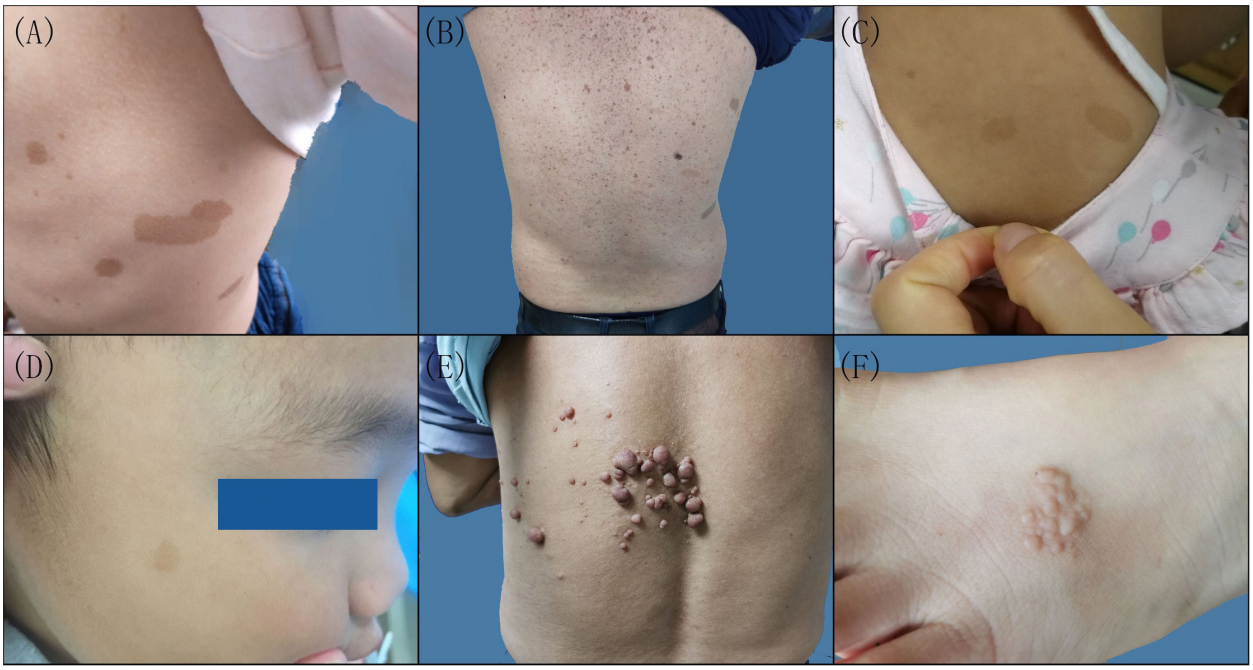


**FIGURE 1 |** Clinical features of the patients with neurofibromatosis (NF). Multiple cafeì-au-lait macules were scattered on the left lateral chest of the proband **(A)** and the back of the proband's father in family 1 **(B)**, the back of the proband in family 2 **(C)**, and the right side of the face of the proband in family 3 **(D)**. **(E)** Cutaneous neurofibroma on the back of the proband in family 4. **(F)** Skin pigmented plaques on the left foot back of the proband in family 5.

**TABLE 1 |** Clinical characteristics of the neurofibromatosis proband study.

| Family no. | Patient no. | Age (years) | Gender | CALMs | Neurofibromas | Intracranial neurogenic tumor | Lisch nodules | Ocular abnormalities |
|---|---|---|---|---|---|---|---|---|
| 1 | III-1 | 3 | F | + | – | – | – | – |
| 2 | II-1 | 2 | F | + | – | – | – | – |
| 3 | II-1 | 2.8 | M | + | – | – | – | – |
| 4 | II-4 | 62 | M | – | + | – | NA | – |
| 5 | II-1 | 4 | F | + | + | + | NA | + |

*"+": affected; "–": unaffected. CALMs, cafeì-au-lait macules; NA, not available.*

library. Then, streptavidin-coated magnetic beads by NimbleGen (Roche NimbleGen, Inc.) were bound to an avidin-labeled probe after the probe had captured the target exons. Next, a hybridization reaction between the DNA library with various index marks and probes with biotin was performed. After linear PCR amplification, the quality of the library was determined. Sequencing was carried out on an Illumina HiSeq X Ten System (Illumina, San Diego, CA, United States) under sequencing efficiency with an average sequencing depth $>$ 200$\times$ and Q30 $>$ 90% according to the manufacturer's instructions. DNA from all of the probands' blood samples and tumor tissues from the proband in family 4 were subjected to multigene panel testing.

## Sanger Sequencing

Sanger sequencing was used to confirm the mutations found by multigene panel testing, which were analyzed to determine whether the variants co-segregated with the disease phenotype in their families. Primers were designed based on the mutation sites found using Primer 3.0. An ABI PRISM 3730XL analyzer (Applied Biosystems, Foster City, CA, United States) was used for Sanger sequencing. The DNA from blood samples of all the probands and their relatives was assessed separately, and the mutation sites of the genes were detected by multigene panel testing.

## Ultradeep Sequencing

When multigene panel testing could detect mutations in the probands' tumor tissues but not in the peripheral blood, ultradeep sequencing was applied to determine the mutation percentage in the peripheral blood, skin lesions, hair, oral mucosa, and tumor tissues. This was performed using the Illumina HiSeq X Ten System (Illumina, San Diego, CA, United States) after DNA quantification and library quality control. The variant allele frequency (VAF) was defined as the number of reads that mapped to whole exons of causal genes, including untranslated and splicing regions. A mutation was considered present when the mutation site VAF was $>$1.0%.

**TABLE 2 |** Variants identified of neurofibromatosis in this study.

| Nucleotide change | Mutation gene | Amino acid change | Variant type | Type of variants | Reference | Inheritance | SIFT_score | Mutation Taster_score |
|---|---|---|---|---|---|---|---|---|
| c.5072_5073insTATAACTGTAACTCCTGGGTCAGGGAGTACACCAA | *NF1* | p.Tyr1692Ilefs | Frameshift | Germline | Novel | Familial | 0 | 0 |
| c.4110 + 1G > T | *NF1* | NA | Splicing | Germline | Reported | Sporadic | 0 | 1 |
| c.3826C > T | *NF1* | p.Arg1276Ter | Missense | Germline | Reported | Sporadic | 1 | 1 |
| c.495_498del | *NF1* | p.Thr165fs | Frameshift | Mosaicism | Reported | Sporadic | 0 | 0 |
| c.36_39del | *NF2* | p.Ser12fs | Frameshift | Germline | Reported | Sporadic | 0 | 0 |

*NA, not available.*

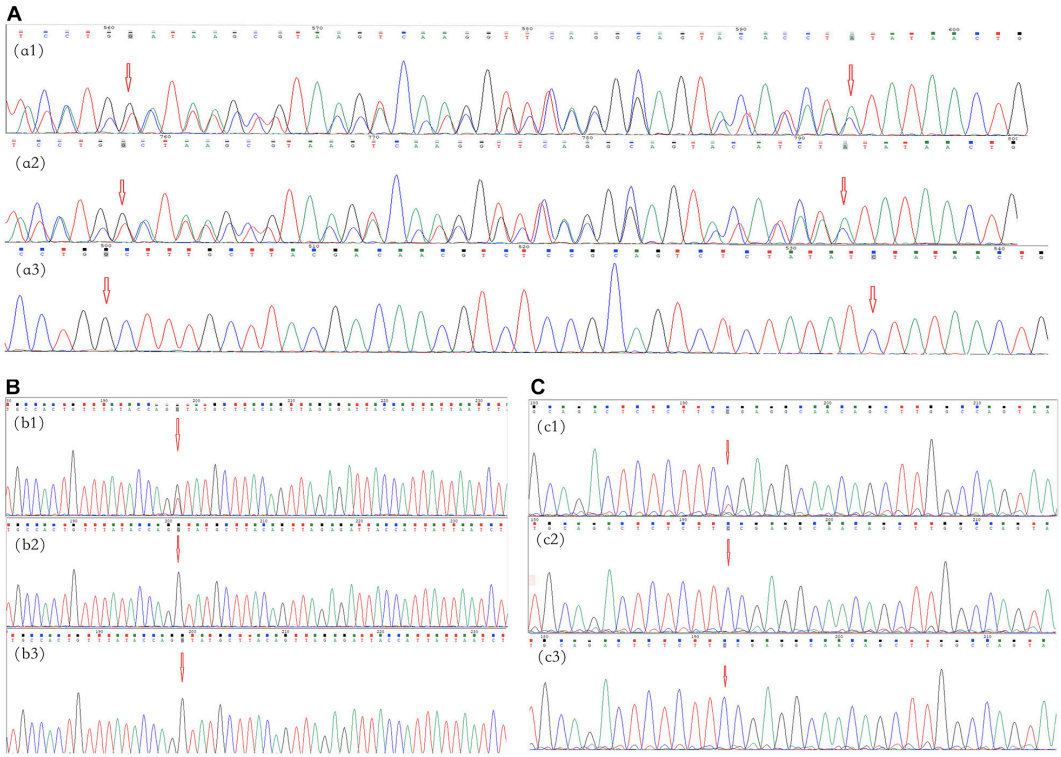


**FIGURE 2 |** Mutational analysis of the neurofibromatosis (NF) patients in families 1–3. The *red arrows* indicate the mutation sites. **(A)** Family 1: the c.5072_5073insTATAACTGTAACTCCTGGGTCAGGGAGTACACCAA:p.Tyr1692Ilefs frameshift variant in *NF1* in exon 37 in proband III-1 ***(a1)*** and her father ***(a2)***; there was no mutation in her mother ***(a3)***. **(B)** Family 2: the c.4110 + 1G > T splicing variant in NF1 at the first base downstream of the 3′-end of exon 30 in proband II-1 **(b1)**; there were no mutations in her father and mother (**b2,b3**, respectively). **(C)** Family 3: the c.3826C > T:p.Arg1276Ter missense variant in NF1 in exon 28 in proband II-1 **(c1)**; there were no mutations in his father and mother (**c1,c2**, respectively).

## RESULTS

Four *NF1* variants in four families and one *NF2* variant in one family were found in our study. All variants were heterozygous, and the genetic findings and analyses are shown in **Table 2**.

A novel frameshift variant, c.5072_5073insTATAACTGTAACTCCTGGGTCAGGGAGTACACCAA:p.Tyr1692Ilefs in exon 37, was found in III-1 and II-3 in family 1 (**Figure 2A**), which inserted 12 amino acids and changed the amino acid sequence starting at position 1692, followed by the production of abnormal neurofibromin. A splicing variant, c.4110 + 1G > T, at the first base downstream of the 3′-end of exon 30 was found in II-1 in family 2 (**Figure 2B**), which resulted in putative aberrant splicing. A missense variant, c.3826C > T:p.Arg1276Ter in exon 28, was identified in II-1 in family 3 (**Figure 2C**), which resulted in the replacement of the arginine residue at 1276 position with a stop codon and premature protein truncation. These variants were not found in the DNA samples from unaffected family members.

In family 4, no variant was found in the peripheral blood of the proband (II-4) by multigene panel testing. However, testing of cutaneous neurofibromas from the proband showed a frameshift variant, c.495_498del:p.Thr165fs, in exon 5 of *NF1* (**Figure 3A**). The pathogenic variant deleted four bases, including thymine, guanine, thymine, and thymine, located from 495–498 in *NF1* exon 5, which caused a change in the amino acid at position 165. This result was confirmed

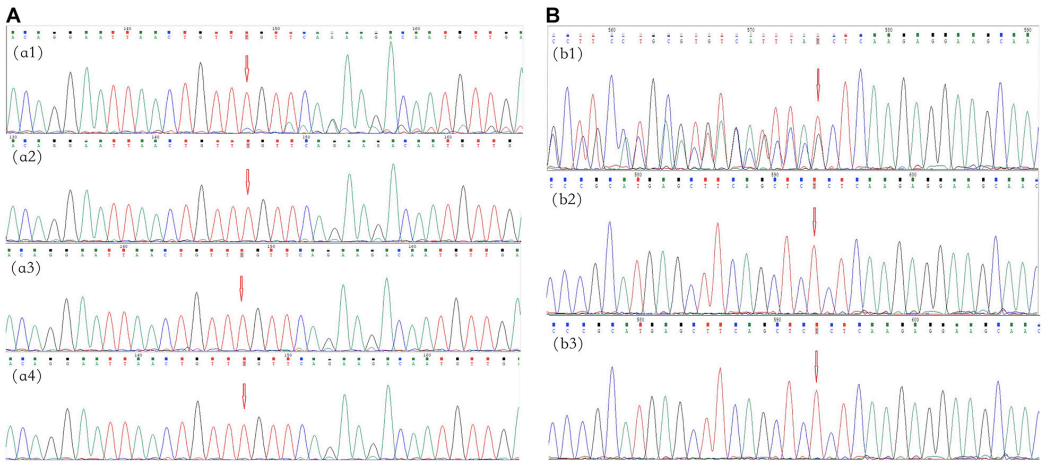


**FIGURE 3 |** Mutational analysis of the neurofibromatosis (NF) patients in families 4 and 5. The *red arrows* indicate the mutation sites. **(A)** Family 4: the c.495_498del:p.Thr165fs frameshift variant in *NF1* in exon 5 in cutaneous neurofibromas from proband II-4 ***(a1)***; there was no mutation in the peripheral blood, oral mucosa, or hair (***a2–a4***, respectively). **(B)** Family 5: the c.36_39del:p.Ser12fs frameshift variant in *NF2* in exon 1 in proband II-1 ***(b1)***; there were no mutations in her father and mother (***b2,b3***, respectively).

in the cutaneous neurofibroma tissue of the proband by Sanger sequencing. Ultradeep sequencing analysis was used to determine the mutation percentage of samples, including from the peripheral blood, the oral mucosa, hair follicles, and cutaneous neurofibromas. The highest mutation rate of 10.81% was observed in the cutaneous neurofibromas, while those of other tissues were less than 0.01% (**Supplementary Table 2**). These results confirmed that the proband had MNF1. This variant was not found in the DNA derived from the peripheral blood of his unaffected daughter.

In family 5, the genetic testing analysis presented a frameshift variant, c.36_39del:p.Ser12fs in exon 1 of *NF2*, in the proband's peripheral blood (**Figure 3B**). The absence of bases 36–39 in exon 1 resulted in the deletion of the serine residue at position 12. The variant was not found in the unaffected family members.

These variants were also not found in the DNA samples from 100 unrelated healthy volunteers.

## DISCUSSION

The main manifestation of CALMs can overlap with that of other disorders, such as Legius syndrome (Brems et al., 2012), Lynch syndrome (Wimmer et al., 2017), and the Piebald trait (Stevens et al., 2012). According to some studies, the incidence rates of *NF1* and *SPRED1* mutations in NF1 patients presenting with familial CALMs are 73 and 19%, respectively (Messiaen and Legius, 2010). In this study, three probands only presented with CALMs. RCM and dermoscopy could provide new ways to help diagnose CALMs, which were used as supplementary diagnostic criteria for NF1 (Duman and Elmas, 2015). The results of the RCM and dermoscopy examination showed pigmentation changes, supporting the observed CALMs.

*NF1* is a highly mutable tumor suppressor gene, and approximately half of affected individuals have *de novo* variants (Yao et al., 2019). Approximately half of children with NF1 have no known family history (Friedman, 1993). Genetic testing could confirm the diagnosis of NF1 in patients suspected of NF1 but only presenting with CALMs (Wang et al., 2019). The variant c.5072_5073insTATAACTGTAACTCCTGGGTCAGGGAGTACACCAA:p.Tyr1692Ilefs in exon 37 was found both in the proband and her father from family 1, so the mutation was inherited from her father. This variant was not reported before.

In family 2, the splicing variant, c.4110 + 1G > T of *NF1* at the first base downstream of the 3′-end of exon 30, affects a donor splice site in intron 30 of the *NF1* gene, which is expected to disrupt RNA splicing and likely result in an absent or disrupted protein product. This mutation was reported in NF1 patients of German or Turkish descent (Fahsold et al., 2000). It was first found in the Chinese NF1 patient in this study. The variant c.3826C > T:p.Arg1276Ter in exon 28 was found in the proband from family 3. This was first reported in two unrelated patients from Spain (Valero et al., 2011) and identified in Chinese and other populations later (Fahsold et al., 2000; Zhang et al., 2015). The sporadic NF1 variant was most likely a *de novo* variant or inherited from the germ cell of one or both of the parents (Friedman, 1993). No genetic testing was performed on the germ cells from the parents of the probands (families 2 and 3), so the source of the mutation is unclear.

MNF1 is an uncommon NF1 subtype with a prevalence rate of approximately 0.0006–0.0027% (Wolkenstein et al., 1995; Ruggieri and Huson, 2001; Ruggieri et al., 2004; Pascual-Castroviejo et al., 2008; Cohen, 2016). In general, affected individuals exhibit milder phenotypes than complete NF1. Fernandez-Rodriguez et al. (2011) revealed the possible biological mechanisms, which were somatic mosaicism and the presence of mild NF1 mutations. Cutaneous neurofibromas are the most common clinical manifestation, with a prevalence of 56% in MNF1 (Ruggieri and Huson, 2001; Wagner et al., 2018). The proband in family 4 only presented

with large cutaneous neurofibromas in some parts of the body. The histopathology results showed wavy spindle cell changes, and immunohistochemical analysis mainly presented strong and diffuse CD34 positivity, which supported the neurofibroma changes.

No variant was found in the peripheral blood of the proband in family 4, but a frameshift variant, c.495_498del:p.Thr165fs in exon 5 of *NF1*, was discovered in his cutaneous neurofibromas, which may produce an abnormal protein product. Ultradeep sequencing showed that the frequency of the mutant *NF1* gene was the highest at 10.81% in cutaneous neurofibromas, though it was very low in the peripheral blood, hair, or the oral mucosa from the patient or normal control. This patient was found to be a somatic mosaic. All three germ layers should carry mutations, and the clinical phenotype will be generalized disease if the mutation occurs earlier than zygote formation. Mutations occurring later in development during embryogenesis may affect fewer cell types or specific tissues. The proband's children might have a risk of classic NF1 if the affected individuals display gonosomal mosaicism (Hardin et al., 2014; Garcia-Romero et al., 2016). However, there was no molecular proof revealing the proband to be an NF1 gonosomal mosaic because the proband refused to provide his semen. Currently, no clinical manifestation of NF has appeared in his offsprings, including a son and two daughters. The variant might be a *de novo* mutation and occurred in the late stage of embryo development after zygote formation. This mutation has been reported in the germline (Osborn and Upadhyaya, 1999; Toliat et al., 2000; Ars et al., 2003; Schaefer et al., 2013; Xu et al., 2014) and saliva (Toliat et al., 2000) from multiple patients with sporadic or familial NF1, which belong to the germline mutation. Interestingly, it is the first report of c.499_502delTGTT appearing as the somatic mosaicism variant.

NF2 is a devastating autosomal-dominant disorder and is characterized by VS (Evans, 1993; Kluwe and Mautner, 1998). The early and typical features of NF2 are meningiomas, ocular abnormalities, or skin plaques in children (Evans et al., 1999; Ruggieri et al., 2015; Gaudioso et al., 2019). The diagnosis of NF2 is easy in adults, but it is often delayed in pediatric patients. The average age of these diagnoses in individuals is 18–24 years, or even earlier (Evans, 1993). The prognosis of younger individuals affected with NF2 might be worse, and severe sporadic NF2 typically occurs in childhood. Skin plaques were the initial manifestation in the proband in family 5. Histological and immunohistochemical analyses showed a dermal plexiform schwannoma with swill spindle cell changes and a strong and diffuse S100 staining. Furthermore, amblyopia was found in her right eye, and an approximately 12-mm tumor was located in the cerebellum medulla oblongata pool of the right brain. Intracranial tumors might become larger, form multiple neurogenic tumors, and further press the tongue base, which could cause epilepsy and affect her ability to speak.

A heterozygous pathogenic frameshift variant, c.36_39del:p.Ser12fs in exon 1 of *NF2*, was found in the proband of family 5, which might result in abnormally truncated proteins because the reading frameshift was predicted to introduce a premature stop codon. It was reported as the somatic inactivating mutation in a study for detecting *SMARCB1* and *NF2* gene mutations (Paganini et al., 2018). It is, for the first time, reported as a germline mutation in this report, which suggests that the same mutation may occur at the different stages of embryo formation.

Approximately 50% of patients with NF2 have an affected parent, while the remaining 50% may have a *de novo* mutation (Mills et al., 2018). Approximately 25–33% of patients with a *de novo NF2* variant have somatic mosaicism (Kluwe et al., 2003; Moyhuddin et al., 2003; Evans et al., 2007, 2013). Genetic testing showed an *NF2* variant in her blood lymphocytes, but no mutation in her parents. However, we did not examine non-hematopoietic tissues from the proband or her parents, specifically germ cells. The presentation may be due to germline mosaicism in a parent or a *de novo* pathogenic variant in the proband. According to genotype–phenotype correlations, frameshift mutations are frequently associated with meningioma (Baser et al., 2004; Smith et al., 2011). Therefore, the prognosis may not be optimistic for the 4-year-old girl.

Multigene panel belongs to next-generation sequencing, and multiple genes can be tested at one time. It has a higher gene mutation detection rate. By applying multigene panel testing methods, the molecular cause has been successfully elucidated in 91% of 35 inherited ichthyosis patients (Cheng et al., 2020) and 90% of 40 suspected epidermolysis bullosa patients (Has et al., 2018). Although it is not a 100% discovery rate, there is undoubtedly an economic and a time advantage to panel genetic testing *versus* a stepwise approach, which is one of the alternative effective methods to help clinical diagnosis. In this study, five affected probands with suspected NF from unrelated families were enrolled. The probands had different clinical manifestations (CALMs, cutaneous neurofibromas, skin plaque, and intracranial neurogenic tumor), and it was difficult to diagnose and determine the type of NF based on clinical manifestations alone. Fortunately, all of them were diagnosed clearly using multigene panel testing combined with Sanger sequencing.

Multigene panel testing combined with Sanger sequencing was used to test five probands suspected of having NF. Three *NF1* mutations were found in three probands with CALMs, one *NF1* mosaic variant was observed in a proband with cutaneous neurofibroma, and an *NF2* variant was found in a proband with skin plaques and an intracranial neurogenic tumor. All of these variants were present in the heterozygous state; one of them has never been reported previously, and one has been reported in the Chinese population for the first time. The additional methods employed in the present study, including multigene panel testing, Sanger sequencing, and ultradeep sequencing, helped to clarify the diagnosis. The novel pathogenic variants expanded the pathogenic variant spectrum of NF.

## DATA AVAILABILITY STATEMENT

The datasets for this article are not publicly available due to concerns regarding participant/patient anonymity. Requests to access the datasets should be directed to the corresponding author.

## ETHICS STATEMENT

The studies involving human participants were reviewed and approved by Institutional Review Board of the First Affiliated Hospital of Anhui Medical University. Written informed consent to participate in this study was provided by the participants' legal guardian/next of kin. Written informed consent was obtained from the minor(s)' legal guardian/next of kin for the publication of any potentially identifiable images or data included in this article.

## AUTHOR CONTRIBUTIONS

F-LX and W-LF conceived and designed the study and revised the manuscript. Z-Y-OZ and Y-YW wrote the manuscript. XC helped perform the experiments and prepared the samples in this study. All the authors reviewed the manuscript.

## FUNDING

This study was funded by the Key Project of Natural Science Research in Colleges and Universities in Anhui Province (No. KJ2016A367), National Natural Science Foundation of China (Nos. 81172838 and 81972926), and scientific research activities of academic and technological leaders of Anhui Province (No. 2017D141).

## ACKNOWLEDGMENTS

We would like to thank the individuals and their families who participated in this project.

## SUPPLEMENTARY MATERIAL

The Supplementary Material for this article can be found online at: https://www.frontiersin.org/articles/10.3389/fgene.2021.603195/full#supplementary-material

**Supplementary Figure 1 |** Family pedigree of the five probands with NF. "■": affected male individual. "●": affected female individual. "□": unaffected male individual. "○": unaffected female individual. "↗": probands in the family "⌀" dead male individual in the family.

**Supplementary Figure 2 |** Pictures of CALMs by reflectance confocal microscopy and dermoscopy examination. High refractive index particles of different sizes in the superficial dermis (red arrow) significantly increased pigment contents in the stratum layer (yellow arrows) under RCM **(A)**. Regular sepia grid-like pigmentation under a microscope with clear boundaries by dermoscopy (100X) **(B)**.

**Supplementary Figure 3 |** Histological and immunohistochemical manifestations of cutaneous neurofibromas in the proband from family 4. A large and isolated nodule in the dermis **(A**, 10X**)** and wavy spindle cell changes (**D**, 40X). Strong and diffuse CD34 staining (**B**, 10X) and strong CD34 staining in the tumor cell cytoplasm (**E**, 40X). Scattered S100 staining (**C**, 10X) and S100 staining in tumor cell nuclei (**F**, 40X).

**Supplementary Figure 4 |** Histological and immunohistochemical manifestations of skin plaques in the proband from family 5. The nodules interconnected with each other (**A**, 10X) and the change in swirly spindle cells (**D**, 40X**)**. Scattered CD34 staining (**B**, 10X) and weak CD34 staining in the tumor cell cytoplasm (**E**, 40X). Strong and diffuse S100 staining (**C**, 10X) and strong S100 staining in the tumor cell nuclei (**F**, 40X).

## REFERENCES

Ars, E., Kruyer, H., Morell, M., Pros, E., Serra, E., Ravella, A., et al. (2003). Recurrent mutations in the NF1 gene are common among neurofibromatosis type 1 patients. *J. Med. Genet.* 40:e82. doi: 10.1136/jmg.40.6.e82

Baser, M. E., Kuramoto, L., Joe, H., Friedman, J. M., Wallace, A. J., Gillespie, J. E., et al. (2004). Genotype-phenotype correlations for nervous system tumors in neurofibromatosis 2: a population-based study. *Am. J. Hum. Genet.* 75, 231–239. doi: 10.1086/422700

Brems, H., Pasmant, E., Van Minkelen, R., Wimmer, K., Upadhyaya, M., Legius, E., et al. (2012). Review and update of SPRED1 mutations causing Legius syndrome. *Hum. Mutat.* 33, 1538–1546. doi: 10.1002/humu.22152

Cheng, R., Liang, J., Li, Y., Zhang, J., Ni, C., Yu, H., et al. (2020). Next-generation sequencing through multi-gene panel testing for diagnosis of hereditary ichthyosis in Chinese. *Clin. Genet.* 97, 770–778. doi: 10.1111/cge.13704

Cohen, P. R. (2016). Segmental neurofibromatosis and cancer: report of triple malignancy in a woman with mosaic Neurofibromatosis 1 and review of neoplasms in segmental neurofibromatosis. *Dermatol. Online J.* 22:13030/qt66k5j4wt.

Dhamija, R., Plotkin, S., Asthagiri, A., Messiaen, L., and Babovic-Vuksanovic, D. (1993). "Schwannomatosis," in *GeneReviews((R))*, eds M. P. Adam, H. H. Ardinger, R. A. Pagon, S. E. Wallace, L. J. H. Bean, K. Stephens, et al. (Seattle, WA: University of Washington).

Duman, N., and Elmas, M. (2015). Dermoscopy of cutaneous neurofibromas associated with neurofibromatosis type 1. *J. Am. Acad. Dermatol.* 73, 529–531. doi: 10.1016/j.jaad.2015.05.021

Evans, D. G. (1993). "Neurofibromatosis 2," in *GeneReviews((R))*, eds M. P. Adam, H. H. Ardinger, R. A. Pagon, S. E. Wallace, L. J. H. Bean, K. Stephens, et al. (Seattle, WA: University of Washington).

Evans, D. G., Birch, J. M., and Ramsden, R. T. (1999). Paediatric presentation of type 2 neurofibromatosis. *Arch. Dis. Child* 81, 496–499. doi: 10.1136/adc.81.6.496

Evans, D. G., Bowers, N., Huson, S. M., and Wallace, A. (2013). Mutation type and position varies between mosaic and inherited NF2 and correlates with disease severity. *Clin. Genet.* 83, 594–595. doi: 10.1111/cge.12007

Evans, D. G., Ramsden, R. T., Shenton, A., Gokhale, C., Bowers, N. L., Huson, S. M., et al. (2007). Mosaicism in neurofibromatosis type 2: an update of risk based on uni/bilaterality of vestibular schwannoma at presentation and sensitive mutation analysis including multiple ligation-dependent probe amplification. *J. Med. Genet.* 44, 424–428. doi: 10.1136/jmg.2006.047753

Fahsold, R., Hoffmeyer, S., Mischung, C., Gille, C., Ehlers, C., Kucukceylan, N., et al. (2000). Minor lesion mutational spectrum of the entire NF1 gene does not explain its high mutability but points to a functional domain upstream of the GAP-related domain. *Am. J. Hum. Genet.* 66, 790–818. doi: 10.1086/302809

Fernandez-Rodriguez, J., Castellsague, J., Benito, L., Benavente, Y., Capella, G., Blanco, I., et al. (2011). A mild neurofibromatosis type 1 phenotype produced by the combination of the benign nature of a leaky NF1-splice mutation and the presence of a complex mosaicism. *Hum. Mutat.* 32, 705–709. doi: 10.1002/humu.21500

Friedman, J. M. (1993). "Neurofibromatosis 1," in *GeneReviews((R))*, eds M. P. Adam, H. H. Ardinger, R. A. Pagon, S. E. Wallace, L. J. H. Bean, K. Stephens, et al. (Seattle, WA: University of Washington).

Garcia-Romero, M. T., Parkin, P., and Lara-Corrales, I. (2016). Mosaic neurofibromatosis type 1: a systematic review. *Pediatr. Dermatol.* 33, 9–17. doi: 10.1111/pde.12673

Gaudioso, C., Listernick, R., Fisher, M. J., Campen, C. J., Paz, A., and Gutmann, D. H. (2019). Neurofibromatosis 2 in children presenting during the first decade of life. *Neurology* 93, e964–e967. doi: 10.1212/WNL.0000000000008065

Hardin, J., Behm, A., and Haber, R. M. (2014). Mosaic generalized neurofibromatosis 1: report of two cases. *J. Cutan. Med. Surg.* 18, 271–274. doi: 10.2310/7750.2013.13116

Has, C., Kusel, J., Reimer, A., Hoffmann, J., Schauer, F., Zimmer, A., et al. (2018). The position of targeted next-generation sequencing in epidermolysis bullosa diagnosis. *Acta Derm .Venereol.* 98, 437–440. doi: 10.2340/00015555-2863

Kluwe, L., Mautner, V., Heinrich, B., Dezube, R., Jacoby, L. B., Friedrich, R. E., et al. (2003). Molecular study of frequency of mosaicism in neurofibromatosis 2 patients with bilateral vestibular schwannomas. *J. Med. Genet.* 40, 109–114. doi: 10.1136/jmg.40.2.109

Kluwe, L., and Mautner, V. F. (1998). Mosaicism in sporadic neurofibromatosis 2 patients. *Hum. Mol. Genet.* 7, 2051–2055. doi: 10.1093/hmg/7.13.2051

Kresak, J. L., and Walsh, M. (2016). Neurofibromatosis: a review of NF1. NF2, and Schwannomatosis. *J. Pediatr. Genet.* 5, 98–104. doi: 10.1055/s-0036-1579766

Le Gallo, M., Lozy, F., and Bell, D. W. (2017). Next-generation sequencing. *Adv. Exp. Med. Biol.* 943, 119–148. doi: 10.1007/978-3-319-43139-0_5

Levy, S. E., and Myers, R. M. (2016). Advancements in next-generation sequencing. *Annu. Rev. Genomics Hum. Genet.* 17, 95–115. doi: 10.1146/annurev-genom-083115-022413

Louvrier, C., Pasmant, E., Briand-Suleau, A., Cohen, J., Nitschke, P., Nectoux, J., et al. (2018). Targeted next-generation sequencing for differential diagnosis of neurofibromatosis type 2, schwannomatosis, and meningiomatosis. *Neuro Oncol.* 20, 917–929. doi: 10.1093/neuonc/noy009

Messiaen, L., and Legius, E. (2010). Error in a study of the clinical and mutational spectrum of neurofibromatosis type 1-like syndrome. *JAMA* 303, 2476–2477. doi: 10.1001/jama.2010.827

Miettinen, M. M., Antonescu, C. R., Fletcher, C. D. M., Kim, A., Lazar, A. J., Quezado, M. M., et al. (2017). Histopathologic evaluation of atypical neurofibromatous tumors and their transformation into malignant peripheral nerve sheath tumor in patients with neurofibromatosis 1-a consensus overview. *Hum. Pathol.* 67, 1–10. doi: 10.1016/j.humpath.2017.05.010

Mills, J. R., Moyer, A. M., Kipp, B. R., Poplawski, A. B., Messiaen, L. M., and Babovic-Vuksanovic, D. (2018). Unilateral vestibular schwannoma and meningiomas in a patient with PIK3CA-related segmental overgrowth: co-occurrence of mosaicism for 2 rare disorders. *Clin. Genet.* 93, 187–190. doi: 10.1111/cge.13099

Moyhuddin, A., Baser, M. E., Watson, C., Purcell, S., Ramsden, R. T., Heiberg, A., et al. (2003). Somatic mosaicism in neurofibromatosis 2: prevalence and risk of disease transmission to offspring. *J. Med. Genet.* 40, 459–463. doi: 10.1136/jmg.40.6.459

Osborn, M. J., and Upadhyaya, M. (1999). Evaluation of the protein truncation test and mutation detection in the NF1 gene: mutational analysis of 15 known and 40 unknown mutations. *Hum. Genet.* 105, 327–332. doi: 10.1007/s004399900135

Paganini, I., Capone, G. L., Vitte, J., Sestini, R., Putignano, A. L., Giovannini, M., et al. (2018). Double somatic SMARCB1 and NF2 mutations in sporadic spinal schwannoma. *J. Neurooncol.* 137, 33–38. doi: 10.1007/s11060-017-2711-6

Pascual-Castroviejo, I., Pascual-Pascual, S. I., and Viano, J. (2008). Segmental neurofibromatosis type 1 (NF1) associated with Cobb syndrome: case report. *Neuropediatrics* 39, 341–343. doi: 10.1055/s-0029-1214422

Ruggieri, M., and Huson, S. M. (2001). The clinical and diagnostic implications of mosaicism in the neurofibromatoses. *Neurology* 56, 1433–1443. doi: 10.1212/wnl.56.11.1433

Ruggieri, M., Pavone, P., Polizzi, A., Di Pietro, M., Scuderi, A., Gabriele, A., et al. (2004). Ophthalmological manifestations in segmental neurofibromatosis type 1. *Br. J. Ophthalmol.* 88, 1429–1433. doi: 10.1136/bjo.2004.043802

Ruggieri, M., Pratico, A. D., and Evans, D. G. (2015). Diagnosis, management, and new therapeutic options in childhood neurofibromatosis Type 2 and related forms. *Semin. Pediatr. Neurol.* 22, 240–258. doi: 10.1016/j.spen.2015.10.008

Schaefer, I. M., Strobel, P., Thiha, A., Sohns, J. M., Muhlfeld, C., Kuffer, S., et al. (2013). Soft tissue perineurioma and other unusual tumors in a patient with neurofibromatosis type 1. *Int. J. Clin. Exp. Pathol.* 6, 3003–3008.

Shin, H. C., Lee, H. B., Yoo, T. K., Lee, E. S., Kim, R. N., Park, B., et al. (2020). Detection of germline mutations in breast cancer patients with clinical features of hereditary cancer syndrome using a multi-gene panel test. *Cancer Res. Treat.* 52, 697–713. doi: 10.4143/crt.2019.559

Smith, M. J., Higgs, J. E., Bowers, N. L., Halliday, D., Paterson, J., Gillespie, J., et al. (2011). Cranial meningiomas in 411 neurofibromatosis type 2 (NF2) patients with proven gene mutations: clear positional effect of mutations, but absence of female severity effect on age at onset. *J. Med. Genet.* 48, 261–265. doi: 10.1136/jmg.2010.085241

Stevens, C. A., Chiang, P. W., and Messiaen, L. M. (2012). Cafe-au-lait macules and intertriginous freckling in piebaldism: clinical overlap with neurofibromatosis type 1 and Legius syndrome. *Am. J. Med. Genet. A* 158A, 1195–1199. doi: 10.1002/ajmg.a.35297

Toliat, M. R., Erdogan, F., Gewies, A., Fahsold, R., Buske, A., Tinschert, S., et al. (2000). Analysis of the NF1 gene by temperature gradient gel electrophoresis reveals a high incidence of mutations in exon 4b. *Electrophoresis* 21, 541–544. doi: 10.1002/(SICI)1522-2683(20000201)21:3<541::AID-ELPS541<3.0.CO;2-L

Valero, M. C., Martin, Y., Hernandez-Imaz, E., Marina Hernandez, A., Melean, G., Valero, A. M., et al. (2011). A highly sensitive genetic protocol to detect NF1 mutations. *J. Mol. Diagn.* 13, 113–122. doi: 10.1016/j.jmoldx.2010.09.002

Wagner, G., Meyer, V., and Sachse, M. M. (2018). [Segmental neurofibromatosis]. *Hautarzt* 69, 487–490. doi: 10.1007/s00105-017-4078-1

Wang, W., Qin, W., Ge, H., Kong, X., Xie, C., Tang, Y., et al. (2019). Clinical and molecular characteristics of thirty NF1 variants in Chinese patients with neurofibromatosis type 1. *Mol. Biol. Rep.* 46, 4349–4359. doi: 10.1007/s11033-019-04888-3

Wimmer, K., Rosenbaum, T., and Messiaen, L. (2017). Connections between constitutional mismatch repair deficiency syndrome and neurofibromatosis type 1. *Clin. Genet.* 91, 507–519. doi: 10.1111/cge.12904

Wolkenstein, P., Mahmoudi, A., Zeller, J., and Revuz, J. (1995). More on the frequency of segmental neurofibromatosis. *Arch. Dermatol.* 131:1465. doi: 10.1001/archderm.1995.01690240131030

Xu, W., Yang, X., Hu, X., and Li, S. (2014). Fifty-four novel mutations in the NF1 gene and integrated analyses of the mutations that modulate splicing. *Int. J. Mol. Med.* 34, 53–60. doi: 10.3892/ijmm.2014.1756

Yao, R., Yu, T., Xu, Y., Yu, L., Wang, J., Wang, X., et al. (2019). Clinical presentation and novel pathogenic variants among 68 Chinese Neurofibromatosis 1 children. *Genes* 10:847. doi: 10.3390/genes10110847

Zhang, J., Tong, H., Fu, X., Zhang, Y., Liu, J., Cheng, R., et al. (2015). Molecular characterization of NF1 and Neurofibromatosis Type 1 genotype-phenotype correlations in a Chinese population. *Sci. Rep.* 5:11291. doi: 10.1038/srep11291

**Conflict of Interest:** The authors declare that the research was conducted in the absence of any commercial or financial relationships that could be construed as a potential conflict of interest.

frontiers in Genetics

REVIEW
published: 12 March 2021
doi: 10.3389/fgene.2021.634789

# Functions of BLM Helicase in Cells: Is It Acting Like a Double-Edged Sword?

*Ekjot Kaur*, Ritu Agrawal and Sagar Sengupta**

*Signal Transduction Laboratory-2, National Institute of Immunology, New Delhi, India*

DNA damage repair response is an important biological process involved in maintaining the fidelity of the genome in eukaryotes and prokaryotes. Several proteins that play a key role in this process have been identified. Alterations in these key proteins have been linked to different diseases including cancer. BLM is a 3′−5′ ATP-dependent RecQ DNA helicase that is one of the most essential genome stabilizers involved in the regulation of DNA replication, recombination, and both homologous and non-homologous pathways of double-strand break repair. BLM structure and functions are known to be conserved across many species like yeast, *Drosophila*, mouse, and human. Genetic mutations in the BLM gene cause a rare, autosomal recessive disorder, Bloom syndrome (BS). BS is a monogenic disease characterized by genomic instability, premature aging, predisposition to cancer, immunodeficiency, and pulmonary diseases. Hence, these characteristics point toward BLM being a tumor suppressor. However, in addition to mutations, *BLM* gene undergoes various types of alterations including increase in the copy number, transcript, and protein levels in multiple types of cancers. These results, along with the fact that the lack of wild-type BLM in these cancers has been associated with increased sensitivity to chemotherapeutic drugs, indicate that BLM also has a pro-oncogenic function. While a plethora of studies have reported the effect of *BLM* gene mutations in various model organisms, there is a dearth in the studies undertaken to investigate the effect of its oncogenic alterations. We propose to rationalize and integrate the dual functions of BLM both as a tumor suppressor and maybe as a proto-oncogene, and enlist the plausible mechanisms of its deregulation in cancers.

**Keywords: BLM helicase, tumor suppressor, oncogene, RecQ helicase, neoplastic transformation**

OPEN ACCESS

***Edited by:***
*Hari S. Misra,*
*Bhabha Atomic Research Centre (BARC), India*

***Reviewed by:***
*Sudha Sharma,*
*Howard University, United States*
*Robert M. Brosh,*
*National Institutes of Health (NIH), United States*

****Correspondence:***
*Ekjot Kaur*
*ekjotkaur@nii.ac.in*
*Sagar Sengupta*
*sagar@nii.ac.in*

***Specialty section:***
*This article was submitted to Genetics of Common and Rare Diseases, a section of the journal Frontiers in Genetics*

***Received:*** *28 November 2020*
***Accepted:*** *11 February 2021*
***Published:*** *12 March 2021*

***Citation:***
*Kaur E, Agrawal R and Sengupta S (2021) Functions of BLM Helicase in Cells: Is It Acting Like a Double-Edged Sword? Front. Genet. 12:634789. doi: 10.3389/fgene.2021.634789*

## INTRODUCTION

Both prokaryotic and eukaryotic genomes continuously accumulate spontaneous and genotoxic agent-induced DNA damages that are generated during the DNA replication process and also when the cells are exposed to multiple types of exogenous factors including exposure to chemicals or ionizing irradiation (IR) (Khanna and Jackson, 2001; Giglia-Mari et al., 2011). DNA repair can be classified as a highly complex biological process that orchestrates to detect and repair these genetic insults. DNA repair processes are evolutionarily conserved across different species, and inability to repair the damage can cause mutations and eventually lead to multiple ailments including neoplastic transformation in mammals. Apart from the DNA repair–cell cycle checkpoints, mechanisms enable the restoration of the damaged DNA by halting the progression of cell cycle

(Barnum and O'Connell, 2014). DNA damage response (DDR) is a multistep process involving detection of DNA damage and cell cycle checkpoint activation, along with DNA repair, that is ultimately responsible for the repair of aberrant DNA structures and resolution of DNA replication stalled forks. Thus, DDR ensures the transmission of identical genomes to subsequent progenies and thereby maintains the genomic integrity.

Double-strand breaks (DSBs) are one of the most lethal forms of DNA damage. Two major distinct pathways have evolved in both prokaryotes and eukaryotes for repairing DSBs. These include the homologous recombination repair (HRR) and non-homologous end joining repair (NHEJ) pathways. Twenty-five percent to 50% of the DSBs generated by nucleases in yeast and mammalian cells are repaired by the classical NHEJ (cNHEJ) pathway that occurs in all phases of the cell cycle. However, NHEJ is an error-prone process (Clikeman et al., 2001; Stinson et al., 2020). In contrast to NHEJ, the HHR pathway is potentially error free and is largely restricted to the S phase and G2 phase of the cell cycle (Jasin and Rothstein, 2013). Each one of them independently operates to restore the DNA integrity; however, the mechanism by which the processing of the damaged DNA ends by these two pathways varies.

Many of the key factors in the DSB repair pathways have been identified. Cells lacking these factors have been implicated in various diseases in humans. Several recent reviews have reiterated the role of RecQ helicases as critical regulators of these repair pathways (Newman and Gileadi, 2020; Ahamad et al., 2021; Datta et al., 2021). This review focuses on delineating the functions of one of the RecQ helicase BLM with a particular emphasis on its dual role in cancer.

## RECQ HELICASES

DNA helicases are a diverse group of proteins that utilizes the energy from ATP hydrolysis to unwind the duplex DNA, with a few of them involved in displacing other proteins from the DNA, making the template accessible to the replication machinery (Xue et al., 2019; Brosh and Matson, 2020). Due to this function, they are known to be involved in a plethora of cellular processes like bacterial conjugation, DNA replication, repair, recombination, and eukaryotic transcription. Of these, RecQ family of helicases are important members of the superfamily 2 (SF2) helicases, which has been found in bacteria, fungi, animals, and plants (Byrd and Raney, 2012). However, the number of *RecQ* genes vary among different species with one homolog found in *Escherichia coli* and budding yeast (*RecQ* and *Sgs1*, respectively), three members in *Drosophila melanogaster* (*DmBlm*, *DmRecQL4*, and *DmRecQL5*) (Cox et al., 2019), and seven in *Arabidopsis thaliana* and *Oryza sativa* (Bachrati and Hickson, 2003; Hartung and Puchta, 2006).

Five different *RecQ* genes have been identified in humans (*BLM, WRN, RECQL1, RECQL4*, and *RECQL5*). The proteins encoded by all these genes have a structurally conserved helicase domain containing Walker A and B boxes and a DEAH box that functions in unwinding of the helical structure in an ATP- and $Mg^{2+}$-dependent manner (Bennett and Keck, 2004). Additional domains such as the RQC domain (RecQ C-terminal) and HRDC (Helicase and RNase D C-terminal) are also found in few of the members of RecQ family of proteins (Bennett and Keck, 2004; Guo et al., 2005). In RECQ1-3, protein–protein interactions are mediated by the RQC domain, whereas the HRDC domain present only in RECQ2-3 ensures protein–DNA interactions (Morozov et al., 1997; Liu et al., 1999). In addition to this, a $3' \rightarrow 5'$ exonuclease domain at the N-terminus of WRN and *Xenopus* FFA-1, a nuclear localization signal at the C-terminal of BLM and WRN (Kaneko et al., 1997; Matsumoto et al., 1997), as well as a mitochondrial localization signal in RECQL4 (De et al., 2012) have also been identified. Different members of the RecQ helicase family are involved in the maintenance of genomic integrity during replication, recombination, and repair in both nucleus (Larsen and Hickson, 2013; Bochman, 2014; Croteau et al., 2014) and mitochondria (De et al., 2012; Gupta et al., 2014). Therefore, mutations in three of the RecQ family members, namely, *BLM, WRN*, and *RECQL4*, lead to Bloom syndrome (BS), Werner syndrome (WS), and Rothmund–Thomson syndrome (RTS), respectively, in humans, whereas in yeast, lack of the Sgs1 induces a hyper-recombination as well as hypersensitivity to a wide range of DNA-damaging agents (Watt et al., 1996). Of the five members in human, this review focuses on the dual role of BLM helicase in the context of cancers.

## BLM HELICASE

BLM is one of the important members of the RecQ family of DNA helicases. It is a 1417-amino-acid protein-coding gene located on the chromosome 15q26.1, possessing a 3'−5' ATP-dependent helicase activity whose expression is tightly regulated in a cell cycle manner with highest levels observed in late S and G2 phases of the cell cycle (Dutertre et al., 2000; Sengupta et al., 2005). The different domains of BLM interact with a number of proteins—some of which are in a cell cycle-dependent manner (summarized in **Figure 1**).

## BLM HELICASE AND REPAIR PATHWAYS

BLM functions primarily in the DNA replication and repair of DSBs by associating with various HHR factors and replication machinery. BLM associates and forms a BTRR complex or "BLM dissolvasome" consisting of topoisomerase IIIα (TopIIIα) and RecQ-mediated genome instability proteins 1 and 2 (RMI1 and RMI2, respectively) to process the Double Holliday Junctions (dHJs) generated during the strand invasion step of the HRR pathway yielding non-crossover recombinants (Hu et al., 2001; Daley et al., 2014; Bythell-Douglas and Deans, 2021). Notably, the interaction between BLM and Topo IIIα is evolutionary conserved—it occurs in yeast (Gangloff et al., 1994), *E. coli* (Harmon et al., 1999), as well as in somatic and meiotic human cells (Johnson et al., 2000; Wu et al., 2000). In the anaphase population of human cells, this interaction at the ultrafine bridges (UFBs) ensures complete sister chromatid decatenation (Chan et al., 2007). BLM preferentially unwinds multiple types of complex DNA structures including G-quartet,

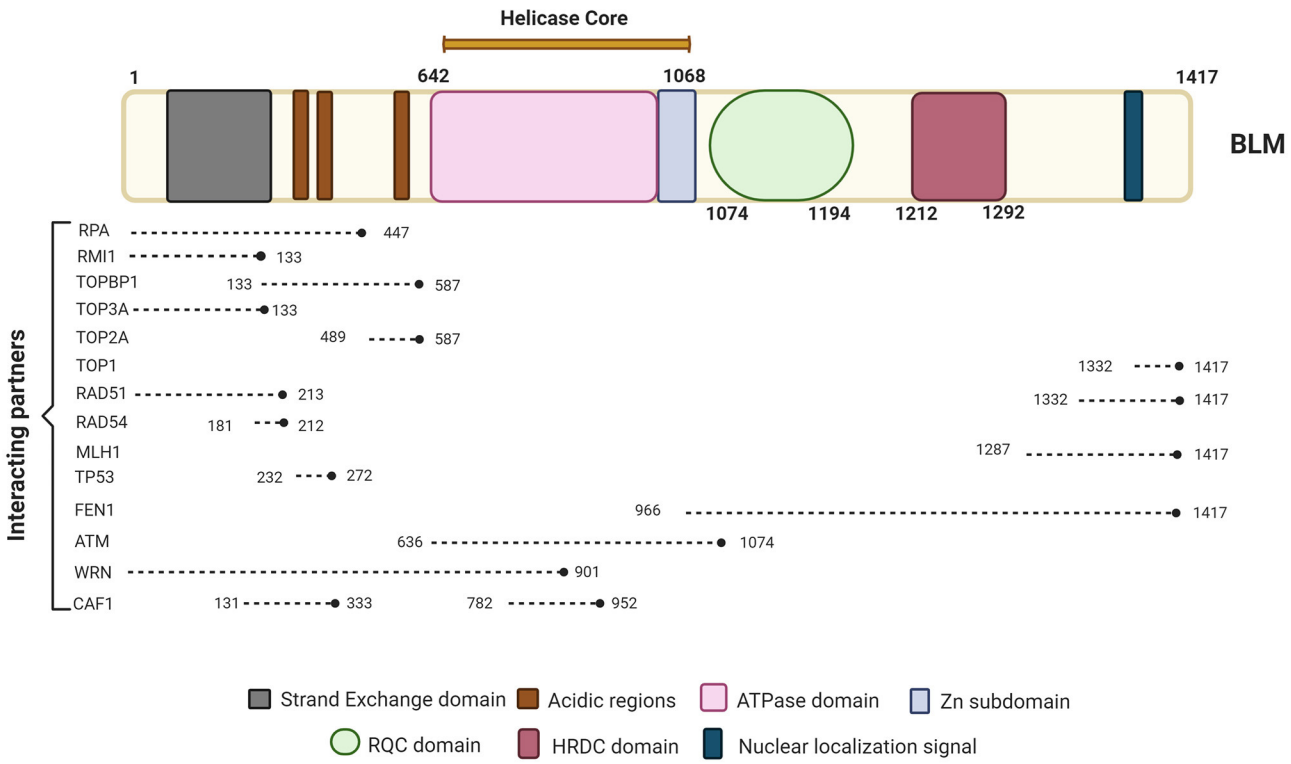


**FIGURE 1 |** Schematic representation of BLM primary protein structure and its interacting partners. BLM is composed of the structurally ordered ATPase/helicase core, RQC, and HRDC domains in the C-terminal of the protein of which helicase domain is conserved across organisms. Key proteins involved in different repair pathways and interacting with BLM are shown along with their approximate binding positions with respect to BLM. The different interacting partners of BLM that are involved in DNA repair processes and chromatin assemble include RPA (Kang et al., 2018; Bythell-Douglas and Deans, 2021), RMI (Blackford et al., 2015; Bythell-Douglas and Deans, 2021), TOPBP1 (Blackford et al., 2015), TOP3A (Hu et al., 2001; Bythell-Douglas and Deans, 2021), TOP2A (Bhattacharyya et al., 2009), TOP1 (Grierson et al., 2013), RAD51 (Bugreev et al., 2007), RAD54 (Srivastava et al., 2009), MLH1 (Pedrazzi et al., 2001), FEN1 (Sharma et al., 2005), ATM (Beamish et al., 2002), WRN (von Kobbe et al., 2002), and CAF1 (Jiao et al., 2004). Figure created with BioRender.com.

D-loop, telomere DNA, and Holliday Junctions (HJs) (Vindigni and Hickson, 2009). It has been reported that BLM possesses a low helicase activity; however, physical interaction with Replication Protein A (RPA) accentuates its unwinding activity on both intact and nicked ssDNAs (Brosh et al., 2000; Kang et al., 2018; Qin et al., 2020). Recent study identified three conserved RPA binding motifs in the BTRR complex (two in BLM and one in RMI1) that interact with the RPA1 N-terminal OB-fold (Shorrocks et al., 2021). This interaction was found to be specifically required in the role of the BTR complex in promoting replication fork restart but not in its roles of suppressing sister chromatid exchanges (SCEs), processing UFBs, or promoting DNA-end resection (Shorrocks et al., 2021). Furthermore, a critical interaction of BLM with RAD51 is responsible for homology search and during the subsequent strand invasion step (Wang et al., 2000; Wu et al., 2001). BLM also promotes DNA end resection by the exonucleases EXO1 and DNA2, generating a 3′ single-stranded substrate for RAD51 recruitment and filament formation (Mimitou and Symington, 2009; Nimonkar et al., 2011). Together, these properties of BLM position it as a pro-recombinogenic protein. Multiple studies have also shown that BLM accumulates at the stalled replication forks, interacting with FANCM and FANCC to dissolve the dHJs and related DNA configurations (Davalos and Campisi, 2003; Wu and Hickson, 2003; Sengupta et al., 2004; Singh et al., 2008; Moder et al., 2017). Further, we have earlier elucidated that the ATR-mediated phosphorylation at Thr99 on BLM is required for its interaction with the signal transducer 53BP1 protein. This interaction is critical for the anti-recombinogenic role of BLM during the HHR pathway and ensures survival post-replicative stress (Tripathi et al., 2007, 2008), thereby providing a hint about the dual roles of this helicase.

Genome-wide guanine-quadruplex (G4) motif analysis has shown that unconventional structures are particularly enriched in telomeres, minisatellites, ribosomal DNA, and, importantly, gene regulatory regions (Drosopoulos et al., 2015). BLM has been shown to bind and unwind G4 structures promoting fork progression through G-rich telomeric DNA (Drosopoulos et al., 2015; Tippana et al., 2016). BLM has also been implicated in repairing the secondary DNA structures including R-loops and G4s induced by reactive oxygen species (ROS) at transcriptionally active sites (Tan et al., 2020). These studies again provide evidence that BLM suppresses recombination at these telomeric sites to

maintain genomic stability (Root et al., 2016; van Wietmarschen et al., 2018).

BLM has also been identified as an early sensor to multiple types of DNA damage (Sengupta et al., 2004; Tripathi et al., 2018). BLM is reported to assemble along with hRAD51 and p53 immediately to the sites of stalled replication (Sengupta et al., 2003; Ouyang et al., 2009) and IR-induced DSBs (Wu et al., 2001). In asynchronously growing cells, Chk1-mediated Ser646 phosphorylation (Kaur et al., 2010) on BLM causes it to colocalize with the promyelocytic leukemia (PML) protein (Bischof et al., 2001). Notably, in response to laser-induced DSBs, BLM co-localizes with γH2AX and ATM within seconds of induction at the sites of damage (Karmakar et al., 2006). The localization of BLM onto the stalled replication forks occurs after its ubiquitylation at lysine residues 105, 225, and 259 by RNF8/RNF168 E3 ligases (Tikoo et al., 2013). The early recruitment of BLM is ATR- and ATM-dependent, and this ensures the optimum formation of pATM and 53BP1 foci during replication stress (Davies et al., 2004). BLM along with BRCA1 and the MRN complex is part of a large complex called BRCA1-associated genome surveillance complex (BASC), which is co-recruited with PCNA during DNA replication-associated repair (Wang et al., 2000). In contrast, BLM recruitment in the later stages of repair is independent of ATM but requires functional interaction between polyubiquitylated BLM and NBS1 for its retention at the DSB site (Tripathi et al., 2018). In addition, BLM has been shown to physically and functionally associated with hp150, the largest subunit of chromatin assembly factor 1 (CAF-1) to promote survival in response to DNA damage and/or replication blockade (Jiao et al., 2004). Furthermore, a functional interaction between BLM and RAD54 enhances the chromatin remodeling activity of RAD54 resulting in its increased recruitment of RAD51 protein onto the HU-induced DNA damage (Srivastava et al., 2009). These results indicate that the role of BLM in the DDR response is a combination of its role as an early DNA damage sensor as well as its multiple functions during the effector stage of the repair.

Recently, we have also demonstrated that BLM is co-recruited with the c-NHEJ factor XRCC4 in a cell cycle-specific manner and regulates the cNHEJ process (Tripathi et al., 2018). In a cell cycle phase-dependent manner, BLM seems to help in making the choice between HR and cNHEJ (Tripathi et al., 2018). Apart from its role in HHR, BLM also has an effect on the other DNA repair pathways operative in human cells. BLM prevents the activation of the error-prone MMEJ pathway in human and mouse. Thus, cells lacking BLM displayed higher genomic rearrangements (Gaymes et al., 2002). In addition, studies have revealed that the C-terminal of human BLM interacts with the mismatch repair protein MLH1; however, this interaction did not seem to affect the post-replicative mismatch repair pathway (Langland et al., 2001; Pedrazzi et al., 2001).

## REGULATION OF BLM

BLM has been shown to undergo various post-translational modifications (PTMs) including phosphorylation, ubiquitination, acetylation, and SUMOylation that are necessary for its function, interaction, turnover, localization, and stability. In turn, these PTMs of BLM have been shown to regulate several DDR signaling cascades. BLM undergoes phosphorylation at Thr99 and Thr122 by ATM/ATR that is crucial for restarting of stalled replication folks after HU or IR treatment (Davies et al., 2004). Constitutive phosphorylation of BLM at Serine 502 by Chk1 during interphase stabilizes its levels, preventing its cullin-3-mediated degradation in colon cancer cells (Petsalaki et al., 2014). Additionally, NEK11-dependent S phase-specific phosphorylation at Serine 338 of BLM mediates its interaction with TopBP1 that functions to stabilize the BLM levels in S and G2 phases of the cell cycle (Wang et al., 2013).

Apart from phosphorylation, K63-linked ubiquitination of BLM at Lys105, Lys225, and Lys259, mediated by RNF8/RNF168, was demonstrated to be essential for BLM to relocate to the sites of stalled replication (Tikoo et al., 2013). K48-linked ubiquitylation of BLM by E3 ligase, Fbw7α, leads to its subsequent degradation during mitosis. This modification, in turn, is regulated by sequential phosphorylation on BLM by multiple kinases at Thr182, Thr171, and Ser175 residues (Kharat et al., 2016). Further, K3 linked BLM ubiquitination by MIB1 E3 ligase that led to its rapid degradation in the G1 phase of the cell cycle (Wang et al., 2013). PTM-like SUMOylation of BLM at Lys317, Lys331, Lys34, and Lys347 is also shown to be necessary for the interaction between BLM and RAD51 promoting HR repair (Eladad et al., 2005; Ouyang et al., 2013).

In addition to its post-translational regulation, recent evidences of its post-transcriptional regulation particularly in cancers have also been demonstrated. miR-522-3p was found to be highly expressed in colorectal cancer (CRC) tissues compared to adjacent non-tumor tissues and negatively regulates the BLM levels, promoting proliferation of colon cancer cells and thus demonstrating its tumor suppressor function (Shuai et al., 2018). In contrast, overexpression of miR-607 and miR-27b-3p in PC3 cells reduced proliferation, colony formation, and invasion capacity by decreasing the BLM mRNA levels and protein levels, respectively (**Figure 2**) (Chen Y. et al., 2019). BLM transcript levels have also been found to undergo epigenetic regulation by CpG island promoter methylation in CRC samples (Votino et al., 2017). CpG island promoter hypomethylation altered its expression, which might contribute to proliferation of poorly differentiated cells (Votino et al., 2017). The different modes by which BLM transcript levels can be regulated are summarized in **Figure 2**.

## CLINICAL MANIFESTATIONS DUE TO ALTERATIONS IN BLM LEVELS

BS is caused by either homozygous or compound heterozygous mutations in the *BLM* gene located at the 15q26.1 locus (Ellis et al., 1995a; German et al., 2007). BS patients display features like proportional pre- and postnatal dwarfism, immunodeficiency, hypersensitivity to sunlight, infertility in males, subfertility in females, and type 2 diabetes mellitus (Bloom, 1954; German and Passarge, 1989; Ellis et al., 2008). Due to its pivotal role as an

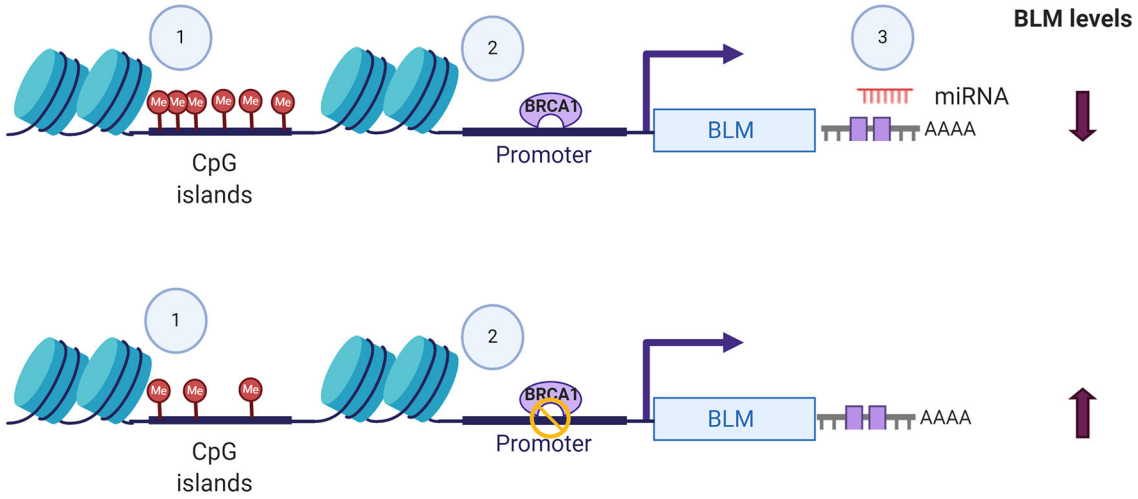


**FIGURE 2 |** Different modes of BLM transcript regulation. The alterations in the expression levels of BLM can be brought about by (1) CpG island methylation, (2) transcriptional regulators like BRCA, and (3) miRNA-mediated targeting of 3′-UTR. Figure created with BioRender.com.

anti-recombinogenic protein, BS patients lacking the functional protein exhibit a significant increase in mitotic recombination, high rates of heterozygosity (Langlois et al., 1989), chromatid gaps, breaks, increased frequency of SCE (Chaganti et al., 1974; German et al., 1974; German, 1993; Ellis et al., 1995b), telomere defects (TD) (Barefield and Karlseder, 2012), and aberrant quadriradial chromosomes (Chaganti et al., 1974; Lonn et al., 1990; Groden and German, 1992). Additionally, BLM defective cells displayed accumulation of anaphase bridges that caused chromosome entanglement (Chan et al., 2007). Since the cells cannot adequately repair the inherent and induced DNA damage, BS patients additionally show increased sensitivity toward DNA-damaging agents like HU, camptothecin (CPT), and IR (Davies et al., 2004; Ouyang et al., 2008; Shastri and Schmidt, 2016).

Most of the BS mutations are either non-sense or frameshift mutations causing premature truncation of the protein. Additionally, several of the missense mutations spreading across the helicase domain and RQC domain have also been identified and reported in the Bloom Syndrome Registry and BLM database (Ellis et al., 1995a; German et al., 2007; Bythell-Douglas and Deans, 2021). These missense mutations have been shown to abolish the ATPase and DNA binding activity with some of them losing ATP binding activity, thus rendering the BLM protein catalytically inactive (Bahr et al., 1998; Rong et al., 2000; Guo et al., 2007). The Ashkenazi Jewish are the most commonly affected population by BS because of the high prevalence of the $BLM^{Ash}$ founder mutation: a 6-bp deletion and 7-bp insertion at the nucleotide position 2281 in BLM cDNA (Li et al., 1998). However, the $BLM^{Ash}$ mutation has also been found in non-Jewish individuals, such as Americans of Spanish descent (Ellis et al., 1998).

Similar to BS patients, individuals harboring mutations in the *TOP3A* (an essential gene in mammals) displayed elevated rates of SCE, unresolved recombination, and replication intermediates, leading to chromosome bridges and thus inducing genomic instability (Martin et al., 2018). Additionally, homozygous truncating variants in RMI1, another important member of the BTR complex, caused growth retardation as seen in the case of BS (Martin et al., 2018). These reports establish that the intact, functionally active BTRR complex is required for the regulation of recombination repair and thus in genome maintenance.

BLM is also postulated to be involved in the development and maintenance of the immune system. In BS patients, abnormal serum concentrations of at least one subclass of serum immunoglobulins with IgM and IgA levels and lowered IgG levels have been documented (Hutteroth et al., 1975; Weemaes et al., 1979; Taniguchi et al., 1982; Kondo et al., 1992). Upon BLM depletion, the number of progenitor B lymphoid cells in the bone marrow and mature B cells in the spleen and peritoneal cavity was significantly decreased in the B cell-specific BLM knockout mice (Babbe et al., 2009). Additionally, ablation of BLM in mice and in BS patients also leads to defect in the T cell lineage (Hutteroth et al., 1975; Taniguchi et al., 1982; Van Kerckhove et al., 1988). It was observed that in some BS patients, the reduced CD4-positive T cell numbers (Van Kerckhove et al., 1988) impaired T cell proliferation, and T helper function has been identified (Hutteroth et al., 1975; Taniguchi et al., 1982; Van Kerckhove et al., 1988). Using the conditional T-cell-specific BLM knockout mice, severe blockage at the β selection checkpoint was observed, which resulted in significantly decreased number of thymocytes (Babbe et al., 2007). Due to an accumulation of damaged DNA and micronuclei in BLM-deficient cells, enhanced expression of *inflammatory interferon-stimulated gene (ISG)* and increased levels in peripheral blood have also been observed. This increased expression is mediated through the Cyclic GMP-AMP synthase–stimulator of interferon genes–interferon regulatory factor-3 (cGAS–STING–IRF3) cytosolic DNA–sensing pathway, thus linking the innate immune system with the DNA damage machinery (Gratia et al., 2019). However,

the specific molecular mechanisms regulated by BLM are not well-elucidated. Altogether, BLM plays an indispensable role in the development, proliferation, maintenance, stability, and function of immune cells and contributes to the immune deficiency in patients afflicted with BS.

## TUMOR-SUPPRESSIVE FUNCTIONS OF BLM

In addition to the aforementioned clinical features, loss of functional BLM increases the risk of developing plethora of solid tumors and hematological malignancies in BS patients (German et al., 2007; Cunniff et al., 2017). BLM-depleted cells lead to amassment of damaged DNA, showed suppressed cell proliferation, and enhanced genomic damage with high response or sensitivity toward various chemotherapeutic drugs like cis-diamminedichloroplatinum (CDDP or cis-Pt), CPT, HU (Arora et al.), and 5-fluorouracil (5-FU) (Mao et al., 2010), suggesting its tumor-suppressive function. Studies using mouse models further demonstrated that haploinsufficiency of BLM led to an early onset of lymphomas and intestinal tumors particularly CRC (Gruber et al., 2002; de Voer et al., 2015). BLM heterozygous mutant mice developed T cell lymphoma at a much more rapid rate when challenged with murine leukemia virus (Goss et al., 2002) and the frequency of intestinal tumor development is higher when crossed with *Adenomatous Polyposis Coli (APC)* gene heterozygous mutant mice. In contrast, BLM transgenic mice expressing human BLM attenuated intestinal tumors when crossed with APC heterozygous mutant mice, thereby indicating that tumor growth can be regulated in a BLM dose-dependent manner (McIlhatton et al., 2015). BLM homozygous null $BLM^{m3/m3}$ mice are viable, fertile, and more cancer prone with and without tumor predisposing factors like gamma irradiation (Warren et al., 2010). This tumorigenic effect was enhanced after irradiation of $BLM^{m3/m3}$ mice (Warren et al., 2010) wherein lymphoma, sarcoma, and carcinoma were the most common cancers arising in this genotype. It is important to note that the hematopoietic system is predominantly affected by the lack of wild-type BLM expression as the frequencies of lymphoma and leukemia in BS are higher than expected, the most common being the T cell lymphoma (Luo et al., 2000; Warren et al., 2010). In patched homolog 1 (Ptch1) heterozygous mutant mice, loss of BLM function significantly enhanced the tumorigenesis of basal cell carcinoma (BCC) (a type of skin cancer) and rhabdomyosarcomas (RMS) (Davari et al., 2010). Conditional BLM knockout mice bearing heat shock promoter cre transgene (HS-cre), prostate-specific antigen promoter-cre transgene (PSA-cre), and ovine beta-lactoglobulin promoter-cre transgene (BLG-cre) develop different types of mammary tumors, i.e., adeno-myoepithelioma and adenocarcinoma (Chester et al., 2006). Cell lines developed from these mammary tumors produce a high number of SCEs and show high chromosomal instability (CIN) (Chester et al., 2006). Thus, in mice, BLM acts as a factor essential for maintaining genomic stability and is involved in the prevention or reduction of tumor development (McDaniel et al., 2003).

Similar to mice models, BS patients also develop a spectrum of cancers at a very early age, of which leukemia and lymphomas are the most common malignancies followed by CRCs (German et al., 2007; Cunniff et al., 2017). This was particularly observed in the Ashkenazi Jews population harboring heterozygous BLM mutation, which displayed a more than a 2-fold increase in colon cancer incidence (Li et al., 1998). Furthermore, hematological malignancies of BS patients have been reported to demonstrate chromosomal rearrangements (Kaneko et al., 1996; Schuetz et al., 2009). Elevated incidence of micronuclei in the exfoliated epithelial cells from the BS patients compared to normal individuals carrying a heterozygous *BLM* gene mutation has also been reported (Rosin and German, 1985), indicative of HHR deregulation and the presence of genomic instability. While investigating its function in during instability in CRC, BLM deficiency was found to induce hyper-recombination in epithelial cells that was associated with loss of heterozygosity (Traverso et al., 2003).

In accordance with its role as a caretaker of the genome, several of the germline mutations in the *BLM* gene have been identified to be associated with CRC risk (Sokolenko et al., 2012; de Voer et al., 2015). The whole exome sequencing data from the CRC patients was used to infer that about 0.11% of the general population were enriched with the heterozygous BLM mutation that confers low-to-moderate penetrance risk for developing CRC. The carrier frequency of this mutation was, however, observed to be higher by about 1% in the people with an Ashkenazi Jewish ancestry (de Voer et al., 2015). Gruber et al. similarly identified that CRC patients were high-frequency carriers of the heterozygous $BLM^{Ash}$ mutation (Gruber et al., 2002). However, in the case of the association of BLM mutation with breast cancer, a contradictory set of reports exists in the literature. While Sokolenko et al. and Prokofyeva et al. identified that truncating mutation of BLM (c.1642 C>T, p.Gln548Ter) conferred a 6-fold increased risk of breast cancer, such association was not observed by Kluzniak et al. in the large cohort of samples obtained from Poland (Sokolenko et al., 2012; Prokofyeva et al., 2013; Kluzniak et al., 2019). A similar observation with the $BLM^{Ash}$ and p.Gln548Ter mutations was observed in the prostate cancer (PC) cells wherein no significant effect on the survival was seen even though the frequency of truncating BLM germline mutations was higher in advanced PC patients as compared to the control populations (Antczak et al., 2013; Bononi et al., 2020; Ledet et al., 2020). Based on these observations, it was hypothesized that the presence of only one functional allele of BLM is incapable of maintaining genomic integrity, which could lead to accumulation of high frequency of deleterious mutations in the cell harboring BLM mutation. In addition, the occurrence of such mutations in the colonic cancer stem cells could potentially generate a hyper-mutated cancer phenotype (Gruber et al., 2002).

Mechanistically, it was demonstrated that in colon cancer cells, BLM enhanced Fbw7α-mediated K48-linked ubiquitylation of proto-oncogene c-Myc (Chandra et al., 2013). This subsequently led to enhanced c-Myc degradation by proteasomal pathway. Additionally, BLM also alleviated c-Jun degradation by E3 ligase Fbw7α, thus attenuating the proliferation of colon

cancer cells in mouse xenograft model (Priyadarshini et al., 2018). Thus, the lack of functional BLM may hamper its ability to regulate the expression of these proto-oncogenes, causing the promotion of tumorigenesis. In addition, BS cells harboring p53 mutations exhibited a lower level of apoptosis and DNA repair and thus may negatively regulate the BLM-dependent repair pathway (Wang et al., 2001). It is noteworthy that BS patients exhibited significant differences in their mRNA expression profile as compared to the normal fibroblasts, with genes involved in cell proliferation and survival being the topmost altered genes (Nguyen et al., 2014; Montenegro et al., 2020).

## EVIDENCE SUPPORTING THE ONCOGENIC FUNCTIONS OF BLM

BLM expression levels are found to be high in testis, ovary, hematopoietic cells, and in all the proliferative cells (like cells of lymphoid origin, in the skin, and digestive tract) (Turley et al., 2001). This upregulation of BLM in forebear cells or undifferentiated cells indicates that BLM may be involved in controlling the differentiation of cells as its overexpression has been associated with the suppression of the differentiating markers (Turley et al., 2001). Taking this evidence into consideration, it can be argued that in contrast to tumor suppressor, BLM may be involved in promoting cancer development. In fact, BLM protein expression was observed in the tumors of both lymphoid and epithelial origin wherein a significant correlation between Ki67 and PCNA was observed with BLM expression (Chandrashekar et al., 2017). Furthermore, an *in silico* examination of the TCGA datasets revealed that BLM mRNA is overexpressed in all types of cancer tissues as compared with normal tissues (**Figure 3**) (Chandrashekar et al., 2017). A recent report utilizing the computation approach has also identified that BLM overexpression was related to poor overall survival (OS) in lung and gastric cancer patients and thus may act as a critical prognostic marker for the detection of these cancers (Alzahrani et al., 2020). In particular, exceedingly high levels of BLM have been demonstrated in all of the hematological malignancies such as intense myeloid leukemia, constant lymphocytic leukemia, lymphoma, and different myeloma (Turley et al., 2001). In acute myeloid leukemia (AML) samples with normal karyotype, high expression of BLM displayed a strong association with poor prognosis, whereas with abnormal karyotype, high expression of BLM associated with better OS (Viziteu et al., 2016a). Further, it was observed that BCR/ABL tyrosine kinase (a common tyrosine kinase fusion in chronic myeloid leukemia) as well as other fusion tyrosine kinases induced the expression of BLM and its helicase function (Slupianek et al., 2005). This in turn potentiated HHR repair capacity via its interaction with RAD51 complex for HR repair in response to chemotherapeutic drugs including cisplatin and mitomycin C, thus playing a role in BCR/ABL-induced resistance to these genotoxic insults (Slupianek et al., 2005).

High levels of BLM protein were also observed in PC cell lines and patients, exhibiting an enhanced rate of cell proliferation whereas BLM depletion resulted in an increased rate of apoptosis due to enhanced ROS generation mediated through the inhibition of AKT and PRAS40 signaling (Chen K. et al., 2019). Thus, BLM may induce oncogenesis through activating pAKT and pPRAS40 in PC (Chen K. et al., 2019). BRCA1 is one of the transcriptional regulators known to be involved in PC (De Luca et al., 2011, 2013). BRCA1 expression hindered tumor development and sensitized these cells to chemotherapy, whereas its suppression promoted chemoresistance. BLM is negatively regulated by BRCA1. Hence, upon BRCA1 suppression, BLM level is elevated, which conceivably leads to chemoresistance upon DNA damage (De Luca et al., 2011; Qian et al., 2017).

Further, BLM mRNA and protein levels are found to be overexpressed in CRC cell lines and patients (Lao et al., 2013). A meta-analysis of the gene expression data sets revealed that BLM levels were significantly upregulated in a subset of poorly differentiated CRC samples wherein shorter relapse-free survival was seen (Votino et al., 2017). In these CRC samples, a positive correlation between BLM expression levels and molecular parameters of the tumors like CpG island methylator phenotype (CIMP) and DNA mismatch repair was observed (Votino et al., 2017). Notably, aberrant overexpression of BLM has been reported to lead to its mis-localization to the cytosol instead of the nucleus and thereby compromising its DNA repair activity (Votino et al., 2017) in CRC cells. CRC samples with low BLM mRNA levels were found to be sensitized with the mitomycin C treatment, thereby showing better survival; in contrast, resistant CRC cell lines had elevated BLM levels (Kwakman et al., 2015).

A study conducted on about 2000 breast tumor samples also revealed that BLM mRNA overexpression was significantly associated with high histologic grade, larger tumor size, estrogen receptor, and progesterone receptor status (Arora et al., 2015). Furthermore, a significant BLM mRNA overexpression along with high BLM cytoplasmic localization was observed in the aggressive molecular phenotypes (including PAM50, which is a 50-gene signature that classifies breast cancer into five molecular intrinsic subtypes: Luminal A, Luminal B, HER2-enriched, Basal-like, and Normal-like) and has been associated with poor breast cancer-specific survival, possibly highlighting BLM transcript level detection as a promising biomarker (Arora et al., 2015).

Re-expression of reverse transcriptase telomerase (Shay and Bacchetti, 1997) or alternative lengthening of telomeres (ALT) (Bryan et al., 1997) have been implicated in the acquisition of replicative immortality by cancer cells. These ALT positive cancer cells display a highly complex karyotype with excessively clustered telomeres localized in specialized PML nuclear bodies called ALT-associated PML bodies (APBs) (Yeager et al., 1999; Draskovic et al., 2009). It is at these sites where ALT-dependent telomere recombination has been shown to occur. BLM has been shown to contribute in telomere maintenance through its capacity of dissolution and alleviating late-replicating structures (LRI) (Barefield and Karlseder, 2012). Using biophysical studies, Min et al. established that BLM helicase activity is vital for the generation of single-stranded

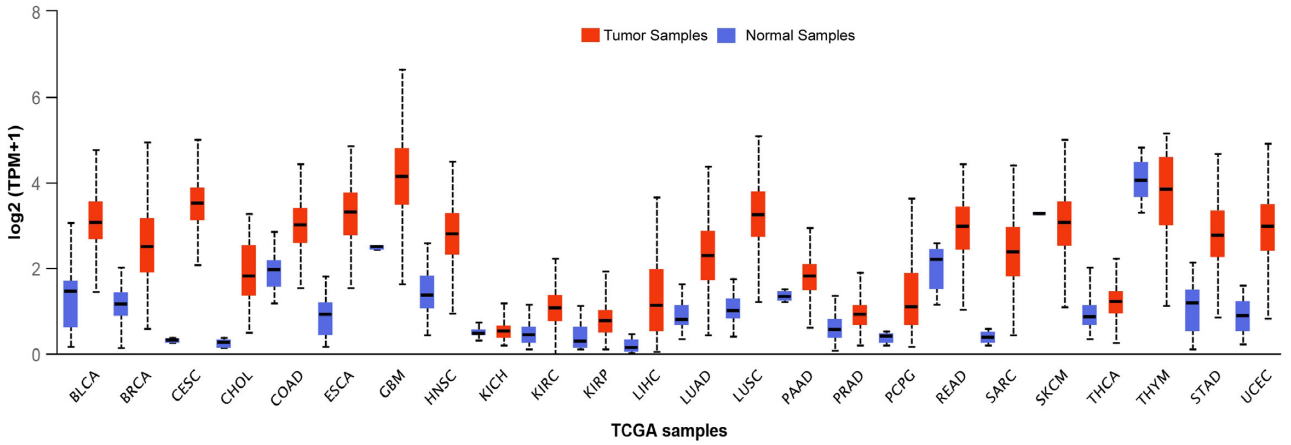


**FIGURE 3 |** Transcript levels of BLM across different types of tumor samples as well as their matched normal samples. The expression levels of BLM in different tumor samples along with their normal samples as analyzed using the TCGA datasets: BLCA (Urothelial Bladder Carcinoma), Breast Invasive Carcinoma (BRCA), CESC (Cervical Squamous Cell Carcinoma and Endocervical Adenocarcinoma), CHOL (Cholangiocarcinoma), COAD (Colon adenocarcinoma), ESCA (Esophageal carcinoma), GBM (Glioblastoma), HNSC (Head-Neck Squamous Cell Carcinoma), KICH (Kidney Chromophobe), KIRP (Kidney renal papillary cell carcinoma), LHC (Liver hepatocellular carcinoma), LUAD (Lung adenocarcinoma), LUSC (Lung squamous cell carcinoma), PAAD (Pancreatic adenocarcinoma), PCPG (Pheochromocytoma and Paraganglioma), READ (Rectum adenocarcinoma), SARC (Sarcoma), SKCM (Skin Cutaneous Melanoma), THCA (Thyroid Cancer), THYM (Thyroid carcinoma), STAD (Stomach adenocarcinoma), and UCEC (Uterine Corpus Endometrial Carcinoma) (Chandrashekar et al., 2017).

telomeric DNAs and accumulation of RPA at telomere clustering scaffolds (Min et al., 2019). Notably, through its interaction with the shelterin protein Telomeric Repeat Binding Factor 2 (TRF2), BLM facilitates efficient telomere extension (Lillard-Wetherell et al., 2004) that is dependent on the PML-mediated localization of the BTR complex in ALT cells (Loe et al., 2020). On the other hand, its association with Telomeric Repeat Factor 1 (TRF1) inhibits BLM unwinding activity of telomeric substrates (Lillard-Wetherell et al., 2004). Further, SLX4 interacting protein (SLX4IP), FANCM, and FANCD2 have been identified as critical regulators of ALT phenotype, limiting the deregulated activity of BLM (BTR complex) on the telomeres, thus ensuring appropriate balance of its resolution activities at the recombining telomeres (Root et al., 2016; Panier et al., 2019; Silva et al., 2019). Loss or inactivation of these regulators may promote growth of ATL cancer cells in a BLM-dependent manner.

Based on the importance of the helicase-dependent function of BLM, a selective small-molecule inhibitor, ML-216, was synthesized and was demonstrated to reduce proliferation and increase SCE in cellular studies on human cultured cells (Rosenthal et al., 2010; Nguyen et al., 2013). The inhibitor has also shown promise in inducing a significant amount of apoptosis in patient-derived primary myeloma cells having aberrant BLM expression as compared to normal bone marrow (Viziteu et al., 2016b). Based on these observations, a class of Isaindigotone derivatives has been found as a novel BLM inhibitor, attenuating DNA damage-dependent recruitment of BLM, thus affecting the HRR process (Yin et al., 2019). In addition, evaluation of quinazolinone derivatives led to the identification of another BLM helicase inhibitor that has shown promise in sensitizing the CRC cell in combination with chemotherapy drugs and PARP inhibitors (Wang et al., 2020). However, these inhibitors may lack specificity requiring further refinement before they can be used as anticancer agents.

## PERSPECTIVE

Nearly 100 years since the identification of the first DNA repair pathway, extensive research in this field has led to the identification of repair factors critical for the survival/fitness of both prokaryotes and eukaryotes. Thus, genetic ablation of these has been associated with various diseases in humans particularly cancer. Notably, several of these critical regulators of repair have been identified as a potential therapeutic target for cancers as well as other genetic abnormalities associated with DDR factors. One such example is that of the early response gene ATM whose role in mediating cancer resistance has been well-elucidated and thus several of the ATM inhibitors are under different phases of the clinical trials (Lavin and Yeo, 2020). BLM helicase has been implicated in various DNA transactions where it acts as a bonafide tumor suppressor gene. However, recent evidence shows BLM mRNA to be overexpressed in a plethora of cancers including colon, breast, and hematological cancers when compared with the normal samples (Alzahrani et al., 2020). Additionally, it has been postulated that non-sense SNP-mediated aberrant BLM activity or its high mRNA expression levels could confer genomic instability in humans, predisposing them to different cancer types (Alzahrani et al., 2020). From the above studies, it can be extrapolated that an optimal level of BLM is necessary to maintain genome stability. Both high and low levels or loss of BLM may lead to

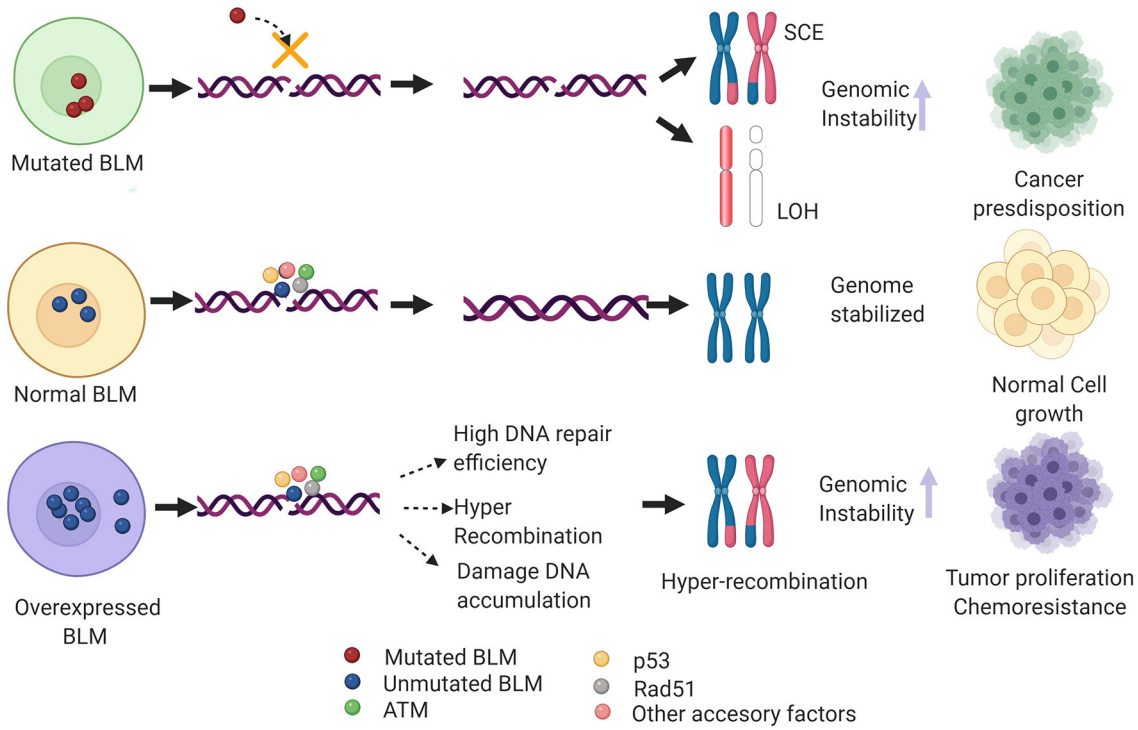


**FIGURE 4 |** Hypothetical model depicting the clinical phenotype of de-regulated BLM levels. In case of mutant *BLM* (as seen in BS patients), inefficient DNA repair via HRR induces formation of sister chromatid exchanges (SCEs) and loss of heterozygosity (LOH), and in turn alleviates genomic instability and thus predisposing to multiple types of cancers. On the other hand, overexpressed BLM mislocalizes to cytoplasm that may heighten the DNA repair capacity and cause hyper-recombination, thus promoting tumor growth and chemoresistance. Additionally, BLM overexpression may dislocate the RAD51 filaments, preventing efficient HRR pathway and eventually causing accumulation of DNA damage. Figure created with BioRender.com.

genomic instability and may eventually promote tumorigenesis (**Figure 4**).

These observations have provoked the question as to whether BLM helicase performs dual functions in different types of cancer. Perhaps a more pertinent query will also be—when does BLM act as a tumor suppressor and when does it convert into a proto-oncogene? In order to address these questions, it becomes imperative to investigate the molecular mechanisms involved in the de-regulation of the *BLM* gene specifically in the cancer cells to gain insights into its "dual role" in humans. The role of PTMs of BLM has been well-elucidated (Bohm and Bernstein, 2014). Ubiquitylation at specific residues of BLM has been found to regulate its stability in a cell cycle-specific manner (Wang et al., 2013; Kharat et al., 2016). However, the status of these PTMs as well as their effect on BLM turnover in the context of cancer progression has not yet been examined. It is also possible that a single or combination of yet undiscovered PTM on BLM acts like a trigger that converts BLM from a tumor suppressor into an oncogene. Recent evidence has also shed light on how BLM undergoes miRNA-mediated post-transcriptional control (Shuai et al., 2018; Chen Y. et al., 2019). It is possible that miRNA-mediated BLM turnover can be altered in specific types of cancers. In addition to this, there has been a growing interest in elucidating the importance of epigenetic regulators in BLM expression in cancers. A recent report identified that hypomethylation of BLM promoter at the CpG islands enhanced the BLM expression in colon cancer cells (Votino et al., 2017). This resulted in high levels of BLM expression, which mis-localized to the cytoplasm due to which a heightened DDR was seen in the tumor samples (Votino et al., 2017). Interaction studies have shown that BLM has functional interactions with two of the chromatin modifiers CAF1 and RAD54 during DDR (Jiao et al., 2004; Srivastava et al., 2009). Whether these interactions also have an effect on the BLM function in cancer needs to be explored further. Deregulation of tumor suppressor and the high risk of cancer development have been well-documented (Sherr, 2004; Giancotti, 2014). Many of these tumor suppressors also function as transcriptional regulators and may inter-regulate each other in a coordinated or backhanded way (el-Deiry et al., 1993; Liu et al., 2008; De Luca et al., 2011). A few of the major tumor suppressors like BRCA1 and RB may impact or regulate BLM or could be a common target of tumor suppressors.

The final pertinent question will be whether other mechanisms exist in cancer cells that allow BLM to act as an oncogene under certain conditions during cancer progression, whether these mechanisms act in conjunction with each other, or whether there are any specific networks that aid BLM to act

as a double-edged sword. Exploration studies on these lines will allow a better understanding of the rewiring of BLM, and its Janus-like character may have important implications in the study of neoplastic transformation and cancer development.

## AUTHOR CONTRIBUTIONS

SS conceptualized the review and gave overall inputs. EK and RA wrote the drafts and generated the figures. EK, RA, and SS together generated the final version. All authors contributed to the article and approved the submitted version.

## ACKNOWLEDGMENTS

SS acknowledges National Institute of Immunology (NII) core funds; the Department of Biotechnology (DBT), India (BT/MED/30/SP11263/2015, BT/PR23545/BRB/10/1593/2017, and BT/PR27681/GET/119/269/2018); the Council of Scientific and Industrial Research (CSIR), India [37(1699)/17/EMR-11]; the Science and Engineering Research Board (SERB), India (EMR/2017/000541); and J. C. Bose Fellowship (JCB/2018/000013) for financial assistance. EK acknowledges DST Inspire Faculty Fellowship (DST/INSPIRE/04/2017/000088) for support.

## REFERENCES

Ahamad, N., Khan, S., Mahdi, A. T. A., and Xu, Y. J. (2021). Checkpoint functions of RecQ helicases at perturbed DNA replication fork. *Curr. Genet.* doi: 10.1007/s00294-020-01147-y

Alzahrani, F. A., Ahmed, F., Sharma, M., Rehan, M., Mahfuz, M., Baeshen, M. N., et al. (2020). Investigating the pathogenic SNPs in BLM helicase and their biological consequences by computational approach. *Sci. Rep.* 10:12377. doi: 10.1038/s41598-020-69033-8

Antczak, A., Kluzniak, W., Wokolorczyk, D., Kashyap, A., Jakubowska, A., Gronwald, J., et al. (2013). A common nonsense mutation of the BLM gene and prostate cancer risk and survival. *Gene* 532, 173–176. doi: 10.1016/j.gene.2013.09.079

Arora, A., Abdel-Fatah, T. M., Agarwal, D., Doherty, R., Moseley, P. M., Aleskandarany, M. A., et al. (2015). Transcriptomic and protein expression analysis reveals clinicopathological significance of bloom syndrome helicase (BLM) in breast cancer. *Mol. Cancer Ther.* 14, 1057–1065. doi: 10.1158/1535-7163.MCT-14-0939

Babbe, H., Chester, N., Leder, P., and Reizis, B. (2007). The Bloom's syndrome helicase is critical for development and function of the alphabeta T-cell lineage. *Mol. Cell. Biol.* 27, 1947–1959. doi: 10.1128/MCB.01402-06

Babbe, H., McMenamin, J., Hobeika, E., Wang, J., Rodig, S. J., Reth, M., et al. (2009). Genomic instability resulting from Blm deficiency compromises development, maintenance, and function of the B cell lineage. *J. Immunol.* 182, 347–360. doi: 10.4049/jimmunol.182.1.347

Bachrati, C. Z., and Hickson, I. D. (2003). RecQ helicases: suppressors of tumorigenesis and premature aging. *Biochem. J.* 374(Pt 3), 577–606. doi: 10.1042/bj20030491

Bahr, A., De Graeve, F., Kedinger, C., and Chatton, B. (1998). Point mutations causing Bloom's syndrome abolish ATPase and DNA helicase activities of the BLM protein. *Oncogene* 17, 2565–2571. doi: 10.1038/sj.onc.1202389

Barefield, C., and Karlseder, J. (2012). The BLM helicase contributes to telomere maintenance through processing of late-replicating intermediate structures. *Nucleic Acids Res.* 40, 7358–7367. doi: 10.1093/nar/gks407

Barnum, K. J., and O'Connell, M. J. (2014). Cell cycle regulation by checkpoints. *Methods Mol. Biol.* 1170, 29–40. doi: 10.1007/978-1-4939-0888-2_2

Beamish, H., Kedar, P., Kaneko, H., Chen, P., Fukao, T., Peng, C., et al. (2002). Functional link between BLM defective in Bloom's syndrome and the ataxia-telangiectasia-mutated protein, ATM. *J. Biol. Chem.* 277, 30515–30523. doi: 10.1074/jbc.M203801200

Bennett, R. J., and Keck, J. L. (2004). Structure and function of RecQ DNA helicases. *Crit. Rev. Biochem. Mol. Biol.* 39, 79–97. doi: 10.1080/10409230490460756

Bhattacharyya, S., Keirsey, J., Russell, B., Kavecansky, J., Lillard-Wetherell, K., Tahmaseb, K., et al. (2009). Telomerase-associated protein 1, HSP90, and topoisomerase IIalpha associate directly with the BLM helicase in immortalized cells using ALT and modulate its helicase activity using telomeric DNA substrates. *J. Biol. Chem.* 284, 14966–14977. doi: 10.1074/jbc.M900195200

Bischof, O., Kim, S. H., Irving, J., Beresten, S., Ellis, N. A., and Campisi, J. (2001). Regulation and localization of the Bloom syndrome protein in response to DNA damage. *J. Cell Biol.* 153, 367–380. doi: 10.1083/jcb.153.2.367

Blackford, A. N., Nieminuszczy, J., Schwab, R. A., Galanty, Y., Jackson, S. P., and Niedzwiedz, W. (2015). TopBP1 interacts with BLM to maintain genome stability but is dispensable for preventing BLM degradation. *Mol. Cell* 57, 1133–1141. doi: 10.1016/j.molcel.2015.02.012

Bloom, D. (1954). Congenital telangiectatic erythema resembling lupus erythematosus in dwarfs; probably a syndrome entity. *AMA. Am. J. Dis. Child* 88, 754–758. doi: 10.1001/archpedi.1954.02050100756008

Bochman, M. L. (2014). Roles of DNA helicases in the maintenance of genome integrity. *Mol. Cell Oncol.* 1:e963429. doi: 10.4161/23723548.2014.963429

Bohm, S., and Bernstein, K. A. (2014). The role of post-translational modifications in fine-tuning BLM helicase function during DNA repair. *DNA Repair* 22, 123–132. doi: 10.1016/j.dnarep.2014.07.007

Bononi, A., Goto, K., Ak, G., Yoshikawa, Y., Emi, M., Pastorino, S., et al. (2020). Heterozygous germline BLM mutations increase susceptibility to asbestos and mesothelioma. *Proc. Natl. Acad. Sci. U.S.A.* 117, 33466–33473. doi: 10.1073/pnas.2019652117

Brosh, R. M. Jr., Li, J. L., Kenny, M. K., Karow, J. K., Cooper, M. P., Kureekattil, R. P., et al. (2000). Replication protein A physically interacts with the Bloom's syndrome protein and stimulates its helicase activity. *J. Biol. Chem.* 275, 23500–23508. doi: 10.1074/jbc.M001557200

Brosh, R. M. Jr., and Matson, S. W. (2020). History of DNA helicases. *Genes* 11:255. doi: 10.3390/genes11030255

Bryan, T. M., Englezou, A., Dalla-Pozza, L., Dunham, M. A., and Reddel, R. R. (1997). Evidence for an alternative mechanism for maintaining telomere length in human tumors and tumor-derived cell lines. *Nat. Med.* 3, 1271–1274. doi: 10.1038/nm1197-1271

Bugreev, D. V., Yu, X., Egelman, E. H., and Mazin, A. V. (2007). Novel pro- and anti-recombination activities of the Bloom's syndrome helicase. *Genes Dev.* 21, 3085–3094. doi: 10.1101/gad.1609007

Byrd, A. K., and Raney, K. D. (2012). Superfamily 2 helicases. *Front. Biosci.* 17, 2070–2088. doi: 10.2741/4038

Bythell-Douglas, R., and Deans, A. J. (2021). A structural guide to the bloom syndrome complex. *Structure* 29, 99–113. doi: 10.1016/j.str.2020.11.020

Chaganti, R. S., Schonberg, S., and German, J. (1974). A manyfold increase in sister chromatid exchanges in Bloom's syndrome lymphocytes. *Proc. Natl. Acad. Sci. U.S.A.* 71, 4508–4512. doi: 10.1073/pnas.71.11.4508

Chan, K. L., North, P. S., and Hickson, I. D. (2007). BLM is required for faithful chromosome segregation and its localization defines a class of ultrafine anaphase bridges. *EMBO J.* 26, 3397–3409. doi: 10.1038/sj.emboj.7601777

Chandra, S., Priyadarshini, R., Madhavan, V., Tikoo, S., Hussain, M., Mudgal, R., et al. (2013). Enhancement of c-Myc degradation by BLM helicase leads to delayed tumor initiation. *J. Cell Sci.* 126(Pt 16), 3782–3795. doi: 10.1242/jcs.124719

Chandrashekar, D. S., Bashel, B., Balasubramanya, S. A. H., Creighton, C. J., Ponce-Rodriguez, I., Chakravarthi, B., et al. (2017). UALCAN: a portal for facilitating tumor subgroup gene expression and survival analyses. *Neoplasia* 19, 649–658. doi: 10.1016/j.neo.2017.05.002

Chen, K., Xu, H., and Zhao, J. (2019). Bloom syndrome protein activates AKT and PRAS40 in prostate cancer cells. *Oxid. Med. Cell. Longev.* 2019:3685817. doi: 10.1155/2019/3685817

Chen, Y., Zhao, J., Duan, Z., Gong, T., Chen, W., Wang, S., et al. (2019). miR27b3p and miR607 cooperatively regulate BLM gene expression by directly targeting the 3'UTR in PC3 cells. *Mol. Med. Rep.* 19, 4819–4831. doi: 10.3892/mmr.2019.10135

Chester, N., Babbe, H., Pinkas, J., Manning, C., and Leder, P. (2006). Mutation of the murine Bloom's syndrome gene produces global genome destabilization. *Mol. Cell. Biol.* 26, 6713–6726. doi: 10.1128/MCB.00296-06

Clikeman, J. A., Khalsa, G. J., Barton, S. L., and Nickoloff, J. A. (2001). Homologous recombinational repair of double-strand breaks in yeast is enhanced by *MAT* heterozygosity through yKU-dependent and -independent mechanisms. *Genetics* 157, 579–589.

Cox, R. L., Hofley, C. M., Tatapudy, P., Patel, R. K., Dayani, Y., Betcher, M., et al. (2019). Functional conservation of RecQ helicase BLM between humans and *Drosophila melanogaster*. *Sci. Rep.* 9:17527. doi: 10.1038/s41598-019-54101-5

Croteau, D. L., Popuri, V., Opresko, P. L., and Bohr, V. A. (2014). Human RecQ helicases in DNA repair, recombination, and replication. *Annu. Rev. Biochem.* 83, 519–552. doi: 10.1146/annurev-biochem-060713-035428

Cunniff, C., Bassetti, J. A., and Ellis, N. A. (2017). Bloom's syndrome: clinical spectrum, molecular pathogenesis, and cancer predisposition. *Mol. Syndromol.* 8, 4–23. doi: 10.1159/000452082

Daley, J. M., Chiba, T., Xue, X., Niu, H., and Sung, P. (2014). Multifaceted role of the Topo IIIalpha-RMI1-RMI2 complex and DNA2 in the BLM-dependent pathway of DNA break end resection. *Nucleic Acids Res.* 42, 11083–11091. doi: 10.1093/nar/gku803

Datta, A., Dhar, S., Awate, S., and Brosh, R. M. Jr. (2021). Synthetic lethal interactions of RECQ helicases. *Trends Cancer* 7, 146–161. doi: 10.1016/j.trecan.2020.09.001

Davalos, A. R., and Campisi, J. (2003). Bloom syndrome cells undergo p53-dependent apoptosis and delayed assembly of BRCA1 and NBS1 repair complexes at stalled replication forks. *J. Cell Biol.* 162, 1197–1209. doi: 10.1083/jcb.200304016

Davari, P., Hebert, J. L., Albertson, D. G., Huey, B., Roy, R., Mancianti, M. L., et al. (2010). Loss of Blm enhances basal cell carcinoma and rhabdomyosarcoma tumorigenesis in Ptch1+/- mice. *Carcinogenesis* 31, 968–973. doi: 10.1093/carcin/bgp309

Davies, S. L., North, P. S., Dart, A., Lakin, N. D., and Hickson, I. D. (2004). Phosphorylation of the Bloom's syndrome helicase and its role in recovery from S-phase arrest. *Mol. Cell. Biol.* 24, 1279–1291. doi: 10.1128/MCB.24.3.1279-1291.2004

De Luca, P., Moiola, C. P., Zalazar, F., Gardner, K., Vazquez, E. S., and De Siervi, A. (2013). BRCA1 and p53 regulate critical prostate cancer pathways. *Prostate Cancer Prostatic Dis.* 16, 233–238. doi: 10.1038/pcan.2013.12

De Luca, P., Vazquez, E. S., Moiola, C. P., Zalazar, F., Cotignola, J., Gueron, G., et al. (2011). BRCA1 loss induces GADD153-mediated doxorubicin resistance in prostate cancer. *Mol. Cancer Res.* 9, 1078–1090. doi: 10.1158/1541-7786.MCR-11-0155

de Voer, R. M., Hahn, M. M., Mensenkamp, A. R., Hoischen, A., Gilissen, C., Henkes, A., et al. (2015). Deleterious germline BLM mutations and the risk for early-onset colorectal cancer. *Sci. Rep.* 5:14060. doi: 10.1038/srep14060

De, S., Kumari, J., Mudgal, R., Modi, P., Gupta, S., Futami, K., et al. (2012). RECQL4 is essential for the transport of p53 to mitochondria in normal human cells in the absence of exogenous stress. *J. Cell Sci.* 125(Pt 10), 2509–2522. doi: 10.1242/jcs.101501

Draskovic, I., Arnoult, N., Steiner, V., Bacchetti, S., Lomonte, P., and Londono-Vallejo, A. (2009). Probing PML body function in ALT cells reveals spatiotemporal requirements for telomere recombination. *Proc. Natl. Acad. Sci. U.S.A.* 106, 15726–15731. doi: 10.1073/pnas.0907689106

Drosopoulos, W. C., Kosiyatrakul, S. T., and Schildkraut, C. L. (2015). BLM helicase facilitates telomere replication during leading strand synthesis of telomeres. *J. Cell. Biol.* 210, 191–208. doi: 10.1083/jcb.201410061

Dutertre, S., Ababou, M., Onclercq, R., Delic, J., Chatton, B., Jaulin, C., et al. (2000). Cell cycle regulation of the endogenous wild type Bloom's syndrome DNA helicase. *Oncogene* 19, 2731–2738. doi: 10.1038/sj.onc.1203595

Eladad, S., Ye, T. Z., Hu, P., Leversha, M., Beresten, S., Matunis, M. J., et al. (2005). Intra-nuclear trafficking of the BLM helicase to DNA damage-induced foci is regulated by SUMO modification. *Hum. Mol. Genet.* 14, 1351–1365. doi: 10.1093/hmg/ddi145

el-Deiry, W. S., Tokino, T., Velculescu, V. E., Levy, D. B., Parsons, R., Trent, J. M., et al. (1993). WAF1, a potential mediator of p53 tumor suppression. *Cell* 75, 817–825. doi: 10.1016/0092-8674(93)90500-P

Ellis, N. A., Ciocci, S., Proytcheva, M., Lennon, D., Groden, J., and German, J. (1998). The Ashkenazic Jewish Bloom syndrome mutation blmAsh is present in non-Jewish Americans of Spanish ancestry. *Am. J. Hum. Genet.* 63, 1685–1693. doi: 10.1086/302167

Ellis, N. A., Groden, J., Ye, T. Z., Straughen, J., Lennon, D. J., Ciocci, S., et al. (1995a). The Bloom's syndrome gene product is homologous to RecQ helicases. *Cell* 83, 655–666. doi: 10.1016/0092-8674(95)90105-1

Ellis, N. A., Lennon, D. J., Proytcheva, M., Alhadeff, B., Henderson, E. E., and German, J. (1995b). Somatic intragenic recombination within the mutated locus BLM can correct the high sister-chromatid exchange phenotype of Bloom syndrome cells. *Am. J. Hum. Genet.* 57, 1019–1027.

Ellis, N. A., Sander, M., Harris, C. C., and Bohr, V. A. (2008). Bloom's syndrome workshop focuses on the functional specificities of RecQ helicases. *Mech. Ageing Dev.* 129, 681–691. doi: 10.1016/j.mad.2008.09.005

Gangloff, S., McDonald, J. P., Bendixen, C., Arthur, L., and Rothstein, R. (1994). The yeast type I topoisomerase Top3 interacts with Sgs1, a DNA helicase homolog: a potential eukaryotic reverse gyrase. *Mol. Cell. Biol.* 14, 8391–8398. doi: 10.1128/MCB.14.12.8391

Gaymes, T. J., North, P. S., Brady, N., Hickson, I. D., Mufti, G. J., and Rassool, F. V. (2002). Increased error-prone non homologous DNA end-joining–a proposed mechanism of chromosomal instability in Bloom's syndrome. *Oncogene* 21, 2525–2533. doi: 10.1038/sj.onc.1205331

German, J. (1993). Bloom syndrome: a mendelian prototype of somatic mutational disease. *Medicine* 72, 393–406. doi: 10.1097/00005792-199311000-00003

German, J., Crippa, L. P., and Bloom, D. (1974). Bloom's syndrome. III. Analysis of the chromosome aberration characteristic of this disorder. *Chromosoma* 48, 361–366. doi: 10.1007/BF00290993

German, J., and Passarge, E. (1989). Bloom's syndrome. XII. Report from the Registry for 1987. *Clin. Genet.* 35, 57–69. doi: 10.1111/j.1399-0004.1989.tb02905.x

German, J., Sanz, M. M., Ciocci, S., Ye, T. Z., and Ellis, N. A. (2007). Syndrome-causing mutations of the BLM gene in persons in the Bloom's Syndrome Registry. *Hum. Mutat.* 28, 743–753. doi: 10.1002/humu.20501

Giancotti, F. G. (2014). Deregulation of cell signaling in cancer. *FEBS Lett.* 588, 2558–2570. doi: 10.1016/j.febslet.2014.02.005

Giglia-Mari, G., Zotter, A., and Vermeulen, W. (2011). DNA damage response. *Cold Spring Harb. Perspect. Biol.* 3:a000745. doi: 10.1101/cshperspect.a000745

Goss, K. H., Risinger, M. A., Kordich, J. J., Sanz, M. M., Straughen, J. E., Slovek, L. E., et al. (2002). Enhanced tumor formation in mice heterozygous for Blm mutation. *Science* 297, 2051–2053. doi: 10.1126/science.1074340

Gratia, M., Rodero, M. P., Conrad, C., Bou Samra, E., Maurin, M., Rice, G. I., et al. (2019). Bloom syndrome protein restrains innate immune sensing of micronuclei by cGAS. *J. Exp. Med.* 216, 1199–1213. doi: 10.1084/jem.20181329

Grierson, P. M., Acharya, S., and Groden, J. (2013). Collaborating functions of BLM and DNA topoisomerase I in regulating human rDNA transcription. *Mutat. Res.* 743–744, 89–96. doi: 10.1016/j.mrfmmm.2012.12.002

Groden, J., and German, J. (1992). Bloom's syndrome. XVIII. Hypermutability at a tandem-repeat locus. *Hum. Genet.* 90, 360–367. doi: 10.1007/BF00220459

Gruber, S. B., Ellis, N. A., Scott, K. K., Almog, R., Kolachana, P., Bonner, J. D., et al. (2002). BLM heterozygosity and the risk of colorectal cancer. *Science* 297, 2013. doi: 10.1126/science.1074399

Guo, R. B., Rigolet, P., Ren, H., Zhang, B., Zhang, X. D., Dou, S. X., et al. (2007). Structural and functional analyses of disease-causing missense mutations in Bloom syndrome protein. *Nucleic Acids Res.* 35, 6297–6310. doi: 10.1093/nar/gkm536

Guo, R. B., Rigolet, P., Zargarian, L., Fermandjian, S., and Xi, X. G. (2005). Structural and functional characterizations reveal the importance of a zinc binding domain in Bloom's syndrome helicase. *Nucleic Acids Res.* 33, 3109–3124. doi: 10.1093/nar/gki619

Gupta, S., De, S., Srivastava, V., Hussain, M., Kumari, J., Muniyappa, K., et al. (2014). RECQL4 and p53 potentiate the activity of polymerase gamma and maintain the integrity of the human mitochondrial genome. *Carcinogenesis* 35, 34–45. doi: 10.1093/carcin/bgt315

Harmon, F. G., DiGate, R. J., and Kowalczykowski, S. C. (1999). RecQ helicase and topoisomerase III comprise a novel DNA strand passage function: a conserved mechanism for control of DNA recombination. *Mol. Cell* 3, 611–620. doi: 10.1016/S1097-2765(00)80354-8

Hartung, F., and Puchta, H. (2006). The RecQ gene family in plants. *J. Plant Physiol.* 163, 287–296. doi: 10.1016/j.jplph.2005.10.013

Hu, P., Beresten, S. F., van Brabant, A. J., Ye, T. Z., Pandolfi, P. P., Johnson, F. B., et al. (2001). Evidence for BLM and Topoisomerase IIIalpha interaction in genomic stability. *Hum. Mol. Genet.* 10, 1287–1298. doi: 10.1093/hmg/10.12.1287

Hutteroth, T. H., Litwin, S. D., and German, J. (1975). Abnormal immune responses of Bloom's syndrome lymphocytes *in vitro*. *J. Clin. Invest.* 56, 1–7. doi: 10.1172/JCI108058

Jasin, M., and Rothstein, R. (2013). Repair of strand breaks by homologous recombination. *Cold Spring Harb. Perspect. Biol.* 5:a012740. doi: 10.1101/cshperspect.a012740

Jiao, R., Bachrati, C. Z., Pedrazzi, G., Kuster, P., Petkovic, M., Li, J. L., et al. (2004). Physical and functional interaction between the Bloom's syndrome gene product and the largest subunit of chromatin assembly factor 1. *Mol. Cell. Biol.* 24, 4710–4719. doi: 10.1128/MCB.24.11.4710-4719.2004

Johnson, F. B., Lombard, D. B., Neff, N. F., Mastrangelo, M. A., Dewolf, W., Ellis, N. A., et al. (2000). Association of the Bloom syndrome protein with topoisomerase IIIalpha in somatic and meiotic cells. *Cancer Res.* 60, 1162–1167.

Kaneko, H., Inoue, R., Yamada, Y., Sukegawa, K., Fukao, T., Tashita, H., et al. (1996). Microsatellite instability in B-cell lymphoma originating from Bloom syndrome. *Int. J. Cancer* 69, 480–483. doi: 10.1002/(SICI)1097-0215(19961220)69:6<480::AID-IJC11>3.0.CO;2-5

Kaneko, H., Orii, K. O., Matsui, E., Shimozawa, N., Fukao, T., Matsumoto, T., et al. (1997). BLM (the causative gene of Bloom syndrome) protein translocation into the nucleus by a nuclear localization signal. *Biochem. Biophys. Res. Commun.* 240, 348–353. doi: 10.1006/bbrc.1997.7648

Kang, D., Lee, S., Ryu, K. S., Cheong, H. K., Kim, E. H., and Park, C. J. (2018). Interaction of replication protein A with two acidic peptides from human Bloom syndrome protein. *FEBS Lett.* 592, 547–558. doi: 10.1002/1873-3468.12992

Karmakar, P., Seki, M., Kanamori, M., Hashiguchi, K., Ohtsuki, M., Murata, E., et al. (2006). BLM is an early responder to DNA double-strand breaks. *Biochem. Biophys. Res. Commun.* 348, 62–69. doi: 10.1016/j.bbrc.2006.07.037

Kaur, S., Modi, P., Srivastava, V., Mudgal, R., Tikoo, S., Arora, P., et al. (2010). Chk1-dependent constitutive phosphorylation of BLM helicase at serine 646 decreases after DNA damage. *Mol. Cancer Res.* 8, 1234–1247. doi: 10.1158/1541-7786.MCR-10-0233

Khanna, K. K., and Jackson, S. P. (2001). DNA double-strand breaks: signaling, repair and the cancer connection. *Nat. Genet.* 27, 247–254. doi: 10.1038/85798

Kharat, S. S., Tripathi, V., Damodaran, A. P., Priyadarshini, R., Chandra, S., Tikoo, S., et al. (2016). Mitotic phosphorylation of Bloom helicase at Thr182 is required for its proteasomal degradation and maintenance of chromosomal stability. *Oncogene* 35, 1025–1038. doi: 10.1038/onc.2015.157

Kluzniak, W., Wokolorczyk, D., Rusak, B., Huzarski, T., Kashyap, A., Stempa, K., et al. (2019). Inherited variants in BLM and the risk and clinical characteristics of breast cancer. *Cancers* 11:1548. doi: 10.3390/cancers11101548

Kondo, N., Motoyoshi, F., Mori, S., Kuwabara, N., Orii, T., and German, J. (1992). Long-term study of the immunodeficiency of Bloom's syndrome. *Acta Paediatr.* 81, 86–90. doi: 10.1111/j.1651-2227.1992.tb12088.x

Kwakman, R., de Cuba, E. M., de Winter, J. P., de Hingh, I. H., Delis-van Diemen, P. M., Tijssen, M., et al. (2015). Tailoring heated intraperitoneal mitomycin C for peritoneal metastases originating from colorectal carcinoma: a translational approach to improve survival. *Br. J. Cancer* 112, 851–856. doi: 10.1038/bjc.2015.18

Langland, G., Kordich, J., Creaney, J., Goss, K. H., Lillard-Wetherell, K., Bebenek, K., et al. (2001). The Bloom's syndrome protein (BLM) interacts with MLH1 but is not required for DNA mismatch repair. *J. Biol. Chem.* 276, 30031–30035. doi: 10.1074/jbc.M009664200

Langlois, R. G., Bigbee, W. L., Jensen, R. H., and German, J. (1989). Evidence for increased *in vivo* mutation and somatic recombination in Bloom's syndrome. *Proc. Natl. Acad. Sci. U.S.A.* 86, 670–674. doi: 10.1073/pnas.86.2.670

Lao, V. V., Welcsh, P., Luo, Y., Carter, K. T., Dzieciatkowski, S., Dintzis, S., et al. (2013). Altered RECQ helicase expression in sporadic primary colorectal cancers. *Transl. Oncol.* 6, 458–469. doi: 10.1593/tlo.13238

Larsen, N. B., and Hickson, I. D. (2013). RecQ helicases: conserved guardians of genomic integrity. *Adv. Exp. Med. Biol.* 767, 161–184. doi: 10.1007/978-1-4614-5037-5_8

Lavin, M. F., and Yeo, A. J. (2020). Clinical potential of ATM inhibitors. *Mutat Res.* 821, 111695. doi: 10.1016/j.mrfmmm.2020.111695

Ledet, E. M., Antonarakis, E. S., Isaacs, W. B., Lotan, T. L., Pritchard, C., and Sartor, A. O. (2020). Germline BLM mutations and metastatic prostate cancer. *Prostate* 80, 235–237. doi: 10.1002/pros.23924

Li, L., Eng, C., Desnick, R. J., German, J., and Ellis, N. A. (1998). Carrier frequency of the Bloom syndrome blmAsh mutation in the Ashkenazi Jewish population. *Mol. Genet. Metab.* 64, 286–290. doi: 10.1006/mgme.1998.2733

Lillard-Wetherell, K., Machwe, A., Langland, G. T., Combs, K. A., Behbehani, G. K., Schonberg, S. A., et al. (2004). Association and regulation of the BLM helicase by the telomere proteins TRF1 and TRF2. *Hum. Mol. Genet.* 13, 1919–1932. doi: 10.1093/hmg/ddh193

Liu, Y., El-Naggar, S., Clem, B., Chesney, J., and Dean, D. C. (2008). The Rb/E2F pathway and Ras activation regulate RecQ helicase gene expression. *Biochem. J.* 412, 299–306. doi: 10.1042/BJ20070975

Liu, Z., Macias, M. J., Bottomley, M. J., Stier, G., Linge, J. P., Nilges, M., et al. (1999). The three-dimensional structure of the HRDC domain and implications for the Werner and Bloom syndrome proteins. *Structure* 7, 1557–1566. doi: 10.1016/S0969-2126(00)88346-X

Loe, T. K., Li, J. S. Z., Zhang, Y., Azeroglu, B., Boddy, M. N., and Denchi, E. L. (2020). Telomere length heterogeneity in ALT cells is maintained by PML-dependent localization of the BTR complex to telomeres. *Genes Dev.* 34, 650–662. doi: 10.1101/gad.333963.119

Lonn, U., Lonn, S., Nylen, U., Winblad, G., and German, J. (1990). An abnormal profile of DNA replication intermediates in Bloom's syndrome. *Cancer Res.* 50, 3141–3145.

Luo, G., Santoro, I. M., McDaniel, L. D., Nishijima, I., Mills, M., Youssoufian, H., et al. (2000). Cancer predisposition caused by elevated mitotic recombination in Bloom mice. *Nat. Genet.* 26, 424–429. doi: 10.1038/82548

Mao, F. J., Sidorova, J. M., Lauper, J. M., Emond, M. J., and Monnat, R. J. (2010). The human WRN and BLM RecQ helicases differentially regulate cell proliferation and survival after chemotherapeutic DNA damage. *Cancer Res.* 70, 6548–6555. doi: 10.1158/0008-5472.CAN-10-0475

Martin, C. A., Sarlos, K., Logan, C. V., Thakur, R. S., Parry, D. A., Bizard, A. H., et al. (2018). Mutations in TOP3A cause a bloom syndrome-like disorder. *Am. J. Hum. Genet.* 103:456. doi: 10.1016/j.ajhg.2018.08.012

Matsumoto, T., Shimamoto, A., Goto, M., and Furuichi, Y. (1997). Impaired nuclear localization of defective DNA helicases in Werner's syndrome. *Nat. Genet.* 16, 335–336. doi: 10.1038/ng0897-335

McDaniel, L. D., Chester, N., Watson, M., Borowsky, A. D., Leder, P., and Schultz, R. A. (2003). Chromosome instability and tumor predisposition inversely correlate with BLM protein levels. *DNA Repair* 2, 1387–1404. doi: 10.1016/j.dnarep.2003.08.006

McIlhatton, M. A., Murnan, K., Carson, D., Boivin, G. P., Croce, C. M., and Groden, J. (2015). Genetic manipulation of homologous recombination *in vivo* attenuates intestinal tumorigenesis. *Cancer Prev. Res.* 8, 650–656. doi: 10.1158/1940-6207.CAPR-15-0001-T

Mimitou, E. P., and Symington, L. S. (2009). Nucleases and helicases take center stage in homologous recombination. *Trends Biochem. Sci.* 34, 264–272. doi: 10.1016/j.tibs.2009.01.010

Min, J., Wright, W. E., and Shay, J. W. (2019). Clustered telomeres in phase-separated nuclear condensates engage mitotic DNA synthesis through BLM and RAD52. *Genes Dev.* 33, 814–827. doi: 10.1101/gad.324905.119

Moder, M., Velimezi, G., Owusu, M., Mazouzi, A., Wiedner, M., Ferreira da Silva, J., et al. (2017). Parallel genome-wide screens identify synthetic viable interactions between the BLM helicase complex and Fanconi anemia. *Nat. Commun.* 8:1238. doi: 10.1038/s41467-017-01439-x

Montenegro, M. M., Quaio, C. R., Palmeira, P., Gasparini, Y., Rangel-Santos, A., Damasceno, J., et al. (2020). Gene expression profile suggesting immunological dysregulation in two Brazilian Bloom's syndrome cases. *Mol. Genet. Genomic Med.* 8:e1133. doi: 10.1002/mgg3.1133

Morozov, V., Mushegian, A. R., Koonin, E. V., and Bork, P. (1997). A putative nucleic acid-binding domain in Bloom's and Werner's syndrome helicases. *Trends Biochem. Sci.* 22, 417–418. doi: 10.1016/S0968-0004(97)01128-6

Newman, J. A., and Gileadi, O. (2020). RecQ helicases in DNA repair and cancer targets. *Essays Biochem.* 64, 819–830. doi: 10.1042/EBC20200012

Nguyen, G. H., Dexheimer, T. S., Rosenthal, A. S., Chu, W. K., Singh, D. K., Mosedale, G., et al. (2013). A small molecule inhibitor of the BLM helicase modulates chromosome stability in human cells. *Chem. Biol.* 20, 55–62. doi: 10.1016/j.chembiol.2012.10.016

Nguyen, G. H., Tang, W., Robles, A. I., Beyer, R. P., Gray, L. T., Welsh, J. A., et al. (2014). Regulation of gene expression by the BLM helicase correlates with the presence of G-quadruplex DNA motifs. *Proc. Natl. Acad. Sci. U.S.A.* 111, 9905–9910. doi: 10.1073/pnas.1404807111

Nimonkar, A. V., Genschel, J., Kinoshita, E., Polaczek, P., Campbell, J. L., Wyman, C., et al. (2011). BLM-DNA2-RPA-MRN and EXO1-BLM-RPA-MRN constitute two DNA end resection machineries for human DNA break repair. *Genes Dev.* 25, 350–362. doi: 10.1101/gad.2003811

Ouyang, K. J., Woo, L. L., and Ellis, N. A. (2008). Homologous recombination and maintenance of genome integrity: cancer and aging through the prism of human RecQ helicases. *Mech. Ageing Dev.* 129, 425–440. doi: 10.1016/j.mad.2008.03.003

Ouyang, K. J., Woo, L. L., Zhu, J., Huo, D., Matunis, M. J., and Ellis, N. A. (2009). SUMO modification regulates BLM and RAD51 interaction at damaged replication forks. *PLoS Biol.* 7:e1000252. doi: 10.1371/journal.pbio.1000252

Ouyang, K. J., Yagle, M. K., Matunis, M. J., and Ellis, N. A. (2013). BLM SUMOylation regulates ssDNA accumulation at stalled replication forks. *Front. Genet.* 4:167. doi: 10.3389/fgene.2013.00167

Panier, S., Maric, M., Hewitt, G., Mason-Osann, E., Gali, H., Dai, A., et al. (2019). SLX4IP antagonizes promiscuous BLM activity during ALT maintenance. *Mol. Cell.* 76, 27–43 e11. doi: 10.1016/j.molcel.2019.07.010

Pedrazzi, G., Perrera, C., Blaser, H., Kuster, P., Marra, G., Davies, S. L., et al. (2001). Direct association of Bloom's syndrome gene product with the human mismatch repair protein MLH1. *Nucleic Acids Res.* 29, 4378–4386. doi: 10.1093/nar/29.21.4378

Petsalaki, E., Dandoulaki, M., Morrice, N., and Zachos, G. (2014). Chk1 protects against chromatin bridges by constitutively phosphorylating BLM serine 502 to inhibit BLM degradation. *J. Cell Sci.* 127(Pt 18), 3902–3908. doi: 10.1242/jcs.155176

Priyadarshini, R., Hussain, M., Attri, P., Kaur, E., Tripathi, V., Priya, S., et al. (2018). BLM potentiates c-Jun degradation and alters its function as an oncogenic transcription factor. *Cell. Rep.* 24, 947–961 e947. doi: 10.1016/j.celrep.2018.06.101

Prokofyeva, D., Bogdanova, N., Dubrowinskaja, N., Bermisheva, M., Takhirova, Z., Antonenkova, N., et al. (2013). Nonsense mutation p.Q548X in BLM, the gene mutated in Bloom's syndrome, is associated with breast cancer in Slavic populations. *Breast Cancer Res. Treat.* 137, 533–539. doi: 10.1007/s10549-012-2357-1

Qian, X., Feng, S., Xie, D., Feng, D., Jiang, Y., and Zhang, X. (2017). RecQ helicase BLM regulates prostate cancer cell proliferation and apoptosis. *Oncol. Lett.* 14, 4206–4212. doi: 10.3892/ol.2017.6704

Qin, Z., Bi, L., Hou, X. M., Zhang, S., Zhang, X., Lu, Y., et al. (2020). Human RPA activates BLM's bidirectional DNA unwinding from a nick. *Elife* 9:e54098. doi: 10.7554/eLife.54098

Rong, S. B., Valiaho, J., and Vihinen, M. (2000). Structural basis of Bloom syndrome (BS) causing mutations in the BLM helicase domain. *Mol. Med.* 6, 155–164. doi: 10.1007/BF03402111

Root, H., Larsen, A., Komosa, M., Al-Azri, F., Li, R., Bazett-Jones, D. P., et al. (2016). FANCD2 limits BLM-dependent telomere instability in the alternative lengthening of telomeres pathway. *Hum. Mol. Genet.* 25, 3255–3268. doi: 10.1093/hmg/ddw175

Rosenthal, A. S., Dexheimer, T. S., Nguyen, G., Gileadi, O., Vindigni, A., Simeonov, A., et al. (2010). "Discovery of ML216, a Small Molecule Inhibitor of Bloom (BLM) Helicase," in *Probe Reports from the NIH Molecular Libraries Program* (Bethesda, MD).

Rosin, M. P., and German, J. (1985). Evidence for chromosome instability *in vivo* in Bloom syndrome: increased numbers of micronuclei in exfoliated cells. *Hum. Genet.* 71, 187–191. doi: 10.1007/BF00284570

Schuetz, J. M., MaCarthur, A. C., Leach, S., Lai, A. S., Gallagher, R. P., Connors, J. M., et al. (2009). Genetic variation in the NBS1, MRE11, RAD50 and BLM genes and susceptibility to non-Hodgkin lymphoma. *BMC Med. Genet.* 10:117. doi: 10.1186/1471-2350-10-117

Sengupta, S., Linke, S. P., Pedeux, R., Yang, Q., Farnsworth, J., Garfield, S. H., et al. (2003). BLM helicase-dependent transport of p53 to sites of stalled DNA replication forks modulates homologous recombination. *EMBO J.* 22, 1210–1222. doi: 10.1093/emboj/cdg114

Sengupta, S., Robles, A. I., Linke, S. P., Sinogeeva, N. I., Zhang, R., Pedeux, R., et al. (2004). Functional interaction between BLM helicase and 53BP1 in a Chk1-mediated pathway during S-phase arrest. *J. Cell Biol.* 166, 801–813. doi: 10.1083/jcb.200405128

Sengupta, S., Shimamoto, A., Koshiji, M., Pedeux, R., Rusin, M., Spillare, E. A., et al. (2005). Tumor suppressor p53 represses transcription of RECQ4 helicase. *Oncogene* 24, 1738–1748. doi: 10.1038/sj.onc.1208380

Sharma, S., Sommers, J. A., Gary, R. K., Friedrich-Heineken, E., Hubscher, U., and Brosh, R. M. Jr. (2005). The interaction site of Flap Endonuclease-1 with WRN helicase suggests a coordination of WRN and PCNA. *Nucleic Acids Res.* 33, 6769–6781. doi: 10.1093/nar/gki1002

Shastri, V. M., and Schmidt, K. H. (2016). Cellular defects caused by hypomorphic variants of the Bloom syndrome helicase gene BLM. *Mol. Genet. Genomic Med.* 4, 106–119. doi: 10.1002/mgg3.188

Shay, J. W., and Bacchetti, S. (1997). A survey of telomerase activity in human cancer. *Eur. J. Cancer* 33, 787–791. doi: 10.1016/S0959-8049(97)00062-2

Sherr, C. J. (2004). Principles of tumor suppression. *Cell* 116, 235–246. doi: 10.1016/S0092-8674(03)01075-4

Shorrocks, A. K., Jones, S. E., Tsukada, K., Morrow, C. A., Belblidia, Z., Shen, J., et al. (2021). The Bloom syndrome complex senses RPA-coated single-stranded DNA to restart stalled replication forks. *Nat. Commun.* 12:585. doi: 10.1038/s41467-020-20818-5

Shuai, F., Wang, B., and Dong, S. (2018). miR-522-3p promotes tumorigenesis in human colorectal cancer via targeting bloom syndrome protein. *Oncol. Res.* 26, 1113–1121. doi: 10.3727/096504018X15166199939341

Silva, B., Pentz, R., Figueira, A. M., Arora, R., Lee, Y. W., Hodson, C., et al. (2019). FANCM limits ALT activity by restricting telomeric replication stress induced by deregulated BLM and R-loops. *Nat. Commun.* 10:2253. doi: 10.1038/s41467-019-10179-z

Singh, T. R., Ali, A. M., Busygina, V., Raynard, S., Fan, Q., Du, C. H., et al. (2008). BLAP18/RMI2, a novel OB-fold-containing protein, is an essential component of the Bloom helicase-double Holliday junction dissolvasome. *Genes Dev.* 22, 2856–2868. doi: 10.1101/gad.1725108

Slupianek, A., Gurdek, E., Koptyra, M., Nowicki, M. O., Siddiqui, K. M., Groden, J., et al. (2005). BLM helicase is activated in BCR/ABL leukemia cells to modulate responses to cisplatin. *Oncogene* 24, 3914–3922. doi: 10.1038/sj.onc.1208545

Sokolenko, A. P., Iyevleva, A. G., Preobrazhenskaya, E. V., Mitiushkina, N. V., Abysheva, S. N., Suspitsin, E. N., et al. (2012). High prevalence and breast cancer predisposing role of the BLM c.1642 C>T (Q548X) mutation in Russia. *Int. J. Cancer* 130, 2867–2873. doi: 10.1002/ijc.26342

Srivastava, V., Modi, P., Tripathi, V., Mudgal, R., De, S., and Sengupta, S. (2009). BLM helicase stimulates the ATPase and chromatin-remodeling activities of RAD54. *J. Cell Sci.* 122(Pt 17), 3093–3103. doi: 10.1242/jcs.051813

Stinson, B. M., Moreno, A. T., Walter, J. C., and Loparo, J. J. (2020). A mechanism to minimize errors during non-homologous end joining. *Mol. Cell* 77, 1080–1091 e1088. doi: 10.1016/j.molcel.2019.11.018

Tan, J., Wang, X., Phoon, L., Yang, H., and Lan, L. (2020). Resolution of ROS-induced G-quadruplexes and R-loops at transcriptionally active sites is dependent on BLM helicase. *FEBS Lett.* 594, 1359–1367. doi: 10.1002/1873-3468.13738

Taniguchi, N., Mukai, M., Nagaoki, T., Miyawaki, T., Moriya, N., Takahashi, H., et al. (1982). Impaired B-cell differentiation and T-cell regulatory function in four patients with Bloom's syndrome. *Clin. Immunol. Immunopathol.* 22, 247–258. doi: 10.1016/0090-1229(82)90041-1

Tikoo, S., Madhavan, V., Hussain, M., Miller, E. S., Arora, P., Zlatanou, A., et al. (2013). Ubiquitin-dependent recruitment of the Bloom syndrome helicase upon replication stress is required to suppress homologous recombination. *EMBO J.* 32, 1778–1792. doi: 10.1038/emboj.2013.117

Tippana, R., Hwang, H., Opresko, P. L., Bohr, V. A., and Myong, S. (2016). Single-molecule imaging reveals a common mechanism shared by G-quadruplex-resolving helicases. *Proc. Natl. Acad. Sci. U.S.A.* 113, 8448–8453. doi: 10.1073/pnas.1603724113

Traverso, G., Bettegowda, C., Kraus, J., Speicher, M. R., Kinzler, K. W., Vogelstein, B., et al. (2003). Hyper-recombination and genetic instability in BLM-deficient epithelial cells. *Cancer Res.* 63, 8578–8581.

Tripathi, V., Agarwal, H., Priya, S., Batra, H., Modi, P., Pandey, M., et al. (2018). MRN complex-dependent recruitment of ubiquitylated BLM helicase to DSBs negatively regulates DNA repair pathways. *Nat. Commun.* 9:1016. doi: 10.1038/s41467-018-03393-8

Tripathi, V., Kaur, S., and Sengupta, S. (2008). Phosphorylation-dependent interactions of BLM and 53BP1 are required for their anti-recombinogenic roles during homologous recombination. *Carcinogenesis* 29, 52–61. doi: 10.1093/carcin/bgm238

Tripathi, V., Nagarjuna, T., and Sengupta, S. (2007). BLM helicase-dependent and -independent roles of 53BP1 during replication stress-mediated homologous recombination. *J. Cell Biol.* 178, 9–14. doi: 10.1083/jcb.200610051

Turley, H., Wu, L., Canamero, M., Gatter, K. C., and Hickson, I. D. (2001). The distribution and expression of the Bloom's syndrome gene product in normal and neoplastic human cells. *Br. J. Cancer* 85, 261–265. doi: 10.1054/bjoc.2001.1874

Van Kerckhove, C. W., Ceuppens, J. L., Vanderschueren-Lodeweyckx, M., Eggermont, E., Vertessen, S., and Stevens, E. A. (1988). Bloom's syndrome. Clinical features and immunologic abnormalities of four patients. *Am. J. Dis. Child* 142, 1089–1093. doi: 10.1001/archpedi.1988.02150100083032

van Wietmarschen, N., Merzouk, S., Halsema, N., Spierings, D. C. J., Guryev, V., and Lansdorp, P. M. (2018). BLM helicase suppresses recombination at G-quadruplex motifs in transcribed genes. *Nat. Commun.* 9:271. doi: 10.1038/s41467-017-02760-1

Vindigni, A., and Hickson, I. D. (2009). RecQ helicases: multiple structures for multiple functions? *HFSP J.* 3, 153–164. doi: 10.2976/1.3079540

Viziteu, E., Kassambara, A., Pasero, P., Klein, B., and Moreaux, J. (2016a). RECQ helicases are deregulated in hematological malignancies in association with a prognostic value. *Biomark Res.* 4:3. doi: 10.1186/s40364-016-0057-4

Viziteu, E., Lin, Y. L., Vincent, L., Seckinger, A., Hose, D., Constantinou, A., et al. (2016b). A small molecule that selectively targets BLM helicase has a therapeutic interest in multiple myeloma. *Blood* 128, 4433–4433. doi: 10.1182/blood.V128.22.4433.4433

von Kobbe, C., Karmakar, P., Dawut, L., Opresko, P., Zeng, X., Brosh, R. M. Jr., et al. (2002). Colocalization, physical, and functional interaction between Werner and Bloom syndrome proteins. *J. Biol. Chem.* 277, 22035–22044. doi: 10.1074/jbc.M200914200

Votino, C., Laudanna, C., Parcesepe, P., Giordano, G., Remo, A., Manfrin, E., et al. (2017). Aberrant BLM cytoplasmic expression associates with DNA damage stress and hypersensitivity to DNA-damaging agents in colorectal cancer. *J. Gastroenterol.* 52, 327–340. doi: 10.1007/s00535-016-1222-0

Wang, C. X., Zhang, Z. L., Yin, Q. K., Tu, J. L., Wang, J. E., Xu, Y. H., et al. (2020). Design, synthesis, and evaluation of new quinazolinone derivatives that inhibit bloom syndrome protein (BLM) helicase, trigger DNA damage at the telomere region, and synergize with PARP inhibitors. *J. Med. Chem.* 63, 9752–9772. doi: 10.1021/acs.jmedchem.0c00917

Wang, J., Chen, J., and Gong, Z. (2013). TopBP1 controls BLM protein level to maintain genome stability. *Mol. Cell* 52, 667–678. doi: 10.1016/j.molcel.2013.10.012

Wang, X. W., Tseng, A., Ellis, N. A., Spillare, E. A., Linke, S. P., Robles, A. I., et al. (2001). Functional interaction of p53 and BLM DNA helicase in apoptosis. *J. Biol. Chem.* 276, 32948–32955. doi: 10.1074/jbc.M103298200

Wang, Y., Cortez, D., Yazdi, P., Neff, N., Elledge, S. J., and Qin, J. (2000). BASC, a super complex of BRCA1-associated proteins involved in the recognition and repair of aberrant DNA structures. *Genes Dev.* 14, 927–939. doi: 10.1101/gad.14.8.927

Warren, M., Chung, Y. J., Howat, W. J., Harrison, H., McGinnis, R., Hao, X., et al. (2010). Irradiated Blm-deficient mice are a highly tumor prone model for analysis of a broad spectrum of hematologic malignancies. *Leuk. Res.* 34, 210–220. doi: 10.1016/j.leukres.2009.06.007

Watt, P. M., Hickson, I. D., Borts, R. H., and Louis, E. J. (1996). SGS1, a homologue of the Bloom's and Werner's syndrome genes, is required for maintenance of genome stability in *Saccharomyces cerevisiae*. *Genetics* 144, 935–945. doi: 10.1093/genetics/144.3.935

Weemaes, C. M., Bakkeren, J. A., ter Haar, B. G., Hustinx, T. W., and van Munster, P. J. (1979). Immune responses in four patients with Bloom syndrome. *Clin. Immunol. Immunopathol.* 12, 12–19. doi: 10.1016/0090-1229(79)90107-7

Wu, L., Davies, S. L., Levitt, N. C., and Hickson, I. D. (2001). Potential role for the BLM helicase in recombinational repair via a conserved interaction with RAD51. *J. Biol. Chem.* 276, 19375–19381. doi: 10.1074/jbc.M009471200

Wu, L., Davies, S. L., North, P. S., Goulaouic, H., Riou, J. F., Turley, H., et al. (2000). The Bloom's syndrome gene product interacts with topoisomerase III. *J. Biol. Chem.* 275, 9636–9644. doi: 10.1074/jbc.275.13.9636

Wu, L., and Hickson, I. D. (2003). The Bloom's syndrome helicase suppresses crossing over during homologous recombination. *Nature* 426, 870–874. doi: 10.1038/nature02253

Xue, C., Daley, J. M., Xue, X., Steinfeld, J., Kwon, Y., Sung, P., et al. (2019). Single-molecule visualization of human BLM helicase as it acts upon double- and single-stranded DNA substrates. *Nucleic Acids Res.* 47, 11225–11237. doi: 10.1093/nar/gkz810

Yeager, T. R., Neumann, A. A., Englezou, A., Huschtscha, L. I., Noble, J. R., and Reddel, R. R. (1999). Telomerase-negative immortalized human cells contain a novel type of promyelocytic leukemia (PML) body. *Cancer Res.* 59, 4175–4179.

Yin, Q. K., Wang, C. X., Wang, Y. Q., Guo, Q. L., Zhang, Z. L., Ou, T. M., et al. (2019). Discovery of isaindigotone derivatives as novel bloom's syndrome protein (BLM) helicase inhibitors that disrupt the BLM/DNA interactions and regulate the homologous recombination repair. *J. Med. Chem.* 62, 3147–3162. doi: 10.1021/acs.jmedchem.9b00083

**Conflict of Interest:** The authors declare that the research was conducted in the absence of any commercial or financial relationships that could be construed as a potential conflict of interest.

frontiers in Genetics

BRIEF RESEARCH REPORT
published: 25 March 2021
doi: 10.3389/fgene.2021.634938

# Prolonged Exposure to Platelet Activating Factor Transforms Breast Epithelial Cells

*Vaishali Chakravarty†‡, Libi Anandi†‡, K. A. Ashiq†‡, K. Abhijith, Rintu Umesh and Mayurika Lahiri**

*Department of Biology, Indian Institute of Science Education and Research, Pune, India*

OPEN ACCESS

**Edited by:**
*Hari S. Misra, Bhabha Atomic Research Centre (BARC), India*

**Reviewed by:**
*Chandrima Das, Saha Institute of Nuclear Physics (SINP), India*
*Constantinos Demopoulos, National and Kapodistrian University of Athens, Greece*

***Correspondence:**
*Mayurika Lahiri*
*mayurika.lahiri@iiserpune.ac.in*
*orcid.org/0000-0001-9456-4920*

*†These authors have contributed equally to this work*

**‡Present address:**
*Vaishali Chakravarty, Enveda Therapeutics India Pvt. Ltd., VCR Park, Vishakhapatnam, India*
*Libi Anandi, Department of Biology, Center for Genomics and Systems Biology, New York University, New York, NY, United States*
*K. A. Ashiq, National Centre for Cell Science, Pune, India*

**Specialty section:**
*This article was submitted to Genetics of Common and Rare Diseases, a section of the journal Frontiers in Genetics*

**Received:** *29 November 2020*
**Accepted:** *03 March 2021*
**Published:** *25 March 2021*

**Citation:**
*Chakravarty V, Anandi L, Ashiq KA, Abhijith K, Umesh R and Lahiri M (2021) Prolonged Exposure to Platelet Activating Factor Transforms Breast Epithelial Cells. Front. Genet. 12:634938. doi: 10.3389/fgene.2021.634938*

Lipid species are known to have various biological functions owing to their structural differences, and each of them possesses a specific role to play depending upon their location and distribution in the cell. Some of these lipids interact with proteins on the cell membrane and acts as second messengers. The level of lipid mediators is generally maintained in the cell by feedback mechanisms; however, their improper degradation or enhanced production leads to their accumulation in the tumor microenvironment and disturbs the homeostasis of the cell. Platelet activating factor (PAF) is a known phospholipid mediator secreted upon immunological challenges by platelets, neutrophils, basophils, and macrophages. PAF, as a potent inflammatory molecule, is well studied, and its role in various cancers and cardiovascular diseases has also been investigated. Interestingly, increased levels of PAF have been found in the blood plasma of smokers, and breast cancer cells have shown the accumulation of PAF in presence of cigarette smoke extract. This accumulation was found to increase tumor cell motility that in turn could promote metastasis. Beyond this, however, the effect of PAF on tumorigenesis has not yet been well explored. Here, we show that the continuous exposure of 3D breast acinar cultures to PAF resulted in the activation of various oncogenic signaling pathways leading to transformation. We also found that the presence of PAF in the micro-environment increased the expression of PAF receptor (PAF-R), which corroborated with the higher expression of PAF-R detected in some epithelial cancers, as per literature. Thus, this study impresses on the fact that the presence of PAF alters the cellular microenvironment and eventually triggers irreversible effects that can cumulatively lead to transformation.

**Keywords: platelet activating factor, transformation, breast cancer, epithelial-mesenchymal transition, polarity**

## INTRODUCTION

Immune system holds a key position in maintaining cellular homeostasis, and an imbalance can lead to various abnormities including cancer. Hence, it is one of the primary targets while designing therapy for malignancies. Tumor infiltrating cells, such as leukocytes and macrophages, are common entities in cancers, and their interaction with the tumor micro-environment components is widely studied (Hanahan and Weinberg, 2011). Such entities are known to promote tumor progression and invasion, and thus hold a clinical relevance in

various cancers (Man et al., 2013). The interaction of the immune cells and the cancer cells could be through direct cell-cell contact or may also be mediated by secretory molecules. One such molecule is platelet activating factor (PAF). PAF is an autacoid phospholipid mediator, which is secreted in response to an agonist by various immune cells and elicits various immunoregulatory reactions such as platelet aggregation, allergy, anaphylaxis, and many more (Foa et al., 1985; Hanahan and Weinberg, 2011). Overall, it is known to induce various physiological and pathological processes that eventually affect the respiratory, vascular, and even reproductive system (Papakonstantinou et al., 2017). PAF production is tightly regulated by biosynthetic and degradative mechanisms since uncontrolled levels can cause various pathologies. PAF acetyl hydrolase (PAF-AH) controls the level of PAF in the system by degradative mechanisms (Chen et al., 2007).

In the early studies, after the role of PAF was established in various pleiotropic activities, its effects were observed in various diseases as well (Lordan et al., 2019). PAF-AH activity was seen to be inhibited when human plasma was treated with cigarette smoke extract (CSE). This was also strengthened by the results that showed increased plasma concentration of PAF in smokers, indicating the role of PAF in the development of cardiovascular diseases in smokers (Miyaura et al., 1992). Kispert et al. (2015) has shown that CSE inhibits PAF-AH activity, thus leading to the accumulation of PAF in the endothelial cells. In a recent study with a bladder cancer cell line, the same group has reported similar results, wherein grade III HT-1376 cells showed higher PAF accumulation followed by greater adherence in presence of CSE, exhibiting highly aggressive manifestations (Kispert et al., 2019). Investigations by Bussolati et al. showed the presence of high amounts of PAF in MCF-7, MDA-MB 231, and T47D cells. This synthesized PAF enhanced cell motility as well as increased proliferation in MDA-MB 231 cells (Bussolati et al., 2000). An early report from Bennett et al. demonstrates that PAF induces phenotypic transformation in rat embryonic cells. They have shown increased cell density, growth in low serum condition, and anchorage-independent growth, which are the indicators of transformation, in the presence of dose-dependent increase in PAF concentration (Bennett et al., 1993).

Although PAF is a lipid mediator, it is not known to freely diffuse through the cell membrane and studies clearly state that PAF activates a G-protein coupled receptor, PAF-R and mediates its activities through this axis. PAF-R is ubiquitously expressed across tissues, and its role in various cancers has been established (Ishii and Shimizu, 2000; Jancar and Chammas, 2014). The PAF-PAFR axis activation suggests a feedback control loop that maintains the PAFR levels in pathological conditions (Chen et al., 2015a; Lv et al., 2017). Two groups in 2015 have shown the role of PAFR in non small cell lung carcinoma (NSCLC) and esophageal squamous cell carcinoma (ESCC). In NSCLC, the activation of PAF-PAF-R axis induces epithelial-mesenchymal transition (EMT), leading to invasion and metastasis of NSCLC cells (Chen et al., 2015a). Role of PAF-R in ESCC malignancy has been stated *via* the activation of oncogenic signaling through FAK/PI3K/AKT/NF-kB axis (Chen et al., 2015b). Previous report from the lab has shown that breast cancer cells in the presence of PAF shows higher motility and when MCF10A, a non-tumorigenic breast epithelial cell line, was grown on an ECM, in presence of PAF, disrupts the luminal phenotype (Anandi et al., 2016). Results from the lab as well as mounting evidence from literature imposed heavily on the necessity to investigate the role of PAF in the transformation of three-dimensional (3D) cultures of MCF10A cells. In the current study, we have focused on elucidating the transformation phenotypes acquired by MCF10A breast acinar cultures in the presence of PAF and the activation of PI3-K/AKT signaling pathway to strengthen the oncogenic potential of PAF.

# MATERIALS AND METHODS

## Cell Lines and Culture Conditions

MCF10A cell line was a generous gift from Prof. Raymond C. Stevens (The Scripps Research Institute, California, United States) and 2D monolayer cultures and 3D cultures were grown according to the standard protocols (Debnath et al., 2003). 3D cultures were maintained for 20 days by supplementing fresh media every 4 days. Methylcarbamyl PAF C-16, procured as a 10 mg/ml solution in ethanol (Cayman chemicals, 60908), was diluted in sterile PBS to make a working stock of 100 μM. Required volume of the working stock was directly added to the desired volume of media, to achieve a final concentration of 200 nM. PAF treatment was given 3 h post seeding and along with every media change.

## Immunoflourescence

Acini from the 3D cultures were extracted using PBS-EDTA treatment for apical proteins and other proteins using normal method of extraction. Immunostaining was done using a previously described protocol (Anandi et al., 2017). Samples were imaged using 40X oil immersion objective of SP8 confocal microscope (Leica, Germany).

Details of chemical, antibodies, and statistical analysis used and methods for 3D "on top" cultures, immunoblot analysis, RNA Extraction, cDNA preparation, semi-quantitative PCR, soft agar assay, DQ collagen invasion assay, and gelatin zymography can be found in **Supplementary Material**.

# RESULTS

## PAF Treatment on 3D Cultures of MCF10A Leads to Increased Proliferation

3D breast acinar cultures, grown on laminin rich matrix, attain a growth arrested state with a monolayer of cells around a hollow lumen, after 12 days of culturing. Cells in such stable structures are usually arrested in the G1 Phase (Fournier et al., 2006). Based on our previous data (Anandi et al., 2016), to ascertain if PAF treatment resulted in the presence of hyperproliferating and actively dividing cells, that resulted in large acini, we immunostained the PAF-treated 20-day cultures with Ki67, a proliferation marker. Acini with more than five

cells positive for Ki67 are considered to be hyperproliferating (Wu and Gallo, 2013). Eighty percent of the PAF treated acini were found to be hyperproliferating (**Figure 1A**). Further, immunoblotting revealed a 1.4-fold upregulation in Ki67 protein levels (**Figure 1B**). This shows that PAF leads to the formation of large multiple layered acini that have evaded the growth-arrested state and are hyperproliferating thus qualifying as a transformation phenotype.

## Apico-Basal Polarity and Cell-Cell Junctions Gets Disrupted in the Presence of PAF Treatment

One of the important features of epithelial architecture is polarization. Epithelial cells attain apico-basal polarity when placed in a 3D environment unlike cells on a 2D plane, which only have front and rear polarities. Alongside, cell-cell junction is an important component in maintaining the epithelial tissue homeostasis. In this study, it is evident that PAF affects the orientation of epithelial polarity and leads to compromised cell-cell junctions. There are various proteins that are known to act as markers of polarity such as integrins, laminins, and also Golgi (Debnath et al., 2003; Debnath and Brugge, 2005). E-cadherin is an adherens junction protein, which is well-established in MCF10A unlike the tight junctions, which are poorly developed (Ivers et al., 2014). E-cadherin is a central component of the zona adherens junction complex, and the loss of E-cadherin is a key indicator of tumor aggressiveness (Kourtidis et al., 2017). The 3D cultures of MCF10A treated with PAF were extracted after 20 days and immunostained with apical and basal markers such as GM130, α6-integrin, and Laminin-V. α6-integrin, receptors for the ECM, marks the basal region of the acini and stains across the basolateral regions. In the presence of PAF, the staining pattern was altered dramatically by change in expression level as well as membrane distribution of the protein (**Figure 2A**). Seventy-three percent of acini treated with PAF exhibited marked loss of α6-integrin from the basal region and also enhanced cytoplasmic staining was observed, which we quantified as loss and mis-localized phenotype. Epithelial cells have a remarkable property of attachment to the ECM *via* the basement membrane (BM). This BM is disrupted in the cases of primary metastasis in breast carcinomas (Shaw et al., 2004). Laminins are a group of BM proteins and LamininV is one of the components of BM (Shaw et al., 2004). Acini grown in the presence of PAF showed gross disruption in LamininV staining, thus indicating loss of BM protein due to PAF treatment. Seventy-two percent of acini show disrupted as well as the loss of membrane localization of LamininV (**Figure 2B**). GM130, which is a cis-Golgi marker, was mislocalized to the basal and lateral regions in PAF-treated acini, whereas in the control acini Golgi localization remained apical. Upon quantifying, it was observed that 100% of Golgi was mislocalized in PAF-treated acini (**Figure 2C**). These results indicate a clear loss of apical as well as basal polarity in MCF10A 3D cultures grown in the presence of PAF. Immunostaining for β-catenin revealed a diffused localization of β-catenin at cell-cell junction as well as in intercellular granular pockets, which is also indicative of aberrant protein trafficking (**Figure 2D**). To further confirm the disruption of the cell-cell junctions, cells from day 20 spheroids were dissociated (referred to as dissociated cells hereafter) and immunostained for E-cadherin and β-catenin. Loss of E-cadherin by immunostaining was observed in the presence of PAF (**Figure 2E**) and analyzed using intensity plot profiling (**Figure 2G**). β-catenin also showed similar diffused patterns in the dissociated cells as was observed in the acinar cultures (**Figure 2F**). The diffused pattern was analyzed using a plot profiling of lines drawn across cell-cell junctions and then calculating Full Width Half Max (FWHM) as depicted in the schematic in **Figure 2H**. The FWHM values were significantly higher in PAF exposed cells as compared to

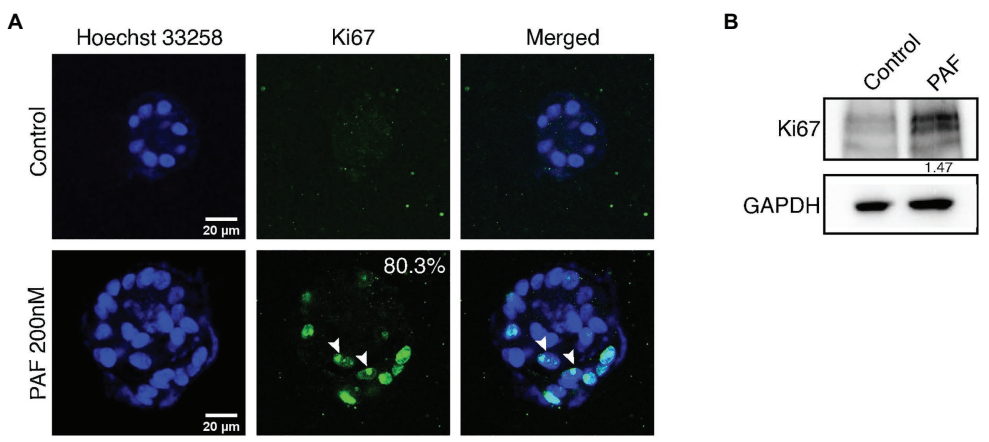


**FIGURE 1 |** PAF treatment on 3D cultures of MCF10A leads to increased proliferation. MCF10A cells grown as 3D cultures for 20 days treated with and without PAF (200 nM) were immunostained with the proliferation marker, Ki67. **(A)** Representative image showing hyperproliferation in PAF-treated acini. The data are from $N = 5$ set of experiments. **(B)** Protein lysates from 20-day cultures were immunoblotted for Ki67. The values represent the relative expression of Ki67 normalized to GAPDH.

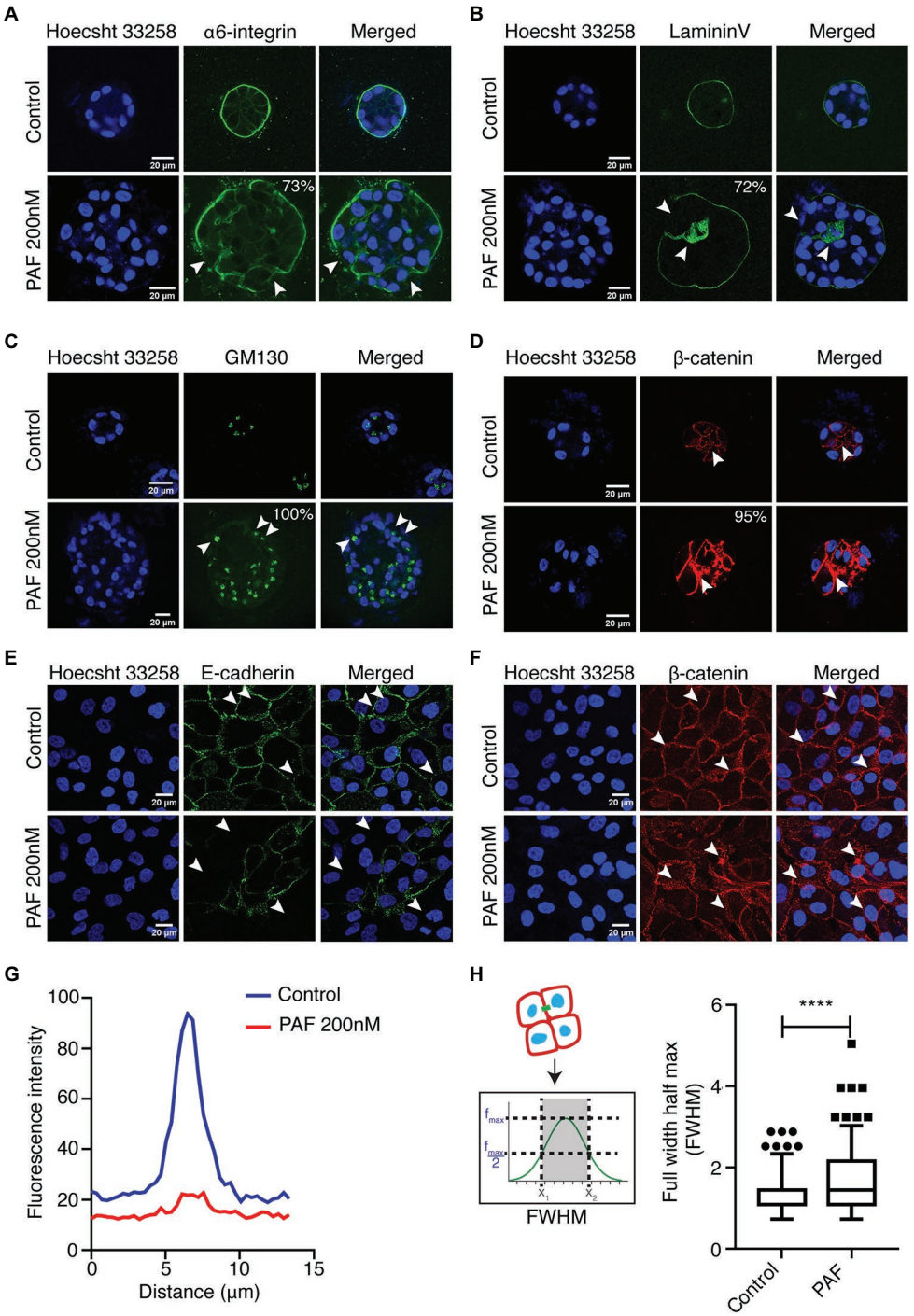


**FIGURE 2 |** PAF treatment alters acinar polarity and leads to the disruption of cell-cell junctions. PAF-treated 20 days 3D cultures of MCF10A were immunostained with polarity and cell-cell junction markers. Nucleus is stained with Hoecsht 33,258 (blue). **(A)** Immunostained images of α6-integrin (green) marks the basal polarity ($N = 4$). **(B)** Immunostained images of LamininV (green) marks the basement membrane of the acini ($N = 4$). **(C)** Immunostained images of GM130 (green) marks apical polarity ($N = 3$). **(D)** Immunostained images of β-catenin (red) marks the cell-cell junctions. **(E)** Dissociated cells of control and PAF-treated acini immunostained with E-cadherin (green), a cell-cell junction marker and the image is a representative of the phenotype ($N = 3$). **(F)** Dissociated cells of control and PAF treated acini immunostained with β-catenin (red), a cell-cell junction marker and the image is a representative of the diffused phenotype ($N = 3$). **(G)** Median fluorescent intensity of E-cadherin line profile showing loss phenotype. **(H)** FWHM profile of β-catenin line profile showing diffused phenotype. The phenotypes are quantified from $N > 3$ set independent experiments. Statistical analysis was performed for **(H)** using Mann Whitney U test; *****$p < 0.0001$.

untreated dissociated cells (**Figure 2H**). This clearly indicated that PAF treatment altered epithelial polarity and also led to a loss and/or disruption of cell-cell junctions.

## PAF Treatment Induces Partial EMT-Like Phenotype

EMT is a process of transition of epithelial cells into mesenchymal cells. This program has been distinctively viewed as a two-stage program with two discrete cell populations of epithelial and mesenchymal cells expressing the cell-type specific proteins (Pastushenko and Blanpain, 2019). However, recent studies indicate that EMT is a gradual process that takes place through stages that are known as intermediate states. This state circumscribes the co-expression of epithelial and mesenchymal markers. It has also been shown in similar studies that this hybrid/incomplete state of EMT is more culpable to poor survival and higher chances of resistance to therapy (Lambert et al., 2017; Pastushenko and Blanpain, 2019).

Vimentin, a known mesenchymal marker, showed an upregulated phenotype in the acini grown in the presence of PAF (**Figures 3A,B**). The protein expression of the different EMT markers was also investigated as shown in (**Figure 3C**). Vimentin and N-cadherin protein levels showed an upregulation in the presence of PAF, and densitometric analysis showed a 2-fold and 1.76-fold increase in the respective protein levels. Fibronectin, which is also a mesenchymal marker, is also upregulated in the presence of PAF. E-cadherin, an epithelial and a cell-cell junction marker showed a 0.5-fold reduction in protein level, which further corroborated the loss that was observed earlier (**Figure 2E**). β-catenin protein levels did not show a significant change probably because there has not been a major loss of the protein but more of cellular redistribution from the junctions to the cytoplasm as granules. Hence, a clear difference in protein level was not observed. Slug, a transcription factor, showed a 1.47-fold increase at protein level.

Transcript levels of the various EMT markers were also investigated in the 20-day PAF-treated 3D cultures. Fibronectin, slug, and twist transcript levels were measured using semi-quantitative PCR. Fibronectin transcript level was more than 2-fold higher in the RNA lysates collected post 20 days of PAF treatment. The transcript levels of slug and twist also showed a 2-fold upregulation in the presence of PAF (**Figure 3D**). The quantifications of the transcript level were performed using densitometric analysis using ImageJ software. The role of tumor micro-environment (TM) is well-established in various cancers including breast cancer (Yu and Elble, 2016). TM is composed of different inflammatory and immune cells, apart from other components, which have been known to induce EMT-like phenotype (Yu and Elble, 2016). As mentioned before, PAF is a phospholipid mediator that is widely known to play a role in the activation of various immune cells. Hence, the above results are indicative of the formation of a link between hybrid state of EMT, TM and PAF; all leading to transformation.

**Figure 3E** shows the phase contrast images of control and PAF-treated dissociated cells grown as monolayer cultures. Control cells appear like MCF10A cells, epithelial-like, and cuboidal, while PAF-treated cells appear spindle-like, large, and elongated. This appearance is retained when cells are both sparsely or densely seeded. This morphology strengthens the fact that PAF has the ability to transform MCF10A breast epithelial cells.

Since the data indicate induction of EMT, this was further supported by performing DQ collagen™ assay. PAF dissociated cells showed increased fluorescence when observed under SP8 confocal microscope (Leica, Germany; **Figure 3F**), which was quantified (**Figure 3G**). To strengthen the hypothesis that PAF induces invasion, gelatin zymography was performed using the conditioned media (CM) from the 3D breast acinar cultures. Increased activation of MMP-2 (1.42-fold) and MMP-9 (2.23-fold) were observed in the conditioned media collected from the PAF-treated samples (**Figure 3H**), thus indicating the ability of PAF stimulation to induce invasion, which is a known marker for transformation. Taken together, our data clearly indicate the induction of partial EMT and invasion in PAF-treated cells thereby leading to a transformation phenotype.

## Effect of PAF on Anchorage Independent Growth of MCF10A Cells and Activation of the PI3K/AKT Pathway

Anchorage independent growth is a key characteristic feature that cells attain when they have undergone transformation, and this ability is considered as a fundamental property of cancer cells. This capacity to grow on a semisolid substratum serves as a proxy for *in vivo* tumorigenicity (Horibata et al., 2015). In our study, soft agar assay was performed to investigate whether prolonged PAF-treatment could transform the cells, thus allowing them to grow in an anchorage-independent manner. Dissociated cells of both control and PAF-treated acini were grown on soft agar for 27 days and then stained with MTT, a tetrazolium dye, to visualize the colonies and to distinguish the dead cells from live ones. **Figures 4A,B** clearly show PAF dissociated cells to have gained the capability to form colonies in an anchorage-independent manner, which supports the hypothesis that PAF induces *in vitro* tumorigenesis.

Our data indicate PAF stimulation of non-tumorigenic breast epithelial cells to undergo transformation; however, the mechanism of this transformation process is not known. In the current study, PAF-R showed a 2-fold upregulation in transcript levels of the PAF-stimulated lysates (**Figure 4C**). Further, PAF-treated 3D culture lysates were immunoblotted and probed for pAKT and total AKT. pAKT showed close to 3-fold increase in activation with concomitant increase in AKT protein expression upon prolonged treatment with PAF (**Figure 4D**).

In support of the existing literature, our data also show MMP-2 and MMP-9 activation downstream of pAKT activation. Increased cellular proliferation observed in the presence of PAF is suggestive of the contribution of the AKT pathway in the PAF-mediated transformation of MCF10A cells grown as 3D cultures. Hence, we predict the following pathway (**Figure 4E**) using existing data and current literature; however, further research is required to delineate the mechanism of transformation through PAF. Since our data are preliminary,

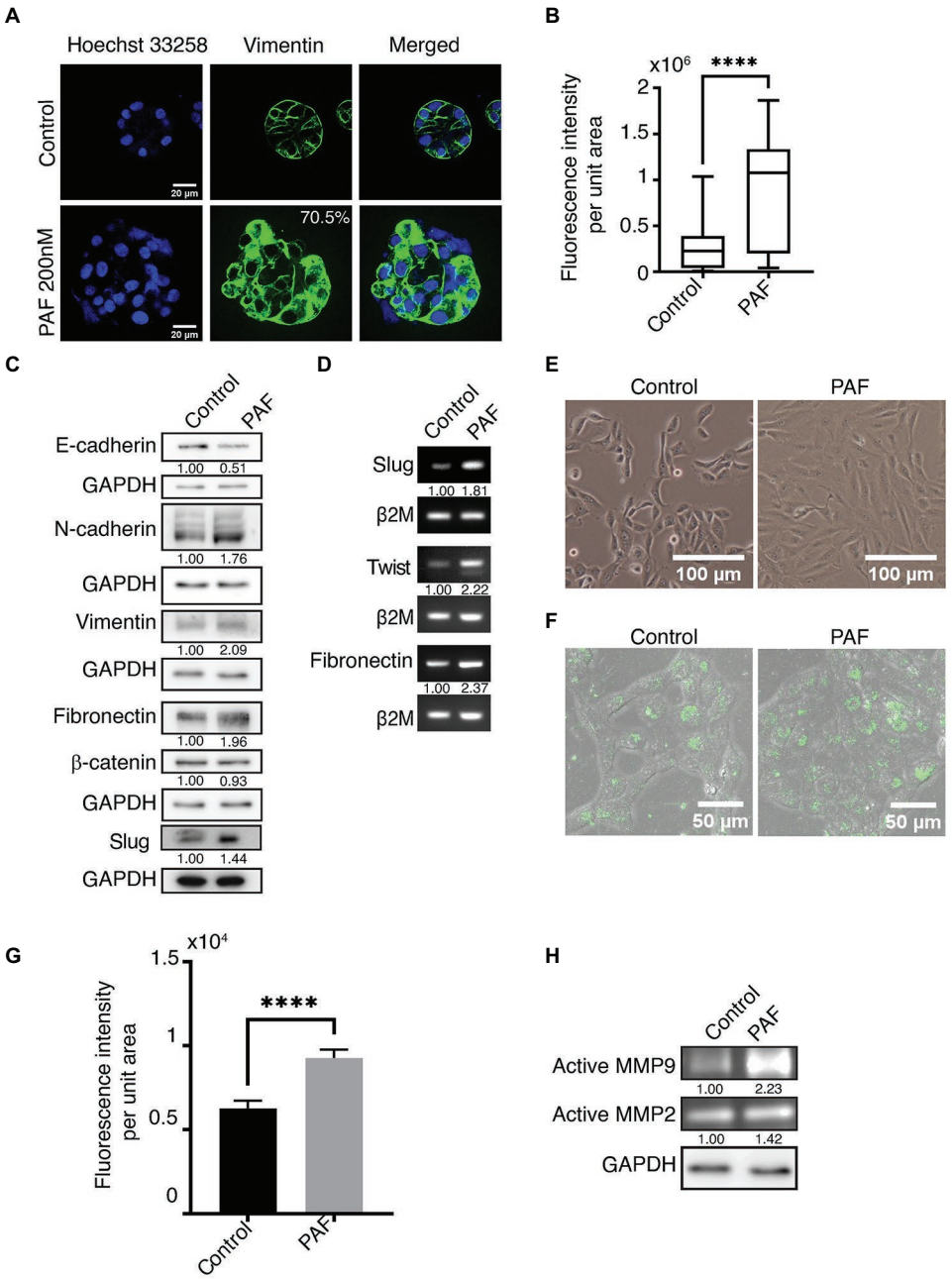


**FIGURE 3 |** PAF treatment induces partial epithelial-mesenchymal transition (EMT)-like phenotype. MCF10A cells grown for 20 days on Matrigel™ treated with and without 200 nM PAF immunostained and immunoblotted with EMT markers. **(A)** PAF-treated acini showed upregulated vimentin expression (green). **(B)** Box plot depicts the acinar fluorescence (CTCF) of vimentin ($N = 4$). **(C)** 20-day 3D culture lysates of control and PAF immunoblotted for various EMT markers. The values represent fold change with respect to control and normalized to GAPDH ($N = 3$). **(D)** mRNA expression analysis done for various EMT markers using RNA lysates. The values represent fold change with respect to control and normalized to β2M ($N = 3$). **(E)** Phase contrast images of dissociated cells of PAF treated acini grown as 2D cultures showed a mesenchymal phenotype. **(F)** Dissociated cells of control and PAF, seeded on rat tail collagen type1 containing DQ™ collagen type1 and fluorescence intensity captured on SP8 confocal microscope (Leica, Germany). **(G)** Quantification of the DQ fluorescence per cell ($n = 150$). **(H)** Coomassie-stained gel showing gelatinase activity using conditioned media from 3D cultures. The values represent fold change with respect control and normalized to GAPDH. Statistical analysis was performed for **(A)** and **(F)** using Mann Whitney U test; $^{****}p < 0.0001$.

further studies are called for using small molecule inhibitors to thoroughly dissect the signaling mechanism. Overall, PAF leads to phenotypic transformation of breast epithelial cells when grown on ECM for 20 days and the activation of the oncogenic molecular players warrants deeper investigations for the mechanism.

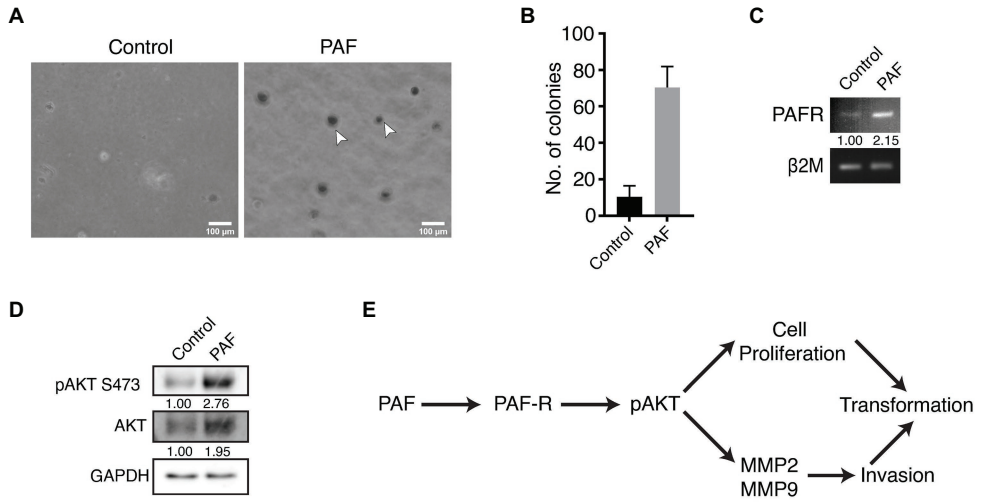


**FIGURE 4 |** Effect of PAF on anchorage independent growth of MCF10A cells and activation of the PI3K/AKT pathway. Dissociated cells were grown on soft agar and stained with MTT to visualize colonies formed and the pathway for PAF induced transformation. **(A)** Phase contrast images showing MTT stained colonies grown on soft agar. **(B)** Quantification of the number of colonies formed on soft agar ($N = 3$). **(C)** Transcript level of PAF-R. The values represent fold change with respect to control and normalized to β2M ($N = 3$). **(D)** Western blot indicating activation of AKT through PAF-R. The values represent fold change with respect to control and normalized to GAPDH ($N = 3$). **(E)** Pathway showing the activation of AKT downstream of PAF-R activation.

## DISCUSSION

PAF is long known as a potent inflammatory bioactive molecule that is unequivocally proven to give rise to aberrant physiological effects (Lordan et al., 2019). Its role in various types of cancer is studied; however, the mechanism that leads to cancer is still understudied (Tsoupras et al., 2009). The current study will be instrumental in defining the mode of action of PAF in transforming non-tumorigenic breast epithelial cells. Health hazards of high levels of PAF in the system were studied earlier by Kispert et al., and although it is known to be naturally present in the living system, improper degradation leads to its accumulation and hence leads to cellular and molecular anomalies (Chen et al., 2007; Kispert et al., 2015, 2019). Bussolati et al. (2000) have shown that the stimulated secretion of PAF promotes migration, proliferation, and neo-angiogenesis in breast cancer cells, clearly indicating its role in carcinogenesis (Bussolati et al., 2000). Cell microenvironment perturbations by exogenous or endogenous sources lead to increased cellular proliferation that results in a loss of hollow lumen followed by the formation of multiple layers of cells in the lumen. Such a phenotype is predictive of transformation and can be a representative model for early stage mammary cancer *in vitro* (Vidi et al., 2013). Formation of a polarized, growth-arrested acinar structure with glandular epithelial cells surrounding a hollow lumen is archetypal of perfectly synchronized cellular and molecular events culminating into a normal breast acinus. When this tissue architecture is disturbed, cell survival, and differentiation processes get largely affected and eventually pave the way to tumor formation (Vidi et al., 2013). Transformation is the initial step to this process, wherein the normal cell signaling goes haywire, and there is an aberrant expression of genes leading to malignant phenotypes, and this phenomenon is nearly recapitulated using the 3D breast acinar model system. Formation of disorganized acinar structures is characteristic of transformation and various phenotypic changes are categorized under lack of growth arrest, loss of cell polarity, disruption of BM and cell-cell junctions, EMT, and ability to grow in anchorage-independent conditions (Debnath et al., 2003). Our study encompasses all the above phenotypes in the zest to investigate the role of PAF in transformation of breast epithelial cells using the 3D breast acinar model.

Investigations revealed that continuous PAF treatment for 20 days leads to the disruption of polarity manifested by loss of apico-basal polarity. Generally, for apical polarity, *in vitro* studies as well as pathologists utilize Golgi marker as a strong identifying marker to understand polarity alteration leading to transformation or cancer (Debnath et al., 2003). Golgi is the hub for signal transduction for various pathways and alteration in its localization affects the polarized secretion of proteins from the ER to the plasma membrane and other compartments that in turn affects the signal transduction pathways (Millarte and Farhan, 2012). Hence, although the global secretory pattern does not change, but the directed trafficking of cargo is impaired. Alongside, breakage of BM is the key to loss of basal polarity. This phenomenon is significant because it provides a hallway to invading cells into the surrounding ECM and further into tissue stroma. The entirety of the BM is necessary to limit tumor growth and invasion and for this reason many solid tumors show discontinuous or a loss of BM (Ioachim et al., 2002). These investigations and the supporting literature revealed a structural loss of tissue architecture and loss of epithelial polarity in the presence of

PAF, indicating that such phenotypes are important components toward the maintenance of polarity and disruption of these leads to transformation and gives direct evidence in cancer development and progression (Lee and Vasioukhin, 2008).

E-cadherin, a cell-cell junction protein is known to maintain epithelial polarity by being a center for the intercommunicating signals between catenins and the cytoskeletal network and disruptions in this contact lead to various morphogenetic and developmental defects apart from loss of epithelial polarity (Olson et al., 2019). E-cadherin complexes with cytoplasmic β-catenin at the junctions and aberrations in this interaction leads to an increased flux of cytoplasmic β-catenin resulting in transformation and such an observation is commonly noted in solid tumors and epithelial cancers (Kourtidis et al., 2017). In our study, the loss of E-cadherin and diffused β-catenin at the junctions was observed in cells treated with PAF. Dissociation of the E-cadherin and β-catenin proteins from the complex leads to aberrant expression at the cell membrane and attributes to malignant progression, as well as has importance as a prognostic marker (Kaur et al., 2013). β-catenin expression leads to the transcription of various EMT inducing genes, thus identifying the various proteins that are under its transcriptional activity that lead to EMT is important (Solanas et al., 2008). EMT is a biological process that is employed during developmental stages; however, carcinoma cells hijack this program and herein the cells tend to lose their epithelial-like characteristics, both morphologically and functionally, and become mesenchymal or express such characteristics. Induction of EMT leads to the activation of various oncogenic programs including enhanced migration, invasion, metastasis, and the evasion of apoptotic stimuli (Kalluri and Weinberg, 2009; Scheel and Weinberg, 2011). Such complex programs are orchestrated by various EMT regulating transcription factors such as Snail, Slug, Twist, Zeb1, to name a few, to culminate into EMT. Apart from transcription factors, loss of cell-cell contacts and aberrant polarity also triggers EMT initiation. As cells fall loose in the cell matrix, they degrade it and attain mobility and this process is an attribute to EMT, which leads to the expression of mesenchymal proteins (Lamouille et al., 2014; Puisieux et al., 2014). Considering SNAIL1 and TWIST, the master regulators of EMT, they are classically known to repress E-cadherin and this opens the gate for tumor cells to migrate, either by mesenchymal movement or by amoeboid movement (Padmanaban et al., 2019). Concurrently, as E-cadherin levels decrease, N-cadherin levels increase and literature suggests that N-cadherin expression is TWIST-dependent (Alexander et al., 2006). Apart from the typical EMT markers, there are other molecules as well that play important roles in pathological EMT pathways. Fibronectin is an extracellular matrix protein, which gets enriched when EMT is induced, as well as various MMP's are expressed, which aid in the degradation of the matrix and enable tumor cells to invade deeper into tissues. Studies show that MMP-2 and MMP-9 deficient mice show impaired tumor cell growth and poor metastasis (Itoh et al., 1998). So, the conjoint efforts of BM disruption, mesenchymal expression, and MMP activation hold key position in inducing EMT, and the study suggests the same. However, inherent heterogeneity that arises in carcinoma cells, the tissue-wise difference in signal that cells receive to drive the EMT program, the signaling pathways that get activated in response to the induction of EMT, and the original state of the normal differentiated cells are few of the factors that deter making a perfect molecular trait chart that describes EMT (Lambert et al., 2017).

Traditionally, anchorage independent growth is a key feature of a transformed cell, and this phenomenon is well studied in the limited scope of *in vitro* culture system through colony formation in low attachment conditions. In our study, we have shown that acinar cultures grown in the presence of PAF attain anchorage independent growth, when grown on soft agar. As a first attempt these investigations gave enough evidence to show that PAF leads to transformation and the molecular players involved in this process is probably pAKT (S473; Chen et al., 2015b). Further studies are necessary to delineate the pathways that are involved in transformation through PAF.

Until now several investigations have shown that PAF plays a leading role in inflammation, platelet aggregation, leukocyte migration, and many such inflammatory mechanisms (Chignard et al., 1979; Bussolati et al., 2000). Cigarette smoke exposure is shown to promote bladder cancer and motility leading to metastasis in breast cancer cells *via* PAF (Kispert et al., 2015, 2019). In our study, we show that continuous exposure of PAF to 3D breast acinar cultures for 20 days leads to the formation of aberrant acinar morphology as well as the functional disruption of acinar morphogenesis, which might be due to activation of the PI3K/AKT pathway.

## DATA AVAILABILITY STATEMENT

The original contributions presented in the study are included in the article/**Supplementary Material**, further inquiries can be directed to the corresponding author.

## AUTHOR CONTRIBUTIONS

LA, VC, and ML: study conceptualization, supervision, study design, and wrote the paper. LA, VC, KAA, KA, and RU: data collection. All authors contributed to the article and approved the submitted version.

## FUNDING

This study was supported by a grant from the Science and Engineering Research Board (SERB), Government of India (EMR/2016/001974) and partly by the IISER, Pune core funding. LA was supported by the INSPIRE fellowship. KAA was supported by the INSPIRE scholarship, Government of India. KA and RU were supported by the CSIR fellowship, Government of India.

## ACKNOWLEDGMENTS

We acknowledge the IISER Pune Microscopy Facility for access to equipment and infrastructure. We thank Lahiri lab members for their timely help with the experiments and comments.

## SUPPLEMENTARY MATERIAL

The Supplementary Material for this article can be found online at: https://www.frontiersin.org/articles/10.3389/fgene.2021.634938/full#supplementary-material

## REFERENCES

Alexander, N. R., Tran, N. L., Rekapally, H., Summers, C. E., Glackin, C., and Heimark, R. L. (2006). N-cadherin gene expression in prostate carcinoma is modulated by integrin-dependent nuclear translocation of Twist1. *Cancer Res.* 66, 3365–3369. doi: 10.1158/0008-5472.CAN-05-3401

Anandi, V. L., Ashiq, K. A., Nitheesh, K., and Lahiri, M. (2016). Platelet-activating factor promotes motility in breast cancer cells and disrupts non-transformed breast acinar structures. *Oncol. Rep.* 35, 179–188. doi: 10.3892/or.2015.4387

Anandi, L., Chakravarty, V., Ashiq, K. A., Bodakuntla, S., and Lahiri, M. (2017). DNA-dependent protein kinase plays a central role in transformation of breast epithelial cells following alkylation damage. *J. Cell Sci.* 130, 3749–3763. doi: 10.1242/jcs.203034

Bennett, S. A., Leite, L. C., and Birnboim, H. C. (1993). Platelet activating factor, an endogenous mediator of inflammation, induces phenotypic transformation of rat embryo cells. *Carcinogenesis* 14, 1289–1296. doi: 10.1093/carcin/14.7.1289

Bussolati, B., Biancone, L., Cassoni, P., Russo, S., Rola-Pleszczynski, M., Montrucchio, G., et al. (2000). PAF produced by human breast cancer cells promotes migration and proliferation of tumor cells and neo-angiogenesis. *Am. J. Pathol.* 157, 1713–1725. doi: 10.1016/S0002-9440(10)64808-0

Chen, J., Lan, T., Zhang, W., Dong, L., Kang, N., Zhang, S., et al. (2015a). Feed-forward reciprocal activation of PAFR and STAT3 regulates epithelial-mesenchymal transition in non-small cell lung cancer. *Cancer Res.* 75, 4198–4210. doi: 10.1158/0008-5472.can-15-1062

Chen, J., Lan, T., Zhang, W., Dong, L., Kang, N., Zhang, S., et al. (2015b). Platelet-activating factor receptor-mediated PI3K/AKT activation contributes to the malignant development of esophageal squamous cell carcinoma. *Oncogene* 34, 5114–5127. doi: 10.1038/onc.2014.434

Chen, J., Yang, L., Foulks, J. M., Weyrich, A. S., Marathe, G. K., and McIntyre, T. M. (2007). Intracellular PAF catabolism by PAF acetylhydrolase counteracts continual PAF synthesis. *J. Lipid Res.* 48, 2365–2376. doi: 10.1194/jlr.M700325-JLR200

Chignard, M., Le Couedic, J. P., Tence, M., Vargaftig, B. B., and Benveniste, J. (1979). The role of platelet-activating factor in platelet aggregation. *Nature* 279, 799–800. doi: 10.1038/279799a0

Debnath, J., and Brugge, J. S. (2005). Modelling glandular epithelial cancers in three-dimensional cultures. *Nat. Rev. Cancer* 5, 675–688. doi: 10.1038/nrc1695

Debnath, J., Muthuswamy, S. K., and Brugge, J. S. (2003). Morphogenesis and oncogenesis of MCF-10A mammary epithelial acini grown in three-dimensional basement membrane cultures. *Methods* 30, 256–268. doi: 10.1016/S1046-2023(03)00032-X

Foa, R., Bussolino, F., Ferrando, M. L., Guarini, A., Tetta, C., Mazzone, R., et al. (1985). Release of platelet-activating factor in human leukemia. *Cancer Res.* 45, 4483–4485.

Fournier, M. V., Martin, K. J., Kenny, P. A., Xhaja, K., Bosch, I., Yaswen, P., et al. (2006). Gene expression signature in organized and growth-arrested mammary acini predicts good outcome in breast cancer. *Cancer Res.* 66, 7095–7102. doi: 10.1158/0008-5472.CAN-06-0515

Hanahan, D., and Weinberg, R. A. (2011). Hallmarks of cancer: the next generation. *Cell* 144, 646–674. doi: 10.1016/j.cell.2011.02.013

Horibata, S., Vo, T. V., Subramanian, V., Thompson, P. R., and Coonrod, S. A. (2015). Utilization of the soft agar colony formation assay to identify inhibitors of tumorigenicity in breast cancer cells. *J. Vis. Exp.* e52727. doi: 10.3791/52727

Ioachim, E., Charchanti, A., Briasoulis, E., Karavasilis, V., Tsanou, H., Arvanitis, D. L., et al. (2002). Immunohistochemical expression of extracellular matrix components tenascin, fibronectin, collagen type IV and laminin in breast cancer: their prognostic value and role in tumour invasion and progression. *Eur. J. Cancer* 38, 2362–2370. doi: 10.1016/S0959-8049(02)00210-1

Ishii, S., and Shimizu, T. (2000). Platelet-activating factor (PAF) receptor and genetically engineered PAF receptor mutant mice. *Prog. Lipid Res.* 39, 41–82. doi: 10.1016/S0163-7827(99)00016-8

Itoh, T., Tanioka, M., Yoshida, H., Yoshioka, T., Nishimoto, H., and Itohara, S. (1998). Reduced angiogenesis and tumor progression in gelatinase A-deficient mice. *Cancer Res.* 58, 1048–1051.

Ivers, L.P., Cummings, B., Owolabi, F., Welzel, K., Klinger, R., and Saitoh, S., et al. (2014). Dynamic and influential interaction of cancer cells with normal epithelial cells in 3D culture. *Cancer Cell Int.* 14:108. doi: 10.1186/s12935-014-0108-6

Jancar, S., and Chammas, R. (2014). PAF receptor and tumor growth. *Curr. Drug Targets* 15, 982–987. doi: 10.2174/1389450115666140903111812

Kalluri, R., and Weinberg, R. A. (2009). The basics of epithelial-mesenchymal transition. *J. Clin. Invest.* 119, 1420–1428. doi: 10.1172/JCI39104

Kaur, J., Sawhney, M., DattaGupta, S., Shukla, N. K., Srivastava, A., Walfish, P. G., et al. (2013). Clinical significance of altered expression of β-catenin and E-cadherin in oral dysplasia and cancer: potential link with ALCAM expression. *PLoS One* 8:e67361. doi: 10.1371/journal.pone.0067361

Kispert, S., Marentette, J., and McHowat, J. (2015). Cigarette smoke induces cell motility via platelet-activating factor accumulation in breast cancer cells: a potential mechanism for metastatic disease. *Physiol. Rep.* 3:e12318. doi: 10.14814/phy2.12318

Kispert, S., Marentette, J., and McHowat, J. (2019). Cigarette smoking promotes bladder cancer via increased platelet-activating factor. *Physiol. Rep.* 7:e13981. doi: 10.14814/phy2.13981

Kourtidis, A., Lu, R., Pence, L. J., and Anastasiadis, P. Z. (2017). A central role for cadherin signaling in cancer. *Exp. Cell Res.* 358, 78–85. doi: 10.1016/j.yexcr.2017.04.006

Lambert, A. W., Pattabiraman, D. R., and Weinberg, R. A. (2017). Emerging biological principles of metastasis. *Cell* 168, 670–691. doi: 10.1016/j.cell.2016.11.037

Lamouille, S., Xu, J., and Derynck, R. (2014). Molecular mechanisms of epithelial-mesenchymal transition. *Nat. Rev. Mol. Cell Biol.* 15, 178–196. doi: 10.1038/nrm3758

Lee, M., and Vasioukhin, V. (2008). Cell polarity and cancer--cell and tissue polarity as a non-canonical tumor suppressor. *J. Cell Sci.* 121, 1141–1150. doi: 10.1242/jcs.016634

Lordan, R., Tsoupras, A., Zabetakis, I., and Demopoulos, C. A. (2019). Forty years since the structural elucidation of platelet-activating factor (PAF): historical, current, and future research perspectives. *Molecules* 24:4414. doi: 10.3390/molecules24234414

Lv, X. X., Liu, S. S., Li, K., Cui, B., Liu, C., and Hu, Z. W. (2017). Cigarette smoke promotes COPD by activating platelet-activating factor receptor and inducing neutrophil autophagic death in mice. *Oncotarget* 8, 74720–74735. doi: 10.18632/oncotarget.20353

Man, Y. G., Stojadinovic, A., Mason, J., Avital, I., Bilchik, A., Bruecher, B., et al. (2013). Tumor-infiltrating immune cells promoting tumor invasion and metastasis: existing theories. *J. Cancer* 4, 84–95. doi: 10.7150/jca.5482

Millarte, V., and Farhan, H. (2012). The Golgi in cell migration: regulation by signal transduction and its implications for cancer cell metastasis. *ScientificWorldJournal* 2012:498278. doi: 10.1100/2012/498278

Miyaura, S., Eguchi, H., and Johnston, J. M. (1992). Effect of a cigarette smoke extract on the metabolism of the proinflammatory autacoid, platelet-activating factor. *Circ. Res.* 70, 341–347. doi: 10.1161/01.RES.70.2.341

Olson, A., Le, V., Aldahl, J., Yu, E. J., Hooker, E., He, Y., et al. (2019). The comprehensive role of E-cadherin in maintaining prostatic epithelial integrity during oncogenic transformation and tumor progression. *PLoS Genet.* 15:e1008451. doi: 10.1371/journal.pgen.1008451

Padmanaban, V., Krol, I., Suhail, Y., Szczerba, B. M., Aceto, N., Bader, J. S., et al. (2019). E-cadherin is required for metastasis in multiple models of breast cancer. *Nature* 573, 439–444. doi: 10.1038/s41586-019-1526-3

Papakonstantinou, V. D., Lagopati, N., Tsilibary, E. C., Demopoulos, C. A., and Philippopoulos, A. I. (2017). A review on platelet activating factor inhibitors: could a new class of potent metal-based anti-inflammatory drugs induce anticancer properties? *Bioinorg. Chem. Appl.* 2017:6947034. doi: 10.1155/2017/6947034

Pastushenko, I., and Blanpain, C. (2019). EMT transition states during tumor progression and metastasis. *Trends Cell Biol.* 29, 212–226. doi: 10.1016/j.tcb.2018.12.001

Puisieux, A., Brabletz, T., and Caramel, J. (2014). Oncogenic roles of EMT-inducing transcription factors. *Nat. Cell Biol.* 16, 488–494. doi: 10.1038/ncb2976

Scheel, C., and Weinberg, R. A. (2011). Phenotypic plasticity and epithelial-mesenchymal transitions in cancer and normal stem cells? *Int. J. Cancer* 129, 2310–2314. doi: 10.1002/ijc.26311

Shaw, K. R., Wrobel, C. N., and Brugge, J. S. (2004). Use of three-dimensional basement membrane cultures to model oncogene-induced changes in mammary epithelial morphogenesis. *J. Mammary Gland Biol. Neoplasia* 9, 297–310. doi: 10.1007/s10911-004-1402-z

Solanas, G., Porta-de-la-Riva, M., Agustí, C., Casagolda, D., Sánchez-Aguilera, F., Larriba, M. J., et al. (2008). E-cadherin controls beta-catenin and NF-kappaB transcriptional activity in mesenchymal gene expression. *J. Cell Sci.* 121, 2224–2234. doi: 10.1242/jcs.021667

Tsoupras, A. B., Iatrou, C., Frangia, C., and Demopoulos, C. A. (2009). The implication of platelet activating factor in cancer growth and metastasis: potent beneficial role of PAF-inhibitors and antioxidants. *Infect. Disord. Drug Targets* 9, 390–399. doi: 10.2174/187152609788922555

Vidi, P. A., Bissell, M. J., and Lelièvre, S. A. (2013). Three-dimensional culture of human breast epithelial cells: the how and the why. *Methods Mol. Biol.* 945, 193–219. doi: 10.1007/978-1-62703-125-7_13

Wu, X., and Gallo, K. A. (2013). The 18-kDa translocator protein (TSPO) disrupts mammary epithelial morphogenesis and promotes breast cancer cell migration. *PLoS One* 8:e71258. doi: 10.1371/journal.pone.0085166

Yu, Y., and Elble, R. C. (2016). Homeostatic signaling by cell-cell junctions and its dysregulation during cancer progression. *J. Clin. Med.* 5:26. doi: 10.3390/jcm5020026

**Conflict of Interest:** The authors declare that the research was conducted in the absence of any commercial or financial relationships that could be construed as a potential conflict of interest.

frontiers in Genetics

ORIGINAL RESEARCH
published: 07 April 2021
doi: 10.3389/fgene.2021.635808

# Human ALKBH6 Is Required for Maintenance of Genomic Stability and Promoting Cell Survival During Exposure of Alkylating Agents in Pancreatic Cancer

*Shengyuan Zhao, Rodan Devega, Aaliyah Francois and Dawit Kidane**

*Division of Pharmacology and Toxicology, College of Pharmacy, Dell Pediatric Research Institute, The University of Texas at Austin, Austin, TX, United States*

Alpha-ketoglutarate-dependent dioxygenase (ALKBH) is a DNA repair gene involved in the repair of alkylating DNA damage. There are nine types of ALKBH (ALKBH1-8 and FTO) identified in humans. In particular, certain types of ALKBH enzymes are dioxygenases that directly reverse DNA methylation damage via transfer of a methyl group from the DNA adduct onto α-ketoglutarate and release of metabolic products including succinate and formaldehyde. Here, we tested whether ALKBH6 plays a significant role in preventing alkylating DNA damage and decreasing genomic instability in pancreatic cancer cells. Using an *E. coli* strain deficient with ALKB, we found that ALKBH6 complements ALKB deficiency and increases resistance after alkylating agent treatment. In particular, the loss of ALKBH6 in human pancreatic cancer cells increases alkylating agent-induced DNA damage and significantly decreases cell survival. Furthermore, *in silico* analysis from The Cancer Genome Atlas (TCGA) database suggests that overexpression of ALKBH6 provides better survival outcomes in patients with pancreatic cancer. Overall, our data suggest that ALKBH6 is required to maintain the integrity of the genome and promote cell survival of pancreatic cancer cells.

**Keywords: alkbh6, alkylating DNA damage, pancreatic cancer, DNA repair, Alkb *E. coli***

OPEN ACCESS

***Edited by:***
*Anthony Davis, University of Texas Southwestern Medical Center, United States*

***Reviewed by:***
*Damian Mielecki, Institute of Biochemistry and Biophysics (PAN), Poland*
*Roy Anindya, Indian Institute of Technology Hyderabad, India*

****Correspondence:***
*Dawit Kidane*
*dawit.kidane@austin.utexas.edu*

***Specialty section:***
*This article was submitted to Genetics of Common and Rare Diseases, a section of the journal Frontiers in Genetics*

***Received:*** *30 November 2020*
***Accepted:*** *08 March 2021*
***Published:*** *07 April 2021*

***Citation:***
*Zhao S, Devega R, Francois A and Kidane D (2021) Human ALKBH6 Is Required for Maintenance of Genomic Stability and Promoting Cell Survival During Exposure of Alkylating Agents in Pancreatic Cancer. Front. Genet. 12:635808. doi: 10.3389/fgene.2021.635808*

## INTRODUCTION

Pancreatic cancer is the seventh leading cause of cancer-related death in the world (Bray et al., 2020). The global cancer statistics estimate 495,773 new cases and 466,003 deaths in 2020. Pancreatic cancer patients are often diagnosed at late stages of the disease, and approximately 20–30% of patients experience relapse after surgical therapy (Mahipal et al., 2015). The 5-year overall survival of patients is less than 10% (Conroy et al., 2011; Von Hoff et al., 2013). The extremely low 5-year overall survival of patients is, in part, due to pancreatic cancer cells having several mechanisms of resistance to different chemotherapeutic treatments, one of which is their capacity to efficiently repair alkylating agent-induced DNA damage. Importantly, alkylating agents induce DNA damage at different genomic sites, which subsequently leads to lethal and/or mutagenic DNA base lesions. The major repair mechanisms for alkylation damage are direct DNA repair, base excision repair (BER), and mismatch repair (MMR) (Kondo et al., 2010). It is critical to uncover the molecular

mechanisms that contribute to carcinogenesis and to identify an effective novel target for therapies directed toward pancreatic cancer.

Direct DNA repair comprises several types of DNA repair enzymes that reversibly remove alkyl groups from damaged DNA bases through oxidative dealkylation processes. The α-ketoglutarate- and Fe (II)-dependent dioxygenases remove alkyl groups from DNA and proteins via oxidative demethylation (Mishina et al., 2004). In several studies in *Escherichia coli*, the induction of the Ada response with alkylating agents results in increased expression of different genes including *ADA*, ALKA, ALKB, and AIDB (Lindahl et al., 1988). In particular *Escherichia coli* (*E. coli*) have shown that certain types of alkylating agent-induced DNA base damage is repaired by AlkB dioxygenase via direct reversal repair pathways (Sedgwick et al., 2007; Yi and He, 2013). Together with $O^6$-methylguanine-DNA methyltransferase (MGMT), the ALKB dioxygenase removes alkyl lesions to protect the genome from mutagenic and/or cytotoxic consequences (Zhang et al., 1993; Rose et al., 2011). Several alkylating agents are commonly used in chemotherapy but may induce DNA damage to cancer cells as well as normal cells. Based on alkylating mechanisms, these agents can be divided as SN1 and SN2. *N*-methyl-*N*'-nitro-*N*-nitrosoguanidine (MNNG), a common SN1 agent, predominantly induces $O^6$-methylguanine ($O^6$mG) and $N^3$-methyladenine ($m^3A$) lesions, which then block the DNA replication fork and generate genotoxic double-stranded DNA (DSBs) breaks (Loechler et al., 1984; Shah and Gold, 2003). In comparison, the SN2 agent methyl methane sulfonate (MMS) induces $N^1$-methyladenine ($m^1A$) and $N^3$-methylcytosine ($m^3C$) lesions, preferably in single-stranded DNA (ssDNA). Overall, accumulation of these unrepaired DNA base lesions and their repair intermediates can lead to cell death (van den Born et al., 2009; Dietlein et al., 2014).

In *E. coli*, the ALKB (EcALKB) protein is involved in DNA and RNA repair in response to environmental stress (Nieminuszczy and Grzesiuk, 2007). Several biochemical and genetic studies have demonstrated that the EcALKB protein initiates repair by promoting oxidative demethylation of the alkyl DNA base lesions, including $m^1A$ and $m^3C$ lesions (Falnes et al., 2002; Trewick et al., 2002). In contrast, in the human genome, there are nine genes that encode EcALKB homologs, including ALKBH1-8 and FTO (fat mass and obesity-associated protein) (Aravind and Koonin, 2001; Sedgwick et al., 2007; Ougland et al., 2015). So far, a significant number of human ALKBH proteins (ALKBH1, ALKBH2, ALKBH3, and FTO) have been characterized *in vitro* to show DNA repair activity and epigenetic as well as RNA post transcription modification on methylated DNA/RNA substrates (Duncan et al., 2002; Aas et al., 2003; Westbye et al., 2008). In particular, ALKBH2 (Nay et al., 2012) and ALKBH3 (Sundheim et al., 2006) complement ALKB-deficient *E. coli in vivo* (Aas et al., 2003). In addition, ALKBH2 and ALKBH3 are involved in the repair of alkylating DNA damage in both cell culture and animal models to protect the integrity of the genome (Calvo et al., 2012; Fu and Samson, 2012; Aihara et al., 2016). Studies conducted in a transgenic knockout mouse model show that ALKBH2 repairs $m^1A$ lesions (Ringvoll et al., 2006), while ALKBH3 plays a role in the repair of $m^3C$ lesions in human cells (Dango et al., 2011). ALKBH2 and ALKBH3 use the same α-KG/Fe(II)-dependent mechanism to oxidize alkyl groups on DNA base lesions, subsequently removing the damage and restoring normal DNA bases (Zheng et al., 2014; Fedeles et al., 2015; Aihara et al., 2016). However, some of the other α-KG/Fe(II)-dependent ALKBH proteins are involved in various other biochemical pathways including RNA metabolism, histone demethylation, and fatty acid metabolism (Rajecka et al., 2019). For example, ALKBH8 and ALKBH5 are involved in processing tRNAs and modifying N(6)-methyladenosine ($N^6$-mA) in mRNA, respectively (Fu et al., 2010). In contrast, ALKBH1 is an important nuclear eraser of $N^6$-mA in unpairing regions of DNA of the mammalian genome (Zhang et al., 2020). These findings suggest additional roles of mammalian ALKBH enzymes in RNA post transcript modification and regulations of epigenetic markers.

However, the role of ALKBH6 in the maintenance of genomic stability and protection from alkylating DNA damage is unknown. In this study, we show that human ALKBH6 is required to prevent genomic instability and to prevent the MMS-induced cytotoxicity seen in pancreatic cancer. Our data show that siRNA silencing of ALKBH6 in pancreatic cancer cell lines increases DSBs and sensitivity to MMS but not MNU. Moreover, our TCGA data analysis shows that a majority of tumor tissues significantly overexpress ALKBH6, as compared to normal tissue, and show poor overall survival in the selected types of human cancers, thus suggesting a pro-carcinogenic role of these proteins (Tan et al., 2015). Specifically, an approximate 4% genetic alteration and 28% mRNA overexpression of ALKBH6 is detected in pancreatic cancer cells compared to other ALKBH genes. In this study, overexpression of ALKBH6 genes improves pancreatic cancer survival rates, compared to pancreatic cancer patients with low expression. However, ALKBH6 overexpression in p53 mutant tumors is associated with poor overall survival. Altogether, these results suggest that ALKBH6 is involved in maintaining genomic integrity during SN2 alkylating agent-mediated DNA damage, and also provides a more favorable prognosis in the overall survival of pancreatic cancer patients.

# MATERIALS AND METHODS

## Bacterial Strains and Media

The following *E. coli* K12 strains (a gift from Dr. Elżbieta Grzesiuk) were used: AB1157 [argE3, hisG4, leuB6, Δ(gpt -proA)62, thr -1, ara -1, galK2, lacY1, mtl-1, xylA5, thi-1, rpsL31, glnV44, tsx-33, rfbD1, mgl-51, kdgK51] as wild-type (WT: $alkB^+$); BS87 (as AB1157 but alkB117:Tn3) as $alkB^-$ (Sedgwick, 1992).

## Construction of Plasmids for ALKBH6 Expression

A human cDNA pool was constructed by reverse transcription-PCR (RT-PCR) with the Transcriptor High Fidelity cDNA Synthesis Kit (Cat. 5081955001, Sigma Aldrich,

St. Louis, MO) from RNA extracted from immortalized non-transformed gastric epithelial cell (GES-1). A 650-bp cDNA, encoding the human ALKBH6 open reading frame (nt 280–786 of XM_024451747), was amplified using PCR (Platinum Taq, Invitrogen, Carlsbad, CA). The primers are: 5′-GCGAAGCTTTCACTTGCCCAGCAGG-3′, and 5′-GCTCTAGAGCGGAAATGGCTGGGAG-3′. The amplified product was cloned into pBAD24 (Addgene) as an *Xba*I-*Not*I fragment. The recombinant plasmid was transformed into BS87 with electroporation to construct BS87-pBAD24-ALKBH6, and the expression of ALKBH6 was induced by the addition of 0.1% arabinose (Cat. A3256, Sigma Aldrich).

## Quantitative Growth Curve and Colony-Forming Assay of *E. coli*

WT, ALKB$^{-}$, and transformed *E. coli* were grown in 3 ml of LB broth (Cat. L3022, Sigma Aldrich) at 37°C overnight, shaking at 250 rpm. For growth curve analysis, 10 μl of bacteria culture was added to 5 ml of LB broth containing 1 mM of MMS or 1 mM of MNU with 0.1% arabinose and was allowed to grow at 37°C overnight, again shaking at 250 rpm. The optical density at 600 nm (OD600) was determined every 30 min until the observed growth curve reached a plateau state. For the colony-forming assay, the bacteria culture following overnight growth was diluted to $10^3$ cells/ml using OD600 quantification. Next, 100 μl of the diluted culture was spread on LB plates containing MMS (0–3 mM) or MNU (0–3 mM) with 0.1% arabinose and were allowed to grow overnight at 37°C overnight. The colonies were counted the next day.

## Small Interfering RNA (siRNA) for Silencing of ALKBH6

ON-TARGETplus human ALKBH6 siRNA duplexes (Cat. L-015030-01-0005) were purchased from Dharmacon Research Inc. (Lafayette, CO). All siRNAs were suspended in RNase-free water to achieve a concentration of 5 μM for each siRNA. A final concentration of 25 nM for siRNA was used for subsequent experiments. The siRNA sequences are as follows: J-015030-09: 5′-GGACGCUGGUGGACGGAUU; J-015030-10: 5′-GCUGUGACUCCGCGACCUA; J-015030-11: 5′-AGGAGUAUUUGCUUCGACA; J-015030-12: 5′-GCAAGGA GUUGGUGUUGAU.

## Cell Lines and Drug Treatment

Human pancreatic cancer cell lines MIA-PaCa-2 and BXPC3 (a gift from Dr. John DiGiovanni) were maintained in EMEM media supplemented with 10% Fetal Bovine Serum (FBS), 1% penicillin/streptomycin, and 1% L-glutamine at 37°C in a 5% $CO_2$ environment. Methyl methanesulfonate (MMS, Cat. 129925, Sigma-Aldrich, St. Louis, MO) and *N*-nitroso-*N*-methylurea (MNU, Cat. N2939, Spectrum Chemical, New Brunswick, NJ) were dissolved in DMSO, and stored at −20°C before use. Forty-eight hours after siRNA treatment, 70% of the confluent cells were treated with either MMS or MNU at various concentrations for 24 h in culture. The cells were then washed with PBS and used for further analysis.

## Clonogenic Survival Assay

A clonogenic survival assay was performed according to the previously published protocol, including minor modifications (Franken et al., 2006). Both the control and ALKBH6-siRNA silenced cells were plated in six-well plates at a density of 500 cells per well and cultured to allow adherence overnight. Seventy percent of confluent cells were then treated with MMS (0–5 mM), or MNU (0–5 mM) for 24 h. Following treatment, the cells were then washed with PBS and supplemented with fresh growth media and allowed to grow for an additional 10 days. The cells were then stained with 0.25% crystal violet in an 80% methanol solution for 30 min. The colonies were finally counted and scored using visual techniques.

## Western Blotting

Cells were lysed with radioimmunoprecipitation assay (RIPA) buffer supplemented with a protease inhibitor (Cat. 25765800, Sigma Aldrich) and a phosphatase inhibitor (Cat. P5726, Sigma Aldrich). Protein concentration was measured using a BCA kit as described by the manufacturer (Cat# 23250 Thermo Fisher Scientific, United States). After denaturing the samples at 95°C for 5 min, 30 μg of the protein samples were separated using SDS-PAGE and transferred onto nitrocellulose membranes (Cat. 1620112, Bio-Rad, Hercules, CA). Next, the membranes were blocked with 5% BSA for 1 h, and then incubated with primary antibodies against γ$H_2$AX (Cat. 07-164, Millipore, Burlington, MA), ALKBH6 (Cat. ab170186, Abcam, Cambridge, MA; antibody dilution 1:1,000), and α-tubulin (Cat. 2125S, Cell Signaling, Danvers, MA; antibody dilution 1:500) overnight. The following day, the membranes were washed with PBST and incubated with anti-mouse (Cat. NXA931, GE healthcare, Chicago, IL) or anti-rabbit (Cat. NA934V, GE Healthcare) secondary antibody for 2 h before developing with ECL substrates (Bio-rad, 170506). The gel images were captured using A Chem-DocXRS image acquisition machine (Bio-Rad).

## Immunofluorescence

The $5 \times 10^4$ cells were seeded in cover slips and cultured for 24 h before siRNA and drug treatment (see above). Cells were then fixed with 3.7% paraformaldehyde (PFA) for 15 min, and permeabilized with 0.5% Triton X-100 in PBS for 10 min. The cells were then blocked with 3% BSA for 1 h, prior to incubation at 4°C overnight with primary antibodies, including γ$H_2$AX (Cat. 07-164, Millipore: dilution 1: 400) and 53BP1 (Cat. Sc-22760, Santa Cruz, Dallas, TX; dilution 1:400). On the following day, the cells were washed with PBS and incubated for 1 h with the secondary antibody, including FITC-conjugated anti-mouse antibody (Cat. 715-095-150, dilution 1:400, Jackson ImmunoResearch Labs, West Grove, PA) and TRITC-conjugated anti-rabbit antibody (Cat. 711-025-152, Jackson ImmunoResearch Labs; dilution 1:400). Finally, the cells were mounted with cover slips using mounting media containing DAPI stain before visualization.

## Cell Cycle Analysis

We performed cell cycle analyses by flow cytometry as previously described (Shimada et al., 2003). Cells were briefly harvested after siRNA and drug treatment, washed with PBS, and then fixed in cold 70% ethanol overnight. Further, these cells were stained with 20 ml/mL of propidium iodide and treated with 1 mg/mL of RNase for at least 30 min. The cell cycle distribution was then analyzed using FlowJo 10.5.3.

## Data Acquisition

TCGA provisional data sets were pulled from cBioPortal[1] between the months of November 2017 and January 2018. The pulled data sets consisted of pancreatic adenocarcinoma (PADC; $n$ = 147). Since ALKBH6 is the primary source of interest for this analysis, only individuals with valid RNA Seq V2 RSEM data for ALKBH6 were included. To group individuals as having either low or high expression of *NEIL3*, the $z$ scores of each individual were considered. Individuals with a $z$ score of $\leq$-0.5 were placed into the low expressing group while individuals with a $z$ score of $\geq$ 0.5 were placed into the high expressing group. Individuals falling between -0.5 and 0.5 were excluded from analyses. In addition, individuals in the low or high expressing group reporting a null value for OS months were excluded from the group analyses.

## Statistical Analysis

Three independent experiments were performed using immunofluorescence, a comet assay, cell proliferation, and a cell survival assay. Data were statistically analyzed using Student's $t$-test. Survival analyses of high and low expression of ALKBH6 were evaluated using the Kaplan–Meier method and the log-rank test using a Graph Pad prism. Results were considered significant at $P < 0.05$.

# RESULTS

## Human ALKBH6 Genes Complement ALKB Deficiency in *E. coli* and Enhance Response for DNA Alkylating Agents

Biochemical and structural studies of *E. coli* ALKB and other human ALKBH proteins provide mechanistic insight into how oxidative dealkylation catalyzed by ALKB dioxygenases proteins with an $Fe^{2+}$ binding site at H131, D133, and H187 active sites (Mishina et al., 2004). In addition, the minor β-sheet, and the major β-sheet, contain the 2OG-binding $R_{204}xNxTxR_{210}$ motif (numbering of the residues as in the ALKB structure). The 1-carboxylate and 2-oxo groups of 2OG bind to the metal in a bidentate manner, whereas the 5-carboxylate of 2OG interacts by means of a hydrogen bond with Arg 210 and by means of a salt bridge with Arg 204 (Yu et al., 2006; Yang et al., 2008; Yi et al., 2010; Feng et al., 2014). However, little is known about the functional domain of ALKBH6 proteins in mammalian cells. Specifically, ALKBH6 contains an Fe (II) metal center in the wild-type enzymes coordinated to the binding site at H114, D116, and H182, with two α-KG binding sites (103–105 aa and 218–224aa), and oxygen (**Figure 1A**, taxonomic identifier 9606, NCBI). To determine whether ALKBH6 plays role in alkylating DNA damage repair, we cloned human ALKBH6 genes and generated an *E. coli* strain to express human ALKBH6 using pBAD-24 plasmids. Our growth assay shows that expression of ALKBH6 in an ALKB-deficient strain increases survival by 50% during 1-mM MMS treatment (**Figure 1B**). In contrast, ALKBH6 complements ALKB-deficient *E. coli* and enhances survival by 1% during 1-mM MNU treatment **(Figure 1C**).

[1]http://cbioportal.org

## ALKBH6-Deficient Pancreatic Cells Accumulate Alkylating Agent-Induced DNA Damage

To determine whether ALKBH6 protects pancreatic cancer cells from accumulating alkylating agent-induced DNA damage, we performed siRNA-mediated silencing of ALKBH6 in BXPC3 and MIA-PaCa-2 pancreatic cancer cell lines and performed an immunofluorescence co-localization assay. Silencing of ALKBH6 with siRNA was confirmed with Western blot which showed a >90% depletion of the target protein (**Figure 2A**). To further explore whether ALKBH6 protects PDAC cells from alkylating DNA damage, we treated BxPC3 and MIA-PaCa-2 cells with MMS or MNU for 1 h and then examined them by immunofluorescence staining for γH2AX and 53BP1 co-localization (**Figure 2B**), both established biomarkers for DSBs. We found that siRNA mediated silencing of ALKBH6 in BXPC3 and MIA-PaCa-2 cell lines led to a significantly increased co-localization of γH2AX/53BP1 in the BXPC3 (80%) and MIA-PaCa-2 cells treated with MMS (75%) versus WT cells (40%) (**Figure 2C**; left panel; $P < 0.001$). In contrast, there was no significant difference found in the cells treated with MNU versus untreated cells (**Figure 2C**; right panel). Furthermore, the neutral comet assay confirmed that DSBs were significantly increased in siRNA-mediated ALKBH6 silencing in BXPC3 and MIA-PaCa-2 cells following their treatment with MMS ($^{**}P < 0.01$) as compared to untreated cells and/or wild-type cells treated with MMS (**Figure 2D**). Our data suggested that ALKBH6 prevents accumulation of MMS-induced DSBs in PDAC cells.

## ALKBH6 Required for Cell Survival During Exposure to Alkylating Agents

To determine whether ALKBH6 promotes cell survival and cellular growth, we performed siRNA-mediated silencing of ALKBH6 in BXPC3 and MIA-PaCa-2 pancreatic cancer cell lines and performed a clonogenic survival assay. We investigated whether siRNA-mediated silencing of ALKBH6 in PDAC cells had decreased cell proliferation and increased cell survival after treatment with MMS or MNU (**Figures 3A,B**). We show that by directly measuring both cell growth and cell survival, we can likely provide evidence on how the pancreatic cells respond to MMS and MNU treatments. Cell viability in the ALKBH6-deficient BXPC3 and MIA-PaCa-2 cells were found to be significantly reduced as compared to the ALKBH6-proficient BXPC3 (60% versus 75%; $P < 0.01$) and MIA-PaCa-2 (55% versus 80%; $P < 0.01$) cells following treatment with MMS, but not

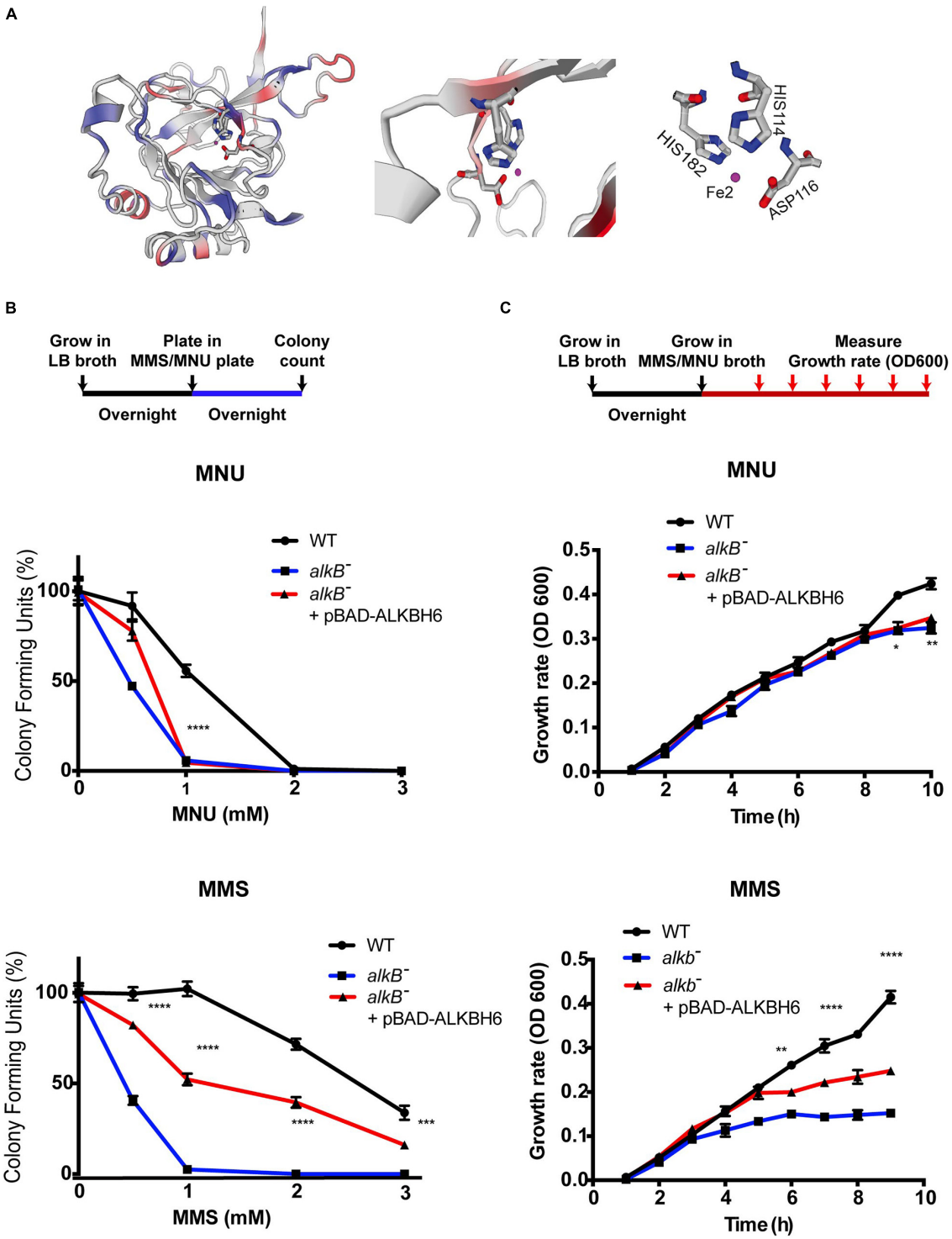


**FIGURE 1 |** ALKBH6 partially restores growth and increases resistance to alkylating DNA-damaging agents. **(A)** Model of ALKBH6 (238 aa) based on SWISS-MODEL indicating metal binding sites labeled in red (HIS114, ASP116, and HIS182). The $Fe^{2+}$ ion in the active site is shown in purple; protein residues (His114 represented by blue/gray ring; His182 represented by blue/gray ring; D116 represented by gray/red) are labeled in white. **(B)** Schematic representation and results of colony-forming assay using *ALKB*-proficient strain (WT), ALKB-deficient strain (*ALKB*$^{-}$), and ALKBH6-complemented *E. coli* strain (ALKB$^{-}$ + pBAD-ALKBH6). Results were normalized with untreated groups. Student's *t*-test was used to determine whether there was significant difference between deficient and complemented strains. **(C)** Schematic representation and results of growth curve assay using the same three strains mentioned above. $^{*}p < 0.05$, $^{**}p < 0.01$, $^{***}p < 0.001$, $^{****}p < 0.0001$ represent *t*-test results. N.S represents non-significant difference, three independent experiments.

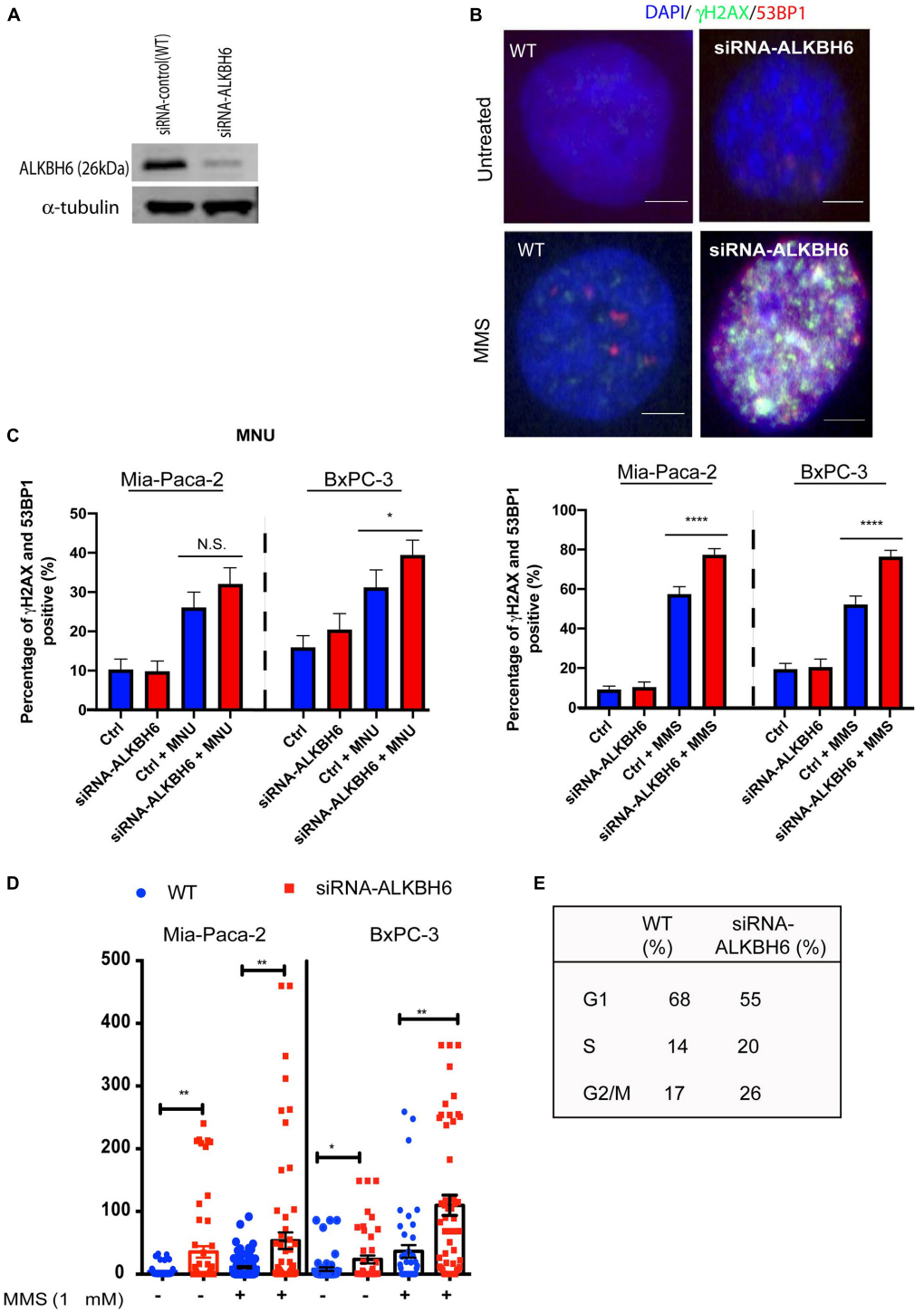


**FIGURE 2 |** Loss of ALKBH6 induces DSBs. **(A)** Western blot of siRNA-mediated silencing of ALKBH6 on MIA-PaCa-2 cells; **(B)** Representative image of siRNA-mediated silencing of BXPC3 and MIA-PaCa-2 cells treated with MMS and examined with co-localization of 53BP1 and γH2AX; note that blue color represents DAPI staining of the cell nuclei; scale bar represents 10 μm; **(C)** Percent of cells positive for co-localization of 53BP1 and γH2AX treated with MMS/MNU; **(D)** Representative image of ALKBH6 knockout; **(D)** results of tail moment of BxPC3 and MIA-PaCa-2 cells treated with MMS and examined with neutral comet assay; **(E)** Cell cycle profile of cells deficient in ALKBH6. Student's *t*-test was applied for data analysis. $^{*}p < 0.05$, $^{**}p < 0.01$), $^{****}p < 0.0001$, N.S represents non-significant difference, three independent experiments.

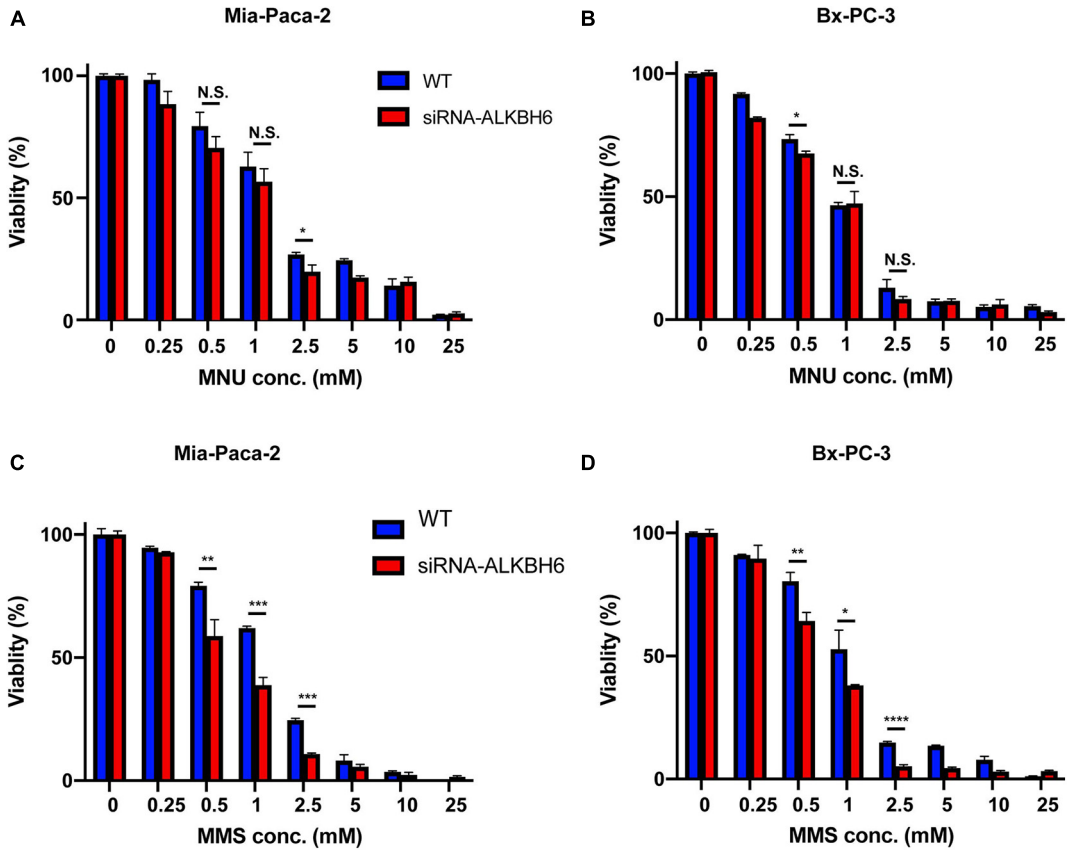


**FIGURE 3 |** ALKBH6 protects pancreatic cells from alkylating agents. **(A,B)** MTT assay results of MIA-PaCa-2 and BxPC-3 cells treated with a different concentration of MNU for 24 h following ALKBH6 knockout; **(C,D)** MTT assay results of MIA-PaCa-2 and BxPC-3 cells treated with a different concentration of MMS for 24 h following siRNA silencing of ALKBH6 cells; Student's *t*-test was applied for data analysis. $^{*}p < 0.05$, $^{**}p < 0.01$, $^{***}p < 0.001$), $^{****}p < 0.0001$, N.S represents non-significant difference, three independent experiments.

with MNU (**Figures 3C,D**). Collectively, these data indicate that ALKBH6 deficiency leaves PDAC cells vulnerable to cytotoxicity resulting from SN2 alkylating agent treatment.

## ALKBH6 Overexpression in p53 Mutant Tumors Induces Poor Overall Survival in Pancreatic Cancer Patients

To correlate our findings to human pancreatic cancer, we quantified the expression data of ALKBH6 in pancreatic cancer using The Cancer Genome Atlas database (TCGA). We observed that 28% of pancreatic cancer patients overexpressed mRNA of ALKBH6 in tumor tissue samples relative to normal pancreatic tissue (**Figure 4A**). Moreover, high expression of ALKBH6 in pancreatic cancer tissue was correlated with favorable overall patient survival (**Figure 4B**). Similar favorable overall survival outcomes were observed in head and neck cancer and skin cutaneous carcinoma. In contrast, we found that the majority of tumor tissues that significantly overexpressed ALKBH6 were associated with poor overall survival in a few types of cancer including low-grade glioma (LGG) and kidney renal clear cell carcinoma (data not shown). Furthermore, mutation in p53 in ALKBH6-overexpressing pancreatic cancer patients significantly decreased the rate of overall survival (**Figure 4C**). Our results show that co-occurrence of ALKBH6 overexpression and loss of tumor suppressor genes status is critical for pancreatic cancer progression and negatively impacts patient overall survival.

## DISCUSSION

Environmental risk factors and metabolic stress within the cell likely induce alkyl and methyl DNA and/or RNA damage. The repair of DNA or RNA base lesions is critical to maintain normal cellular functions, including genomic stability. It is important to identify the biological significance of the mammalian proteins involved in the repair of DNA alkylation adducts. Alkylating agents induce different types of DNA base lesions, and each substrate is likely repaired by different types of enzymes to prevent mutagenesis (Sedgwick et al., 2007; Fu et al., 2012). Humans have nine different ALKBH proteins, with some involved in direct repair of alkylating DNA damage. However, the type of substrates used for the transfer of alkyl groups determines

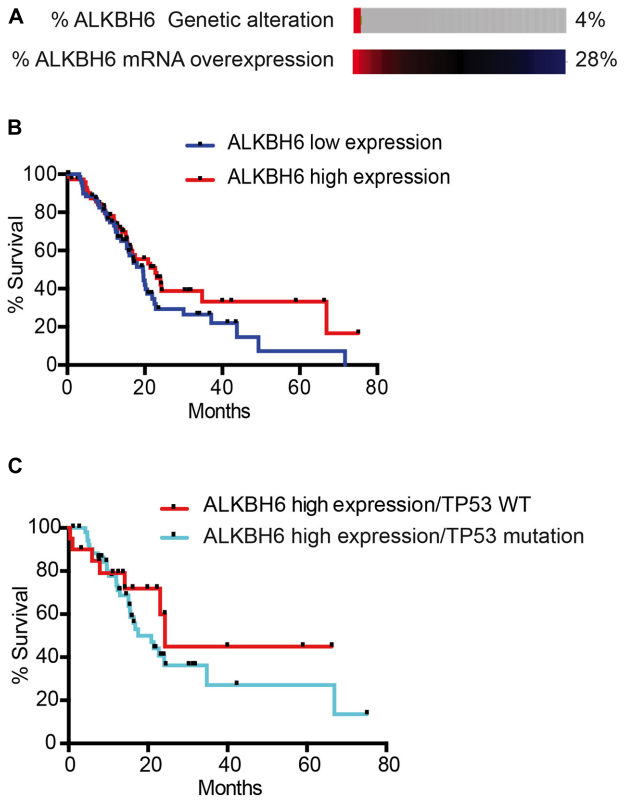


**FIGURE 4 |** ALKBH6 overexpressed in pancreatic cancer patients positively correlates with patient survival. **(A)** Schematic representation of ALKBH6 gene amplification and expression levels of ALKBH6 mRNA in normal versus tumor samples. mRNA expression was analyzed from TCGA database and the RNA Seq dataset was analyzed using the log scale expression. An expression of >0.5 denotes the high expressed group ($n$ = 76) versus < –0.5 for the low expressed group ($n$ = 71); **(B)** Survival curve of pancreatic cancer patients with high ALKBH6-expressing versus low ALKBH6-expressing pancreatic tumors. Kaplan-Meier survival graph of patients with high and low expression of ALKBH6; **(C)** Survival of patients with ($n$ = 56) and without ($n$ = 20) TP53 mutation-driven ALKBH6-overexpressing tumors promotes worse prognosis in pancreatic cancer.

which ALKBH protein is involved at the DNA base lesions (Li et al., 2013), thus indicating the importance of different types of oxidative demethylation for cell survival. In this study, we have demonstrated that ALKBH6 partially complements ALKB-deficient *E. coli* and restores survival and growth, following the SN2 type of alkylating DNA damage-induced cytotoxicity. Similarly, previous studies have demonstrated that ALKBH2 and ALKBH3 contribute to the repair of alkylating DNA damage and restore cellular survival of *E. coli* ALKB-deficient cells *in vitro* (Falnes et al., 2002; Trewick et al., 2002; Aas et al., 2003; Tasaki et al., 2011). Further, ALKBH2 and 3 complement ALKB-deficient E. coli strains and restore the transformation efficiency of plasmids bearing MMS-induced DNA damage up to 90% (Mishina et al., 2004). In particular, our data show that the loss of ALKBH6 increased MMS-induced DSBs and enhanced the cytotoxicity of MMS in human pancreatic cancer cells. In contrast, no significant difference was observed in pancreatic cells treated with SN1 type alkylating agents (MNU). It is also possible that DSBs in ALKBH6-deficient pancreatic cells likely arise from unrepaired SSBs that carry over to the S-phase of the cell cycle. Alternatively, it is also possible that a loss of ALKBH6 causes the accumulation of SSBs in close proximity to replication forks or processing of the DNA end-blocking groups with nucleases (Ma et al., 2009), which likely contributes to MMS-induced DSBs. Similarly, our data support that MMS-induced DNA base lesions in ssDNA are repaired by EcALKB *in vivo* and *in vitro* (Dinglay et al., 2000). Further, previous works have shown that ALKBH1-3 protect cells against MMS-induced damage (Ougland et al., 2004; Vagbo et al., 2013) and repair $m^1A$ and $m^3C$ DNA base lesions, preventing replication and transcription-related stress that could trigger cell cycle checkpoint activation and apoptosis (Wei et al., 1996; Duncan et al., 2002; Aas et al., 2003; Falnes et al., 2004; Westbye et al., 2008). It is known that both chemicals actually cause a similar range of methylated residues. The only substantial difference in dsDNA is that MNU methylates much more backbone phosphate and O6 guanine residues, compared to MMS, with the latter causing slightly increased 1 meA and 3 meA levels. On the other hand, in ssDNA, 1 meA and 3 meC appear to much more apparent in MMS-treated cells. However, our observations are in contrast with other DNA damaging agents, such as ionization radiation (Ward, 1994) which causes clustered DNA damage in close proximity. Consistent with the above evidence, results of this study suggest that ALKBH6 is critical in protecting pancreatic cancer cells from MMS-induced DNA base damage. Therefore, treatment of cells with MMS may lead to an increase in substrates recognized by ALKBH6. Further studies are warranted to define the precise role of ALKBH6 to protect mutagenesis-mediated genomic instability.

Our data demonstrated that there is no significant difference in spontaneous DNA damage between siRNA-silenced ALKBH6 cells and wild-type pancreatic cancer cells. However, siRNA-silenced ALKBH6 leads to the accumulation of cells in the G2/M phase of the cell cycle (**Figure 2E**) suggesting that ALKBH6 may contribute to the mitotic cellular growth of pancreatic cancer cells. Further, our data show that siRNA-mediated silencing of ALKBH6 impacts cell viability. In contrast, silencing of ALKBH2, 3, and 8 or both ALKBH2 and 3, did not affect cancer cell viability (Pilžys et al., 2019). Our results also demonstrated that MMS treatment compromises the survival of pancreatic cancer cells, suggesting the involvement of ALKBH6 in DNA repair. These findings are in agreement with previous studies, showing that deletion of ALKBH repair results in reduced cell survival (Ringvoll et al., 2006; Sikora et al., 2010; Dango et al., 2011; Pilžys et al., 2019).

Considering the clinical relevance of our study, ALKBH6 is significantly overexpressed in pancreatic cancer and is associated with favorable overall survival. In addition, a high level of ALKBH6 expression has been detected in adenocarcinomas of other organs, such as head and neck squamous cell carcinoma, malignant melanoma, and renal cell carcinoma, with favorable overall survival as well. In contrast, overexpression of ALKBH6 is associated with poor overall patient survival in LGG. The relatively high expression of ALKBH6 in tumor tissues correlate with cancer development in some cancer types, and may provide

an opportunity to use ALKBH6 as a potential target for anticancer therapy (Chen et al., 2019; Li et al., 2019). Other members of the ALKBH family, such as ALKBH3, are essential for cancer progression and present themselves as potential targets for effective therapy in prostate cancer (Konishi et al., 2005; Shimada et al., 2008). In addition, ALKBH2 plays a crucial role in the treatment of pediatric brain tumors during chemotherapy (Cetica et al., 2009). In summary, our results suggest that ALKBH6 is involved in protecting pancreatic cancer from alkylating-induced DNA damage and promotes cell survival. Further biochemical characterizations are required to determine whether ALKBH6 repairs $m^1A$ or $m^3C$. Our data provide a basis for future studies to uncover the clinical benefit of ALKBH6 in certain cancers as a prognostic marker or a potential target for therapy.

## DATA AVAILABILITY STATEMENT

The original contributions presented in the study are included in the article/supplementary material, further inquiries can be directed to the corresponding author/s.

## AUTHOR CONTRIBUTIONS

SZ perform the experiment. RD perform DNA damage experiment on *E. coli*. AF perform DNA damage localization in human pancreatic cancer cells. DK and SZ perform data analysis and wrote the manuscript. All authors contributed to the article and approved the submitted version.

## REFERENCES


Aas, P. A., Otterlei, M., Falnes, P. O., Vågbø, C. B., Skorpen, F., Akbari, M., et al. (2003). Human and bacterial oxidative demethylases repair alkylation damage in both RNA and DNA. *Nature* 421, 859–863. doi: 10.1038/nature01363

Aihara, E., Matthis, A. L., Karns, R. A., Engevik, K. A., Jiang, P., Wang, J., et al. (2016). Epithelial regeneration after gastric ulceration causes prolonged cell-type alterations. *Cell. Mol. Gastroenterol. Hepatol.* 2, 625–647. doi: 10.1016/j.jcmgh.2016.05.005

Aravind, L., and Koonin, E. V. (2001). The DNA-repair protein AlkB, EGL-9, and leprecan define new families of 2-oxoglutarate- and iron-dependent dioxygenases. *Genome Biol.* 2:RESEARCH0007. doi: 10.1186/gb-2001-2-3-research0007

Bray, F., Ferlay, J., Soerjomataram, I., Siegel, R. L., Torre, L. A., and Jemal, A. (2020). Global cancer statistics 2018: GLOBOCAN estimates of incidence and mortality worldwide for 36 cancers in 185 countries (vol 68, pg 394, 2018). *CA Cancer J. Clin.* 70, 313–313. doi: 10.3322/caac.21609

Calvo, J. A., Meira, L. B., Lee, C. Y., Moroski-Erkul, C. A., Abolhassani, N., Taghizadeh, K., et al. (2012). DNA repair is indispensable for survival after acute inflammation. *J. Clin. Invest.* 122, 2680–2689. doi: 10.1172/JCI63338

Cetica, V., Genitori, L., Giunti, L., Sanzo, M., Bernini, G., Massimino, M., et al. (2009). Pediatric brain tumors: mutations of two dioxygenases (hABH2 and hABH3) that directly repair alkylation damage. *J. Neurooncol.* 94, 195–201. doi: 10.1007/s11060-009-9837-0

Chen, Z., Qi, M., Shen, B., Luo, G., Wu, Y., Li, J., et al. (2019). Transfer RNA demethylase ALKBH3 promotes cancer progression via induction of tRNA-derived small RNAs. *Nucleic Acids Res.* 47, 2533–2545. doi: 10.1093/nar/gky1250

Conroy, T., Desseigne, F., Ychou, M., Bouche, O., Guimbaud, R., Becouarn, Y., et al. (2011). FOLFIRINOX versus gemcitabine for metastatic pancreatic cancer. *N. Engl. J. Med.* 364, 1817–1825. doi: 10.1056/NEJMoa1011923

Dango, S., Mosammaparast, N., Sowa, M. E., Xiong, L. J., Wu, F., Park, K., et al. (2011). DNA unwinding by ASCC3 helicase is coupled to ALKBH3-dependent DNA alkylation repair and cancer cell proliferation. *Mol. Cell* 44, 373–384. doi: 10.1016/j.molcel.2011.08.039

Dietlein, F., Thelen, L., and Reinhardt, H. C. (2014). Cancer-specific defects in DNA repair pathways as targets for personalized therapeutic approaches. *Trends Genet.* 30, 326–339. doi: 10.1016/j.tig.2014.06.003

Dinglay, S., Trewick, S. C., Lindahl, T., and Sedgwick, B. (2000). Defective processing of methylated single-stranded DNA by E. coli AlkB mutants. *Genes. Dev.* 14, 2097–2105.

Duncan, T., Trewick, S. C., Koivisto, P., Bates, P. A., Lindahl, T., and Sedgwick, B. (2002). Reversal of DNA alkylation damage by two human dioxygenases. *Proc. Natl. Acad. Sci. U.S.A.* 99, 16660–16665. doi: 10.1073/pnas.262589799

Falnes, P. O., Bjoras, M., Aas, P. A., Sundheim, O., and Seeberg, E. (2004). Substrate specificities of bacterial and human AlkB proteins. *Nucleic Acids Res.* 32, 3456–3461. doi: 10.1093/nar/gkh655

Falnes, P. O., Johansen, R. F., and Seeberg, E. (2002). AlkB-mediated oxidative demethylation reverses DNA damage in *Escherichia coli*. *Nature* 419, 178–182. doi: 10.1038/nature01048

Fedeles, B. I., Singh, V., Delaney, J. C., Li, D., and Essigmann, J. M. (2015). The AlkB Family of Fe(II)/alpha-ketoglutarate-dependent dioxygenases: repairing nucleic acid alkylation damage and beyond. *J. Biol. Chem.* 290, 20734–20742. doi: 10.1074/jbc.R115.656462

Feng, C., Liu, Y., Wang, G. Q., Deng, Z. Q., Zhang, Q., Wu, W., et al. (2014). Crystal structures of the human RNA demethylase Alkbh5 reveal basis for substrate recognition. *J. Biol. Chem.* 289, 11571–11583. doi: 10.1074/jbc.M113.546168

Franken, N. A. P., Rodermond, H. M., Stap, J., Haveman, J., and van Bree, C. (2006). Clonogenic assay of cells in vitro. *Nat. Protoc.* 1, 2315–2319. doi: 10.1038/nprot.2006.339

Fu, D., Brophy, J. A. N., Chan, C. T. Y., Atmore, K. A., Begley, U., Paules, R. S., et al. (2010). Human AlkB Homolog ABH8 is a tRNA methyltransferase required for wobble uridine modification and DNA damage survival. *Mol. Cell. Biol.* 30, 2449–2459. doi: 10.1128/Mcb.01604-09

Fu, D., Calvo, J. A., and Samson, L. D. (2012). Balancing repair and tolerance of DNA damage caused by alkylating agents. *Nat. Rev. Cancer* 12, 104–120. doi: 10.1038/nrc3185

Fu, D., and Samson, L. D. (2012). Direct repair of 3,N(4)-ethenocytosine by the human ALKBH2 dioxygenase is blocked by the AAG/MPG glycosylase. *DNA Repair (Amst.)* 11, 46–52. doi: 10.1016/j.dnarep.2011.10.004

Kondo, N., Takahashi, A., Ono, K., and Ohnishi, T. (2010). DNA damage induced by alkylating agents and repair pathways. *J. Nucleic Acids* 2010:543531. doi: 10.4061/2010/543531

Konishi, N., Nakamura, M., Ishida, E., Shimada, K., Mitsui, E., Yoshikawa, R., et al. (2005). High expression of a new marker PCA-1 in human prostate carcinoma. *Clin. Cancer Res.* 11, 5090–5097. doi: 10.1158/1078-0432.CCR-05-0195

Li, D., Fedeles, B. I., Shrivastav, N., Delaney, J. C., Yang, X., Wong, C., et al. (2013). Removal of N-alkyl modifications from N(2)-alkylguanine and N(4)-alkylcytosine in DNA by the adaptive response protein AlkB. *Chem. Res. Toxicol.* 26, 1182–1187. doi: 10.1021/tx400096m

Li, J., Han, Y., Zhang, H., Qian, Z., Jia, W., Gao, Y., et al. (2019). The m6A demethylase FTO promotes the growth of lung cancer cells by regulating the m6A level of USP7 mRNA. *Biochem. Biophys. Res. Commun.* 512, 479–485. doi: 10.1016/j.bbrc.2019.03.093

Lindahl, T., Sedgwick, B., Sekiguchi, M., and Nakabeppu, Y. (1988). Regulation and expression of the adaptive response to alkylating-agents. *Ann. Rev. Biochem.* 57, 133–157. doi: 10.1146/annurev.bi.57.070188.001025

Loechler, E. L., Green, C. L., and Essigmann, J. M. (1984). In vivo mutagenesis by O6-methylguanine built into a unique site in a viral genome. *Proc. Natl. Acad. Sci. U.S.A.* 81, 6271–6275. doi: 10.1073/pnas.81.20.6271

Ma, W. J., Panduri, V., Sterling, J. F., Van Houten, B., Gordenin, D. A., and Resnick, M. A. (2009). The transition of closely opposed lesions to double-strand breaks during long-patch base excision repair is prevented by the coordinated action of DNA polymerase delta and Rad27/Fen1. *Mol. Cell. Biol.* 29, 1212–1221. doi: 10.1128/Mcb.01499-08

Mahipal, A., Frakes, J., Hoffe, S., and Kim, R. (2015). Management of borderline resectable pancreatic cancer. *World J. Gastroint. Oncol.* 7, 241–249. doi: 10.4251/wjgo.v7.i10.241

Mishina, Y., Chen, L. X., and He, C. (2004). Preparation and characterization of the native iron(II)-containing DNA repair AlkB protein directly from *Escherichia coli*. *J. Am. Chem. Soc.* 126, 16930–16936. doi: 10.1021/ja045066z

Nay, S. L., Lee, D. H., Bates, S. E., and O'Connor, T. R. (2012). Alkbh2 protects against lethality and mutation in primary mouse embryonic fibroblasts. *DNA Repair (Amst.)* 11, 502–510. doi: 10.1016/j.dnarep.2012.02.005

Nieminuszczy, J., and Grzesiuk, E. (2007). Bacterial DNA repair genes and their eukaryotic homologues: 3. AlkB dioxygenase and Ada methyltransferase in the direct repair of alkylated DNA. *Acta Biochim. Pol.* 54, 459–468. doi: 10.18388/abp.2007_3221

Ougland, R., Rognes, T., Klungland, A., and Larsen, E. (2015). Non-homologous functions of the AlkB homologs. *J. Mol. Cell. Biol.* 7, 494–504. doi: 10.1093/jmcb/mjv029

Ougland, R., Zhang, C. M., Liiv, A., Johansen, R. F., Seeberg, E., Hou, Y. M., et al. (2004). AlkB restores the biological function of mRNA and tRNA inactivated by chemical methylation. *Mol. Cell* 16, 107–116. doi: 10.1016/j.molcel.2004.09.002

Pilžys, T., Marcinkowski, M., Kukwa, W., Garbicz, D., Dylewska, M., Ferenc, K., et al. (2019). ALKBH overexpression in head and neck cancer: potential target for novel anticancer therapy. *Sci. Rep.* 9:13249.

Rajecka, V., Skalicky, T., and Vanacova, S. (2019). The role of RNA adenosine demethylases in the control of gene expression. *Biochim. Biophys. Acta Gene Regul. Mech.* 1862, 343–355. doi: 10.1016/j.bbagrm.2018.12.001

Ringvoll, J., Nordstrand, L. M., Vagbo, C. B., Talstad, V., Reite, K., Aas, P. A., et al. (2006). Repair deficient mice reveal mABH2 as the primary oxidative demethylase for repairing 1meA and 3meC lesions in DNA. *EMBO J.* 25, 2189–2198. doi: 10.1038/sj.emboj.7601109

Rose, N. R., McDonough, M. A., King, O. N., Kawamura, A., and Schofield, C. J. (2011). Inhibition of 2-oxoglutarate dependent oxygenases. *Chem. Soc. Rev.* 40, 4364–4397. doi: 10.1039/c0cs00203h

Sedgwick, B. (1992). Oxidation of methylhydrazines to mutagenic methylating derivatives and inducers of the adaptive response of <em>*Escherichia coli*</em> to alkylation damage. *Cancer Res.* 52:3693.

Sedgwick, B., Bates, P. A., Paik, J., Jacobs, S. C., and Lindahl, T. (2007). Repair of alkylated DNA: recent advances. *DNA Repair (Amst.)* 6, 429–442. doi: 10.1016/j.dnarep.2006.10.005

Shah, D., and Gold, B. (2003). Evidence in *Escherichia coli* that N3-methyladenine lesions and cytotoxicity induced by a minor groove binding methyl sulfonate ester can be modulated in vivo by netropsin. *Biochemistry* 42, 12610–12616. doi: 10.1021/bi035315g

Shimada, K., Nakamura, M., Ishida, E., Higuchi, T., Yamamoto, H., Tsujikawa, K., et al. (2008). Prostate cancer antigen-1 contributes to cell survival and invasion though discoidin receptor 1 in human prostate cancer. *Cancer Sci.* 99, 39–45. doi: 10.1111/j.1349-7006.2007.00655.x

Shimada, K., Nakamura, M., Ishida, E., Kishi, M., Yonehara, S., and Konishi, N. (2003). c-Jun NH2-terminal kinase-dependent Fas activation contributes to etoposide-induced apoptosis in p53-mutated prostate cancer cells. *Prostate* 55, 265–280. doi: 10.1002/pros.10227

Sikora, A., Mielecki, D., Chojnacka, A., Nieminuszczy, J., Wrzesinski, M., and Grzesiuk, E. (2010). Lethal and mutagenic properties of MMS-generated DNA lesions in *Escherichia coli* cells deficient in BER and AlkB-directed DNA repair. *Mutagenesis* 25, 139–147. doi: 10.1093/mutage/gep052

Sundheim, O., Vagbo, C. B., Bjoras, M., Sousa, M. M., Talstad, V., Aas, P. A., et al. (2006). Human ABH3 structure and key residues for oxidative demethylation to reverse DNA/RNA damage. *EMBO J.* 25, 3389–3397. doi: 10.1038/sj.emboj.7601219

Tan, A., Dang, Y., Chen, G., and Mo, Z. (2015). Overexpression of the fat mass and obesity associated gene (FTO) in breast cancer and its clinical implications. *Int. J. Clin. Exp. Pathol.* 8, 13405–13410.

Tasaki, M., Shimada, K., Kimura, H., Tsujikawa, K., and Konishi, N. (2011). ALKBH3, a human AlkB homologue, contributes to cell survival in human non-small-cell lung cancer. *Br. J. Cancer* 104, 700–706. doi: 10.1038/sj.bjc.6606012

Trewick, S. C., Henshaw, T. F., Hausinger, R. P., Lindahl, T., and Sedgwick, B. (2002). Oxidative demethylation by *Escherichia coli* AlkB directly reverts DNA base damage. *Nature* 419, 174–178. doi: 10.1038/nature00908

Vagbo, C. B., Svaasand, E. K., Aas, P. A., and Krokan, H. E. (2013). Methylation damage to RNA induced in vivo in *Escherichia coli* is repaired by endogenous AlkB as part of the adaptive response. *DNA Repair (Amst.)* 12, 188–195. doi: 10.1016/j.dnarep.2012.11.010

van den Born, E., Bekkelund, A., Moen, M. N., Omelchenko, M. V., Klungland, A., and Falnes, P. O. (2009). Bioinformatics and functional analysis define four distinct groups of AlkB DNA-dioxygenases in bacteria. *Nucleic Acids Res.* 37, 7124–7136. doi: 10.1093/nar/gkp774

Von Hoff, D. D., Ervin, T., Arena, F. P., Chiorean, E. G., Infante, J., Moore, M., et al. (2013). Increased survival in pancreatic cancer with nab-paclitaxel plus gemcitabine. *N. Engl. J. Med.* 369, 1691–1703. doi: 10.1056/NEJMoa1304369

Ward, J. F. (1994). The complexity of dna-damage–relevance to biological consequences. *Int. J. Radiat. Biol.* 66, 427–432. doi: 10.1080/09553009414551401

Wei, Y. F., Carter, K. C., Wang, R. P., and Shell, B. K. (1996). Molecular cloning and functional analysis of a human cDNA encoding an *Escherichia coli* AlkB homolog, a protein involved in DNA alkylation damage repair. *Nucleic Acids Res.* 24, 931–937. doi: 10.1093/nar/24.5.931

Westbye, M. P., Feyzi, E., Aas, P. A., Vagbo, C. B., Talstad, V. A., Kavli, B., et al. (2008). Human AlkB homolog 1 is a mitochondrial protein that demethylates 3-methylcytosine in DNA and RNA. *J. Biol. Chem.* 283, 25046–25056. doi: 10.1074/jbc.M803776200

Yang, C. G., Yi, C. Q., Duguid, E. M., Sullivan, C. T., Jian, X., Rice, P. A., et al. (2008). Crystal structures of DNA/RNA repair enzymes AlkB and ABH2 bound to dsDNA. *Nature* 452, 961–965. doi: 10.1038/nature06889

Yi, C., and He, C. (2013). DNA repair by reversal of DNA damage. *Cold Spring Harb. Perspect. Biol.* 5:a012575. doi: 10.1101/cshperspect.a012575

Yi, C. Q., Jia, G. F., Hou, G. H., Dai, Q., Zhang, W., Zheng, G. Q., et al. (2010). Iron-catalysed oxidation intermediates captured in a DNA repair dioxygenase. *Nature* 468, 330–333. doi: 10.1038/nature09497

Yu, B., Edstrom, W. C., Benach, J., Hamuro, Y., Weber, P. C., Gibney, B. R., et al. (2006). Crystal structures of catalytic complexes of the oxidative DNA/RNA repair enzyme AlkB. *Nature* 439, 879–884. doi: 10.1038/nature04561

Zhang, M., Yang, S. M., Nelakanti, R., Zhao, W. T., Liu, G. C., Li, Z., et al. (2020). Mammalian ALKBH1 serves as an N-6-mA demethylase of unpairing DNA. *Cell Res.* 30, 197–210. doi: 10.1038/s41422-019-0237-5

Zhang, Y., Chen, F. X., Mehta, P., and Gold, B. (1993). Groove- and sequence-selective alkylation of DNA by sulfonate esters tethered to lexitropsins. *Biochemistry* 32, 7954–7965. doi: 10.1021/bi00082a017

Zheng, G., Fu, Y., and He, C. (2014). Nucleic acid oxidation in DNA damage repair and epigenetics. *Chem. Rev.* 114, 4602–4620. doi: 10.1021/cr400432d

**Conflict of Interest:** The authors declare that the research was conducted in the absence of any commercial or financial relationships that could be construed as a potential conflict of interest.

frontiers in Cell and Developmental Biology

ORIGINAL RESEARCH
published: 16 April 2021
doi: 10.3389/fcell.2021.663411

# USP44 Stabilizes DDB2 to Facilitate Nucleotide Excision Repair and Prevent Tumors

*Ying Zhang[1], Imke K. Mandemaker[2], Syota Matsumoto[3], Oded Foreman[4], Christopher P. Holland[1], Whitney R. Lloyd[1], Kaoru Sugasawa[3], Wim Vermeulen[2], Jurgen A. Marteijn[2] and Paul J. Galardy[1,5,6]**

[1] Department of Pediatric and Adolescent Medicine, Mayo Clinic, Rochester, MN, United States, [2] Department of Molecular Genetics, Oncode Institute, Erasmus MC, Rotterdam, Netherlands, [3] Biosignal Research Center, Kobe University, Hyogo, Japan, [4] Department of Pathology, Genentech, South San Francisco, CA, United States, [5] Division of Pediatric Hematology-Oncology, Mayo Clinic, Rochester, MN, United States, [6] Department of Biochemistry and Molecular Biology, Mayo Clinic, Rochester, MN, United States

OPEN ACCESS

**Edited by:**
*Hari S. Misra, Bhabha Atomic Research Centre (BARC), India*

**Reviewed by:**
*Hanspeter Naegeli, University of Zurich, Switzerland*
*Vesna Rapić Otrin, University of Pittsburgh, United States*
*Qianzheng Zhu, The Ohio State University, United States*

***Correspondence:**
*Paul J. Galardy*
*galardy.paul@mayo.edu*

**Specialty section:**
*This article was submitted to Cell Death and Survival, a section of the journal Frontiers in Cell and Developmental Biology*

**Received:** *02 February 2021*
**Accepted:** *29 March 2021*
**Published:** *16 April 2021*

**Citation:**
*Zhang Y, Mandemaker IK, Matsumoto S, Foreman O, Holland CP, Lloyd WR, Sugasawa K, Vermeulen W, Marteijn JA and Galardy PJ (2021) USP44 Stabilizes DDB2 to Facilitate Nucleotide Excision Repair and Prevent Tumors. Front. Cell Dev. Biol. 9:663411. doi: 10.3389/fcell.2021.663411*

Nucleotide excision repair (NER) is a pathway involved in the repair of a variety of potentially mutagenic lesions that distort the DNA double helix. The ubiquitin E3-ligase complex UV-DDB is required for the recognition and repair of UV-induced cyclobutane pyrimidine dimers (CPDs) lesions through NER. DDB2 directly binds CPDs and subsequently undergoes ubiquitination and proteasomal degradation. DDB2 must remain on damaged chromatin, however, for sufficient time to recruit and hand-off lesions to XPC, a factor essential in the assembly of downstream repair components. Here we show that the tumor suppressor USP44 directly deubiquitinates DDB2 to prevent its premature degradation and is selectively required for CPD repair. Cells lacking USP44 have impaired DDB2 accumulation on DNA lesions with subsequent defects in XPC retention. The physiological importance of this mechanism is evident in that mice lacking *Usp44* are prone to tumors induced by NER lesions introduced by DMBA or UV light. These data reveal the requirement for highly regulated ubiquitin addition and removal in the recognition and repair of helix-distorting DNA damage and identify another mechanism by which USP44 protects genomic integrity and prevents tumors.

**Keywords: ubiquitin, animal model, DNA damage, deubiquitinating enzyme, tumor supperssor gene**

## INTRODUCTION

Maintenance of the accuracy of encoded genetic information is essential to guard the integrity of genomic identity across cell division and organism reproduction. A wide array of environmental insults leads to physical or chemical DNA damage that must be efficiently recognized and repaired to safeguard against cell dysfunction and disease. The nucleotide excision repair (NER) pathway of DNA repair is responsible for correcting helix-distorting DNA lesions that result from a range of chemical insults (e.g., cisplatin) or exposure to ultraviolet (UV) light (Kamileri et al., 2012; Scharer, 2013; Marteijn et al., 2014; Zhu and Wani, 2017). The recognition of damage in NER varies depending on the location of the lesion, lesions within an actively transcribed region are recognized by the transcription-coupled NER (TC-NER) pathway of NER, while global-genome NER (GG-NER) is capable of recognizing DNA damage throughout the entire genome. The

physiological importance of these mechanisms is underscored by the diseases Cockayne syndrome (CS) and xeroderma pigmentosum (XP) that exhibit severe UV hypersensitivity due to defects in the TC-NER and GG-NER pathways, respectively (DiGiovanna and Kraemer, 2012; Natale and Raquer, 2017). While damage in the TC-NER pathway is detected indirectly by the stalling of RNA polymerase II (Fousteri et al., 2006), GG-NER involves the direct detection of damage through the protein products of the genes XP group C (XPC) and XP group E (XPE; DDB2). Cyclobutane pyrimidine dimers (CPDs) and 6-4 photoproducts (6-4PPs) are the predominant lesions introduced by UV light, with CPDs being more abundant and repaired more slowly compared with 6-4PPs. CPDs have also been shown to be the predominant mutagen responsible for the development of UV induced skin cancer in mice (Jans et al., 2005). These lesions are also distinguished by the mechanisms of their detection. While XPC can detect and promote the repair of both CPDs and 6-4PPs *in vitro*, it has a very low affinity for CPDs *in vivo* necessitating a separate pathway for their recognition (Sugasawa et al., 2001; Wakasugi et al., 2002; Scrima et al., 2008). DDB2, as part of the UV-DDB ubiquitin ligase complex that also includes DDB1 and CUL4A, has a high affinity for CPDs *in vivo* and cells with mutated DDB2 have a selective deficit in their repair (Sugasawa et al., 2001). UV-DDB, however, cannot recruit the downstream TFIIH complex that is required to coordinate strand excision. To accomplish this then, DDB2 forms a direct complex with XPC after binding to CPDs (Fitch et al., 2003; Sugasawa et al., 2005; Fei et al., 2011; Matsumoto et al., 2015). Both DDB2 and XPC are substrates of the Ub ligase activity of UV-DDB with differing results. DDB2 ubiquitination leads to reduced affinity for DNA and its proteasomal degradation while ubiquitination of XPC increases its affinity for DNA but does not lead to its destruction (Sugasawa et al., 2005; Matsumoto et al., 2015). The result then of the ubiquitination event is the "pass-off" of CPDs from DDB2 to XPC, which then recruits the TFIIH complex. This model, however, leaves open the question of how DDB2 ubiquitination and degradation is prevented to allow time for XPC recruitment.

We previously demonstrated that the deubiquitinase USP44 is a potent tumor suppressor in mice and that reduced *USP44* levels are also seen in human cancers (Zhang Y. et al., 2012). First characterized as a component of the mitotic spindle assembly checkpoint (Stegmeier et al., 2007), we found that USP44 ensures the timely separation of centrosomes in G2 through a direct complex with the centriole protein centrin. While initially discovered as a component of the centriole structure (Salisbury, 1995), the majority of centrin is not localized to this organelle, instead localizing diffusely through the cytosol and nucleus (Paoletti et al., 1996). Centrin forms a direct complex with XPC, which together with the protein RAD23, forms a trimeric complex that is required for NER activity (Araki et al., 2001; Popescu et al., 2003). USP44 and XPC share a centrin binding motif that is anchored by an invariant tryptophan in both proteins (Zhang Y. et al., 2012). The binding of USP44 with centrin, together with the predominant nuclear localization of USP44 (Zhang Y. et al., 2011; Zhang Y. et al., 2012), led us to question the potential role of USP44 in NER.

Here we show that USP44 is an essential component of NER that is required for the efficient repair of CPDs, but not 6-4 photoproducts. Consistent with the selective CPD repair defect in *Usp44* null cells, we find that USP44 deubiquitinates the recognition protein DDB2 to facilitate its accumulation on DNA lesions and facilitate the subsequent recruitment of XPC. Reinforcing the physiological significance of this mechanism, we find that *Usp44* null mice are hypersensitive to tumors induced by two NER-dependent carcinogens—DMBA and UVB. These findings have important implications for understanding the molecular mechanisms of damage recognition in NER and for the understanding of the tumor suppressive functions of USP44.

# MATERIALS AND METHODS

## Reagents

CPD and 6-4PP quantitation was performed using commercial ELISA kits (CosmoBio, Carlsbad, CA, United States) according to the manufacturer's instructions. Antibodies used in this study include anti-DDB2 (#5416), FLAG (DYKDDDDK, #2368), histone H2B (#5546), α-actin (#4970) (Cell Signaling Inc. Danvers, MA, United States), HA (3F10, Millipore-Sigma, St. Louis, MO, United States), V5 (Bethyl Laboratories, Montgomery, TX, United States), CPD (clone TDM-2; CosmoBio) XPC (graciously supplied by Jeff Salisbury) (Acu et al., 2010).

## Mice

All procedures involving mice were reviewed and approved by the Mayo Clinic institutional animal care and use committee (IACUC). Mice carrying hypomorphic or null alleles of *Usp44* were generated and genotyped as previously described (Zhang Y. et al., 2012). The DMBA carcinogen bioassay was performed as described (Serrano et al., 1996). The ultraviolet light tumor assay was performed was adapted from published procedures (Itoh et al., 2004). Briefly, the dorsal skin was shaved twice weekly and the mice were exposed to UVB (312 nm) 2,500 J/$m^2$/day on 5 days per week for 20 weeks using a Spectroline E-series lamp equipped with two 8-watt bulbs. Humane endpoints used in addition to standard institutional guidelines include the development of any tumor and moderate-severe dermatitis.

## Cell Lines, Fractionation, Immunoprecipitation

Murine embryonic fibroblasts (MEFs) carrying combinations of hypomorphic or null alleles of *Usp44* were generated and cultured as previously described (Zhang Y. et al., 2012). The human cell line VH10 expressing DDB2-GFP was generated and cultured as previously described (Pines et al., 2012; Ribeiro-Silva et al., 2020). The XPC deficient cell line XP4PA expressing XPC-GFP was generated and cultured as previously described. RNA interference was performed using smart pool reagents from Dharmacon according to manufacturer's instructions (Hoogstraten et al., 2008; Ribeiro-Silva et al., 2020). Cell fractionation was performed as described (Robu et al., 2013). Immunoprecipitation was

performed on extracts generated with 0.1% NP-40, 10% glycerol in PBS as described (Kasper et al., 1999; Zhang Y. et al., 2012).

## Ultraviolet Light Treatment

For quantitative DNA damage repair experiments, cells were washed with PBS and were exposed to 10 J/m$^2$ UVC (254 nm) following PBS aspiration using a Mineralight XX-15S lamp (UVP) with two 15-watt bulbs. The exposure time was calibrated using a radiometer (UVX, UVP) prior to each experiment. For subnuclear foci analysis, cells were washed with PBS and a 5 micron micropore filter (Millipore) was overlaid on the cells prior to exposure to 50 J/m$^2$ UVC. Cells were fixed with 3% paraformaldehyde at the indicated times after exposure and stained with the antibodies indicated in each figure. The accumulation of DDB2-GFP and the fluorescence recovery after photobleaching (FRAP) of XPC-GFP were performed as described (van Cuijk et al., 2015). The immobilized fraction of XPC-GFP was calculated by comparing the average relative fluorescence intensity measured after recovery was complete (35–45 s after bleaching) expressed as a percentage of the intensity measured prior to bleaching. The relative recovery observed in un-irradiated cells was considered as 100% mobile. The mobility was then similarly calculated in other conditions and normalized to the control cells.

## *In vitro* Deubiquitination Assay

The DDB2-based ubiquitin E3 ligase (CRL-DDB2) was purified as described (Nishi et al., 2005; Sugasawa et al., 2005; Matsumoto et al., 2015). HA-tagged wild-type and catalytic mutant (C281A) USP44 was purified from two 10 cm dishes of MEFs transduced with the respective constructs using the HA tagged protein purification kit (MBL International Corporation, Woburn, MA, United States) according to the manufacturer's recommendations (Zhang Y. et al., 2012). UbE1 and UBCH5a were obtained from Boston Biochem (Cambridge, MA, United States). CRL-DDB2 (40 ng) was ubiquitinated for 60 min at room temperature (21°C) by incubating UbE1 (200 ng), UBCH5a (800 ng), ubiquitin (10 μg) in a final volume of 30 μl of buffer containing 50 mM Tris-HCl pH 7.6, 10 mM MgCl2, 0.2 mM CaCl2, 4 mM ATP, 1 mM DTT, BSA (3 μg). When this reaction was completed, varying amounts of purified USP44 (2.5, or 5 μl from the 40 μl final volume of protein purified as above) and incubated for an additional 60 min at room temperature (21°C). This reaction was terminated by the addition of SDS sample buffer and boiling.

## Rigor, Reproducibility, Statistics, and Graphing

Unless specified, all experiments were performed at least three times with similar results. All experiments with MEFs were performed with at least three independently derived lines. All immunoblots represent similar findings from at least three independent experiments. Statistical calculations were performed using functions embedded in GraphPad Prism as indicated in each figure legend. Unless specified, all graphs represent the means ± SEM for at least 3 independent experiments. Outlier values were identified and excluded using the Grubbs test at 0.05 alpha. Unless specified, *p*-values were considered significant if $<0.05$. All graphs were prepared using GraphPad Prism.

# RESULTS

## USP44 Is Required for the Repair of CPDs

Because of the direct interaction between USP44 and centrin, and the known function of centrin as a cofactor in NER, we asked whether USP44 loss affects the response to UV induced DNA damage. To address this, we exposed wild-type or *Usp44* null MEFs to ultraviolet light (UVC) and monitored the repair kinetics of the predominant UVC induced lesions 6-4 photoproducts (6-4PPs) and CPDs by ELISA. As has been observed by others, 6-4PPs are rapidly repaired in wild-type cells while CPD repair kinetics are slower (**Figures 1A,B**). Compared to wild-type cells, *Usp44* null MEFs repaired 6-4PPs with normal kinetics, but had a selective defect in the repair of CPDs. Consistent with this finding; we observed strong continued CPD immunostaining of *Usp44* null MEFs 24-h after UVC exposure—a time when most damage has been repaired in wild-type cells (**Figure 1C**). There was no significant difference in cell survival following UVC exposure, regardless of genotype (data not shown). We next examined the effect of *Usp44* gene dosage on NER through the use of mice carrying a combination of wild-type (+), hypomorphic (h), or null (–) alleles (Zhang Y. et al., 2012). By combining these alleles we generated a series of mice predicted to have graded expression of USP44 and we examined CPD repair in MEFs derived from these animals. There was a strong inverse relationship between the *Usp44* genotype and the amount of CPDs that remained after a 24-h repair period following UV exposure (**Figure 1D**) though only the difference between wild-type and null is significant. The degree of CPDs remaining bore a striking similarity with the incidence of spontaneous tumors in these mice, though all spontaneous tumors occurred within internal organs similar to that previously reported for *Usp44* null mice (**Figure 1E**; Zhang Y. et al., 2012).

## USP44 Deubiquitinates and Prevents the Premature Degradation of DDB2

Because of the selective defect in CPD repair in *Usp44* null cells, we examined the level and degradation kinetics of DDB2 that is required for the *in vivo* repair of CPDs, but not 6-4PPs. As expected, DDB2 levels decline after exposure to UV in wild-type cells with levels returning to—or exceeding baseline levels by 24 h (**Figures 2A,B**). In comparison, DDB2 underwent a more rapid and profound degradation and failed to recover to wild-type levels in cells lacking USP44. Consistent with a possible enzyme-substrate relationship, we also repeatedly observed USP44 to co-precipitate with DDB2 (**Figure 2C**), though we were unable to reproducibly demonstrate the reciprocal co-precipitation of DDB2 with USP44. To determine if DDB2 is a direct substrate of USP44, we established an *in vitro* deubiquitination assay. We observed robust ubiquitination of DDB2 when we combined purified CRL-DDB2 with ubiquitin E1 activating enzyme UBE1,

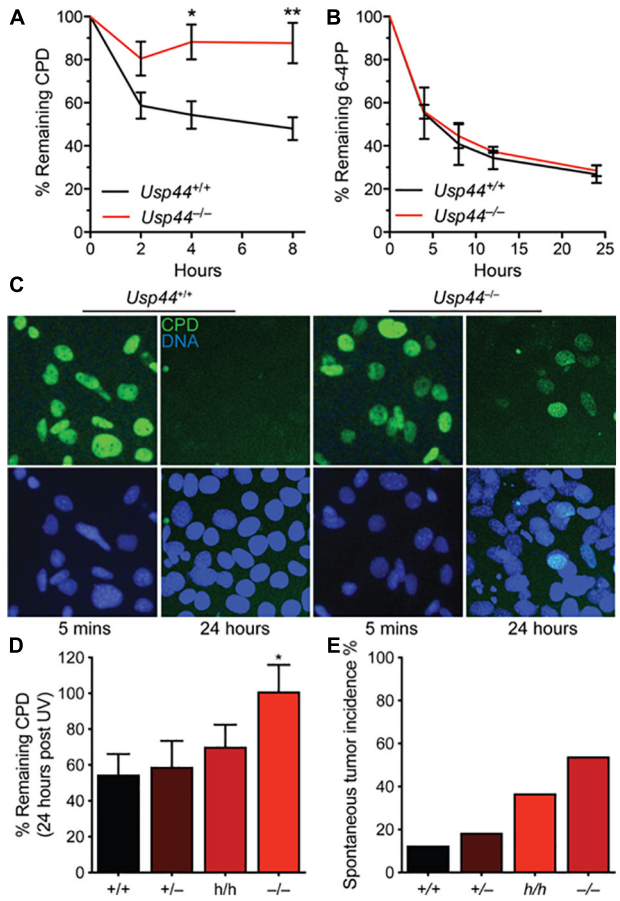


**FIGURE 1 |** USP44 is selectively required for the repair of cyclobutene pyrimidine dimers. **(A,B)** MEFs of the indicated genotypes were exposed to UVC (10 J/m$^2$) and the presence of cyclobutene pyrimidine dimers (CPDs) or 6-4 photoproducts (6-4PPs) were monitored by ELISA at the times shown. The graph represents the mean ± SEM at each time point for three independent MEF lines. **(C)** MEFs from A were stained as indicated 5 min or 24 h after exposure to UVC as in **(A,B)**. **(D)** CPDs were monitored as in **(A)** in MEFs of the indicated genotypes. "*" indicates $p < 0.05$. E. Mice of the indicated genotypes were aged for 18 months and the incidence of tumors detected at necropsy is shown. Note: data for *Usp44* +/+, +/-, and -/- were previously published and included for comparison with the results from *Usp44* h/h mice.

the E2 conjugating enzyme UBCH5a, Ub, and ATP (**Figure 2D**). Following auto-ubiquitination of DDB2, we conducted a second incubation with immunopurified wild-type or mutant USP44. Ubiquitination of DDB2 was reversed by the inclusion of wild-type USP44 but not the catalytically inactive USP44$^{C281A}$ (Zhang Y. et al., 2012). These data lead us to conclude that USP44 deubiquitinates DDB2 following UV exposure and prevents its premature degradation.

## USP44 Promotes the Accumulation of DDB2 on Damaged DNA

To better understand the impact of USP44 loss on DDB2 localization, we examined the kinetics of DDB2 accumulation on chromatin using live-cell fluorescent microscopy. As the level of DDB2 affects the NER reaction, these experiments were performed in human VH10 fibroblasts expressing DDB2-GFP at near endogenous levels (Pines et al., 2012; Ribeiro-Silva et al., 2020). Subnuclear DNA damage was induced using an UVC laser (266 nm) and the level of DDB2-GFP at the damage was monitored over time. In cells transfected with control siRNA, DDB2-GFP rapidly accumulates at local UV-induced damage sites reaching a plateau approximately 100 s after damage (**Figures 3A,B** and **Supplementary Figure 1**). In contrast, cells transfected with USP44 targeting siRNA had a significant defect in the DDB2-GFP accumulation kinetics. This suggests that in the absence of USP44, either DDB2 is more quickly degraded upon binding to DNA damage, or that its ubiquitination prevents efficient chromatin association on damage sites. To further investigate the impact of DDB2 degradation, we examined the ability of various constructs to rescue the CPD repair defect in a complementation assay. As expected, reintroducing wild-type USP44, but not the catalytically inactive USP44$^{C281A}$ (Zhang Y. et al., 2012) completely restored CPD repair in *Usp44* null MEFs (**Figure 3C**). Similarly, and demonstrating a requirement for the USP44-Centrin complex, the centrin binding mutant USP44$^{W162A}$ (which is fully catalytically active; Zhang Y. et al., 2012) failed to rescue CPD repair. Overexpressing FLAG-DDB2 completely restored CPD repair in *Usp44* null MEFs, consistent with it being a limiting factor in cells lacking USP44. We conclude that the rapid degradation of DDB2 upon DNA damage is responsible for the defective repair of CPDs in *Usp44* null MEFs.

## XPC Recruitment to DNA Damage Is Impaired in the Absence of USP44

While DDB2 is important for the initial recognition of CPDs, the "hand-off" of these lesions to XPC is ultimately required for their repair. To examine the impact of USP44 loss on XPC recruitment we examined the colocalization of XPC with CPDs by confocal immunofluorescence microscopy. As we observed with DDB2, there was a decrease in the localization of XPC on CPD lesions in *Usp44* null MEFs compared with wild-type (**Figures 4A,B**). To further investigate this, we again used live-cell fluorescence microscopy. *XPC* deficient human fibroblasts expressing endogenous levels of XPC-GFP were analyzed with fluorescence recovery after photobleaching (FRAP) to examine the immobilization of XPC on chromatin after UVC exposure. In control cells, as expected, exposure to UVC leads to a strong immobilization of XPC indicating increased residence time at sites of damage. Comparing control cells with those depleted of USP44, showed a reduction in the UV-induced XPC immobilization, indicating impaired binding of XPC at damage sites (**Figures 4C,D**). This is particularly noteworthy as only the immobilization of XPC on CPDs would be expected to be impaired in the absence of USP44. Deficient XPC binding to chromatin was confirmed by subcellular fractionation in wild-type or *Usp44* null MEFs. We observed a decreased amount of XPC-V5 in the chromatin fraction in USP44 null MEFs 20 min after UVC exposure (**Figure 4E**). Similar results were also obtained by assessing the chromatin binding of endogenous XPC (**Figure 4F**). Taken together these data indicate that USP44

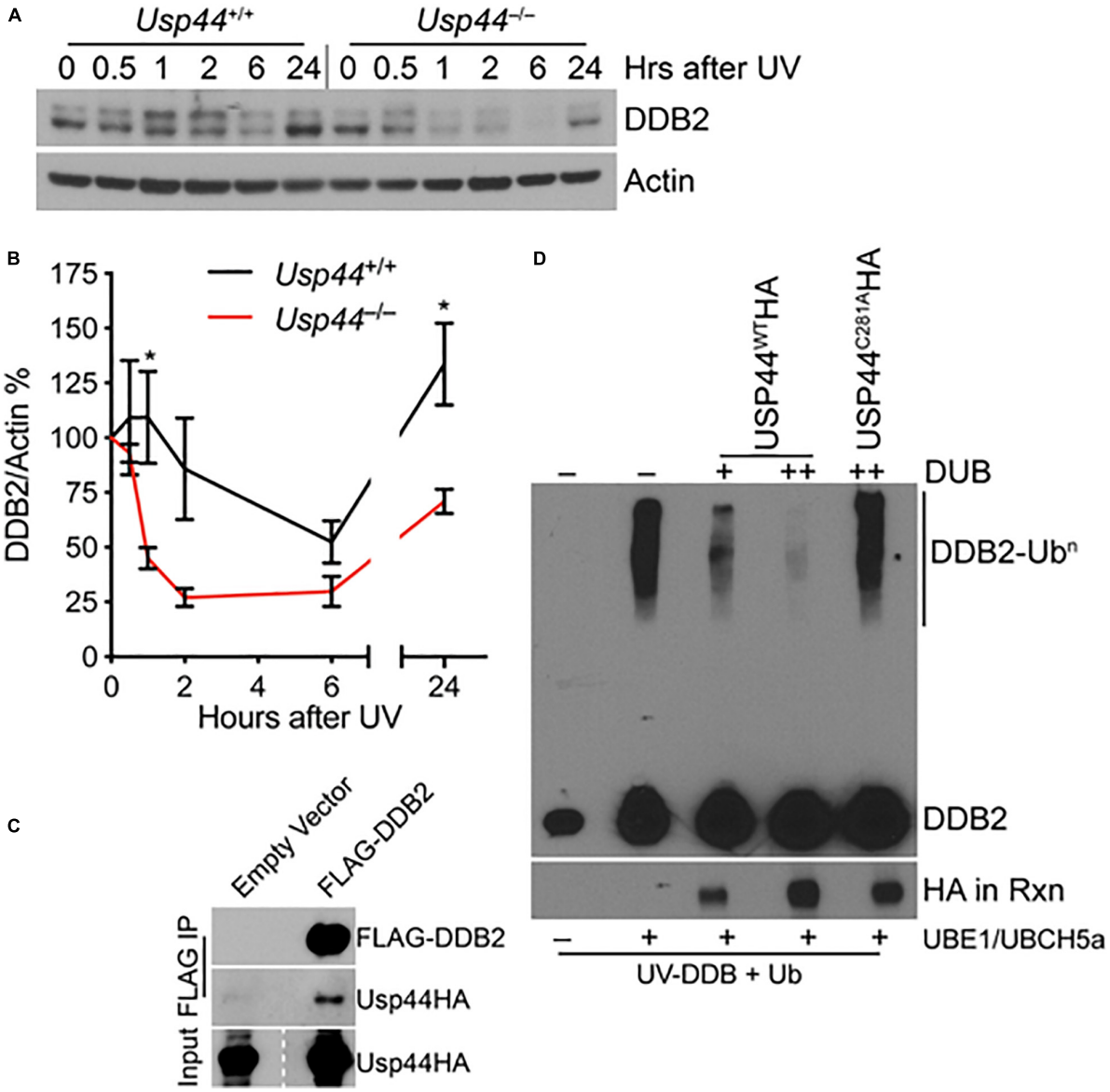


**FIGURE 2 |** USP44 deubiquitinates DDB2 following UVC exposure. **(A,B)** MEFs of the indicated genotype were exposed to 30 J/m$^2$ UVC and samples were collected for immunoblot at the indicated times. The doublet bands were consistently observed in these mouse cells, and were both quantitated to represent DDB2 using imageJ. The graph represents the mean ± SEM for three independent MEF lines. "*" denotes $p < 0.05$. **(C)** MEFs were transduced with the indicated constructs and subjected to immunoprecipitation for the FLAG epitope and probed as indicated. **(D)** Purified CRL-DDB2 was auto-ubiquitinated by the addition of UbE1, UBCH5a, and ubiquitin, and subsequently incubated with either wild type or catalytic mutant (C281A) immunopurified USP44 as indicated. Rxn = reaction.

assists in the recruitment of DDB2 to damaged chromatin and that this defective DDB2 accumulation results in reduced XPC localization to these lesions.

## USP44 Is Required to Protect Mice From Tumors Following NER Pathway Carcinogens

To examine the impact of the identified NER defect on tumorigenesis, we exposed pups of *Usp44*$^{\pm}$ intercrosses to a single dose of the carcinogen DMBA that induces DNA adducts that are repaired by NER (Wijnhoven et al., 2001). Animals were scored for tumors at 5 months of age. We found a significant increase in skin tumors in *Usp44* null mice compared with wild-type (**Figure 5A**). To further examine the role of USP44 in preventing DNA damage induced tumors, wild-type or *Usp44* null mice were exposed to UVB for 5 days per week for 20 weeks and were monitored for skin tumors. There was a significant increase in the rate of skin tumors in *Usp44* null mice (**Figures 5B,C**). Of note, there were also a number of internal tumors that developed in *Usp44* null mice during the observation period, including some discovered in moribund animals. As these do not appear

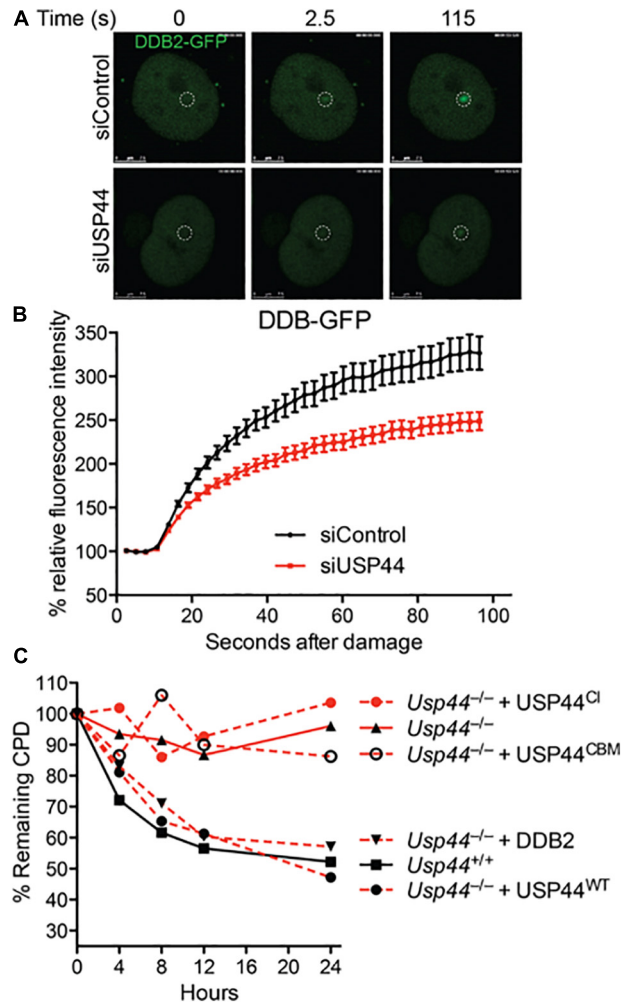


**FIGURE 3 |** Incomplete CPD repair in *Usp44* null cells associated with inadequate DDB2 recruitment to sites of damage. **(A,B)** VH10 cells expressing DDB2-GFP were transfected with control or USP44 targeting siRNA and then locally irradiated. The DDB-GFP fluorescence was monitored over time using live-cell confocal imaging and quantified to pre-damage intensity set at 100. The graph represents the mean ± SEM for 31–36 cells per condition. **(C)** MEFs of the indicated genotypes were transduced with wild-type, catalytic mutant (USP44$^{CI}$; C281A), centrin-binding deficient (USP44$^{CBM}$; W162A) USP44, or DDB2 as indicated. The cells were exposed to UVC (10 J/m$^2$) and CPD levels were monitored at the indicated times. The graph represents the means of three independent experiments for each condition.

to be metastatic tumors from the skin (no skin tumors identified in these mice) it seems unlikely that these are related to the UVB exposure. However, we have not otherwise observed life-threatening tumors in the first year of life in *Usp44* null mice. We conclude that the NER activity of USP44 is important in its ability to suppress tumors resulting from UV exposure.

## DISCUSSION

Targeted ubiquitination plays an important role in many aspects of the repair of DNA damage, including lesion recognition and repair during the NER pathway. Based on our observation that USP44 binds the XPC partner centrin, we hypothesized that it played a role in NER. Our results demonstrate that USP44 is an important component of this pathway and is required specifically for the repair CPDs—a lesion that is dependent on recognition by DDB2. Based on our data, we envision a model in which USP44 counteracts the UV-induced DDB2 ubiquitylation. After UV exposure, DDB2 binds to CPDs on chromatin where it becomes auto-ubiquitinated. This ubiquitination lowers the affinity of DDB2 for DNA and results in its dissociation and degradation. Based on the data presented in this manuscript USP44 could be involved in two processes. One possibility is that USP44 de-ubiquitinates DDB2 once it has been released, allowing it to be recycled back onto persisting CPDs. In cells proficient for USP44, the DDB2 is rapidly de-ubiquitinated, resulting in an increase protein lifetime, allowing efficient re-association with chromatin. DDB2 recruits XPC to CPDs that it cannot efficiently recognize itself. Therefore, in the presence of USP44, the de-ubiquitination of DDB2 allows it to iteratively cycle back onto damaged chromatin until XPC is recruited. In contrast, cells lacking USP44 cannot recycle the released DDB2 back onto the chromatin—leading to reduced DDB2 residency on CPDs, impairing recruitment of XPC and the repair of these lesions.

A second scenario is that USP44 may remove ubiquitin from DDB2 bound to CPDs. This would suppress DDB2 dissociation and degradation and enhance XPC recruitment. The lack of USP44 enrichment at sites of localized DNA damage might suggests it preferentially acts in the soluble phase to stabilize damage-evicted DDB2, rather than acting directly at damaged chromatin. However, as DUB-substrate interactions may be transient, we cannot exclude a role of USP44 at chromatin bound DDB2. Data supporting this model is the finding that USP44 stimulates DDB2 accumulation directly upon DNA damage induction (**Figure 3B**). The severe reduction of DDB2 accumulation kinetics at damage sites in living cells is most consistent with a direct effect of USP44 on chromatin-bound DDB2 rather than enhanced recycling. In compliance with this latter model, it was recently found that XPC competitively suppresses ubiquitination of DDB2 and this effect is significantly promoted by centrin-2, which may be explained by the recruitment of USP44 via its centrin binding domain (Matsumoto et al., 2015). In line with this, our data demonstrate the requirement for centrin binding by USP44, suggesting that DDB2 is de-ubiquitinated while bound at the UV-induced lesion by XPC-centrin recruited USP44. Importantly, USP44 may be involved in both mechanisms, by de-ubiquitinating chromatin bound DDB2 and by stabilizing the damage-evicted DDB2, both important for efficient XPC damage binding (Fig XX). While mechanistic details remain, our data provide compelling evidence that USP44 stabilizes DDB2 and that this mechanism is crucial for efficient XPC recruitment and has physiological relevant roles in tumor prevention.

As CPDs represents only one DDB2-dependent substrate repaired through NER, and given that we lack a clear understanding of other DDB2-dependent lesions, it remains possible that USP44 may be involved more generally in

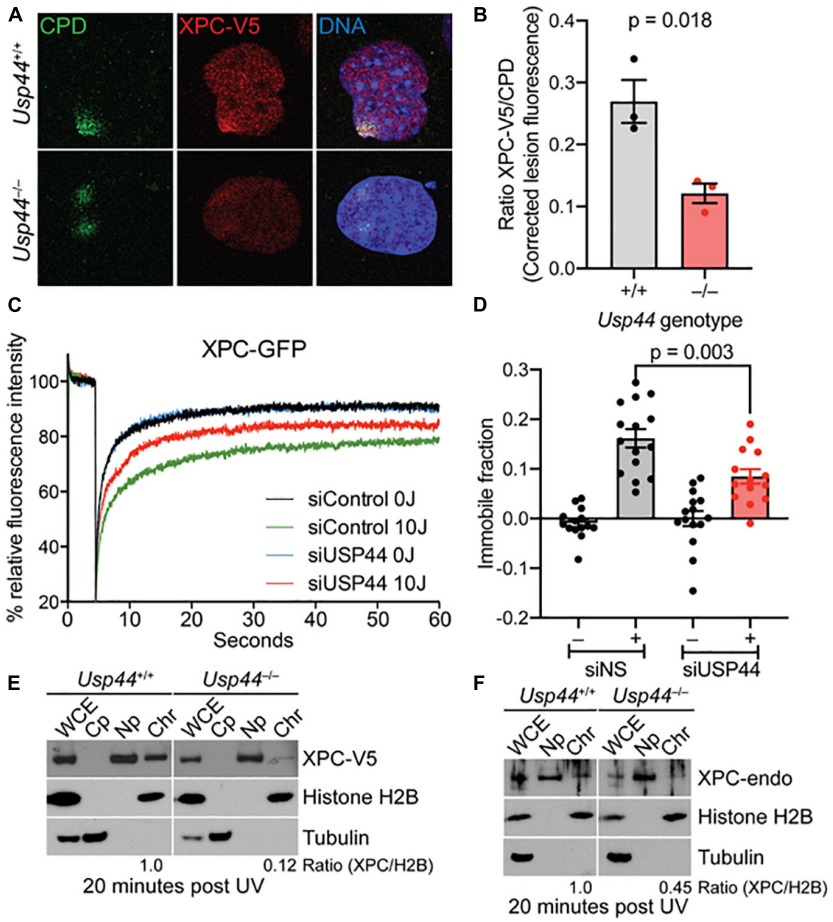


**FIGURE 4 |** Recruitment of XPC to UV induced DMA damage sites requires USP44. **(A,B)** MEFs of the indicated genotype fixed and stained as indicated 20 min after exposure to UVC (50 J/m$^2$) through a micropore filter (5 μM), The intensity of XPC to CPD lesions was quantitated using imageJ and was normalized to the intensity of the corresponding CPD. The graph represents the mean of the means from three independent experiments, *n* = 64–65 individual lesions total per genotype. **(C)** XPC deficient human fibroblasts expressing XPC-GFP were transfected with control or USP44 targeting siRNA. After exposure (or not) to UVC, cells were photobleached and the recovery of fluorescence was monitored by live-cell fluorescence microscopy, plotted relative fluorescence was normalized to prebleach values set at 100. Note the reduced recovery of control cells reflecting XPC immobilization and the enhanced recovery seen in USP44 depleted cells. The graph represents the mean of 15 cells per condition. **(D)** Immobile fractions of XPC-GFP in cells transfected with the indicated siRNA and analyzed by FRAP in **(C)**. **(E,F)** MEFs of the indicated genotypes were exposed to UVC (30 J/m$^2$)and cells were harvested and separated into fractions as indicated (WCE, whole cell extract; Cp, cytoplasm; Np, nucleoplasm; Chr, chromatin). The presence of V5-tagged XPC **(D)** or endogenous XPC **(E)** in the chromatin fraction relative to histone H2B (chromatin marker) was determined using image J, The blots are representative of 2–3 independent experiments of each type.

facilitating DNA damage repair through this pathway. In support of this notion, the increased susceptibility to DMBA induced tumors is not explained by the accelerated destruction of DDB2. *Ddb2* or *Xpc* deficient mice do not have increased tumor susceptibility following DMBA exposure. In contrast, mice lacking the *Ercc6* gene critical for early steps of transcription-coupled NER, as well as components involved in damage verification (*Xpa*) downstream of both the GG- and TC-NER pathways lead to increased DMBA sensitivity (Nakane et al., 1995; van der Horst et al., 1997; de Boer et al., 1998). This may suggest USP44 also participates in the de-ubiquitination in these other NER events. It is also noteworthy in this regard that mouse models lacking XPC and/or DDB2 are prone to tumors in internal organs in addition to being sensitive to UV-induced skin tumors (Itoh et al., 2004; Hollander et al., 2005; Yoon et al., 2005). Recently, DDB2 was found to be a critical component of the base excision repair of 8-oxo-guanine and abasic sites (Jang et al., 2019), potentially accounting for these observations. Additional evidence for NER protecting against internal tumors comes from the large number of genome association studies that have linked polymorphisms in several NER pathway genes with the development or therapeutic response of non-skin tumors (Matakidou et al., 2006; Qiu et al., 2008). This likely reflects the defective repair of other forms of DNA damage (e.g., environmental chemical adducts or oxidative lesions). The additional role of USP44 in the prevention of aneuploidy makes it difficult to say whether the tumors seen in the internal organs of *Usp44* null mice are related to NER defects, particularly since mutation induced tumors may be accelerated through the loss of heterozygosity induced by aneuploidy.

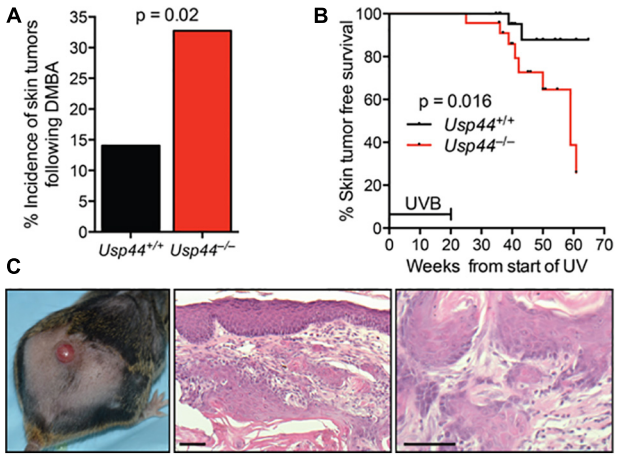


**FIGURE 5 |** *Usp44* null mice have increased sensitivity to UVB-induced skin tumors. **(A)** Newborn pups (1–3 days of live; n = 55–57 per genotype) were exposed to a single topical dose of DBMA. Mice were monitored for 5 months at which point the incidence of skin tumors was determined. **(B)** Mice of the indicated genotypes (*n* = 25 each) were exposed to UVB (2,500 J/m$^2$/day) 5 days per week for 20 weeks. The incidence of skin tumors was monitored. The graph represents the Kaplan-Meier estimated skin tumor free survival for the cohorts. **(C)** Representative images of skin -gross (left) H&E stained (right) of tumors observed in *Usp44* null mice from **(B)**. Scale bar = 50 μm.

Although it has been known for some time that DDB2 undergoes ubiquitin-dependent degradation after UV exposure, there has been recent attention on understanding how this process may be regulated. Recently, DDB2-dependent poly(ADP-ribosyl)ation (PARylation) at DNA damage lesions was identified (Pines et al., 2012; Robu et al., 2013). One of the targets of this modification was found to be DDB2 itself. As PARylation and ubiquitination occur on lysine residues and both modifications cluster in the N-terminal region of DDB2, a model of PARylation competing for ubiquitination sites was forwarded. In support of this model, PARP inhibition led to increase ubiquitination and accelerated degradation of DDB2. Surprisingly, PARP inhibition had no impact on DDB2 accumulation at damage loci. Whether there are other mechanisms that regulate the timing of DDB2 ubiquitination and degradation is not known.

De-ubiquitinating enzymes play other roles in NER. The best described is USP7 (HAUSP) that is involved both in the TC-NER and GG-NER pathways. USP7 was identified to be the primary enzyme removing ubiquitin from XPC following its ubiquitination by UV-DDB (He et al., 2014), and subsequently was found to be critical for maintaining levels of ERCC6 in the early steps of the TC-NER pathway (Schwertman et al., 2012). Additionally, recent reports identify another DUB, USP24 that plays a role in deubiquitinating DDB2 (Zhang L. et al., 2012). USP24 does not seem to be an essential component of the NER machinery, however, as CPD repair was found to be unperturbed in cells depleted of USP24. This may be due to USP24 not influencing the rate of DDB2 degradation following UV, but rather only at steady state. Interestingly, we find that in the absence of USP44 the levels of DDB2 are preserved at baseline but decline rapidly after UV exposure. This suggests that these DUBs act on DDB2 at different phases of its function in a non-redundant fashion. In another recent report, XPC was found to negatively affect the ubiquitination of DDB2—an effect amplified in the presence of centrin (Matsumoto et al., 2015). The model arising from this data is that the presence of XPC-HR23-Centrin diverts UV-DDB mediated ubiquitination away from DDB2 onto XPC. The proposed model further postulates that the ubiquitin-independent dissociation of DDB2 from chromatin allows its persistence for subsequent rounds of CPD recognition prior to its ultimate degradation. This model is not mutually exclusive with our work as we propose that DDB2 remains ubiquitin-free in part due to the activity of USP44 until XPC arrives, and that its activity may further facilitate the survival of DDB2 for subsequent rounds of damage recognition.

We previously reported the tumor prone phenotype of *Usp44* null mice in the context of its role in the protection against aneuploidy (Zhang Y. et al., 2012). Here we now demonstrate a second distinct tumor suppressive function of USP44. While our current data do not allow us to determine which if either of these roles is most important in its role as tumor suppressor, it raises the intriguing possibility that in fact these functions act in concert to protect against tumors. Aneuploidy is thought to drive tumors, at least in part, through its ability to promote the loss of heterozygosity at the loci of mutated tumor suppressor genes (Baker et al., 2009). The missegregation of chromosomes in mitosis may lead to the loss of the remaining wild-type tumor suppressor locus. In some instances, this may even be followed by the subsequent gain of an additional copy of the chromosome carrying the mutated gene, resulting in so-called copy neutral loss of heterozygosity, a process that also results in uniparental disomy. This model is predicated on the pre-existence of mutated tumor suppressor loci on which the chromosome missegregation may act. It is easy to appreciate how the loss of USP44, resulting in both increased mutagenesis and increased chromosome missegregation, may therefore act as a powerful tumor suppressor. Future work is needed to separate these functions and to determine their relative importance.

## DATA AVAILABILITY STATEMENT

The raw data supporting the conclusions of this article will be made available by the authors, without undue reservation.

## ETHICS STATEMENT

The animal study was reviewed and approved by the Mayo Clinic Institutional Animal Use and Care Committee.

## AUTHOR CONTRIBUTIONS

PG: conceptualization, formal analysis, writing – original draft preparation, project administration, and funding acquisition. YZ, IM, SM, KS, WV, JM, and PG: methodology. YZ,

IM, SM, OF, CH, and WL: investigation. SM and KS: resources. YZ, IM, SM, OF, CH, WL, KS, WV, JM, and PG: writing – review and editing. YZ, IM, KS, JM, and PG: visualization. KS, WV, JM, and PG: supervision. All authors have read and agreed to the published version of the manuscript.

## FUNDING

This work was funded by support provided to PG from Mayo Clinic and the Hyundai Hope of Wheels Foundation.

## ACKNOWLEDGMENTS

We would like to thank Dr. Jan van Deursen and the members of his laboratory for fruitful discussions regarding the data.

## SUPPLEMENTARY MATERIAL

The Supplementary Material for this article can be found online at: https://www.frontiersin.org/articles/10.3389/fcell.2021.663411/full#supplementary-material

## REFERENCES


Acu, I. D., Liu, T., Suino-Powell, K., Mooney, S. M., D'Assoro, A. B., Rowland, N., et al. (2010). Coordination of centrosome homeostasis and DNA repair is intact in MCF-7 and disrupted in MDA-MB 231 breast cancer cells. *Cancer Res.* 70, 3320–3328. doi: 10.1158/0008-5472.CAN-09-3800

Araki, M., Masutani, C., Takemura, M., Uchida, A., Sugasawa, K., Kondoh, J., et al. (2001). Centrosome protein centrin 2/caltractin 1 is part of the xeroderma pigmentosum group C complex that initiates global genome nucleotide excision repair. *J. Biol. Chem.* 276, 18665–18672. doi: 10.1074/jbc.M100855200

Baker, D. J., Jin, F., Jeganathan, K. B., and van Deursen, J. M. (2009). Whole chromosome instability caused by Bub1 insufficiency drives tumorigenesis through tumor suppressor gene loss of heterozygosity. *Cancer Cell* 16, 475–486. doi: 10.1016/j.ccr.2009.10.023

de Boer, J., de Wit, J., van Steeg, H., Berg, R. J., Morreau, H., Visser, P., et al. (1998). A mouse model for the basal transcription/DNA repair syndrome trichothiodystrophy. *Mol. Cell* 1, 981–990. doi: 10.1016/S1097-2765(00)80098-2

DiGiovanna, J. J., and Kraemer, K. H. (2012). Shining a light on xeroderma pigmentosum. *J. Invest. Dermatol.* 132, 785–796. doi: 10.1038/jid.2011.426

Fei, J., Kaczmarek, N., Luch, A., Glas, A., Carell, T., and Naegeli, H. (2011). Regulation of nucleotide excision repair by UV-DDB: prioritization of damage recognition to internucleosomal DNA. *PLoS Biol.* 9:e1001183. doi: 10.1371/journal.pbio.1001183

Fitch, M. E., Nakajima, S., Yasui, A., and Ford, J. M. (2003). In vivo recruitment of XPC to UV-induced cyclobutane pyrimidine dimers by the DDB2 gene product. *J. Biol. Chem.* 278, 46906–46910. doi: 10.1074/jbc.M307254200

Fousteri, M., Vermeulen, W., van Zeeland, A. A., and Mullenders, L. H. (2006). Cockayne syndrome A and B proteins differentially regulate recruitment of chromatin remodeling and repair factors to stalled RNA polymerase II in vivo. *Mol. Cell* 23, 471–482. doi: 10.1016/j.molcel.2006.06.029

He, J., Zhu, Q., Wani, G., Sharma, N., Han, C., Qian, J., et al. (2014). Ubiquitin-specific protease 7 regulates nucleotide excision repair through deubiquitinating XPC protein and preventing XPC protein from undergoing ultraviolet light-induced and VCP/p97 protein-regulated proteolysis. *J. Biol. Chem.* 289, 27278–27289. doi: 10.1074/jbc.M114.589812

Hollander, M. C., Philburn, R. T., Patterson, A. D., Velasco-Miguel, S., Friedberg, E. C., Linnoila, R. I., et al. (2005). Deletion of XPC leads to lung tumors in mice and is associated with early events in human lung carcinogenesis. *Proc. Natl. Acad. Sci. U.S.A.* 102, 13200–13205. doi: 10.1073/pnas.0503133102

Hoogstraten, D., Bergink, S., Ng, J. M., Verbiest, V. H., Luijsterburg, M. S., Geverts, B., et al. (2008). Versatile DNA damage detection by the global genome nucleotide excision repair protein XPC. *J. Cell Sci.* 121, 2850–2859. doi: 10.1242/jcs.031708

Itoh, T., Cado, D., Kamide, R., and Linn, S. (2004). DDB2 gene disruption leads to skin tumors and resistance to apoptosis after exposure to ultraviolet light but not a chemical carcinogen. *Proc. Natl. Acad. Sci. U.S.A.* 101, 2052–2057. doi: 10.1073/pnas.0306551101

Jang, S., Kumar, N., Beckwitt, E. C., Kong, M., Fouquerel, E., Rapic-Otrin, V., et al. (2019). Damage sensor role of UV-DDB during base excision repair. *Nat. Struct. Mol. Biol.* 26, 695–703. doi: 10.1038/s41594-019-0261-7

Jans, J., Schul, W., Sert, Y. G., Rijksen, Y., Rebel, H., Eker, A. P., et al. (2005). Powerful skin cancer protection by a CPD-photolyase transgene. *Curr. Biol.* 15, 105–115. doi: 10.1016/j.cub.2005.01.001

Kamileri, I., Karakasilioti, I., and Garinis, G. A. (2012). Nucleotide excision repair: new tricks with old bricks. *Trends Genet.* 28, 566–573. doi: 10.1016/j.tig.2012.06.004

Kasper, L. H., Brindle, P. K., Schnabel, C. A., Pritchard, C. E., Cleary, M. L., and van Deursen, J. M. (1999). CREB binding protein interacts with nucleoporin-specific FG repeats that activate transcription and mediate NUP98-HOXA9 oncogenicity. *Mol. Cell Biol.* 19, 764–776. doi: 10.1128/MCB.19.1.764

Marteijn, J. A., Lans, H., Vermeulen, W., and Hoeijmakers, J. H. (2014). Understanding nucleotide excision repair and its roles in cancer and ageing. *Nat. Rev. Mol. Cell Biol.* 15, 465–481. doi: 10.1038/nrm3822

Matakidou, A., Eisen, T., Fleischmann, C., Bridle, H., and Houlston, R. S. (2006). Evaluation of xeroderma pigmentosum XPA, XPC, XPD, XPF, XPB, XPG and DDB2 genes in familial early-onset lung cancer predisposition. *Int. J. Cancer* 119, 964–967. doi: 10.1002/ijc.21931

Matsumoto, S., Fischer, E. S., Yasuda, T., Dohmae, N., Iwai, S., Mori, T., et al. (2015). Functional regulation of the DNA damage-recognition factor DDB2 by ubiquitination and interaction with xeroderma pigmentosum group C protein. *Nucleic Acids Res.* 43, 1700–1713. doi: 10.1093/nar/gkv038

Nakane, H., Takeuchi, S., Yuba, S., Saijo, M., Nakatsu, Y., Murai, H., et al. (1995). High incidence of ultraviolet-B-or chemical-carcinogen-induced skin tumours in mice lacking the xeroderma pigmentosum group A gene. *Nature* 377, 165–168. doi: 10.1038/377165a0

Natale, V., and Raquer, H. (2017). Xeroderma pigmentosum-Cockayne syndrome complex. *Orphanet J. Rare Dis.* 12:65. doi: 10.1186/s13023-017-0616-2

Nishi, R., Okuda, Y., Watanabe, E., Mori, T., Iwai, S., Masutani, C., et al. (2005). Centrin 2 stimulates nucleotide excision repair by interacting with xeroderma pigmentosum group C protein. *Mol. Cell Biol.* 25, 5664–5674. doi: 10.1128/MCB.25.13.5664-5674.2005

Paoletti, A., Moudjou, M., Paintrand, M., Salisbury, J. L., and Bornens, M. (1996). Most of centrin in animal cells is not centrosome-associated and centrosomal centrin is confined to the distal lumen of centrioles. *J. Cell Sci.* 109(Pt 13), 3089–3102.

Pines, A., Vrouwe, M. G., Marteijn, J. A., Typas, D., Luijsterburg, M. S., Cansoy, M., et al. (2012). PARP1 promotes nucleotide excision repair through DDB2 stabilization and recruitment of ALC1. *J. Cell Biol.* 199, 235–249. doi: 10.1083/jcb.201112132

Popescu, A., Miron, S., Blouquit, Y., Duchambon, P., Christova, P., and Craescu, C. T. (2003). Xeroderma pigmentosum group C protein possesses a high affinity binding site to human centrin 2 and calmodulin. *J. Biol. Chem.* 278, 40252–40261. doi: 10.1074/jbc.M302546200

Qiu, L., Wang, Z., and Shi, X. (2008). Associations between XPC polymorphisms and risk of cancers: a meta-analysis. *Eur. J. Cancer* 44, 2241–2253. doi: 10.1016/j.ejca.2008.06.024

Ribeiro-Silva, C., Sabatella, M., Helfricht, A., Marteijn, J. A., Theil, A. F., Vermeulen, W., et al. (2020). Ubiquitin and TFIIH-stimulated DDB2 dissociation drives DNA damage handover in nucleotide excision repair. *Nat. Commun.* 11:4868. doi: 10.1038/s41467-020-18705-0

Robu, M., Shah, R. G., Petitclerc, N., Brind'Amour, J., Kandan-Kulangara, F., and Shah, G. M. (2013). Role of poly(ADP-ribose) polymerase-1 in the removal of

UV-induced DNA lesions by nucleotide excision repair. *Proc. Natl. Acad. Sci. U.S.A.* 110, 1658–1663. doi: 10.1073/pnas.1209507110

Salisbury, J. L. (1995). Centrin, centrosomes, and mitotic spindle poles. *Curr. Opin. Cell Biol.* 7, 39–45. doi: 10.1016/0955-0674(95)80043-3

Scharer, O. D. (2013). Nucleotide excision repair in eukaryotes. *Cold Spring Harb Perspect Biol.* 5:a012609. doi: 10.1101/cshperspect.a012609

Schwertman, P., Lagarou, A., Dekkers, D. H., Raams, A., van der Hoek, A. C., Laffeber, C., et al. (2012). UV-sensitive syndrome protein UVSSA recruits USP7 to regulate transcription-coupled repair. *Nat. Genet.* 44, 598–602. doi: 10.1038/ng.2230

Scrima, A., Konickova, R., Czyzewski, B. K., Kawasaki, Y., Jeffrey, P. D., Groisman, R., et al. (2008). Structural basis of UV DNA-damage recognition by the DDB1-DDB2 complex. *Cell* 135, 1213–1223. doi: 10.1016/j.cell.2008.10.045

Serrano, M., Lee, H., Chin, L., Cordon-Cardo, C., Beach, D., and DePinho, R. A. (1996). Role of the INK4a locus in tumor suppression and cell mortality. *Cell* 85, 27–37. doi: 10.1016/S0092-8674(00)81079-X

Stegmeier, F., Rape, M., Draviam, V. M., Nalepa, G., Sowa, M. E., Ang, X. L., et al. (2007). Anaphase initiation is regulated by antagonistic ubiquitination and deubiquitination activities. *Nature* 446, 876–881. doi: 10.1038/nature05694

Sugasawa, K., Okamoto, T., Shimizu, Y., Masutani, C., Iwai, S., and Hanaoka, F. (2001). A multistep damage recognition mechanism for global genomic nucleotide excision repair. *Genes Dev.* 15, 507–521. doi: 10.1101/gad.866301

Sugasawa, K., Okuda, Y., Saijo, M., Nishi, R., Matsuda, N., Chu, G., et al. (2005). UV-induced ubiquitylation of XPC protein mediated by UV-DDB-ubiquitin ligase complex. *Cell* 121, 387–400. doi: 10.1016/j.cell.2005.02.035

van Cuijk, L., van Belle, G. J., Turkyilmaz, Y., Poulsen, S. L., Janssens, R. C., Theil, A. F., et al. (2015). SUMO and ubiquitin-dependent XPC exchange drives nucleotide excision repair. *Nat. Commun.* 6:7499. doi: 10.1038/ncomms8499

van der Horst, G. T., van Steeg, H., Berg, R. J., van Gool, A. J., de Wit, J., Weeda, G., et al. (1997). Defective transcription-coupled repair in Cockayne syndrome B mice is associated with skin cancer predisposition. *Cell* 89, 425–435. doi: 10.1016/S0092-8674(00)80223-8

Wakasugi, M., Kawashima, A., Morioka, H., Linn, S., Sancar, A., Mori, T., et al. (2002). DDB accumulates at DNA damage sites immediately after UV irradiation and directly stimulates nucleotide excision repair. *J. Biol. Chem.* 277, 1637–1640. doi: 10.1074/jbc.C100610200

Wijnhoven, S. W., Kool, H. J., Mullenders, L. H., Slater, R., van Zeeland, A. A., and Vrieling, H. (2001). DMBA-induced toxic and mutagenic responses vary dramatically between NER-deficient *Xpa, Xpc* and *Csb mice*. *Carcinogenesis* 22, 1099–1106. doi: 10.1093/carcin/22.7.1099

Yoon, T., Chakrabortty, A., Franks, R., Valli, T., Kiyokawa, H., and Raychaudhuri, P. (2005). Tumor-prone phenotype of the DDB2-deficient mice. *Oncogene* 24, 469–478. doi: 10.1038/sj.onc.1208211

Zhang, L., Lubin, A., Chen, H., Sun, Z., and Gong, F. (2012). The deubiquitinating protein USP24 interacts with DDB2 and regulates DDB2 stability. *Cell Cycle* 11, 4378–4384. doi: 10.4161/cc.22688

Zhang, Y., Foreman, O., Wigle, D. A., Kosari, F., Vasmatzis, G., Salisbury, J. L., et al. (2012). USP44 regulates centrosome positioning to prevent aneuploidy and suppress tumorigenesis. *J. Clin. Invest.* 122, 4362–4374. doi: 10.1172/JCI63084

Zhang, Y., van Deursen, J., and Galardy, P. J. (2011). Overexpression of ubiquitin specific protease 44 (USP44) induces chromosomal instability and is frequently observed in human T-cell leukemia. *PLoS One* 6:e23389. doi: 10.1371/journal.pone.0023389

Zhu, Q., and Wani, A. A. (2017). Nucleotide excision repair: finely tuned molecular orchestra of early pre-incision events. *Photochem. Photobiol.* 93, 166–177. doi: 10.1111/php.12647

**Conflict of Interest:** PG owns stock in Abbott laboratories, Abbvie, and Johnson and Johnson. OF is employed by the company Genentech. These companies had no influence on the design or interpretation of the study—nor the writing of the manuscript.

The remaining authors declare that the research was conducted in the absence of any commercial or financial relationships that could be construed as a potential conflict of interest.

frontiers in Pediatrics

CASE REPORT
published: 01 July 2021
doi: 10.3389/fped.2021.574402

# Case Report: Pansynostosis, Chiari I Malformation and Syringomyelia in a Child With Frontometaphyseal Dysplasia 1

*Jaewon Kim, Dong-Woo Lee and Dae-Hyun Jang**

*Department of Rehabilitation Medicine, College of Medicine, The Catholic University of Korea, Seoul, South Korea*

Frontometaphyseal dysplasia 1 (FMD1) is a rare otopalatodigital spectrum disorder (OPDSD) that is inherited as an X-linked trait and it is caused by gain-of-function mutations in the *FLNA*. It is characterized by generalized skeletal dysplasia, and craniofacial abnormalities including facial dysmorphism (supraorbital hyperostosis, hypertelorism, and down-slanting palpebral fissures). The involvement of the central nervous system in patients with OPDSD is rare. Herein, we present the case of a 12-year-old boy with facial dysmorphism, multiple joint contractures, sensorineural hearing loss, scoliosis, craniosynostosis, and irregular sclerosis with hyperostosis of the skull. Brain and whole-spine magnetic resonance imaging revealed Chiari I malformation with extensive hydrosyringomyelia from the C1 to T12 levels. Targeted next-generation sequencing identified a hemizygous pathologic variant (c.3557C>T/p.Ser1186Leu) in the *FLNA*, confirming the diagnosis of FMD1. This is the first report of a rare case of OPDSD with pansynostosis and Chiari I malformation accompanied by extensive syringomyelia.

**Keywords: frontometaphyseal dysplasia 1, otopalatodigital spectrum disorder, syringomyelia, Chiari I malformation, FLNA gene mutation, pansynostosis**

OPEN ACCESS

***Edited by:***
*Hari S. Misra,*
*Bhabha Atomic Research Centre (BARC), India*

***Reviewed by:***
*Rita Selvatici,*
*University of Ferrara, Italy*
*Stephen Robertson,*
*University of Otago, New Zealand*

****Correspondence:***
*Dae-Hyun Jang*
*dhjangmd@naver.com*

***Specialty section:***
*This article was submitted to Genetics of Common and Rare Diseases, a section of the journal Frontiers in Pediatrics*

***Received:*** *19 June 2020*
***Accepted:*** *08 June 2021*
***Published:*** *01 July 2021*

***Citation:***
*Kim J, Lee D-W and Jang D-H (2021) Case Report: Pansynostosis, Chiari I Malformation and Syringomyelia in a Child With Frontometaphyseal Dysplasia 1. Front. Pediatr. 9:574402. doi: 10.3389/fped.2021.574402*

## INTRODUCTION

Otopalatodigital spectrum disorder (OPDSD), which is characterized by skeletal dysplasia, includes six disorders, OPD type 1 (OMIM #311300) and 2 (OMIM #304120), frontometaphyseal dysplasia 1 (FMD1; OMIM #305620), Melnick–Needles syndrome (MNS; OMIM #309350), digitocutaneous dysplasia (DCD; OMIM #300244), and a disorder characterized by keloid scarring, joint contractures, and cardiac valvulopathy (1, 2). Patients with these diseases commonly have mutations in the filamin A (*FLNA*) (3). The *FLNA* is located on chromosome Xq28 and is known to cause OPDSD (4). It encodes a 280-kDa cytoskeletal protein containing an actin-binding domain, which is important for cytoplasmic signaling. This protein interacts with transmembrane receptors or intracellular signaling molecules as well as filamentous actin and anchors transmembrane proteins to the actin cytoskeleton (5–8). The diseases accompanying the pathogenic variant of *FLNA* are termed X-linked filaminopathies. Disorders with a pathogenic variant of *FLNA* are classified as either a gain-of-function or a loss-of-function *FLNA* disorder, and OPDSD is classified as a gain-of-function disorder (2). Patients with OPDSD show various clinical manifestations, such as skeletal dysplasia, craniofacial dysmorphism, or sensorineural and/or conductive hearing loss (3, 9). Although clinical manifestations vary in females, the severity of this disease is generally milder in females than in males (10). The cardinal criteria for the diagnosis of FMD1 are craniofacial

abnormalities including facial dysmorphism such as supraorbital hyperostosis, hypertelorism, and down-slanting palpebral fissures (2, 11). FMD2 caused by *MAP3K7* mutations and FMD3 caused by *TAB2* mutations exhibit clinical features similar to those of FMD1, but show autosomal dominant trait (2, 12, 13). Among the clinical manifestations of OPDSD, the involvement of central nervous system (CNS) is relatively rare. The presence of Chiari I malformation (CM1), cerebellar hypoplasia, hydrocephalus, and cerebellar tonsillar herniation have been previously reported in a few patients with OPDSD (14–17); however, these cases were only clinically reported and did not undergo genetic confirmation. Herein, we report for the first case of FMD1, with pansynostosis and Chiari I malformation accompanied by extensive syringomyelia.

## CASE PRESENTATION

### Clinical Presentation

A 12-year-old boy visited our clinic with complaints of back pain since 2 years. His medical history included bilateral sensorineural hearing loss and multiple joint contractures on both wrists and fingers, most prominently in the proximal interphalangeal joint of the left fifth finger. He has two male cousins who resemble him in appearance. His parents and sister show no obvious anomalies (**Figure 1**).

Physical examination revealed facial dysmorphism with micrognathia, frontal bossing, prominent supraorbital ridge, and hypertelorism. Furthermore, hypodontia, hypoplasia of the left fifth digital phalanx and great toes, and thoracic scoliosis were noted. The intrinsic muscles of both hands were graded as 2/5 based on the manual muscle test. There was no sensory impairment. Knee and ankle jerks were hyperreflexic and ankle clonus was evoked. His height was 154 cm (63.9 percentile).

Whole-spine X-ray revealed thoracic scoliosis (Cobb angle of 17°) and flattening of the vertebral body. X-ray of the upper and lower extremities revealed valgus deformity of the elbow and knee joints with mild humerus and tibia bone bowing. Computed tomography (CT) of the skull revealed irregular sclerosis with hyperostosis, obliteration of the frontal sinus, frontal bone thickening and protrusion. Three-dimensional (3D) CT of skull demonstrated premature closure of all cranial sutures (pansynostosis) (**Figure 2**). Brain and whole-spine magnetic resonance imaging (MRI) revealed cerebellar tonsillar inferior herniation, which clinically translates to CM1, with extensive hydrosyringomyelia from the C1 to T12 levels and C2 spina bifida occulta (**Figure 3**). Laboratory test, including complete blood cell count, blood chemistry, and immunochemistry, were normal. Electrodiagnostic tests, including nerve conduction study, electromyography, and somatosensory and motor-evoked potential tests, were within the normal range.

### Cytogenetic and Molecular Analyses

Chromosomal study revealed a karyotype of 46,XY without anomalies. No significant microdeletion or duplication was detected *via* the chromosomal microarray test. Targeted gene panel sequencing was performed using the Illumina MiSeqDxTM Platform (Illumina Inc., San Diego, CA, USA) with 150-bp paired-end sequencing. The targeted gene panel was custom-made and included 124 genes spanning a 461,040-bp region related to skeletal dysplasia (see **Supplementary Material**). Exomes were captured using a customized Target Enrichment Kit (Celemics, Seoul, Korea). The enrichment of sequenced target genes was hybridized with oligonucleotide probes. The reference genome used was hg19. Alignment was performed using BWA-mem (version 0.7.10), and variant annotation was performed using Variant Effect Predictor and dbNSFP (18, 19).

A hemizygous missense variant (c.3557C>T/p.Ser1186Leu) in *FLNA* (NM_001456.3), which was previously reported as being pathogenic and related to FMD1, was detected (11, 20, 21). Family gene analysis revealed that his mother, aunt, and sister (who had no symptoms) carried the same heterozygous *FLNA* variant and that his maternal male cousin with similar facial dysmorphism had the same hemizygous *FLNA* variant as the proband. Finally, the patient was diagnosed with FMD1 inherited from the asymptomatic maternal carrier (**Figure 4**).

## DISCUSSION

OPDSD was first described in 1962 by Taybi, and FMD1 was reported in 1969 by Gorlin and Cohen (22, 23). Since then, various clinical features related to OPDSD have been reported. In the past, molecular genetic studies found a relationship between OPDSD and the distal Xq28 chromosome in the form of allelic variants of the *FLNA* (10, 24). The diagnosis of FMD1 is based on X-linked inheritance, clinical manifestations, and radiological studies and can be confirmed by detecting a *FLNA* pathogenic variant *via* molecular cytogenetic studies. Recently, technological advances, such as next-generation sequencing, have increased the accessibility and accuracy of diagnosis. The *FLNA* is not only associated with OPDSD caused by gain-of-function but also with loss-of-function diseases that do not cause skeletal dysplasia, such as periventricular heterotopia 1 (OMIM #300049), X-linked cardiac valvular dysplasia (OMIM #314400), and congenital short-bowel syndrome (OMIM #300048) (25).

FMD1 account for ∼50% of all the FMD patients, and the other 50% are diagnosed with FMD2 or FMD3, with pathogenic variants of *MAP3K7* or *TAB2*, respectively (2). FMD1 shows X-linked recessive inheritance, whereas other OPDSDs show X-linked dominant inheritance. Dozens of unrelated families with FMD1 have been reported to date; they mostly carry single-nucleotide variants of *FLNA*, resulting in missense mutations. Among the missense mutations, the c.3557C>T transition, which causes Ser1186Leu substitution (as detected in the current patient) is the most frequent mutation. The clinical manifestations of FMD1 include hyperostosis of the skull, supraorbital hyperostosis, sensorineural and/or conductive hearing loss, hypertelorism, agenesis of the sinuses in the skull, oligohypodontia, distal phalangeal hypoplasia, progressive joint contracture, scoliosis, limb bowing, shoulder girdle and hand intrinsic muscle underdevelopment, and hydronephrosis (11). FMD1 is distinguished from other OPDSDs based on the presence of a cleft palate, a joint contracture, or a

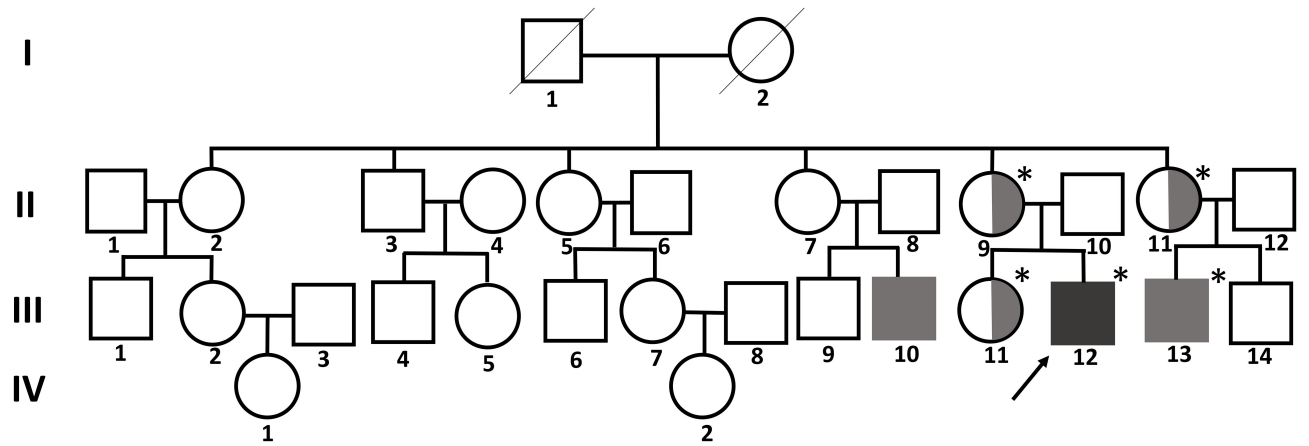


**FIGURE 1 |** Pedigree chart of the family with FMD1. The asterisk indicates people tested for the *FLNA* pathogenic variant. The affected members are indicated by gray shading. Symbols divided into halves indicate heterozygous carriers of FMD1. The arrow indicates the proband.

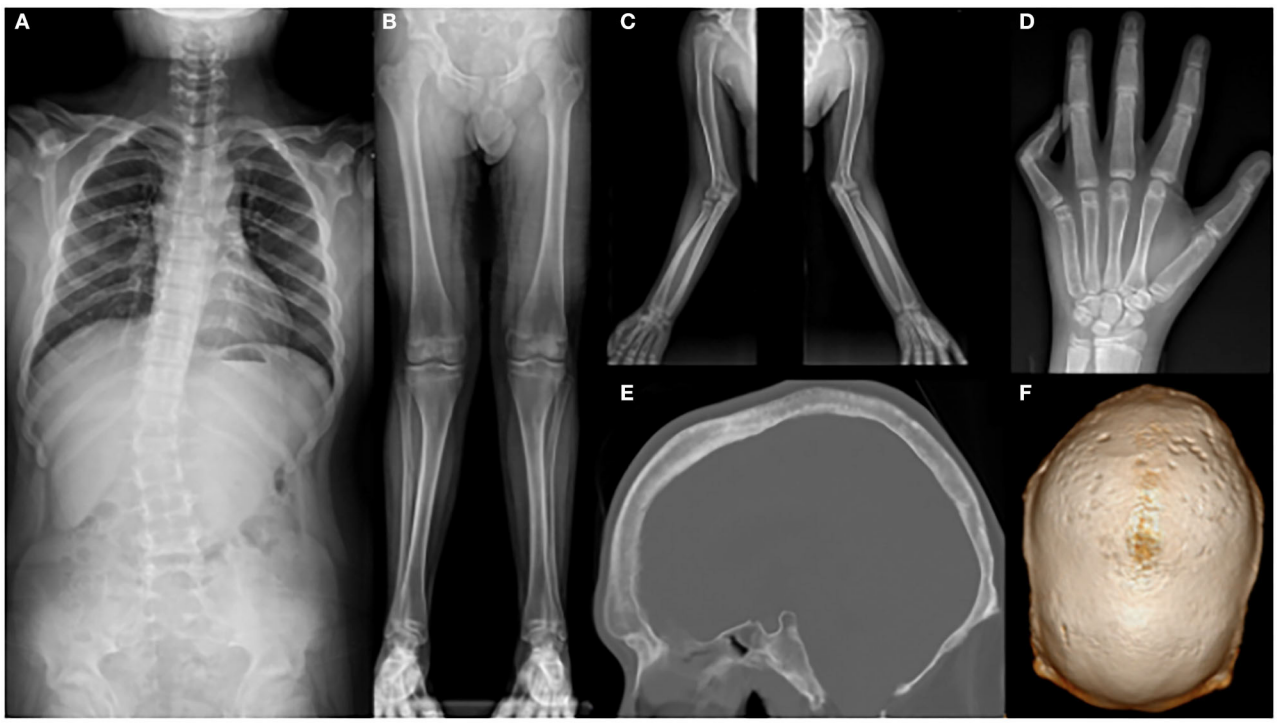


**FIGURE 2 |** X-ray showing **(A)** scoliosis of the whole spine; **(B)** mild bowing of the tibia and **(C)** humerus; **(D)** flexion contracture of the left fifth proximal phalangeal joint; **(E)** hyperostosis, irregular sclerosis, frontal bone thickening, and protrusion; and **(F)** craniosynostosis.

tracheobronchial tree malformation (3). To date, only one case of CNS involvement, i.e., a CM1, has been reported in FMD1 in 1999 (26). However, the author was unsure whether the CM1 was a characteristic of FMD1 or an incidental finding because it was the first report of such an occurrence. In addition, many previous reports of FMD1 did not mention whether brain MRI was performed, and it is not clear whether CM1 was present. Because CM1 was observed in our patient with FMD1, there is a possibility that this type of malformation is a manifestation of this disease.

CM1 is defined as a cerebellar tonsillar herniation below the foramen magnum >5 mm. The common neurological symptoms caused by CM1 include headache, gait disturbance, weakness, sensory disturbance, poor coordination, or hypo- or hyper-reflexia. Two-third of the patients with CM1 show small and shallow posterior fossa and foramen magnum

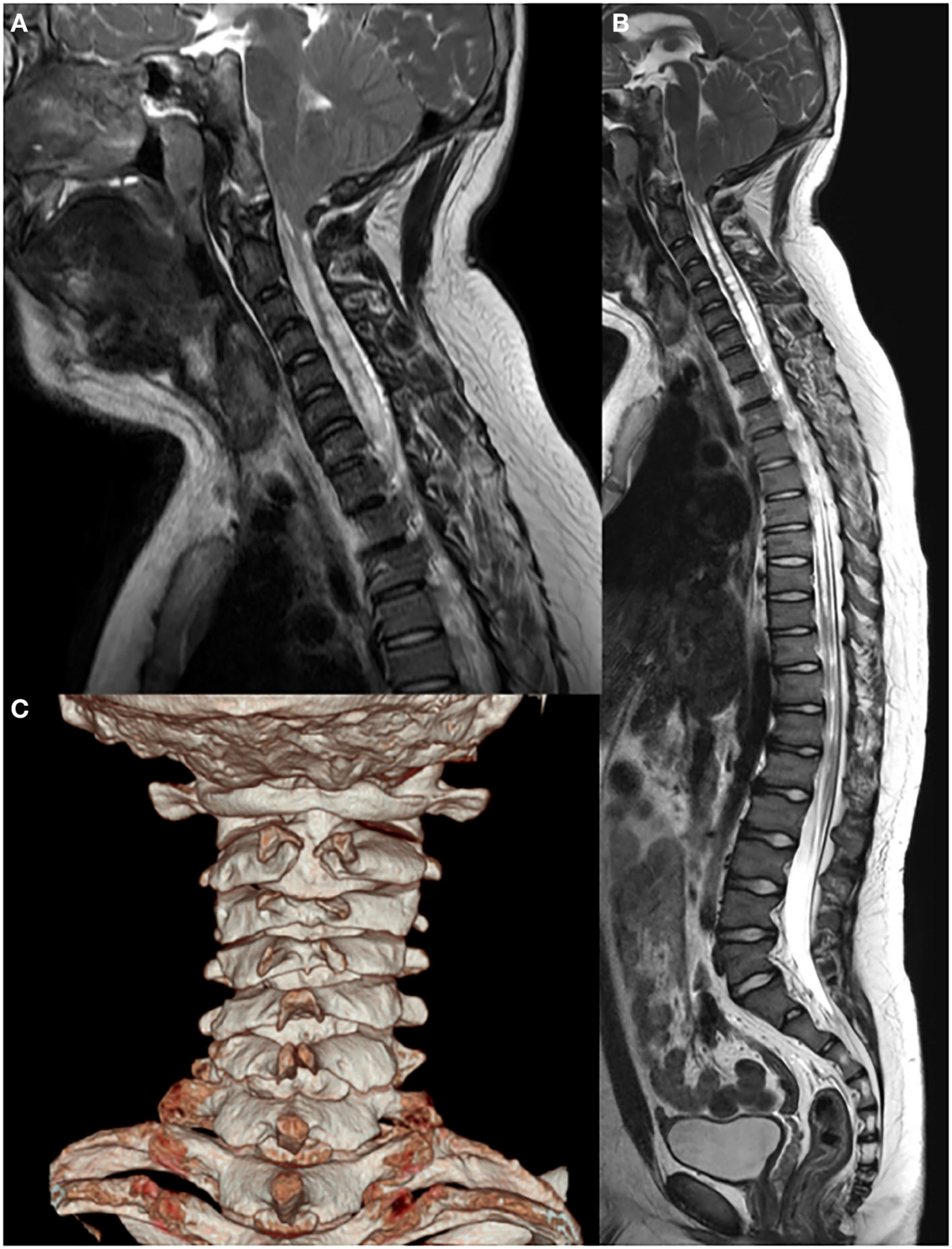


**FIGURE 3 |** Brain and whole-spine magnetic resonance imaging and computed tomography showing **(A,B)** Chiari I malformation with extensive hydrosyringomyelia from the C1 to T12 levels and **(C)** C2 spina bifida.

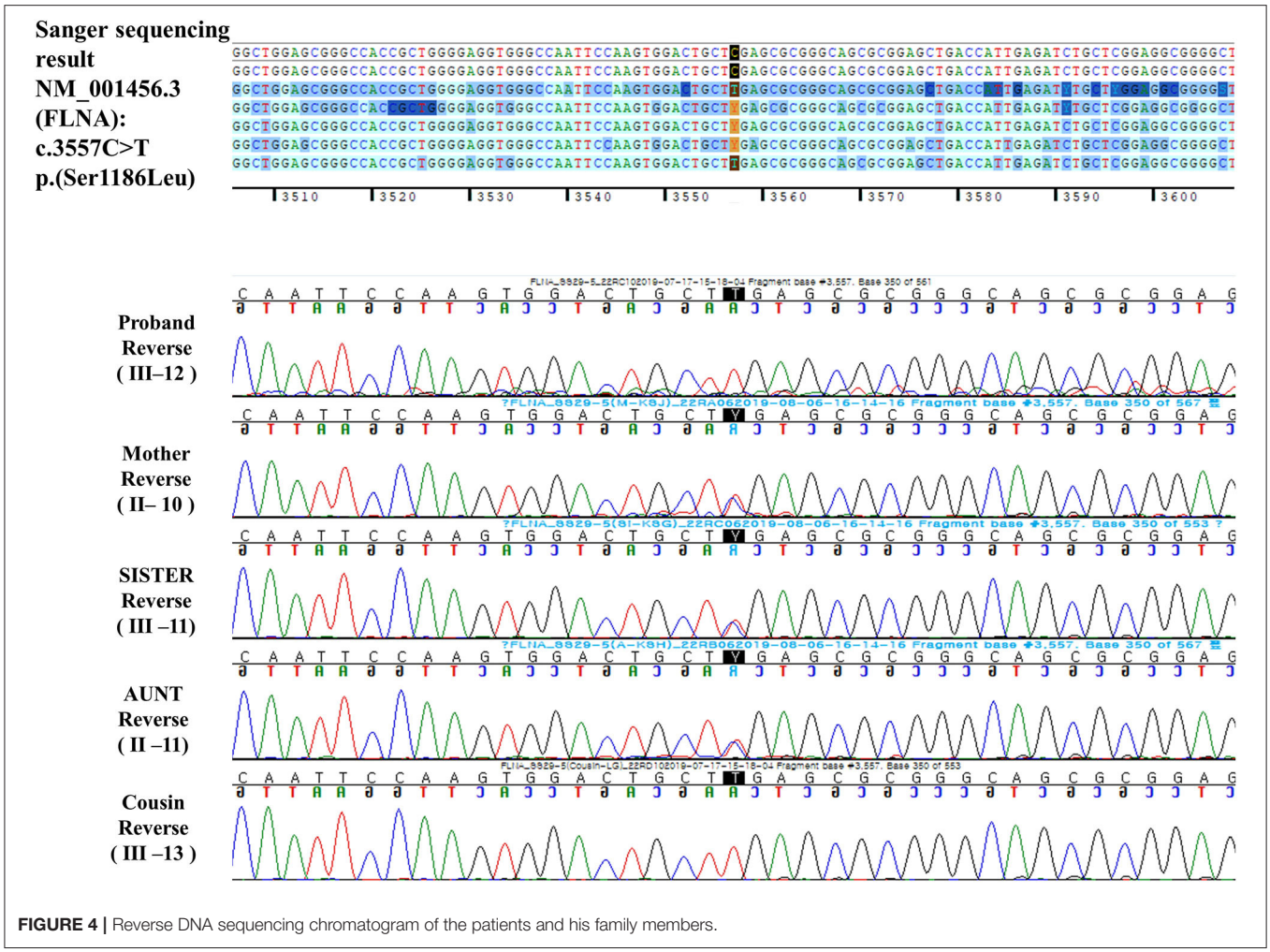


**FIGURE 4 |** Reverse DNA sequencing chromatogram of the patients and his family members.

overcrowding, possibly resulting from craniocervical bony dysplasia caused by a paraxial mesodermal defect (27–29). Moreover, CM1 can be observed as secondary to other pathology causing increased intracranial pressure, overcrowding in the posterior fossa with space-occupying lesions, or lower intrathecal pressure (e.g., leaking of spinal fluid or lumbar-to-peritoneal shunt) (30). Bidot et al. revealed that idiopathic intracranial hypertension can be accompanied by CM1 (31). In addition, CMs have been reported in patients with craniosynostosis similar to that in our patient. Cinalli et al. reported that ∼70% of the Crouzon's syndrome, which is characterized by craniosynostosis, had CMs, particularly in the lambdoid suture premature closure (32, 33). Several genetic studies revealed that CM1 is related to genetic factors and candidate genes include *FGFR2, PAX1, DFNB1, GDF3, CDX1, FLT1,* and *ALDH1A2* (34–37). Several syndromic disorders, such as Klippel–Feil syndrome, achondroplasia, Crouzon's syndrome, neurofibromatosis are found to be related to CM1 (38, 39). Most genetic predispositions for CM1 have been found to be caused by genetic factors related to the overcrowding of posterior fossa or underdevelopment of occipital bone. However, the genetic background is still uncertain and various factors are considered to be combined (40). Approximately 15–26% of CM1 patients suffer from lower brain stem or cranial nerve dysfunction, such as vocal cord paralysis, sensorineural hearing loss, sleep apnea, recurrent aspiration, or sinus bradycardia (41–43). Our patient also showed mild dysarthria, possibly owing to an association with cranial nerve involvement. However, sensorineural hearing loss appears to have little correlation with cranial nerve dysfunction secondary to CM1 because sensorineural or conductive hearing loss is commonly observed in patients with OPDSDs (44).

Extensive hydrosyringomyelia associated with CM1 was observed in the present case. To date, there have been no reports of hydrosyringomyelia in patients with OPDSD. Pathophysiologically, CM1 may be accompanied by syringomyelia. A study reported that 65% of patients with symptomatic CM1 exhibited syringomyelia (45). In the presence of CM1, cerebellar tonsil occlude the narrow subarachnoid space located around the foramen magnum. The propagation of existing syringomyelia may occur *via* the expansion of the brain during systole, which obstructs the subarachnoid space

across the foramen magnum; moreover, the piston-like rapid movement of CSF during systole generates pressure, which propels the fluid inferiorly (46). However, the mechanism underlying syringomyelia formation remains unclear, although several hypotheses have been proposed based on the narrowed space and high subarachnoid space pressure; nevertheless, this cannot explain the rare passage between the fourth ventricle and syrinx and has not been confirmed (47).

Craniofacial anomaly is one of the major features of OPDSD, and several cases with craniosynostosis have been reported. To date, six patients with gain-of-function variants of *FLNA* have been reported to show craniosynostosis, and there was only one patient who was diagnosed with FMD1 with pansynostosis similar to our patient (48). Our case is the seventh case of craniosynostosis in OPDSD and second for pansynostosis, emphasizing that FMD1 can be associated with craniosynostosis. Therefore, if the patient is diagnosed as having gain-of-function variants of *FLNA*, craniosynostosis should be promptly checked, and if necessary, immediate surgical treatment can prevent CM1 and thus, complications such as syringomyelia.

Several reported FMD1 cases exhibit hypoplasia of hand intrinsic muscles (11). Similarly, the strength of the hand intrinsic muscles was graded as 2/5 in our patient. The development of hand weakness has not been explored in previous studies. Therefore, it is currently difficult to determine whether extensive syringomyelia, as observed in our patient, is the direct cause of hand weakness or whether hand weakness can appear without any CNS lesions because it is a clinical characteristic of FMD1. Additional research is warranted to address this issue.

OPDSD is an allelic condition, and the mutations identified to date are in-frame mutations that preserve the reading frame and length of the translated filamin A protein. Robertson et al. performed genotypic and phenotypic correlation in 41 unrelated patients with OPDSD (10). All five disorders of OPDSDs were caused by 17 mutations in four regions of *FLNA*. All mutations resulted in OPD1 and OPD2 were located in the calponin homology domains of the N-terminal actin-binding domain of *FLNA*. Some common and frequent mutations were 620C>T in OPD1, 760G>A in OPD2, and 3562G>A and 3596C>T in MNS. In addition, patients with the same mutations showed similar phenotypes. For example, four males with OPD2, possessing the 760G>A mutation, exhibited omphalocele and perinatal death. However, although they carried the same mutation, two of four patients showed hydrocephalus, while the others did not (10). Our patient exhibited CM1 with syringomyelia; however, CNS anomalies were not reported in other patients with FMD1 who carried the same missense mutation. The genotypic and phenotypic correlation in patients with OPDSD is complex and difficult to define. Further genotypic and phenotypic correlation studies are needed to address these issues.

## CONCLUSION

We reported a rare case of FMD1 resulting from a pathogenic variant (c.3557C>T) of *FLNA*. This case was distinguished from those previously reported in that the patient had pansynostosis and showed CNS involvement in the form of Chiari I malformation accompanied by extensive syringomyelia. If OPDSD is diagnosed, evaluation of craniosynostosis and CM1 malformation may be essential and proper treatment is critical for the prognosis of these patients. Further studies are warranted to determine whether CNS involvement is a phenotype of FMD1.

## DATA AVAILABILITY STATEMENT

The original contributions presented in the study are included in the article/**Supplementary Material**, further inquiries can be directed to the corresponding author.

## ETHICS STATEMENT

The studies involving human participants were reviewed and approved by the Catholic University of Korea, Incheon St. Mary's hospital, South Korea. Written informed consent to participate in this study was provided by the participants' legal guardian/next of kin. Written informed consent was obtained from the parent of the patient for publication of this case report.

## AUTHOR CONTRIBUTIONS

JK: acquisition of data, analysis and interpretation of data, writing, and critical revision of manuscript. D-WL: acquisition of data, analysis, and interpretation of data. D-HJ: study concept and design, acquisition of data, analysis and interpretation of data, study supervision, and critical revision of manuscript for intellectual content. All authors contributed to the article and approved the submitted version.

## SUPPLEMENTARY MATERIAL

The Supplementary Material for this article can be found online at: https://www.frontiersin.org/articles/10.3389/fped.2021.574402/full#supplementary-material

## REFERENCES

1. Atwal PS, Blease S, Braxton A, Graves J, He W, Person R, et al. Novel X-linked syndrome of cardiac valvulopathy, keloid scarring, and reduced joint mobility due to filamin A substitution G1576R. *Am J Med Genet A.* (2016) 170A:891–5. doi: 10.1002/ajmg.a.37491
2. Wade EM, Halliday BJ, Jenkins ZA, O'Neill AC, Robertson SP. The X-linked filaminopathies: synergistic insights from clinical and molecular analysis. *Hum Mutat.* (2020) 41:865–83. doi: 10.1002/humu.24002
3. Robertson SP. Otopalatodigital syndrome spectrum disorders: otopalatodigital syndrome types 1 and 2, frontometaphyseal dysplasia

and Melnick-Needles syndrome. *Eur J Human Genet.* (2007) 15:3–9. doi: 10.1038/sj.ejhg.5201654
4. Gorlin JB, Henske E, Warren ST, Kunst CB, D'Urso M, Palmieri G, et al. Actin-binding protein (ABP-280) filamin gene (FLN) maps telomeric to the color vision locus (R/GCP) and centromeric to G6PD in Xq28. *Genomics.* (1993) 17:496–8. doi: 10.1006/geno.1993.1354
5. Maestrini E, Patrosso C, Mancini M, Rivella S, Rocchi M, Repetto M, et al. Mapping of two genes encoding isoforms of the actin binding protein ABP-280, a dystrophin like protein, to Xq28 and to chromosome 7. *Hum Mol Genet.* (1993) 2:761–6. doi: 10.1093/hmg/2.6.761
6. Nakamura F, Kumeta K, Hida T, Isono T, Nakayama Y, Kuramata-Matsuoka E, et al. Amino- and carboxyl-terminal domains of Filamin-A interact with CRMP1 to mediate Sema3A signalling. *Nat Commun.* (2014) 5:5325. doi: 10.1038/ncomms6325
7. Nakamura F, Stossel TP, Hartwig JH. The filamins: organizers of cell structure and function. *Cell Adh Migr.* (2011) 5:160–9. doi: 10.4161/cam.5.2.14401
8. Stossel TP, Condeelis J, Cooley L, Hartwig JH, Noegel A, Schleicher M, et al. Filamins as integrators of cell mechanics and signalling. *Nat Rev Mol Cell Biol.* (2001) 2:138–45. doi: 10.1038/35052082
9. Robertson S. X-linked otopalatodigital spectrum disorders. In: Adam MP, Ardinger HH, Pagon RA, et al., editors. *GeneReviews*. Seattle, WA: University of Washington, Seattle (2005).
10. Robertson SP, Twigg SR, Sutherland-Smith AJ, Biancalana V, Gorlin RJ, Horn D, et al. Localized mutations in the gene encoding the cytoskeletal protein filamin A cause diverse malformations in humans. *Nat Genet.* (2003) 33:487–91. doi: 10.1038/ng1119
11. Robertson SP, Jenkins ZA, Morgan T, Ades L, Aftimos S, Boute O, et al. Frontometaphyseal dysplasia: mutations in FLNA and phenotypic diversity. *Am J Med Genet A.* (2006) 140:1726–36. doi: 10.1002/ajmg.a.31549
12. Wade EM, Jenkins ZA, Daniel PB, Morgan T, Addor MC, Ades LC, et al. Autosomal dominant frontometaphyseal dysplasia: delineation of the clinical phenotype. *Am J Med Genet A.* (2017) 173:1739–46. doi: 10.1002/ajmg.a.38267
13. Wade EM, Daniel PB, Jenkins ZA, McInerney-Leo A, Leo P, Morgan T, et al. Mutations in MAP3K7 that alter the activity of the TAK1 signaling complex cause frontometaphyseal dysplasia. *Am J Hum Genet.* (2016) 99:392–406. doi: 10.1016/j.ajhg.2016.05.024
14. Stratton RF, Bluestone DL. Oto-palatal-digital syndrome type II with X-linked cerebellar hypoplasia/hydrocephalus. *Am J Med Genet.* (1991) 41:169–72. doi: 10.1002/ajmg.1320410206
15. Hung PC, Wang HS, Lui TN. Coexistence of oto-palato-digital syndrome type II and Arnold-Chiari I malformation in an infant. *Brain Dev.* (1999) 21:488–90. doi: 10.1016/S0387-7604(99)00044-3
16. Hidalgo-Bravo A, Pompa-Mera EN, Kofman-Alfaro S, Gonzalez-Bonilla CR, Zenteno JC. A novel filamin A D203Y mutation in a female patient with otopalatodigital type 1 syndrome and extremely skewed X chromosome inactivation. *Am J Med Genet A.* (2005) 136:190–3. doi: 10.1002/ajmg.a.30792
17. Naudion S, Moutton S, Coupry I, Sole G, Deforges J, Guerineau E, et al. Fetal phenotypes in otopalatodigital spectrum disorders. *Clin Genet.* (2016) 89:371–7. doi: 10.1111/cge.12679
18. Liu X, Wu C, Li C, Boerwinkle E. dbNSFP v3.0: a one-stop database of functional predictions and annotations for human nonsynonymous and splice-site SNVs. *Hum Mutat.* (2016) 37:235–41. doi: 10.1002/humu.22932
19. McLaren W, Gil L, Hunt SE, Riat HS, Ritchie GR, Thormann A, et al. The ensembl variant effect predictor. *Genome Biol.* (2016) 17:122. doi: 10.1186/s13059-016-0974-4
20. Zenker M, Nahrlich L, Sticht H, Reis A, Horn D. Genotype-epigenotype-phenotype correlations in females with frontometaphyseal dysplasia. *Am J Med Genet A.* (2006) 140:1069–73. doi: 10.1002/ajmg.a.31213
21. Crary MA, Humphrey JL, Carnaby-Mann G, Sambandam R, Miller L, Silliman SJD. Dysphagia, nutrition, and hydration in ischemic stroke patients at admission and discharge from acute care. *Dysphagia.* (2013) 28:69–76. doi: 10.1007/s00455-012-9414-0
22. Taybi H. Generalized skeletal dysplasia with multiple anomalies. A note on Pyle's disease. *Am J Roentgenol Radium Ther Nucl Med.* (1962) 88:450–7.
23. Gorlin RJ, Cohen MM Jr. Frontometaphyseal dysplasia. A new syndrome. *Am J Dis Child.* (1969) 118:487–94. doi: 10.1001/archpedi.1969.02100040489014
24. Biancalana V, Le Marec B, Odent S, Van den Hurk J, Hanauer A. Oto-palato-digital syndrome type I: further evidence for assignment of the locus to Xq28. *Human Genet.* (1991) 88:228–30. doi: 10.1007/BF00206078
25. Robertson SP. Filamin A: phenotypic diversity. *Curr Opin Genet Dev.* (2005) 15:301–7. doi: 10.1016/j.gde.2005.04.001
26. Boduroglu K, Tuncbilek E. Frontometaphyseal dysplasia: a case with Arnold-Chiari malformation and bracket epiphysis of the first metacarpal bone. *Pediatr Int.* (1999) 41:181–3. doi: 10.1046/j.1442-200X.1999.4121025.x
27. Schijman E. History, anatomic forms, and pathogenesis of Chiari I malformations. *Childs Nerv Syst.* (2004) 20:323–8. doi: 10.1007/s00381-003-0878-y
28. Nishikawa M, Sakamoto H, Hakuba A, Nakanishi N, Inoue Y. Pathogenesis of Chiari malformation: a morphometric study of the posterior cranial fossa. *J Neurosurg.* (1997) 86:40–7. doi: 10.3171/jns.1997.86.1.0040
29. Schady W, Metcalfe RA, Butler P. The incidence of craniocervical bony anomalies in the adult Chiari malformation. *J Neurol Sci.* (1987) 82:193–203. doi: 10.1016/0022-510X(87)90018-9
30. Buell TJ, Heiss JD, Oldfield EH. Pathogenesis and cerebrospinal fluid hydrodynamics of the Chiari I malformation. *Neurosurg Clin N Am.* (2015) 26:495–9. doi: 10.1016/j.nec.2015.06.003
31. Bidot S, Saindane AM, Peragallo JH, Bruce BB, Newman NJ, Biousse V. Brain imaging in idiopathic intracranial hypertension. *J Neuroophthalmol.* (2015) 35:400–11. doi: 10.1097/WNO.0000000000000303
32. Cinalli G, Renier D, Sebag G, Sainte-Rose C, Arnaud E, Pierre-Kahn A. Chronic tonsillar herniation in Crouzon's and Apert's syndromes: the role of premature synostosis of the lambdoid suture. *J Neurosurg.* (1995) 83:575–82. doi: 10.3171/jns.1995.83.4.0575
33. Cinalli G, Spennato P, Sainte-Rose C, Arnaud E, Aliberti F, Brunelle F, et al. Chiari malformation in craniosynostosis. *Childs Nerv Syst.* (2005) 21:889–901. doi: 10.1007/s00381-004-1115-z
34. Schanker BD, Walcott BP, Nahed BV, Kahle KT, Li YM, Coumans JV. Familial Chiari malformation: case series. *Neurosurg Focus.* (2011) 31:E1. doi: 10.3171/2011.6.FOCUS11104
35. Markunas CA, Soldano K, Dunlap K, Cope H, Asiimwe E, Stajich J, et al. Stratified whole genome linkage analysis of Chiari type I malformation implicates known Klippel-Feil syndrome genes as putative disease candidates. *PLoS ONE.* (2013) 8:e61521. doi: 10.1371/journal.pone.0061521
36. Urbizu A, Toma C, Poca MA, Sahuquillo J, Cuenca-Leon E, Cormand B, et al. Chiari malformation type I: a case-control association study of 58 developmental genes. *PLoS ONE.* (2013) 8:e57241. doi: 10.1371/journal.pone.0057241
37. Fric R, Eide PK. Chiari type 1-a malformation or a syndrome? A critical review. *Acta Neurochir.* (2020) 162:1513–25. doi: 10.1007/s00701-019-04100-2
38. Saletti V, Vigano I, Melloni G, Pantaleoni C, Vetrano IG, Valentini LG. Chiari I malformation in defined genetic syndromes in children: are there common pathways? *Childs Nerv Syst.* (2019) 35:1727–39. doi: 10.1007/s00381-019-04319-5
39. Speer MC, George TM, Enterline DS, Franklin A, Wolpert CM, Milhorat TH. A genetic hypothesis for Chiari I malformation with or without syringomyelia. *Neurosurg Focus.* (2000) 8:E12. doi: 10.3171/foc.2000.8.3.12
40. Abbott D, Brockmeyer D, Neklason DW, Teerlink C, Cannon-Albright LA. Population-based description of familial clustering of Chiari malformation Type I. *J Neurosurg.* (2018) 128:460–5. doi: 10.3171/2016.9.JNS161274
41. Ruff ME, Oakes WJ, Fisher SR, Spock A. Sleep apnea and vocal cord paralysis secondary to type I Chiari malformation. *Pediatrics.* (1987) 80:231–4.
42. Sclafani A, DeDio R, Hendrix R. The Chiari-I malformation. *Ear Nose Throat J.* (1991) 70:208–12.
43. Tubbs RS, Lyerly MJ, Loukas M, Shoja MM, Oakes WJ. The pediatric Chiari I malformation: a review. *Childs Nerv Syst.* (2007) 23:1239–50. doi: 10.1007/s00381-007-0428-0
44. Chen H, Chen H. *Atlas of Genetic Diagnosis and Counseling*. Totowa, NJ: Humana Press (2006).
45. Milhorat TH, Chou MW, Trinidad EM, Kula RW, Mandell M, Wolpert C, et al. Chiari I malformation redefined: clinical and radiographic findings for 364 symptomatic patients. *Neurosurgery.* (1999) 44:1005–17. doi: 10.1097/00006123-199905000-00042

46. Oldfield EH, Muraszko K, Shawker TH, Patronas NJ. Pathophysiology of syringomyelia associated with Chiari I malformation of the cerebellar tonsils. Implications for diagnosis and treatment. *J Neurosurg.* (1994) 80:3–15. doi: 10.3171/jns.1994.80.1.0003
47. Oldfield EH. Pathogenesis of Chiari I - pathophysiology of syringomyelia: implications for therapy: a summary of 3 decades of clinical research. *Neurosurgery.* (2017) 64:66–77. doi: 10.1093/neuros/nyx377
48. Fennell N, Foulds N, Johnson DS, Wilson LC, Wyatt M, Robertson SP, et al. Association of mutations in FLNA with craniosynostosis. *Eur J Hum Genet.* (2015) 23:1684–8. doi: 10.1038/ejhg.2015.31

**Conflict of Interest:** The authors declare that the research was conducted in the absence of any commercial or financial relationships that could be construed as a potential conflict of interest.

# Advantages of publishing in Frontiers

**OPEN ACCESS**
Articles are free to read for greatest visibility and readership

**FAST PUBLICATION**
Around 90 days from submission to decision

**HIGH QUALITY PEER-REVIEW**
Rigorous, collaborative, and constructive peer-review

**TRANSPARENT PEER-REVIEW**
Editors and reviewers acknowledged by name on published articles

**Frontiers**
Avenue du Tribunal-Fédéral 34
1005 Lausanne | Switzerland

**Visit us:** www.frontiersin.org
**Contact us:** frontiersin.org/about/contact

**REPRODUCIBILITY OF RESEARCH**
Support open data and methods to enhance research reproducibility

**DIGITAL PUBLISHING**
Articles designed for optimal readership across devices

**FOLLOW US**
@frontiersin

**IMPACT METRICS**
Advanced article metrics track visibility across digital media

**EXTENSIVE PROMOTION**
Marketing and promotion of impactful research

**LOOP RESEARCH NETWORK**
Our network increases your article's readership